



Assefa M. Melesse *Editor*

# Nile River Basin

Hydrology, Climate and Water Use

# Nile River Basin

Assefa M. Melesse  
Editor

# Nile River Basin

Hydrology, Climate and Water Use



Springer

*Editor*

Dr. Assefa M. Melesse  
Florida International University  
Department of Earth and Environment  
Modesto A. Maidique Campus  
33199 Miami Florida  
USA  
melessea@fiu.edu

ISBN 978-94-007-0688-0

e-ISBN 978-94-007-0689-7

DOI 10.1007/978-94-007-0689-7

Springer Dordrecht Heidelberg London New York

Library of Congress Control Number: 2011922985

© Springer Science+Business Media B.V. 2011

All Rights Reserved for Chapter 11

No part of this work may be reproduced, stored in a retrieval system, or transmitted in any form or by any means, electronic, mechanical, photocopying, microfilming, recording or otherwise, without written permission from the Publisher, with the exception of any material supplied specifically for the purpose of being entered and executed on a computer system, for exclusive use by the purchaser of the work.

Printed on acid-free paper

Springer is part of Springer Science+Business Media ([www.springer.com](http://www.springer.com))

# Foreword

The River Nile Water is the lifeblood for 180 million people who live in the river basin. Nile water supports hydropower, agriculture, navigation, and a multitude of ecosystem services all essential for economic growth, poverty reduction, and stability in the region. The region has the potential for rapid growth, and many individuals, communities, companies, and countries have high hopes that the Nile waters can support growth and prosperity. While the future expectation of what the Nile can deliver to its people is extremely high, in fact the resource is limited, and there is a real danger that ill-planned development can lead to degradation and conflict.

Underpinning good planning and development is knowledge about the hydrology of the Nile system. While there has been millions spent on development, and there are large plans for more development, it is surprising how little basic data and analysis is readily available, especially data for the upstream countries in the basin. For historic reasons, Egypt and Sudan possess a wealth of knowledge about the Nile waters and its use. This is not true for upstream countries who have tapped very little of the Nile River water resource, but who are looking to gain more benefits from the Nile in the future. Information in the book plays an important role to bridge this gap. There is a wealth of new modeling and information techniques that can really help build a better picture of water resources in the region. This book makes an advance in bringing these techniques to bear on the Nile basin.

The book covers a range of biophysical issues important for the Nile basin. For example, fundamental to water management are the water budgets of the major lakes in the region which are revisited in this book. Ultimately rain is the source of water for the Nile River basin, yet the knowledge of historic, let alone real time rainfall across the huge basin is scant. Satellite rainfall estimation provides some exciting opportunities to fill in this void, and there is a great opportunity for their application in planning and real time management as the book reveals. Ultimately many decisions are made in a watershed context, and GIS and remote sensing provide the spatial tools needed for communities and countries to explore options for development. Climate variability and climate change are major unknowns in the region, but people have to contend with climate variability in their day to day lives. Chapters in the book shed light on basic processes and provide tools which are useful to better analyze and understand the implications of climate change and climate variability.

Ultimately decisions have to be made about the allocation of Nile waters amongst different users, and different countries. While it can be argued that these decisions are largely political, science has an important role in informing better ways to serve all, to highlight tradeoffs that need to be made, and to minimize negative consequences. Making better water decisions requires better knowledge of water availability, how water is accessed now, what is the productivity of its use, environmental flows, and the implications of future demands and development scenarios. The book, *Nile River Basin: Hydrology, Climate and Water Use* represents an important milestone for work on Nile waters. It is an important reference for professionals, policy makers, practitioners, researchers and students who are required to find solutions for the people dependent on Nile waters, and their children. It provides a critical resource for the people managing this transboundary river, and thus the people dependent on its water. It is an important milestone for those addressing one of the most pressing challenges of our time, water scarcity.

David Molden

# Introduction: Hydrology of the Niles in the Face of Climate and Land-Use Dynamics

Assefa M. Melesse, Seleshi Bekele, and P. McCornick

## 1 Nile River Basin Overview

The Nile River, at about 6,825 km, is the longest river in the world. It comprises two major tributaries, the White Nile and the Blue Nile (known as the Abbay in Ethiopia). The White Nile rises in the Great Lakes region of central Africa, with the most distant source in southern Rwanda and flows north from there through Tanzania, Lake Victoria, Uganda and southern Sudan. The Blue Nile starts at Lake Tana in Ethiopia, and flows into Sudan from the southeast. The two rivers meet at the Sudanese capital Khartoum and flow north through Sudan and Egypt to drain into the Mediterranean Sea. The drainage area estimate varies between 3.1 million km<sup>2</sup> (FAO, 2007) to 3.3 million km<sup>2</sup> (CPWF, 2007). The variation is due to difficulty in delineation of the sub-basin in the flat slope parts of Sudan and Egypt. Ten countries fall within the Nile basin and these include Burundi, Democratic Republic of Congo, Egypt, Eritrea, Ethiopia, Kenya, Rwanda, Sudan, Tanzania, and Uganda (Molden et al., 2010). The Nile River basin is home to approximately 180 million people, while over 350 million (based on World Bank, 2006b) live within the 10 riparian states. The Nile region is characterized by high population growth and considerable development challenges (Awulachew et al., 2008). The benefits of the Nile River need to be shared among these 10 countries, but the issues are hard to encompass. The unbalanced distribution of water, wealth, and power have made the issues even more challenging for gaining information and creating appropriate interventions (Molden et al., 2010).

---

A.M. Melesse (✉)

Department of Earth and Environment, Florida International University,  
Modesto A. Maidique Campus, Miami, FL 33199, USA  
e-mail: melessea@fiu.edu

## 2 Hydrometeorological Variability

Historical hydro-meteorological data analysis of the basin showed a high variability in the river flows and rainfall pattern. The variability of dry season precipitation hence river flows is higher than that of the wet season rainfall and river discharges. The spatial variability of rainfall and river discharges is also high with the upper basin receiving more rainfall and thereby generating most of the runoff than downstream, with virtually no flow generated in the lower basin. The relative contribution to the mean natural Nile River at Aswan of  $84.1 \text{ Gm}^3/\text{year}$  (mean of 1900–1950) is approximately 4/7 from the Blue Nile, 2/7 from the White Nile (of which 1/7 is from the Sobat), and 1/7 is from the Atbara River (Molden et al., 2010), signifying that over 85% of the Nile flow is generated in the Ethiopian highlands. The long term mean flow of the Nile at Aswan is in fact higher than  $84.1 \text{ Gm}^3/\text{year}$  (Awulachew et al., 2010).

A close examination of the seasonality of rainfall and flow using wavelet analysis showed different frequency recurrence for the rainfall and river flows for the upper Blue Nile River basin (Figs. 1 and 2). Figures 1 and 2 show the Continuous Wavelet

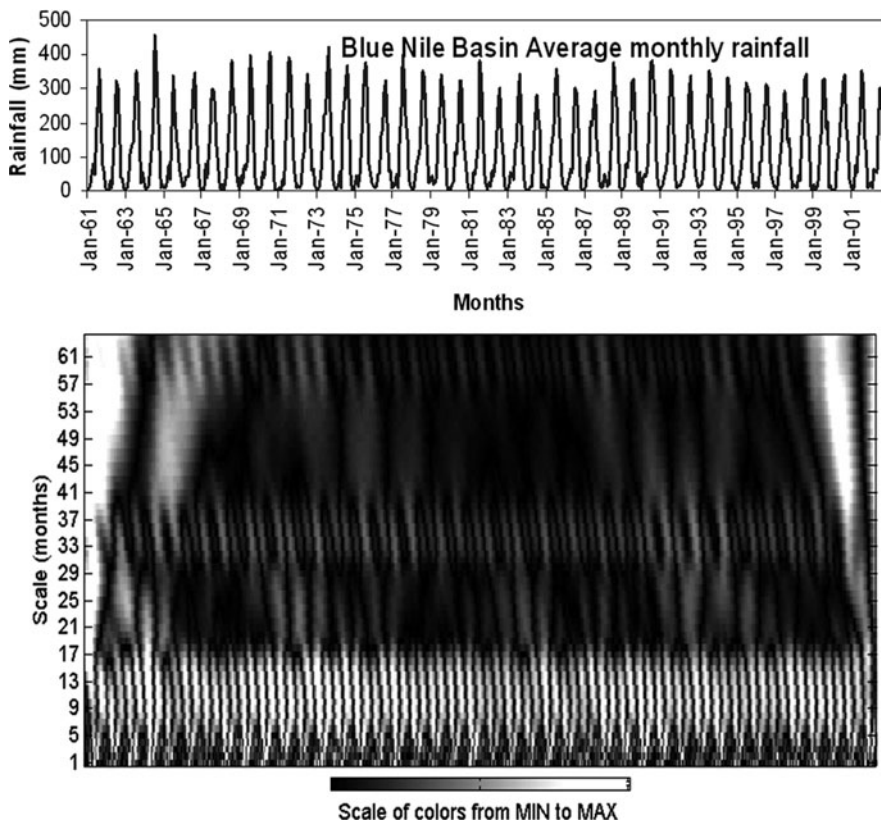


**Fig. 1** Continuous wavelet transform for Blue Nile basin-wide Rainfall (Melesse et al., 2009)

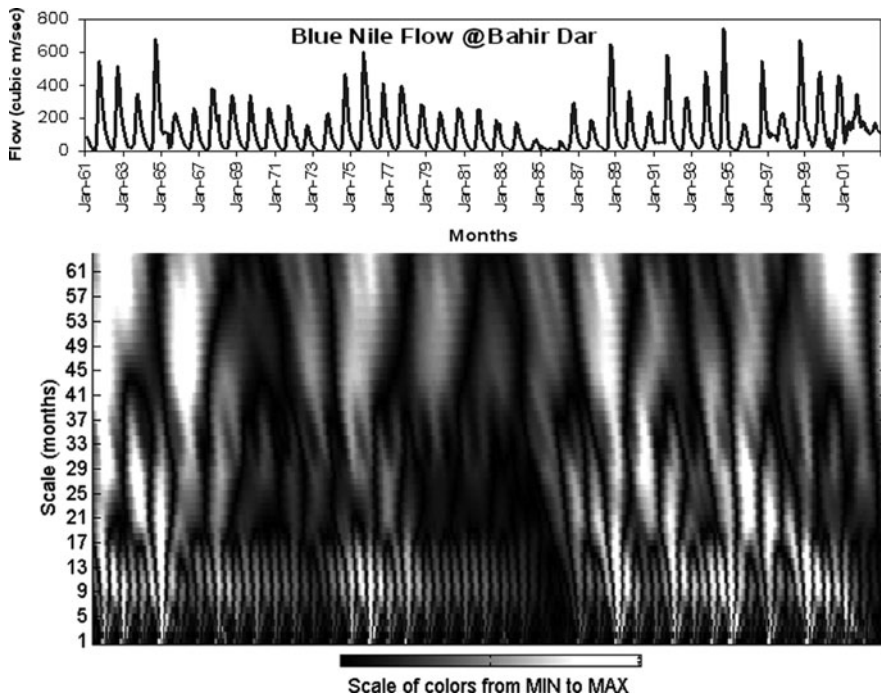


**Fig. 2** Continuous wavelet transform for the monthly average flow Blue Nile at Bahir Dar (Melesse et al., 2009)

Transform (CWT) maps of the basin-wide average monthly rainfall and Blue Nile flow at Bahir Dar, respectively. The wavelet time-frequency analysis of the rainfall and flow in the upper Blue Nile River basin has shown various trends at different time scales. As depicted in Fig. 1, approximately a 10-year trend is shown for the Blue Nile basin wide rainfall around 1963, 1973, 1983, 1993 and 2003 at a scale of 17–30 months. The wavelet spectral power of the Blue Nile basin-wide average rainfall was also strong for the period of 1961–1963 at a scale of 41–64 months. The time-frequency representation for the monthly average flow of Blue Nile River at Bahir Dar (Fig. 2) for the period from 1987–2003 has shown some trend which is consistent at different scales (9–17, 17–30 and 30–61 months). The 17–30 months scale trend was very strong for the 1987–1997 period.

Scale represents the width or frequency of the signal. When the scale factor is relatively low (high frequency), the signal is more contracted which in turn results in a more detailed time series graph. However, low scale does not last for the entire duration of the signal. On the other hand, when the scale factor is high (low frequency), the signal is stretched out which means that the resulting graph will be presented in less detail. Nevertheless, it usually lasts the entire duration of the signal.

The Gravity Recovery and Climate Experiment (GRACE) (GRACE, 2010) satellite-based monthly changes in gravity converted to equivalent water in the Nile River basin is shown in Fig. 3. These maps demonstrate that the stored water and

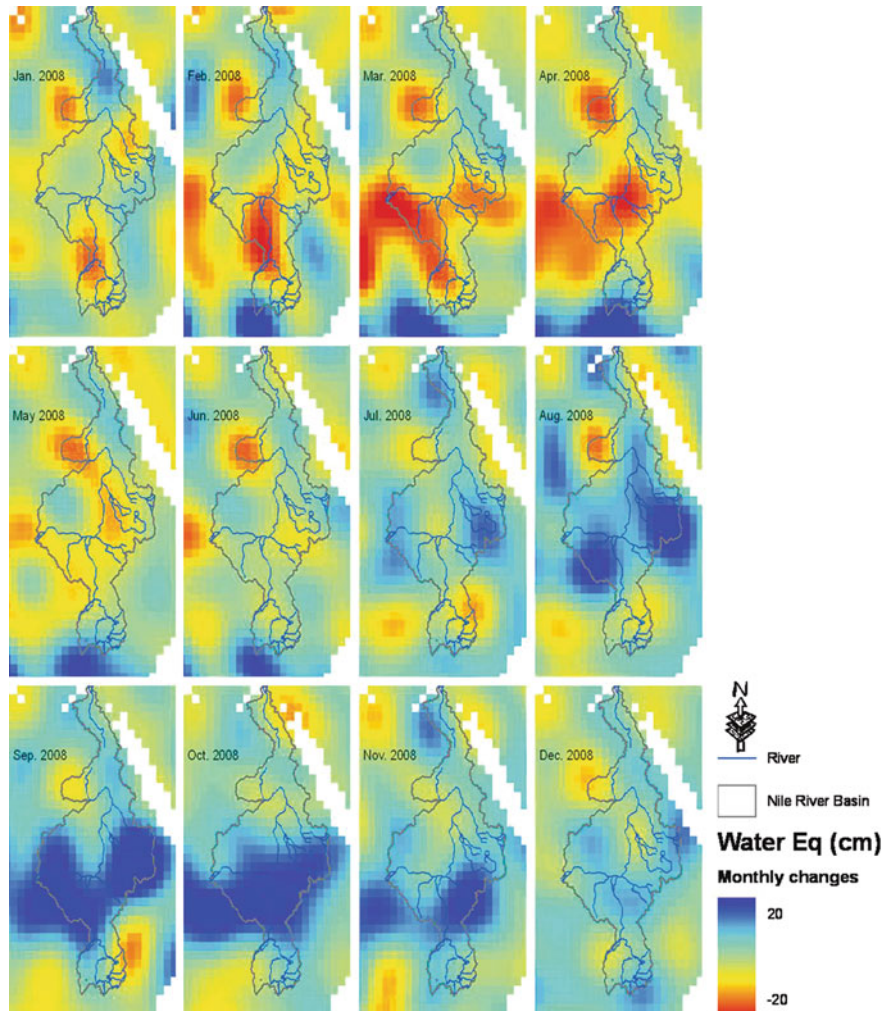


**Fig. 3** GRACE-based monthly changes of water equivalent for the Nile River basin in 2008

monthly moisture flux within the basin are highly seasonal as well as spatially variable. The Blue Nile (Lake Tana) and middle part of the Nile River basin receives large amount of water in the July-September period resulting in positive monthly changes (see Fig. 3). On the other hand, the maps for January-May indicate a negative moisture flux, due to limited rainfall and increasing evaporation.

The potential evapotranspiration (PET) maps of the Nile River Basin (Fig. 4) based on the Penman-Monteith (PM) equation (FEWS NET, 2010) demonstrates the considerable temporal and spatial variation in potential evaporation across the basin.

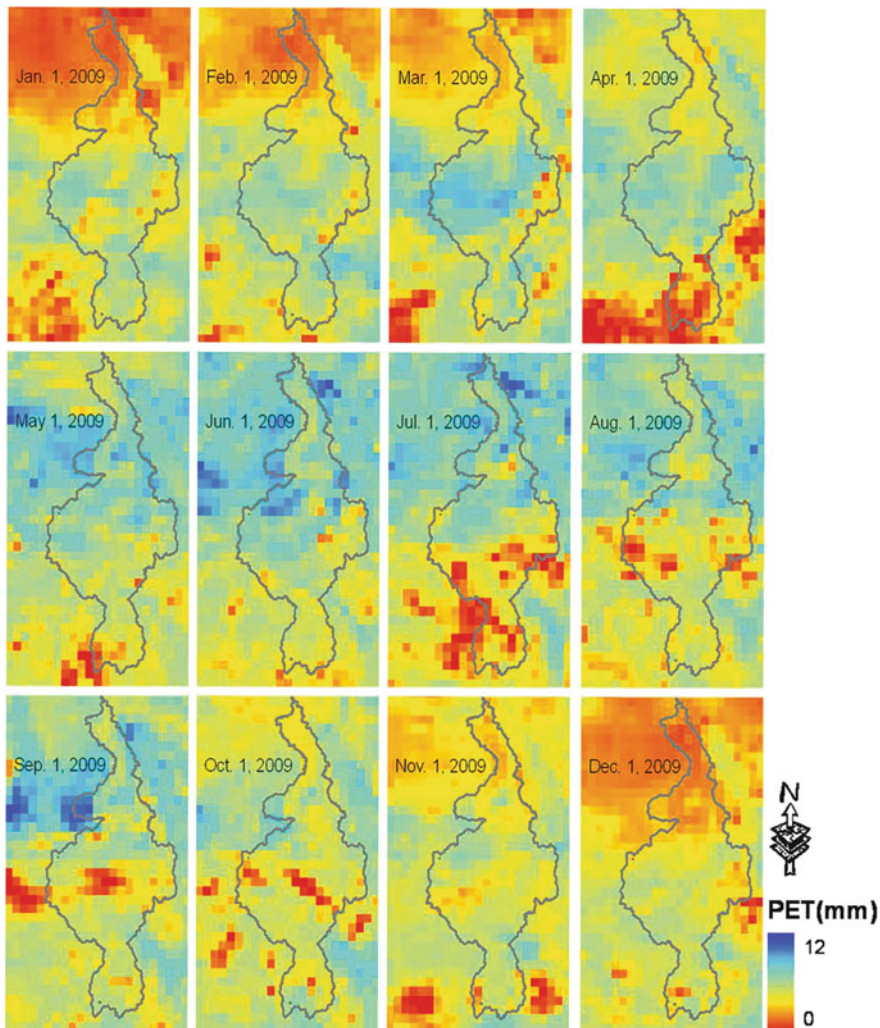


**Fig. 4** Daily potential evapotranspiration (PET) across the Nile River basin

### 3 Land Use/Land Covers Change and Land Degradation

Although the Nile River is the longest river in the world, the total volume of water in the Nile River system is much smaller than the Amazon (2%), Mississippi (15%) and Mekong (20%) Rivers. But the river is historically important and the livelihood of many people depends on it. The basin is characterized as one of the most degraded mainly due to rapid population growth, poverty, political instability, poor watershed management, poor or absence of effective water use policy and frequent natural disasters. Home of the second and the third populous countries of Africa, the Nile

basin is under continuous pressure to provide the water needs of the basin. The population pressure in the Blue Nile River part of the basin has led to serious land degradation and land conversion to agricultural areas. This has led to increased soil erosion, loss of soil fertility and reduction in dry season flows. Although there is no a reliable basin wide systematic analysis of land use and land cover change, satellite images shows land cover changes in the upper Blue Nile River and other parts of the basin.

Numerous challenges face the basin. Fifty percent of the countries in the basin such as Burundi, DR Congo, Eritrea, Ethiopia and the Sudan face the challenge of food security due to poor agricultural productivity, climate change, degradation and conflicts. Subsistence and rain-fed agriculture, together with high rainfall variability is one of the main causes of food insecurity and the most daunting challenge the basin faces. Degradation is extensive in the upstream countries such as Ethiopia, Eritrea, Rwanda and the Lake Victoria region. Drought and floods are critical issues in most of the upstream countries, including Sudan, with the potential to be exacerbated by climate change.

Large wetlands are found in eight of the Nile basin countries. Preservation of some of these wetlands such as the Sudd is a topic of considerable transboundary and international importance. The benefits of the Nile River need to be shared among the 10 riparian countries, but the issues are hard to encompass and often appear as sources of disagreements and conflicts. On the other hand, many believe that if the difficulties of the Nile basin hydro-political impasse is resolved, the significant potential of the water resources (i.e. hydropower) can benefit the people of all riparian countries.

Over 70% of the basin's people depend on subsistence, rain-fed agriculture (<http://eastafrika.iwmi.org/>) (IWMI, 2010). However, the resource base of land and water is not well utilized, nor appropriately managed, and is degrading very rapidly due to population pressure and poor agricultural practices. Water related diseases are common and a major cause of the relatively low life expectancy in the region. Livestock, fisheries and aquaculture are fundamental in the daily lives of people along the Nile, but have been neglected topics in the water discourse (Molden et al., 2010). Livestock are essential to many groups in the Nile basin; they establish the wealth of a family, determine the ability to marry and indicate the social standing of several groups within the basin. Water, food and health issues for animals and humans are crucial. The potential to develop fisheries along the Nile River is very promising (Molden et al., 2010).

## 4 Climate Change and Predicted Impacts on Available Water

There is generally good agreement on anticipated temperature increases across the Nile basin over the course of the coming century (Beyene et al., 2010; Jeuland, 2009; and Conway, 2005), but for the projections on likely trends in precipitation and runoff, there is less concurrence. Jeuland (2009) concluded that, while there remains considerable disagreement on the likely effects of climate change on the

water resources in the basin, the research to date suggests that the rainfall and runoff in the Lake region (White Nile) is likely to increase, the Eastern Nile (including the Blue Nile) is highly uncertain, and even where precipitation increases the increased temperatures may reduce runoff.

Recognizing that there are considerable differences in results, using the mean output from a number (ensemble) of models results does greatly reduce the range of projections (Jeuland, 2009). Using this approach with the results from 11 GCMs, Beyene, et al. (2010)<sup>1</sup> suggested that the effects of climate change would cause the basin to become wetter over the next three decades, and thereafter drier. Furthermore, the average results suggest a wetter winter (DJF) in both the Blue and White Nile, and mixed results in the summer (JJA).

We should recognize that there are other changes in the basin that are likely to have a greater effect on the water resources over this same time-scale, especially the increasing demand for agriculture and other productive uses.

According to Kim et al. (2008), the increased rainfall and resultant water supply in the upper Blue Nile that is anticipated through the middle of the century, is likely to be positive in a region regularly beset by drought. However, according to ElShamy et al. (2009), over the longer term (2081–2098), the Blue Nile basin may become drier. Using the outputs from 17 GCM for the A1B scenario their predictions varied between a -15% and +14% change in precipitation, with the ensemble mean suggesting little change. However, the projected increase in temperature and evaporation is projected to reduce the runoff.

Based on 15 GCMs, Setegn et al. (2011) (Chapter 12 by Setegn et al. this book) downscaled the temperature and precipitation to a watershed scale for the upper Blue Nile River basin for the 2046–2065 and 2080–2100 periods and assessed the impact on the hydrology of the Blue Nile River at selected gauge stations. The Soil and Water Assessment Tool (SWAT) model output based on the downscaled data shows that flow, soil moisture, evapotranspiration and groundwater levels can change significantly but also were highly variable across the different GCMs leading to high uncertainty and less conformity in the predication.

The seasonal distribution of these possible increases also needs to be considered. According to the analysis by Beyene et al. (2010), much of the precipitation increases in the Blue Nile are anticipated in the winter (DJF) months, which may be of less value in this region, where the majority of the agricultural production systems are presently rainfed. However, the projections from Soliman et al. (2009)<sup>2</sup> suggest that by the middle of the century the annual discharge from the Blue Nile

---

<sup>1</sup>Beyene et al. (2010) compared the results of eleven Global Change Models (GCM) on water resources in the Nile basin for both the A2 and B1 IPCC climate change scenarios. The B1 scenario assumes continuing economic growth and global trade, population growth gradually slowing down to a maximum of close to 9 billion people by 2050 and the adoption of clean and resource efficient technologies, and the A2 assumes less globalization and cooperation, relatively slow economic and technological development, and the continuing expansion of the world's population that would reach 15 billion by the end of the century.

<sup>2</sup> This analysis used in the A1B emissions scenario and the ECHAM5 (Max Planck Institute) GCM and considered the 2034–2055 timeframe.

would be similar to recent historic levels, but with appreciable changes in the seasonality and spatial variability. This analysis suggested higher flows at the onset of the wet season, and reduction in flows at the end of the wet season and through the dry season.

Where there is irrigated agriculture, the anticipated effects of climate change on the already highly variable seasonal and spatial variation is likely to be a complicating factor. While overall the eastern portion of the Nile basin is likely to be wetter in coming decades, the expectation is that there will be a greater frequency and magnitude of extreme and localized climatic events (e.g., heavy precipitation, flooding and drought).

Similarly on the White Nile, the effects of climate change on the spatial variability of the water resources at the lower scales are expected to be relatively high. The lakes are expected to have a moderating effect on the downstream flows, although lake level changes are anticipated to be modified with climate change (Beyene, et al., 2010).

## **5 Impacts of Climate Change to Economic and Other Sectors (Agriculture, Health, Energy)**

The predicted changes in climate discussed above, while potentially beneficial in some cases, add further uncertainty to water resources systems in the Nile basin that are already naturally highly variable. In addition to the impact on the existing situation, this increases the uncertainty associated with major investments in water and other related sectors, especially agriculture, energy, transportation (i.e. roads) and urban development.

Based on the projections by Beyene et al. (2010), the annual inflows into the High Aswan Dam would increase by approximately 10% above recent historic averages through 2040, which would allow for approximately 6% increase in annual irrigation over this time period. However, using the same predictions, inflow into the reservoir is projected to decline to 15% less than the historical average by the end of the century due to the drying trend and increased evaporative demand. Should this occur, by around the middle of the century the irrigation releases are predicted to decline to 87% of recent historical averages and remain at this level thereafter. Hydropower is expected to follow a similar trend over the same time period that is increase through 2040 and then decline thereafter.

The situation becomes more ambiguous upstream of the High Aswan Dam, in part because of the existing spatial and temporal variation of the precipitation and runoff, the increased uncertainty of the projections at lower scales, a higher dependency on rainfed agriculture, and the relatively low levels of development of water resources. The more vulnerable countries and communities are in many cases the least able to cope and adapt. Securing and sustaining water supply to these communities, creating the resilience to survive extreme events, and enhancing the capacity to use water productively will be a challenge (Sadoff and Muller, 2009). This is

of particular concern where there is a strong correlation between the hydrologic shocks, and reduced economic growth and increasing poverty, as is the case in many of the countries within the basin (World Bank, 2006a).

The future impacts of climate change would introduce additional risks of negative health impacts from the increasingly limited and poor-quality global water supply (WHO, 2009), especially in parts of the basin where significant portions of the population continue to be exposed to the disease burden brought on by poor water quality, water shortages and the effects of floods. The anticipated climate change conditions that include a greater frequency and magnitude of extreme climatic events (e.g., heavy precipitation, flooding and drought) will have potential impacts on population health as such conditions make securing clean drinking water more difficult. In addition, these same extreme events can further destabilize an already food-insecure situation and the nutritional status of the local population, even where the overall climate is wetter.

## 6 Adaptation Strategies to Future Climate Change Related Disasters

Effective water resources management is fundamental to successful adaptation, and adaption efforts need to be appropriately integrated into on-going development and resource management systems, in a fashion that compliments climate change mitigation. Failure to do this not only means missed opportunities, but could result in mal-adaptation, including infrastructure that is not designing for the conditions or institutional (i.e. water rights) and organizational arrangements that don't have the flexibility or capacity to respond.

Efforts to adapt to climate change need to recognize and integrate with the broader sustainable development and the effects of the other drivers affecting the particular context; implement good water management practices, such as improving efficiency, enhancing storage and risk management, that will improve resilience to cope with the uncertainties of climate change; improve governance from communities up to basin or national level frameworks; recognize the economic consequences of inaction and securing the necessary financing (economics and financing); and enhance and disseminate the knowledge and information required for local adaptation, and to reduce uncertainties, including early warning (adapted from the Nairobi Principles<sup>3</sup>)

The planning, development and management of water resources in the Nile basin, which has historically been undertaken in a highly variable and relatively data sparse environment, must further allow for the uncertainty associated with the potential

---

<sup>3</sup>The Nairobi Statement on Land and Water Management for Adaptation to Climate Change Nairobi, 17 April 2009. Dialogue on Land and Water Management for Adaptation to Climate Change. <http://landwaterdialogue.um.dk>

non-stationarity of the resource and disagreement in predictions. Given that the spatial and temporal changes are expected to be relatively extreme, and that there is more uncertainty on the impacts of the water resources, adaptation approaches in the sub-basins of both the Blue and White Niles need to be more nuanced.

The book, “Nile River Basin: Hydrology, Climate and Water Use” is a collection of various reviews, analysis and study results covering a wide range of topics and issues. The chapters cover from the physical hydrology and climate change to water use and allocation. The chapters are organized in 6 thematic areas (Hydrology and water budget, Satellite rainfall estimation, GIS and Remote sensing in watershed modeling, Climate variability and hydrologic response and Water resources management, allocation and policy I and II).

## References

Awulachew SB, McCartney M, Steenhuis T, Ahmed AA (2008) A review of hydrology, sediment and water resource use in the Blue Nile basin. IWMI working paper 131. International Water Management Institute, Colombo

Awulachew S, Rebelo L, Molden D (2010) The Nile basin: tapping the unmet agricultural potential of Nile waters. *Water Int* 35(5):623–654

Beyene T, Lettenmaier DP, Kabat P (2010) Hydrologic impacts of climate change on the Nile River Basin: implications of the 2007 IPCC scenarios. *Clim Change* 100:433–461

Challenge Program on Water and Food (CPWF) (2007) <http://www.cpnile.net>. Accessed 14 Jan 2010

Conway D (2005) From headwater tributaries to international river: observing and adapting to climate variability and change in the Nile basin. *Glob Environ Change* 15:99–114

Elshamy ME, Seierstad IA, Sorteberg A (2009) Impacts of climate change on Blue Nile flows using bias corrected GCM scenarios. *Hydrol Earth Syst Sci* 13:551–565

FAO (2007) <http://www faonile org/nbs/nilesystem html>. Accessed 15 Aug 2010

FEWS NET (Famine early warning System Network) (2010) Potential evapotranspiration map. <http://earlywarning.usgs.gov/Global/product.php?image=pt>. Accessed May 2010

GRACE (2010) Gravity recover and climate experiment. <http://www.csr.utexas.edu/grace/> Accessed 23 Apr 2010

IWMI (2010) <http://eastafrica.iwmi.org/> Accessed 15 June 2010

Jeuland M (2009) Planning water resources development in an uncertain climate future: a hydro-economic simulation framework applied to the case of the Blue Nile. PhD Dissertation, Department of Environmental Sciences and Engineering, University of North Carolina, Chapel Hill, NC

Kim U, Kaluarachchi JJ, Smakhtin VU (2008) Climate change impacts on hydrology and water resources of the Upper Blue Nile River Basin, Ethiopia. (IWMI Research Report 126), International Water Management Institute, Colombo, p 27

Melesse A, Abtew W, Desalegn T, Wang X (2009) Low and high flow analysis and wavelet application for characterization of the Blue Nile River system. *Hydrol Processes* 24(3): 241–252

Molden D, Awulachew SB, Conniff K, Rebelo LM, Mohamed Y, Peden D, Kinyangi J, van Breugel P, Mukherji A, Cascão A, Notenbaert A, Demissie SS, Neguid MA, el Naggar G (2010) Nile basin Focal Project, synthesis report. The CGIAR Challenge Program on Water and Food, Colombo (in press)

Sadoff C, Muller M (2009) Water management, water security and climate change adaptation: early impacts and essential responses. Technical Committee (TEC) Background Paper No. 14, Global Water Partnership (GWP), Stockholm

Setegn S, Rayner D, Melesse AM, Dargahi B, Srinivasan R (2011) Impact of climate change on the hydro-climatology of Lake Tana basin. *Ethiopia Water Resources Research*. doi:10.1029/2010WR009248, in press

Soliman ESA, Sayed MAA, Jeuland M (2009) Impact assessment of future climate change for the Blue Nile basin, using a RCM nested in a GCM. *Nile Basin Water Eng Sci Mag* 2:15–30

World Bank (2006a) Ethiopia: managing water resources to maximize sustainable growth: country water resources assistance strategy. The World Bank, Washington, DC

World Bank (2006b) Africa development indicators 2006. International Bank, Washington, DC

World Health Organization (WHO) (2009) Vision 2030: the resilience of water supply and sanitation in the face of climate change. World Health Organization, Geneva

# Contents

## Part I Hydrology and Water Budget

<b>1</b>	<b>Hydrological Variability and Climate of the Upper Blue Nile River Basin</b>	3
	Assefa M. Melesse, Wossenu Abtew, Shimelis G. Setegn, and Tibebe Dessalegne	
<b>2</b>	<b>Hydro-Meteorology and Water Budget of the Mara River Basin Under Land Use Change Scenarios</b>	39
	Liya M. Mango, Assefa M. Melesse, Michael E. McClain, Daniel Gann, and Shimelis G. Setegn	
<b>3</b>	<b>Hydrological Balance of Lake Tana, Upper Blue Nile Basin, Ethiopia</b>	69
	Tom H.M. Rientjes, Janaka B.U. Perera, Alemseged T. Haile, Ambro S.M. Gieske, Martijn J. Booij, and Paolo Reggiani	

## Part II Satellite Rainfall Estimation

<b>4</b>	<b>Satellite Based Cloud Detection and Rainfall Estimation in the Upper Blue Nile Basin</b>	93
	Tom H.M. Rientjes, Alemseged T. Haile, Ambro S.M. Gieske, Ben H.P. Maathuis, and Emad Habib	
<b>5</b>	<b>Evaluation of Satellite Rainfall Estimates and Gridded Gauge Products over the Upper Blue Nile Region</b>	109
	Tufa Dinku, Stephen Connor, and Pietro Ceccato	
<b>6</b>	<b>Are Satellite-Gauge Rainfall Products Better than Satellite-Only Products for Nile Hydrology?</b>	129
	Menberu M. Bitew and Mekonnen Gebremichael	

**Part III GIS and Remote Sensing in Watershed Modeling**

7 **Watershed Hydrology of the (Semi) Humid Ethiopian Highlands** . . . . 145  
Tegenu A. Engda, Haimanote K. Bayabil, Elias S. Legesse,  
Essayas K. Ayana, Seifu A. Tilahun, Amy S. Collick,  
Zachary M. Easton, Alon Rimmer, Seleshi B. Awulachew,  
and Tammo S. Steenhuis

8 **Evapotranspiration Modeling Using Remote Sensing  
and Empirical Models in the Fogera Floodplain, Ethiopia** . . . . . 163  
Temesgen Enku, Christiaan van der Tol, Ambro S.M. Gieske,  
and Tom H.M. Rientjes

9 **Flood Hazard and Risk Assessment Using GIS and Remote  
Sensing in Fogera Woreda, Northwest Ethiopia** . . . . . 179  
Woubet Gashaw and Dagnachew Legesse

10 **Soil Erosion Mapping and Hotspot Area Identification  
Using GIS and Remote Sensing in Northwest Ethiopian  
Highlands, Near Lake Tana** . . . . . 207  
Mulatie Mekonnen and Assefa M. Melesse

**Part IV Climate Variability and Hydrologic Response**

11 **Application of Hydrological Models for Climate Sensitivity  
Estimation of the Atbara Sub-basin** . . . . . 227  
Eman Hasan and Mohamed Elshamy

12 **Climate Change Impact on Agricultural Water Resources  
Variability in the Northern Highlands of Ethiopia** . . . . . 241  
Shimelis G. Setegn, David Rayner, Assefa M. Melesse,  
Bijan Dargahi, Ragahavan Srinivasan, and Anders Wörman

13 **Climatic Factors Modulating Nile River Flow** . . . . . 267  
Mark R. Jury

**Part V Water Resources Management, Allocation and Policy I**

14 **Hydrological Water Availability, Trends and Allocation  
in the Blue Nile Basin** . . . . . 283  
Seleshi B. Awulachew, Fasikaw Dessie Wubet,  
Matthew McCartney, and Yilma Sileshi Shiferaw

15 **Livestock-Water Productivity in the Nile Basin: Solutions  
for Emerging Challenges** . . . . . 297  
Tilahun Amede, Katrien Descheemaeker, Everisto Mapedza,  
Don Peden, Paulo van Breugel, Seleshi B. Awulachew,  
and Amare Haileslassie

<b>16 Blue Nile (Abbay) Hydropower Potential, Prioritization, and Trade-Offs on Priority Investments . . . . .</b>	<b>321</b>
Dereje T. Desalegn, Seleshi B. Awulachew, and Semu A. Moges	
<b>Part VI Water Resources Management, Allocation and Policy II</b>	
<b>17 Concepts of Environmental Flow Assessment and Challenges in the Blue Nile Basin, Ethiopia . . . . .</b>	<b>337</b>
Bianca Reitberger and Matthew McCartney	
<b>18 Geospatial Mapping and Analysis of Water Availability, Demand, and Use Within the Mara River Basin . . . . .</b>	<b>359</b>
Christina Hoffman, Assefa M. Melesse, and Michael E. McClain	
<b>19 Impacts of Irrigation on Soil Characteristics in Selected Irrigation Schemes in the Upper Blue Nile Basin . . . . .</b>	<b>383</b>
Mekonnen Getahun, Enyew Adgo, and Asmare Atalay	
<b>20 Critical Water Resources Issues in the Nile River Basin . . . . .</b>	<b>401</b>
Muluneh Yitayew and Assefa M. Melesse	
<b>Index . . . . .</b>	<b>417</b>

# Contributors

**Wossenu Abtew** South Florida Water Management District, West Palm Beach, FL, USA, [wabtew@sfwmd.gov](mailto:wabtew@sfwmd.gov)

**Enyew Adgo** Bahir Dar University, Bahir Dar, Ethiopia, [enyewadgo@gmail.com](mailto:enyewadgo@gmail.com)

**Tilahun Amede** International Livestock Research Institute (ILRI), International Water Management Institute (IWMI) and Challenge Programme on Water for Food (CPWF), Addis Ababa, Ethiopia; International Livestock Research Institute (ILRI), Addis Ababa, Ethiopia, [t.amede@cgiar.org](mailto:t.amede@cgiar.org)

**Asmare Atalay** Virginia Tech University, Blacksburg, VA, USA

**Seleshi B. Awulachew** International Water Management Institute (IWMI), Addis Ababa, Ethiopia, [s.bekele@cgiar.org](mailto:s.bekele@cgiar.org)

**Essayas K. Ayana** Department of Water Resources and Environmental Engineering, Bahir Dar University, Bahir Dar, Ethiopia; Department of Biological and Environmental Engineering, Cornell University, Ithaca, NY, USA, [ekk45@cornell.edu](mailto:ekk45@cornell.edu)

**Haimanote K. Bayabil** Cornell Master's program in Integrated Watershed Management and Hydrology, Bahir Dar, Ethiopia; Amhara Regional Agricultural Research Institute, Debra Tabor, Ethiopia, [hkb24@cornell.edu](mailto:hkb24@cornell.edu)

**Menberu M. Bitew** Department of Civil and Environmental Engineering, University of Connecticut, Storrs, CT, USA, [menberu@engr.uconn.edu](mailto:menberu@engr.uconn.edu)

**Martijn J. Booij** Water Engineering and Management, Faculty of Engineering Technology, Twente University, 7500, AE Enschede, The Netherlands, [M.J.Booij@ctw.utwente.nl](mailto:M.J.Booij@ctw.utwente.nl)

**Pietro Ceccato** International Research Institute for Climate and Society, The Earth Institute at Columbia University, New York, NY, USA, [pceccato@iri.columbia.edu](mailto:pceccato@iri.columbia.edu)

**Amy S. Collick** Cornell Master's Program in Integrated Watershed Management and Hydrology, Bahir Dar, Ethiopia; Department of Water Resources and Environmental Engineering, Bahir Dar University, Bahir Dar, Ethiopia;

Department of Biological and Environmental Engineering, Cornell University, Ithaca, NY, USA, asc38@cornell.edu

**Stephen Connor** International Research Institute for Climate and Society, The Earth Institute at Columbia University, New York, NY, USA, sjconnor@iri.columbia.edu

**Bijan Dargahi** Department of Land and Water Resources Engineering, The Royal Institute of Technology (KTH), Stockholm, Sweden, bijan@kth.se

**Dereje T. Desalegn** Water Works Design and Supervision Enterprise, Addis Ababa, Ethiopia, der\_tadesse@yahoo.com

**Katrien Descheemaeker** International Water Management Institute (IWMI), Addis Ababa, Ethiopia; International Livestock Research Institute (ILRI), Addis Ababa, Ethiopia; Current Address: CSIRO Ecosystem Sciences, Glen Osmond, SA 5064, Australia

**Tibebe Dessalegne** Natural and Water Resources Department, BEM Systems, Inc., West Palm Beach, FL, USA, tdessalegne@bemsys.com

**Tufa Dinku** International Research Institute for Climate and Society, The Earth Institute at Columbia University, New York, NY, USA, tufa@iri.columbia.edu

**Zachary M. Easton** Department of Biological and Environmental Engineering, Cornell University, Ithaca, NY, USA, zme2@cornell.edu

**Mohamed Elshamy** Nile Forecast Center, Ministry of Water Resources and Irrigation, Cairo, Egypt, meame\_69@yahoo.com

**Tegenu A. Engda** Cornell Master's Program in Integrated Watershed Management and Hydrology, Bahir Dar, Ethiopia; Amhara Regional Agricultural Research Institute, Debra Tabor, Ethiopia, tegenu@gmail.com

**Temesgen Enku** Department of Water Resources Engineering, Bahir Dar University, Bahir Dar, Ethiopia, enku\_te@yahoo.com; temesgenku@gmail.com

**Daniel Gann** Geographic Information Systems-Remote Sensing Center, Florida International University, Miami, FL 33199, USA

**Woubet Gashaw** Department of Natural Resources Management, Bahir Dar University, Bahir Dar, Ethiopia, wubetga@gmail.com

**Mekonnen Gebremichael** Department of Civil and Environmental Engineering, University of Connecticut, Storrs, CT, USA, mekonnen@engr.uconn.edu

**Mekonnen Getahun** Amhara Design and Supervision Works Enterprise, Bahir Dar, Ethiopia, mekonnengetahun2001@gmail.com

**Ambro S.M. Gieske** Department of Water Resources, Faculty of Geoinformation Science and Earth Observation (ITC), Twente University, 7500 AA Enschede, The Netherlands, gieske@itc.nl

**Emad Habib** Department of Civil Engineering, University of Louisiana at Lafayette, Lafayette, LA 70504, USA, [exh5102@louisiana.edu](mailto:exh5102@louisiana.edu)

**Alemseged T. Haile** Department of Water Resources, Faculty of Geoinformation Science and Earth Observation (ITC), Twente University, 7500 AA Enschede, The Netherlands, [haile07634@itc.nl](mailto:haile07634@itc.nl)

**Amare Haileslassie** International Livestock Research Institute (ILRI), Addis Ababa, Ethiopia, [A.Haileslassie@cgiar.org](mailto:A.Haileslassie@cgiar.org)

**Eman Hasan** National Water Research Center, Cairo, Egypt, [Dr\\_eman30@hotmail.com](mailto:Dr_eman30@hotmail.com)

**Christina Hoffman** School of Natural Resources, University of Nebraska, Lincoln NE, USA; Department of Earth and Environment, Florida International University, Miami, FL, USA, [christina.hoffman@huskers.unl.edu](mailto:christina.hoffman@huskers.unl.edu)

**Mark R. Jury** Physics Dept, University of Puerto Rico, Mayagüez, Puerto Rico; University of Zululand, KwaDlangezwa, South Africa, [mark.jury@upr.edu](mailto:mark.jury@upr.edu)

**Elias S. Legesse** Cornell Master's program in Integrated Watershed Management and Hydrology, Bahir Dar, Ethiopia; Department of Water Resources and Environmental Engineering, Bahir Dar University, Bahir Dar, Ethiopia, [2003sime@gmail.com](mailto:2003sime@gmail.com)

**Dagnachew Legesse** Department of Earth Sciences, Addis Ababa University, Addis Ababa, Ethiopia, [dagnachewl@yahoo.com](mailto:dagnachewl@yahoo.com)

**Ben H.P. Maathuis** Department of Water Resources, Faculty of Geoinformation Science and Earth Observation (ITC), Twente University, 7500 AA Enschede, The Netherlands, [maathuis@itc.nl](mailto:maathuis@itc.nl)

**Liya M. Mango** Department of Earth and Environment, Florida International University, Miami, FL 33199, USA, [lmango@fiu.edu](mailto:lmango@fiu.edu)

**Everisto Mapedza** International Water Management Institute (IWMI), Addis Ababa, Ethiopia; International Water Management Institute (IWMI), Pretoria, South Africa

**Matthew McCartney** International Water Management Institute (IWMI), Addis Ababa, Ethiopia, [m.mccartney@cgiar.org](mailto:m.mccartney@cgiar.org)

**Michael E. McClain** Department of Earth and Environment, Florida International University, Miami, FL, USA; UNESCO-IHE Institute for Water Education, Delft, The Netherlands, [michael.mcclain@fiu.edu](mailto:michael.mcclain@fiu.edu)

**P. McCornick** Nicholas Institute for Environmental Policy Solutions, Duke University, Durham, NC, USA, [P.McCornick@duke.edu](mailto:P.McCornick@duke.edu)

**Mulatie Mekonnen** Bureau of Agriculture and Rural Development, Amhara Region, Bahir Dar, Ethiopia, [mulatemekonnen@yahoo.com](mailto:mulatemekonnen@yahoo.com)

**Assefa M. Melesse** Department of Earth and Environment, Florida International University, Modesto A. Maidique Campus, Miami, FL 33199, USA, melessea@fiu.edu

**Semu A. Moges** Department of Civil Engineering, Addis Ababa University, Addis Ababa, Ethiopia, semu\_moges\_2000@yahoo.com

**Don Peden** International Livestock Research Institute (ILRI), Addis Ababa, Ethiopia

**Janaka B.U. Perera** National Water Supply and Drainage Board, Ratmalana, Sri Lanka, upuljanaka@gmail.com

**David Rayner** Department of Earth Sciences, University of Gothenburg, 405 30 Gothenburg, Sweden, David.Rayner@gvc.gu.se

**Paolo Reggiani** Unit Inland Water Systems, Hydrology, DELTARES, 1772600 MH Delft, The Netherlands, paolo.reggiani@deltares.nl

**Bianca Reitberger** Faculty of Biology and Geography, Applied Hydrogeology/Hydrobiology, University of Duisburg-Essen, Essen, Germany, bianca.reitberger@gmail.com

**Tom H.M. Rientjes** Department of Water Resources, Faculty of Geoinformation Science and Earth Observation (ITC), Twente University, 7500 AA Enschede, The Netherlands, t.h.m.rientjes@utwente.nl

**Alon Rimmer** The Kinneret Limnological Laboratory, Migdal, Israel, alon@ocean.org.il

**Shimelis G. Setegn** Department of Earth and Environment, Florida International University, Miami, FL 33199, USA, ssetegn@fiu.edu

**Yilma Sileshi Shiferaw** Department of Civil Engineering, Addis Ababa University, Addis Ababa, Ethiopia, base\_et@ethiopiet.t

**Raghavanan Srinivasan** Spatial Science Laboratory, Texas A&M University, College Station, TX, USA, r-srinivasan@tamu.edu

**Tammo S. Steenhuis** Cornell Master's Program in Integrated Watershed Management and Hydrology, Bahir Dar, Ethiopia; Department of Water Resources and Environmental Engineering, Bahir Dar University, Bahir Dar, Ethiopia; Department of Biological and Environmental Engineering, Cornell University, Ithaca, NY, USA, tss1@cornell.edu

**Seifu A. Tilahun** Department of Water Resources and Environmental Engineering, Bahir Dar University, Bahir Dar, Ethiopia; Department of Biological and Environmental Engineering, Cornell University, Ithaca, NY, USA, sat86@cornell.edu

**Paulo van Breugel** International Livestock Research Institute (ILRI), Addis Ababa, Ethiopia

**Christiaan van der Tol** Department of Water Resources, Faculty of Geo-Information Science and Earth Observation (ITC), University of Twente, 7500 AA Enschede, The Netherlands, vandertol@itc.nl

**Anders Wörman** Land and Water Resources Engineering, Stockholm, Sweden, worman@kth.se

**Fasikaw Dessie Wubet** Arba Minch University, Arba Minch, Ethiopia, fasiwork@yahoo.com

**Muluneh Yitayew** Agricultural and Biosystems Engineering Department, University of Arizona, Tucson AZ, USA, myitayew@email.arizona.edu

# **Part I**

## **Hydrology and Water Budget**

# Chapter 1

## Hydrological Variability and Climate of the Upper Blue Nile River Basin

Assefa M. Melesse, Wossenu Abtew, Shimelis G. Setegn,  
and Tibebe Dessalegne

**Abstract** This chapter discusses the hydrometeorology, land use, soils, topography, agroecological zones, extreme flows, climatic variability and climatic teleconnections of the upper Blue Nile River basin. The basin has a varied topography, rainfall and temperature resulting in different agroclimatic zones. Spatial distribution of annual rainfall over the basin shows high variation with the southern tip receiving as high as 2,049 mm and the northeastern tip as low as 794 mm annual average rainfall. The analysis of the basin's river flow and El Niño Southern Oscillation (ENSO) index connectivity indicates that the upper Blue Nile River basin rainfall and flows are teleconnected to the ENSO index. Based on event correspondence analysis, high rainfall and high flows are likely to occur during La Niña years and dry years are likely to occur during El Niño years at a confidence level of 90%. Low and high flow analysis for selected tributaries and flow at the Blue Nile River flow shows different recurrence intervals of the high and low flows.

**Keywords** Blue Nile River basin · Rainfall frequency analysis · Climatic teleconnections · ENSO · Lake Tana · Blue Nile River flow

### 1.1 Introduction

The Blue Nile River basin is the main source of the Nile River with a drainage area of 324,530 km<sup>2</sup> (Peggy and Curtis, 1994). Degefu (2003) states that 86% of the annual flow of the Nile comes from the Blue Nile River basin (59%), from the Barro-Akobo-Sobat sub-system (14%), and from the Tekeze/Atbara/Gash sub-system (13%). The remaining 14% comes from the equatorial lakes after losses of evaporation in the Sudd region and Machar marshes (Degefu, 2003). The upper Blue Nile River basin (Fig. 1.1) is 176,000 km<sup>2</sup> in area (Conway, 2000). The

---

A.M. Melesse (✉)

Department of Earth and Environment, Florida International University, Modesto A. Maidique Campus, Miami, FL 33199, USA  
e-mail: melessea@fiu.edu

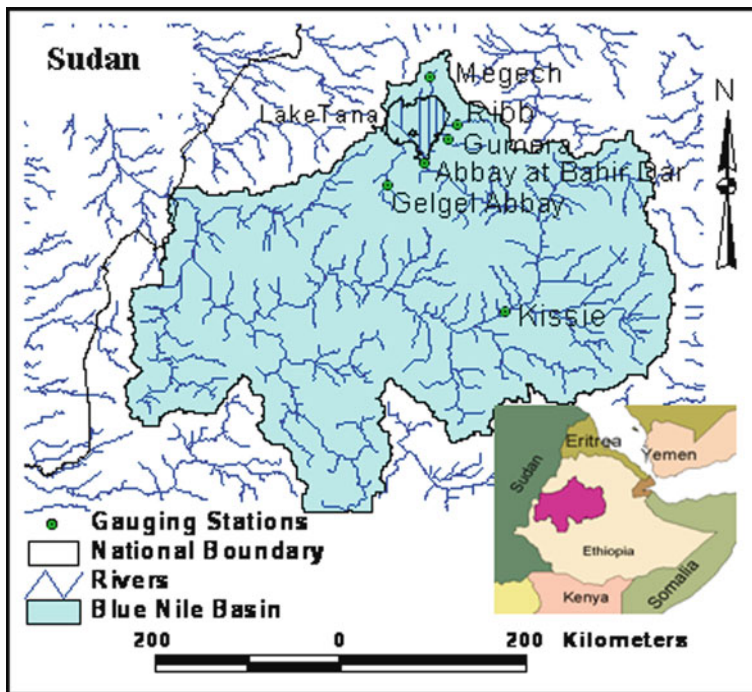


**Fig. 1.1** Location of the upper Blue Nile River basin in Ethiopia (Abtew et al., 2009a)

major tributaries of the Blue Nile River in Ethiopia are Gilgel Abbay, Megech, Ribb, Gumera, Beshlo, Woleka, Jemma, Muger, Guder, Chemoga, Finch, Dedessa, Angar, Dura and Beles. The upper Blue Nile River basin is relatively wet when compared to the lower basin (part of the Blue Nile drainage basin outside Ethiopia until it joins the White Nile River). Annual rainfall ranges from over 2,000 mm in the Southwest of the basin to a 1,000 in the northeast (Conway, 2000). Bewket and Conway (2007) reported mean annual point rainfall of 1,445, 1,665, 1,542, 1,349 mm rainfall at Bahir Dar, Chagni, Dangla and Debremarkos, respectively. Peggy and Curtis (1994) reported 1,521 and 1,341 mm long-term average annual rainfall for Bahir Dar and Debremarkos, respectively. Kebede et al. (2006) reported 1,451 mm average annual rainfall for Bahir Dar based on observations from 1960 to 1992. Analysis of spatial variation of annual rainfall over the upper Blue Nile River basin showed the southern tip receiving as high as 2,049 mm and the northeastern tip as low as 794 mm (Abtew et al., 2009a).

In Ethiopia, rain-fed agriculture is the main source of food production. Temporal and spatial fluctuations of rainfall result in low food production from droughts or unfavorable wet conditions. Point rainfall frequency analysis characterizes the temporal and spatial variation of rainfall at a gauge and analysis from many gauges can help detect temporal trends. Spatial mapping of the characteristics of all gauges in a region provides the spatial characteristics of rainfall. Regionally averaged rainfall frequency analysis characterizes rainfall over the region. Sufficient data length and

quality is needed for temporal and spatial characterization of rainfall. Conway et al. (2004) studied the history of rainfall and temperature monitoring network and available records in Ethiopia and concluded that there are very few numbers of sites where continuous rainfall and temperature measurement records are available. In the absence of long term concurrent rainfall observations in a basin, the use of available data is warranted to conduct as much analysis as possible.

## 1.2 Hydrometeorology

### 1.2.1 Air Temperature

Air temperature of the Blue Nile River basin was analyzed using monthly minimum and maximum data from nine stations (Fig. 1.2). The period of record varies from 13 to 44 years for Jiga (1978–1990) and Bahr Dar (1961–2004) stations, respectively, and the average length of record is 23 years. Table 1.1 summarizes average monthly air temperature for the nine stations in the Blue Nile River basin. As shown in Table 1.1, the majority of the stations have maximum average air temperature in

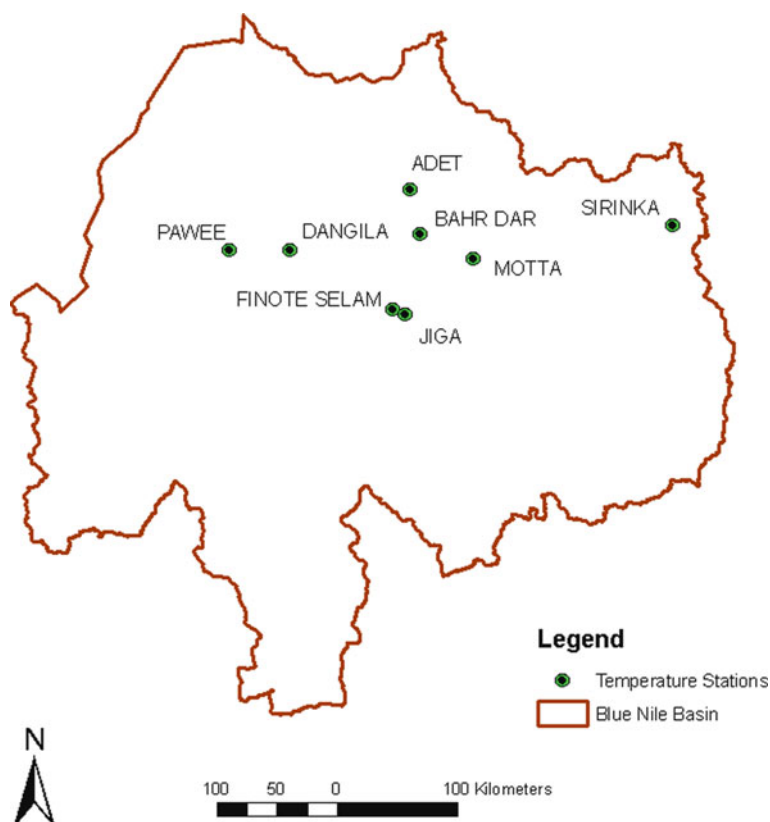


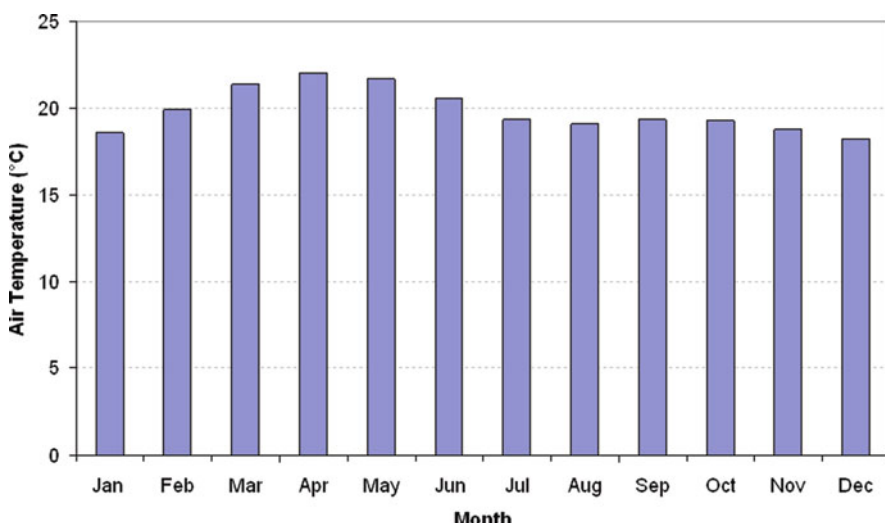
Fig. 1.2 Air temperature measurement stations of the upper Blue Nile River basin

**Table 1.1** Summary of average air temperature in the Blue Nile basin (°C)

	Bahir			Finote selam					
	Adet	Dar	Deddessa	Dangila	Jiga	Motta	Pawee	Sirinka	
Jan	15.85	16.90	22.09	15.27	19.08	22.45	15.48	23.23	17.05
Feb	17.51	18.49	23.46	16.68	20.06	22.88	16.94	25.23	17.90
Mar	19.01	20.66	25.36	17.95	21.03	23.44	18.07	27.44	19.41
Apr	19.56	21.43	25.61	19.05	21.34	23.50	18.68	28.14	20.61
May	19.67	21.60	23.94	18.84	20.91	23.23	18.81	26.51	21.99
Jun	18.30	20.22	22.40	17.58	19.42	22.14	17.63	23.91	23.60
Jul	16.89	18.78	21.39	16.71	17.89	21.65	15.84	22.54	22.30
Aug	16.83	18.61	21.29	16.70	17.68	21.50	15.61	22.49	21.24
Sep	16.98	18.90	22.00	16.89	18.21	21.64	15.65	23.09	20.76
Oct	16.93	19.22	22.18	16.67	18.43	21.80	15.57	23.36	19.17
Nov	16.16	18.28	21.88	15.56	18.64	21.95	15.31	23.18	17.99
Dec	15.64	16.98	21.60	15.02	18.43	21.77	15.09	22.93	17.04
Min	15.64	16.90	21.29	15.02	17.68	21.50	15.09	22.49	17.04
Max	19.67	21.60	25.61	19.05	21.34	23.50	18.81	28.14	23.60
Avg	17.44	19.17	22.77	16.91	19.26	22.33	16.56	24.34	19.92

the months of April or May and the minimum in the months of August or December. The average annual temperature at the nine stations ranges from a minimum of 16.6°C to a maximum of 24.3°C for Motta (eastern part of the basin) and Pawee (western part of the basin) stations, respectively.

Further, to summarize the upper Blue Nile River basin air temperature, mean monthly temperature was calculated using simple averaging of air temperatures at the nine stations (Fig. 1.3). As depicted in Fig. 1.3, the monthly distribution of the upper Blue Nile River basin temperature suggest that the maximum occurs in the month of April (22.0°C) and the minimum in the month of December (18.3°C).

**Fig. 1.3** Monthly distribution of mean air temperature in the Blue Nile basin

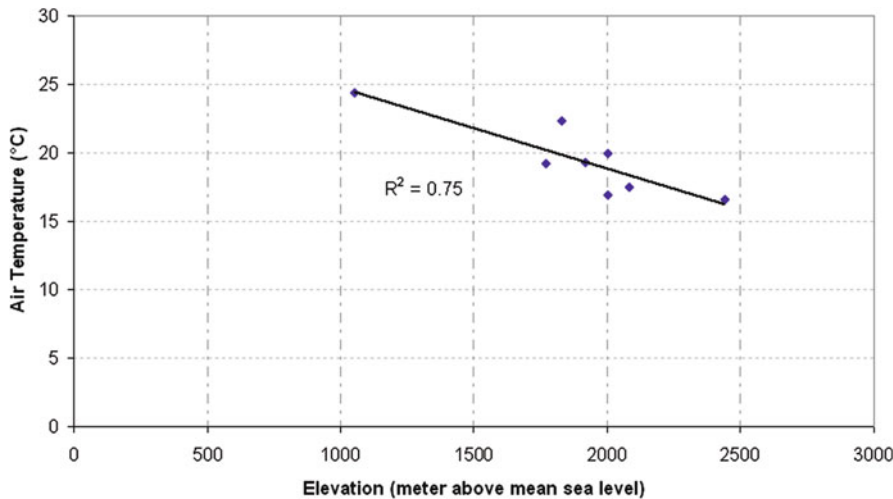


**Fig. 1.4** Air temperature and elevation relationships in the Blue Nile basin

In an attempt to study the nature and strength of relationship that may exist between average air temperature and elevation, a simple linear regression analysis was conducted. As depicted in Fig. 1.4, there is a strong relationship ( $R^2 = 0.75$ ) between average air temperature and elevation in the Blue Nile River basin. On the average in the Blue Nile River basin there is a drop in average air temperature of  $1^{\circ}\text{C}$  for every 168 m increase in elevation.

### 1.2.2 Seasons

The major seasons in the upper Blue Nile River basin are divided into wet (*Kiremt*) and dry (*Bega*). The wet season runs from June to September and about 70 % of the annual rainfall occurs during this period (Conway, 2000). The dry season spans from October to May. However, in some part of the basin, there is a third season with moderate rainfall (*Belg*) occurring from mid-February to mid-May.

### 1.2.3 Rainfall

#### 1.2.3.1 Rainfall Data

Monthly rainfall data was available from 32 monitoring stations in the upper Blue Nile River basin. The period of record was from 1960 to 2002 with varying record length. The length of record varies due to differences in site establishment and data gaps. The rainfall station network is shown in Fig. 1.5. Generally, the south-central

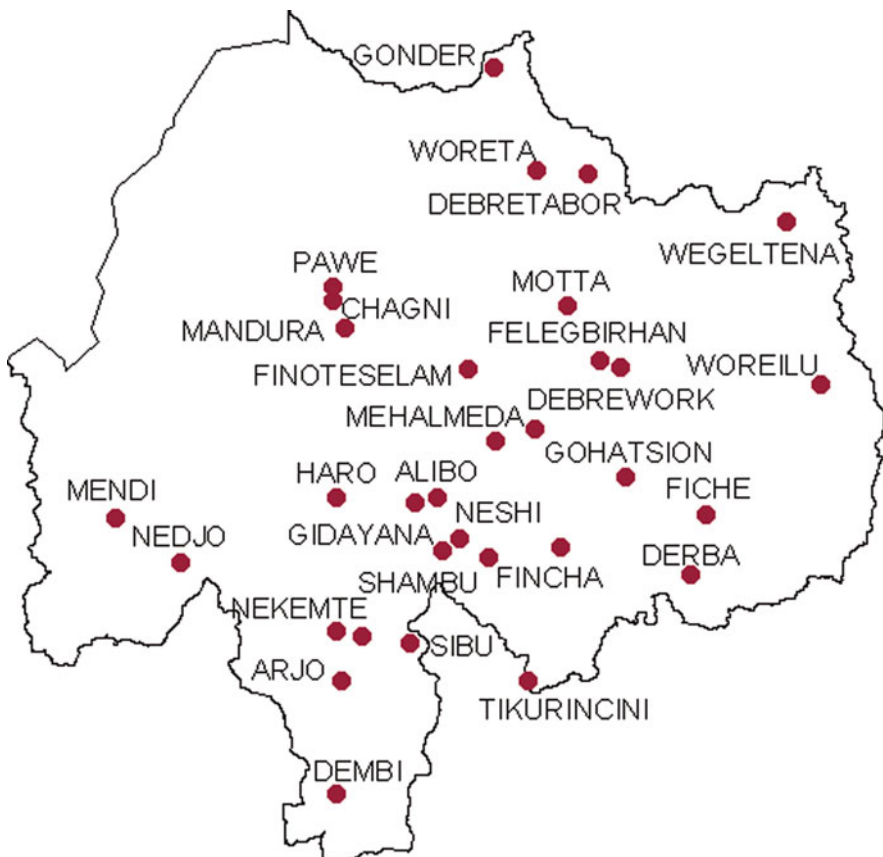


**Fig. 1.5** Rainfall gauge network in the upper Blue Nile River (Abtew et al., 2009a)

area has higher gauge density with sparse gauge concentration or none to the west. In the analysis, for each month in a year, spatial rainfall statistics was computed using all gauges with available data for the period. As a result, the network size varies from year to year.

#### 1.2.3.2 Monthly Rainfall Statistics

Spatially averaged monthly rainfall over the upper Blue Nile River basin ranges from a low of 10 mm in January to a high of 332 mm in July. Spatially averaged monthly rainfall spread is shown in Fig. 1.6. Figure 1.6 shows monthly spatial average rainfall, with temporal mean, 25 and 75 percentile. The ranges of spatial observations for the period of record can be discerned from Fig. 1.6. As shown in Table 1.2 and Fig. 1.6, the wet season months are June, July, August and September and the dry season months are January, February, March, April, November and

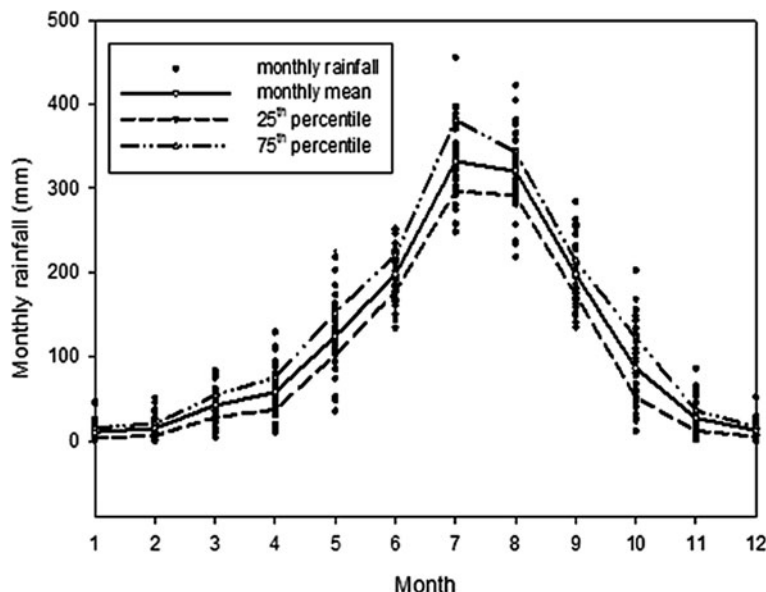


**Fig. 1.6** Temporal variation of upper Blue Nile River monthly rainfall

December. May is the transition month from the dry season to the wet season and October is the transition month from the wet season to the dry season. January has the lowest and July has the highest monthly mean ( $\mu$ ) rainfall. The standard deviation ( $\sigma$ ) is relatively high for the dry season and transition months. The coefficient of variation, c.v. ( $\sigma/\mu$ ) of the wet season months is small indicating that these months have low variation (Table 1.2). January, February, November and December have relatively higher positive skewness. The dry season months have higher coefficient of variation indicating that the year-to-year variation for these

**Table 1.2** Upper Blue Nile River basin monthly rainfall statistics

Month	Mean (mm)	STDEV (mm)	CV (%)	Skewness	Kurtosis
Jan	10.4	10.4	100	1.90	7.4
Feb	15.0	12.3	82	1.14	4.3
Mar	42.0	21.2	51	0.26	2.6
Apr	57.9	28.6	49	0.31	2.9
May	124.6	42.2	34	0.19	3.4
Jun	197.2	28.6	15	-0.10	2.6
Jul	331.9	42.0	13	0.38	3.8
Aug	320.2	42.7	13	-0.07	3.6
Sep	197.6	35.4	18	0.57	2.9
Oct	86.8	43.9	51	0.51	2.8
Nov	26.9	20.6	76	1.09	3.6
Dec	12.7	10.4	83	1.45	6.5

months is high. January, February, May, July, August, November and December are Leptokurtic (Kurtosis > 3). March, April, June, September and October are Platykurtic (kurtosis < 3).

### 1.2.3.3 Monthly Rainfall Probability Distribution

Frequency of rainfall depths and duration can be determined from point, single gauge measurements or from spatially averaged rainfall data. In this case, the distribution of monthly rainfall time series averaged over the basin is analyzed. The density function characterizes a continuous probability of monthly rainfall of a given value and less than the given value, such that the area under the curve bounded by the horizontal axis is equal to 1. Figures 1.7, 1.8, 1.9, and 1.10 depict density function for all 12 months.

Theoretical probability distribution fittings with a Chi-square test resulted in January, July, October and November basin rainfall fit the Gamma-2 probability distribution. February, June and December fit Weibull distribution. March, April, May and August fit Normal distribution. September fits Log-Normal distribution. For the Gamma and Weibull distributions the shape and scale parameters vary from month to month. Each model was fitted to each month rainfall and the best-fit model was selected based on the ratio of computed Chi-square ( $\chi^2$ ) to the tabular  $\chi^2$ . Chi Square ratio is computed as follows:

$$\chi^2 \text{ ratio} = \frac{\chi^2 \text{ computed}}{\chi^2 \text{ table}} \quad (1.1)$$

When  $\chi^2$  ratio is less than 1, the model is accepted and greater than 1, the model is rejected at 90% confidence level.

The 2-parameter Gamma distribution is presented as follows (Haan, 1977):

$$f(P) = \frac{\beta^\alpha P^{\alpha-1} e^{-\beta P}}{\Gamma(\alpha)} \quad (1.2)$$

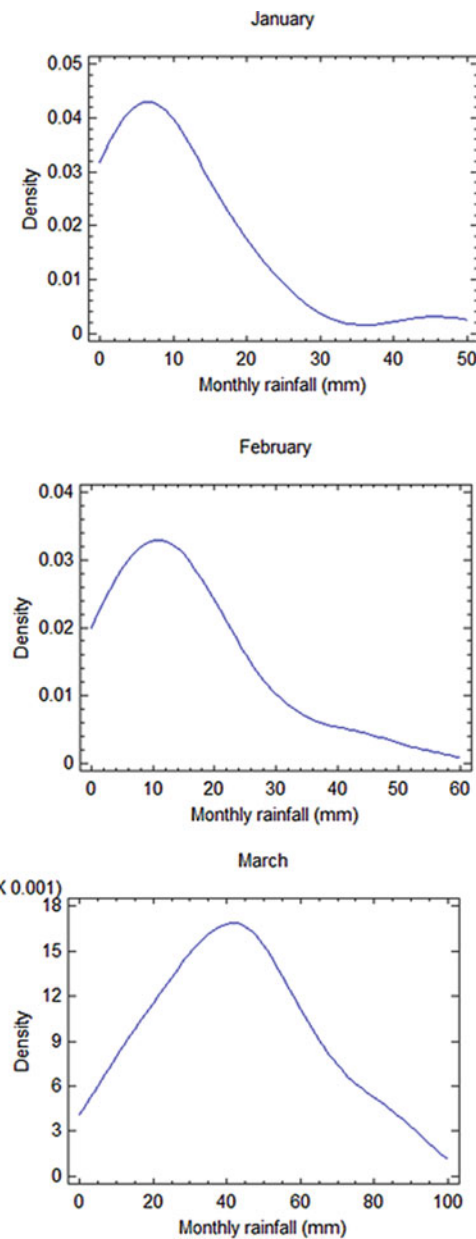
Where  $f(P)$  is the probability density function of  $P$  (rainfall amount),  $\alpha$  is a shape parameter,  $\beta$  is a scale parameter, and  $\Gamma(\alpha)$  is the Gamma function of  $\alpha$ . The shape and scale parameters were calculated using software STATGRAPHICS Centurion XV Version 15.2. The shape ( $\alpha$ ) and scale ( $\beta$ ) can be similarly computed as follows (Greenwood and Durand, 1960):

$$\alpha = \frac{0.500876 + 0.1648852Y - 0.0544274Y^2}{Y} \quad (1.3)$$

$$Y = \ln \frac{X_m}{G} \quad (1.4)$$

Where  $X_m$  is the arithmetic mean and  $G$  is the geometric mean for non-zero monthly rainfall values. Zero monthly values were replaced with 0.01 inches (0.254 mm).

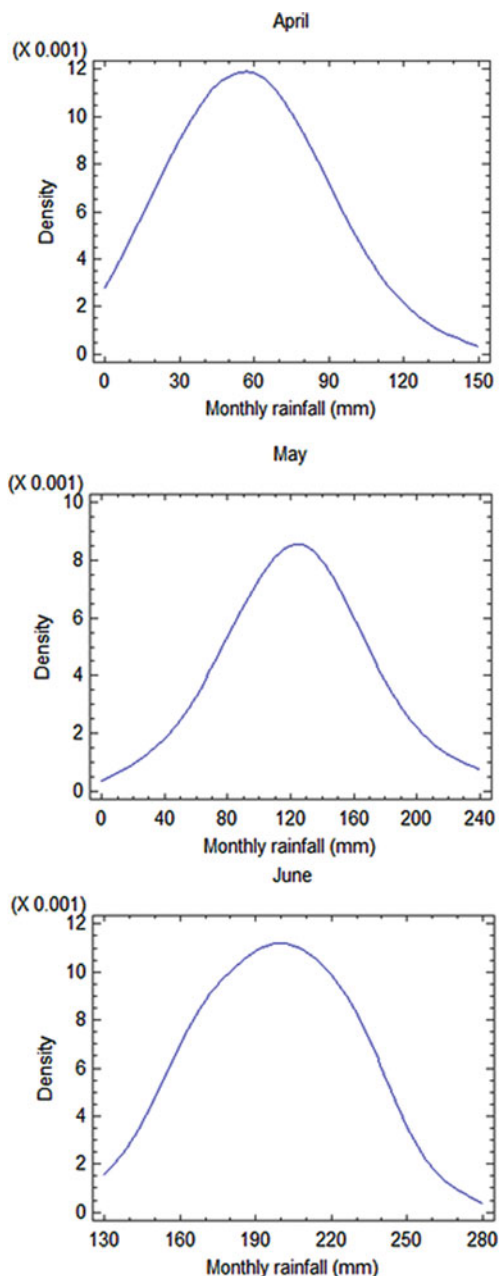
**Fig. 1.7** Probability density functions for January, February and March



$$\beta = \frac{\alpha}{X_m} \quad (1.5)$$

The remaining probability density functions (Normal, Weibull and Log-Normal) are discussed in Walpole and Myers (1985) and Maidment (1993).

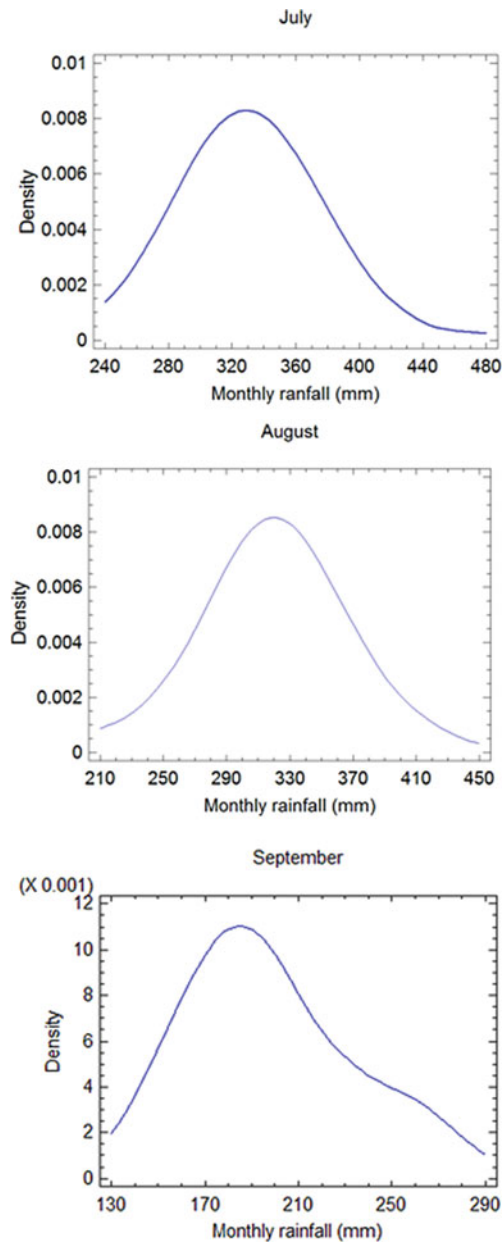
**Fig. 1.8** Probability density functions for April, May and June



#### 1.2.3.4 Monthly Rainfall Return Periods

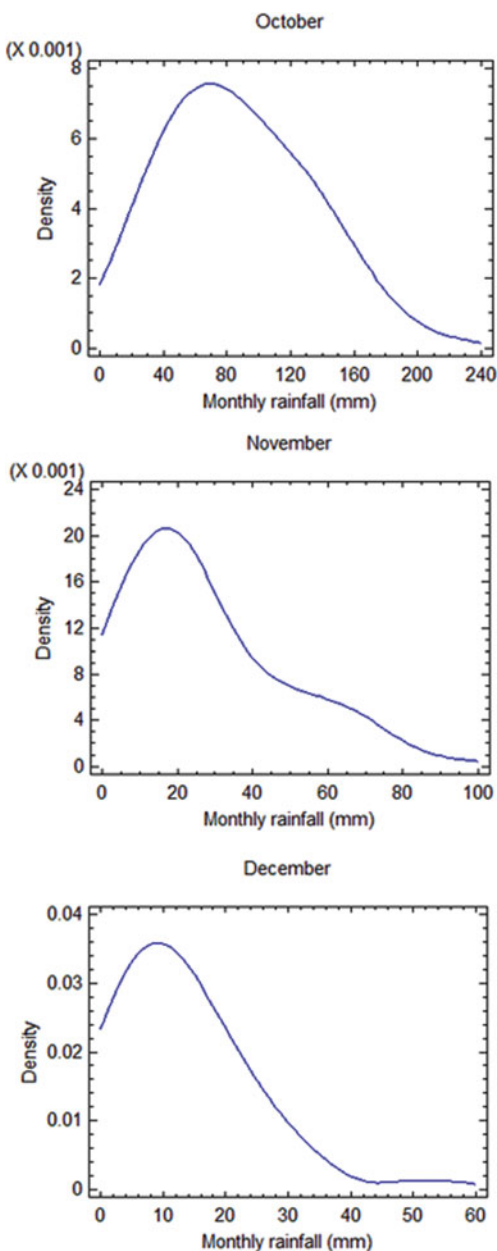
Probabilistic measure of the likelihood of occurrence of a given depth of rainfall is measured in return periods. Return periods are the expected interval of years a given

**Fig. 1.9** Probability density functions for July, August and September



depth of rainfall is expected to occur. Return periods in years were computed from the Cumulative Density Function (CDF) of each month's respective distribution fitting Eqs. (1.6) and (1.7). Return periods for dry (below average) and wet (above average) rainfall patterns were computed for return periods of 2, 5, 10, 25, 50 and 100-year.

**Fig. 1.10** Probability density functions for October, November and December



$$\text{Dry Return Period} = \frac{1}{\text{CDF}} \text{ for } \text{CDF} \leq 0.5 \quad (1.6)$$

$$\text{Wet Return Period} = \frac{1}{1 - \text{CDF}} \text{ for } \text{CDF} \geq 0.5 \quad (1.7)$$

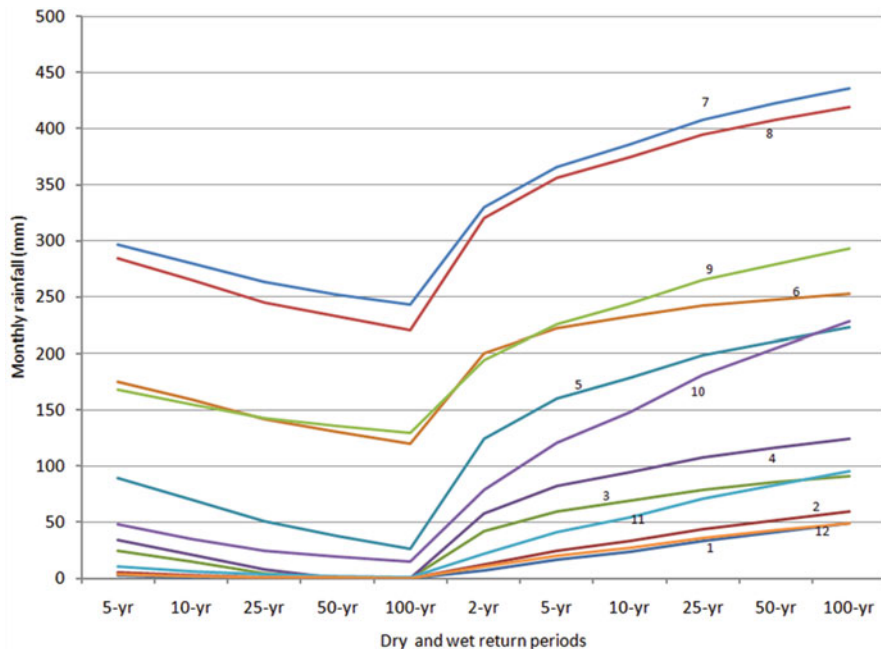


**Fig. 1.11** Dry and wet return period rainfall for each month

Return period for dry and wet pattern rainfall for each month is depicted in Fig. 1.11. The six dry months' (November–April) rainfall for dry and wet return periods show that for drought return periods of 50 years and higher, all the 6 months experience no rainfall. But for wet return periods, distinct groups emerge with December, January and February producing lower rainfall amount than November, March and April. The wet season months are separated into two, with July and August being closely related. June and September are rainfalls far lower than July and August. The two transitional months, May and October lie between the June and September of the wet season months and the dry seasons confirming the transitional characteristic.

#### 1.2.3.5 Annual Rainfall Statistics and Probability Distribution

With mean annual rainfall of 1,423 mm, the upper Blue Nile River basin is relatively wet. Figure 1.12 depicts basin annual rainfall (1960–2002), mean annual rainfall, and  $\pm 1$  standard deviation (125 mm) basin annual rainfall. The upper Blue Nile River basin annual rainfall has a normal distribution (Abtew et al., 2009a). The coefficient of the temporal variation of annual rainfall is 0.09 which is relatively small. The rainfall statistics is based on 32 rainfall stations with varying length of record (Fig. 1.5). For each year, spatial mean annual rainfall analysis was computed

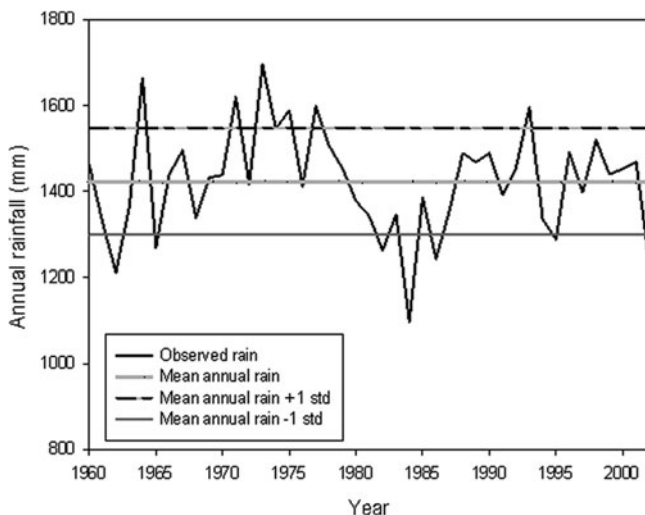


**Fig. 1.12** Upper Blue Nile River basin average annual rainfall (1960–2002)

**Table 1.3** Dry and wet return periods for the upper Blue Nile River basin annual rainfall

Return period (years)	Annual rainfall (mm)
100	1,132
50	1,166
25	1,204
10	1,263
5	1,318
2	1,423
5	1,528
10	1,583
25	1,642
50	1,714
100	1,745

as a sum of spatial monthly average rainfalls for the year. An arithmetic spatial mean monthly rainfall is computed from all gauges with monthly rainfall record for each month. The sum of the monthly spatial average rainfall produces the spatial average rainfall for the year under consideration. Conway (2000) reported a mean annual basin rainfall of 1,421 mm based on 11 gauges for the period 1900–1998. Annual dry and wet return periods were computed from Normal probability cumulative density functions as shown in Table 1.3 for dry and wet return periods of 2, 5, 10, 25, 50 and 100-year. The 100-year drought annual basin rainfall is 1,132 mm while the 100-year wet annual rainfall is 1,745 mm. A basin wide anomaly of  $\pm 300$  mm of rainfall would result in extreme drought or high stream flows.

### 1.2.3.6 Spatial Variation of Rainfall Over the Upper Blue Nile River Basin

Spatial variation of rainfall over a basin is essential knowledge for water resources planning and management at basin and sub-basin level. Mapping spatial distribution of rainfall from data set observed at a limited number of sites provides the means to infer estimates of point (local) and areal (regional) values from the map. Spatial variation of annual rainfall over the upper Blue Nile River basin is high with a coefficient of variation of 0.25. The highest annual average rainfall of 2,049 mm is in the southern tip of the basin and the lowest average annual rainfall of 794 mm is in the northeast. Rainfall amount varies generally from the southwest to the northeast, decreasingly. Average rainfall over the basin is spatially mapped using 28 rain gauge records eliminating 4 gauges which are very close to other gauges. Isohyetal map was produced using the Kriging interpolation package in SURFER Version 8 with linear variogram (Fig. 1.13). Since the Kriging method is a best linear unbiased estimator, the spatial distribution of average annual rainfall over the basin is the best reflection of spatial variation of annual rainfall for the given rain gauge network. Variation associated with elevation was not evaluated in this study.

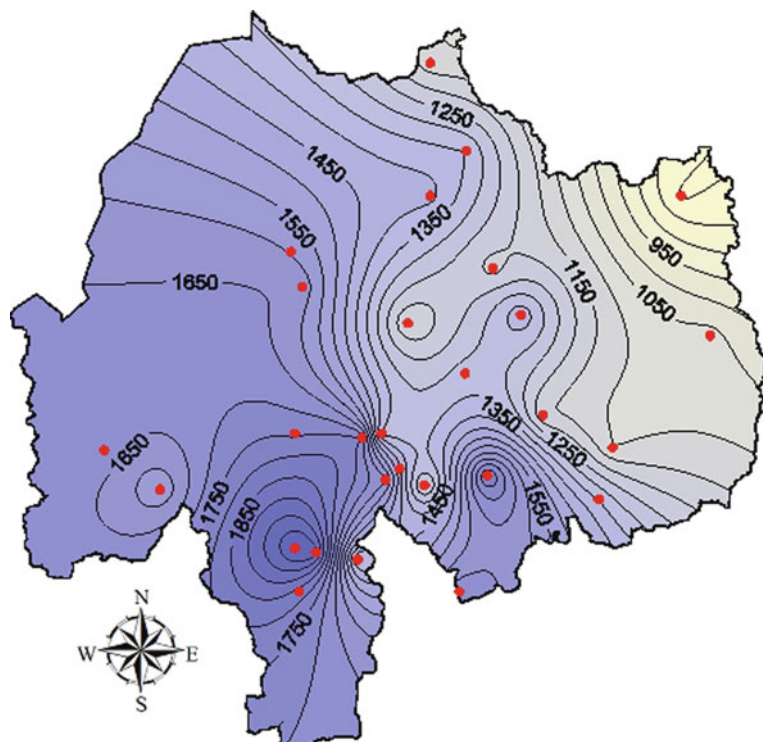


**Fig. 1.13** Spatial variation of the Upper Blue Nile River basin average annual rainfall with rain gauge locations (Abtew et al., 2009a)

## 1.3 Upper Blue Nile River Basin Features

### 1.3.1 Topography and Agroclimatic Zones

The topography in the upper Blue Nile River basin is highly varied ranging from low lands to mountain ranges. This variation coupled with rainfall variability leads to the occurrence of different climatic zones within the basin. The relationship between topography, rainfall and temperature in the basin is shown to be a factor that is used to classify different agroclimatic zones. As the altitude increases rainfall increases and temperature decreases. This variation is also one factor that dictates the suitability of different areas for different agricultural practices, presence of certain plant community and forest cover and also dominant soil types. Figure 1.14 shows the digital elevation model (DEM) of the upper Blue Nile River basin from the ASTER (Advanced Spaceborne Thermal Emission and Reflection radiometer) Global DEM dataset (NASA, 2009). The elevation grid has a 30-m horizontal resolution and shows a large variability of topography in the basin. The altitude ranges from 590 m above sea level to more than 4,000 m. In addition, the near equator latitude of the basin contributes to the climatic variations in the basin. These factors determine the occurrence of different local climates ranging from hot and desert-like along the Sudan border, to temperate on the high plateaux, and cold on the mountain peaks.

The main rainy season in the basin is June to September during which south-west winds bring rains from the Atlantic Ocean. About 70% of total rainfall occurs during this season which is also typified by minimum levels of sunshine, low variation in daily temperatures and high relative humidity. The dry season lasts from October to January during which clear skies are associated with maximum sunshine, high daily temperature variation, and low relative humidity. The short rainy season lasts from February to May during which south-east winds bring the small rains from the

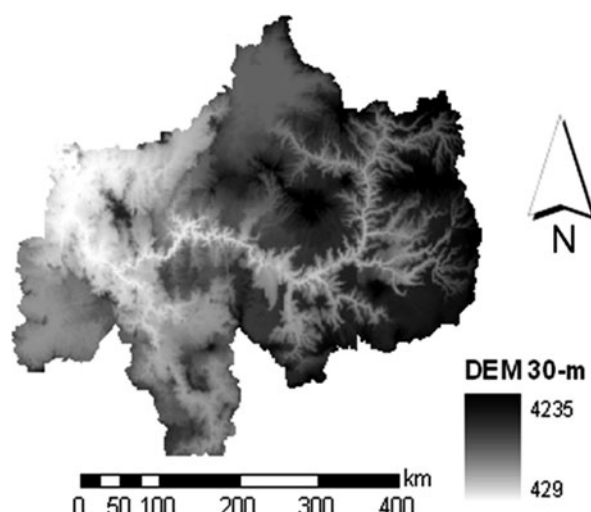


**Fig. 1.14** A 30-m Digital elevation model (DEM) of the upper Blue Nile River basin from ASTER data

Indian Ocean and temperatures are at their highest. The timing and duration of these seasons varies considerably by location.

Based on rainfall distribution and altitude, traditionally the basin is classified into various agroclimatic zones. This classification can be different depending on different reports. The basin is classified into 5 agroclimatic zones. Each agro-climatic zone is described below (USDA-FAS, 2003).

1. *Wurch (Cold highlands)*: Areas above 3,000 m where barley is the dominant crop and light frost often forms at night.
2. *Dega (Cool, humid, highlands)*: Areas from 2,500 to 3,000 m where barley and wheat are the dominant crops.
3. *Weina Dega (Temperate, cool sub-humid, highlands)*: Areas between 1,500 and 2,500 m where most of the population lives and all regional types of crops are grown, especially teff.
4. *Kolla (Warm, semi-arid lowlands)*: Areas below 1,500 m where sorghum and corn are grown, with teff grown in the better areas. The *kolla* is warm year round and temperatures range from 27 to 50°C.

According to Azene et al. (1993), the basin is also classified into six agroecological zones based on rainfall and altitude classes as shown in Table 1.4. Figure 1.15 shows the traditional classification of the agroecological zones of the basin.

According to De Pauw and Bruggeman (1988), agro-ecological zones are natural physical regions which are sufficiently large to be mapped at very small scales and which are sufficiently uniform in climate, physiography and soil patterns for generalised descriptions and evaluation of the agricultural potential and constraints to be meaningful at a national planning level.

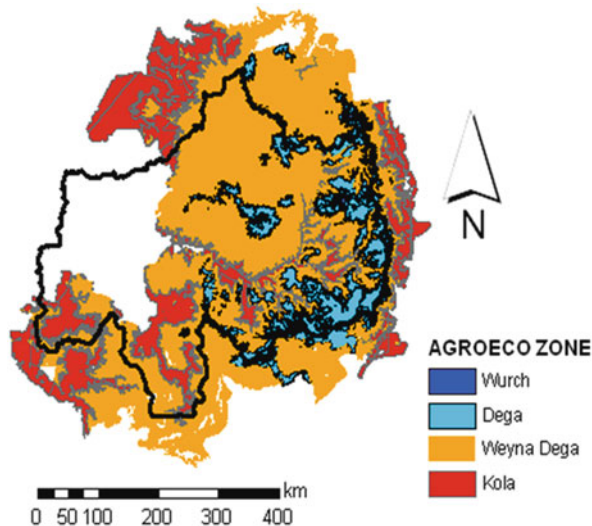
De Pauw and Bruggeman (1988) identified 140 agro-ecological zones in the basin, grouped into 15 agroecological regions based on thermal zone, growing

**Table 1.4** Agroclimatic zones of Ethiopia

Altitude (m)	Annual rainfall		
	<900 mm	900–1,400 mm	>1,400 mm
>3,700			High wurch (afro-alpine)
3,200–3,700		Moist wurch (sub-alpine)	Wet wurch (sub-alpine)
2,300–3,200		Moist dega (afro-montane forest-woodland)	Wet dega (Afro-montane forest-bamboo)
1,500–2,300	Dry weyna dega (savannah)	Moist weyna dega	Wet weyna dega
500–1,500	Dry kolla	Moist kolla	Wet kolla
<500	Bereha		

After Azene et al. (1993).

**Fig. 1.15** Agroecological zones within the upper Blue Nile River basin



period (cropping period determined from length of growing period and management characteristics), physiography, and soils.

### 1.3.2 Soils

The soils of the upper Blue Nile River basin can be divided into four or five broad groups for agro-ecological purposes.

- The shallow soils, with limited or zero agricultural potential are generally grouped as Leptosols and Regosols and are commonly associated with steep slopes. These cover large areas of the basin, and their depth is determining in recognition of the associated agro-ecological units.
- The moderately deep soils, classed as Cambisols and some Luvisols include most of the lighter textured soils of the basin and they are therefore suitable for cultivation. However, the limited depth demands careful management to avoid erosion leading to further depth constraints.
- The heavy textured vertisols are deep soils with poor drainage and properties of swelling and cracking. Under careful management, and assuming that drainage is not too problematic, they can be highly productive. Due to the clayey texture, they are difficult to manage with traditional agricultural management and even pose problems for mechanised production.
- The deeply leached red soils including Alisols, Acrisols and Nitisols have low pH, deficiencies in phosphorus and other nutrients, and a potential for

**Table 1.5** Morphological characteristics for the major soils of upper Blue Nile River basin

Soil group	Depth	Colour	Texture	Drainage
Acrisols	Deep to very deep	Very dark greyish brown	Clay	Well
Alisols	Deep to very deep	Reddish brown	Clay/clay loam/silty clay	Well
Arenosols	Shallow to moderately deep	Dark yellowish brown	Loamy sand	Well to excessive
Cambisols	Moderately deep	Brown/dark brown	Silty clay	Well
Fluvisols	Deep to very deep	Variable	Clay/silty clay	Well
Leptosols	Shallow to very shallow	Brown to yellowish brown	Loam/clay loam/clay	Well
Luvisols	Deep to very deep	Brown/reddish brown	Clay/silty clay	Well
Nitisols	Deep to very deep	Reddish brown	Clay/clay loam/silty clay loam	Well
Phaeozems	Deep	Dark grey	Clay loam/clay	Moderately well to poor
Regosols	Shallow to moderately deep	Brown	Clay/silt/loamy sand/loam/silty clay/sandy loam	Well

Source: FAO, 2002

aluminium toxicity. Most of their fertility tends to be tied up in the upper soil layers; loss of these layers due to erosion leave the subsoils of low fertility.

(e) Luvisols are generally deep soils with a horizon of clay accumulation. They are not so deeply leached of their nutrients as the red soils, and generally have a better distribution of nutrients through the soil. Conversely, the clay accumulation layers can lead to some drainage restrictions. Table 1.5 shows the morphological characteristics of the major soil types in the upper Blue Nile River basin.

### 1.3.3 Land Cover/Use

The upper Blue Nile River basin has a varied land use/land cover including agriculture, grassland, forest, barrenland and water. Due to the variation in the topography, rainfall distribution and landscape, the basin has a mosaic of land cover. According to the 2004–2006 land cover maps from Globcover (Globcover, 2008) based on the Medium Resolution Imaging Spectrometer (MERIS) sensor aboard the Meteosat, the basin has a varied land cover including 37.2% (agriculture), 30.3% (grassland

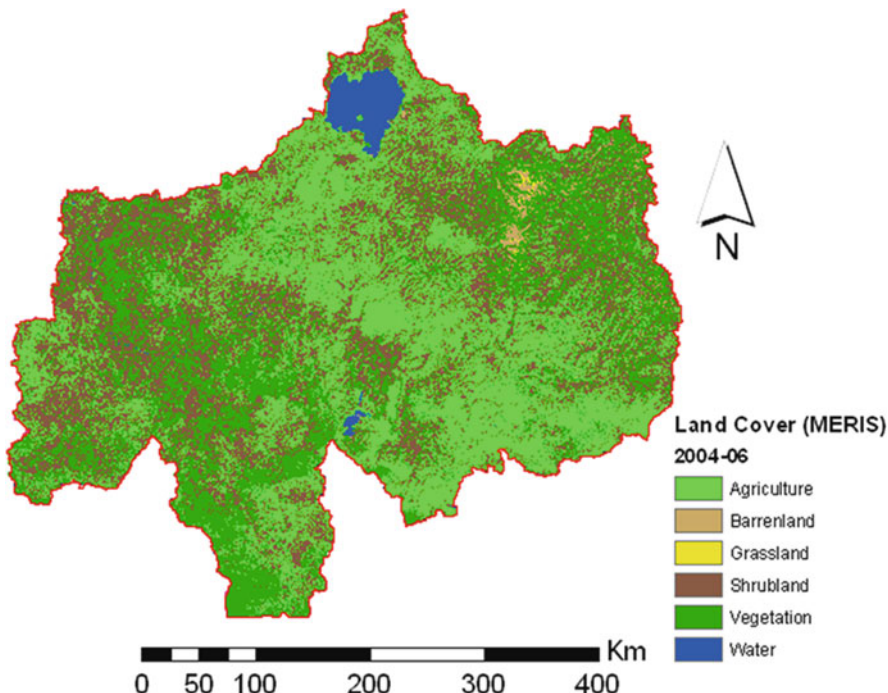


**Fig. 1.16** Land cover map of the upper Blue Nile River basin (2004–2006) based on the MERIS sensor (300-m)

and brushland) and 1.96% (water). Figure 1.16 shows land cover map of the upper Blue Nile River basin from the MERIS sensor.

The Globcover initiative produces a global land cover map for year 2005/2006 using remotely sensed data from MERIS with a spatial resolution of 300-m data acquired between mid 2005 and mid 2006. MERIS is a sensor aboard Envisat-1 satellite which was launched in March 2002 with a standard 15 band setting acquiring images in the VIS and NIR part of the electromagnetic spectrum. Data are acquired at 300 m (full resolution) and 1,200 m (reduced resolution) spatial resolution over land, thus vegetation can be monitored at regional to global scales (Verstraete et al., 1999).

## 1.4 Blue Nile River Basin Hydrology and Climate Teleconnections

### 1.4.1 Climatic Teleconnections

Variation in the weather in the short term and climate in the long term has been a mystery for man kind for a long time and many cultures attribute the

phenomena to super natural forces. In the last century, significant progress has been made in understanding the ocean, the atmosphere and land processes, inter-relationships and regional teleconnections. Modeling of these complex systems and prediction of weather and climate has achieved significant progress with a lot more work left for more understanding of the various processes and reduction of uncertainties in weather forecasting and climatic predictions for practical applications. Weather is defined as the state of the atmosphere or meteorological conditions as temperature, humidity, atmospheric pressure, wind speed and precipitation. Weather forecasts are made up to 10 days into the future with forecasting error increasing for longer periods. Climate is the weather averaged over longer temporal and spatial domain for months to years to centuries (Garbrecht and Piechota, 2006).

Prediction of hydrometeorology using global climate indices or other methods has become a necessity for water resources management in a future where water supply per capita declines and the impact of variability of the resource increase. Prediction of temporal and spatial variation of precipitation and runoff is necessary for water resource management and planning to mitigate impacts of droughts and floods.

Analysis of climate variation is based on directly measured hydrometeorology data such as rainfall, stream flow, stream water level, groundwater level, and air and water temperature. Significant climatologic variation can be derived from historical events of droughts and floods. Ice cores and tree rings analysis have been used to derive long-term climatic data. Sea surface temperature variation and pressure gradient records have been correlated to regional weather and climatic variations. One of the earliest works done on global climatic relationships is by Walker and Bliss in the early 1930s (Walker and Bliss, 1930). They studied world weather and developed statistical correlation equations to predict a weather parameter at a part of the world using different weather parameters from other parts of the globe as variables. In one case, they related Honolulu and Port Darwin atmospheric pressure, the Nile flood and Indian monsoon to air temperature in western Canada. Sun spot number was one of the variables in their studies.

Wind patterns over the globe and moisture distribution patterns are controlled by the interaction of the atmosphere, ocean and land caused by differentials in temperature and pressure. Regional climatic variations have been explained by cyclic temperature and pressure anomalies of the oceans. One of the well known systems is the El Niño Southern Oscillation (ENSO) which is a measure of sea surface temperature (SST) anomalies in tropical Pacific. ENSO has teleconnections to the variation of the hydro-climatology of many parts of the world. The Atlantic Multidecadal Oscillation (AMO) is a long-term pattern of SST anomalies in the northern Atlantic between the equator and Greenland with decadal oscillation between warm and cool phase. The AMO cycle between warm phase and cool phase is shown to explain 10% of the Mississippi River outflow and 40% of Lake Okeechobee inflow in the United States. ENSO, AMO and Pacific Decadal Oscillation have been linked to the climate of South Florida (Enfield et al., 2001; Zhang and Trimble, 1996). Not only atmospheric, oceanic and land processes affect the climate, but also solar activity has a link to climate variation (Trimble et al., 1997; Soon et al., 2000).

Relevant to the study region, Seleshi and Zanke (2004), in their analysis of recent changes of rainfall in Ethiopia, concluded that Ethiopian highlands June-September rainfall is positively correlated to the Southern Oscillation Index and negatively correlated to the equatorial eastern pacific sea surface temperature. The variables for linear regression equations developed to forecast Ethiopian summer rains included SST anomalies of the western Indian Ocean, the tropical eastern Indian Ocean, and Niño3.4 SST anomalies for the preceding March, April and May rainfall (Gissila et al., 2004).

### 1.4.2 Climatic Indices

#### 1.4.2.1 El Niño-Southern Oscillation (ENSO) Indices

El Niño is an ocean-atmosphere phenomenon where the cooler eastern pacific warms up once every 2–7 years. The increase in eastern pacific SST is attributed to the weakening of the easterly trade winds which results in warm water from the western pacific moving to the east. An average of  $+0.4^{\circ}\text{C}$  deviation from average SST for three or more consecutive months indicates El Niño event. An average of  $-0.04^{\circ}\text{C}$  indicate La Niña conditions. Based on cumulative SST anomalies in Niño 3.4 region ( $5^{\circ}\text{N}$ – $5^{\circ}\text{S}$ ,  $120$ – $170^{\circ}\text{W}$ ), El Niño and La Niña years shown in Table 1.6 mostly correspond to periods presented in Trenberth (1997) and ENSO classifications on the web (<http://iri.columbia.edu/climate/ENSO/background/pastevent.html>, <http://ggweather.com/enso/years.htm>, <http://www.atmos.washington.edu/~mantua/TABLES2.html>).

The weather impact of El Niño varies with the strength of ENSO. In South Florida there is strong correlation between dry season rainfall (November–May) and ENSO events. Rainfall is significantly higher during El Niño and drier during La Niña events. Climatic prediction based on this correlation has become part of water management decision (Obeysekera et al., 2007; Abtew and Trimble 2009). Thomas (2007) developed regression equations forecasting Colorado River

**Table 1.6** El Niño and La Niña years (1871–2008)

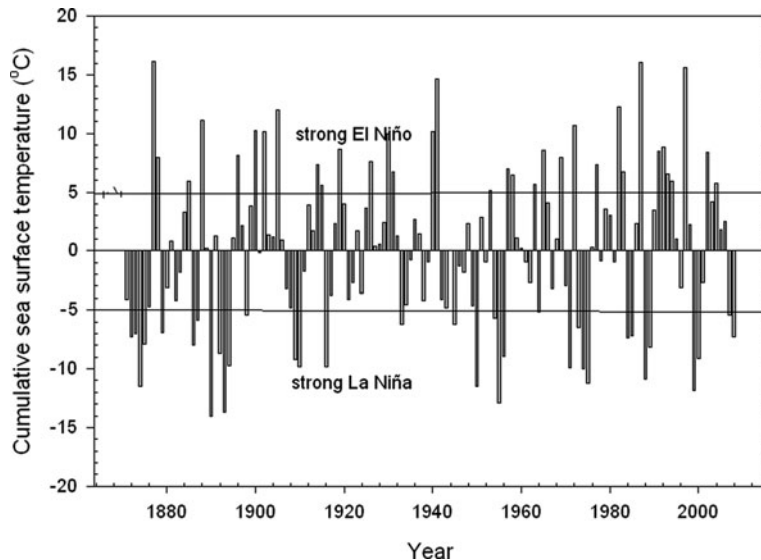


**Fig. 1.17** Cumulative annual sea surface temperature (Niño 3.4) Index (1871–2008)

stream flow using climatic indices as variables for application in water resource management.

Monthly climatic index as ENSO do not amplify the seasonal strength of the event. Cumulative index clearly indicate the comparative strength of a climatic phenomenon such as SST (Abtew et al., 2009b, 2008). In this study, cumulative climatic index is used for analysis of relationship of annual rainfall and stream flow and climatic indices. Based on historical records of ENSO events, a cumulative SST index of  $\geq 5$  indicates strong El Niño and a cumulative SST index of  $\leq -5$  indicates strong La Niña. SST cumulative annual index is shown in Fig. 1.17 for Niño 3.4.

Southern Oscillation (SO) is the variation in air pressure between the western and eastern tropical pacific. The SO index (SOI) is a measure of air pressure difference between Tahiti in the east and Darwin, Australia to the west as compared to historical average of the differences. Negative differences indicate El Niño conditions as lower pressure in the eastern Pacific is associated to warmer water and weakened easterly trade winds. Positive SOI correspond to negative SST index and La Niña. The ENSO event strength indicators are cumulative values of 7 and -7 for La Niña and El Niño, respectively (Abtew et al., 2009b). Figure 1.18 depicts cumulative annual SOI.

#### 1.4.2.2 Sunspot Numbers

Sun spots are dark spots on the surface of the sun. Observation and recording of sunspot numbers has been maintained since the seventeenth century. Solar sunspot

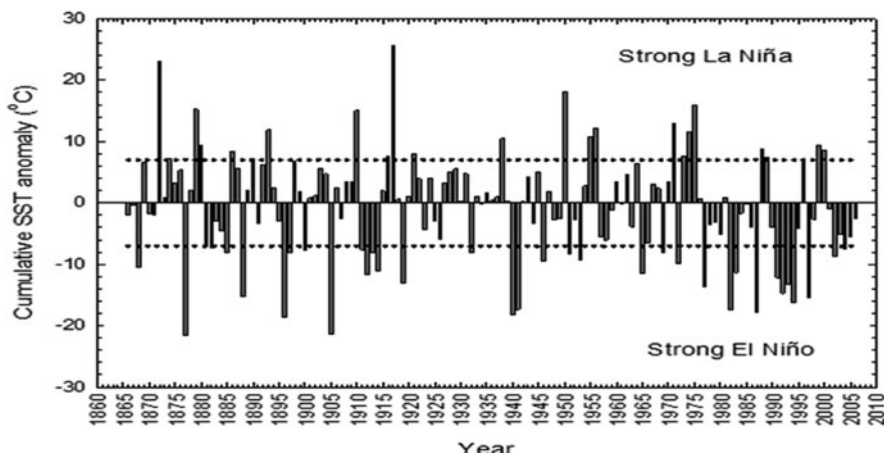


**Fig. 1.18** Cumulative annual southern oscillation index (1866–2006)

activity is measured by the number of sunspots and by the magnitude of geomagnetic activity. Solar sunspot activity has an average cycle of 11 years with reversal in the sun's magnetic field between cycles. Trimble et al. (1997) have shown that the runoff inflows into Lake Okeechobee of South Florida are associated to solar activity as estimated by the number of sunspots and geomagnetic activity. Other researchers have also shown evidence in the connection between solar activity and the earth's climate (Friis-Christensen and Lassen, 1991). In a study of decadal periodicities of the Nile River historical discharge (A.D. 622–1,470), it was suggested that both ENSO and solar periods were related factors (Putter et al., 1998). A study of the influence of decadal solar oscillation on July and August rainfall in the tropics for the period 1979–2002 reported that precipitation maxima are intensified during solar maxima than solar minima (Loon et al., 2004). A study based on diatom series, suggest that Lake Victoria lake level peaked during every peak of the 11-year sunspot cycle since the late nineteenth century (Stager et al., 2005).

#### 1.4.3 Upper Blue Nile River Basin Rainfall and ENSO Relations

The upper Blue Nile River basin is relatively wet with annual mean rainfall of 1,423 mm (1960–2002) with standard deviation of 125 mm (Fig. 1.12). The rainfall statistics is based on 36 rainfall stations with varying length of record (Abtew et al., 2009b). Out of the eight strongest El Niño years (1987, 1997, 1982, 1972, 1992, 1965, 1991 and 2002) all produced below average annual rainfall except 1992. All of the seven strongest La Niña years (1999, 1975, 1988, 1974, 1971, 2000 and 1989) produced above average rainfall. Conway (2000) reported that dry years show a degree of association with low values of SOI (El Niño). Eldaw et al. (2003) reported that the July to October flows of the Nile are correlated to the Pacific SST and

Guinea rainfall. Other studies that relate El Niño events to Ethiopian droughts are reviewed in Gissila et al. (2004). Jury and Enfield (2002) have shown that African rainfall variation is related to El Niño-Southern Oscillation Indices (ENSO).

A scatter plot of cumulative annual ENSO index and annual upper Blue Nile River basin rainfall deviations shows that wet years are more likely to occur in La Niña years and dry years occur during El Niño years (Abtew et al., 2009b). In 27 years out of 42 years of record, below average rainfall corresponded with El Niño years and above average rainfall occurred during La Niña years. A test of significance of a binomial proportion was applied to show that the events are not random (Snedecor and Cochran, 1980). With an assumed probability of 0.5 that correspondence of ENSO events to rainfall deviations in a year is a random event as the null hypothesis, Chi square ( $\chi^2$ ) test of goodness of fit was performed. The following equation expresses the test.

$$\chi^2 = \frac{\sum (f - F)^2}{F} = \frac{(r - np)^2}{np} + \frac{(n - r - np)^2}{nq} \quad (1.8)$$

Where  $n$  is the number of years of analysis (42);  $f$  is observed number of years where annual rainfall deficit corresponds to ENSO event ( $r = 27$ );  $n-r$  is the number of years where rainfall deficit does not correspond to ENSO event ( $n-r = 15$ );  $F$  is expected frequency of random correspondence assuming a probability of 0.5 ( $np = 21$ );  $F$  is also expected number of years rainfall deficit not corresponding with any ENSO events ( $nq = 21$ ). The computation results in  $\chi^2 = 3.41$ . Compared to the expected ( $\chi^2$  Table) value at 1° of freedom, the null hypothesis that the rainfall deficit has 50/50 chance to correspond to any ENSO event is rejected at 0.10 significant test level. Table 1.7 depicts the summary of the correspondence analysis.

Anecdotal records of Ethiopian droughts correspond to ENSO events. The great Ethiopian famine of 1888–1892 (Pankhurst, 1966) corresponds to one of the strong El Niño years, 1888. In recent years, 1965, 1972–1973, 1983–1984, 1987–1988 and 1997 were drought years with low agricultural production and impacts on millions of people and the environment (Seleshi and Zanke, 2004). Years 1965, 1972, 1983, 1987 and 1997 correspond to strong El Niño years. Analysis of the Nile flows at Aswan from 1872 to 1972 showed correspondence of high flows with negative SST and low flows with positive SST anomalies for the months of September, October and November (Eltahir, 1996).

**Table 1.7** Relationship of cumulative annual ENSO indices and upper Blue Nile River basin annual rainfall and flows

Events	ENSO		Significant test level
	Correspondence	Non-correspondence	
Annual rainfall (42 years)	27	15	0.1
Annual flow (44 years)	28	16	0.1

#### 1.4.4 Upper Blue Nile River Flow at Bahr Dar and ENSO Relations

Flow data with some missing data and few questionable data was available for the Blue Nile River flow at Bahr Dar for the period 1961–2003. Questionable data and missing data were estimated by interpolation and filling with flows of similar pattern months in other years. An example of questionable data is data where the mean is less than the minimum. The annual flow ranged from a maximum of 6,489 million  $m^3$  to a minimum of 975 million  $m^3$ . The mean annual flow is 3,850 million  $m^3$  and the standard deviation is 1,353 million  $m^3$ . Figure 1.19 depicts annual flow (1960–2002), mean annual flow, and  $\pm 1$  standard deviation (1353 million  $m^3$ ) of the Blue Nile River flow at Bahr Dar. Seventy one percent of the flows are from July through November while 70% of the rainfall at Bahr Dar occurs between June and September. Seventy three percent of the Blue Nile River basin areal average rainfall occurs between May and September. Comparison of annual flow deviations with cumulative Nino 3.4 sea surface temperature index shows that wet years are likely to occur during La Niña years and dry years are likely to occur during El Niño years (Abtew et al., 2009). Seven of the nine highest annual flow years occurred during La Niña years (1964, 1999, 1988, 2000, 2001, 1975 and 1962). Also, nine of the driest 10 years occurred during El Niño years (1994, 1983, 1972, 1982, 1987, 1990, 2003, 1980, 1979, 1995 and 1972).

The Chi square value based on equation 8 with  $n$ ,  $r$ ,  $F$  values of 43, 29, 21.5 is 5.25. This test is significant at 5% level indicating that below average flows correspond to El Niño years and above average flows correspond to La Niña years.

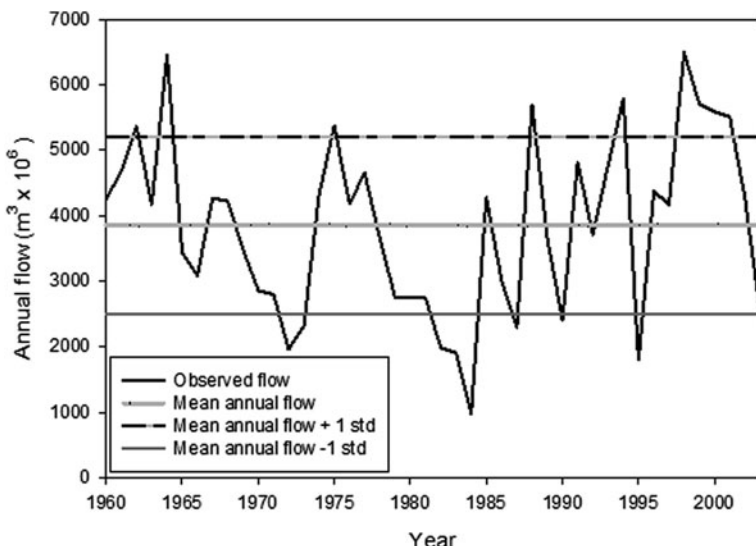
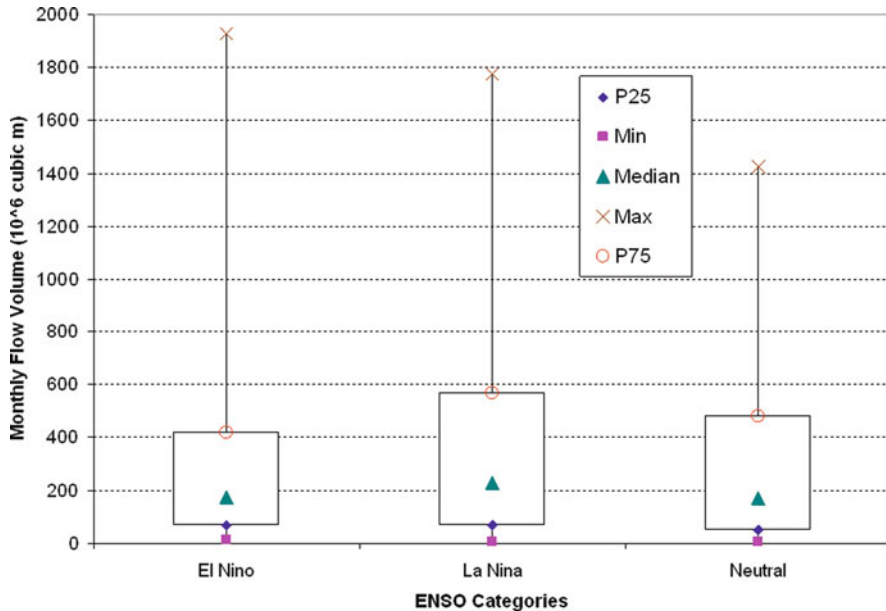


Fig. 1.19 Blue Nile River annual flows at Bahr Dar



**Fig. 1.20** Relationship of month moving average ENSO (SST) index and Blue Nile River at Bahir Dar monthly flow

Figure 1.20 shows comparison of monthly flows of the Blue Nile River at Bahir Dar with 3 months moving average ENSO (SST). El Niño events occur when sea surface temperature deviation is greater or equal to  $+0.50^{\circ}\text{C}$  and La Niña events occur when sea surface temperature deviation is less than or equal to  $-0.50^{\circ}\text{C}$  for this analysis. Average flows during La Niña years are 25% higher than flows during El Niño and neutral years.

In this analysis, monthly average sunspot numbers were summed to annual sunspot numbers. Relationship of the Blue Nile River flow to solar sunspots was evaluated by comparing annual flows to annual cumulative sunspot numbers (Fig. 1.21). The peak flows generally correspond to solar maxima in a solar cycle. The relationship warrants further evaluation of the relationship, with longer period data sets.

## 1.5 Lake Tana

### 1.5.1 Lake Tana Stage Variation

Lake Tana is located in the northwestern part of Ethiopia with a surface area of  $3,156 \text{ km}^2$ , accounting 20% of the  $15,096 \text{ km}^2$  drainage area of the Lake Tana basin. The lake is a natural type which covers  $3,000\text{--}3,600 \text{ km}^2$  area at an elevation of

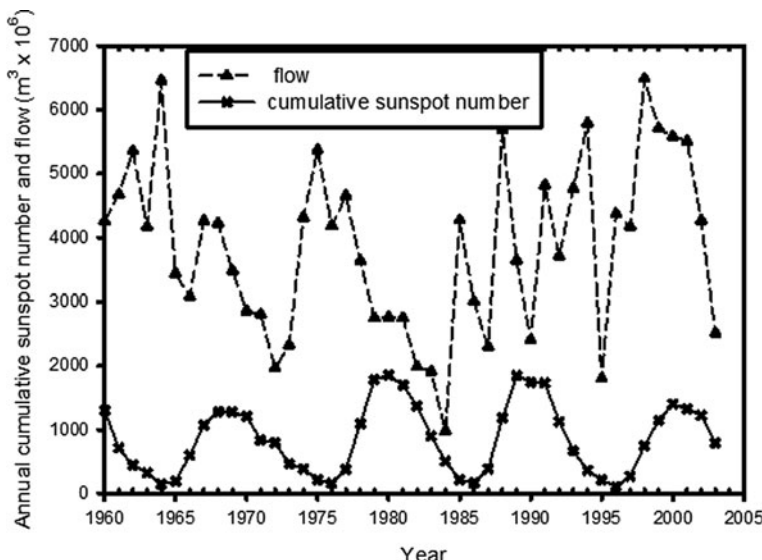


**Fig. 1.21** Relationship of Blue Nile River flow and sunspot numbers

1,800 m and with a maximum depth of 15 m. It is approximately 84 km long, 66 km wide. It is the largest lake in Ethiopia and the third largest in the Nile River basin. It is the main source of the Blue Nile River that is the only surface outflow for the Lake.

The lake receives perennial flow from four major rivers: Gilgel Abay, Rib, Gumera, and Megech contributing 93% of the inflow, and at the outlet starts the Blue Nile River. The mean annual rainfall of the catchment area is about 1,280 mm. The annual mean actual evapotranspiration and water yield of the catchment area is estimated to be 773 and 392 mm, respectively (Setegn et al., 2009). Records show that Lake Tana had a historical variation in its level believed to stem from hydrologic alterations within its basin due to reduction in dry season flows attributed to human and climate-induced changes.

Stage monitored data and satellite data from TOPEX/POSEIDON and Jason-1 Altimetry (NOAA, 2008) has also shown good correspondence indicating radar altimetry's application in large lake stage monitoring (Fig. 1.22). Figure 1.22 shows the deviation of the monitored Lake Tana stage from the 10-year average monthly lake stage as monitored from TOPEX/POSEIDON and Jason-1 Altimetry. Lake Tana has shown historical variation in its stage responding to the rainfall signal and river inflows to the lake. The lake receives large volumes of water during the wet season in June, July and August. Figure 1.23 shows Lake Tana stage measured by radar altimetry. The stage has shown seasonality and also inter-annual variability responding to rainfall variation (Fig. 1.23). The lake has also shown a decline in its stage in 2001 responding to an intake of more water for hydroelectric power generation.

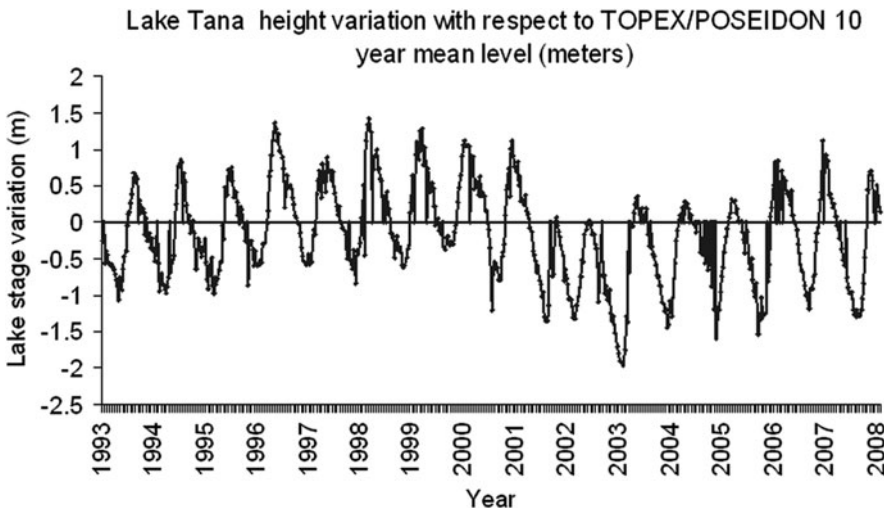


Fig. 1.22 Measured and a 10-year mean radar altimetry lake stage variation

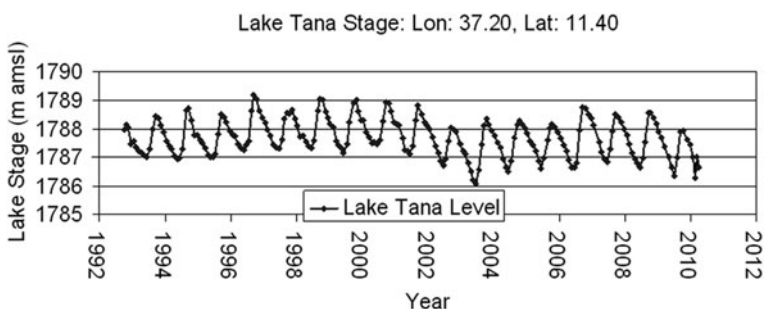
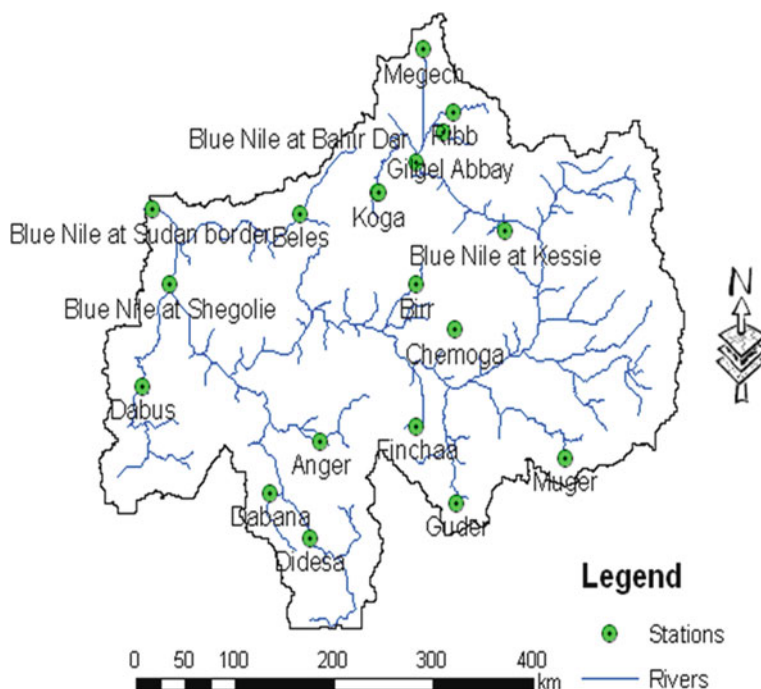


Fig. 1.23 Radar altimetry based stage of Lake Tana

## 1.6 Blue Nile River and Tributaries Flow Patterns

### 1.6.1 High and Low Flow Analysis

In order to understand the behavior of the extreme flows and their recurrence interval, monthly high and low flow records from the Ethiopian Ministry of Water Resources were acquired and analyzed for selected representative stations (Fig. 1.24). The data has some gaps and also different length of records. The recurrence interval (in months) for the high and low flows based on the recorded data for selected rivers in the upper Blue Nile River basin is shown in Figs. 1.25, 1.26, 1.27 and 1.28. It is shown that, based on the flow size and river, different lengths of recurrence intervals are found. Blue Nile River (Abbay) at Kessie has large flows



**Fig. 1.24** River flow monitoring stations of the upper Blue Nile River basin

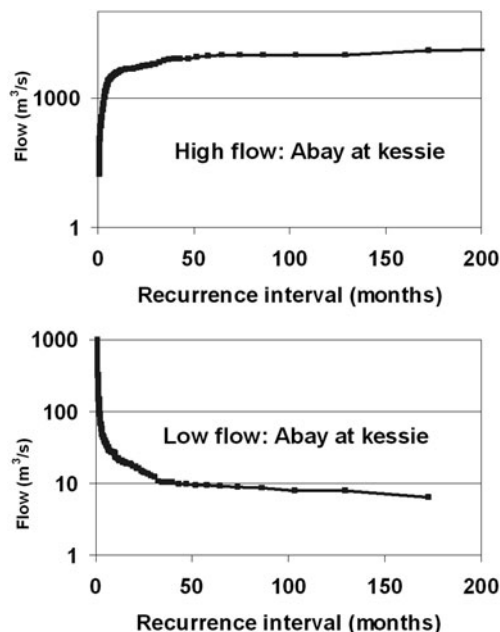
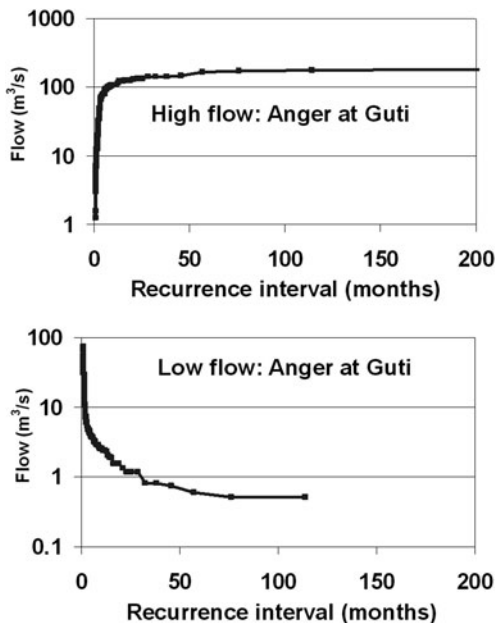


**Fig. 1.25** Monthly high and low flow recurrence interval for Blue Nile River flow at Kessie (a) high flow and (b) low flow. Flow is in logarithmic scale

**Fig. 1.26** Monthly high and low flow recurrence interval for Anger River flow at Guti (a) high flow and (b) low flow. Flow is in logarithmic scale



compared to the other three rivers and corresponding high flow of  $9,910 \text{ m}^3/\text{s}$  with the recurrence interval of 10.8 years,  $380 \text{ m}^3/\text{s}$  for Gilgel Beles,  $180 \text{ m}^3/\text{s}$  for Anger at Guti and  $130 \text{ m}^3/\text{s}$  for Megech (Melesse et al., 2009). Low flow analysis for the monthly records at the four rivers also showed a varied low flow for a recurrence

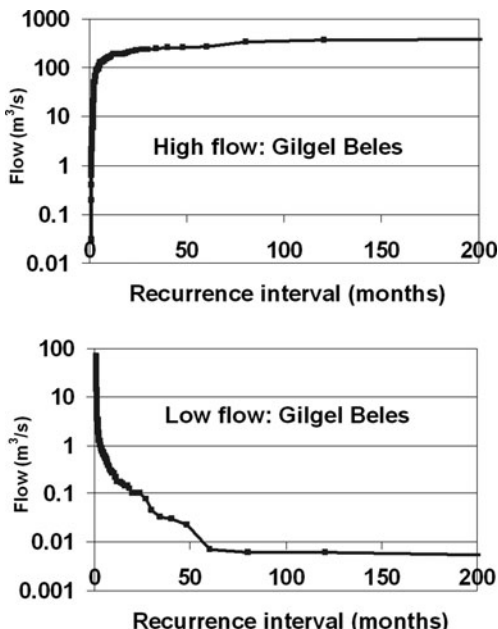
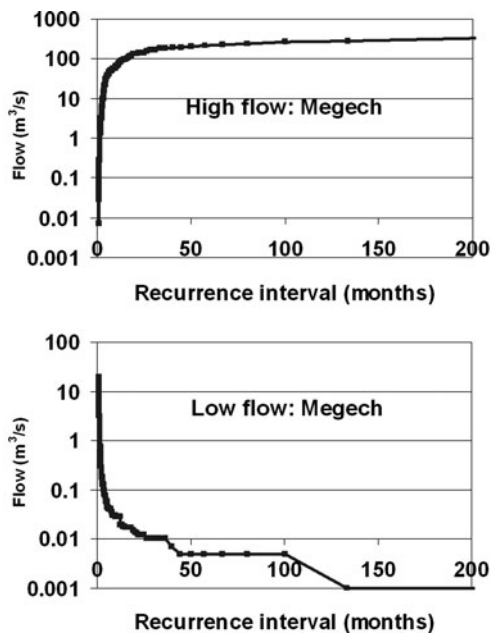


**Fig. 1.27** Monthly high and low flow recurrence interval for Gilgel Beles River flow (a) high flow and (b) low flow. Flow is in logarithmic scale

**Fig. 1.28** Monthly high and low flow recurrence interval for Megech River flow  
**(a)** high flow and **(b)** low flow. Flow is in logarithmic scale



interval of 10–11 years as  $129.5 \text{ m}^3/\text{s}$  for Blue Nile River (Abbay) at Kessie,  $0.006 \text{ m}^3/\text{s}$  for Gilgel Beles,  $0.5 \text{ m}^3/\text{s}$  for Anger at Guti and  $0.015 \text{ m}^3/\text{s}$  for Megech.

## 1.7 Summary

With an annual average rainfall of 1,423 mm and standard deviation of 125 mm, the upper Blue Nile River basin is relatively wet. The rainfall statistics is based on 32 rainfall stations with varying length of record from 1960 to 2002. This mean rainfall is similar to a mean annual rainfall study for a longer period (1900–1998). The wet season months are June, July, August and September and the dry season months are January, February, March, April, November and December. May is the transition month from the dry season to the wet season and October is the transition month from the wet season to the dry season. January has the lowest and July has the highest monthly rainfall. Monthly rainfall probability distribution varies from month to month fitting Gamma-2, Normal, Weibull and Lognormal distributions. January, July, October and November basin average rainfall fit the Gamma-2 probability distribution. February, June and December fit Weibull distribution. March, April, May and August fit Normal distribution. September fits Log-Normal distribution. The annual basin rainfall has a Normal probability distribution. The year-to-year (temporal) basin rainfall variation is relatively small with a coefficient of temporal variation of 0.09 while the spatial variation is high with coefficient of spatial variation of 0.25. The 100-year drought basin annual rainfall is 1,132 mm and the 100-year wet basin

annual rainfall is 1,745 mm. The dry season is from November through April. The wet season runs from June through September with 74% of the annual rainfall and with low variation and skewness. October and May are transition months. Monthly and annual rainfalls for return periods 2, 5, 10, 25, 50 and 100-year dry and wet patterns are presented. Spatial distribution of annual rainfall over the basin is mapped and shows high variation with the southern tip receiving as high as 2,049 mm and the northeastern tip as low as 794 mm annual average rainfall.

Climatic teleconnections to the Blue Nile River hydrology was evaluated using basin average rainfall and Blue Nile River flows at Bahir Dar. The El Niño Southern Oscillation index (ENSO) relationship using sea surface temperature anomalies in region Niño 3.4 and variation in air pressure between the western and eastern tropical pacific was used for analysis. The analysis indicates that the upper Blue Nile River basin rainfall and flows are connected to the ENSO index. High rainfall and high flows are likely to occur during La Niña years and dry years are likely to occur during El Niño years. Extreme dry years are highly likely to occur during El Niño years and extreme wet years are highly likely to occur during La Niña years. The prediction of El Niño and La Niña relatively has higher certainty than predicting basin rainfall and runoff. Identifying teleconnections to a region's hydrology has practical applications for water resources management. There are indications that the hydrology of the Blue Nile River basin may correspond to sunspot numbers with wet conditions occurring during solar maxima and dry conditions prevailing during solar minima.

Analysis of low and high recorded monthly flows for selected stations in the basin resulted in different return periods based on river size and flows. For the return period of 10–11 years, the high flows for the selected stations varied from 130 m<sup>3</sup>/s for Megech to 9,910 m<sup>3</sup>/s for Blue Nile River (Abbey) at Kessie. Similarly, the low flows for the same return period were 0.006 m<sup>3</sup>/s for Gilgel Beles to 129.5 m<sup>3</sup>/s for Blue Nile River (Abbey) at Kessie.

**Acknowledgments** We would like to extend our appreciation to the Ministry of Water Resources of Ethiopia and Ethiopian Meteorological Agency for the river flow and meteorological data of the study area.

## References

Abtew W, Melesse A, Dessalegne T (2009a) Spatial, inter and intra-annual variability of the upper Blue Nile River basin rainfall. *Hydrol Process* 23:3075–3082

Abtew W, Melesse AM, Dessalegne T (2008) Characteristics of monthly and annual rainfall of the upper Blue Nile Basin. In Abtew W, Melesse AM (ed) *Proceedings of the 2008 workshop on the Nile basin hydrology and ecology under extreme climatic condition*. Aardvark Global Publishing, Salt Lake City, UT

Abtew W, Melesse AM, Dessalegne T (2009b) El Niño Southern Oscillation link to the Blue Nile River basin hydrology. *Hydrol Process* 23:3653–3660

Abtew W, Trimble P (2009) El Niño Southern Oscillation link to South Florida hydrology and water management applications. Technical Paper SFWMD # 106, South Florida Water Management District, West Palm Beach, FL

Azene B, Birnie A, Tengnas B (1993) Useful trees and shrubs for Ethiopia. Identification, propagation and management for agricultural and pastoral communities. Regional Soil Conservation Unit, SIDA, Nairobi

Bewket W, Conway D (2007) A Note on the temporal and spatial variability of rainfall in the drought-prone Amhara region of Ethiopia. *Int J Climatol* 27:1467–1477

Conway D, Mould C, Bewket W (2004) Over one century of rainfall and temperature observations in Addis Ababa, Ethiopia. *Int J Climatol* 24:77–91

Conway D (2000) The Climate and hydrology of the Upper Blue Nile River. *Geogra J* 166(1): 49–62

De Pauw E, Bruggeman HY (1988) A Summary of the agricultural ecology of Ethiopia. Prepared under FAO projects food information systems (GCP/ETH/044/NOR), zonation and calibration for project planning (TCP/ETH/6658), Master Land Use Plan (ETH/82/010), FAO, Rome

Degefu GT (2003) The Nile historical legal and developmental perspectives. Trafford Publishing, St. Victoria, BC, Canada

Eldaw AK, Salas JD, Garcia LA (2003) Long-range forecasting of the Nile River flows using climatic forcing. *J Appl Meteorol* 42:890–904

Eltahir EAB (1996) El Niño and the natural variability in the flow of the Nile River. *Water Resour Res* 32(1):131–137

Enfield DB, Nunez AM, Trimble PJ (2001) The AMO and its relationship to rainfall and river flow in the continental US. *Geophys Res Lett* 28(10):2077–2080

FAO (2002) Major Soils of the World. Land and Water Digital Media Series (CD-ROM). Food and Agricultural Organization of the United Nations, Rome

Friis-Christensen E, Lassen K (1991) Length of the solar cycle: an indicator of solar activity closely associated with climate. *Science* 254:698–700

Garbrecht JD, Piechota TC (2006) Climatic variations, climate change, and water resources engineering, ASCE, Reston, Virginia

Gissila T, Black E, Grimes DIF, Slingo JM (2004) Seasonal forecasting of the Ethiopian summer rains. *Int J Climatol* 24:1345–1358

GlobCover (2008) [http://ionia1.esrin.esa.int/images/GLOBCOVER\\_Product\\_Specification\\_v2.pdf](http://ionia1.esrin.esa.int/images/GLOBCOVER_Product_Specification_v2.pdf). Accessed on 10 Jan 2010

Greenwood JA, Durand D (1960) Aids for fitting the gamma distribution by maximum likelihood. *Technometrics* 2(1):55–65

Haan C (1977) Statistical methods in hydrology. The Iowa State University Press, Ames, IA

Jury MR, Enfield DB (2002) Tropical monsoons around Africa: stability of El Niño-Southern Oscillation associations and links with continental climate. *J Geophys Res* 107(C10):3151

Kebede S, Travi Y, Alemayehu T, Marc V (2006) Water balance of Lake Tana and its sensitivity to fluctuations in rainfall, Blue Nile basin, Ethiopia. *J Hydrol* 316:233–247

Loon HV, Meehl GA, Arblaster JM (2004) A decadal solar effect in the tropics in July-August. *J Atmos Sol Terr Phys* 22(18):1767–1778

Maidment DR (1993) Handbook of hydrology. McGraw-Hill, Inc., New York, NY

Melesse A, Abtew W, Desalegn T, Wang X (2009) Low and high flow analysis and wavelet application for characterization of the blue Nile River system, *Hydrol Process* 24(3):241–252

NASA (2009). ASTER Global DEM. <http://asterweb.jpl.nasa.gov/gdem-wist.asp>. Accessed on Nov 2009

NOAA (2008) Global reservoir and lake elevation database. <http://www.cpc.ncep.noaa.gov/products/fews/africa/briefing.html>. Accessed on 20 Sept 2008

Obeysekera J, Trimble P, Neidrauer C, Pathak C, VanArman J, Strowd T, Hall C (2007) Consideration of long-term climatic variability in regional modeling for SFWMD planning and operations. In: Redfield G (ed) The 2007 South Florida environmental report. Chapter 2: hydrology of the South Florida environment. South Florida Water Management District, West Palm Beach, FL

Pankhurst R (1966) The great Ethiopian famine of 1888–1892: a new assessment part one. *J Hist Med Allied Sci* XXI:95–124

Peggy AJ, Curtis D (1994) Water Balance of Blue Nile Basin in Ethiopia. *J Irrig Drain Eng* 120(3):573–590

Putter TD, Loutre MF, Wansard G (1998) Decadal periodicities of Nile River historical discharge (A.D. 622–1470) and climate implications. *Geophys Res Lett* 25(16):3193–3196

Seleshi Y, Zanke U (2004) Recent changes in rainfall and rainy days in Ethiopia. *Int J Climatol* 24:973–983

Setegn SG, Srinivasan R, Melesse A, Dargahil B (2009) SWAT model application and prediction uncertainty analysis in the Lake Tana Basin, Ethiopia. *Hydrol Process* 24(3):357–367

Snedecor GW, Cochran WG (1980) Statistical methods. The Iowa State University Press, Ames, IA

Soon W, Baliunas S, Posmentier ES, Okeke P (2000) Variations of solar coronal hole area and terrestrial lower tropospheric air temperature from 1979 to mid-1998: astronomical forcings of change in earth's climate. *New Astronomy* 4(8):563–579

Stager JC, Ryves D, Cumming BF, Meeker LD, Beer J (2005) Solar variability and the levels of Lake Victoria, East Africa, during the last millennium. *J Paleolimnol* 33(2):243–251

Thomas BE (2007) Climatic fluctuations and forecasting of streamflow in the lower Colorado River basin. *J Am Water Resour Assoc* 43(6):550–1569

Trenberth KE (1997) The Definition of El Niño. *Bull Am Meteorol Soc* 78(12):2771–2777

Trimble P, Santee ER, Neidrauer C (1997) Including the effects of solar activity for more efficient water management: an application of neural networks. Special Report, South Florida Water Management District, West Palm Beach, FL

USDA-FAS (2003) Agroecological zones of Ethiopia. [http://www.fas.usda.gov/pecad2/highlights/2002/10/ethiopia/baseline/Eth\\_Agroeco\\_Zones.htm](http://www.fas.usda.gov/pecad2/highlights/2002/10/ethiopia/baseline/Eth_Agroeco_Zones.htm). Accessed 12 Dec 2009

Verstraete MM, Pinty B, Curran PJ (1999) MERIS potential for land applications. *Int J Rem Sens* 20:1747–1756

Walker GT, Bliss EW (1930) World weather IV 3(24):81–95

Walpole RE, Myers RH (1985) Probability and statistics for engineers and scientists. Macmillan Publishing Co., New York, NY

Zhang EY, Trimble P (1996) Forecasting water availability by applying neural networks with global and solar indices. In: Proceedings of the 16th Annual American Geophysical Union. Hydrology Days, Atherton, pp 1–13

# Chapter 2

## Hydro-Meteorology and Water Budget of the Mara River Basin Under Land Use Change Scenarios

**Liya M. Mango, Assefa M. Melesse, Michael E. McClain, Daniel Gann, and Shimelis G. Setegn**

**Abstract** Mara is a transboundary river located in Kenya and Tanzania and considered to be an important life line to the inhabitants of the Mara-Serengeti ecosystem. It is also a source of water for domestic water supply, irrigation, livestock and wildlife. The alarming increase of water demand as well as the decline in the river flow in recent years has been a major challenge for water resource managers and stakeholders. This has necessitated the knowledge of the available water resources in the basin at different times of the year. Historical rainfall, minimum and maximum stream flows were analyzed. Inter and intra-annual variability of trends in streamflow are discussed. Landsat imagery was utilized in order to analyze the land use land cover in the upper Mara River basin. The semi-distributed hydrological model, Soil and Water Assessment Tool (SWAT) was used to model the basin water balance and understand the hydrologic effect of the recent land use changes from forest-to-agriculture. The results of this study provided the potential hydrological impacts of three land use change scenarios in the upper Mara River basin. It also adds to the existing literature and knowledge base with a view of promoting better land use management practices in the basin.

**Keywords** Mara River · Hydro-meteorology · SWAT · Land use change · Water budget

### 2.1 Introduction

The 395-km long Mara River is transboundary and drains an area of about 13,750 km<sup>2</sup> across the Kenya-Tanzania border (Mati et al., 2005). Widespread human activities such as cultivation and deforestation of the Mau catchment in the highlands have led to erratic flow in the Mara River in both the dry and wet seasons.

---

L.M. Mango (✉)

Department of Earth and Environment, Florida International University, Miami, FL 33199, USA  
e-mail: lmango@fiu.edu

This is a major problem given the high demand for water by the different sectors in the Mara River basin where Mara is the only perennial river. Downstream of the Mara River are human settlements, agricultural areas, protected areas that support immense wildlife populations and wetlands that are dependent on the availability of water in adequate quality and quantity. Activities such as deforestation, irrigation and the construction of weirs on the Amala River, which is a tributary of the Mara, contribute to the reduction of Mara River flow during severe droughts. This reduction negatively impacts wildlife-water interactions and consequently, the ecosystems (Gereta and Wolanski, 1998; Gereta et al., 2002). Serneels et al. (2001) noted that climatic, anthropogenic and other factors shape the vegetation, ecology and biodiversity of an ecosystem. According to Mutie et al. (2006), modification of natural land cover and soil conditions have brought about changes in the river flow regime such as high peak flows, reduced base flows, enlarged river channels and silt deposition downstream. Reliable data is needed to develop policies and comprehensive management principles for sustainable resource utilization (Mati et al., 2005). Therefore, determining the water balance of the main tributaries of the Mara River basin (Amala and Nyangores Rivers) is considered to be an important step in analyzing the different hydrological resources that is believed to be used by different sectors.

The main objectives of the study reported in this chapter are to (1) understand the hydro-meteorological variability within the Mara River basin, (2) evaluate the performance of the Soil and Water Assessment Tool (SWAT) model in the hydrological analysis of the Amala sub-basin utilizing two different sources of rainfall data and (3) quantify the water balance of the upper Mara basin under different land use change scenarios. To achieve these objectives, the physically based, semi-distributed SWAT model was calibrated and applied for prediction of streamflow and other hydrological parameters in the basin.

The modeling, land use change and hydrological response results presented in this chapter are those of the Amala watershed. Amala has experienced high level of forest-to-agriculture conversion in recent years and has been the focus of the study due to the hydrologic alterations and impacts it has exhibited. The Amala watershed had a short dataset and this as in any other hydrological study was a constraint in terms of calibration and validation of the model.

## 2.2 Study Area

The transboundary Mara River basin is shared between Kenya and Tanzania and is located between longitudes 33.88372° and 35.907682° West, latitudes –0.331573° and –1.975056° South (Fig. 2.1). It covers about 13,750 km<sup>2</sup> (Mati et al., 2005) and is characterized by different types of land use/cover as a result of different human activities carried out by the stakeholders in various parts of the basin. The land uses include; settlements and villages, subsistence and large scale agriculture, forestry, livestock, fisheries, tourism, conservation areas, mining and other industries. The

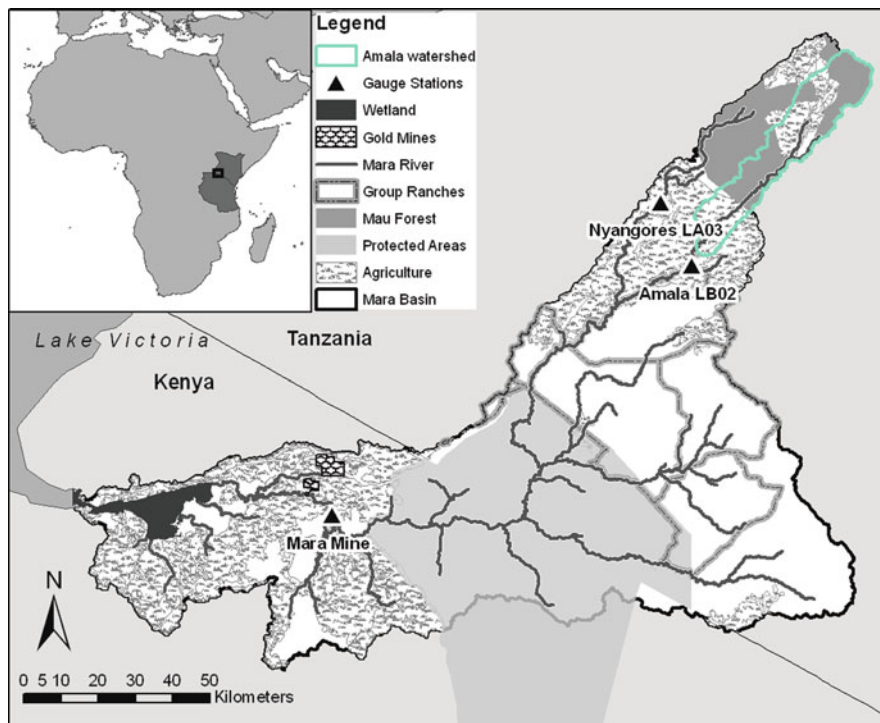


**Fig. 2.1** Mara River basin, Kenya/Tanzania

Mara River flows 395 km from its source in the high altitude of Mau Forest in Kenya across different landscapes and finally drains into Lake Victoria at Musoma Bay in Tanzania. Mara is formed by the convergence of its two main perennial tributaries, the Amala and Nyangores Rivers that flow from the Enapuiyapui swamp in the Mau Escarpment. Other tributaries include the Talek River, the Engare Engito and the Sand River which is the last main tributary on the Kenyan side of the basin joining the Mara River in the Serengeti plains on the Kenya-Tanzania border. On the Tanzanian side of the basin, the main tributary is the Bologonja River, the Mara River then flows through the Mosirori Swamp, into the Mara Bay, Lake Victoria at Musoma.

### 2.3 Hydrological Modeling and Water Balance

Physically-based models are most suited for studying catchment change scenarios. Prediction of discharge from catchments and monitoring of pollutant and sediment dispersal are well suited for physical models (Abbot and Refsgaard, 1996). There are different physically based hydrological models designed and applied to simulate the

rainfall runoff relationship under different temporal and spatial dimensions. In this study, the physically based, semi-distributed SWAT model was used. This model is one of the watershed models that play a major role in analyzing the impact of land management practices on water, sediment, and agricultural chemical yields in large complex watersheds. It simulates impacts over a long time and requires inputs of weather, soil properties, topography, vegetation and land management practices in the watershed. It is also computationally efficient and can be used to simulate processes over very large areas like the Mara River basin without excessive data and investment of time and resources (Neitsch et al., 2005).

The Mara River basin is a gauged river basin with four gauging stations but there is a substantial amount of data missing in the stations. Moreover, in the process of simulation, gauging station data is required at the outlets of the sub-basins or sub-watersheds in simulations in order to calibrate the model by fitting the simulated or predicted values to the observed or measured values.

Setegn et al. (2009a, b) applied the SWAT model to Lake Tana basin, Ethiopia to model the hydrological processes aiming at testing the performance and feasibility of the model in streamflow and sediment yield prediction in the basin. The SWAT model produced good simulation results for daily and monthly time steps. Jayakrishnan et al. (2005) used SWAT to model the hydrology of Sondu River basin in Western Kenya. This study demonstrated that the application of detailed hydrologic models, developed and studied widely in the United States, to African river basins is possible given proper and adequate input data collection to improve model parameter calibration and simulation results.

### ***2.3.1 Description of SWAT Model***

SWAT is a hydrological model that can be applied at the river basin, or watershed scale. It was developed by the United States Department of Agriculture (USDA) Agricultural research Service (ARS) for the purpose of simulation of impact of land management practices on water, sediment and agrochemical yields in large watersheds with varying soils, land use and agricultural conditions over extended time periods (Neitsch et al., 2005). It is used to simulate processes affecting water quantity, sediment and nutrient loads in a catchment (Abbaspour et al., 2007). Arnold et al. (1998) defines SWAT as a semi-distributed, time continuous simulator operating on a daily time step. It is developed for assessment of the impact of land management and climate on water supplies, sediment, and agricultural chemical yields in sub-basins and larger basins.

It allows simulation with a high level of spatial detail by dividing the watershed into a large number of sub-watersheds which are characterized by one or more hydrological response units (HRUs). Each HRU corresponds to a particular combination of soil and land use within the sub-basin. Only soil types and land use classes exceeding the user-defined threshold area are considered to set the overlay combination. The program is provided with an interface in ArcView GIS (Di Luzio et al.,

2002) for the definition of watershed hydrologic features and storage, as well as the organization and manipulation of the related spatial and tabular data.

### 2.3.1.1 Hydrological Component of SWAT

The simulation of the hydrology of a watershed is done in two separate phases. One is the land phase of the hydrological cycle that controls the amount of water, sediment, nutrient and pesticide loadings to the main channel in each sub-basin. Hydrological components simulated in land phase of the hydrological cycle are canopy storage, infiltration, redistribution, evapotranspiration, lateral subsurface flow, surface runoff, ponds, tributary channels and return flow. The second division is routing phase of the hydrologic cycle that can be defined as the movement of water, sediments, nutrients and organic chemicals through the channel network of the watershed to the outlet. In the land phase of hydrological cycle, SWAT simulates the hydrological cycle based on the water balance equation.

$$SW_t = SW_0 + \sum_{i=1}^t R_{day} - Q_{surf} - E_a - W_{seep} - Q_{gw} \quad (2.1)$$

Where;  $SW_t$  is the final soil water content (mm),  $SW_0$  is the initial soil water content on day  $i$  (mm),  $t$  is the time (days),  $R_{day}$  is the amount of precipitation on day  $i$  (mm),  $Q_{surf}$  is the amount of surface runoff on day  $i$  (mm),  $E_a$  is the amount of evapotranspiration on day  $i$  (mm),  $W_{seep}$  is the amount of water entering the vadose zone from the soil profile on day  $i$  (mm), and  $Q_{gw}$  is the amount of return flow on day  $i$  (mm).

More detailed descriptions of the different model components are shown in (Arnold et al., 1998; Neitsch et al., 2005).

Surface runoff or overland flow generally occurs on a slope whenever the rate of precipitation exceeds the rate of infiltration. SWAT uses two methods for estimating the surface runoff: the SCS curve number method (USDA-SCS, 1972) and the Green & Ampt infiltration method (Green and Ampt, 1911). The Green & Ampt infiltration method makes use of sub-daily precipitation and calculates the infiltration as a function of the wetting front matric potential and effective hydraulic conductivity. Using daily or sub-daily rainfall data, the SWAT model simulates surface runoff volumes peak runoff rates for each HRU. In this study, the SCS curve number method is used to estimate surface runoff because of the unavailability of sub-daily rainfall data for Green & Ampt method.

SWAT calculates the peak runoff rate with a modified rational method. There are many methods that are developed to estimate potential evapotranspiration (PET). Three methods are incorporated into SWAT: the Penman-Monteith method (Monteith, 1965), the Priestley-Taylor method (Priestley and Taylor, 1972) and the Hargreaves method (Hargreaves and Samani, 1982). For this study, the Hargreaves method was used due to lack of weather data such as wind speed, humidity and sunshine hours.

### 2.3.1.2 Routing Phase of the Hydrological Cycle

Once SWAT determines the loadings of water, sediment, nutrients and pesticides to the main channel, the loadings are routed through the stream network of the watershed. Routing in the channel is divided into four components: water, sediment, nutrients and organic chemicals. In flood routing, flow is routed through the channel and possible losses are taken into consideration such as evaporation and transmission through the channel bed. Another potential loss is the abstraction or removal of water from the channel for human or agricultural use. Flow may be supplemented by rain falling directly on the channel or addition of water from a point source discharge. Flow through the channel is routed using a variable storage coefficient method developed by Williams (1969) or the Muskingum routing method.

## 2.4 Materials and Methods

### 2.4.1 Land Use Data Classification

The SWAT model requires a spatially explicit land use map as an input in order to simulate the hydrology of a watershed. Land use data was obtained by the classification of satellite imagery from the Landsat 4/5 Thematic Mapper (TM) sensor that is built for earth observation purposes. Both its spatial resolution of 30 m pixel and 7 band radiometric resolutions makes it suitable for land cover classification (Van der Meer, 2000). Two images of Path 169, Row 61 and Path 169, Row 60 from the 5th of September 2008 were selected for the classification (Fig. 2.2).

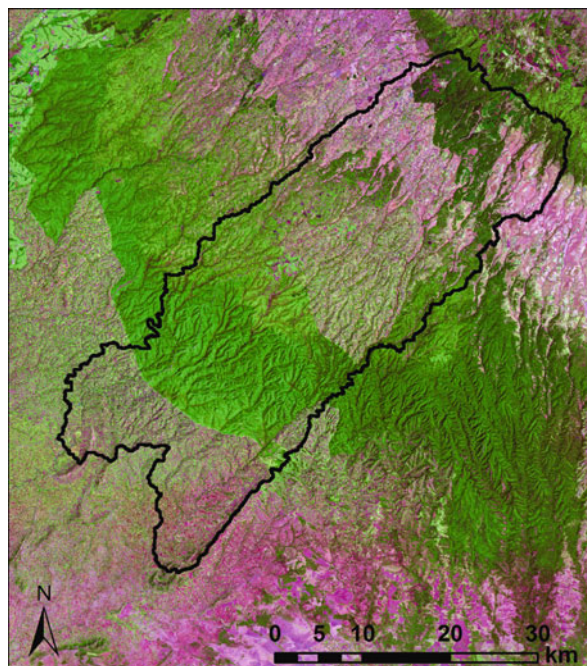


**Fig. 2.2** A 2008 Landsat TM image of the Upper Mara River basin

The expert classifier was constructed using the Knowledge Engineer Tool in Earth Resources Data Analysis Systems (ERDAS, 2009) which involved identification of the hypotheses which are the classes identified in the study area; Cloud, Bushland, Cropland, Grassland, Bare soil, Shadow, Water and Forest. The expert system rules (variables) and conditions were specified based on remote sensing multispectral reflectance characteristics and derivatives including the Kauth Thomas Tasseled Cap transformation and texture bands. The recursive partitioning process carried out beforehand resulting in the decision tree and production rules significantly reduced the time and effort required to construct the expert classifier which was then used to classify the image.

A land use/land cover classification scheme was formulated that would accurately and adequately represent the land cover/land use within the Mara River basin. This scheme however follows the basic principles of the USGS Land use/land cover classification system (LULCCS) for use with remote sensor data level classification (Anderson et al., 1976).

### **2.4.2 Model Input**

To setup a hydrological SWAT model, basic data are required: topography, soil, land use and climatic data.

#### **2.4.2.1 Digital Elevation Model**

The 90-m digital elevation model (DEM) of the study area obtained from the Shuttle Radar Topography Mission (SRTM) was used (Fig. 2.3). The DEM gives the elevation of a particular point at a particular spatial resolution and was used in the delineation of the watershed and analysis of the land surface characteristics and drainage patterns. Terrain preprocessing was performed with ArcSWAT in ArcMap 9.2 (ESRI, 2006) using the digital elevation model to delineate the catchments and drainage line.

#### **2.4.2.2 Soil Data**

Soil data was obtained from the Soil Terrain Database of East Africa (SOTER) (Fig. 2.4). Geographic Information System (GIS) layers were obtained and used in the hydrological model as one of the main inputs to the SWAT model which requires soil property data such as the texture, chemical composition, physical properties, available moisture content, hydraulic conductivity, bulk density and organic carbon content for the different layers of each soil type (Setegn et al., 2009a). A user table specific for the Mara River basin soil layer was appended to the soil table in the SWAT database since the soil types found in the study area are not included in the US soils database. Table 2.1 shows the texture of the soils in the upper Mara River basin.

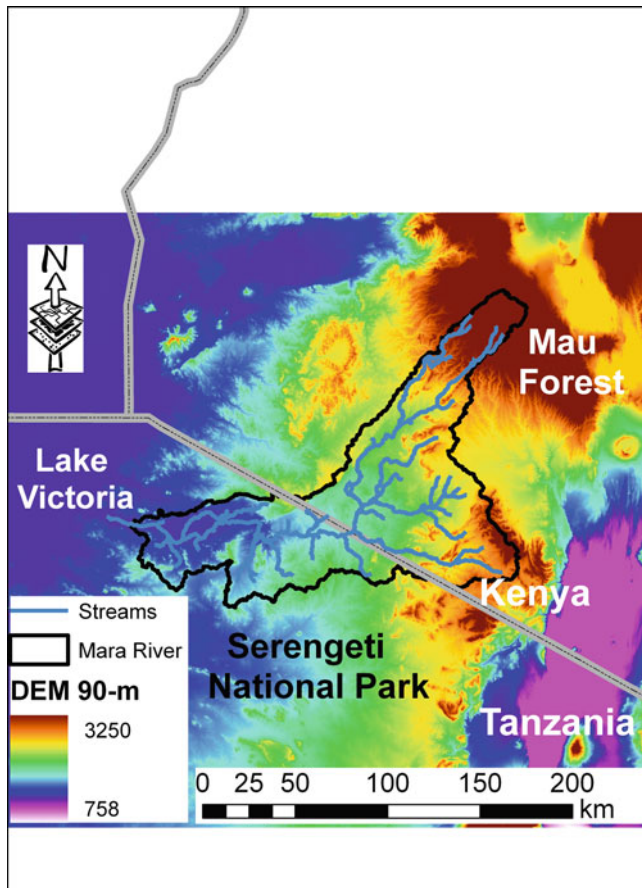


**Fig. 2.3** Digital elevation model (DEM) of Mara River basin

#### 2.4.2.3 Land Use

Land use data for the year 2008 was obtained from classified Landsat TM imagery following the process described previously in this chapter. The land cover map was then converted to a GIS layer and aggregated to make them easier to input into the model for use in the hydrological modeling exercise. An existing land use data set for the year 2002 were also used and this was obtained from the FAO-Africover project (FAO, 2005). Figure 2.5 shows the 2008 land cover maps for the upper Mara.

Land use and management is an important factor affecting different processes in the watershed such as surface runoff, erosion and evapotranspiration. Reclassification of the land use map is done in order to present them in a form that is acceptable in the model and this is the USGS Land use/Land cover classification scheme for Use with Remote Sensor data level classification (Anderson et al., 1976).

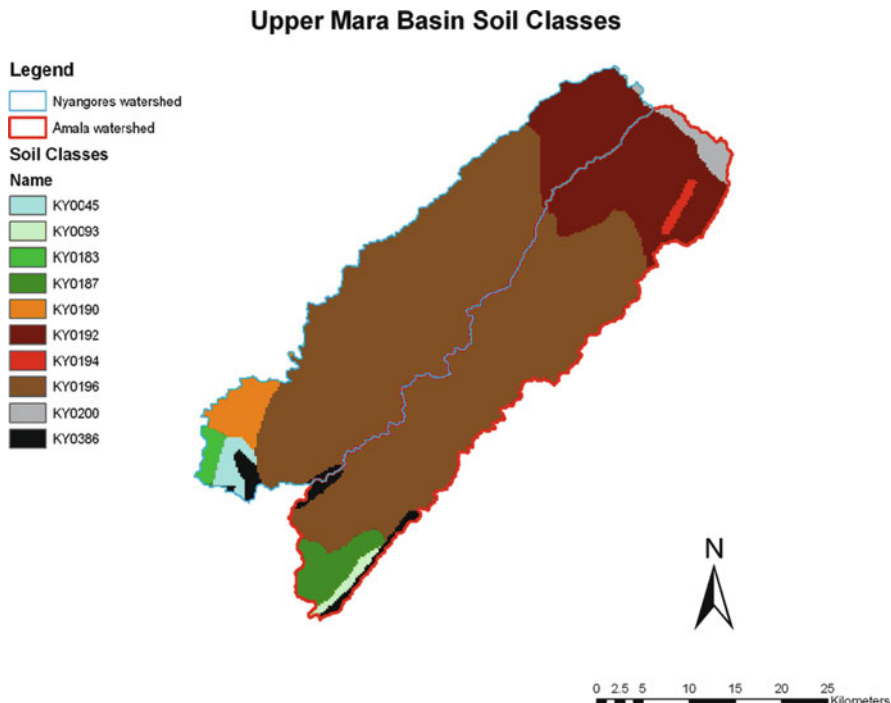


**Fig. 2.4** Soil classes for the Upper Mara River basin

**Table 2.1** Texture of the soils in the Upper Mara River

Soil type code	Clay (%)	Silt (%)	Sand (%)
KE200	31	29	40
KE196	42	42	16
KE386	41	29	30
KE45	9	67	24
KE93	15	70	15
KE194	22	50	28
KE187	38	35	27
KE183	30	26	44
KE190	10	28	62
KE192	20	48	32

#### 2.4.2.4 Climate Data

Weather data used in the SWAT model consists of daily rainfall, temperature, wind speed, humidity and evapotranspiration data. In this study, the weather variables used were the daily precipitation values obtained from the Bomet Water Supply Office Station located at Bomet Town and Kiptunga Forest Station located in Elburgon District, and also minimum and maximum air temperature values for

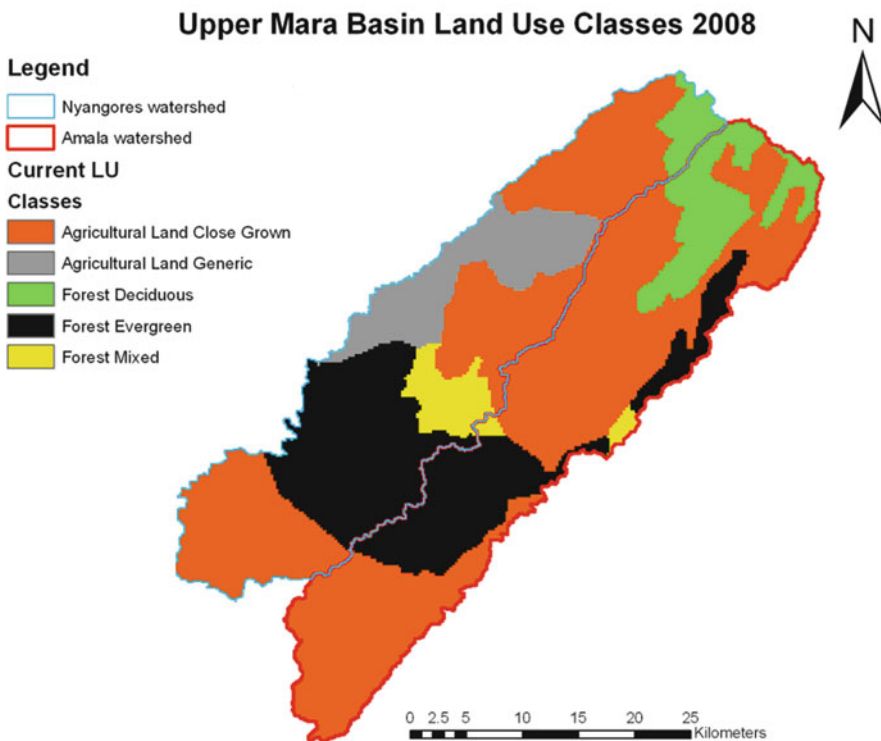


**Fig. 2.5** Land use types for the Upper Mara River basin

the period of 1996–2003 obtained from the Kericho Hail Research and Narok Meteorological weather stations. These data were obtained from the Ministry of Water Resources of Kenya and the Lake Victoria South Water Resource Management Authority in Kenya. The available weather data is of high importance as it determines what methods and equations the SWAT model uses in the calculation of different climatic and hydrological parameters in the simulation. Figures 2.6a, b show selected meteorological stations within the Mara River basin.

Another source of rainfall data for the hydrological modeling was obtained from the Famine Early Warning System (FEWS) Rainfall Estimation (RFE) product. This is a computer generated product that uses Meteosat infrared data at a horizontal resolution of 10 km (Xie and Arkin, 1997). The gridded rainfall was converted to point values based on preferences and generates artificial rain gauge stations. Output is formatted to be compatible with input file format of ArcSWAT, in this case daily time series data tables. This process resulted in the creation of 30 artificial rain gauges as the centroids of the 30 sub-watersheds making up the Amala and Nyangores watersheds. The Amala watershed was assigned 15 RFE artificial rain gauges (Fig. 2.6b) for use in the hydrological modeling process. The RFE data was able to provide continuous and complete data ranging from the years 2002–2008 which were used in the model simulations.

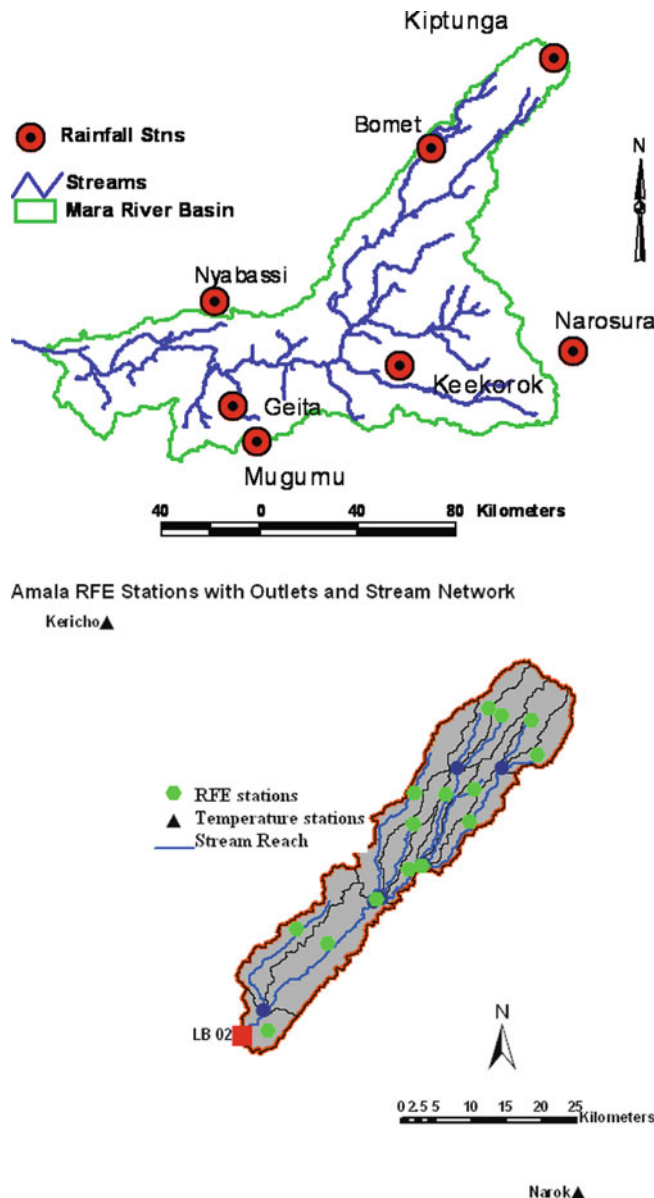


**Fig. 2.6** Hydro-meteorological stations in the study area

#### 2.4.2.5 River Discharge

Daily river discharge data was obtained for the Amala River from the gauging station located at the outlet of the basin (Fig. 2.1). The discharge values for the Amala were used for calibration and validation of the model. In the Amala watershed,

observed discharge data spanned from the year 2000–2006 and for the rain gauge model, 2 years were used for calibration and 2 years were used for validating the model. For the RFE model, 3 years were used for the calibration and 2 years for validation of the model. The length of the simulations was determined by the availability and length of time series data for discharge, air temperature and rainfall which are key inputs in the model simulation.

To conduct the hydrological analysis of flow data across the basin, average, minimum and maximum recorded historical data were collected for the Mara Mines, Nyangores and Amala stations. The location of these stations is shown in Fig. 2.1.

### **2.4.3 Model Setup**

The model setup involved five steps: (1) data preparation, (2) sub-basin discretization, (3) HRU definition, (4) parameter sensitivity analysis, (5) calibration and uncertainty analysis.

The DEM was projected to the required projection parameter which is UTM Zone 37 South. A mask was used to reduce the area for stream delineation and analysis of terrain drainage patterns of the land surface. The streams were delineated from the DEM. The land use/land cover layer was reclassified into the SWAT/USGS land use code linked to a user table with the land use code. Since the SWAT database includes only soils from the United States and not from the study area, the soil types and their qualities from the study area had to be entered manually and thereafter the soil layer was added and linked to its various soil types in the database via a lookup table.

Watershed and sub-watershed delineation was carried out using the DEM and has various steps including: DEM setup, stream definition, outlet and inlet definition, watershed outlets selection and definition and calculation of sub-basin parameters. For the stream definition, the threshold based stream definition option in the Graphic User Interface was used to define the minimum size of the sub-basin. By choosing a threshold area of 2,000 ha, much less than the default value of 15,000 ha, the stream definition is more enhanced and much more likely to delineate all the existing streams in the watershed of interest.

The sub-watersheds are then divided into units based on their unique combination of land use, soils and slope combinations and these units are known as HRUs (hydrologic response units). The model was then run on a default simulation of 8 years from 1996 to 2003 for the rain gauge data and from 2002 to 2003 a period of 2 years for the RFE data.

#### **2.4.3.1 Sensitivity Analysis**

Sensitivity analysis and calibration techniques are generally manual or automated, and can be evaluated with a wide range of graphical and/or statistical procedures. Uncertainty can be defined as the estimated amount by which an observed or calculated value may depart from the true value (Shirmohammadi et al., 2006). Parameter

reduction is very important in distributed watershed models. All these parameters are cumbersome to deal with therefore a sensitivity analysis is carried out in order to determine which of these parameters are critical for an efficient calibration.

The parameter sensitivity analysis for the Amala watershed was carried out using the ArcSWAT interface. The model uses the Latin Hypercube One factor At a Time (LH-OAT) analysis method. The LH-OAT method combines the One-factor-At-a-Time (OAT) design and Latin Hypercube (LH) sampling by taking the Latin Hypercube samples as initial points for an OAT design.

#### 2.4.3.2 Latin Hypercube One Factor At a Time (LH-OAT) Analysis

The LH-OAT method combines the One-factor-At-a-Time (OAT) design and Latin Hypercube (LH) sampling by taking the Latin Hypercube samples as initial points for an OAT design. The concept of Latin Hypercube simulation (McKay et al., 1979; McKay, 1988) is based on the Monte Carlo simulation but uses a stratified sampling instead of random sampling. It subdivides the distribution of each parameter into  $n$  ranges, each with a probability of occurrence equal to  $1/n$ . Random values of the parameters are generated such that each range is sampled only once. Then, the model is run  $n$  times with the random combinations of the parameters. The exact steps involved are given below.

Let  $Y = f(x_1, x_2, \dots, x_k)$ , with  $x_1, x_2, \dots, x_k$  – are the independent variables

- Range of each variable is divided into  $n$  non-overlapping interval and one value from each interval is chosen.
- Then,  $n$  values of  $x_1$  is randomly paired to  $n$  values of  $x_2$
- Next,  $n$  pairs of  $x_1$  and  $x_2$  are randomly combined to  $n$  values of  $x_3$  to form  $n$  triplets.
- The procedure is continued to form  $n$   $k$ -tuplets
- This  $n$   $k$ -tuple is called LH Sample.
- From this LHS, sensitivity analysis is carried out by following OAT scheme.

The sensitivity of individual parameters of the model is determined by changing one factor or parameter at a time. So, the change in the output in each model run can be unambiguously attributed to the input parameter changed without the assumptions of relatively few inputs having important effects. The measure of sensitivity can be computed using sensitivity index ( $I$ ) as

$$I = \frac{\frac{y_2 - y_1}{y_1}}{\frac{x_{i2} - x_{i1}}{x_{i1}}} \quad (2.2)$$

Where  $y_1, y_2$  are the output corresponding to the parameter inputs  $x_{i1}$  and  $x_{i2}$  respectively.

Sensitivity ranking prepared by this criterion is especially helpful for calibration of parameters.

#### 2.4.4 Model Calibration and Validation

Calibration is the process of estimating model parameters by comparison of model predictions or output for a given set of assumed conditions with observed or measured data for the same conditions (Moriasi et al., 2007).

Calibration of physically based distributed watershed models should be done before they are used in the simulation of hydrologic processes in order to reduce the uncertainty associated with the model prediction. Watershed scale model calibration is challenging and is impeded by uncertainties like watershed processes unknown to the modeler, processes not captured by the model and simplification of the processes by the model (Abbaspour et al., 2007). Hence, a thorough attempt was made to tune the parameters of the model so that the predicted values were in very close agreement with available measured data before going for the determination of the hydrologic components (Mango, 2010).

For the Amala watershed, discharge data from the year 2000 to 2001 were used for calibration and 2002–2003 were used for validation for the rain gauge model. Autocalibration was carried out and this resulted in the best parameter values for the sensitive parameters; in this particular case, 10 most sensitive parameters.

For this study, the algorithm used was the Parameter Solutions (Parasol) method (Van Griensven et al., 2006) which is integrated in the ArcSWAT interface. Parasol method involves optimization and uncertainty analysis in a single run. The ParaSol method calculates objective functions based on model outputs and observation time series, it aggregates these objective functions to a global optimization criterion (GOC) and minimizes the objective functions or a GOC using the Shuffled Complex Evolution (SCE-UA) algorithm. According to Sorooshian and Gupta (1983), this algorithm selects an initial ‘population’ by means of random sampling throughout the feasible parameters space for  $p$  parameters to be optimized (delineated by given parameter ranges). The population is portioned into several “complexes” that consist of  $2p+1$  points. Each complex evolves independently using the simplex algorithm. The complexes are periodically shuffled to form new complexes in order to share the gained information. It searches over the whole parameter space and finds the global optimum with a success rate of 100%. This algorithm has been found to be robust, effective and efficient and is widely used in watershed model calibration, remote sensing and land surface modeling (Gupta et al., 2003). According to van Griensven et al. (2006), it has also been applied with success on SWAT for the hydrologic and water quality parameters.

The objective function chosen for use is the Sum of Squared Residuals (SSQ) which aims at matching a simulated series to a measured time series.

$$SSQ = \sum_{i=1,n} [x_{i,m} - x_{i,s}]^2 \quad (2.3)$$

With  $n$  the number of pairs of measured ( $x_m$ ) and simulated ( $x_s$ ) variables.

### 2.4.5 Model Evaluation

SWAT hydrologic predictions have been evaluated by means of a wide range of statistics. The coefficient of determination ( $R^2$ ) and the Nash-Sutcliffe model efficiency (NSE) coefficient (Nash and Sutcliffe, 1970) are the most commonly used statistics for evaluation of model performance in hydrologic calibration and validation.

The NSE is a normalized statistic determining the relative magnitude to the residual variance compared to the measured data variance (Nash and Sutcliffe, 1970). This method can be used to describe the predicative accuracy of other models as long as there is observed data to compare the model results to. The NSE is considered fit for model evaluation because it is found to be the best objective function for reflecting the overall fit of a hydrograph (Moriasi et al., 2007).

## 2.5 Results and Discussions

The results of this study are divided into four categories: (i) hydro-meteorological analysis for selected rain gauge and flow gauging stations, (ii) land cover classification and (iii) hydrological modeling evaluation and (iv) water budget analysis under three land use change scenarios in Amala watershed.

### 2.5.1 Hydro-Meteorological Analysis

The average monthly rainfall graphs for the downstream of the Mara River basin (Nyabassi station in Tanzania) and upstream of Mara River basin (Kiptunga Forest station in Kenya) are shown in Figs. 2.7 and 2.8.

For the Nyabassi rainfall station, the average rainfall for the month of January, April and July (1944–1993) did not show any clear trends (Fig. 2.7). It is also noted that the average rainfall at Nyabassi station are relatively low compared to the Kiptunga Forest in the upper Mara which is located at high altitude showing upstream part of the watersheds receives more rainfall than the downstream.

The average monthly rainfall at Kiptunga Forest station, significantly increased for the month of January. In recent years, there has been a significant decrease in rainfall in the months of April and July. January and April fall in the short and long rain periods of the basin, respectively. This reduction in rainfall averages has an impact on the flow of the Amala and Nyangores Rivers which originate from the upper Mara River. Figure 2.9 show the spatial variability of rainfall at different stations. The Olenguruone vs. Nyabassi graph (Fig. 2.9) shows that the rainfall at Olenguruone is higher than at Nyabassi station. Fig. 2.10 (Olenguruone vs Kiptunga) shows that the rainfall received at Olenguruone is higher than that received at Kiptunga Forest. Both Olenguruone and Kiptunga Forest are located in

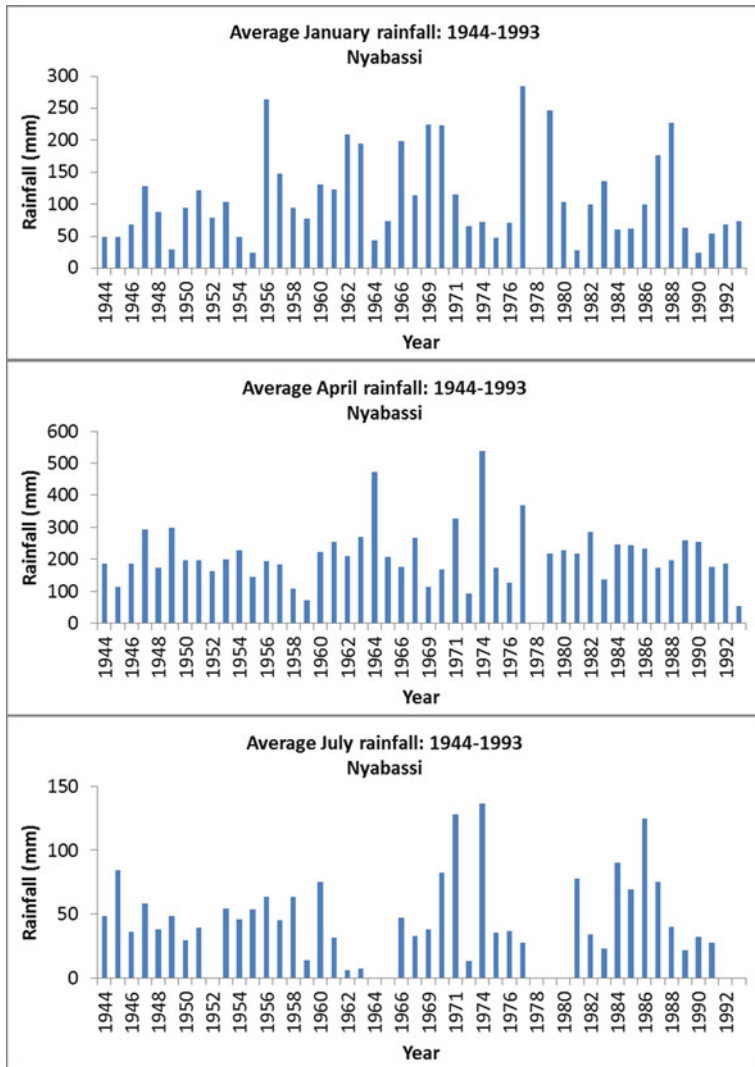


**Fig. 2.7** Average monthly rainfall for selected months at Nyabassi station

the Upper Mara River basin, Kenya whereas Nyabassi is located in the lower Mara, Tanzania. This shows the highly spatial variability of rainfall across the basin.

Figure 2.10 shows the minimum, average and maximum or high flows at the Mara Mines gauging station in the Tanzanian side of the basin. The average flows at the Mara Mines station show a resemblance to the rainfall patterns. The flow of the Mara Mines varies throughout the year and is highest during the two rainy months; April and May, which are a part of the long rainy season and October which fall in

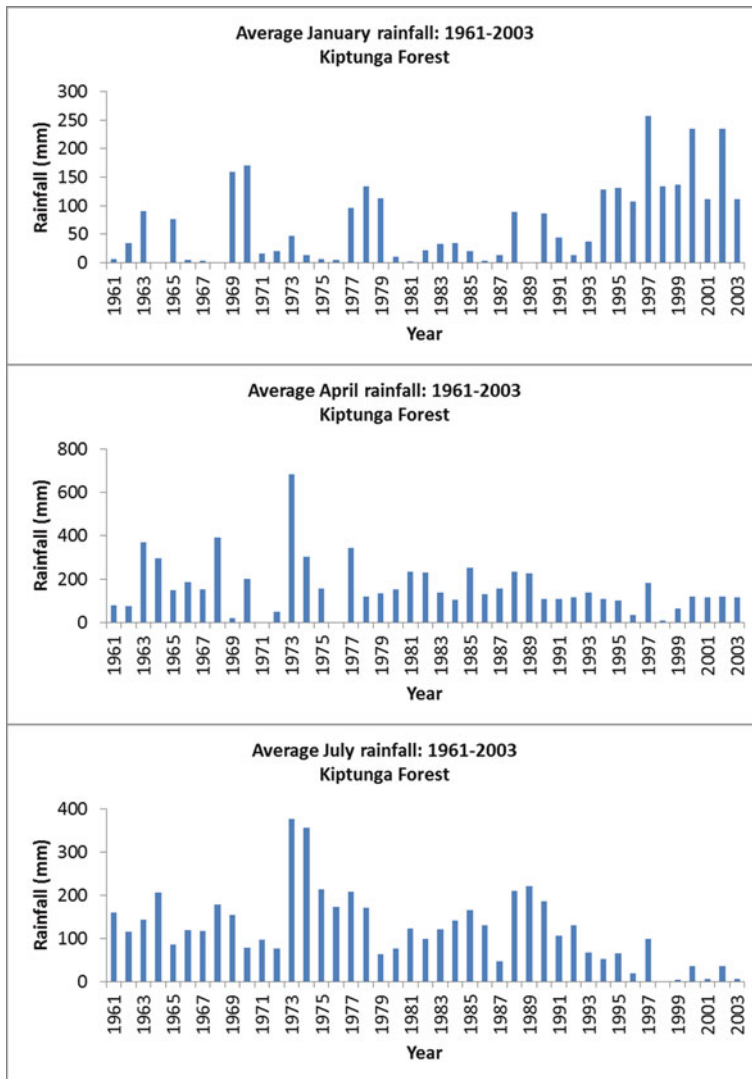
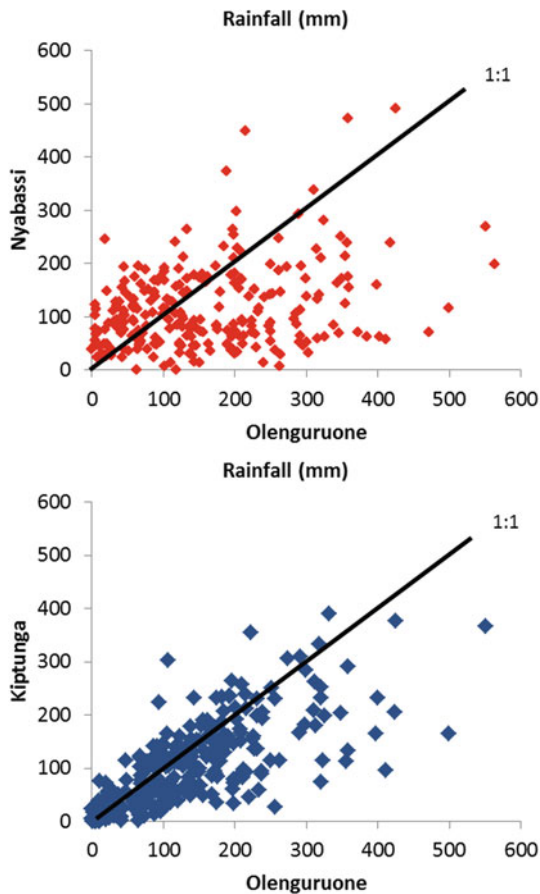


**Fig. 2.8** Average monthly rainfall for selected months at Kiptunga station

the short rainy season. The flows are reflective of the rainfall received in the area and upstream.

The average flow for the Nyangores watershed (Fig. 2.11) is at the maximum during the two rainy seasons meaning it is a system that is highly responsive to rainfall. During dry season it has very low minimum flows and this is mainly due to low groundwater contribution to the stream flow attributed to upstream land degradation in the forested areas.

**Fig. 2.9** Rainfall comparison for the Olenguruone vs. Nyabassi and Kiptunga Forest



The Amala River dry season flows appear to be very low compared to the Nyangores (Fig. 2.12). The Amala watershed drains part of the deforested Mau Forest resulting in low dry season flow and a quick response to rainfall during wet months. This may be due to the fact that the forest cover in this watershed has undergone deforestation and natural land has been converted to agricultural land. This results in reduced groundwater recharge and increased high flow or flooding.

The analysis of annual maximum flows of the Nyangores and Amala Rivers indicated that there is an increasing trend of the streamflow for the most recent years (Fig. 2.13). This may be due to the effect of land use change that has altered the hydrology of the watersheds and resulted in higher maximum flows and flooding downstream due to increased surface runoff and reduced groundwater recharge. In particular, Amala River which is highly deforested watershed has a higher peak flows as compared to the Nyangores, which is less deforested than the former.

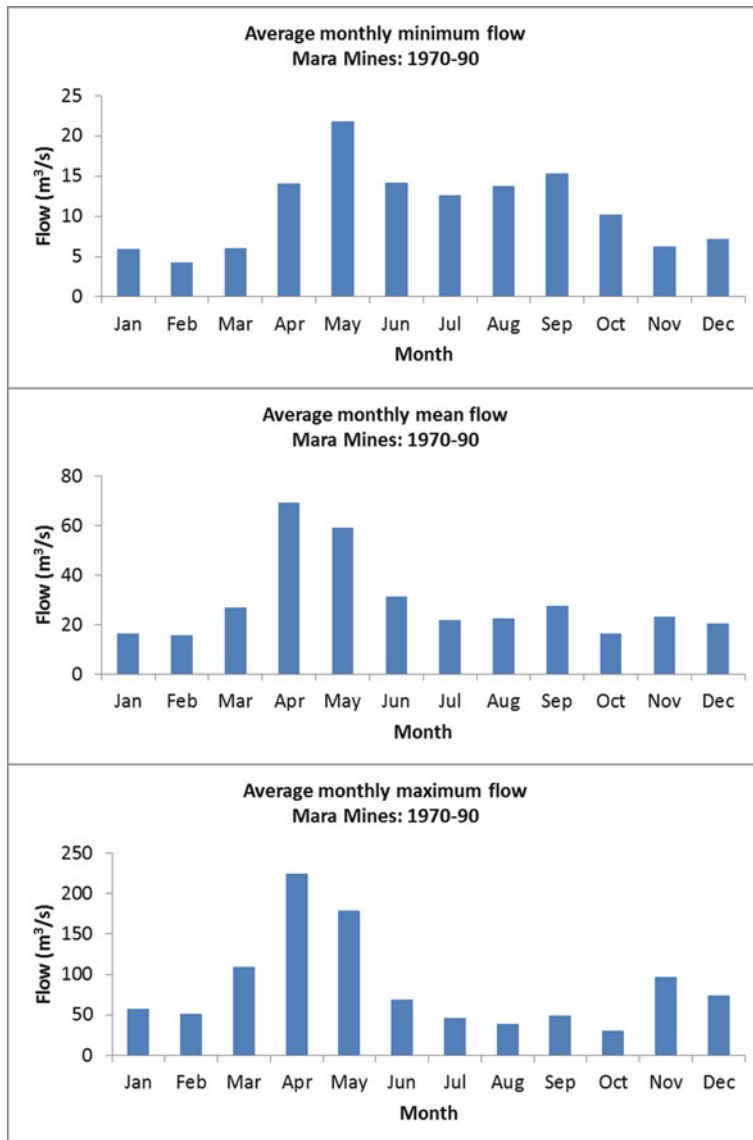


**Fig. 2.10** Average flows for Mara River at Mara Mines gauging station

### 2.5.2 Land Cover Mapping

The expert classifier was built and this involved the generation of a decision tree by recursive linear partitioning and the process resulted in the production of decision trees based on the training data that was specified for input into the statistical

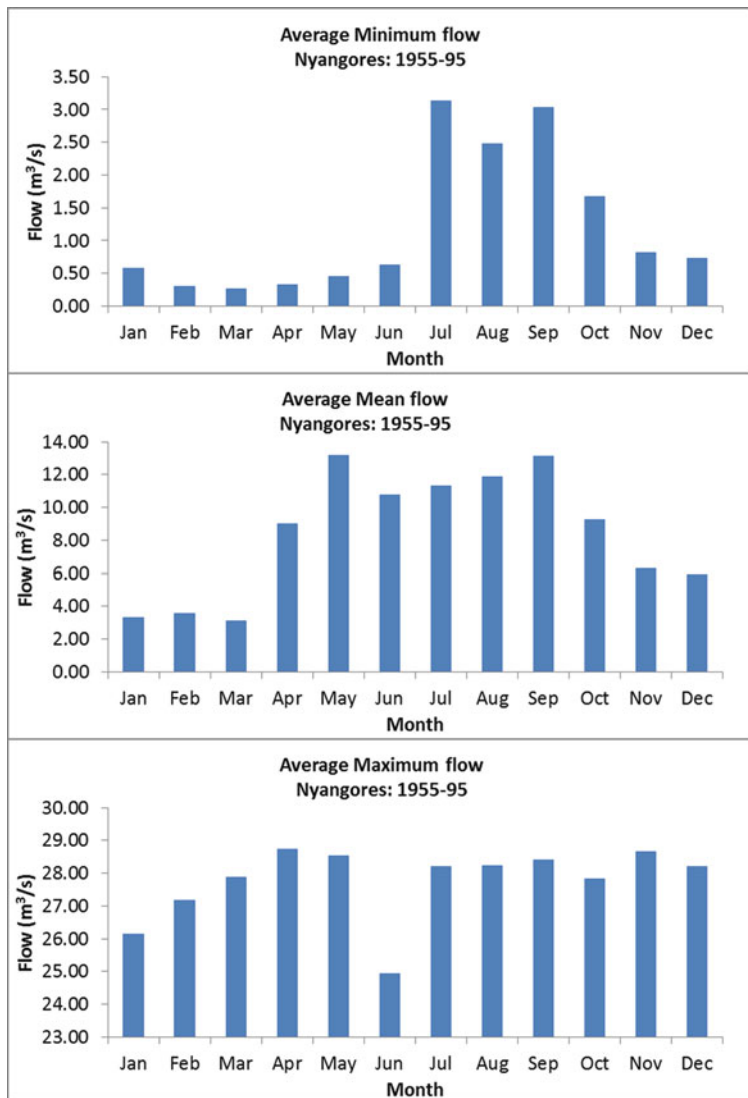


**Fig. 2.11** Average flows for Mara River at Nyangores gauging station

package R. This resulted in production rules used in the expert classifier to classify the image. The classification was successful in distinguishing different land cover classes in the image and the accuracy of the classification was determined by the use of an error or confusion matrix.

The resultant error matrix gave a  $\hat{K}$  statistic value of 82.5% while the overall accuracy for the classification was 84.7%. These values were taken as a fairly good accuracy considering the heterogeneity of the study area that may pose significant

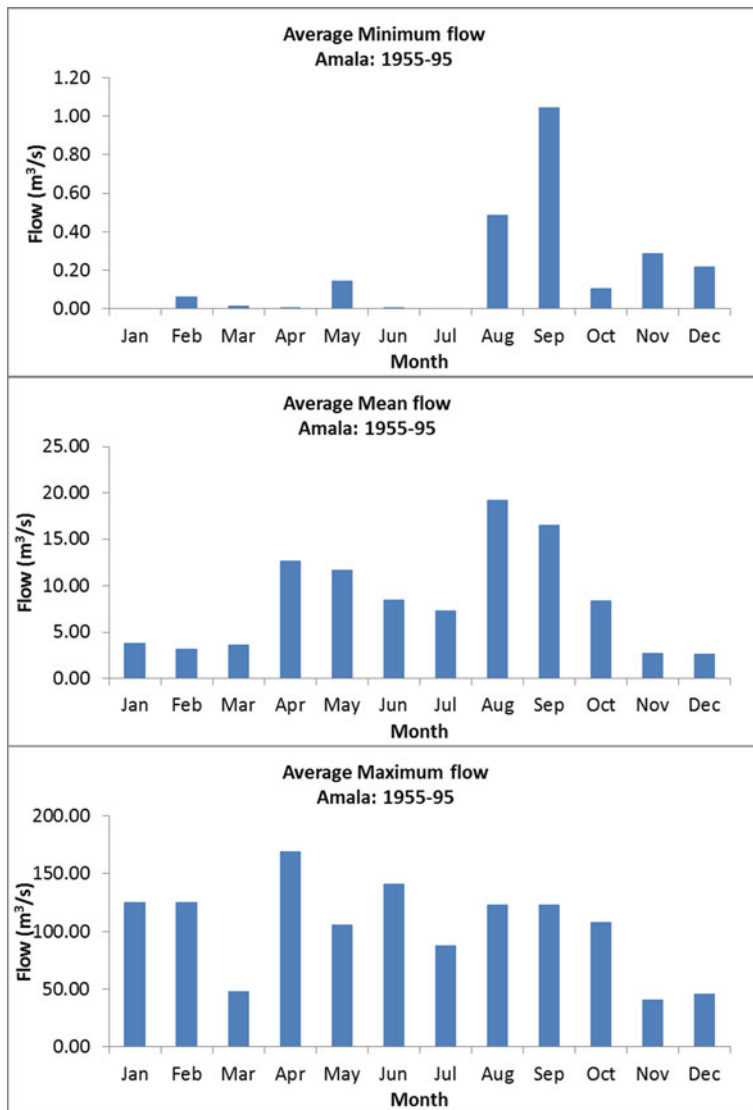


**Fig. 2.12** Average flows for Amala River at Amala gauging station

difficulties using different classification methods. The error matrix indicated that there was substantial confusion between bushland, forest and grassland which was attributed to the selection of training data and also the fact that use of spectral and texture data alone were not capable of accurately distinguishing these three classes. The land use map based on Landsat image from 2008 (Fig. 2.2) was reclassified into SWAT land use/land cover classes to be used in the hydrological modeling process (Fig. 2.5).

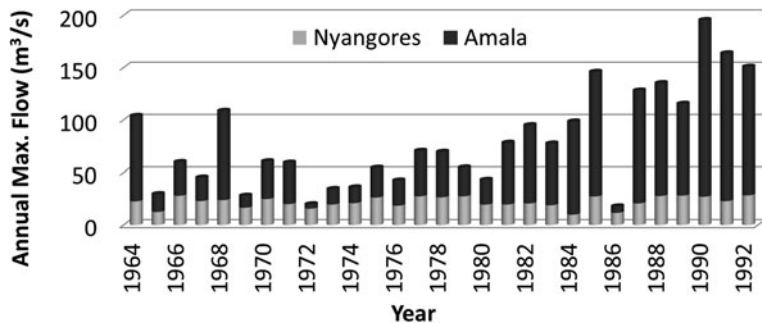


**Fig. 2.13** Maximum flows for the Amala and Nyangores rivers

### 2.5.3 Hydrological Modeling

Twenty six hydrological parameters were tested for sensitivity analysis for the simulation of the stream flow in the study area. The most ten sensitive flow parameters (Table 2.2) were chosen for calibration of the model. The hydrological modeling exercise involved the calibration of the SWAT model in the Amala watersheds for prediction of stream flow using different rainfall inputs; Rain gauge measurements and satellite-based rainfall estimates (RFE). The discharge hydrographs for daily and monthly data were compared for calibration and scenario analysis.

**Table 2.2** Sensitivity ranking of flow parameters for rain gauge and RFE rainfall conditions

Sensitivity rank	Amala		Description
	Rain gauge	RFE	
1	ESCO	CN2	Initial curve number (II) value
2	CN2	GWQMN	Threshold water depth in the shallow aquifer for flow (mm)
3	GWQMN	ESCO	Soil evaporation compensation factor
4	SOL_Z	SOL_Z	Soil depth (mm)
5	ALPHA_BF	ALPHA_BF	Baseflow alpha factor (days)
6	REVAPMN	SOL_AWC	Available water capacity (mm water/mm soil)
7	SOL_AWC	REVAPMN	water in the shallow aquifer for re-evaporation
8	CANMX	CANMX	Maximum canopy storage (mm)
9	BLAI	GW_REVAP	ground water revap coefficient
10	GW_REVAP	SOL_K	Saturated hydraulic conductivity (mm/h)

#### 2.5.3.1 Model Calibration and Validation

Parameter variation was carried out in conjunction with the statistical evaluation until an acceptable correlation or resemblance between the predicted and observed

**Table 2.3** Model evaluation statistics for monthly discharge for Amala watershed

Statistics	RFE		Rain gauge	
	Calibration	Validation	Calibration	Validation
NSE	0.62	0.39	0.08	0.41
$R^2$	0.65	0.46	0.30	0.41

flow was achieved. Comparison was carried out for the rainfall datasets (rain gauge and RFE) obtained and the resulting statistics for the monthly simulations are shown in the Table 2.3. Statistics such as the Nash-Sutcliffe Efficiency (NSE) and the Coefficient of determination ( $R^2$ ) were used to compare the simulated hydrographs from the different datasets to observed flow data.

In the case of the Amala rain gauge data model, there was a clear underperformance of the models as shown by the different model evaluation statistics. Calibration and validation of the rain gauge data produced NSE values of 0.08 and 0.41, respectively. For the rain gauge model, the low calibration results are an indication that the model was unable to accurately or even adequately simulate the discharge of the Amala River. This can be attributed to the fact that; the short calibration period of 2 years was not long enough to capture the long term variability of the discharge and, the limited rain gauge stations and their locations were not well representative of the actual rainfall distribution across the basin thus the high discrepancy between the simulated and observed discharge. Due to the above reasons, the rain gauge data model was therefore determined to be unfit for simulation of discharge and land use change scenarios in the Amala watershed regardless of the adequate NSE for the validation period that may appear suitable but could not be relied on since the calibration process was unsuccessful. The RFE data on the other hand produced NSE values of 0.62 and 0.39 for the calibration and validation periods, respectively which were considered fair results.

Validation was carried out to determine whether these models were suitable for evaluating the impact of land use change on the hydrology of the Amala watershed. For the RFE model, the comparison between the observed and simulated streamflow during validation period indicated that there is relatively good agreement between the observed and simulated discharge which was verified by coefficient of determination ( $R^2$ ) and Nash Sutcliffe efficiency (NSE) better than the rain gauge based rainfall model.

### 2.5.3.2 Changes in Water Balance Components

Figure 2.14 below shows the plotted monthly discharge for the Amala River for the observed and simulated stream flow for both the rain gauge and RFE sources of data. The simulated discharge is lower than the observed discharge especially in the rainy season months of May and January. Figure 2.15 on the other hand

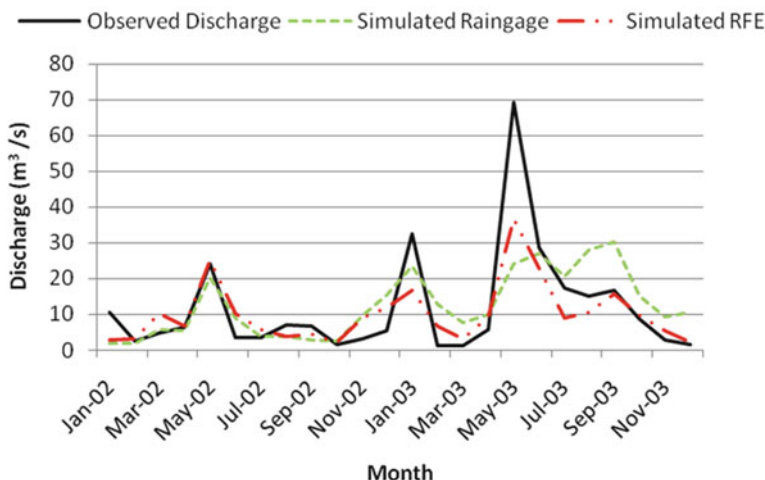


**Fig. 2.14** Observed vs simulated monthly discharge for Amala RFE and rain gauge data

shows the calibrated model results for the RFE-based simulation of monthly flows at Amala.

The water balance components (Table 2.4) account for how the model partitions the available water input from precipitation and by converting them into percent increase and reductions provided an effective way to assess the effect of different climatic inputs and land use on the water balance of the Amala watershed. The water budget analysis based on the two rainfall products having different spatial

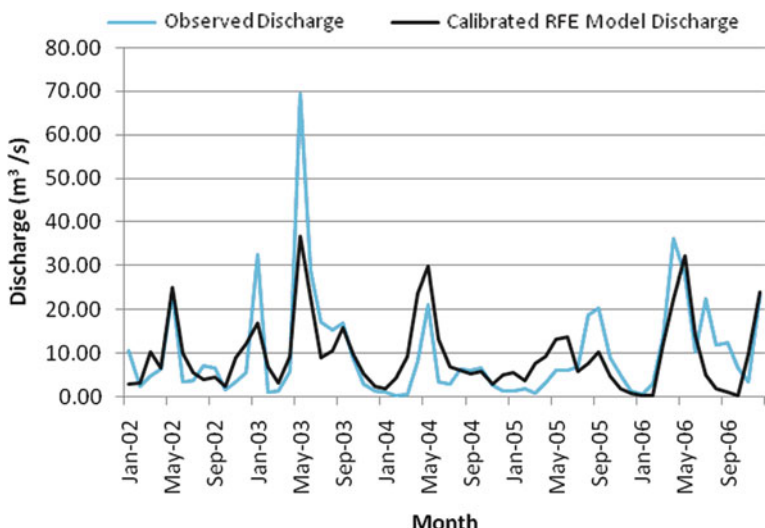


**Fig. 2.15** Amala observed vs simulated discharge for the calibrated RFE model (2002–2006)

**Table 2.4** Annual average water balance components for the calibrated Amala watershed models

Components	Rain gauge 2000–2003	RFE 2002–2006	Percent rainfall: rain gauge	Percent rainfall: RFE
PRECIP (mm)	1,235.3	1,009.8	100.00	100.00
SURQ (mm)	25.64	12.22	2.08	1.21
LATQ (mm)	37.68	30.99	3.05	3.07
GW_Q (mm)	367.85	394.26	29.78	39.04
REVAP (mm)	0	46.86	0.00	4.64
DA_RCHG (mm)	28.63	20.82	2.32	2.06
GW_RCHG (mm)	572.62	416.41	46.35	41.23
WYLD (mm)	429.58	436.52	34.78	43.22
PERC (mm)	577.94	444.37	46.79	44.00
ET (mm)	581.1	508.8	47.04	50.38
PET (mm)	1,258	1,171.4	101.84	115.99
TLOSS (mm)	1.59	0.95	0.13	0.09
SEDYLD (T/HA)	0.641	0.307		

PRECIP = Average total precipitation on sub-basin, PET = Potential evapotranspiration, ET = Actual evapotranspiration, PERC = Amount of water percolating out of the root zone, SURQ = Surface runoff, GW\_Q = Groundwater discharge into reach or return flow, WYLD = Net water yield to reach, TLOSS = Amount of water removed from tributary channels by transmission, DA\_RCHG = Amount of water entering deep aquifer from root zone, REVAP = Water in shallow aquifer returning to root zone, GW\_RCHG = amount of water entering both aquifers, SEDYLD = Sediment yield, LATQ = Lateral flow contribution to reach.

coverage has shown that rainfall distribution and source can influence the predicted components of the water budget.

The main water balance components of the Amala basins includes: the total amount of precipitation falling on the sub-basin during the time step, actual evapotranspiration from the basin and the net amount of water that leaves the basin and contributes to streamflow in the reach (water yield) which includes surface runoff contribution to streamflow, lateral flow contribution to streamflow (water flowing laterally within the soil profile that enters the main channel), groundwater contribution to streamflow (water from the shallow aquifer that returns to the reach) minus the transmission losses (water lost from tributary channels in the HRU via transmission through the bed and becomes recharge for the shallow aquifer during the time step). The water balance estimation indicated that 47% of the annual precipitation is lost by evapotranspiration in the basin for the rain gauge rainfall source as compared to 50% for the RFE. The net water yield (WYLD) contributes 35 and 43% of the water budget during calibration for the rain gauge and RFE rainfall data, respectively (Table 2.4). Table 2.4 lists the simulated water balance components on an annual average basis for the Amala watershed over the calibration period for both rainfall data products.

### 2.5.4 Land Use Change Scenarios

Figure 2.16 below shows the three land use change scenarios considered in this study to assess the impact of the hypothetical future changes from the 2008 land use on the river discharge and water budget for the Amala watershed. These scenarios were selected based on the current trends and also from discussions with area experts. The three land use change scenarios are partial deforestation, complete deforestation and also complete conversion of the forest to agriculture in the Amala watershed. The extent of the land use changes under each scenario are shown in Fig. 2.16.

From Table 2.5 below, the different land use change scenarios affect the water balance components in various ways and; these differences are most pronounced in the surface runoff and groundwater recharge.

From Table 2.5, it is shown that the surface runoff and transmission losses are responsive to the land use change with a significant increase observed in the

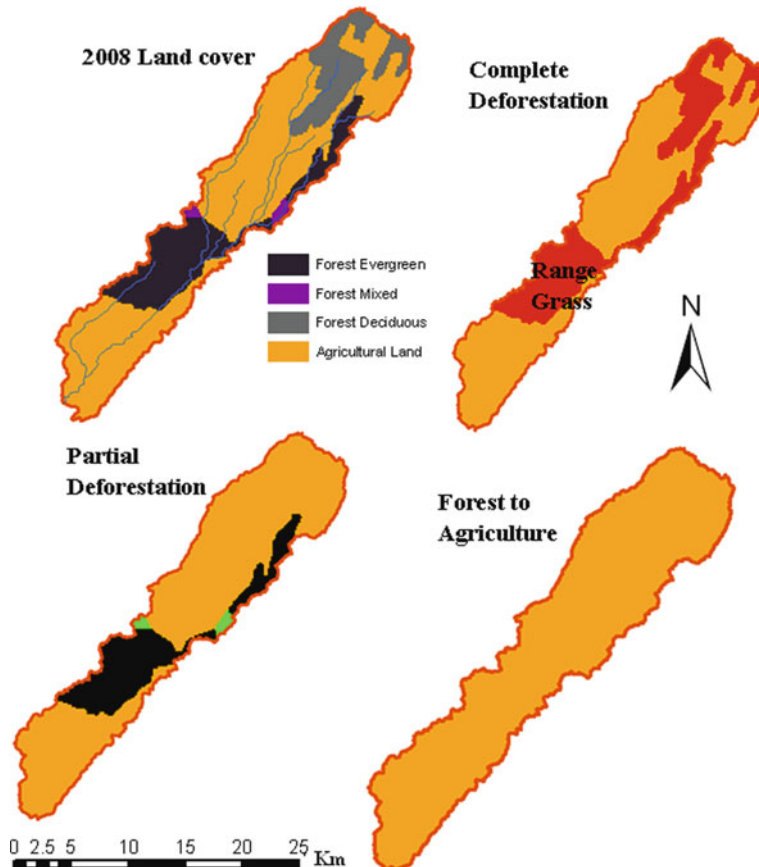


**Fig. 2.16** Land use change scenarios of the Amala watershed

**Table 2.5** Percent changes from the 2008 flow in the annual averages of Amala watershed water balance components for land use change scenarios

Water balance components	Partial deforestation	Complete deforestation	Forest-agriculture conversion
PREC	0.00	0.00	0.00
SURQ	3.15	12.40	13.70
LATQ	-2.55	-2.70	0.80
GW_Q	-6.28	-3.54	-10.51
REVAP	-2.51	-2.73	-4.02
DP AQ RCHRG	-6.03	-3.60	-10.07
TOTAL AQ RCHRG	-5.99	-3.59	-10.02
WYLD	-3.88	0.25	-4.28
PERC	-5.95	-3.93	-10.41
ET	2.57	0.24	3.05
PET	0.00	0.00	0.00
TLOSS	10.83	14.86	38.00
SED	15.72	14.38	55.02

complete deforestation and the conversion of forest to agriculture. The conversion of forest to agriculture scenario experiences the highest reduction in groundwater discharge into the reach, deep aquifer recharge, total aquifer recharge, and percolation with percentage reduction in these components of up to 10%. The sediment yield from the forest to agriculture conversion was over threefold than that of the partial and complete deforestations. The complete deforestation scenario also results in a similar variation in water balance components at a magnitude that is a bit lower with the partial deforestation scenario impacting the water balance components least.

Therefore, the changes in land use have impacts on the water balance components. The conversion of forest to agriculture scenario impacts the water balance components the most and this is due to the fact that the conversion of a land use to agriculture results in the removal of a permanent vegetation cover (forest) and replacing it with cropland which varies from bare soil during the planting season and small crop size when growing to mature crops and back to bare soil after harvesting. The different stages of crop growth result in increased evapotranspiration, surface runoff, transmission losses and higher decreases in groundwater discharge into the reach, deep aquifer recharge, total aquifer recharge and percolation. Increased sediment loss per unit area is also a major issue and this results from the exposure of bare soil to precipitation and surface runoff and also the fact that the crop cover's leaf area index and root depth is significantly less than that of the forest canopy and this results in increased displacement of soil by rainfall and surface runoff hence increased soil erosion. Reduced infiltration and percolation of water into lower soil levels is experienced when the forests that reduce the impact of raindrops and overland flow are replaced by agricultural croplands that do not have the same water holding and conservation properties.

## 2.6 Conclusions

The study results reported in this chapter assessed the hydro-meteorological variability across the basin using historical rainfall and river flow data. The chapter also presents results of land use/cover classification using Landsat imagery and results from the calibration/validation of SWAT model. Comparison between the rain gauge and satellite-based rainfall estimate (RFE) rainfall data and the corresponding simulated flow is also discussed. The effect of land use change scenarios on the hydrological response of the Amala watershed is also assessed using three plausible scenarios.

The hydro-meteorological analysis of historical records for the upper and lower part of the Mara River basin shows high spatial variability. Seasonal trends were also evident from the upstream rainfall data as the short rainy season (January) rainfall slightly increasing and a slight decline in the long rain records (April). The historical high and low flows were also spatiotemporally variable even for adjacent similar size watersheds of the Nyangores and Amala in the upstream Mara River basin. The Amala, a deforested and partly degraded watershed due to the recent deforestation and land conversion to agriculture, has shown a low dry season (minimum) flow and high (maximum) flows during the rainy season compared to the adjacent Nyangores watershed.

This study revealed that land use change scenarios will significantly impact the water flux in the upper Mara River. The land use change scenarios revealed that the variation has an impact on the amount of discharge, sediment yield, surface runoff and baseflow. The model simulations predict that the upper Mara River flow will be significantly affected in the possible increased reduction in vegetation or forest cover or forest-to-agriculture land use change scenarios posing difficulties in adaptation to the altered flow regimes of the Amala River. It is therefore prudent to work towards establishing and maintaining adequate minimum flows that would mitigate the effects of reduced baseflow and put in place measures to maintain adequate sustained river flows to the benefit of the stakeholders of the Mara River basin.

**Acknowledgements** The authors acknowledge the Global Water for Sustainability Program and the United States Agency for International Development (USAID) that funded the study. Authors thank the Worldwide Fund for Nature Offices, Kenya and Tanzania Ministries of Water and Irrigation, and Lake Victoria South Catchment Management Authority (of Kenya's Water Resources Management Authority). We also thank the Kenyan Meteorological Agency for the meteorological data used in the study.

## References

Abbaspour KC, Yang J, Maximov I et al (2007) Modelling hydrology and water quality in the pre-alpine/alpine Thur watershed using SWAT. *J Hydrol* 333:413–430

Abbot MB, Refsgaard JC (eds) (1996) Distributed hydrological modelling. Kluwer Academic Publishers, Dordrecht

Anderson RJ, Hardy EE, Roach JT et al (1976) A land use and land cover classification system for use with remote sensor data. United States Geological Survey. United States Government Printing Office, Washington, DC

Arnold JG, Srinivasan R, Muttiah RS et al (1998) Large area hydrologic modeling and assessment. Part I: model development. *J Am Water Resour Assoc* 34:73–89

Di Luzio M, Srinivasan R, Arnold JG (2002) Integration of watershed tools and the SWAT Model into BASINS. *J Am Water Resour Assoc* 38(4):1127–1141

ERDAS (2009) ERDAS Field guide ERDAS. Inc. Atlanta, GA

ESRI (2006) What is ArcGIS 9.2? ESRI. Redlands, California, CA

Food and Agriculture Organization (FAO) of the United Nations (2005) Kenya Country report in: irrigation in Africa in Figures, AQUASTAT Survey 2005. FAO, Rome

Gereta E, Wolanski E, Borner M et al (2002) Use of an ecohydrology model to predict the impact on the Serengeti ecosystem of deforestation, irrigation and the proposed Amala Weir water Diversion Project in Kenya. *Ecohydrol Hydrobiol* 2(1–4):135–142

Gereta E, Wolanski E (1998) Water quality-wildlife interaction in the Serengeti national park, Tanzania. *Afr J Ecol* 36(1):1–14

Green WH, Ampt GA (1911) Studies on soil physics, 1. The flow of air and water through soils. *J Agric Sci* 4:11–24

Gupta HV, Sorooshian S, Hogue TS et al (2003) Advances in automatic calibration of watershed models. In: Duan Q, Gupta HV, Sorooshian, Rousseau, AN, Turcotte R (eds) Calibration of watershed models, water science and application 6. American Geophysical Union, Washington, DC, pp 9–28

Hargreaves GH, Samani ZA (1982) Estimating potential evapotranspiration. *Tech Note J Irrig Drain Eng* 111(2):113–124

Jayakrishnan R, Srinivasan R, Santhi C et al (2005) Advances in the application of the SWAT model for water resources management. *Hydrol Process* 19:749–762

Mango LM (2010) Modeling the effect of land use and climate change scenarios on the water flux of the Upper Mara River flow, Kenya. M.Sc Thesis. Florida International University, Miami, FL, USA, p 189

Mati BM, Mutie S, Home P et al (2005) Land use changes in the transboundary mara basin: a threat to pristine wildlife sanctuaries in East Africa. A Paper presentation at the: 8th International River Symposium, Brisbane, Australia, 6–9 September 2005

McKay MD, Beckman RJ, Conover WJ (1979) A comparison of three methods for selecting values of input variables in the analysis of output from a computer code. *Technometrics* 21(2): 239–245

McKay MD (1988) Sensitivity and uncertainty analysis using a statistical sample of input values. In: Ronen Y (ed) Uncertainty analysis. CRC Press, Inc. Boca Raton, FL, pp 145–186

Moriasi DN, Arnold JG, Van Liew MW et al (2007) Model evaluation guidelines for systematic quantification of accuracy in watershed simulations. *Trans ASABE* 50(3):885–900

Monteith JL (1965) Evaporation and the environment. In: The state and movement of water in living organisms, XIXth Symposium. Soc For Exp Biol, Swansea. Cambridge University Press, Cambridge, pp 205–234

Mutie S, Mati B, Gadain H et al (2006) Evaluating land use change effects on river flow using USGS geospatial stream flow model in Mara River basin, Kenya. A Paper presentation at the 2nd Workshop of the EARSeL SIG on Land Use and Land Cover, Bonn, 28–30 Sept 2006

Nash JE, Sutcliffe JV (1970) River flow forecasting through conceptual models part I-A discussion of principles. *J Hydrol* 10(3):282–290

Neitsch SL, Arnold JG, Kiniry JR et al (2005) Soil and water assessment tool, theoretical documentation: version 2005. USDA Agricultural Research Service and Texas A&M Blackland Research Center, Temple, TX

Priestley CHB, Taylor RJ (1972) On the assessment of surface heat flux and evaporation using large-scale parameters. *Mon Weather Rev* 100:81–92

Serneels S, Said MY, Lambin EF (2001) Land cover changes around a major east African wildlife reserve: the Mara Ecosystem (Kenya). *Int J Rem Sens* 22(17):3397–3420

Setegn SG, Srinivasan R, Dargahi B et al (2009a) Spatial delineation of soil erosion vulnerability in the Lake Tana Basin, Ethiopia. *Hydrol Process* 23(26):3738–3750

Setegn SG, Srinivasan R, Melesse AM et al (2009b) SWAT model application and prediction uncertainty analysis in the Lake Tana basin, Ethiopia. *Hydrol Process* 24(3):357–367

Sorooshian S, Gupta VK (1983) Evaluation of maximum likelihood parameter estimation techniques for conceptual rainfall-runoff models: influence of calibration data variability and length on model credibility. *Water Resour Res* 19(1):251–259

Shirmohammadi A, Chu TW, Montas H et al (2006) SWAT model and its applicability to watershed nonpoint-source pollution assessment. ASAE Paper No. 012005. ASAE, St. Joseph, MI

USDA Soil Conservation Service (SCS) (1972) National engineering handbook, Section 4 hydrology, Chapters 4–10

Van der Meer F (2000) Imaging spectrometry for geological applications. In: Meyers RA (ed) *Encyclopaedia of analytical chemistry: applications, theory and instrumentation*, vol A2310. Wiley, New York, NY, 31pp

Van Griensven A, Meixner T, Grunwald S et al (2006) A global sensitivity analysis tool for the parameters of multi-variable catchment models. *J Hydrol* 324(1–4):10–23

Williams JR (1969) Flood routing with variable travel time or variable storage coefficients. *Trans ASAE* 12(1):100–103

Xie P, Arkin AP (1997) Global precipitation: a 17-Year monthly analysis based on gauge observations, Satellite Estimates, and numerical model outputs. *Bull Am Meteorol Soc* 78:11 2539–11 2558

# Chapter 3

## Hydrological Balance of Lake Tana, Upper Blue Nile Basin, Ethiopia

**Tom H.M. Rientjes, Janaka B.U. Perera, Alemseged T. Haile, Ambro S.M. Gieske, Martijn J. Booij, and Paolo Reggiani**

**Abstract** In recent years, few studies are presented on the water balance of Lake Tana. In these studies, the water balance is closed by unknown runoff contributions from ungauged catchments. Studies relied on simple procedures of area comparison to estimate runoff from ungauged catchments. In this study, emphasis is on regionalisation approaches by the use of physical catchment characteristics and a regional model. For runoff modelling, the HVB-96 model is selected while automated calibration is applied as based on a Monte Carlo procedure. Closure of the lake water balance was established by comparing measured to estimated lake levels. Results of daily lake level simulation show a relative volume error of 2.17% and a Nash–Sutcliffe coefficient of 0.92. Results show runoff from ungauged catchments of 527 mm/year for the simulation period 1994–2003 while the closure term only is 85 mm. Compared to previous works this closure term is smallest.

**Keywords** Regionalisation · Lake Tana · Bathymetry · Water balance closure

### 3.1 Introduction

During the past decades only few studies on the water balance of Lake Tana have been reported in literature. Reference is made to Conway (1997) who studied the hydrology of the Blue Nile and the studies by Kebede et al. (2006), SMEC (2007) and Wale et al. (2009) who specifically focussed on the hydrology of Lake Tana basin. The latter three studies are reviewed here. Studies show different outcomes when estimating the major terms of the lake water balance. Particularly the estimated inflows from ungauged systems differ significantly as a result of applied procedures. According to Kebede et al. (2006), the four major catchments contribute

---

T.H.M. Rientjes (✉)

Department of Water Resources, Faculty of Geoinformation Science and Earth Observation (ITC), Twente University, 7500 AA Enschede, The Netherlands  
e-mail: t.h.m.rientjes@utwente.nl

93% of the inflow and only 7% of the lake inflow is from ungauged catchments. SMEC (2007) indicates that some 29% of the lake inflow is from ungauged catchments while Wale et al. (2009) indicate that 42% of the lake inflow is from ungauged systems. In the study by Wale et al. (2009), closure of the water balance of Lake Tana is achieved by detailed estimation of flows from ungauged systems through principles of regionalisation. Based on a bathymetric survey, closure of Lake Tana balance was as accurate as 5.0% of the annual inflow.

The work presented here resembles the approach by Wale et al. (2009). Principally different, however, is the procedure of modelling of gauged systems to estimate parameters that are to be used for modelling stream flows from ungauged systems. For the gauged catchments, Wale et al. (2009) relied on manual calibration (i.e. trial and error) while in this study an automated procedure by Monte Carlo simulation was used. In such procedure a very large number of parameter sets are automatically randomly drawn from parameter space by an automated procedure and best performing parameter sets need to be selected.

In this study, Lake Tana's water balance is solved at a daily time step by considering rainfall, evaporation, runoff from gauged and ungauged catchments and Blue Nile river outflow. For simulation of daily lake-level fluctuations, data from a bathymetric survey of Lake Tana in 2006 that was undertaken by the Faculty of Geoinformation Science and Earth Observation (ITC) of Twente University is used. By this survey, lake volume - lake area and lake volume - lake level relations are established to serve for assessing the water balance closure term.

## 3.2 Study Area

Lake Tana (1,786 m.a.s.l.) is the source lake of the Blue Nile River and has a total drainage area of approximately 15,000 km<sup>2</sup>, of which the lake covers around 3,000 km<sup>2</sup>. The lake is located in the north-western highlands at 12°00'N and 37°15'E and receives runoff from more than 40 rivers. Major rivers feeding the lake are Gilgel Abay from the south, Ribb and Gumara from the east and Megech River from the north. From the western side of the lake only small river systems drain into the lake (Fig. 3.1).

A digital elevation model (DEM) of 90 m resolution from Shuttle Radar Topography Mission (SRTM, version 4) (<http://srtm.csi.cgiar.org/>) has been used to delineate the gauged and ungauged catchments. The hydroprocessing tool in ILWIS software (<http://52north.org/>) has been used for this purpose. Nine catchments that are gauged and 10 catchments that are ungauged are extracted (see Fig. 3.1).

Results from catchment delineation show that among the nine catchments seven catchments are partially gauged while catchments in the north-western part are ungauged. Nine catchments are selected as gauged catchments based on the availability of runoff data from 1994 to 2003.

By its large size, Lake Tana has a large storage capacity that only responds slowly to the various processes of the hydrological cycle. Annual lake level

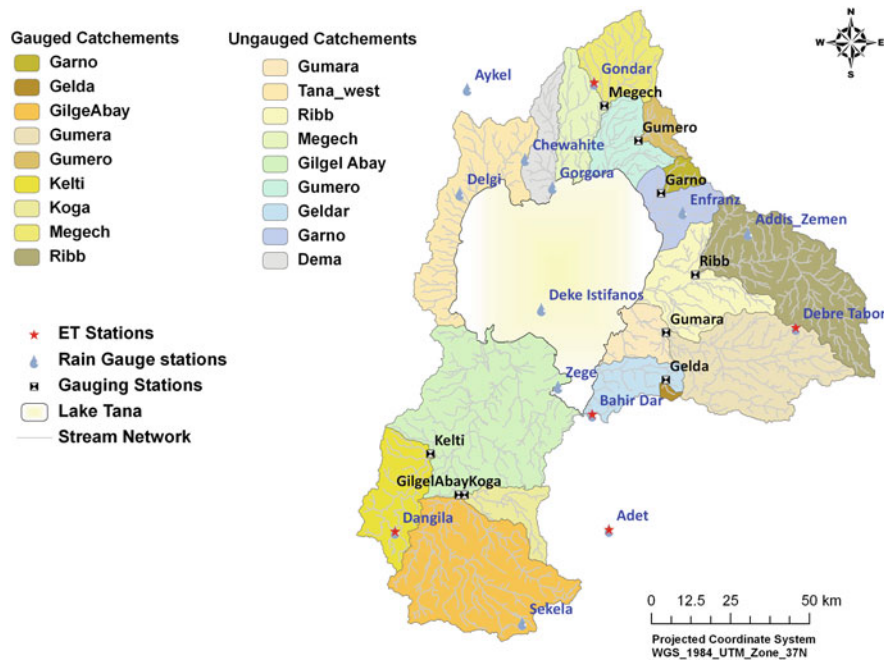


**Fig. 3.1** Gauged and ungauged catchments in Lake Tana basin

fluctuations are approximately 1.6 m where lake level fluctuations primarily respond to seasonal influences by the rainy and dry season. Lake levels reach maxima around September and minima around June with historic maximum and minimum water levels of 1,788.02 m (21 September 1998) and 1,784.46 m (30 June 2003), respectively. The only river that drains Lake Tana is the Blue Nile River (Abay River) with a natural outflow that ranges from a minimum of 1,075 Mm<sup>3</sup> (1984) to a maximum of 6,181 Mm<sup>3</sup> (1964). For the period 1976–2006, the average outflow was estimated to be 3,732 Mm<sup>3</sup>.

### 3.3 Water Balance Terms from Observed Data

In this study, the Lake Tana water balance is solved for the period 1994–2003 on a daily base. In the lake water balance equation (3.1), observation time series are available for rainfall (five stations), evaporation (two stations) and runoff from gauged catchments (five catchments). For both rainfall and evaporation, area averaged estimates are taken after spatial interpolation of the gauged data. Gauged runoff time series are used directly in the water balance after data has been screened and corrected for consistency. Time series data of Lake Tana outflow by the Blue Nile River (Abay River) also have been screened and corrected for consistency.

$$\frac{\Delta S}{\Delta T} = P - E_{\text{vap}} + Q_{\text{gauged}} + Q_{\text{ungauged}} - Q_{\text{BNR}} \quad (3.1)$$

where  $\Delta S/\Delta T$  denotes the change in storage over time,  $P$  is lake areal rainfall,  $E_{\text{vap}}$  is open water evaporation,  $Q_{\text{gauged}}$  is gauged river inflow,  $Q_{\text{ungauged}}$  is ungauged river inflow and  $Q_{\text{BNR}}$  is the Blue Nile River outflow (all terms in  $\text{Mm}^3/\text{day}$ ).

Runoff from ungauged catchment is estimated by three procedures that are further described in Section 3.4. Following SMEC (2007), in this study it is assumed that the groundwater system is decoupled from the lake and any lake leakage may be ignored in the balance. Kebede et al. (2006), however, estimated lake leakage to be some 7% of the total annual lake budget. Obviously, our assumption on lake leakage may be wrong and possibly accounts for an error in the established lake balance.

### 3.3.1 Meteorologic Balance Terms

For this study, rain gauge data from the National Meteorological Agency (NMA) in Ethiopia was collected for 15 stations in and close to the study area for the period 1994–2003. Daily rainfall over Lake Tana has been estimated through inverse distance weighted interpolation. For interpolation, data for the period 1992–2003 from Bahir Dar, Chawhit, Zege, Deke Estifanos and Delgi stations (Fig. 3.2) is used. Inverse distance with power 2 resulted in lake precipitation of 1,290 mm/year. We

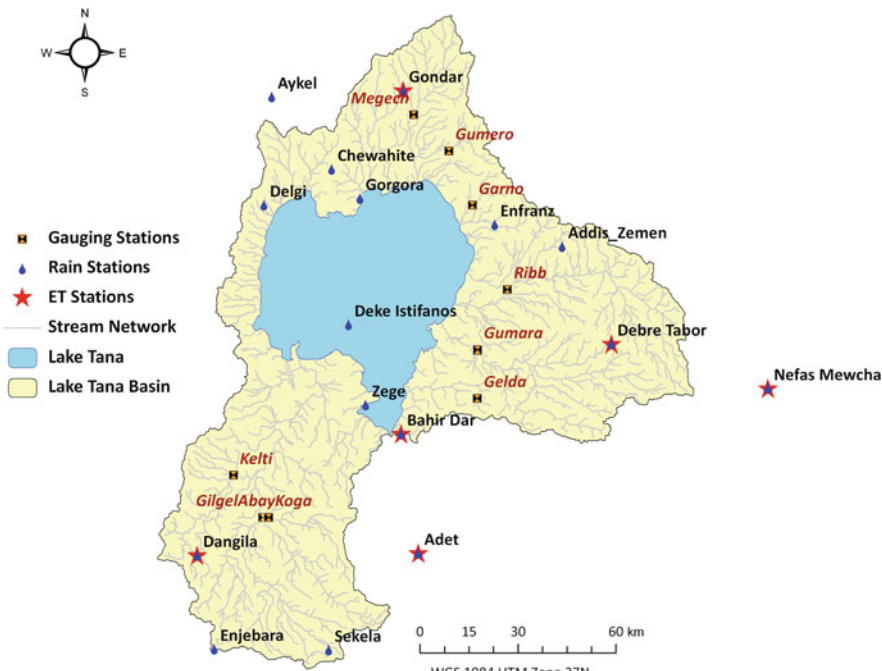


**Fig. 3.2** Weather and gauge stations in Lake Tana basin

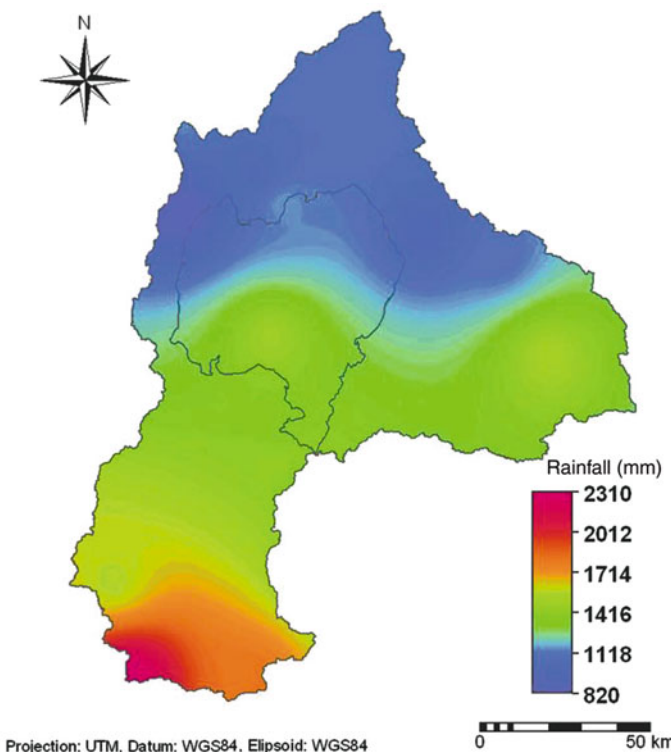


**Fig. 3.3** Annual average rainfall (mm) distribution in Lake Tana basin

selected the weight power of 2 as compared to smaller values to better represent spatial variability of rainfall that generally is high in the basin (see Haile et al., 2009, 2010). As such the spatial effect of rainfall observations at Gurer Island is accounted for. Figure 3.3 shows annual rainfall by accumulation of interpolated daily rainfall.

For estimating lake evaporation the Penman combination equation (see Maidment, 1993) is selected. For estimation of Albedo, Terra MODIS Level 1 products were acquired for the years 2000 and 2002 from the LAADS Web (<http://ladsweb.nascom.nasa.gov/data/search.html>). Albedo was estimated by the Surface Energy Balance System (SEBS) (see Su, 2002). On daily base the results show that in the lake area the Albedo ranged from 0.08 to 0.16. The daily estimated value was used for calculation of open water evaporation. Calculated daily evaporation showed an average value of 4.6 mm/day for the period 1992–2003 and a long-term averaged annual evaporation of 1,563 mm/year.

### 3.3.2 Runoff from Gauged Catchments

In the Lake Tana basin, nine gauged catchments have daily runoff records for the period 1992–2003. By an SRTM digital elevation model (DEM) of 90 m resolution

the area gauged covers some 39% of the total basin area. Runoff time series data is analysed for consistency, and analysis indicated that records from the smaller sub-basins were unreliable. The area gauged as such now only covers for the six sub-catchments (Ribb, Gilgel Abay, Gumara, Megech, Koga and Kelti) that make up approximately 32% of the Lake Tana catchment area.

### ***3.3.3 Tana Outflow by the Blue Nile River***

Outflow from Lake Tana is through the Blue Nile River that originates from the lake. For lake-level simulation, daily observation records of runoff discharges for the period 1995–2001 are used. Data, however, is screened and outliers are corrected to fit a newly constructed stage–discharge relationship (see Wale et al., 2009).

## **3.4 Methodology**

The regionalisation approach selected for this study comprised the following steps. First the HBV-96 model was calibrated for gauged catchments against observed discharges to establish good performing parameter sets to simulate catchment runoff. Next, relationships were established between the model parameters (MPs) and physical catchment characteristics (PCCs) to develop the so-called regional model. The regional model is used to establish model parameters for ungauged catchments where MPs are defined based on the PCCs of the ungauged catchments. Then the HBV-96 model was used to simulate the runoff from the ungauged catchments. Finally, the water balance of Lake Tana was solved by a bathymetric survey, and the closure term was calculated. In the following sections a description of the procedure is presented.

### ***3.4.1 HBV-96***

For this study, the conceptual hydrologic model HBV-96 (Lindström et al., 1997) is selected that has many applications in regionalisation studies (see, e.g. Seibert, 1999; Merz and Blöschl, 2004; Booij, 2005; Wale et al., 2009; Deckers et al., 2010). The model simulates river discharge and requires precipitation, actual temperature and potential evapotranspiration as inputs. In this study the model is used with a fixed time step of 1 day and with a spatially lumped model domain. The model used here consists of four routines, which are a precipitation accounting routine, a soil moisture routine, a quick runoff routine and a base flow routine which together transform excess water from the soil moisture zone to local runoff. A detailed description of the HBV model approach is ignored for reasons of brevity and the reader is referred to Lindström et al. (1997). A simple diagram of the approach is shown in Fig. 3.4.

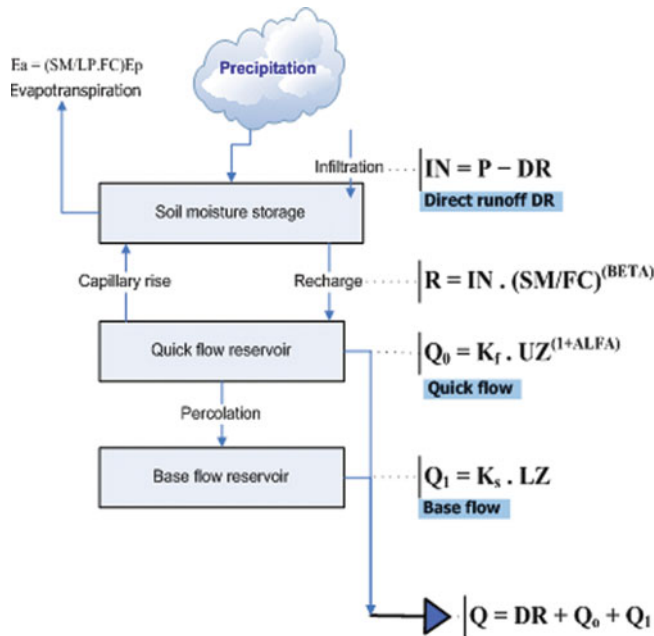


**Fig. 3.4** A diagram of the HBV-96 approach (modified after Lindström, 1997)

### 3.4.2 Model Calibration

In this study, model calibration is accomplished by a Monte Carlo simulation (MCS) procedure. MCS is a technique where numerous model simulations are executed by randomly generated model parameter sets with the objective to find the best performing parameter. Such set yields a minimum or maximum value for selected objective function(s). Principle to MCS is the large number of parameter sets that are drawn for which the model is tested. Good performing parameter sets are selected for further use, and unsatisfactory performing sets are denied for further use. After some tests the number of parameter sets to be tested (i.e. run number) has been set to 60,000 and averaged parameter values of the best 25 performing sets are taken. In the procedure, the same randomly drawn parameter sets are applied to all gauged catchments. A more detailed description on the calibration procedure is added below.

#### 3.4.2.1 Objective Functions

In runoff model calibration, parameter sets are optimised to match simulated model output to observed system output. Goodness of fit commonly is evaluated not only by visual inspection but also by use of an objective function that highlights some specific aspect of the hydrograph. Such aspects can be low flows, high flows, the overall shape of a hydrograph, the rising limb of a hydrograph (see de Vos and

Rientjes, 2007) but also the volumetric error. In this work, we selected two objective functions that are the relative volumetric error (RVE) and the Nash–Sutcliffe efficiency (NS). RVE is a measure that indicates a mass balance error while NS is a measure that indicates overall fit. The RVE requires minimisation and reads

$$\text{RVE} = \left( \frac{\sum_{i=1}^n Q_{\text{sim},i} - Q_{\text{obs},i}}{\sum_{i=1}^n Q_{\text{obs},i}} \right) \times 100\% \quad (3.2)$$

where  $Q_{\text{sim}}$  is simulated flow,  $Q_{\text{obs}}$  is observed flow,  $i$  is time step and  $n$  is total number of time steps used during the calibration. RVE may range between  $-\infty$  and  $+\infty$  but indicates an excellent performing model when a value of 0 is generated. An error between +5 and -5% indicates a well-performing model while error values between +5 and +10% or between -5 and -10% indicate reasonable performance. The NS objective function requires maximisation and reads

$$\text{NS} = 1 - \frac{\sum_{i=1}^n (Q_{\text{sim},i} - Q_{\text{obs},i})^2}{\sum_{i=1}^n (Q_{\text{obs},i} - \bar{Q}_{\text{obs}})^2} \quad (3.3)$$

where  $\bar{Q}_{\text{obs}}$  is mean of observed flow. NS can range between  $-\infty$  and 1 where the value of 1 indicates a perfect fit. NS values between 0.6 and 0.8 indicate reasonably to good performance. A model often is said to perform very good when values are between 0.8 and 0.9. We note, however, that Interpretation of values is not straightforward and reference is made to Gupta et al. (2008).

### 3.4.2.2 Optimum Parameter Set

The objective of MCS is to explore the entire parameter space to find the best performing parameter sets. For each parameter, a prior space has to be defined that reflects on the feasible parameter value range. After testing for 60,000 parameter sets the 10% best performing sets were selected and minimum and maximum values for each parameter were selected to narrow parameter ranges. So parameter ranges were narrowed down to arrive at the posterior range for which the model performance is satisfactory. For optimal parameter estimation, the entire procedure with 60,000 runs was repeated for the narrowed range to select the best performing parameter sets. The average values of parameters of the best 25 performing parameter sets were selected and make up the optimal parameter set for establishing the regional model. In Table 3.1 prior parameter ranges are shown. A simple description of the model parameters is given in Section 3.6.2.

In the procedure for each parameter set, both objective functions are calculated and compared. To evaluate which objective function indicates best performance, the value of each criterion was scaled over the range of objective function values by the 60,000 model runs. The NS value was scaled based on its minimum and maximum values Eq. (3.4).

**Table 3.1** Prior parameter ranges (following Booij et al., 2007)

Parameter	FC	BETA	CFLUX	LP	ALFA	$K_f$	$K_s$	PERC
Unit	mm	—	mm	—	—	1/day	1/day	mm/day
Minimum	100	1	0	0.1	0.1	0.0005	0.0005	0.1
Maximum	800	4	0	1	3	0.15	0.15	2.5

$$C'_{NS,i,n} = \frac{C_{NS,i,n} - \min(C_{NS,i,ntot})}{\max(C_{NS,i,ntot}) - \min(C_{NS,i,ntot})} \quad (3.4)$$

where  $C_{NS}$  is value for the NS criterion,  $i$  is NS value for specific catchment,  $n$  is calibration run number,  $ntot$  is run number.

Since RVE varies between  $-\infty$  and  $+\infty$  positive values as well as negative values can occur. The RVE scaling equation reads

$$C'_{RVE,i,n} = \frac{|C_{RVE,i,n}| - \max |C_{RVE,i,ntot}|}{\min |C_{RVE,i,ntot}| - \max |C_{RVE,i,ntot}|} \quad (3.5)$$

where  $C_{RVE}$  is value for the RVE criterion. Other terms are as defined above.

After scaling of NS and RVE, for each calibration run, the lowest value of the two was selected:

$$C'_{i,n} = \min\{C'_{NS,i,n}, C'_{RVE,i,n}\} \quad (3.6)$$

where  $C'$  is scaled value of the criteria.

The optimum parameter set for each catchment is now determined by selecting the highest values of all selected minimum values as determined through Eq. (3.7). The equation for selecting the optimal parameter set reads

$$C_i = \max\{\min(C'_{i,ntot})\} \quad (3.7)$$

It is noted that the procedure does not aim at selecting a parameter set with a highest possible objective function value but, through selection and averaging over 25 sets, simply serves to select a well-performing parameter set. This procedure aims to prevent that outliers in parameter space may result in highest objective functions values. Such parameter values, however, are not suitable for establishing the regional model.

### 3.4.3 Establishing the Regional Model

The aim of developing a regional model is to establish statistically and hydrologically relevant relationships between MPs and PCCs. PCCs are characteristics of the catchment that affect runoff responses. Such characteristics relate to topography,

climate, soils and land use. In this work, only 22 PCCs are selected that are available from databases in the public domain or that can be obtained from processing of satellite images. Table 3.5 shows the list of PCCs.

Knowledge on the relation between HBV model parameters and PCCs allows us to understand and perhaps quantitatively predict how a change in physical properties of a catchment will affect hydrological response (Mwakalila, 2003). To set up a regional model for estimation of model parameters in ungauged catchments, statistically significant relations have to be established between the calibrated MPs and the PCCs that preferably are hydrologically meaningful. For such it is common to use regression analysis (see Bastola et al., 2008, Heuvelmans et al., 2006, Kim et al., 2008, Mwakalila, 2003, Young, 2005, Xu, 2003, Deckers et al., 2010) that also is used in this study.

### 3.4.3.1 Regression Analysis

Multiple linear regression is performed for each model parameter. To guarantee that regression equations can be used, statistical significance and strength were tested. Also the correlation ( $r$ ) was tested by the  $t$ -test [Eq. (3.8)].

$$t_{\text{cor}} = \frac{|r| \sqrt{n-2}}{\sqrt{1-r^2}} \quad (3.8)$$

where,  $t_{\text{cor}}$  is the  $t$  value of the correlation,  $r$  is correlation coefficient,  $n$  is sample size.

The following hypothesis was tested. The null hypothesis  $H_0$  and the specific hypothesis  $H_1$  are

$H_0$ : The correlation between the PCC and MPs is zero,  $\rho = 0$

$H_1$ : The correlation between the PCC and MPs is not zero,  $\rho \neq 0$

If  $t_{\text{cor}} > t_{\text{cr}}$  the null hypothesis is rejected (MPs are associated with PCCs in the population).

To determine the critical value  $t_{\text{cr}}$ , the number of degrees of freedom  $df$  and  $\alpha$ , a number between 0 and 1 to specify the significance level, has to be determined. In this study a significance level of  $\alpha = 0.1$  was chosen that was applied to a two-tail test with  $n-2$  degrees of freedom. Using this information, for  $t_{\text{cr}}$ , a value of 2.132 was found (critical value from  $t$  distribution table). In order to determine at what  $r$  value the hypothesis is rejected the test statistic was solved. An  $r$  of 0.72 was established and thus  $r > 0.72$  and  $r < -0.72$  results in a statistically significant relationship.

The second method applied was based on multiple regression analysis to optimise the linear relation with forward selection and with the backward removal method. Multiple linear regression was used to predict MPs from several independent PCCs. In the forward entry approach the initially established regression model that incorporates the most significant PCC will be extended by entering a second independent variable in the regional model. This step will be accepted if the entry statistic (i.e.

significance level  $\alpha$ ) of both independent variables is not exceeded. The statistical tools are used to choose the most significant independent variable to be added. Additional steps are executed until the last added independent variable does not significantly contribute to the regression model. In addition to the forward entry method, also the backward removal method is applied. In this method, all expected PCCs are entered into the model. Based on the removal statistic (i.e. significance level  $\alpha$ ), independent variables are stepwise removed from the model. The significance of the multiple linear regression equations is tested by a test of significance of individual coefficients and by a test of overall significance. First, a hypothesis test is applied to determine if the regression equation is significant. For such test, it is assumed that the error term,  $\varepsilon$ , is not correlated and normally distributed. Further they have an average of zero and a constant variance. In this study, these assumptions were made and two hypothesis tests were executed to test the significance of the regression equation. Those are the null hypothesis and the specific hypothesis. Further, the strength of the determined regression equation is tested by the coefficient of determination,  $r^2$ . For detailed descriptions on the significance of the regression equation with hypothesis test and strength, reference is made to Perera (2009).

## 3.5 Runoff Modelling

### 3.5.1 Runoff from Ungauged Catchments

Runoff from ungauged catchments is estimated by three regionalisation procedures that are of different complexity. The first procedure applies a procedure where a regional model is established between catchment characteristics and model parameters that as such are used for ungauged catchment modelling (see Merz and Blöschl, 2004; Deckers et al., 2010; among others). A second procedure simply transfers model parameters from neighbouring or (very) nearby catchments to ungauged catchments to allow for runoff simulation. In the third procedure, parameter sets of gauged catchments are transferred to ungauged catchments by a simple area comparison. In all three procedures, the HBV-96 model is selected to simulate catchment runoff.

### 3.5.2 Results of Gauged Systems

#### 3.5.2.1 Model Calibration

The HBV-96 model was calibrated against the observed daily discharge for the period 1994–2000 using the procedure described in Section 3.4.2. After first calibration runs, several catchments resulted in poor model performance with respect to the RVE as caused by unreliable runoff time series. After screening the observed catchment runoff data, unreliable and spurious data were identified that as such have been corrected (Fig. 3.5).

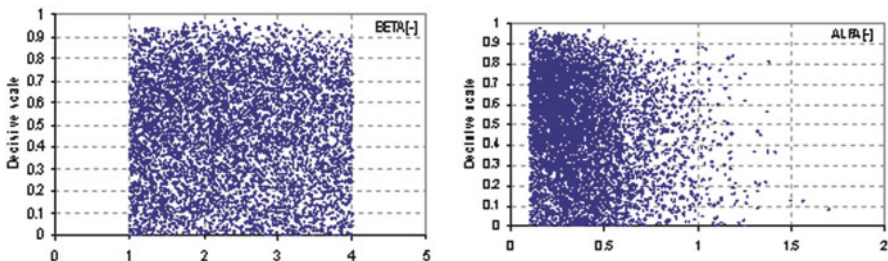


**Fig. 3.5** Scatter plots of scaled objective function values against optimised parameter values for BETA and ALFA for Gilgel Abay catchment (prior range is used)

It can be concluded that the model is much more sensitive to ALFA as compared to BETA. The model performed best for a relatively small parameter range for ALFA while the model performed equally well for a wide range of BETA values. As such, plots suggest that parameter ALFA is much better identified as compared to BETA. In the case of ALFA the scatter plot shows that the model performed well for lower values and hence the parameter space of ALFA can be narrowed. The above procedure is applied to all gauged catchments, and we note that for each catchment, specific posterior parameter ranges and specific optimum parameter values are defined. For details we refer to Perera (2009).

After finishing the procedure, we tested if parameter estimates possibly could be further improved by additional runs to test robustness of the entire MCS procedure. Figure 3.6 shows results for 15 MCS calibration runs of 60,000 runs each. Results indicate that each run has a different optimal parameter set that is the average of

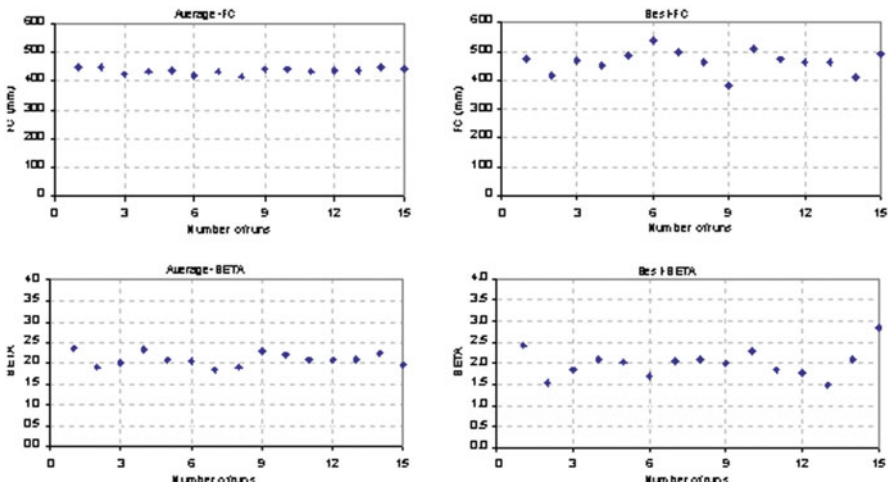


**Fig. 3.6** Plots on the left show the average of best 25 parameters in each 15 calibration run. The plots on the right show the single best parameter value in each of the 15 calibration runs

the 25 best performing parameter sets. Results indicate that optimal parameter sets cannot uniquely be defined but somehow converge to an optimal value. As such the optimum parameter set was finally selected by taking the average of these 15 parameter values.

This procedure was applied to all catchments and optimum parameter sets were established. Finally, the model was run and checked whether the NS and RVE values are acceptable. The model calibration results shown in Table 3.2 indicate that the model performance of Ribb, Gilgel Abay, Gumara, Megech, Koga and Kelti catchments is satisfactory with RVE within  $\pm 5\%$  and NS  $> 0.6$ . For Ribb and Kelti catchments, rainfall was corrected by 20 and 18%, respectively.

The result of the calibration was not satisfactory for catchments with a relatively small area such as Gumero ( $163 \text{ km}^2$ ), Garno ( $98 \text{ km}^2$ ) and Gelda ( $26 \text{ km}^2$ ). Hence these model parameters were ignored in establishing the regional model. Wale et al. (2009) suggested that the time of concentration, which is defined as the time period for water to travel from the most hydrologically remote point in the catchment to the outlet, is small and as such the quick runoff responses are difficult to represent at the daily simulation time step. Time of concentration is measured following Eq. (3.9) and is shown in Table 3.3 for all gauged catchments.

$$T_c = 0.7 \left( \frac{L \cdot L_c}{\sqrt{S}} \right)^{0.38} \quad (3.9)$$

where  $T_c$  is the time of concentration (h),  $L_c$  is the distance from the outlet to the centre of the catchment (km),  $L$  is the length of the main stream (km) and  $S$  is the slope of the maximum flow distance path (Dingman, 2002).

**Table 3.2** Calibrated model parameters for gauged catchments (1994–2000)

	Ribb	Gilgel Abay	Gumara	Megech	Koga	Kelti	Gumero	Garno	Gelda
FC	309	434	349	193	730	196	469	221.25	141.14
BETA	1.23	2.08	1.31	1.56	1.34	1.60	1.10	2.58	1.20
LP	0.73	0.63	0.87	0.71	0.42	0.62	0.26	0.23	0.86
ALFA	0.31	0.24	0.25	0.29	0.41	0.28	1.08	0.27	0.51
KF	0.07	0.08	0.03	0.03	0.07	0.03	0.03	0.10	0.003
KS	0.10	0.09	0.07	0.09	0.05	0.10	0.13	0.11	0.15
PERC	1.09	1.02	1.44	1.47	1.63	1.53	2.32	1.61	1.41
CFLUX	0.60	1.09	0.72	0.79	0.74	0.83	0.39	1.35	1.00
NS	0.78	0.85	0.72	0.61	0.67	0.66	0.16	0.33	0.41
RVE%	-1.61	-0.35	-2.44	2.91	-0.06	-2.00	0.01	0.00	-0.06

**Table 3.3** Time of concentration for selected gauged catchments in Lake Tana basin (Wale et al., 2009)

Catchment	Ribb	Gilgel Abay	Gumara	Megech	Koga	Kelti	Gumero	Garno	Gelda
$T_c$ (h)	32.63	28.64	30.15	19.49	16.38	24.29	9.56	8.27	4.66

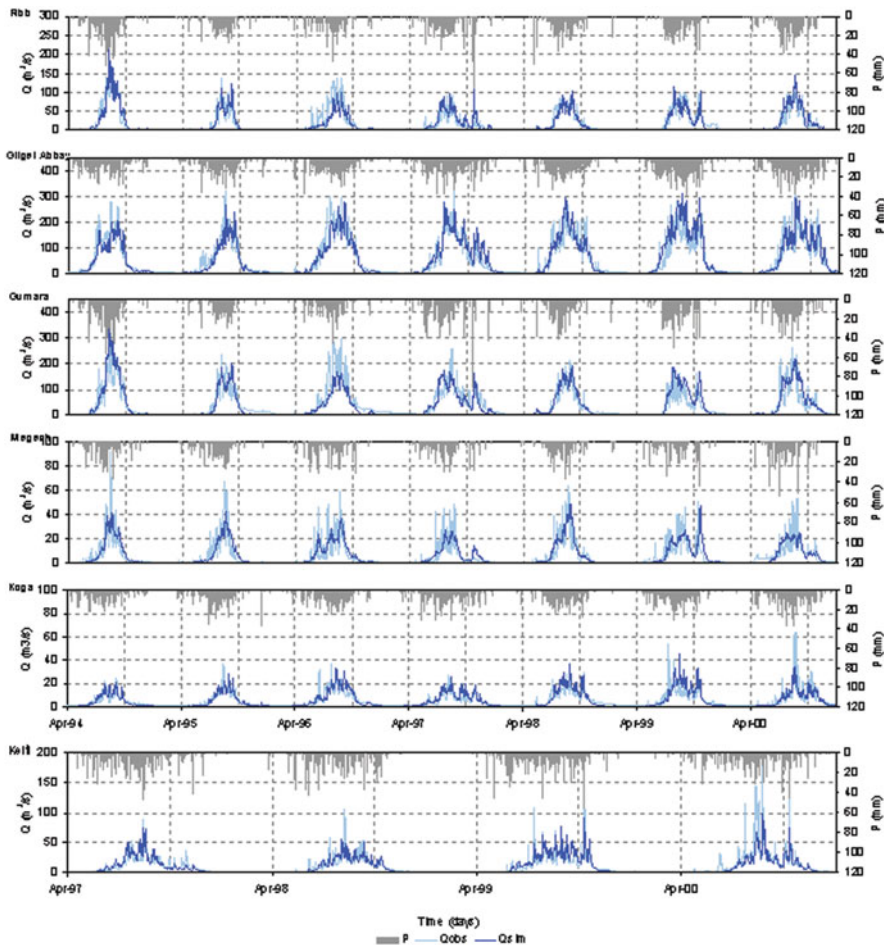


**Fig. 3.7** Model calibration results of Ribb, Gilgel Abay, Gumara, Megech, Koga (1994–2000) and Kelti (1997–2000) catchments

Further, in Wale (2008) it is mentioned that some gauging stations are not placed at the catchment outlet but at some location upstream because of easy road access. As such it is assumed that rainfall-runoff time series of those catchments cannot be considered reliable. Figure 3.7 shows the model calibration results for catchments used for developing the regional model.

### 3.5.2.2 Model Validation

Representing the real-world system by a model approach may not be accurate. Models therefore are uncertain, and models cannot be stated reliable when only one field situation is simulated. As such, it may occur that under different meteorologic

and hydrologic stress conditions the model does not accurately represent the real-world behaviour, despite the fact that optimal and calibrated model parameters are used (Rientjes, 2007).

Therefore a calibrated model requires validation using the time series of meteorological variables that were not used for calibration. In this study the model validation covers the period 2001–2003 and model validation results are shown in Table 3.4. Results for NS values in general slightly deteriorate as compared to the calibration results. RVE values in general are somewhat higher indicating larger errors in the water balance. Values for NS and RVE, however, are relatively close to calibration values and indicate a good to satisfactory model performance.

**Table 3.4** Model validation results for the period 2001–2003

	Ribb	Gilgel Abay	Gumara	Megech	Koga	Kelti
NS	0.87	0.85	0.79	0.51	0.65	0.67
RVE	3.6	-2.3	-9.9	2.9	-9.8	-5.3

## 3.6 Results on Regionalisation

### 3.6.1 Simple Linear Regression

Correlation between PCCs and MPs was established to determine the significance of each relationship (Table 3.5). When the correlation coefficient lies outside critical values of  $-0.72$  to  $0.72$ , the corresponding correlation is significant. Thus, the null hypothesis is rejected. In Table 3.5 the significant correlation coefficients are highlighted.

### 3.6.2 Multiple Linear Regression

It is assumed that by using multiple PCCs, a better relation can be established than when only one PCC is used. Therefore relations between PCCs and MPs were assessed through multiple linear regression analysis. This was done by the forward entry method and the backward removal method as described in Section 3.4.3. The established regional model is shown in Table 3.6. For a more extensive description reference is made to Perera (2009) where statistical characteristics of all regression equations are shown.

### 3.6.3 Validation of the Regional Model

The regional model is established to predict the discharge from the ungauged catchment. Prior to its use, the regional model is assessed by comparing the predicted and observed discharges from the gauged test catchments. It is not possible to carry

**Table 3.5** Correlation matrix between model parameters and PCCs for six selected catchments; significant correlation coefficients are highlighted and in bold

	FC (mm)	BETA (-)	LP (-)	ALFA (-)	$K_f$ (1/day)	$K_s$ (1/day)	PERC (mm/day)	CFLUX (mm/day)
AREA	-0.18	-0.01	0.49	<b>-0.77</b>	0.13	0.62	<b>-0.82</b>	0.07
LFP	-0.17	-0.15	0.53	-0.51	0.25	0.52	<b>-0.74</b>	-0.16
MDEM	0.04	-0.58	0.33	-0.64	-0.11	0.66	-0.51	-0.51
HI	<b>-0.81</b>	-0.03	<b>0.77</b>	<b>-0.76</b>	-0.44	<b>0.77</b>	-0.44	-0.07
AVGSLOPE	-0.30	-0.48	0.39	<b>-0.75</b>	-0.31	<b>0.92</b>	-0.52	-0.45
SHAPE	0.65	<b>-0.90</b>	-0.42	0.12	-0.29	-0.04	0.43	<b>-0.83</b>
CI	<b>0.78</b>	-0.37	-0.55	0.58	0.37	-0.46	0.28	-0.37
EL	0.54	<b>-0.59</b>	-0.32	0.59	-0.01	-0.48	0.57	-0.66
DD	<b>-0.74</b>	0.23	0.64	-0.35	0.30	<b>0.77</b>	<b>-0.83</b>	0.06
CROPD	-0.39	<b>0.77</b>	-0.04	0.35	0.10	-0.36	0.20	0.69
CROPM	0.47	-0.71	0.03	-0.52	-0.22	0.27	-0.16	-0.55
GL	-0.18	-0.54	0.36	-0.19	0.08	0.61	-0.42	-0.67
URBAN	-0.53	-0.19	0.42	-0.71	<b>-0.72</b>	0.59	-0.05	-0.13
FOREST	0.67	-0.61	-0.60	0.47	0.20	-0.09	0.23	-0.63
LEP	-0.50	-0.36	0.20	-0.23	-0.59	0.57	0.14	-0.44
NIT	0.26	-0.31	-0.56	0.26	-0.49	-0.16	0.69	-0.26
VER	0.65	0.07	<b>-0.73</b>	<b>0.81</b>	0.18	<b>-0.88</b>	0.71	0.09
LUV	0.04	0.40	0.30	0.15	0.37	-0.55	-0.08	0.38
SAAR	0.45	0.52	-0.31	0.12	<b>0.75</b>	-0.29	-0.42	0.62
PWET	0.45	0.39	-0.21	0.07	<b>0.73</b>	-0.24	-0.46	0.49
PDRY	0.41	0.69	-0.45	0.20	0.71	-0.36	-0.31	<b>0.81</b>
PET	-0.13	-0.11	-0.23	-0.09	-0.59	0.13	0.43	-0.05

**Table 3.6** The regional model

Regression equation	$R^2$ (%)
$FC = \beta_0 + \beta_1 \cdot HI$	66.3
$BETA = \beta_0 + \beta_1 \cdot SHAPE + \beta_2 \cdot HI$	96.02
$LP = \beta_0 + \beta_1 \cdot HI + \beta_2 \cdot LUV$	91.1
$ALFA = \beta_0 + \beta_1 \cdot AREA + \beta_2 \cdot URBAN$	95.1
$KF = \beta_0 + \beta_1 \cdot SAAR$	56.35
$KS = \beta_0 + \beta_1 \cdot AVGSLOPE$	85.25
$PERC = \beta_0 + \beta_1 \cdot DD + \beta_2 \cdot SAAR$	89.9
$CFLUX = \beta_0 + \beta_1 \cdot SHAPE + \beta_2 \cdot PDRY + \beta_3 \cdot PET$	96.27

out a formal validation on independent (gauged) catchments as too limited number of gauged catchments is available in this study. Therefore validation is done for the calibrated gauged catchments but for the period 2001–2003 that is different from the calibration period.

The established regional model was used to estimate the model parameters of ungauged catchments using their PCCs. Next the discharge was simulated based on the estimated parameters and the model performance was evaluated with respect to NS and RVE. Table 3.7 shows the parameters derived from the regional model and the model performances.

**Table 3.7** Validation of the regional model of gauged catchments (2001–2003)

	FC	BETA	LP	ALFA	$K_F$	$K_S$	PERC	CFLUX	NS (-)	RVE (%)
Ribb	298	1.17	0.71	0.29	0.055	0.098	1.10	0.62	0.85	-1.3
Gilgel Abay	333	1.99	0.72	0.25	0.086	0.084	1.13	1.10	0.83	0.1
Gumara	307	1.48	0.83	0.28	0.057	0.079	1.40	0.71	0.75	-22.8
Megech	201	1.54	0.70	0.29	0.031	0.085	1.52	0.79	0.54	13.3
Koga	659	1.32	0.41	0.43	0.068	0.061	1.63	0.75	0.65	-1.1
Kelti	437	2.45	0.72	0.39	0.072	0.054	1.18	1.06	0.53	-42.0

### 3.6.3.1 Spatial Proximity

The regression method is the most widely used regionalisation technique but alternative much less complex methods are also in use such as the spatial proximity method. In this method, the choice of catchments from which information is to be transferred is usually based on some sort of similarity measure. The rationale of the method is that catchments that are close to each other will have a similar runoff regime as climate and catchment conditions will only vary smoothly in space (Merz and Blöschl, 2004). Van de Wiele and Elias (1995) used a similar approach to estimate parameters of a monthly water balance model for 75 catchments from neighbouring gauged catchments. In the approach, the complete set of model parameters is transferred from one or more gauged catchments to ungauged catchments. In this study, parameter values as derived for gauged catchments in upstream areas were transferred to downstream areas that are ungauged. Also catchments which are not gauged or failed to be simulated were assigned parameters from a neighbouring catchment. In Fig. 3.8, catchment transfer linkages by the spatial proximity method are shown.

### 3.6.3.2 Area Ratio

This method considers only catchment areas by assuming that the catchment area is the dominant factor that controls the volume of water as produced by rainfall. The simulated annual average runoff in gauged catchments showed correlation with  $R^2$  of 72.5% for catchment area. Hence parameter sets of gauged catchments were transferred to ungauged catchments of a comparable area. In Fig. 3.8, catchment transfer linkages by the area ratio method are shown.

### 3.6.3.3 Sub-basin Mean

The sub-basin mean represents the arithmetic mean (Kim et al., 2008) of calibrated parameter set of six catchments to simulate the flow from ungauged catchments.

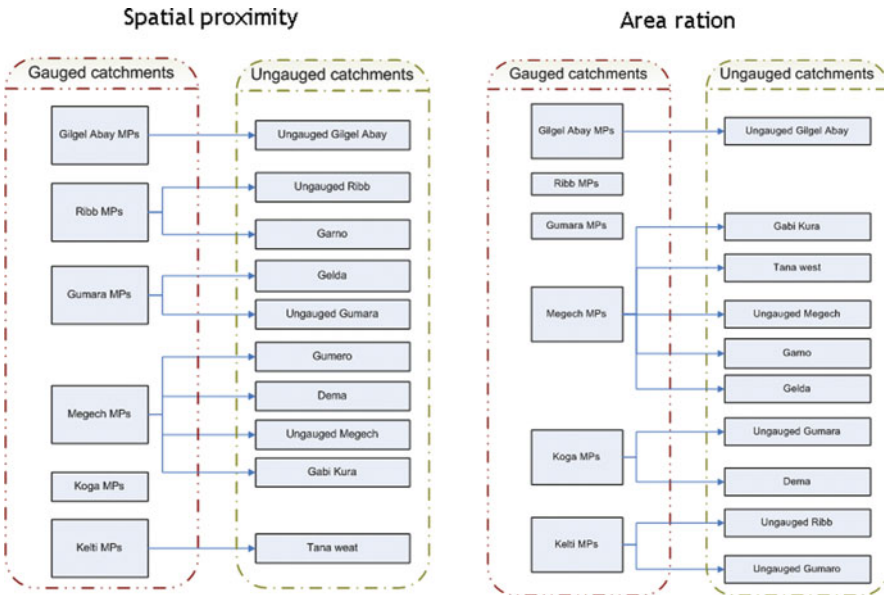


Fig. 3.8 Catchment linkages for the spatial proximity and area ratio methods

### 3.7 Discussion and Conclusion

A well established water balance often leads to a better understanding of a hydrological system. Studies by Gieske et al. (2008), Kebede et al. (2006) and Wale et al. (2009) report on solving Lake Tana's water balance. Dingman (2002) refers to a water balance as “the amount of a conservative quantity entering a control volume during a defined period minus the amount of quantity leaving the control volume during the same period equals the change in the amount of the quantity stored in the control volume during the same time period”. The simple water balance equation is formulated as follows:

$$\frac{\Delta S}{\Delta T} = \text{Inflow} - \text{Outflow} \quad (3.10)$$

The general water balance equation of a lake can be written as follows:

$$\frac{\Delta S}{\Delta T} = (P + Q_{\text{gauged}} + Q_{\text{ungauged}} + GW_{\text{in}}) - (E + Q_{\text{out}} + GW_{\text{out}}) + ss \quad (3.11)$$

where  $P$  is lake areal rainfall,  $Q_{\text{gauged}}$  is surface water inflow from gauged catchment,  $Q_{\text{ungauged}}$  is surface water inflow from ungauged catchment,  $GW_{\text{in}}$  is subsurface water inflow,  $E$  is open water evaporation from the lake surface,  $Q_{\text{out}}$  is surface water outflow,  $GW_{\text{out}}$  is subsurface outflow and  $ss$  is sink source term.

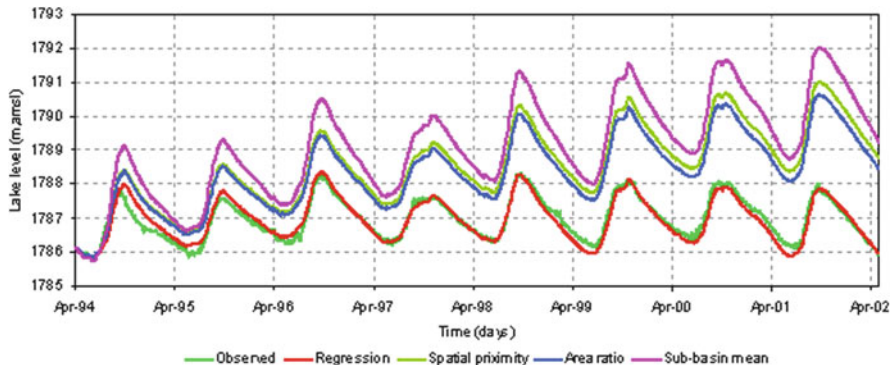


**Fig. 3.9** Comparison of lake-level simulation in different ungauged flow estimation techniques

Based on the above procedures, the water level of Lake Tana was simulated by use of a bathymetric survey and the river discharges that are estimated from ungauged catchments by three regionalisation methods. Figure 3.9 shows a comparison of lake levels using the bathymetric survey by Wale (2008) and a survey by Pietrangeli (1990). Performance results are shown in Table 3.8.

**Table 3.8** Results of NS and RVE for selected bathymetric relations

	NS	RVE (%)
Wale (2008)	0.92	-2.2
Pietrangeli (1990)	0.60	-3.2

One of the uncertain components of the Lake Tana water balance is the discharge from ungauged catchments. The discharges of ungauged catchments are estimated using three different regionalisation techniques and discharges that are used to simulate the lake-level fluctuations. Results are also shown when parameter values are averaged and applied to ungauged catchment systems. Among the four techniques, the regression method gave the best results while poorest results are obtained for the sub-basin mean method.

Except for the regression method, other regionalisation techniques show relatively large deviation between observed and simulated lake levels that gradually increase over the simulation period. Hence the result from the regression method is used to calculate the Lake Tana water balance component and results are shown in Table 3.9. It shows that the balance closure term is 85 mm. This error accounts for 2.7% of the total lake inflow, while the lake relative volume error is 2.17%. The errors may be due to uncertainty in lake–groundwater interaction, uncertainty in estimating open water evaporation and lake areal rainfall and runoff from gauged and ungauged catchments.

**Table 3.9** Lake Tana water balance components simulated for the period 1994–2003

Water balance components	mm/year	MCM/year
Lake areal rainfall	+1,347	+4,104
Gauged river inflow	+1,254	+3,821
Ungauged river inflow	+527	+1,605
Lake evaporation	-1,563	-4,762
River outflow	-1,480	-4,508
Closure term	+85	+260

## References

Bastola S, Ishidaira H, Takeuchi K (2008) Regionalisation of hydrological model parameters under parameter uncertainty: A case study involving TOPMODEL and basins across the globe. *J Hydrol* 357(3–4):188–206

Booij MJ (2005) Impact of climate change on river flooding assessed with different spatial model resolutions. *J Hydrol* 303:176–198

Booij MJ, Deckers DLEH, Rientjes THM, Krol MS (2007) Regionalisation for uncertainty reduction in flows in ungauged basins, vol 313. IAHS, Wallingford, CT, pp 329–337. ISBN 978-1-90150278-09-1

Conway D (1997) A water balance model of the Upper Blue Nile in Ethiopia. *Hydrol Sci J* 42(2):265–286

Deckers DLEH, Booij MJ, Rientjes THM, Krol MS (2010) Catchment variability and parameter estimation in multi-objective regionalisation of a rainfall-runoff model. *Water Resour Manage* P25. doi:10.1007/s11269-010-9642-8

de Vos NJ, Rientjes THM (2007) Multi-objective performance comparison of an artificial neural network and a conceptual rainfall-runoff model. *Hydrol Sci J* 52:397–413

Dingman SL (2002) Physical hydrology, 2nd edn. Prentice Hall, Upper Saddle River, NJ

Gieske ASM, Abeyou WW, Getachew HA, Alemseged TH, Rientjes THM (2008) Non-linear parameterization of Lake Tana's flow system. Proceedings of the workshop on Hydrology and Ecology of the Nile River Basin under Extreme Conditions, Addis Ababa, Ethiopia, pp 127–144

Gupta HV, Wagener T, Liu Y (2008) Reconciling theory with observations: elements of a diagnostic approach to model evaluation. *Hydrol Process* 22:3802–3813. doi:10.1002/hyp.6989

Haile AT, Rientjes THM, Gieske M, Gebremichael M (2009) Rainfall variability over mountainous and adjacent lake areas: the case of Lake Tana basin at the source of the Blue Nile River. *J Appl Meteorol Climatol* 48:1696–1717

Haile AT, Rientjes TH, Gieske A, Gebremichael M (2010) Rainfall estimation at the source of the Blue Nile: a multispectral remote sensing approach. *Int J Appl Earth Obs Geoinf* JAG 12(Suppl. 1):S76–S82

Heuvelmans G, Muys B, Feyen J (2006) Regionalisation of the parameters of a hydrological model: comparison of linear regression models with artificial neural nets. *J Hydrol* 319(1–4):245–265

Kebede S, Travi Y, Alemayehu T, Marc V (2006) Water balance of Lake Tana and its sensitivity to fluctuations in rainfall, Blue Nile basin, Ethiopia. *J Hydrol* 316(1–4):233–247

Kim U, Kaluarachchi JJ, Smakhtin U (2008) Generation of monthly precipitation under climate change for the Upper Blue Nile river basin Ethiopia. *J Am Water Resour Assoc* 44(4):1–17. doi:10.1111/j.1752-1688.2008.00220

Lindström G, Johansson B, Persson M, Gardelin M, Bergstrom S (1997) Development and test of the distributed HBV-96 hydrological model. *J Hydrol* 201:272–288

Maidment DR (ed) (1993) Handbook of hydrology. McGraw-Hill, New York, NY

Merz R, Blöschl G (2004) Regionalisation of catchment model parameters. *J Hydrol* 287:95–123

Mwakalila S (2003) Estimation of stream flows of ungauged catchments for river basin management. *Phys Chem Earth Parts A/B/C* 28(20–27):935–942

Perera BUJ (2009) Ungauged catchment hydrology: the case of Lake Tana. MSc thesis ITC, Enschede, The Netherlands, p 61

Pietrangeli (1990) Studio pietrangeli, hydrological report. Government of Ethiopia, Addis Abeba

Rientjes THM (2007) Modelling in hydrology. ITC, Enschede, The Netherlands, p 234

Seibert J (1999) Regionalisation of parameters for a conceptual rainfall-runoff model. *Agric For Meteorol* 98–99:279–293

SMEC (2007) Hydrological study of the Tana-Beles sub-basins (part 1). Snowy Mountains Engineering Corporation, Australia, p 77

Su Z (2002) The surface energy balance system (SEBS) for estimation of turbulent heat flux. *Hydrol Earth Syst Sci* 6(1):85–89

Vallet-Coulomb C, Legesse D, Gasse F, Travi Y, Chernet T (2001) Lake evaporation estimates in tropical Africa (Lake Ziway, Ethiopia). *J Hydrol* 245(1–4):1–18

Van de Wiele GL, Elias A (1995) Monthly water balance of ungauged catchments obtained by geographical regionalization. *J Hydrol* 170(1–4):277–291

Wale AW (2008) Estimation of flow from ungauged catchments by regionalisation procedures – Lake Tana, Ethiopia. MSc Thesis ITC, The Netherlands, p 94

Wale A, Rientjes THM, Gieske ASM, Getachew HA (2009) Ungauged catchment contributions to Lake Tana's water balance. *Hydrol Proc Int J* 23(26):3682–3693

Xu CY (2003) Testing the transferability of regression equations derived from small sub-catchment to a large area in central Sweden. *Hydrol Earth Syst Sci* 7(3):317–324

Young AR (2005) Stream flow simulation within UK ungauged catchments using a daily rainfall-runoff model. *J Hydrol* 320(1–2):155–172

**Part II**  
**Satellite Rainfall Estimation**

# Chapter 4

## Satellite Based Cloud Detection and Rainfall Estimation in the Upper Blue Nile Basin

**Tom H.M. Rientjes, Alemseged T. Haile, Ambro S.M. Gieske,  
Ben H.P. Maathuis, and Emad Habib**

**Abstract** In this study remote sensing for rainfall estimation is evaluated. For the Lake Tana basin in Ethiopia the diurnal cycle of rainfall is assessed using satellite observations at high temporal resolution and ground based observations. Also convective activity of a cloud system on the lake has been observed through satellite imagery and shows a potential to observe characteristics of a cloud that produced extreme rainfall intensity. These characteristics include the cloud area and a volume index as well as temporal evolution of distance and direction of the centroid of a cloud mass from a rain gauge at the Guret Island in Lake Tana. In this work it is concluded that remote sensing can be very helpful in estimating rainfall, assessing the diurnal cycle and monitoring heavy rainfall producing clouds. The high potential of remote sensing observations is mainly because the observations are consistently available with spatially continuous coverage.

**Keywords** Satellite rainfall estimation · Diurnal cycle · Cloud tracking · Lake Tana

### 4.1 Introduction

Rainfall studies often are restricted by data availability. Estimation of rainfall is challenging in particular when rainfall largely varies over small time and space domains. Under such conditions, ground based rain gauge networks are commonly too sparse to satisfactorily capture the real world spatial distribution of rainfall properties such as rainfall intensity, duration and frequency. To overcome such limitation, the use of meteorological satellites is often advocated. Such satellites have applications in cloud detection and rainfall estimation. Examples of missions are the Tropical Rainfall Measuring Mission (TRMM) and the series of Meteosat satellites from which the Meteosat Second Generation (MSG-2) satellite is used in this study.

---

T.H.M. Rientjes (✉)

Department of Water Resources, Faculty of Geoinformation Science and Earth Observation (ITC),  
Twente University, 7500 AA Enschede, The Netherlands  
e-mail: t.h.m.rientjes@utwente.nl

Meteorological satellites serve to detect rain producing clouds as well as to estimate rainfall over selected time-space domains. These satellites can be in orbit or can be geostationary. The first group overpasses a certain geographic area with a revisit time of ones or twice per day while the second group allows observations at frequency of  $\geq 15$  min. Orbital satellites such as TRMM observe a continuously changing geographic area while geostationary satellites such as MSG-2 observed the same area for the live time of the satellite. Earth orbiting satellites commonly fly at an altitude of hundreds of kilometers (e.g. 403 km for TRMM) while geostationary satellites commonly are positioned at high altitudes (e.g. 36,000 km for MSG-2 satellite).

In remote sensing based rainfall estimation, the most commonly utilized parts of the electromagnetic wave spectrum are the thermal infrared (TIR) and the microwave (MW) channels. These channels produce complementary information regarding rainfall that resulted in the development of combined TIR-MW based approaches. Currently, MW sensors are mounted only on orbiting satellites while TIR sensors are carried by orbiting as well as by geostationary satellites. It is noted that other channels such as the Visible (VIS) and the Water vapor (WV) channels are available as well but these are not used frequently despite that the channels have a potential to provide additional and complementary information about cloud characteristics (see, Lovejoy and Austin, 1979; Tsionis et al., 1996; and Tsintikidis et al., 1999).

In TIR based rainfall estimation, rainfall rates are inferred from cloud top surfaces. The underlying physical assumption is that relatively cold clouds are associated with thick and high clouds that tend to produce high rainfall rates. (Haile et al., 2010) described the limitation of these approaches: (i) different vertical profiles of clouds that result in different rainfall rates can have the same cloud top temperature, and (ii) TIR based approaches assume that rain occurs when the cloud top temperature is less than a selected threshold, e.g. (Griffith et al., 1978; Arkin 1979; Arkin and Meisner, 1987). As a result, the use of a constant temperature threshold introduces errors to the rainfall estimation procedure. (Todd et al., 1995) suggested the use of a TIR threshold that varies with geographic location and terrain elevation.

MW based approaches are based on the concept that observed radiation in the microwave frequencies is affected by atmospheric hydrometeors such as cloud and precipitation droplets that cause augmentation of radiation due to emission and attenuation of radiation due to absorption and scattering. As such, MW sensors respond primarily to precipitation-size hydrometeors in the cloud profile and therefore information from MW channels is much more direct as compared to information from TIR channels. However, we note that in MW approaches rainfall at the land surface cannot be retrieved directly. Currently, MW sensors are mounted only on low-altitude orbiting satellites and therefore the observations are snapshots that are available once or twice a day. Such observation frequency makes it difficult to capture the temporal dynamics of clouds.

The need to improve the performance of TIR and MW based rainfall retrieval approaches resulted in the development of combined approaches that benefit from

the strengths of both data sources. Such algorithms combine and benefit from TIR images at high temporal resolution and MW images that, compared to TIR, carry more direct information about cloud and rainfall characteristics. Examples of such approaches are PERSIANN (Hsu et al., 1997; Sorooshian, et al., 2000; Hong et al., 2005), NRLgeo (Turk and Miller, 2005), TRMM 3B42 (Huffman et al., 2007). As stated by (Haile et al., 2010), most of the rain products by these approaches are available at spatial resolutions  $\geq 0.25^\circ$  and temporal resolutions  $\geq 1$  day which is coarser than what is typically needed in hydrology and water resources. In addition, the validation of these products is still a topic of ongoing research.

Reviews by (Stephens and Kummerow, 2007; Levizzani et al., 2002; Barrett and Martin, 1991; Kidder and Vonder Haar, 1995; Petty, 1995) show that remote sensing based approaches of rainfall estimation have several limitation that lead to inaccurate rainfall estimates. In these reviews, the difficulty of validating remote sensing based estimates is noted since the use of rain gauge data is too poor in terms of resolution, reliability and in providing the spatial coverage of rainfall. Despite the poor performance, remote sensing has found applications in rainfall studies mainly since it provides a spatial coverage of rain producing clouds. Some applications of remote sensing include: rainfall detection to study the diurnal cycle of rainfall (Dai, 2001; Imaoka and Spencer, 2000), to monitor and characterize clouds that produce heavy rainfall (e.g. Feidas and Cartalis, 2001) and to analyze the scaling behaviour of rainfall (Gebremichael et al., 2008).

Nesbitt and Zipser (2003) noted that the limitations of diurnal cycle studies of rainfall revolve around (i) our inability to observe and quantify the true tropics wide diurnal cycle of rainfall amount and convective intensity, and (ii) the use of numerical model simulations that do not allow the true representation of the diurnal cycle. These limitations can be partly overcome by using remote sensing observations which are consistently available with spatially continuous coverage.

In this study, first we evaluate the use of remote sensing observations for rainfall estimation. Next, we present the diurnal cycle of rainfall using ground based observations and the diurnal cycle of convective activity using remote sensing observations in the Lake Tana basin, Ethiopia. Finally, the characteristics of a cloud that produced extreme rainfall intensity over Lake Tana are derived from MSG-2 observations. These characteristics include cloud area and volume index as well as temporal evolution of distance and direction of the centroid of a cloud mass from a rain gauge at the Gurer Island in Lake Tana.

## 4.2 Methods

### 4.2.1 Rainfall Diurnal Cycle

The diurnal cycle of rainfall is commonly analysed by estimating the frequency of rainfall occurrences that shows the percentage of rainy hours in a specific Local Standard Time (LST) of a selected time period, see (Haile et al., 2009; Gebremichael et al., 2007). The frequency of rainfall occurrences reads:

$$F_j = 100 \frac{\sum_{i=1}^N X_{ji}}{N} \quad (4.1)$$

where:  $F$  is the frequency of rainfall occurrences in specific LST (%),  $X$  is a flag for rainfall occurrence with  $X = 0$  for non-rainy hours and  $X = 1$  for rainy hours where a rainy hour in this study is defined based on the observation resolution of the rain gauges that is 0.2 mm. The index  $j$  indicates the LST under consideration while  $N$  is the number of days in the selected time period.

Remote sensing images also have found applications in diurnal cycle assessments of rainfall. For instance (Gebremichael et al., 2007) applied TRMM observations for detection of the rainfall cycle. However, TRMM provides intermittent observations of once or twice per day for a specific geographic location. Such introduces sampling error to the assessments of the diurnal cycle. For such assessment, MSG-2 is much more suitable since it observes a particular geographic location every 15 min. The large number of observations allow for statistical analysis. It is noted that TIR observations are proxy variables for the surface rainfall rate but by analysis of these observations we can infer patterns of convective activity, see (Ohsawa et al., 2001; Barros et al., 2004; Ba and Nicholson, 1998). In this study, the 10.8  $\mu\text{m}$  brightness temperatures are analysed to study the temporal and spatial patterns of convective activity through a convective index ( $CI$ ) that is defined as:

$$CI_h = 100 \left[ \sum_{i=1}^N t_i \right] N^{-1} \quad (4.2)$$

where  $t = 1$  for  $T_l < T_{10.8} \leq T_u$ ,  $t = 0$  for  $T_{10.8} \leq T_l$  and  $T_{10.8} > T_u$ ;  $N$  is the number of observations at a specific LST over a selected time period. In this study, the time period is from June 1 to August 25, 2007. We established indices that correspond to (i)  $T_u < 210$  k, (ii)  $T_u = 225$  k and  $T_l = 210$  k and (iii)  $T_u = 240$  k and  $T_l = 225$  k to account for high, mid and low level clouds, respectively.

#### 4.2.2 Convective Cloud Tracking

Through the MSG-2 satellite, we monitored a single cloud system that produced extreme rainfall in Lake Tana. Characteristics of the cloud that are monitored include the distance and the direction of the cloud centroid from the exact location of an automated rain recorder at Gurer Island in the lake, the cloud area and a cloud volume index. The cloud characteristics are derived following the procedure suggested by (Feidas and Cartalis, 2001); (Arnaud et al., 1992). The September 18, 2008 rain event is selected since the event produced extremely high intensity.

First, the centre of mass of the cloud is estimated. The coordinates of the centre of mass read:

$$X_c = \frac{\sum_{i=1}^N (Tb_{(TIR)i} + Tb_{(WV)i})X_i}{\sum_{i=1}^N (Tb_{(TIR)i} + Tb_{(WV)i})}, \quad (4.3)$$

$$Y_c = \frac{\sum_{i=1}^N (Tb_{(TIR)i} + Tb_{(WV)i})Y_i}{\sum_{i=1}^N (Tb_{(TIR)i} + Tb_{(WV)i})}$$

where  $X_c$  and  $Y_c$  are the coordinates of the centre of mass of the cloud, respectively;  $i$  is a space index representing a pixel covered by a cloud;  $N$  is the number of cloudy pixels;  $Tb$  is the brightness temperature at the 6.2 and 10.8  $\mu\text{m}$  channels that are the water vapour (WV) and thermal infrared (TIR) channels; and  $X_i$  and  $Y_i$  are the coordinates of the  $i$ th pixel covered by a cloud.

Next, the distance is measured from the centre of mass of the cloud to the location of the island rain gauge in Lake Tana. This is repeated for each time step. The direction is expressed in terms of an inclination, i.e. angle, which is measured from a Y-axis, with its origin at the rain gauge location, to the line that joins the rain gauge location and the centre of mass of the cloud. Positive direction indicates a clockwise angle from the Y-axis.

Cloud area is estimated as the number of pixels covered by a cloud multiplied by the size of a single pixel, i.e.  $9 \text{ km}^2$  for MSG-2. Cloud area indicates the potential of the cloud to produce rainfall. Another indicator of the potential of a cloud to produce rainfall is the volume index (VI) which reads:

$$VI = \sum_{i=1}^N k_i(Tb_0 - Tb_i) \quad (4.4)$$

where  $k$  is the number of pixels with equal brightness temperature while the other terms are defined in previous paragraphs. Equation (4.4) is applied for both the TIR and WV channel and the average VI is used to measure the cloud potential to produce rainfall. We applied an arbitrarily chosen temperature threshold ( $Tb_0$ ) of 240 K.

## 4.3 Results

### 4.3.1 Rainfall Estimation

The results in this section are based on the work by (Haile and Rientjes, 2007). Figures 4.1 and 4.2 illustrate that both daily minimum TIR brightness temperature (Tmin) and the Cold Cloud Duration (CCD) carry relevant information that

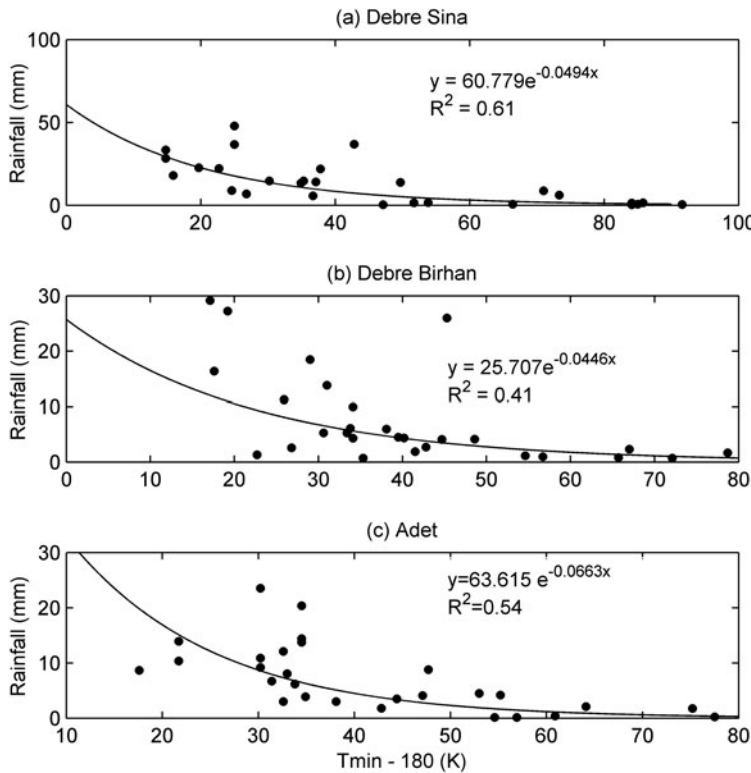


**Fig. 4.1** Daily rainfall vs. daily minimum TIR brightness temperature observations for August, 2005. **a** For D/Sina meteorological station. **b** For D/Birhan meteorological station. **c** For Adet meteorological station

could be related to daily rainfall amounts. CCD is defined here as the duration over which a cloud top temperature of less than 260 K is observed. As it is shown in Fig. 4.1, a power law relationship between daily rainfall and daily minimum brightness temperature ( $T_{min}$ ) observations can be established. Although the coefficient of determination (i.e.  $R^2$ ) is not very low, the relationship between the two variables is not very strong. Also the observed scattering indicates that the relation is non-unique since single brightness temperatures can be related to unequal daily rainfall depths. Nevertheless, the minimum brightness temperature is indicative towards daily rainfall amounts. For instance, for the considered stations,  $T_{min}$  of less than 210 K is most likely associated to a rainfall amount higher than 10 mm while  $T_{min}$  of greater than 230 K corresponds to a rainfall amount of lower than 5 mm.

The CCD is used as one of the indices for retrieval of daily rainfall amounts from images. A major limitation with the CCD is that rainfall amount is related mainly to the cloud duration. However, such assumptions could fail when convective clouds of high rainfall intensity occur over a short period of time. In addition and as observed

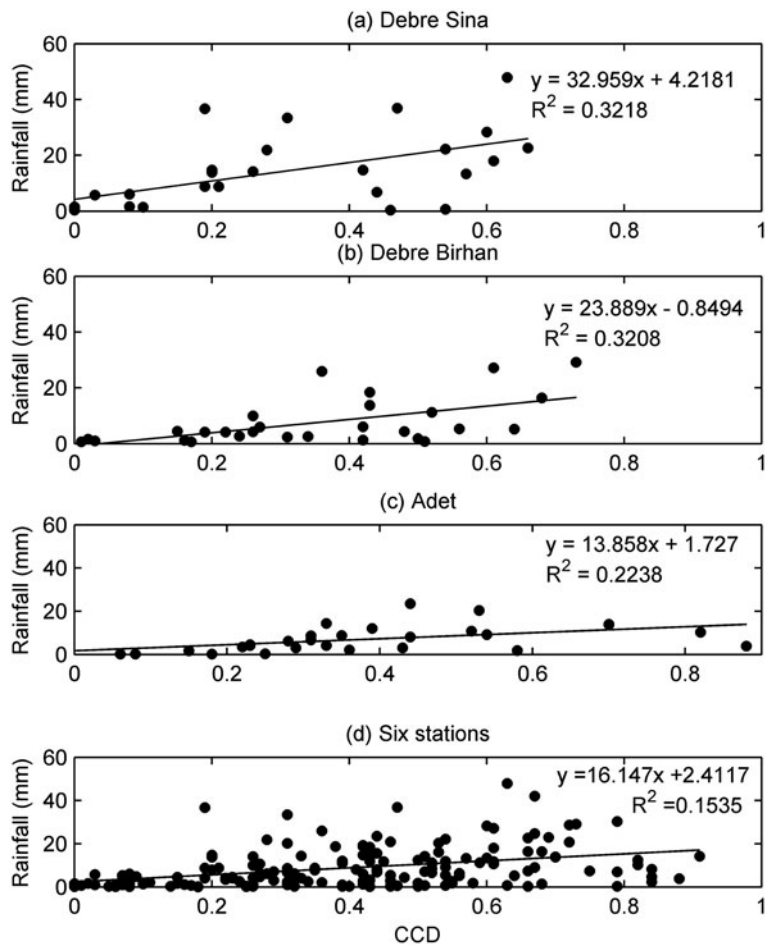


**Fig. 4.2** Observed daily rainfall vs. daily CCD. **a** D/Sina. **b** D/Birhan. **c** Adet. **d** Six stations in the Upper Blue Nile basin

in similar studies, results from our approach are affected by the applied temperature threshold that varies with season and geographic position. In this study, the CCD values are computed based on a brightness temperature threshold of 260 K to detect rainfall from all types of clouds. It should however be understood that the threshold is affected by many factors and also changes over meso-scale spatial domains and season. However, several cloud indexing approaches use a constant threshold. Figure 4.2 shows that the  $R^2$  value becomes lower when the relationship between observed daily rainfall and CCD values is established for combined observations from six stations as compared when the relationship is based on observations from a single station.

**Table 4.1** Performance assessment of rainfall retrieval equations

Station	Equation	RE	RMSE	Rvar
D/Birhan	23.889 CCD-0.8494	0.66	6.82	0.32
	$2 \times 10^{24} \text{ Tmin}^{-10.104}$	0.55	7.00	0.16
D/Sina	35.28+15.55 CCD-0.15 Tmin	0.64	6.59	0.37
	32.959 CCD+4.2181	0.56	10.74	0.32
Adet	$4 \times 10^{27} \text{ Tmin}^{-11.398}$	0.48	10.25	0.54
	72.82+16.81 CCD-0.3 Tmin	0.57	9.92	0.61
Six stations	13.858 CCD+1.727	0.53	5.28	0.22
	$5 \times 10^{35} \text{ Tmin}^{-14.962}$	0.53	5.58	0.71
Adet	54.72+3.42 CCD-0.22 Tmin	0.48	4.60	0.41
	16.147 CCD + 2.4117	0.71	9.59	0.02
Six stations	$6 \times 10^{22} \text{ Tmin}^{-9.4653}$	0.64	9.30	0.11
	44.56+6.95 CCD-0.18 Tmin	0.68	8.10	0.22
Six stations	30.64+12.66 CCD-0.19 Tmin+0.006 Elv	0.62	7.44	0.34

Table 4.1 shows the least square based regression equations and the performance indicators for rainfall estimation based on Tmin and/or CCD as explanatory variables. The performance of the applied regression equations is evaluated in terms of the Relative Error (RE), Root mean Square Error (RMSE) and the Relative variance (Rvar). RE is the ratio of the absolute error to the average of the observed data while Rvar is the ratio of the variance of the estimates to that of the observations. The optimal value for RE is zero and that for Rvar is one. As it is shown in Table 4.1 the errors of the estimates are relatively high and are about half of the averages of the observations. For the stations at D/Birhan and D/Sina, the Rvar and the RMSE become closer to the desired value when the estimates are based on both Tmin and CCD as compared to when only one of the two variables is considered. For the station at Adet, the RMSE becomes smaller when both Tmin and CCD are used, although the Rvar becomes closer to one when only Tmin is used.

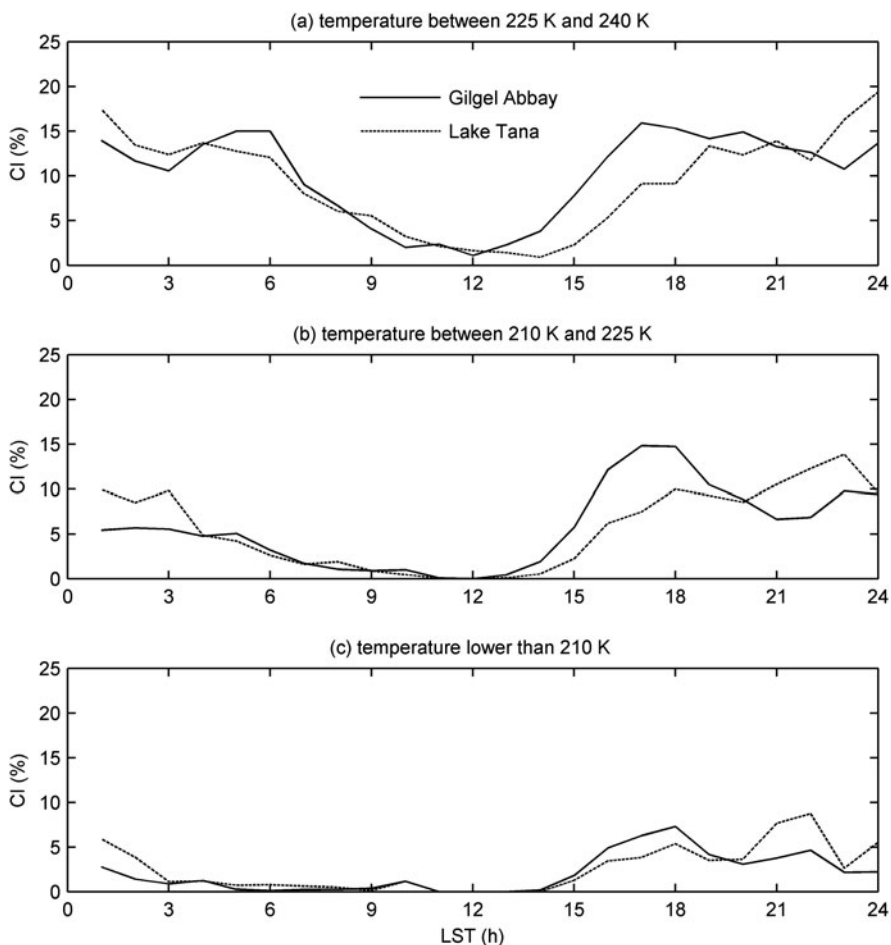
Hydrological modeling requires spatial rainfall inputs that match the scale of the surface spatial units that make up the model domain. This requires formulation of a single relationship that is applicable to all elements that make up the land surface domain. Table 4.2 shows such equations for the Upper Blue Nile basin as based on rainfall observations for the month of August 2005 from six stations. The performance indicator values in Table 4.2 illustrate that formulation of a single best equation for the entire spatial domain requires additional explanatory variables for instance elevation (Elv.) in order to yield better performance.

### 4.3.2 Diurnal Cycle

The diurnal cycle of the convective index over Lake Tana and Gilgel Abbay watershed is shown in Fig. 4.3. Gilgel Abbay is the major contributor to the inflow of Lake

**Table 4.2** Performance assessment of a single best rainfall retrieval equation

Equations	RE	RMSE	Rvar
44.56+6.95 CCD-0.18 Tmin			
D/Sina	0.68	6.79	0.22
D/Sina	0.62	12.17	0.18
Adet	0.52	4.8	0.39
30.64+12.66 CCD-0.19 Tmin+0.0056 Elv			
D/Birhan	0.68	6.69	0.36
D/Sina	0.54	10.68	0.27
Adet	0.55	5.07	0.69

**Fig. 4.3** Diurnal cycle of convective index for various temperature ranges of cloud top surface

Tana (see Wale et al., 2009). Figure 4.3a shows the diurnal cycle of CI for a temperature range between 225 and 240 K that represents low level clouds (LLC). The figure shows that the diurnal cycle of LLC over the land surface of Gilgel Abbay and over the lake area are somewhat different. The number indicates that cloud occurrence peaks at 1700 LST over the land surface and at 2300 LST over the lake. The figure shows that CI values in Gilgel Abbay vary within a small range between 1700 and 2400 LST. Such suggests that LLC probably has long duration in the watershed. Figure 4.3b shows the diurnal cycle of CI for a temperature range between 210 and 225 K which represent middle level clouds (MLC). The values of CI for MLC are much smaller than the values for HLC. The pattern of the CI of Lake Tana for MLC is similar to the pattern for LLC but over Gilgel Abbay, the diurnal cycle of CI for these two types of clouds is somewhat different.

The heaviest rain rates are commonly produced by high level clouds (HLC) that are thick. As such, understanding the diurnal cycle of HLC is important for many applications. Figure 4.3c shows the diurnal cycle of MLC occurrence in terms of CI for temperatures below 210 K. The figure shows that CI values are much smaller than those for MLC and LLC but the pattern is similar to that of the MLC except for small shifts in the time to peak. The CI of HLC peaks at 1800 LST and 2200 LST in Gilgel Abbay and Lake Tana respectively, suggesting the difference in the time of occurrence of heavy rainfall over the land and water surfaces.

#### 4.3.3 Convective Cloud Tracking

In this section, we present the characteristic of the September 18, 2008 cloud that produced extreme rainfall intensity. We used the brightness temperature difference (BTD) which is defined as the difference between the brightness temperature at the 10.8  $\mu\text{m}$  channel and the 6.2  $\mu\text{m}$  channels ( $T_{10.8} - T_{6.2}$ ). Figure 4.4 shows the distribution of the 1-min intensity ( $I_1$ ) and BTD of the (extremely) high that was observed at the Island. The recorded rainfall intensity mostly ranges between 50 and 240 mm/h suggesting that the event had extremely heavy intensity throughout its duration with the highest intensities observed towards the end of the event. The BTD rapidly decreased towards zero when the rainfall commenced and became negative for most of the event duration. Then, the BTD immediately increased when the rainfall ceased.

The September 18 cloud was initiated between 1500 and 1600 LST at a distance of about 90 km from the island, see Figs. 4.5a and 4.6. The minimum Euclidean distance between the centre of mass of the cloud and the location of the rain gauge at the island is about 58 km which is observed at 1930 LST that is about 4 h after the initiation of the cloud. Note that the extreme rainfall at the island was observed between 1800 and 1937 LST. From 1930 onwards, the centroid of the cloud has moved away from the island. As such, although an extreme rainfall is observed at the Island, the center of mass of the cloud has never been over the Island. This suggests the heaviest rainfall presumably occurred at locations other than the Island.

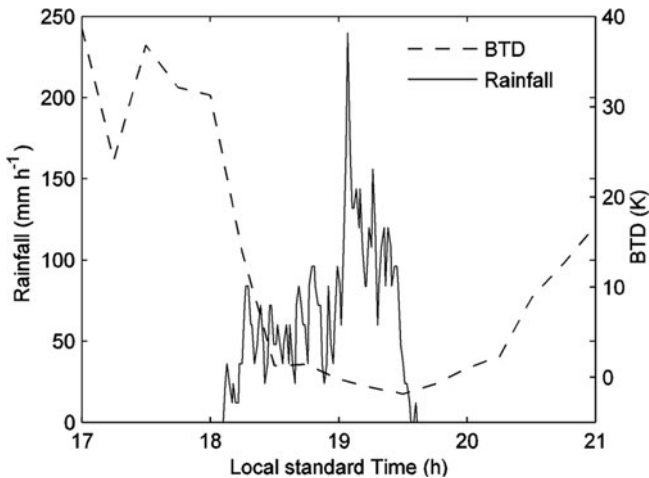


**Fig. 4.4** The 1-min intensity and the brightness temperature difference (BTD) of the extreme rainfall that was observed on September 18, 2008

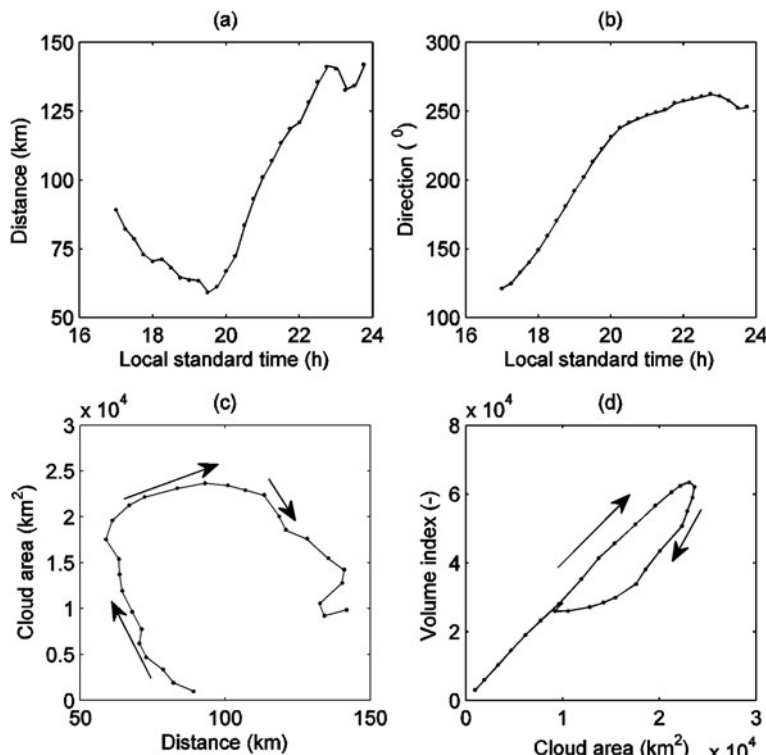


**Fig. 4.5** Characteristics of the September 18, 2008 cloud that produced an extreme rainfall. Note: distance is measured from the island. The direction is expressed in terms of the angle that is measured from a y-axis, with its origin at the rain gauge location, to the line that joins the rain gauge location and the centre of mass of the cloud. Positive angle indicates clockwise direction

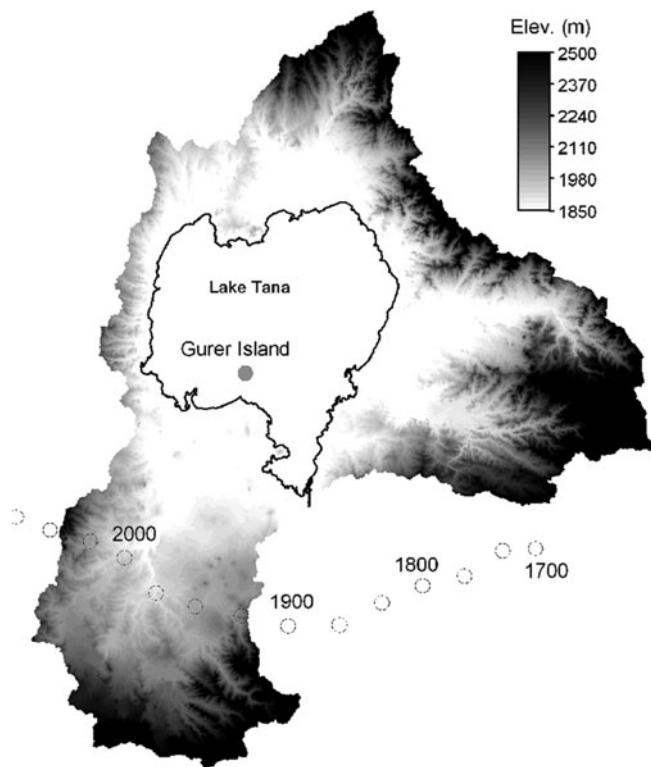


**Fig. 4.6** The movement of the centroid of the cloud system with time. Note that: the centroids are represented by hollow circles and the local standard time for each centroid is also shown

Figure 4.5b shows the direction of the centre of mass of the cloud with respect to the rain gauge location at the island. Initially, the cloud centre was located south-east that is  $120^\circ$  of the island. The cloud centre was located south of the island during the time period, i.e. 18:00–19:37, at which the extreme rainfall was recorded. The cloud moved to south-east of the island afterwards. Both the distance and the direction of the cloud centroid show some trend suggesting that the timing and location of the September 18, 2008 extreme event could have been predicted when applying a technique of cloud tracking.

Figure 4.5c shows that the cloud area increases relatively rapidly as the cloud approaches the island. However, the area increases relatively slowly as the cloud moves away from the island and then it decreases afterwards. This suggests that although the cloud lost some rainwater at the island, its potential to produce heavy rainfall did not decrease immediately. We speculate that water vapour was extracted from the lake area to condense at higher altitude in the cloud to become cloud water. Such feedback causes the cloud to produce high rainfall rates.

The relation between cloud area and volume index is shown in Fig. 4.5d. The relation shows a loop suggesting that the volume increases with an increase in cloud

area during the cloud growth stage. The volume index decreased with a decrease in the cloud area during the cloud dissipation stage. The relation suggests that the volume index indicates the potential of a cloud to produce heavy rainfall however the index can have two values for an equal cloud area with the higher potential occurring during the growth stage. The largest value of the volume index occurred 15 min before the time to the largest value of the cloud area. This indicates that the potential of the cloud to produce heavy rainfall decreases although the cloud area increases towards the end of the growth stage. A similar observation is reported in (Feidas and Cartalis, 2001).

## 4.4 Discussion and Conclusion

We assessed the potential of remote sensing to characterise rainfall and clouds. Three topics are addressed: (i) rainfall estimation, (ii) rainfall detection for diurnal cycle analysis, and (iii) monitoring of extreme rainfall producing clouds.

For rainfall estimation, 2 indexes are derived from TIR observations: Cold Cloud Duration (CCD) and daily minimum temperature (Tmin) of cloud top surface. CCD indicates the duration over which a cloud is observed in a day while Tmin indicates the altitude of a cloud top surface. It is shown that CCD and daily rainfall are directly related but the  $R^2$  values are found to be small and range between 0.15 and 0.32. The relationship between Tmin and daily rainfall are inversely related by a power law relation. The  $R^2$  between Tmin and daily rainfall is relatively large and ranges between 0.42 and 0.61. The analysis indicates that daily rainfall exceeds 10 mm when Tmin of a cloud top surface is lower than 210 K while rainfall amounts of lower than 5 mm are generated by clouds with Tmin of higher than 230 K. Results indicate that formulation of a single best equation of rainfall estimation for the entire spatial domain requires additional explanatory variables, for instance, terrain elevation.

The diurnal cycle of rainfall over Lake Tana and over its major tributary (Gilgel Abbay watershed) is compared using a convective index (CI) that is established using TIR observations. The CI shows a clear difference between the pattern of the rainfall diurnal cycle over the lake and the land surface which suggests a difference in the rain generation mechanisms over the two surfaces. CI peaks in the night over the lake while it peaks in the afternoon over the land surface. The analysis also shows that low level clouds occur much more frequently in the study area than high level clouds.

Although TIR observations are the most commonly used remote sensing observations in rainfall estimation, we showed that brightness temperature difference (BTD) between TIR and WV channels provides additional information about surface rainfall intensities. It is shown that the BTD values rapidly decreases towards zero when the rainfall commences and becomes negative for most of the rain event duration. Then, the BTD value increases directly when the rainfall ceased. Such information is relevant for remote sensing based rainfall estimation.

We used TIR and WV brightness temperatures to monitor the characteristics of a cloud that produced extreme rainfall over Lake Tana. These characteristics are the distance and the direction of the cloud centre of mass with respect to the location of Gurer Island in Lake Tana. The analysis indicates that the heaviest rainfall from the cloud is generated at locations somewhat far from the Island although extreme rainfall is recorded at the Island.

The area covered by the cloud is monitored by using remote sensing observations. The analysis showed that the centre of mass of the cloud increased despite a loss of rain water when the cloud approaches Lake Tana. Such an increase in cloud area suggests the supply of moisture by Lake Tana that enhanced the water content of the cloud. The relationship between the volume index and the cloud area shows that although the potential of the cloud to produce rainfall decreases during the dissipation stage of the cloud, the cloud area still increases.

Overall, the results indicate the potential of remote sensing observations for rainfall studies. Remote sensing can be very helpful in estimating rainfall, assessing diurnal cycle and monitoring heavy rainfall producing clouds. Such potential of remote sensing observations is mainly because the observations are consistently available with spatial continuous coverage.

## References

Arkin PA (1979) The relationship between fractional coverage of high cloud and rainfall accumulations during the GAGE over the B-scale array. *Mon Wea Rev* 107:1382–1387

Arkin PA, Meisner BN (1987) The relationship between large scale convective rainfall and cold cloud over the Western Hemisphere during 1982–1984. *Mon Wea Rev* 115:51–74

Arnaud Y, Desbois M, Maizi J (1992) Automatic tracking and characterization of African convective systems on Meteosat pictures. *J Appl Meteor* 31:443–453

Ba MB, Nicholson SE (1998) Analysis of convective activity and its relationship to the rainfall over the Rift Valley lakes of East Africa during 1983–1990 using meteosat infrared channel. *J Appl Meteor* 37:1250–1264

Barrett EC, Martin DW (1991) The use of satellite data in rainfall monitoring. Academic press, London, 340pp

Barros AP, Kim G, Williams E, Nesbitt SW (2004) Probing orographic controls in the Himalayas during the monsoon using satellite imagery. *Nat Hazards Earth Syst Sci* 4:29–51

Dai A (2001) Global precipitation and thunderstorm frequencies. Part II: diurnal variations. *J Climate* 14:1112–1128

Feidas H, Cartalis C (2001) Monitoring mesoscale convective cloud systems associated with heavy storms using meteosat imagery. *J Appl Meteor* 40:491–512

Gebremichael M, Krajewski WF, Over TM, Takayabu YN, Arkin P, Katayama M (2008) Scaling of tropical rainfall as observed by TRMM precipitation radar. *Atmos Res* 88:337–354

Gebremichael M, Vivoni ER, Watts CJ, Rodríguez JC (2007) Submesoscale spatiotemporal variability of North American monsoon rainfall over complex terrain. *J Climate* 20:1751–1773

Griffith CG, Woodley WL, Grube PG, Martin DW, Stout J, Sikdar DN (1978) Rain estimation from geosynchronous satellite imagery – visible and infrared studies. *Mon Wea Rev* 106:1153–1171

Haile AT, Rientjes THM (2007) Spatio-temporal rainfall mapping from space: setbacks and strengths. Proceedings of the 5th International symposium on Spatial Data Quality SDQ, Modelling qualities in space and time, ITC, Enschede, The Netherlands, 13–15 June, 2007, 9 p

Haile AT, Rientjes THM, Gieske A, Gebremichael M (2009) Rainfall variability over mountainous and adjacent lake areas: the case of Lake Tana basin at the source of the Blue Nile River. *J Appl Meteorol Climatol* 48:1696–1717

Haile AT, Rientjes TH, Gieske A, Gebremichael M (2010) Rainfall estimation at the source of the Blue Nile: a multispectral remote sensing approach. *Int J Appl Earth Obs Geoinf JAG* 12(Suppl. 1):S76–S82

Hong Y, Hsu KL, Sorooshian S, Gao X (2005) Improved representation of diurnal variability of rainfall retrieved from the tropical rainfall measurement mission MW imager adjusted precipitation estimation from remotely sensed information using artificial neural networks PERSIANN system. *J Geophys Res* 110:1–13

Hsu KL, Gao X, Sorooshian S, Gupta HV (1997) Precipitation estimation from remotely sensed imagery using an artificial neural network. *J Appl Meteorol* 36:1176–1190

Huffman GJ, Adler RF, Bolvin DT, Gu G, Nelkin EJ, Bowman KP, Hong Y, Stocker EF, Wolff DB (2007) The TRMM multisatellite precipitation analysis (TMPA): quasi-global, multiyear, combined-sensor precipitation estimates at fine scales. *J Hydrometeorol* 8:38–55

Imaoka K, Spencer RW (2000) Diurnal variation of precipitation over the tropical oceans observed by TRMM/TMI combined with SSM/I. *J Climate* 13:4149–4158

Kidder SQ, Vonder Haar TH (1995) Satellite meteorology: an introduction. Academic Press, New York, 466pp

Levizzani V, Amorati R, Meneguzzo F (2002) A review of satellite-based rainfall estimation methods. European commission project MUSIC report EVK1-CT-2000-00058. 66pp. <http://www.isac.cnr.it/~meteosat/pub.html>

Lovejoy S, Austin GL (1979) The delineation of rain areas from visible and IR satellite data from GATE and mid-latitudes. *Atmos Ocean* 17:77–92

Nesbitt SW, Zipser EJ (2003) The diurnal cycle of rainfall and convective intensity according to the 3 years of TRMM measurements. *J Climate* 16:1456–1475

Ohsawa T, Ueda H, Hayashi T, Watanabe A, Matsumoto J (2001) Diurnal variations of convective activity and rainfall in Tropical Asia. *J Meteor Soc Japan* 79:333–352

Petty GW (1995) The status of satellite-based rainfall estimation over land. *Remote Sens Environ* 51:125–137

Sorooshian S, Hsu KL, Gao X, Gupta HV, Imam B, Braithwaite D (2000) Evaluation of PERSIANN system satellite-based estimates of tropical rainfall. *Bull Am Meteor Soc* 81:2035–2046

Stephens GL, Kummerow CD (2007) The remote sensing of clouds and precipitation from space: a review. *J Atmos Sci* 64:3742–3765

Todd MC, Barrett EC, Beaumont MJ, Green JL (1995) Satellite identification of rain days over the upper Nile River basin using an optimum IR rain/no-rain threshold temperature model. *J Appl Meteorol* 34(12):2600–2611

Tsintikidis D, Georgakakos KP, Artan GA, Tsionis AA (1999) A feasibility study on mean areal rainfall estimation and hydrologic response in the Blue Nile region using METEOSAT images. *J Hydrol* 221:97–116

Tsionis AA, Triantafyllou GN, Geogaakakos KP (1996) Hydrological applications of satellite data 1. Rainfall estimation. *J Geophys Res* 101:26517–26525

Turk FJ, Miller SD (2005) Toward improving estimates of remotely-sensed precipitation with MODIS/AMSR-E blended data techniques. *IEEE Trans Geosci Rem Sens* 43:1059–1069

Wale A, Rientjes THM, Gieske ASM, Getachew HA (2009) Ungauged catchment contributions to Lake Tana's water balance. *Hydrol Process* 23(26):3682–3693

# Chapter 5

## Evaluation of Satellite Rainfall Estimates and Gridded Gauge Products over the Upper Blue Nile Region

Tufa Dinku, Stephen Connor, and Pietro Ceccato

**Abstract** A relatively dense station network over the Ethiopian highlands is used to evaluate the accuracy of some satellite rainfall estimates and gridded raingauge products. The satellite rainfall estimates evaluated are GPCP, CMAP, RFE, TRMM-3B42, and CMORPH. These products are evaluated at monthly, ten-daily, and daily accumulations and spatial resolutions of  $2.5^\circ$ ,  $1^\circ$ ,  $0.5^\circ$  and  $0.25^\circ$  lat/long. The two gridded raingauge analyses evaluated are from the Global Precipitation Climatology Centre and University of East Anglia. These monthly products were evaluated at spatial resolutions of  $2.5^\circ$ ,  $1^\circ$ , and  $0.5^\circ$ . While satellite rainfall estimates at monthly and ten-daily time scale showed good agreements with the reference raingauge data, results for daily accumulations were not as good. However, the daily products performed reasonably well in detecting the occurrence of rainfall. Very good agreements were observed between the gridded raingauge analyses and the reference raingauge data.

**Keywords:** Satellite · Rainfall estimation · Gridded products

### 5.1 Introduction

Rainfall data is the main input into any hydrological model. However, there are two main problems with regards to access to rainfall data over most of Africa. The first problem is that the available station network is very sparse. Second, access to the available data is very limited particularly outside the individual countries. As a result, many researchers use either satellite data or gridded rainfall products, which are freely available from different centers. However, the qualities of these products need to be evaluated. An extensive evaluation of different satellite rainfall estimates at different temporal and spatial scales, and gridded monthly rainfall products at different spatial scales has been performed over the upper Blue Nile basin (Dinku et al.,

---

T. Dinku (✉)

International Research Institute for Climate and Society, The Earth Institute  
at Columbia University, New York, NY, USA  
e-mail: tufa@iri.columbia.edu

2007, 2008a, b). This chapter is a summary of these papers with some more additional analyses. The additional analyses include comparison of the satellite rainfall estimates and the gridded raingauge products.

The satellite products were evaluated in three different groups. The first group consists of monthly products at a spatial resolution of  $2.5^\circ$  lat/long. Here results are presented for the Global Precipitation Climatology Project (GPCP, Huffman et al., 2007; Adler et al., 2003) from the National Aeronautic and Space Administration (NASA), and the National Oceanographic and Atmospheric Administration-Climate Prediction Centre (NOAA-CPC) Merged Analysis (CMAP, Xie and Arkin, 1997; Xie et al., 2007). The second group of the satellite products were evaluated at ten-daily aggregation and spatial resolution of  $1^\circ$  lat/long. Results are summarized for NOAA-CPC African Rainfall Estimation Algorithm (RFE, Herman et al., 1997; Xie et al., 2002), the “TRMM and Other Satellites” product (TRMM-3B42, Huffman et al., 2007), and the CPC morphing technique (CMORPH, Joyce et al., 2004). In third group, the same satellite products are evaluated at daily time scale and spatial resolutions of  $1^\circ$ ,  $0.5^\circ$  and  $0.25^\circ$ .

Results are also presented for two monthly gridded raingauge products at spatial resolutions of  $0.5^\circ$ ,  $1^\circ$  and  $2.5^\circ$ . These products are the Global Precipitation Climatology Centre (GPCC, Fuchs et al., 2007) and a product from the Climate Research Unit at the University of East Anglia (UEA, Mitchell and Jones, 2005) in UK. The GPCC has three different products, which include the monitoring, full-data analysis, and 50-year climatology. Here only the full-data analysis, which uses the most number of gauges, is evaluated. The reader may refer to Dinku et al. (2008b) for the detailed evaluation of the other GPCC products.

## 5.2 Study Region

The study region is located over the Ethiopian highlands (box in Fig. 5.1) and includes the source of the Blue Nile. This region has a very complex topography. The main topographic features of the region are mountain chains, the Blue Nile gorge and part of the East African Rift Valley. Topography plays a significant role in the climate of the region by creating diverse microclimates ranging from hot deserts in the Blue Nile gorge to relatively cold temperature over the Semen Mountains. The main rainy season is June to August, when most of the country receives its rainfall. Part of the validation region also receives rainfall during March to May. Most of the rainfall is associated with the south-north movement of the Inter Tropical Convergence Zone (ITCZ). However, the spatial and temporal distributions of the rainfall over this region are very much modulated by the very complex topography.

### 5.2.1 Raingauge Data

Raingauge data for about 150 stations were obtained from the National Meteorological Agency (NMA) of Ethiopia. The distribution of the raingauge stations used in the current investigation is shown Fig. 5.1. Monthly rainfall data from

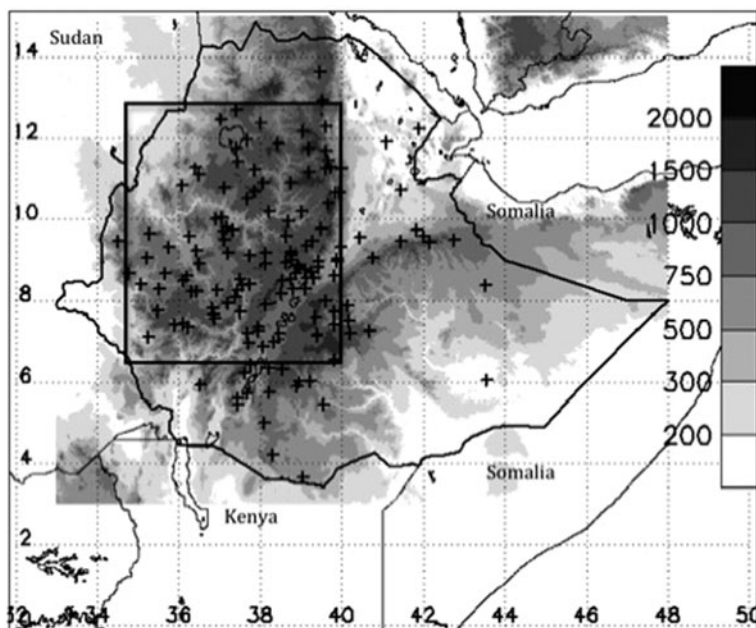


**Fig. 5.1** Geographic location of the study region, the “+” signs represent station locations, while shading shows the elevation. The *dark box* shows stations used for the current validation work

1981 to 2004 were used to evaluate the monthly satellite and gridded products, while data from summer months of 2003 and 2004 were used for evaluating satellite rainfall estimates at daily and ten-daily time scales. The NMA performs routine quality check on their data, but further quality checks were performed to insure the quality of the reference data. The different quality check procedure applied to the rain-gauge data are described in Dinku et al. (2008a, b). After the quality control, the raingauge data were gridded onto regular  $0.1^\circ \times 0.1^\circ$  lat/long grids using climatologically aided interpolation (Willmott and Robeson, 1995). Then the  $0.1^\circ$  pixels were averaged over  $0.25^\circ$ ,  $0.5^\circ$ ,  $1.0^\circ$ , and  $2.5^\circ$  grids for comparison with the satellite estimates and the gridded raingauge products. Only  $0.25^\circ$ ,  $0.5^\circ$ ,  $1.0^\circ$ , and  $2.5^\circ$  grid boxes with at least, 1, 1, 3 and 20 gauges, respectively, were used to evaluate the different products. The minimum number of gauges per grid used here is just intuitive, and was done in order to improve the quality of the reference data.

### 5.2.2 Satellite Data

This section provides brief descriptions of the different satellite rainfall products evaluated here. References are provided for readers interested in more details of the different products. Readers interested in the different aspects of satellite rainfall estimation may also refer to, among many others, Levizzani et al. (2002, 2007) and Gruber and Levizzani (2008).

Five satellite rainfall products are evaluated here. The first two products, GPCP and CMAP, are available at monthly time scale and spatial resolution of  $2.5^{\circ}$  lat/long. The other three products are RFE, TRMM-3B42, and CMORPH. RFE is provided at a spatial resolution  $1.0^{\circ}$ , and daily accumulation, while TRMM-3B42 and CMORPH are available as three-hourly accumulations and spatial resolution of  $0.25^{\circ}$  lat/long. The later three products are selected for presentations here because they are widely used products. These satellite estimates also represent different levels of algorithm sophistication with RFE being a relatively simple one, while 3B42 and CMORPH employ more sophisticated algorithms. The RFE and 3B42 products utilize raingauge data obtained through the Global Telecommunication System (GTS) for adjusting the satellite estimates. However, the use of gauge observations in 3B42 is indirect. The current version of CMORPH does not have any gauge inputs. The other difference among these products is that CMORPH does not include thermal infrared (TIR) rainfall estimates, while TIR rainfall estimates are the main component of the RFE and 3B42 products. Some characteristics of these satellite products are presented in Table 5.1.

The GPCP algorithm combines precipitation estimates from TIR and passive microwave (PM) sensors, and raingauge observations (Huffman et al., 1997; Adler et al., 2003). The main sources of the TIR data are the different Geostationary Meteorological Satellites though data from polar-orbiting satellites are also used to fill in the gaps at higher latitudes. The PM data come mainly from the Special Sensor Microwave Imager (SSM/I). The PM estimates are used to adjust the TIR-based GPI (Global precipitation index) estimates. Then the multi-satellite estimate is adjusted toward the large-scale gauge average for each grid box. The gauge-adjusted multi-satellite estimates are then combined with gauge analysis using a weighted average, where the weights are the inverse error variances of the respective estimates. The current version (V2.1) uses raingauge analyses from GPCC. The GPCC full-data analysis product (Fuchs et al., 2007) is used from 1979 to 2007, while the monitoring product is used thereafter (Huffman et al., 2009). The use of the GPCC full-data analysis product, which contains much more number stations than the other GPCC products (Fuchs et al., 2007) is the main strength of the current version of GPCP.

The CMAP algorithm combines TIR estimates, PM retrievals and raingauge observations (Xie and Arkin, 1997; Xie et al., 2007). The merging technique involves two major steps: first, TIR and PM rain estimates are merged using a

**Table 5.1** Summary of the satellite products evaluated here; the PM and Gauge columns indicate whether the product includes passive microwave or gauge observations

Product	Time aggregation	Space res.	Starting date	PM	Gauge
GPCP	Monthly	$2.5^{\circ}$	1979	Y	Y
CMAP	Monthly	$2.5^{\circ}$	1979	Y	Y
RFE	Daily	$0.10^{\circ}$	1995	Y	Y
TRMM-3B42	3-hourly	$0.25^{\circ}$	1998	Y	Y
CMORPH	3-hourly	$0.08^{\circ}$	2003	Y	N

maximum likelihood approach, where the linear coefficients are inversely proportional to the squares of the local random error of the individual estimate. Raingauge observations are used in the second step to remove biases and are also merged with the product from first step. The implemented blending technique assumes that the combined satellite estimates represent the spatial structure of the precipitation distribution and that there is no bias in gauge observations.

The RFE algorithm combines PM rain retrieval, rainfall estimates from METEOSAT TIR data, and daily rainfall observations from GTS. The TIR algorithm uses a single threshold (235 K) to discriminate between raining and non-raining clouds. This threshold is used to compute cold cloud duration (CCD) from half-hourly TIR observations. Then a single parameter set is used to convert CCD into rain rates.

The TRMM-3B42 product is one of the outputs from the TRMM multi-satellite precipitation analysis (TMPA) algorithm (Huffman et al., 2007). This algorithm combines TIR data from geostationary satellites, PM data from different sources, and GTS gauge reports. The PM sources include TRMM microwave imager (TMI), SSM/I, Advanced Microwave Sounding Unit (AMSU), and Advanced Microwave Sounding Radiometer-Earth Observing System (AMSR-E). The TRMM-3B42 product is created in four steps: (1) the PM estimates are calibrated and combined, (2) TIR precipitation estimated are created using the PM estimates for calibration, (3) PM and TIR estimates are combined, and (4) the data is rescaled to monthly totals whereby gauge observations are also used indirectly.

The CMORPH algorithm (Joyce et al., 2004) is a technique whereby PM rainfall estimates are interpolated in space and time using motion vectors derived from half-hourly TIR observations. This algorithm starts with the time sequence of feature motions from the TIR data, and then this information is used to compute the displacement vector for morphing from one instantaneous microwave estimate to the next. This enables CMORPH to combine the better rainfall estimation accuracy of PM estimates with TIR observations at higher temporal and special resolution. The final output from the CMORPH algorithm is still a PM-only product.

### 5.2.3 *Gridded Gauge Products*

Two gridded raingauge products are compared here. These are GPCC full-data analysis product (GPCC for short), and the product from the Climate Research Unit at the University of East Anglia (UEA). The GPCC also has other products (Fuchs et al., 2007; Schneider et al., 2008). Here we use the full-data analysis, which is a product with the maximum number of raingauge input. The other GPCC products have also been evaluated over the current validation region (Dinku et al., 2008b). The GPCC and UEA products are selected for evaluation here because of their wide use. Also the GPCC products are updated from time to time, though irregularly. Dinku et al. (2008b) have also compared these two products over the current validation region with another similar gridded product.

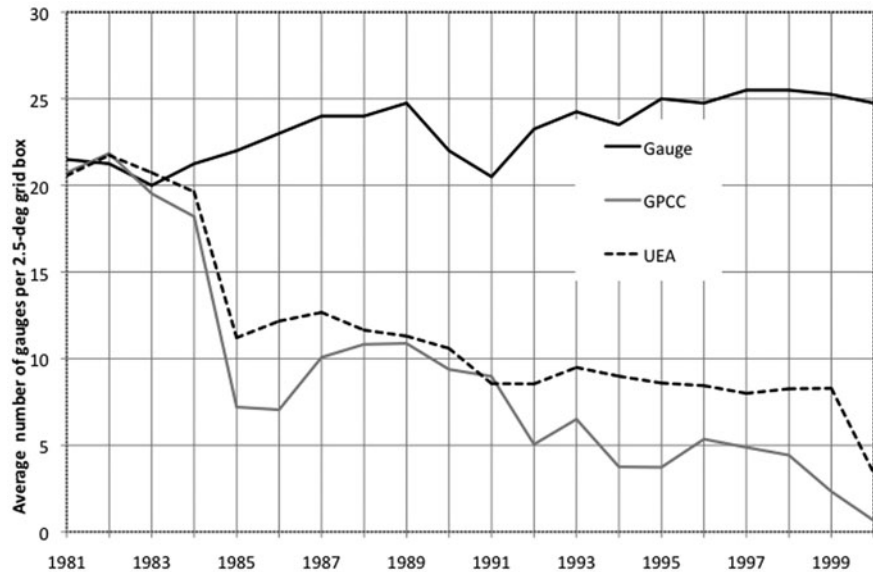


**Fig. 5.2** Average number of gauges per  $2.5^\circ$  grid box for reference data and the two gridded products (modified from Dinku et al., 2008b)

The GPCC full-data product uses significant number of stations (10,000–45,000) from near-real-time and non-real-time data in the GPCC database (Fuchs et al., 2007; Schneider et al., 2008). The GPCC product is updated irregularly, and the current version (V4), covers the period from 1901 to 2007 at spatial resolutions of  $0.5^\circ$ ,  $1^\circ$  and  $2.5^\circ$  (Schneider et al., 2008). The UEA product used here is the CRU TS 2.1 (Mitchell and Jones, 2005). Precipitation is one of the nine climate variables generated by UEA, and it is available at a spatial resolution of  $0.5^\circ$ . Both the GPCC and UEA processing includes rigorous quality checking procedures. The number of gauges used in these products varies significantly for different regions and over different years. The mean number of gauges used by these products between 1981 and 2004 over the current study region is shown in Fig. 5.2. Comparison with the number of gauges used in the reference data set shows that, at least for this region, the products do not have access to all available gauges in a timely manner. And the number of raingauge stations used in the reference data is only a small fraction of the stations managed by NMA.

### 5.3 Evaluation of Gridded and Satellite Rainfall Products

The different rainfall products are evaluated in two groups. The first group consists of monthly accumulations of satellite rainfall estimates (GPCP and CMAP) and gridded raingauge products (GPCC and UAE). The two satellite products

are compared with each other and the gridded products at a spatial resolution of  $2.5^{\circ}$  lat/long. The gridded products are also compared with each other at spatial resolutions of  $1^{\circ}$  and  $0.5^{\circ}$ . The second comparison deals with daily and ten-daily accumulations of satellite rainfall estimates (RFE, 3B42 and CMORPH). The ten-daily products are compared at  $1^{\circ}$  spatial resolution, while the daily products are evaluated at  $0.25^{\circ}$ ,  $0.5^{\circ}$ , and  $1^{\circ}$ .

Standard validation statistics are used to evaluate the different products. These include linear correlation coefficient (CC), multiplicative bias (Bias), mean absolute error (MAE), probability of detection (POD), false alarm ratio (FAR), and Heidke Skill Score (HSS). The description of these statistics is given in different references (e.g. Wilks, 2006) including a good online document at ([http://www.bom.gov.au/bmrc/wefor/staff/eee/verif/verif\\_web\\_page.html](http://www.bom.gov.au/bmrc/wefor/staff/eee/verif/verif_web_page.html)). The CC, Bias, MAE and Eff are used to evaluate the performance of the products in estimating the amount of rainfall, while POD, FAR, and HSS are used only for daily rainfall to asses the rainfall detection capabilities of the satellite products.

Here one may wonder why the gridded reference gauges should be used to evaluate another gridded product (GPCC or UEA). The main advantage of the reference data is that it uses more number of gauges compared to the global products (Fig. 5.2). Additional strengths of the reference data include (Dinku et al., 2008b):

- Monthly rainfall totals of the reference data were constructed from daily values, which helped to avoid the problem of missing data;
- The data were obtained directly from NMA archives, which helped to avoid using data from different sources and problems associated with transmitting data via GTS;
- Local knowledge was used during the rigorous quality checking procedures. This may not be available to the global products; and
- Only grid boxes with raingauges were used for comparison.

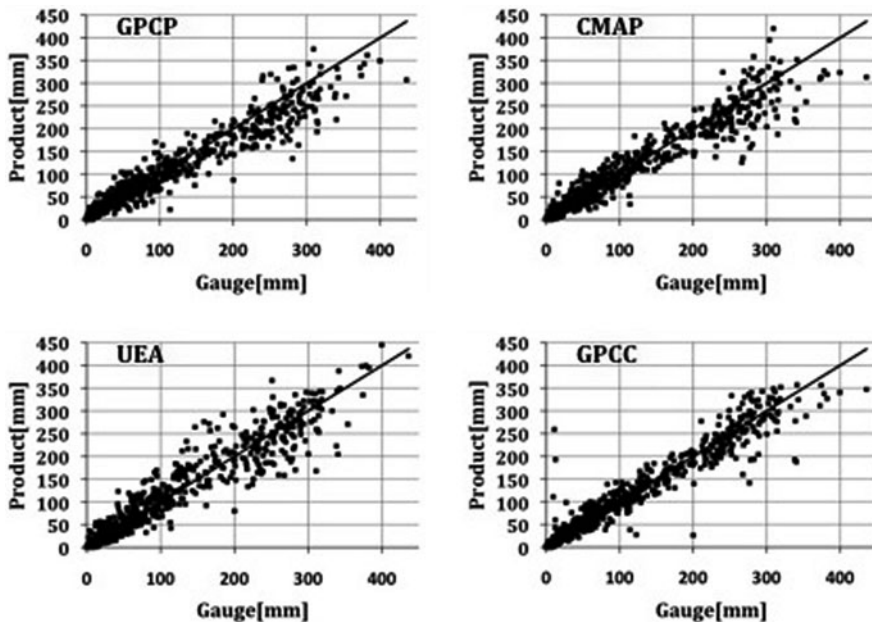
### **5.3.1 Evaluation of Monthly Satellite and Gridded Rainfall Products**

Table 5.2 compares error statistics for the two gridded products and the two satellite estimates at monthly time scale and a spatial resolution of  $2.5^{\circ}$ . All the products exhibit good agreement with the reference raingauge data with high correlations, low biases, low random errors, and good skills (high Eff values). There are no significant differences among the different products except that the satellite estimates exhibit some underestimation. These products are also compared in Fig. 5.3. The satellite products underestimate rainfall over 200 mm while the gridded products do not show any bias. The UEA product has more scatter compared to GPCC, which is also reflected in the MAE values in Table 5.2.

The strength of the satellite products is the better spatial coverage while the gridded products are based on actual raingauge observation. Thus, optimal combination of the two different products may yield a better data product than the individual

**Table 5.2** Comparison of error statistics for the two gridded products (UEA and GPCC) and the two satellite products (GPCP and CMAP) at monthly time scale and a spatial resolution of  $2.5^{\circ}$  lat/long

	UEA	GPCC	GPCP	CMAP
CC	0.95	0.97	0.96	0.96
Bias	1.02	1.00	0.95	0.97
MAE	19.7	15.0	18.7	17.5
Eff	0.91	0.93	0.92	0.92



**Fig. 5.3** Comparison of GPCP, CMAP, UEA, and GPCC products with validation raingauge data at monthly time scale and spatial resolution of  $2.5^{\circ}$

satellite or gridded products. The two satellite products evaluated here already use some raingauge observation to remove biases and then combine the gauge observations with the satellite estimates. However, these satellite products use only data obtained through the Global Telecommunication System (GTS), which is a very small fraction of what is used in the GPCC and UEA products. Thus, it would be very interesting to see what difference it would make if the GPCC product were combined with one of the satellite products. This has already been done for the latest version (V2.1) of GPCP, which incorporates the GPCC full-data product (Huffman et al., 2009). The GPCP product we have already seen is version 2(V2). The two GPCP versions are compared with GPCC in Figs. 5.4 and 5.5 and Table 5.3. The two Figures show that in most cases the latest version (V2.1) of GPCP performs

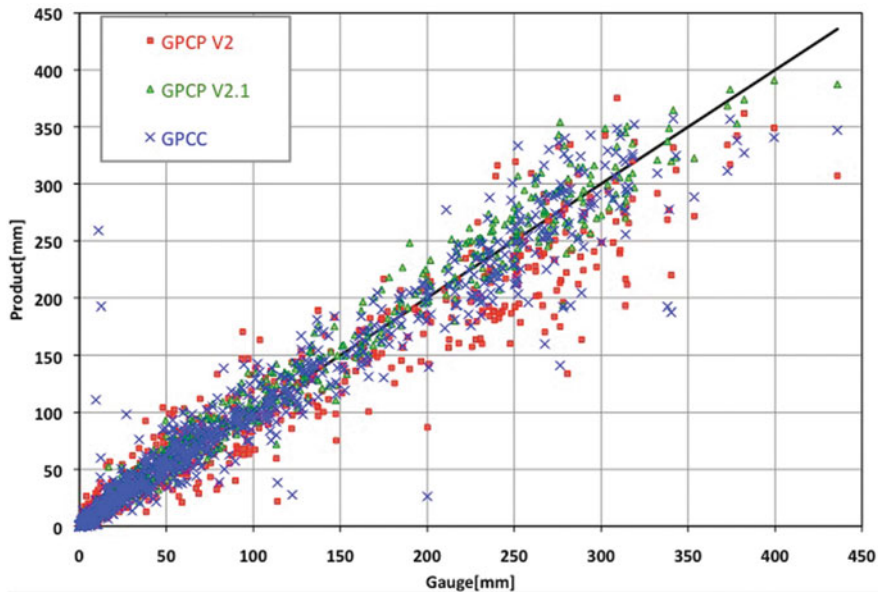


**Fig. 5.4** Comparison of the current (V2.1) and previous (V2) versions the GPCP product and GPCC at monthly accumulation and  $2.5^\circ$  spatial resolution

better than both the previous version (V2) and the gauge-only product (GPCC). To start with, the underestimation of high rainfall rates observed in V2 does not appear in V2.1. In fact V2.1 shows slight overestimation (Table 5.3). The scatter plot shows that GPCP V2 and GPCC have higher random errors compared to GPCP V2.1, which is also reflected in the higher MAE values in Table 5.3. GPCC V2.1 has also higher CC and Eff values. These results show the value of combining the satellite estimates with available raingauge observations.

Figure 5.5 compares the time series of the two GPCP versions and GPCC with the reference raingauge data for two different periods. The top panel represents the period 1981–1983 with relatively more number of gauges used in the GPCC product (Fig. 5.2). The lower panel represents the period 1998–2000, where the GPCC product used less number of stations over Ethiopia. Both panels show that the products do represent the monthly variation of the rainfall reasonably well. As expected, the discrepancy between the reference raingauge data and the products is more during the second period. But the performance of GPCP V2.1 is very good even during the second period, except for the slight overestimation of wet season rainfall amounts. Figure 5.6 compares the performance of the three products for the two main rainy seasons, March to May (MAM) and June to August (JJA). There are no significant differences except that the biases are slightly higher during MAM.

The monthly gridded raingauge products are also available at spatial resolutions of  $1^\circ$  and  $0.5^\circ$  lat/long. Table 5.4 and Fig. 5.7 compare the performance of the two gridded products at  $1.0^\circ$  resolution. The results are similar except that GPCC

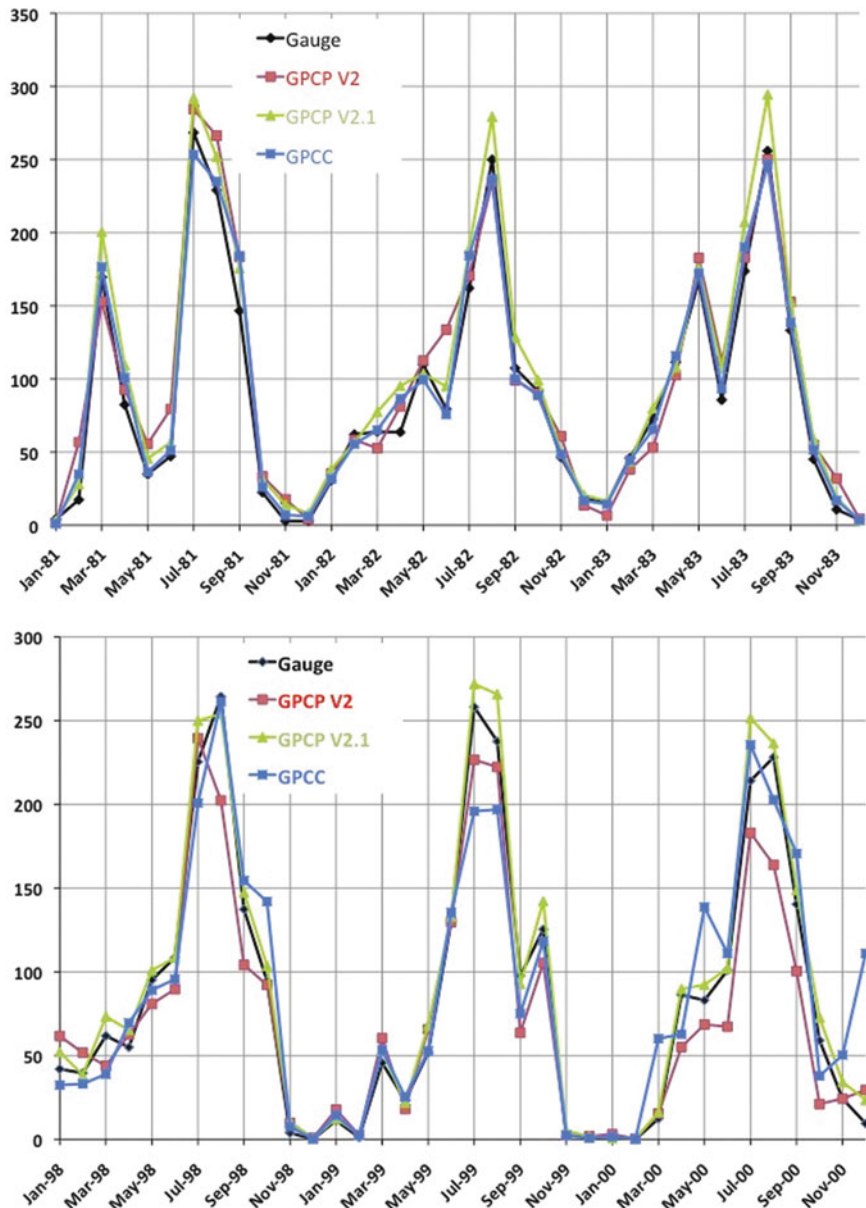


**Fig. 5.5** Time series of area-average rainfall for the different products during two different periods: the number of gauges used in the products is much higher in upper panel as compared to the lower one

**Table 5.3** Comparison of the previous (V2) and current (V2.1) versions of GPCP and the GPCC products at monthly time scale and a spatial resolution of  $2.5^{\circ}$

	GPCP V2	GPCP V2.1	GPCC
CC	0.96	0.99	0.96
Bias	0.95	1.05	1.00
MAE	18.7	11.0	15.0
Eff	0.92	0.98	0.93

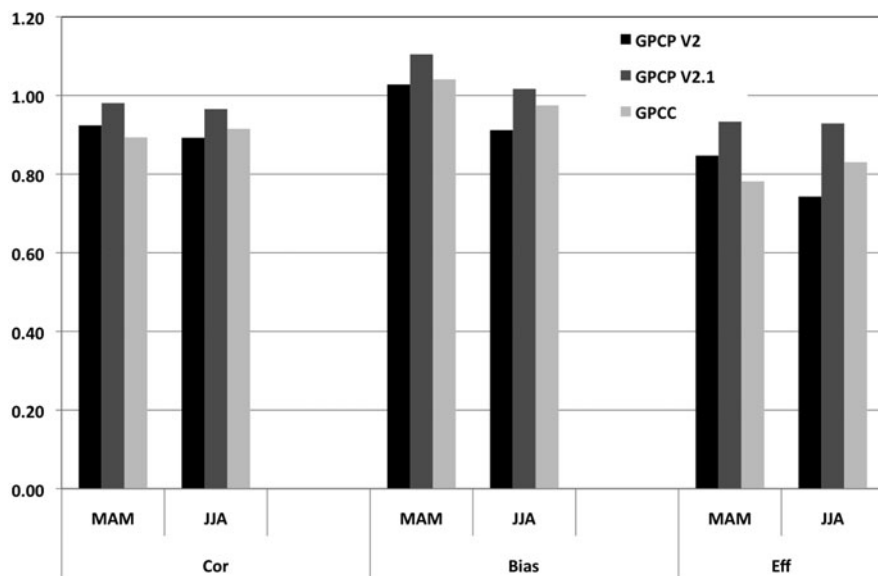


**Fig. 5.6** Comparison of the correlation coefficient, bias, and Eff statistics for the different products and for two rainy seasons (March to May (MAM), and June to August (JJA))

exhibits slightly lower random error and better skill. Figure 5.8 compares the time series of different statistics (correlation, Efficiency, and MAE) for UAE and GPCC. This comparison is done for a single  $1^{\circ} \times 1^{\circ}$  grid with a maximum number of stations; thus, it may not represent the whole region. The first observation is that for this specific pixel GPCC consistently outperforms UAE. The second observation is that though the performances of the products seem to vary from year to year, there are no significant trends in correlation and Eff. The random error (MAE) does show an increasing trend, and all values for the year 2000 are bad particularly for GPCC. This is because of the small number of gauges used in the products (Fig. 5.2). The evaluation of the UAE and GPCC products at a spatial resolution of  $0.5^{\circ}$  is presented in Table 5.5 and Fig. 5.9. Again GPCC has a slightly better performance. As expected, the accuracy of the products has deteriorated compared to results at the coarser resolutions. The scatter in Fig. 5.9 is wider compared to those in Figs. 5.3 and 5.7. The statistics in Tables 5.2 and 5.4 are also better than those in Table 5.5.

**Table 5.4** Comparison of UAE and GPCC products at spatial resolution of  $1^{\circ}$

	UEA	GPCC
CC	0.91	0.92
Eff	0.81	0.84
Bias	1.02	0.99
MAE	28.3	21.9

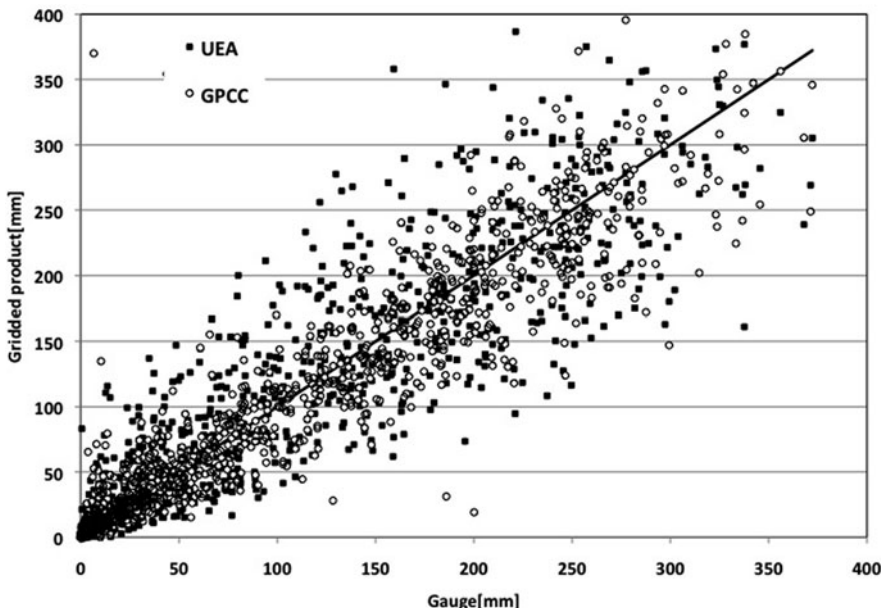


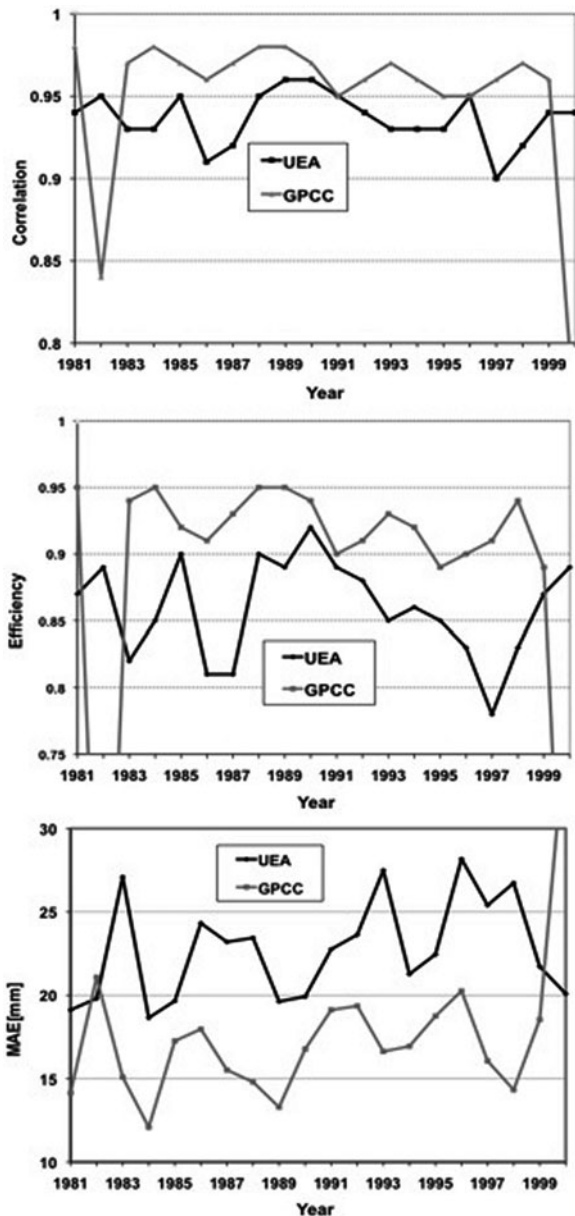
**Fig. 5.7** Scatter plot comparing the performance of UAE and GPCC with respect to the reference data at a spatial resolution of  $1.0^{\circ}$

But the differences are larger between results for  $2.5^{\circ}$  and  $1.0^{\circ}$  resolutions than between  $1.0^{\circ}$  and  $0.5^{\circ}$  resolutions, which corresponds to the differences in spatial resolutions.

### 5.3.2 Evaluation of Ten-Daily and Daily Satellite Rainfall Products

Three satellite products are evaluated at different spatial and temporal resolutions. First, 10-day (dekadal) totals are evaluated at spatial resolution of  $1.0^{\circ}$  lat/long. Then daily estimates are compared at spatial resolutions of  $0.25^{\circ}$ ,  $0.5^{\circ}$ , and  $1^{\circ}$ . The satellite products evaluated in this section are RFE, CMORPH, and TRMM-3B42 (3B42 for short). The evaluation of ten-daily estimates at  $1^{\circ}$  spatial resolution is presented in Table 5.6 and Figs. 5.10 and 5.11. The CMORPH and 3B42

**Fig. 5.8** Year-to-year variations of the correlation coefficient, bias and MAE statistics for the UEA and GPCC products at  $2.5^{\circ}$  spatial resolution



estimates exhibit good performance with good correlation coefficients, low biases, and good skills (Table 5.6). The random error increases with rainfall amount (Fig. 5.10). Though not as good as the monthly aggregations, the satellite estimates do capture the decadal variation of the rainfall (Fig. 5.11). On the other hand, the

**Table 5.5** Comparison of UAE and GPCC products at spatial resolution of  $0.5^\circ$

Error Stat for $0.5^\circ$		
	UEA	GPCC
CC	0.89	0.90
Eff	0.78	0.80
Bias	1.02	0.99
MAE	47.4	44.6

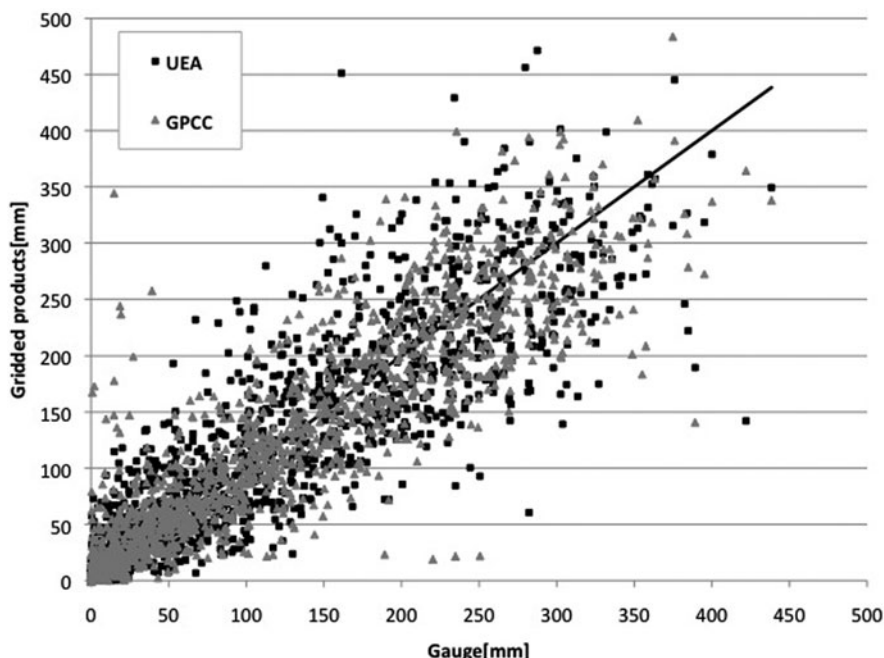


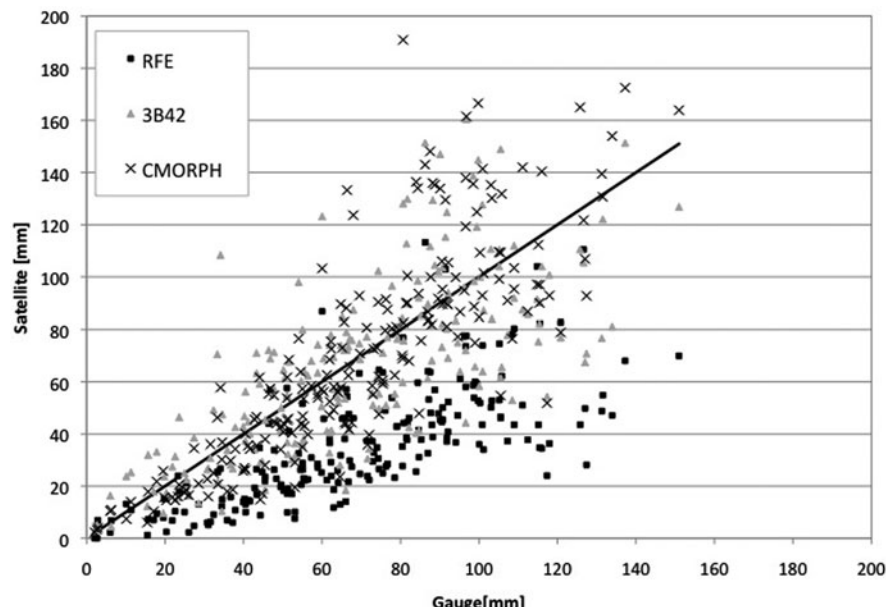
**Fig. 5.9** Comparing the performances of UEA and GPCC gridded products at a spatial resolution of  $0.5^\circ$

performance of RFE is very poor. Both Table 6 and Figs. 5.10 and 5.11 show severe underestimation by RFE. Table 5.6 also shows that RFE does not seem to have any skill (negative Eff values). The problem with RFE is the fixed temperature threshold used in the algorithm and that fact that the validation region is dominated by warm orographic rainfall process (Dinku et al., 2008a). The CMORPH product shows the best performance with high correlation and Eff values, low bias values (Table 5.6) and better correspondence with gauge in Figs. 5.10 and 5.11.

The comparison of daily satellite rainfall estimates at spatial resolutions of  $0.25^\circ$ ,  $0.5^\circ$  and  $1.0^\circ$  lat/long is presented in Fig. 5.12. The upper panel uses correlation coefficient and bias statistics to assess the capability of the different products

**Table 5.6** Validation satellite rainfall estimates at ten-daily accumulation and spatial resolution of 1°

	RFE	3B42	CMORPH
CC	0.72	0.72	0.83
Bias	0.52	0.95	1.01
RMS (%)	57.43	35.40	32.76
EFF	-0.63	0.38	0.47

**Fig. 5.10** Comparison of RFE, 3B42 and CMORPH at ten-daily accumulation and spatial resolution of 1°

to estimate rainfall amount, while the lower panel uses POD, FAR and HSS to assess how good the products are in detecting rainfall. All the statistics, except bias, improve with more spatial averaging (coarser resolution). The improvement is more so for CC and FAR. The correlation coefficients show poor agreement between the satellite estimates and the raingauge measurements. All products underestimate rainfall amount with sever underestimation by RFE. However, all the products, including RFE, show good skill in detecting the occurrence of rainfall. The POD values range from 73 to 82% at 0.25° resolution, and 76–89% at 1°. The FAR values are low at all the three resolutions. The HSS values also show that the skill of the satellite rainfall products in detecting rainfall occurrence is much better than random chance. Again the CMORPH exhibits the best performance while RFE's performance is the poorest for the current validation region.

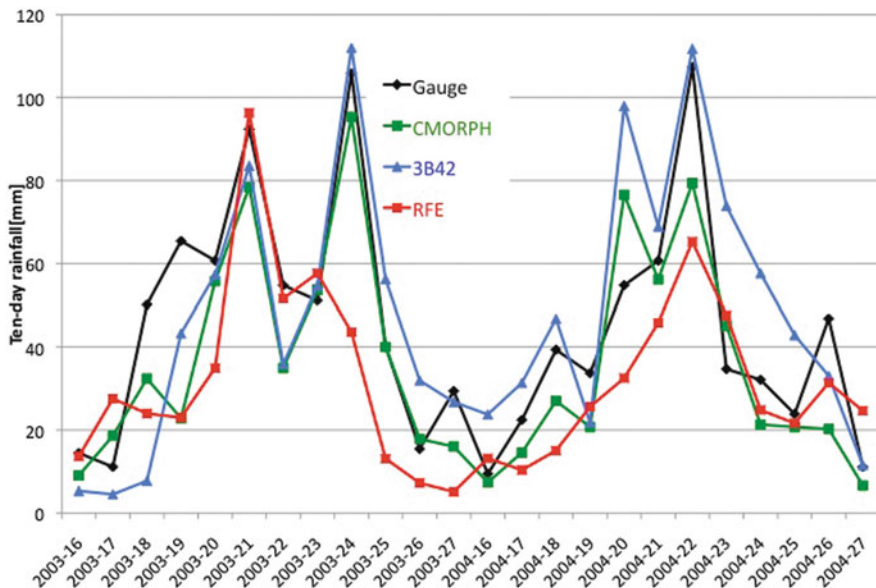


**Fig. 5.11** Comparison of ten-daily variation of the satellite rainfall estimates with the reference raingauge data for a  $1^\circ \times 1^\circ$  grid box. The horizontal axis represents dekads (10- or 11-day periods) from dekad 16 (June 1st dekad) to dekad 27 (August 3rd dekad) for 2003 and 2004

## 5.4 Summary and Conclusions

Five satellite rainfall estimates and two gridded raingauge products were evaluated over the upper Blue Nile basin. The validation region is located over part of the Ethiopian highlands. The evaluated satellite rainfall estimates were GPCP, CMAP, RFE, TRMM-3B42, and CMORPH. The GPCP and CMAP products were evaluated at monthly time scale and spatial resolution of  $2.5^\circ$ , while the rest of the satellite products were evaluated at ten-daily, and daily accumulations and spatial resolutions of  $1^\circ$ ,  $0.5^\circ$  and  $0.25^\circ$  lat/long. The two gridded rainfall products (GPCC UEA) were compared with the reference gauge data and with GPCP and CMAP at monthly accumulation and spatial resolution of  $2.5^\circ$ . These two gridded products were also compared with the reference gauge data at spatial resolutions of  $1.0^\circ$  and  $0.5^\circ$ .

The performances of GPCP and CMAP were very good with high correlation coefficient (0.96) and very good skill ( $Eff = 0.92$ ). The performances of TRMM-3B42 and CMORPH were reasonably good at ten-daily time scale. At daily time scale, these products are good only in detecting the occurrence of rainfall, and poor in estimating rainfall amounts. The RFE product performed very poorly both at ten-daily and daily time scales. The poor performance was ascribed to RFE's fixed temperature threshold, which does not take orographic rainfall into account. Good agreements were observed between the gridded products and the reference rain-gauge data with average correlation coefficients of 0.99, 0.92, and 0.90 at spatial

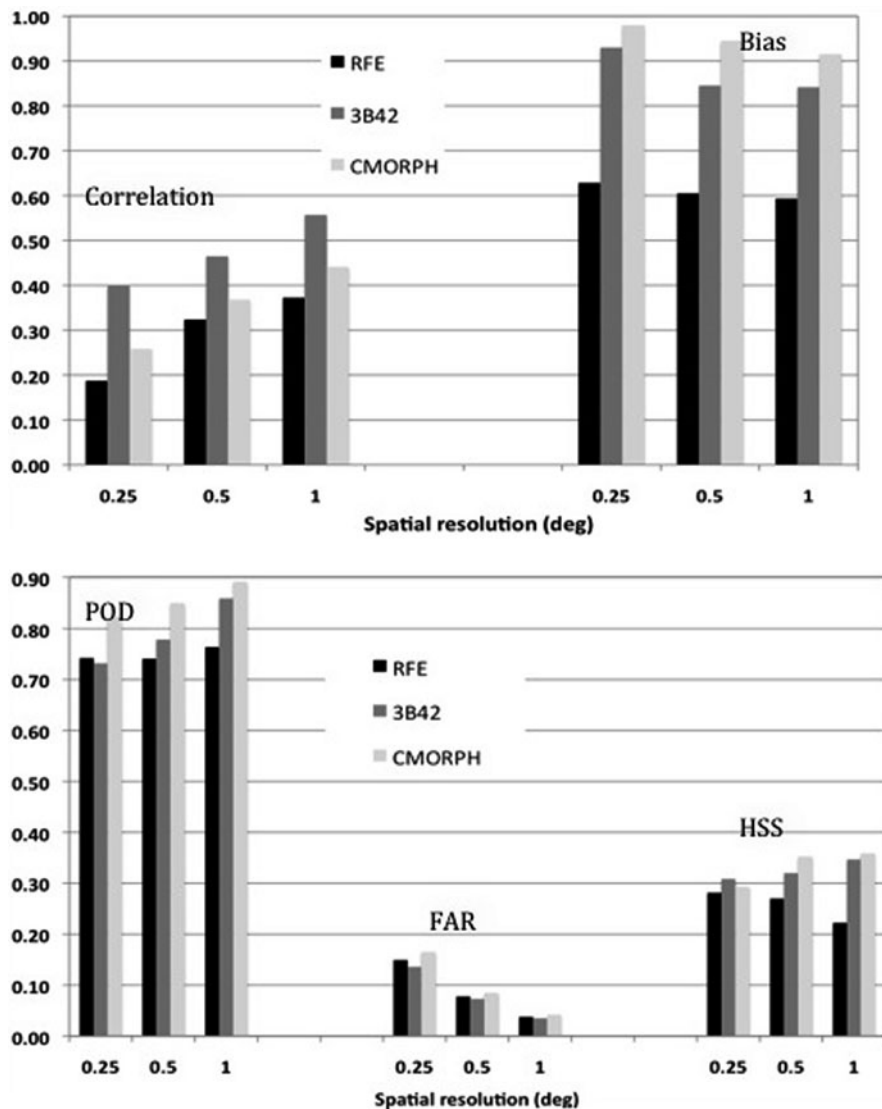


**Fig. 5.12** Comparison of daily satellite rainfall estimates at spatial resolutions of  $0.25^{\circ}$ ,  $0.5^{\circ}$  and  $1.0^{\circ}$  lat/long. The upper panel uses correlation coefficient and bias statistics to assess the capability of the different products in estimating rainfall amount, while the lower panel uses POD, FAR and HSS to assess how good the products are in detecting the occurrence of rainfall

resolutions of  $2.5^{\circ}$ ,  $1.0^{\circ}$ , and  $0.5^{\circ}$ , respectively. The skills of the two products were also very good with average Eff values of 0.92, 0.83, and 0.79 at spatial resolutions of  $2.5^{\circ}$ ,  $1.0^{\circ}$ , and  $0.5^{\circ}$ , respectively. There were no significant differences between the monthly satellite estimates and the gridded raingauge products.

Comparison of the current version of GPCP with its previous version and the GPCC product has shown that combining satellite estimates and gridded raingauge products could yield a more accurate data product. As many countries in Africa have much more stations than the maximum number of stations used in the gridded products, these could be used to improve the accuracy satellite estimates (including ten-daily and daily estimates) over the individual countries. There is an ongoing project in Ethiopia to do just that. Here all available gauges are used for calibrating a selected satellite algorithm and then blending with the satellite estimate. The final product will be a 30-year time series of blended rainfall product at ten-daily time scale and spatial resolution of 10 km.

**Acknowledgements** This work is funded by a grant/cooperative agreement from the National Oceanic and Atmospheric Administration, NA050AR4311004. The views expressed herein are those of the author(s) and do not necessarily reflect the views of NOAA or any of its sub-agencies.

We gratefully acknowledge the National Meteorological Agency of Ethiopia for providing us with all the rain gauge data free of any charges.

## References

Adler RF, Huffman GH, Chang A, Ferraro R, Xie P, Janowiak J, Rudolf B, Schneider U, Curtis S, Bolvin D, Gruber A, Susskind J, Arkin PA, Nelkin E (2003) The version-2 global precipitation climatology project (GPCP) monthly precipitation analysis (1979–present). *J Hydrometeorol* 4:1147–1167

Dinku T, Ceccato P, Grover-Kopec E, Lemma M, Connor SJ, Ropelewski CF (2007) Validation of satellite rainfall products over East Africa's complex topography. *Int J Rem Sens* 28(7): 1503–1526

Dinku T, Chidzambwa S, Ceccato P, Connor SJ, Ropelewski CF (2008a) Validation of high-resolution satellite rainfall products over complex terrain in Africa. *Int J Rem Sens* 29(14):4097–4110

Dinku T, Connor SJ, Ceccato P, Ropelewski CF (2008b) Intercomparison of global gridded rainfall products over complex terrain in Africa. *Int J Climatol* 28:1627–1638

Fuchs T, Schneider U, Rudolf B (2007) Global precipitation analysis products of the GPCC. Available online at: [gpcc.dwd.de](http://gpcc.dwd.de)

Gruber A, Levizzani V (2008) Assessment of global precipitation products, WMO/TD-NO. 1430. Available online at: <http://www.isao.bo.cnr.it/~meteosat/papers/AssessmentGlobalPrecipitation-2008.pdf>

Herman A, Kumar VB, Arkin PA, Kousky JV (1997) Objectively determined 10-day African rainfall estimates created for famine early warning. *Int J Rem Sens* 18(10):2147–2159

Huffman GH, Adler RF, Arkin PA, Chang A, Ferraro R, Gruber G, Janowiak J, McNab A, Rudolf B, Schneider U (1997) The global precipitation climatology project (GPCP) combined precipitation data set. *Bull Am Meteorol Soc* 78:5–20

Huffman GJ, Adler RF, Bolvin DT, Gu G, Nelkin EJ, Bowman KP, Hong Y, Stocker EF, Wolf DB (2007) The TRMM multisatellite precipitation analysis (TMPA): quasi-global, multiyear, combined-sensor precipitation estimates at fine scales. *J Hydrometeorol* 8:38–55

Huffman GJ, Adler RF, Bolvin DT, Gul G (2009) Improving the global precipitation record: GPCP Version 2.1. *Geophys Res Lett* 36:L17808

Joyce RJ, Janowiak JE, Arkin PA, Xie P (2004) CMORPH: a method that produces global precipitation estimates from passive microwave and infrared data at high spatial and temporal resolution. *J Hydrometeorol* 5:487–503

Levizzani V, Amorati R, Meneguzzo F (2002) A review of satellite-based rainfall estimation methods, Consiglio Nazionale delle Ricerche Istituto di Scienze dell'Atmosfera e

del Clima. Available online at. <http://www.isao.bo.cnr.it/~meteosat/papers/MUSIC-Rep-Sat-Precip-6.1.pdf>

Levizzani V, Bauer P, Turk JF (eds) (2007) Measuring precipitation from space: EURAINSAT and the Future. Springer, Netherlands, 724pp

Mitchell TD, Jones PD (2005) An improved method of constructing a database of monthly climate observations and associated high-resolution grids. *Int J Climatol* 25:693–712. DOI:10.1002/joc.1181

Schneider U, Fuchs T, Meyer-Christoffer A, Rudolf B (2008) Global precipitation analysis products. Available at. [gpcc.dwd.de](http://gpcc.dwd.de)

Wilks DS (2006) statistical methods in the atmospheric sciences. Academic Press, Burlington (USA) 627pp

Willmott CJ, Robeson SM (1995) Climatologically aided interpolation (CAI) of terrestrial air temperature. *Int J Climatol* 15(2):221–229

Xie P, Arkin PA (1997) Global precipitation: a 17-year monthly analysis based on gauge observations, satellite estimates, and numerical model outputs. *Bull Am Meteorol Soc* 78:2539–2558

Xie P, Arkin PA, Janowiak JE (2007) CMAP: the CPC merged analysis of precipitation. In: Levizzani et al (eds) Measuring precipitation from space. Springer, Netherlands, 724pp

# Chapter 6

## Are Satellite-Gauge Rainfall Products Better than Satellite-Only Products for Nile Hydrology?

Menberu M. Bitew and Mekonnen Gebremichael

**Abstract** The objective of this study is to compare the performances of two rainfall products (with resolutions of 3-h,  $0.25^\circ \times 0.25^\circ$ ) developed by the Tropical Rainfall Measuring Mission (TRMM) Multi-satellite Precipitation Analysis (TMPA) method: TMPA 3B42RT (a real-time version that does not include any rain gauge data) and TMPA 3B42 (a research version that combines TMPA 3B42RT with global rain gauge data). These products are separately used as input into the SWAT hydrological model to simulate daily streamflow for two adjoining watersheds (Koga with drainage area of  $299 \text{ km}^2$ , and Gilgel Abay with a drainage area of  $1,656 \text{ km}^2$ ) in the Ethiopian part of the Nile basin, and the simulations are then compared to observed streamflow. Results turn the conventional notion on its head: the satellite-only TMPA 3B42RT products are found to be much better than the satellite-gauge TMPA 3B42 products in terms of their ability in reproducing daily streamflow. Nile hydrologist are advised to use TMPA 3B42RT over TMPA 3B42. Algorithm developers are advised to take a deeper look into their bias adjustment techniques especially in mountainous topography and rain gauge sparse regions.

**Keywords** Satellite rainfall · TMPA · SWAT · Uncertainty

### 6.1 Introduction

The growing availability of high resolution satellite rainfall products is making them an alternative source of rainfall data for rainfall-runoff modeling, especially in regions such as the Nile basin where ground-based rainfall measuring instruments are lacking. The concept behind the high resolution satellite rainfall algorithms is to combine information from the more accurate (but infrequent) microwave (MW)

---

M.M. Bitew (✉)

Department of Civil and Environmental Engineering, University of Connecticut, Storrs, CT, USA  
e-mail: menberu@engr.uconn.edu

with the more frequent (but indirect) infrared (IR) to take advantage of the complementary strengths. The combination has been done in a variety of ways leading to a variety of satellite rainfall products. Probably the most popular products are derived based on the Tropical Rainfall Measuring Mission (TRMM) Multi-satellite Precipitation Analysis (TMPA; Huffman et al., 2007) method developed at the National Aeronautics and Space Administration (NASA) Goddard Space Flight Center (GSFC). The TMPA rainfall products, covering the global latitude belt 50°S–50°N at a high resolution (3-h,  $0.25^\circ \times 0.25^\circ$ ), are available in two versions: a real-time version (TMPA 3B42RT, or 3B42RT for short) and a gauge-adjusted post-real-time research version (TMPA 3B42, or 3B42 for short). The main difference between the two versions is the use of monthly rain gauge data for bias adjustment in the 3B42 version. The 3B42 products are released 10–15 days after the end of each month, and the 3B42RT are released about 9 h after overpass.

Given a variety of satellite rainfall products, an important question users often face is which product(s) to use. Herein, our focus is on assessment of the added value, or its lack, from incorporating rain gauge information into the 3B42 product relative to the 3B42RT. Very recently, Habib et al. (2009) compared the performances of 3B42 and 3B42RT rainfall estimates during six heavy rainfall events in Louisiana, United States, by using rainfall data from a dense rain gauge network and weather radar as a ground reference. They reported that the 3B42 product had better performance than the 3B42RT, and that both products underestimated large rain rates. Nonetheless, there is a concern that the improved accuracy of 3B42 over 3B42RT is attributable to the reasonably dense rain gauge network of the United States, and that similar level of improvement may not be achieved in many parts of the world where dense rain gauge networks do not exist.

Our objective is to compare the performances of 3B42 and 3B42RT products in a rain gauge sparse region, with the goal of providing insight to the user community on the appropriate satellite rainfall product for hydrological applications and to the algorithm developers on the consequence of incorporating rain gauge data into satellite rainfall products where such rain gauge data are sparse. Our approach is to use 3B42 and 3B42RT rainfall estimates separately as inputs in the hydrological modeling of two watersheds with drainage areas of  $299 \text{ km}^2$  (Koga) and  $1,656 \text{ km}^2$  (Gilgel Abay) in the mountainous part of the Nile basin in Ethiopia, and compare the simulations to the observed streamflow. The hydrologic model chosen for this study is the Soil and Water Assessment Tool (SWAT), which is popular freely available software with comprehensive functionalities.

## 6.2 Data and Method

### 6.2.1 Study Region

The study region consists of two gauged adjoining watersheds located in the mountainous part of the Nile basin in Ethiopia (Fig. 6.1): Koga has a drainage

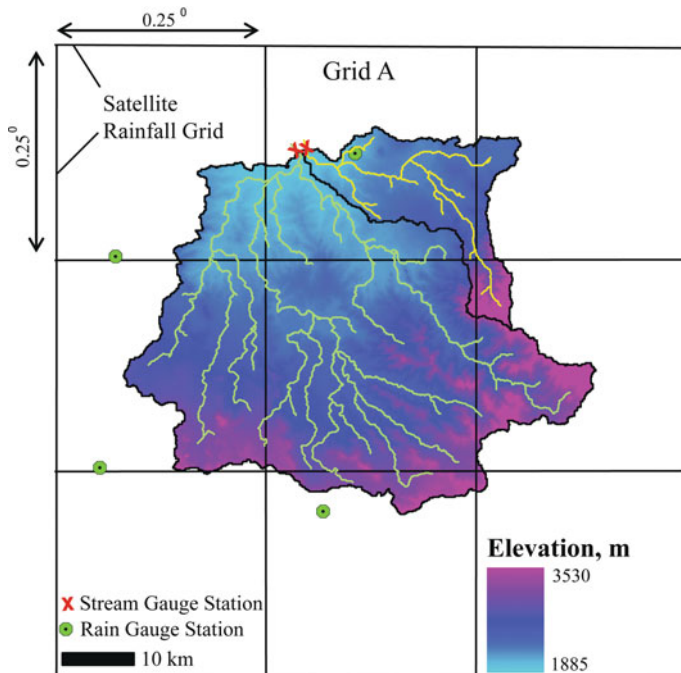


**Fig. 6.1** Koga and Gilgel watersheds in the mountainous part of the Nile basin in Ethiopia: topographic elevation, 3B42 and 3B42RT grids, and stream gauge location

area of  $299 \text{ km}^2$  and is located within  $37^{\circ}2'E - 37^{\circ}20'E$  and  $11^{\circ}8'N - 11^{\circ}25'N$ , Gilgel Abay has a drainage area of  $1,656 \text{ km}^2$  and is located within  $36^{\circ}48'E - 37^{\circ}24'E$  and  $10^{\circ}56'N - 11^{\circ}23'N$ . The climate is semi-humid with a mean annual rainfall of 1,300 mm, more than 70% of which falls in the summer monsoon season. The watersheds have complex topography with elevations ranging from 1,880 m.a.s.l. to 3,530 m. Land use is dominated by cropland and grassland, and soil is predominantly fine-textured.

### 6.2.2 SWAT Hydrologic Model

SWAT, developed by the United States Department of Agriculture (USDA) – Agricultural Research Service (ARS) (Arnold et al., 1998), is a continuous, semi-distributed hydrologic model that runs on a daily time step. Over 250 peer-reviewed published articles have reported SWAT-related research and applications worldwide (Gassman et al., 2007). SWAT requires data on soil, land use and elevation to drive flows and direct sub-watershed routing. While these data may be spatially distributed, SWAT lumps the parameters into hydrologic response units (HRUs),

effectively ignoring the underlying spatial distribution. HRUs are defined by combinations of land cover and soil combinations. The daily water budget in each HRU is computed based on daily precipitation, runoff, evapotranspiration, percolation, and return flow from the subsurface and groundwater flow. Runoff volume in each HRU is computed using the Soil Conservation Service (SCS) curve number method (SCS, 1986). A complete description of the SWAT model can be found in Arnold et al. (1998). Inputs required in SWAT modeling are data on elevation, soil, land use, and meteorology. We obtained elevation data from the 30-m USGS NED digital elevation model dataset, soil texture from the FAO East Africa dataset, land use from the Ethiopian Woody Biomass Inventory Strategic Planning Project, and meteorological data from the nearby meteorological station. We obtained rainfall data from satellite rainfall estimates and rain gauge measurements.

Automatic calibration of all the SWAT model parameters could be time consuming and less practical (Eckhardt and Arnold, 2001). In order to reduce the number of calibration parameters, we performed sensitivity analysis using the LH-OAT method available within SWAT. The LH-OAT method combines the Latin Hypercube (LH) sampling method with the One-factor-At-a-Time (OAT) method (van Griensven et al., 2006). We found nine significantly sensitive parameters, which are shown ranked in their descending order of sensitivity in Table 6.1. Following the identification of the most sensitive parameters, we conducted calibration (automatic at first and then manual) of these parameters using data from 2003 to 2004. Our objective function was to maximize the Nash-Sutcliffe efficiency between simulated and measured daily streamflow.

**Table 6.1** Output of sensitivity analysis of SWAT model parameters in terms of order of sensitivity. The rank shows order of sensitivity, with 1 being most sensitive

Parameter type	Model parameter	Variable	Unit	Ranking	
				Koga	Gilgel Abay
Routing	Hydraulic conductivity of main channel alluvium	CH_K2	mm/h	1	5
Groundwater	Base flow alpha factor	Alpha_BF	1/day	2	1
HRU	Curve number	CN2	—	3	2
Basin	Surface runoff lag coefficient	Surlag	—	4	8
Routing	Manning's "n" value for main channel	CH_N2	—	5	9
HRU	Soil hydraulic conductivity	Sol_K	mm/h	6	
HRU	soil evaporation compensation factor	ESCO	—	7	
HRU	Maximum canopy storage	canmx	—	8	6
Groundwater	Deep aquifer percolation fraction	Rchrg_dp	—		3
Groundwater	Groundwater delay	Gw_delay	day		4
Groundwater	Threshold depth of water in the shallow aquifer for return flow to occur	Gwqmn	Mm		7

### 6.2.3 Performance Statistics

We conducted model performance evaluations based on comparison of simulated and observed streamflow hydrographs through the following statistics: relative bias (Rbias), Nash-Sutcliffe efficiency (NSE), and coefficient of determination ( $R^2$ ):

$$Rbias = \frac{\sum_{i=1}^n [(SIM_i) - OBS_i]}{\sum_{i=1}^n OBS_i},$$

$$NSE = 1 - \left[ \frac{\sum_{i=1}^n (SIM_i - OBS_i)^2}{\sum_{i=1}^n (OBS_i - \overline{OBS})^2} \right],$$

$$R^2 = \left[ \frac{\sum_{i=1}^n (SIM_i - \overline{SIM})(OBS_i - \overline{OBS})}{\sqrt{\sum_{i=1}^n (SIM_i - \overline{SIM})^2} \sqrt{\sum_{i=1}^n (OBS_i - \overline{OBS})^2}} \right]^2,$$

where SIM is the simulated daily streamflow, OBS is the observed daily streamflow,  $n$  is the total number of pairs of simulated and observed data, and the bar indicates average value over  $n$ . NSE indicates how well the plot of the observed value versus the simulated value fits the 1:1 line, and ranges from  $-\infty$  to 1, with higher values indicating better agreement (Legates and McCabe, 1999).  $R^2$  measures the variance of observed values explained by the simulated values.

## 6.3 Results and Discussion

### 6.3.1 Comparison of Rainfall Inputs

We begin by comparing watershed-averaged rainfall estimates derived from 3B42 to 3B42RT, for both watersheds during 2006–2007 (the validation period of the model). Figure 6.2 presents scatter plots at both daily and monthly timescales. The coefficient of determination ( $R^2$ ) between 3B42 and 3B42RT was 0.41 at the daily timescale and 0.43–0.50 at the monthly timescale, indicating that there is tremendous variability between the time series of 3B42 and 3B42RT. On average, 3B42RT rainfall estimates were twice as much as 3B42. Figure 6.3 presents the time series plots at the monthly scale. The difference between 3B42 and 3B42RT varied tremendously from month to month and from year to year. The difference in annual rainfall estimates between 3B42 and 3B42RT was 35–40% of the 3B42RT estimates in 2006, surging to 70% in 2007. Based on the above results, we conclude that the two satellite rainfall estimates were very different from each other in the way they estimated the time series and total depth of rainfall. Obviously, both cannot be correct simultaneously, and one of them must be closer to the truth than the other.

To assess which product was closer to the truth, we compared the watershed-averaged rainfall estimates to the streamflow accumulations at the outlets of the

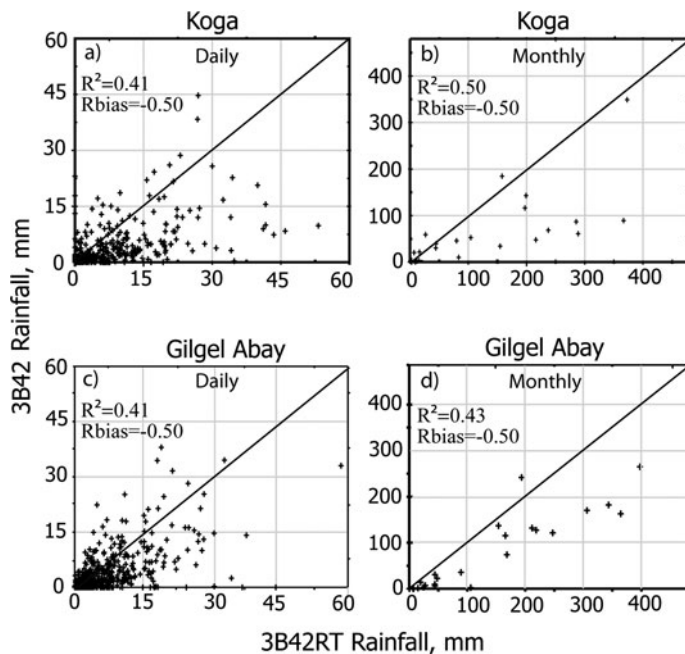


**Fig. 6.2** Inter-comparison of watershed-average 3B42 and 3B42RT rainfall estimates at (a, c) daily and (b, d) monthly timescales, for (a, b) Koga and (c, d) Gilgel Abay watersheds, during 2006–2007

watersheds. Figure 6.4 compares the accumulations at the yearly time scale for each watershed. The annual 3B42 rainfall estimates were lower than the annual streamflow accumulations by 60% in 2007 for Gilgel Abay; earlier years also saw smaller 3B42 rainfall estimates than corresponding streamflow. Since the major source of streamflow in Gilgel Abay is the rainfall that falls over this watershed, the consistently lower 3B42 annual rainfall estimates than the observed annual streamflow points to the underestimation bias in 3B42 rainfall estimates. The 3B42RT annual estimates were consistently higher than the annual observed streamflow.

### 6.3.2 SWAT Calibration Results (2003–2004)

In order to assess the utility of satellite rainfall estimates for hydrologic simulations, the hydrologic model must first be calibrated. We calibrated SWAT model parameters separately for each rainfall input (3B42 and 3B42RT) and watershed (Koga and Gilgel Abay), for the calibration period 2003–2004. The parameter values are tabulated in Table 6.2. Comparisons (using time series and exceedance probability plots) between observed and simulated streamflow are shown in Fig. 6.5. In the case of Koga, both 3B42 and 3B42RT simulations captured the overall shape

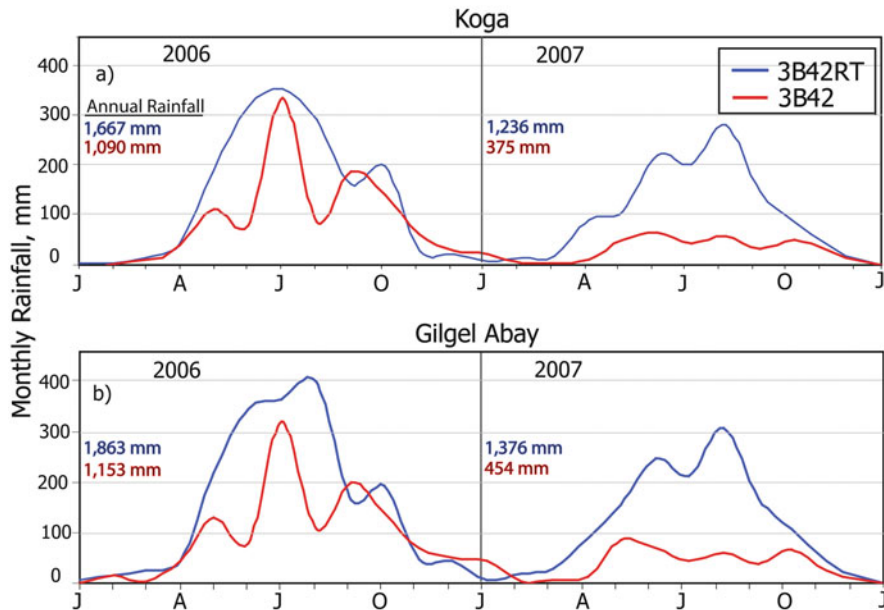


**Fig. 6.3** Inter-comparison of monthly watershed-average time series of rainfall derived from 3B42 to 3B42RT, for (a) Koga and (b) Gilgel Abay watersheds, during 2006–2007. Annual rainfall estimates are texted in the plots

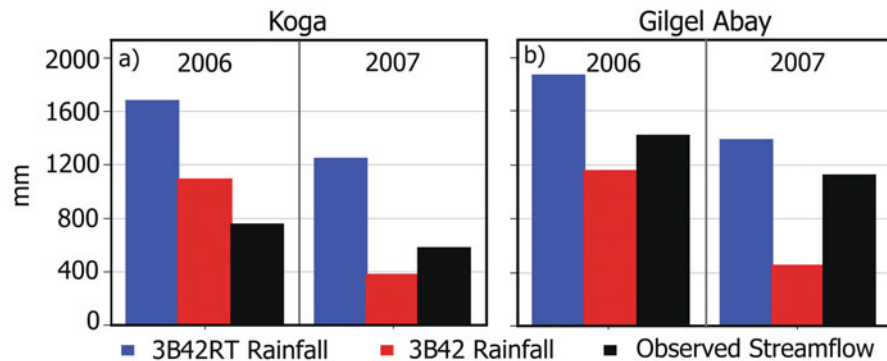


**Fig. 6.4** Comparisons of annual depth of rainfall estimates derived from 3B42 to 3B42RT to observed streamflow, for (a) Koga and (b) Gilgel Abay watersheds

of the observed hydrograph but significantly underestimated the large flood events. In the case of Gilgel Abay, 3B42RT simulations performed way better than 3B42 although both underestimated the large flood events. According to the calibration performance statistics (not shown), 3B42RT yielded better calibration results than 3B42 for both watersheds.

**Table 6.2** SWAT model parameter values obtained by calibrating the model separately for each rainfall input type and watershed, during the calibration period of 2003–2004

Model variable	Unit	Parameter values			
		Koga		Gilgel Abay	
		3B42RT	3B42	3B42RT	3B42
CH_K2	mm/h	29.3	0.01	60	60
Alpha_BF	1/day	0.92	0.99	0.75	1.0
CN2 <sup>a</sup>	–	69	72	65	74
Surlag	–	0.001	0.001	0.8	0.1
CH_N2	–	0.07	0.04	0.04	0.04
Sol_K <sup>a</sup>	mm/h	0.02	0.02	0.0175 <sup>b</sup>	0.0175 <sup>b</sup>
ESCO	–	0.99	1.0	0.0 <sup>b</sup>	0.0 <sup>b</sup>
canmx	–	0.0	0.0	0.0	0.0
Rchrg_dp	–	0.01 <sup>b</sup>	0.01 <sup>b</sup>	0	0
Gw_delay	day	31 <sup>b</sup>	31 <sup>b</sup>	25	3
Gwqmn	mm	0 <sup>b</sup>	0 <sup>b</sup>	0	0

<sup>a</sup>Values represent average values of spatial distribution.

<sup>b</sup>Parameters for which default/literature values were used.

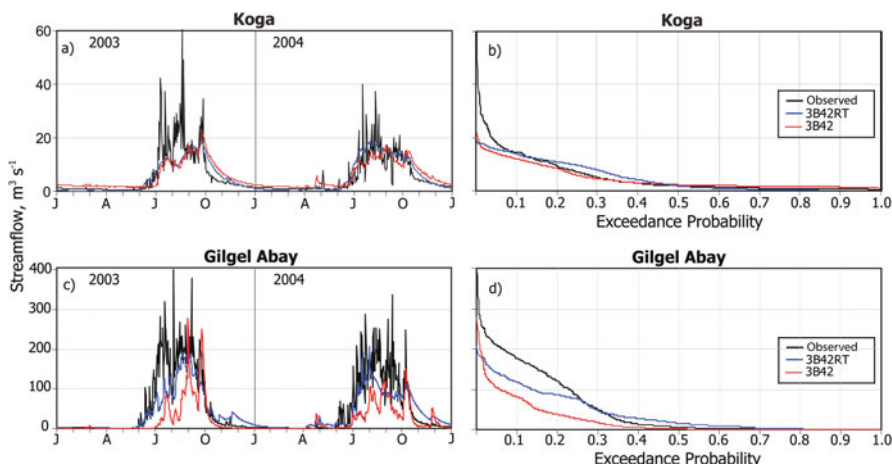


**Fig. 6.5** Comparisons of SWAT simulated (based on 3B42 and 3B42RT rainfall inputs, separately) and observed daily streamflow during 2003–2004, in terms of (a, c) time series and (b, d) exceedance probabilities, for (a, b) Koga and (c, d) Gilgel Abay watersheds

### 6.3.3 SWAT Validation Results (2006–2007)

The purpose of these simulations was to assess the effects of satellite rainfall estimates on streamflow when SWAT was calibrated with corresponding satellite

rainfall data. We simulated daily streamflow for the validation period (2006–2007) using 3B42 and 3B42RT rainfall inputs separately in SWAT calibrated with corresponding rainfall type.

### 6.3.3.1 Simulation Results for Koga

Comparisons of observed and simulated streamflow for Koga watershed are given in Fig. 6.6. Let us first look at the 2006 comparisons. Both 3B42 and 3B42RT captured the overall shapes of observed hydrograph but with significant underestimation of the large flood events especially those with exceedance probabilities under 20%. The average simulations underestimated the average observations by 16–21%. The NSE values (0.42–0.50) indicated modest skill in simulated streamflows. In general, 3B42 and 3B42RT simulations exhibited similar performances in 2006. On the other hand, 2007 saw striking differences between the performances of 3B42 and 3B42RT simulations: 3B42 missed almost all runoff events while 3B42RT captured all runoff events albeit with underestimation, 3B42 had negative NSE value indicating no skill in the simulations compared to simply using the mean as a predictor while 3B42RT had modest skill in reproducing observed streamflow. So in 2007, 3B42RT simulations exhibited much better performance than 3B42 simulations.

### 6.3.3.2 Simulation Results for Gligel Abay

Comparisons of observed and simulated streamflow for Gilgel Abay watershed are given in Fig. 6.7. In 2006, both 3B42 and 3B42RT simulations exhibited skills in predicting streamflow with 3B42RT simulations showing much better performance. In 2007, 3B42 simulations missed all runoff events and showed no skills at all. On the other hand, the 3B42RT simulations in 2007 showed good performance overall although they underestimated the large flood events.

### 6.3.3.3 Comparison of Koga and Gilgel Abay Simulation Results

Let us now discuss the effect of watershed area on the performance of 3B42 and 3B42RT simulations. Figure 6.8 compares the performance statistics (NSE and Rbias) for the two adjoining watersheds with drainage areas of  $299 \text{ km}^2$  (Koga) and  $1,656 \text{ km}^2$  (Gilgel Abay). In both years, 3B42RT simulations showed better performance for the larger watershed than for the small watershed. This is as expected due to the additional averaging process in larger watersheds that tends to dampen the random error in rainfall input and/or hydrological process approximation. On the other hand, 3B42 simulations showed worse performance for the larger watershed than for the small watershed, indicating that larger watershed size brought much more error from the included 3B42 rainfall estimates.

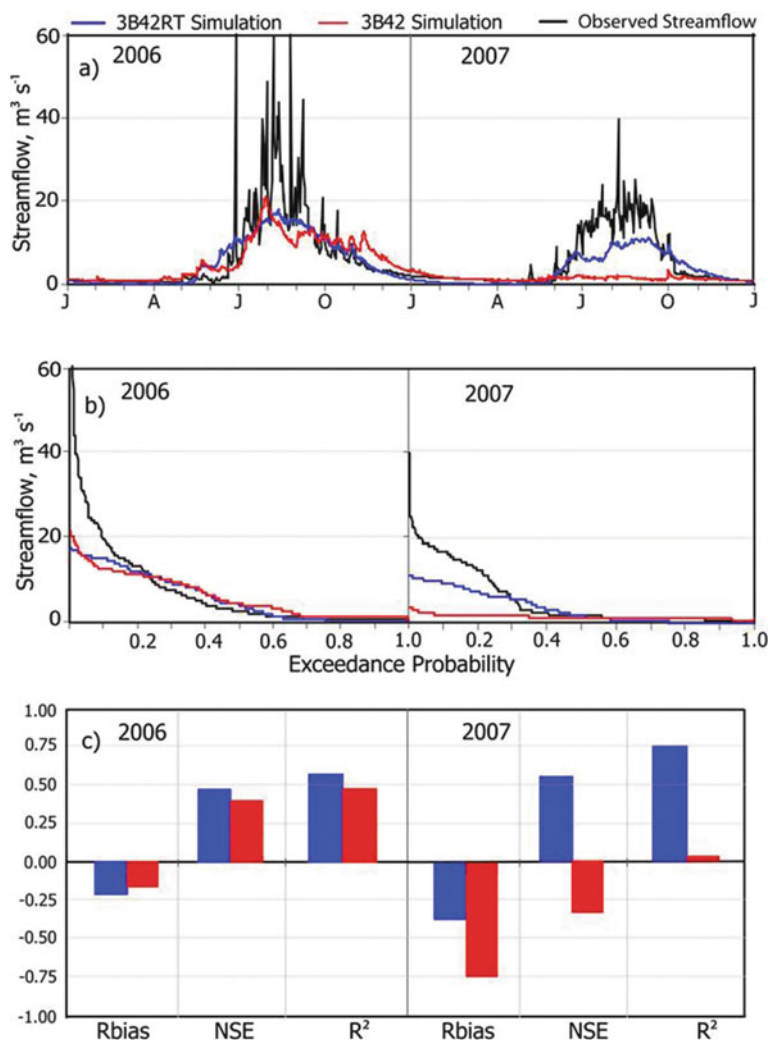


**Fig. 6.6** Comparisons of SWAT simulated (based on 3B42 and 3B42RT rainfall inputs, separately) and observed daily streamflow during the validation period (2006–2007) for Koga watershed, in terms of (a) time series and (b) exceedance probabilities, and (c) performance statistics (Blue bars for 3B42RT and red is for 3B42 rainfall)

## 6.4 Conclusions

The notion that the combination of rain gauge data with satellite rainfall estimates performs better than satellite-only estimates has led to the incorporation of rain gauge data into global satellite rainfall products. This study compared the performance (from streamflow simulation perspective) of two widely-used satellite rainfall products, where the major difference between them is the inclusion or exclusion

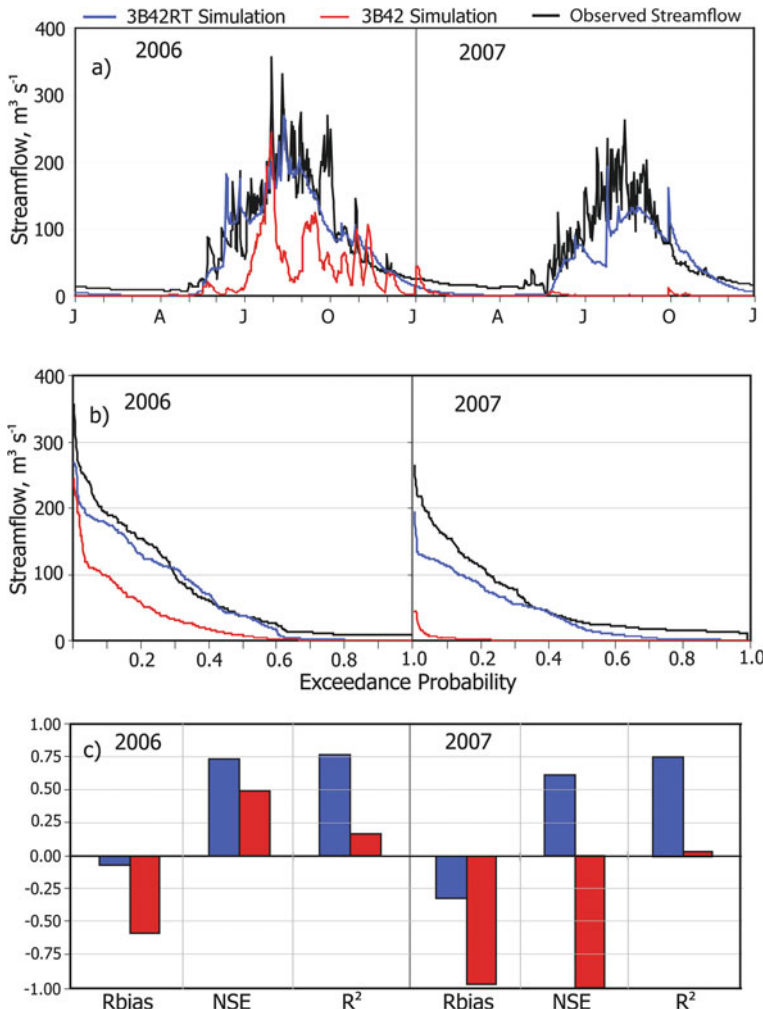


**Fig. 6.7** Same as in Fig. 6.6 but for Gilgel Abay watershed (Blue bars are for 3B42RT and red is for 3B42 rainfall)

of rain gauge data, in a mountainous region in Ethiopia where rain gauge data are sparse. The goal was to provide the user community in Ethiopia with some insight on the selection and limitation of satellite rainfall products for hydrological applications, and to provide feedback to the algorithm developers on the consequence of incorporating rain gauge data into satellite rainfall products in regions where rain gauge data are sparse. The two satellite rainfall products evaluated were: TMPA 3B42RT (a real-time version that does not include any rain gauge data) and TMPA 3B42 (a research version that combines TMPA 3B42RT with global rain gauge data). These products were separately used as input into the SWAT hydrological model to simulate daily streamflow for two adjoining watersheds with

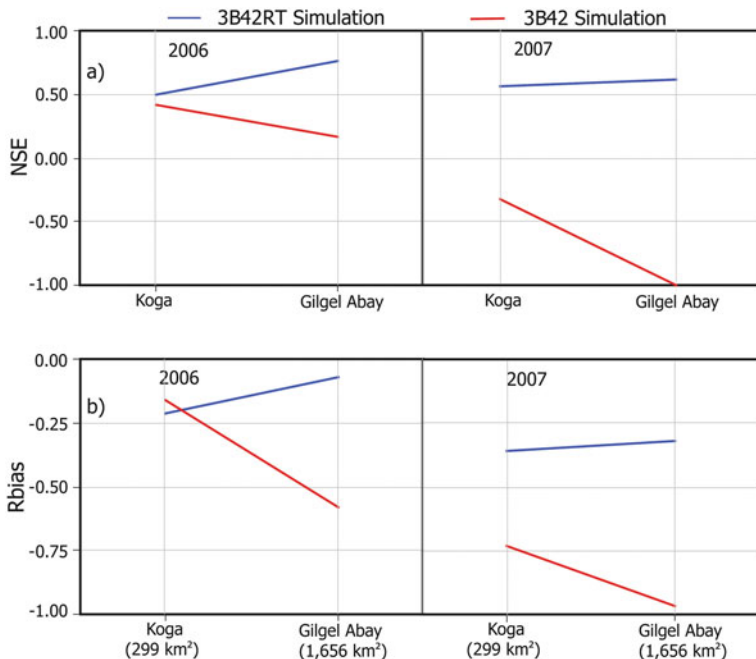


**Fig. 6.8** Comparisons of the performance statistics (NSE and Rbias) of 3B42 and 3B42RT SWAT simulations as a function of watershed size, for (a) NSE and (b) Rbias

drainage areas of 299 km<sup>2</sup> (Koga) and 1,656 km<sup>2</sup> (Gilgel Abay) in Ethiopia, and the simulations were compared to observed streamflow. Our major findings were as follows:

- The rainfall estimates from the two satellite rainfall products were very different from each other in every respect.
- Both satellite rainfall products substantially underestimated the large flood events, and therefore caution must be exercised when using any of these data for flood-related applications.
- TMPA 3B42RT showed consistently some level of skill in reproducing observed streamflow.
- The performance of TMPA 3B42 highly fluctuated from time to time. In 2007, TMPA 3B42 missed almost all runoff hydrographs. In 2006, TMPA 3B42 showed some skills but underperformed 3B42RT.
- As the size of the watershed increased, the accuracy of TMPA 3B42RT simulations increased. However, the TMPA 3B42 products resulted in larger errors with increasing watershed size.

Therefore, we conclude that the TMPA 3B42RT products are by far better than the TMPA 3B42 products in the study region in Ethiopia. Incorporating rain gauge

data in satellite rainfall products has the undesired consequence of deteriorating the quality of the satellite rainfall products in this region. Apparently, the use of rain gauge information from sparsely distributed network is introducing additional error in the satellite rainfall products, and therefore, the algorithm developers must take a deeper look into their algorithms. Users, on the other hand, must forego the conventional notion that satellite rainfall products that incorporate rain gauge data have better performance accuracy than the satellite-only products.

**Acknowledgments** Support for this study came from two NASA Grants (Award #: NNX08AR31G and NNX10AG77G) to the University of Connecticut.

## References

Arnold JG, Srinivasan R, Muttiah RS, Allen PM (1998) Large-area hydrologic modeling and assessment: Part I. model development. *J Amer Water Resour Assoc* 34(1):73–89. Doi: 10.1111/j.1752-1688.1998.tb05961.x

Eckhardt K, Arnold JG (2001) Automatic calibration of a distributed catchment model. *J Hydrol* 251(1–2):103–109. Doi: 10.1016/S0022-1694(01)00429-2

Gassman PW, Reyes MR, Green CH, Arnold JG (2007) The soil and water assessment tool: historical development, applications, and future research directions. *Trans ASABE* 50(4):1211–1250

Habib E, Henschke A, Adler RF (2009) Evaluation of TMPA satellite-based research and real-time rainfall estimates during six tropical-related heavy rainfall events over Louisiana, USA. *Atmos Res* 94(3):373–388. Doi:10.1016/j.atmosres.2009.06.015

Huffman GJ, Adler RF, Bolvin DT, Gu G, Nelkin EJ, Bowman KP, Hong Y, Stocker EF, Wolff DB (2007) The TRMM multisatellite precipitation analysis (TMPA): quasi-global, multilayer, combined-sensor, precipitation estimates at fine scale. *J Hydrometeorol* 8:38–55

Legates DR, McCabe GJ (1999) Evaluating the use of “goodness of fit” measures in hydrologic and hydroclimatic model validation. *Water Resour Res* 35(1):233–241

Soil Conservation Service (1986) TR-55, Urban hydrology for small watersheds. Natural Resources Conservation Service, Washington, DC

van Griensven A, Meixner T, Grunwald S, Bishop T, DiLuzio M, Srinivasan R (2006) A global sensitivity analysis tool for the parameters of multi-variable catchment models. *J Hydrol* 324:10–23. Doi: 10.1016/j.jhydrol.2005.09.008

**Part III**

**GIS and Remote Sensing in Watershed  
Modeling**

# Chapter 7

## Watershed Hydrology of the (Semi) Humid Ethiopian Highlands

Tegenu A. Engda, Haimanote K. Bayabil, Elias S. Legesse, Essayas K. Ayana, Seifu A. Tilahun, Amy S. Collick, Zachary M. Easton, Alon Rimmer, Seleshi B. Awulachew, and Tammo S. Steenhuis

**Abstract** Understanding the basic relationships between rainfall, runoff and soil loss is vital for effective management and utilization of water resources and soil conservation planning. A study was conducted in three small watersheds in or near the Blue Nile basin in Ethiopia, with long-term records of rainfall and discharge. To better understand the water movement within the watershed, piezometers were installed and infiltration rates were measured in the 2008 rainy season. We also reanalyzed the discharge from small plots within the watersheds. Infiltration rates were generally in excess of the rainfall rates. Based on this and plot discharge measurements, we concluded that most rainfall infiltrated into the soil, especially in the upper, steep and well-drained portions of the watershed. Direct runoff is generated either from saturated areas at the lower and less steep portions of the hill slopes or from areas of exposed bedrock. Using these principles, a simple distributed watershed hydrology model was developed. The models reproduce the daily discharge pattern reasonably well for the small watershed and the 10-day discharge values for the whole Blue Nile Basin in Ethiopia. The simplicity and scalability of the model hold promise for use in un-gauged catchments.

**Keywords** Variable source area · Perched water table · Saturation excess · Infiltration excess · Hillslope hydrology

### Abbreviations

GPS	Global Positioning System
SCRP	Soil Conservation Research Program
SCS	Soil Conservation Service

---

T.S. Steenhuis (✉)

Department of Biological and Environmental Engineering, Cornell University,  
Ithaca, NY 14853, USA  
e-mail: tss1@cornell.edu

## 7.1 Introduction

A better understanding of the hydrological characteristics of different watersheds in the headwaters of the Ethiopian highlands is of considerable importance because only 5% of Ethiopia's surface water (0.6% of the Nile Basin's water resource) is being currently utilized by Ethiopia while cyclical droughts cause food shortages and intermittent famine (Arseno and Tamrat, 2005). At the same time the Ethiopian highlands are the origin, or source, of much of the river flow reaching the Nile River, contributing greater than 60% of Nile flow (Ibrahim, 1984; Conway and Hulme, 1993) possibly increasing to 95% during the rainy season (Ibrahim, 1984). In addition, there is a growing anxiety about climate and human-induced changes of the river discharge (Sutcliffe and Parks, 1999), especially because there have been limited studies on basin characteristics, climate conditions, and hydrology of the Upper Nile Basin in Ethiopia (Arseno and Tamrat, 2005).

To predict future water availability three general model types have been used in the Blue Nile basin. Simple engineering approaches such as the Rational Method (Desta, 2003), pure water balance models, and semi distributed models. Pure water balance approaches have been made by Ayenew and Gebreegziabher (2006) for Lake Awassa, Conway (1997) and Kim and Kaluarachchi (2008) at the upper Blue Nile, and Kebede et al. (2006) at Lake Tana. These models provide only information on water quantity at the watershed outlet and perform best at a monthly time scale. Semi distributed models that have been applied in the Nile basin are SWAT (Setegn et al., 2008), Water Erosion Prediction Project (WEPP) (Zeleke, 2000), the Agricultural Non-Point Source model (AGNPS) (Haregeweyn and Yohannes, 2003; Mohammed et al., 2004), and for South Central Ethiopia PRMS (Legesse et al., 2003).

Most semi distributed models use the SCS runoff equation for determining surface runoff. The SCS curve number method is based on a statistical analysis of plot runoff data from the mid-west USA with a temperate climate. When applied to Ethiopia with a monsoon climate, it has been a bit problematic. While most of these models were run on a daily time step, the results are presented on a monthly time step, which indicates these models do not work well at the daily scale. By integrating the result over a monthly time step, errors in daily surface runoff are compensated for by opposite errors in interflow predictions. Thus, the monthly validation indicates that the monthly water balances are met but not necessarily that the daily rainfall-runoff relationship for landscape units in the watershed are correct. In order to understand why a statistically derived and widely used SCS curve number fails to predict the daily direct runoff in monsoonal climates, the effect of climate on the hydrology during the dormant and growing seasons must be considered. The similarity between temperate and monsoonal climate types is that both have a dormant period and a growing period. However, the similarity between the two climates stops there. In the temperate climates, the growth in the dormant season is limited by the temperature. There is usually sufficient precipitation and there is little evaporation with the result that the soils wet up and watershed outflow increases. In monsoonal climates, the limiting factor is insufficient rainfall with the consequence

that the soils dry out and therefore during the dormant season, discharge out of the watershed decreases. Understanding the effect of climate on the hydrology during the growing season is more complicated. We can simply make the observation that the landscape dries out in temperate climates and the opposite is true for monsoonal climate. These differences in how climate interacts with the hydrology, indicates that only physically sound models can be applied in both climates and statistical techniques will be less successfully transferred.

Thus, in order to refine the estimates of watershed outflow in the Ethiopian highlands with a monsoonal climate, a better understanding is needed of rainfall and runoff relationships of the various landscape units. In this chapter, we will use recently collected information by Engda (2009), Legesse (2009) and Bayabil (2009) in three Soil Conservation Research Program (SCRP) watersheds in the Ethiopian highlands – Andit Tid, Anjeni, and Maybar – to derive how interflow, surface runoff, and baseflow are generated spatially. This information then will be used to develop a physically sound model that can be used in the Ethiopian highlands.

## 7.2 Watershed Descriptions

Soil Conservation Research Program (SCRP) watersheds have the longest and most accurate record of both rainfall and runoff data available for small watersheds in Ethiopia. Three of the watersheds are located in the Amhara region either in or close to the Nile Basin: Andit Tid, Anjeni, and Maybar (Fig. 7.1). All three sites are dominated by agriculture with soil erosion control structures built to assist the

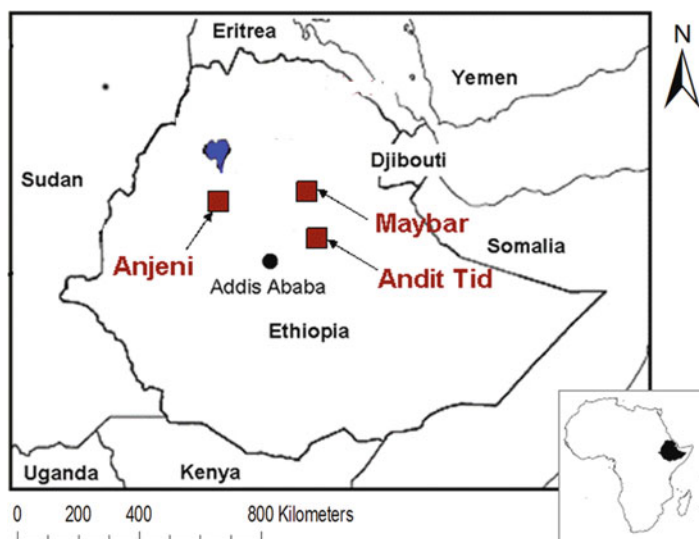


Fig. 7.1 Locations of the three SCRP watersheds in Amhara, Ethiopia

**Table 7.1** Location, description, and data used in the model from the three SCRP research sites

Research site	Location (region)	Area (ha)	Elevation (masl)	Precipitation mm/year	Length of data
Andit Tid	39°43'E, 9°48'N (Shewa)	477.3	3,040–3,548	1,467	1987–2004 (1993, 1995–1996 incomplete)
Anjeni	37°31'E, 10°40'N (Gojam)	113.4	2,407–2507	1,675	1988–1997
Maybar	37°31'E, 10°40'N (South Wollo)	112.8	2,530–2,858	1,417	1988–2001 (1990–1993 incomplete)

rain-fed subsistence farming but the watersheds differ in size, topographic relief, and climate (Table 7.1).

The Andit Tid watershed unit covers a total area of 481 ha, with a hydrological surface area of 477 ha. It is situated 180 km northeast of Addis Ababa at 39°43' east and 9°48' north in the Blue Nile Basin. The topography of Andit Tid ranges from 3,000 m near the research station in the western reach of the research unit to 3,500 m in the southeast. Andit Tid, the largest watershed, is also the highest and least populated. It receives more than 1,500 mm/year and has a bimodal rainfall pattern, smaller/belg from March to May, and main/kerent from June to October. Hill slopes are very steep and degraded, resulting in 54% of the long-term precipitation becoming runoff. Despite its larger size, stream flow quickly returns to nearly zero during the typically dry months of November through March. Some of the contour bunds constructed at the start of the project were destroyed after installation because, according to farmers, they increased erosion (Engda, 2009). Terraces and small contour drainage ditches were installed by the farmers to carry off excess rainfall. From 1987 to 2004, rainfall was measured and discharge was recorded at the outlet and from four runoff plots. Evaporation was measured using the standard pan. During the 2008 main rainy season, soil infiltration rates were determined at 10 different locations throughout the watershed using a 30-cm diameter single-ring infiltrometer. In addition, piezometers were installed in transects to measure the water table depths. Finally, soil depth estimations were taken by field technicians throughout the watershed and registered using Global Positioning System (GPS) points. Further information can be found in Hurni (1984), Bosshart (1997), and Engda (2009).

The Anjeni watershed is located in the Blue Nile basin of Amhara Region in one of the country's more productive agricultural areas and is dominated by highlands. The watershed is oriented north-south and is flanked on three sides by plateau ridges. It is located at 37°31'E and 10°40'N and lies 370 km NW of Addis Ababa to the south of the Choke Mountains. Minchet, a perennial river, starts in the watershed and flows towards the Blue Nile Gorge. The Anjeni watershed covers a total area of 113 ha. It is the most densely populated among the three watersheds. The topography of Anjeni ranges from 3,000 m near the research station in the western reach of the research unit to 3,500 in the southeast. This site receives more rain than the other two watersheds and has only one rainy season, typically May through October.

This watershed has extensive soil and water conservation measures, mainly terraces and small contour drainage ditches, installed each year by the farmers to carry off excess rainfall. From 1987 to 2004, rainfall was measured at five different locations, discharge was recorded at the outlet and from four runoff plots. Forty-five percent of the rainfall becomes runoff. During the 2008 rainy season, soil infiltration rate was measured at 10 different locations throughout the watershed using a 30-cm diameter single-ring infiltrometer. In addition, piezometers were installed in transects to measure the water table depths. Finally, soil depth estimations were taken by field technicians throughout the watershed and registered using GPS points.

Finally, Maybar is located in the northeastern part of the central Ethiopian highlands situated in Southern Wollo Administrative Zone near Dessie Town. It is the first of the SCRP research sites. The gauging station lies at 39°39'E and 10°51'N. The area is characterized by highly rugged topography with steep slopes ranging between 2,530 and 2,860 m, a 330 m altitude difference within a 112.8 ha catchment area. From 1988 to 2004, rainfall data was available using an automatic rain gage and two manual rain gage at two different locations, one in the upper part of the catchment and the other near the office. Discharge was measured with a flume installed in the Kori River using two methods: float-actuated recorder and manual recording. During the main rainy season in 2008, 34% of the long-term precipitation in Maybar became discharge at the outlet. The ground water table levels were measured with 29 piezometers. The saturated area in the watershed was delineated and mapped using combined information collected using GPS instrument, field observation, and ground water level data (piezometer head readings).

## 7.3 Rainfall Runoff Characteristics for Monsoonal Climates

### 7.3.1 Analysis of Rainfall Discharge Data

In order to understand the rainfall/runoff relations in monsoonal climates, Liu et al. (2008) examined how the watershed outflow changed as a function of precipitation for the three SCRP sites. To find the most appropriate representation of watershed behavior, daily rainfall, evaporation, and discharge data were summed over biweekly periods; only with longer time periods could the total stream responses to a rainfall event be determined because interflow lasts several days.

To investigate runoff response patterns, the biweekly sums of discharge were plotted as a function of effective rainfall (i.e., precipitation-evapotranspiration) during the rainy season and dry season, respectively. In Fig. 7.2a, an example is given for the Anjeni watershed. As shown from Fig. 7.2a, the watershed response behavior changes as the wet season progresses, with precipitation later in the season generally producing a greater percentage of runoff. As rainfall continues to accumulate during the rainy season, the watershed eventually reaches a threshold point where runoff response can be predicted by a linear relationship with effective precipitation,

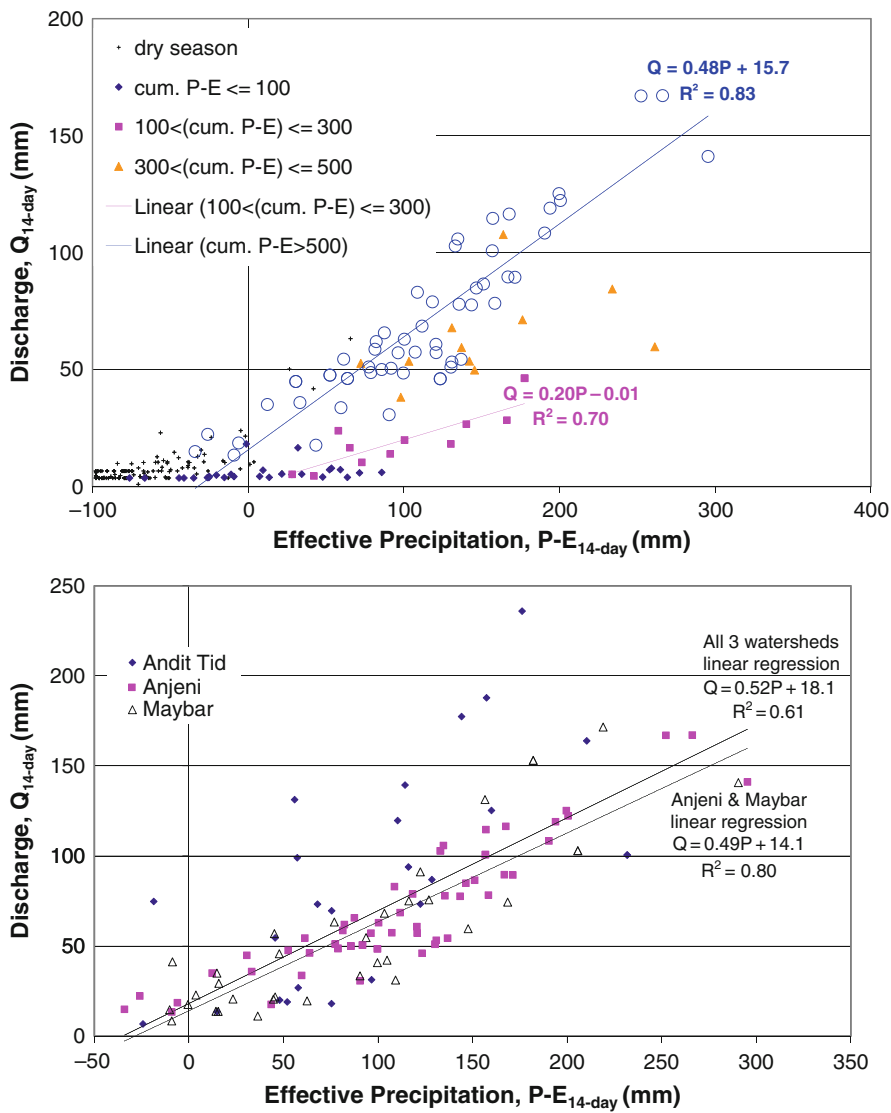


**Fig. 7.2** Fourteen day discharge vs. effective precipitation in (1) the Anjeni watershed, and (2) all three SCRP watersheds with cumulative effective precipitation in excess of 500 mm since the beginning of the rainy season (Liu et al., 2008)

indicating that the proportion of the rainfall that became runoff was constant during the remainder of the rainy season. For the purpose of this study, an approximate threshold of 500 mm of effective cumulative rainfall,  $P-E$ , was selected after iteratively examining rainfall vs. runoff plots for each watershed. The proportion  $Q/(P-E)$  varies within a relative small range for the three SCRP watersheds despite their

differing characteristics. In Anjeni, approximately 48% of late season effective rainfall, P-E, became runoff, while ratios for Andit Tid and Maybar were 56 and 50%, respectively (Liu et al., 2008). There was no correlation between biweekly rainfall and discharge during the dry seasons at any of the sites.

Since each of the SCRP watersheds showed a similar linear response after the threshold cumulative rainfall was satisfied, the latter parts of the wet seasons were all plotted in the same graph (Fig. 7.2b). Despite the great distances between the watersheds and the different characteristics, the response was surprisingly similar. The Anjeni and Maybar watersheds had almost the same runoff characteristics, while Andit Tid had more variation in the runoff amounts but, on average, the same linear response was noted with a higher intercept (Fig. 7.2b). Linear regressions were generated for both the combined results of all three watersheds and for the Anjeni and Maybar watersheds in combination (Fig. 7.2b). The regression slope did not change significantly, but this is due to the more similar Anjeni and Maybar values dominating the fit (note that these regressions are only valid for the end of rainy seasons when the watersheds are wet).

Why these watersheds behave so similarly after the threshold rainfall has fallen is an interesting question to explore. It is imperative to look at various time scales, since focusing on just one type of visual analysis can lead to erroneous conclusions. For example, looking only at storm hydrographs of the rapid runoff responses prevalent in Ethiopian storms, one could conclude that infiltration excess is the primary runoff generating mechanism. However, looking at longer time scales in Fig. 7.2a, it can be seen that the ratio of  $Q/(P-E)$  is increasing with cumulative precipitation and consequently the watersheds behave differently depending on how much moisture is stored in the watershed. This suggests that saturation excess processes play an important role in the watershed runoff response. If infiltration excess was controlling runoff responses, discharge would only depend on the rate of rainfall, and there would be no clear relationship with antecedent cumulative precipitation, as is clearly the case in Fig. 7.2a.

### 7.3.2 *Infiltration and Precipitation Intensity Measurements*

To further investigate the likelihood of infiltration excess, the infiltration rates are compared with rainfall intensities in the Andit Tid watershed where infiltration rates were measured in 2008 by Engda (2009) and rainfall intensity records were available from the SCRP project for 1986–2004 on the pluviometric charts. These were transcribed to digital form by Engda (2009). The exceedance probability of the average intensities of 23,764 storm events is plotted in Fig. 7.3 (dotted black line). These intensities were calculated by dividing the rainfall amount on each day by the duration of the storm. In addition, the exceedance probability for actual intensities of short periods ranging from 5 to 10 min are plotted in Fig. 7.3 (red line). Since there were bursts of high intensity rainfall within each storm, the rainfall intensities for short periods exceeded that of the storm averaged intensities in Fig. 7.3.

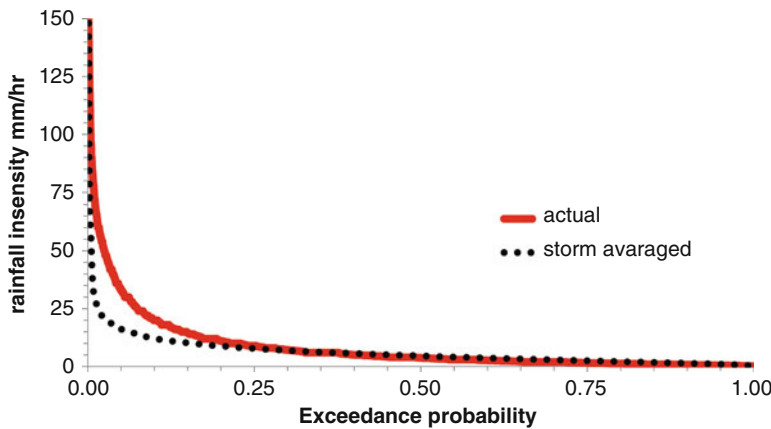


**Fig. 7.3** Rainfall intensity exceedance probability for the Andit Tid watershed

**Table 7.2** Average soil infiltration rate at different soil types, slope range and land use types

Testing sites	Location in the watershed	Average IR (mm/h)	Location slope (°)	Soil type	Soil depth	Land use
3	Top	25	15	Andosol	Medium	Fallow grass
5	Top	24	15	Andosol	Medium	Fallow grass
8	Top	594	29	Andosol	Shallow	Bush land
1	Middle	226	30	Regosol	Shallow	Terraced and cultivated
2	Middle	26	21	Regosol	Deep	Terraced and cultivated
4	Middle	140	21	Andosol	Medium	Fallow
7	Middle	29	21	Humic andosol	Shallow	Fallow
6	Bottom	43	10	Andosol	Deep	Fallow
9	Bottom	53	2	Eutric regosol	Medium	Cultivated
10	Bottom	870	18	Eutric cambisol	Medium	Terraced and cultivated

The infiltration rates for 10 locations measured with the 30-cm diameter singlering infiltrometer (shown in Table 7.2) varied between a maximum of 87 cm/h on a terraced eutric cambisol in the bottom of the watershed to a low of 2.5 cm/h on a shallow soil near the top of the hill slope. This low infiltration rate was mainly caused by the compaction of free roaming grazing animals. Bush lands, which are dominant on the upper watershed, have significantly higher infiltration rates. Terraced and cultivated lands in general have also higher infiltration rates. The average infiltration rate of all 10 measurements indicates that the storm intensities were 20.3 cm/h and the medium 4.8 cm/h. The median infiltration rate of 4.8 cm/h is the most meaningful number to compare with the rainfall intensity since it represents

a spatial average. This median intensity has an exceedance probability of 0.03 for the actual storm intensities and 0.006 for the storm averaged intensities. Thus, the medium intensity was exceeded only 3% of the time and for less than 1% of the storms. Storms with greater intensities were all of short duration with amounts of less than 1 cm of total precipitation, except once, in which almost 4 cm of rain fell over a 40 min period. The runoff generated during short duration intense rainfall can infiltrate into the soil in the subsequent period down slope when the rainfall intensity is less or the rain has stopped. In the Maybar watershed, Derib (2005) performed 16 infiltration tests and observed even greater infiltration rates than in Andit Tid. The final steady state infiltration rates ranged from 1.9 to 60 cm/h with a median of 17.5 cm/hr.

Thus, the infiltration measurements confirmed that infiltration excess runoff is not a common feature in these watersheds. Consequently, most runoff that occurs in these watersheds is from degraded soils where the top soil is removed and by saturation excess in valley bottoms where the interflow accumulates. Since the degraded soils have little storage, the runoff can be classified as either infiltration excess or saturation excess.

The finding that saturation excess is occurring in watersheds with a monsoonal climate is not unique. For example, Hu et al. (2005), Lange et al. (2003), and Merz et al. (2006) found that saturation excess could describe the flow in a monsoonal climate in China, Spain, and Nepal. There are no previous observations published for Ethiopia on the suitability of these saturation excess models to predict runoff even though attempts to fit regular models based on infiltration excess principles were not always satisfactory (Haregeweyn and Yohannes, 2003; Zeleke, 2000).

### **7.3.3 Piezometers and Ground Water Table Measurements**

Ground water table height measurements allow us to determine how the rain that falls on the upslope areas reaches the river. In all three watersheds, transects of piezometers were installed and ground water tables were observed in the 2008 main rainy season.

Both Andit Tid and Maybar have hill slopes with shallow to medium depth soils (0.5–2.0 m depth) above a sloping slowly permeable layer (either a hardpan or bedrock). Consequently, the water table height above the slowly permeable horizon (as indicated by the piezometers) behaved similarly for both watersheds. An example is given for the Maybar watershed where ground water table levels were measured with 29 piezometers across eight transects. The whole watershed was divided into three slope ranges: upper steep slope [25.1°–53.0°], mid slope [14.0°–25.0°], and relatively low-lying areas [0°–14.0°]. For each slope class, the daily perched ground water depths were averaged (i.e., the height of the saturated layer above the restricting layer, Fig. 7.4a). The depth of the perched ground water above the restricting layer in the steep and upper parts of the watershed is very small and disappears if there is no rain for a few days. The depth of the perched water table on

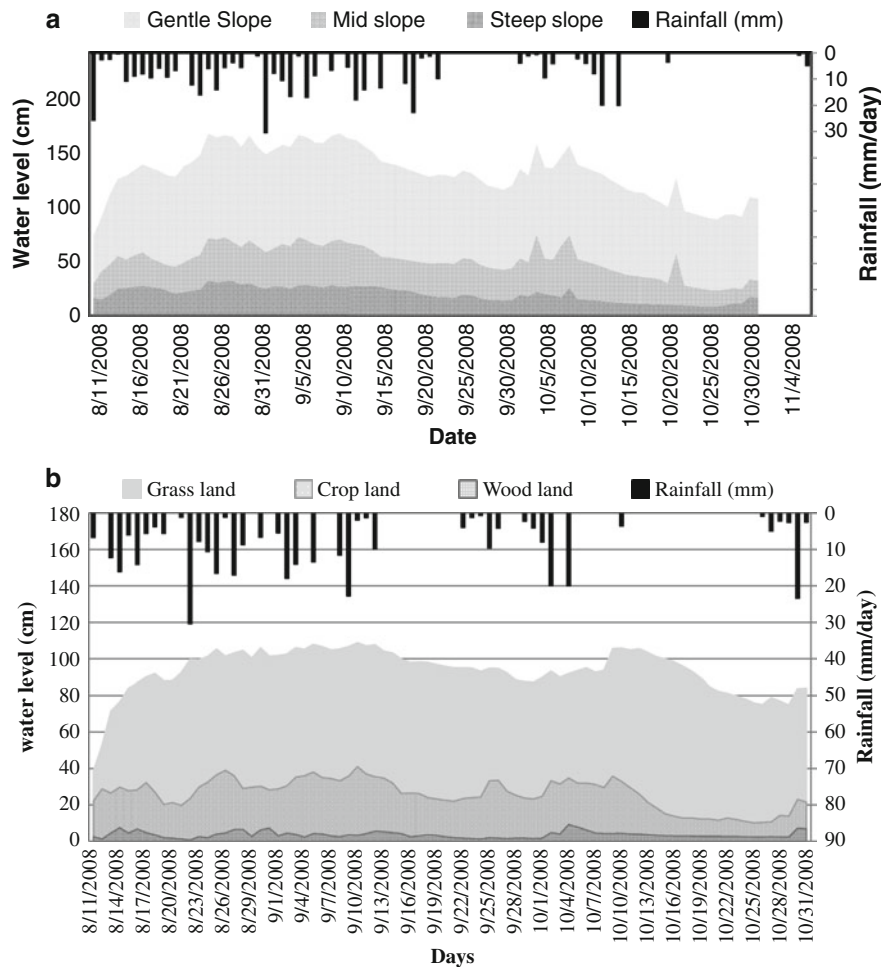


**Fig. 7.4** Water table height measured in the Maybar watershed during the 2008 rainy season and start of dry season. **a** Effect of slope on water table heights; **b** land use effects on the water table heights

the mid slopes is greater than upslope areas. The perched ground water depths are, as expected, the greatest in relatively low-lying areas. Springs occur at the locations where the depth from the surface to the impermeable layer is the same as the depth of the perched water table and are the areas that the surface runoff is generated.

The water table behavior is consistent with what one would expect if interflow is the dominant conveyance mechanism. All else being equal, the greater the driving force (i.e., the slope of the impermeable layer), the smaller the perched ground water depth required to transport a given quantity of water downslope. Moreover, the drainage area and the discharge increase with down slope position. Consequently,

one expects that the perched groundwater table depth increases with down slope position as both slope decreases and drainage area increases.

These findings are different than those generally believed to be the case, i.e., that the vegetation determines the amount of runoff in the watershed. We therefore plotted the average daily depth of the perched water table under the different crop types (Fig. 7.4b). Unexpectedly, there was a strong correlation of perched water depth with crop type as well. The grassland had the greatest perched water table depth, followed by cropland and bush land with the lowest ground water level. However, some local knowledge was needed to interpret these data, as the grasslands are mainly located in the often saturated lower lying areas (too wet to grow a crop), the croplands are in the mid-slope (with a consistent water supply but not saturated) and the bush lands are in the upper steep slope areas (too droughty for good yield). Since land use is related to slope class, we expect the same relationship between crop type and soil water table height as slope class and water table height. Thus, there is an indirect relationship between land use and hydrology determined by the landscape features. The landscape determines the water availability and thus the land use.

In the Anjeni watershed, which had relatively deep soils and no flat bottom land, the only water table that was found was near the stream. The water table level was above the stream level indicating that the rainfall infiltrates the landscape first and then flows laterally to the stream. Although more measurements are needed, we speculate that there was a portion of the watershed that had a hard pan at a relative shallow depth causing saturation excess overland flow.

These findings are consistent with the measurements taken by McHugh (2006) in the Lenche Dima watershed near Woldea where the surface runoff of the flat bottom lands was much greater than the runoff (and erosion) from the hillsides. Thus, in summary, the generally held opinion that the hill slopes are the high surface runoff producing areas is not true, at least at a minimum, for the season of observation in the three watersheds. The only areas that are expected to produce surface runoff are the severely eroded areas where the bedrock or subsoil is exposed and other areas that saturate during the storms.

### 7.3.4 *Conceptual Model for Predicting Watershed Discharge*

In order to develop a realistic hydrological model, the interflow and saturation excess flow phenomena must be included. In our conceptual watershed model, the watershed is divided into three areas based on slope steepness, soil depth, and infiltration capacity of the soil. Surface runoff source areas include areas near the river and the degraded hillsides with little or no soil cover. The well-drained hillsides transmit water as interflow to the stream and are modeled as the third component. Both the degraded and the bottom lands produce surface runoff after they are saturated. For a better understanding of the processes, the three areas are schematically superimposed on a photograph of the upper part of the Andit Tid watershed (Fig. 7.5). In addition to the three surface areas modeled, we included a subsurface reservoir that generates baseflow.

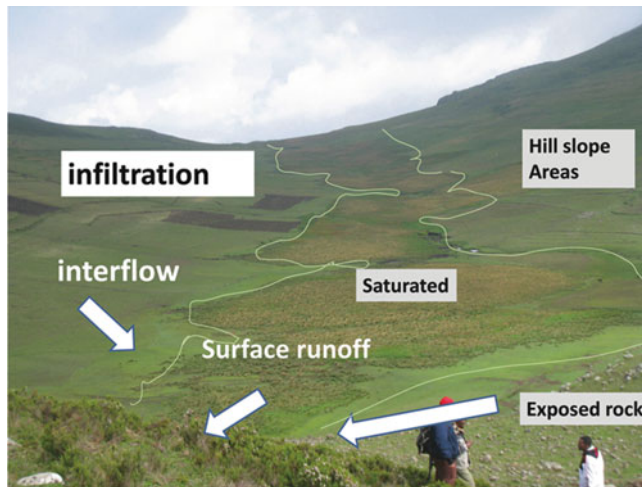


**Fig. 7.5** Conceptual model for predicting watershed discharge superimposed on the upper Andit Tid watershed

For each of the three source areas, a water balance is kept in the model

$$S = S_{t-\Delta t} + (P - AET - R - Perc)\Delta t \quad (7.1)$$

where  $P$  is precipitation (mm/day);  $AET$  is the actual evapotranspiration (mm/day),  $S_{t-\Delta t}$ , previous time step storage (mm),  $R$  saturation excess runoff (mm/day),  $Perc$  is percolation to the subsoil (mm/day) and  $\Delta t$  is the time step.

Based on a linearly decreasing evaporation rate from the maximum moisture content at saturation or field capacity to wilting point, the surface soil layer moisture storage can be written as:

$$S_s = S_{t-\Delta t} \left[ \exp \frac{(P - PET\Delta t)}{S_{max}} \right] \text{ when } p < PET \quad (7.2)$$

where  $S_{max}$  (mm) is the maximum available soil storage capacity and is defined as the difference between the amount of water stored in the topsoil layer at wilting point and the maximum moisture content, equal to either the field capacity for the hill slope soils or saturation (e.g., soil porosity) in runoff contributing areas.  $S_{max}$  varies according to soil characteristics (e.g., porosity, bulk density) and soil layer depth.

By assigning a maximum storage to each of the three source areas, a water balance is maintained for each of the watershed source areas. Surface runoff occurs from the degraded hillsides and the valley bottom when the water balance indicates that the soil is saturated. The flatter areas remain wet even during dry months of the year; only the top most soil layer will dry due to small amounts of water percolating downward from the hills. Hence, these areas need only a small amount of rainfall to

start generating surface runoff. There is even less rainfall needed at the beginning of the rainy season for the degraded hillsides to produce surface runoff

Interflow is generated by the excess rainfall when the hillside is at field capacity. Because these hillsides drain fully and are at or near the wilting point before the rainy season, a significant amount (on the order of 300–400 mm) of effective rainfall (defined as precipitation minus potential evapotranspiration) is needed before the interflow starts to contribute to the lower slope areas. The interflow can be modeled as a zero reservoir. This means that the same quantity of water drains from the hillside each day for each storm. The result is in a linear recession curve. The outflow from different storms is superimposed. Finally, the baseflow is modeled as a linear reservoir with a maximum storage. This base flow reservoir adds water to the stream during the dry period.

This model is similar to that developed by Steenhuis et al. (2009) for the whole Ethiopian Blue Nile Basin but slightly different from Collick et al. (2009) who tested a similar water balance model for the same three SCRP watersheds. Collick et al. (2009), using the semi distributed model, did not have particular landscape units in mind but fitted four areas that produced runoff and interflow based on specific ratios. Our current semi distributed model for the Ethiopian Highlands is more physical based and we do not need to specify a ratio between surface runoff and percolation of water.

## 7.4 Simulation Results

The mathematics for this conceptual model is presented in Steenhuis et al. (2009). The mathematical model was calibrated for each of the three watersheds by Legesse (2009) for Anjeni, by Bayabil (2009) for Maybar, by Engda (2009) for Andit Tid, and by Steenhuis et al. (2009) for the whole Blue Nile Basin. We will present in this chapter the results for two of the years between 1992 and 1995 depending on what quality data was available for each of the three SCRP watersheds. Parameters were slightly adjusted to represent the period after which the conservation practices were in place.

Parameters needed to simulate discharge include potential evaporation (PET), which varies little between years and between watersheds. On average, PET was 5 mm/day during the dry season and 3 mm/day during the rainy season. The precipitation values used were measured for the small SCRP watershed with rain gauges in the watershed itself and for the whole Blue Nile Basin, the average of 10 stations were used.

For calibration, the maximum storage values,  $S_{max}$ , for the contributing areas and hill slopes were based initially on the values of Steenhuis et al. (2009) for the whole Blue Nile Basin.  $S_{max}$  values for the three source areas were then varied around these values to obtain the best fit. Subsurface parameters were adjusted at the same time to fit the recession flows. The parameter set with the highest Nash Sutcliff efficiency was selected. The validation used the most optimum parameter set.

**Table 7.3** Model input values for surface flow components for the three SCRP watersheds and the Nile upstream of the border with Sudan. The watershed is divided into regions with different characteristics: exposed bedrock and saturated areas that contribute surface runoff when the soil is saturated or hillsides that produce recharge when the soil is above field capacity. Maximum storage of water is the amount of water needed above wilting point to become either saturated (runoff contributing areas) or to reach field capacity (*hill slopes*). Model input values for the baseflow and interflow reservoirs are the maximum storage of the linear base flow reservoir; the time in days to reduce the volume of the baseflow reservoir to half under no recharge conditions,  $t^*$  is the duration of the period after a single rainstorm until interflow ceases, Nash-Sutcliffe efficiency for simulated daily averaged discharge for the three SCRP watersheds and 10 day average values for the Blue Nile basin were calculated for the periods of calibration and validation

	Maybar	Andit Tid	Anjeni	Nile in <sup>1</sup> Ethiopia	Type of source area
Valley bottom portion of area	0.23	0.1	0	0.1	Surface runoff
Max storage (mm)	110	90	—	250	
Degraded hill portion of area	0.01	0.05	0.2	0.2	Surface runoff
Max storage (mm)	20	20	150	10	
Hillside portion of area	0.50	0.85	0.6	0.7	Interflow and baseflow
Max storage (mm)	150	150	250	500	
Max storage linear reservoir (mm)	80	90	70	20	
Half life linear reservoir (days)	60	70	70	140	
Drainage time hillsides (days)	3	10	20	35	
Nash Sutcliff	0.78	0.80	0.88	0.60	

<sup>1</sup>Ten day intervals.

The optimum parameter set for each of the three basins and for the Ethiopian highlands are shown in Table 7.3 and the comparison of observed versus predicted values for the SCRP watersheds are shown in Fig. 7.6a, b, c. The model fit the observed data well for the SCRP watersheds with Nash Sutcliffe efficiencies for daily values in the range of 0.78–0.88 (Table 7.3) for the small watersheds. Due to difficulties with obtaining a true average rainfall for the whole Blue Nile Basin, Nash Sutcliffe efficiency for the Blue Nile Basin was lower.

The parameter values for all three SCRP watersheds fall in the same range: 0–23% for the saturated bottom lands with a maximum storage of 110 mm; 0–20% for the degraded lands with storage values less than 150 mm; and 50–75% for the hillsides with storages up to 250 mm. The degraded land in the Anjeni watersheds consists of agricultural soils on terraced land, which soil has a restricting layer at shallow depths. In Maybar and Andit Tid, the degraded soils consist of both exposed hardpan areas and slipping hillside areas. Maybar has less of the soils than Andit Tid. This is the reason that the maximum storage for Anjeni is greater than for the other two watersheds.

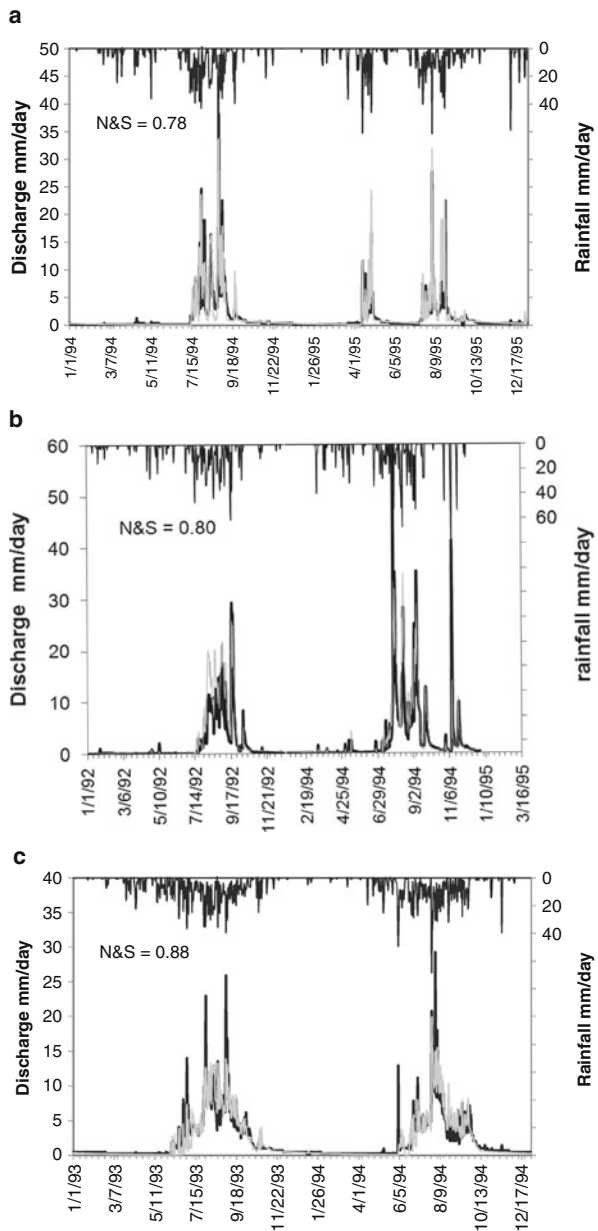


**Fig. 7.6** Measured and modeled streamflow for the (a) Maybar watershed, (b) Andit Tid watershed and (c) Anjeni watershed. The *light grey line* is the simulated discharge values and the *thick black curve* is observed runoff. The *thin black line* is the surface runoff. N&S is the Nash Sutcliffe efficiency

Good fits were obtained between simulated and observed values for both the daily calibration and validation periods. However, the model underestimates most peak flow periods for Anjeni and Andit Tid (Fig. 7.6b, c). Water balance type models have difficulty handling intense convective storms or events of very short duration but high intensity rainfall. In addition, it is likely that a larger part of the hillside contributed to the flow than initialized in the model structure in which the watershed is divided in three regions. Seasonal variations in rainfall amount and distribution may affect the extent of saturated areas and thereby stream flow generation. Several researchers point out that the dynamic variation of stream zone saturated areas due to accumulation of lateral water flow from upslope and the ground water system is responsible for a highly non-linear catchment response during storm events (Todini, 1995; Bari and Smettem, 2004). Adding a fourth region that can saturate during large storm events may produce better estimates for these high runoff events.

The variation among the parameters was in agreement with the landscape characteristics. In Maybar, the model fitting indicated that there were almost no degraded hill slopes. For the Anjeni watershed that had a deep gully and ground water tables generally at least 2 m below the surface, the model fit the data best if there was no saturated area included. Note also that for the two smallest watersheds, Maybar and Anjeni, the portions of the three modeled areas (Table 7.3) of the total watershed area did not add up to one because of regional flows where water drained under the gage. But, for the whole Blue Nile Basin and Andit Tid, the water balance closed and the portions of the total area summed to one. Finally, the magnitude of the subsurface parameters increased with the size of the watershed as expected because as watershed size increases, more deep flow paths become activated in transport.

## 7.5 Conclusions

Direct runoff is generated either from saturated areas at the lower portions of the hill slopes or from areas of exposed bedrock while the upper hill slopes are infiltration zones. As a result, the watersheds were divided into variable saturated areas, exposed rock and hill slopes. This was verified by high measured infiltration rates on hill slope areas and shallow ground water depth at the bottom flat lands. Other findings showed that the lower slope areas produced high runoff compared to high slopes for a given rainfall event. The discharge in each of three watersheds was modeled by separately using a simple water balance type model for degraded hillsides, saturated areas, and non-degraded hillsides. The main input data for the model are rainfall, evaporation, the relative magnitude of the three areas, and soil water holding capacity for the three areas. In addition, interflow and baseflow constants are needed. The model results were encouraging, not only for the three small watersheds, but for the Blue Nile watershed at the Ethiopian-Sudan border as well. The model has the potential to predict runoff in ungauged basins using a small amount of field data.

**Acknowledgments** Funding of the assistantship of the senior author was made available by SWHISA (Sustainable Water Harvesting and Institutional Strengthening in Amhara Region). Funding was made available by Bahir Dar University through the World Bank funded DIF program and by the CGIAR Challenge Program on Water and Food. The research was carried out under the auspices of the International Water Management Institute managed project, PN19 “Improved Water and Land Management in the Ethiopian Highlands and its Impact on Downstream Stakeholders Dependent on the Blue Nile”. The runoff data were graciously available by Amhara Regional Agricultural Research Institute. The help and cooperation of the field technicians and farmers in the three watersheds is greatly appreciated. Without their help, this research would have been impossible to carry out. Finally, we would like to thank professor Hurni for his foresight in establishing the three watersheds for the collection of runoff data collection.

## References

Arseno Y, Tamrat I (2005) Ethiopia and the Eastern Nile basin. *Aquat Sci* 16:15–27

Ayenew T, Gebreegziabher Y (2006) Application of a spreadsheet hydrological model for computing the long-term water balance of Lake Awassa, Ethiopia. *Hydrol Sci* 51(3):418–431

Bari M, Smettem KJR (2004) Modeling monthly runoff generation processes following land use changes: ground water-surface runoff interactions. *Hydrol Earth Sys Sci* 8(5):903–922

Bayabil HK (2009) Modeling rainfall runoff relationships at Maybar watershed, Wollo, Ethiopia. Master Thesis, Integrated Watershed Management and Hydrology Program, Cornell University, Bahir Dar Ethiopia and Ithaca, NY

Bosshart U (1997) Measurement of River discharge for the SCRP research Catchments: gauging station profiles. Soil conservation research project, Research reports 31 University of Bern, Bern

Collick AS, Easton ZM, Engda TA, Ashagrie BB, Adgo E, Awulachew SB, Zeleke G, Steenhuis TS (2009) Application of physically based water balance model on four watersheds throughout the upper Nile basin in Ethiopia. *Hydrol Process* 23:3718–3727

Conway D (1997) A water balance model of the upper Blue Nile in Ethiopia. *Hydrol Sci* 42: 265–282

Conway D, Hulme M (1993) Recent fluctuations in precipitation and runoff over the Nile sub-basins and their impact on main Nile discharge. *Clim Change* 25:127–151

Derib SD (2005) Rainfall-runoff processes at a hill-slope watershed: case of simple models evaluation at Kori-Sheleko Catchments of Wollo, Ethiopia. M.Sc. Thesis

Desta G (2003) Estimation of runoff coefficient at different growth stages of crops in the highlands of Amhara Region. M.Sc. Thesis, Alemaya University, Ethiopia

Engda TA (2009) Modeling rainfall-runoff-soil loss relationships of North-eastern Highlands of Ethiopia, Andit Tid watershed, Ethiopia. Master Thesis, Integrated Watershed Management and Hydrology Program, Cornell University, Bahir Dar Ethiopia and Ithaca, NY

Haregeweyn N, Yohannes F (2003) Testing and evaluation of the agricultural non-point source pollution model (AGNPS) on Augucho catchment, western Hararghe, Ethiopia. *Agric Ecosyst Environ* 99:201–212

Hu CH, Guo SL, Xiong LH, Peng DZ (2005) A modified Xinanjiang model and its application in northern China. *Nordic Hydrol* 3:175–192

Hurni H (1984) The third progress report. Soil conservation research project, Vol.4. University of Bern and the United Nations University. Ministry of Agriculture, Addis Ababa, Ethiopia

Ibrahim AM (1984) The Nile – description, hydrology, control and utilization. *Hydrobiologia* 110:1–13

Kebede S, Travi Y, Alemayehu T, Marc V (2006) Water balance of Lake Tana and its sensitivity to fluctuations in rainfall, Blue Nile basin, Ethiopia. *J Hydrol* 316:233–247

Kim U, Kaluarachchi JJ (2008) Application of parameter estimation and regionalization methodologies to ungauged basins of the Upper Blue Nile River Basin, Ethiopia. *J Hydrol* 362:39–52

Lange J, Greenbaum N, Husary S, Ghanem M, Leibundgut C, Schick AP (2003) Runoff generation from successive simulated rainfalls on a rocky, semi-arid, Mediterranean hillslope. *Hydrology Process* 17:279–296

Legesse D, Vallet-Coulob C, Gasse F (2003) Hydrological response of a catchment to climate and land use changes in tropical Africa: case study south central Ethiopia. *J Hydrol* 275:67–85

Legesse ES (2009) Modeling rainfall-runoff relationships for the Anjeni watershed in the Blue Nile basin, Ethiopia. Master Thesis, Integrated Watershed Management and Hydrology Program, Cornell University, Bahir Dar Ethiopia and Ithaca, NY, USA

Liu BM, Abebe Y, McHugh OV, Collick AS, Gebrekidan B, Steenhuis TS (2008) Overcoming limited information through participatory watershed management: case study in Amhara, Ethiopia. *Phys Chem Earth* 33:13–21

McHugh OV (2006) Integrated water resources assessment and management in a drought-prone watershed in the Ethiopian highlands. PhD dissertation, Department of Biological and Environmental Engineering. Cornell University, Ithaca, NY

Merz J, Dangol PM, Dhakal MP, Dongol BS, Nakarmi G, Weingartner R (2006) Rainfall-runoff events in a middle mountain catchment of Nepal. *J Hydrol* 331(3–4):446–458

Mohammed A, Yohannes F, Zeleke G (2004) Validation of agricultural non-point source (AGNPS) pollution model in Kori watershed, South Wollo, Ethiopia. *Int J Appl Earth Obs Geoinf* 6: 97–109

Setegn SG, Srinivasan R, Dargahi B (2008) Hydrological modeling in the Lake Tana Basin, Ethiopia using SWAT model. *Open Hydrol J* 2:49–62

Steenhuis TS, Collick AS, Easton ZM, Legesse ES, Bayabil HK, White ED, Awulachew SB, Adgo E, Ahmed AA (2009) Predicting discharge and erosion for the Abay (Blue Nile) with a simple model. *Hydrology Process* 23:3728–3737

Sutcliffe JV, Parks YP (1999) The hydrology of the Nile. IAHS Special Publication 5, Wallingford, 180pp

Todini E (1995) The ARNO rainfall-runoff model. *J Hydrol* 175:339–382

Zeleke G (2000). Landscape dynamics and soil erosion process modeling in the North-western Ethiopian Highlands. African Studies Series A 16, Geographica Bernensis, Berne

## Chapter 8

# Evapotranspiration Modeling Using Remote Sensing and Empirical Models in the Fogera Floodplain, Ethiopia

**Temesgen Enku, Christiaan van der Tol, Ambro S.M. Gieske, and Tom H.M. Rientjes**

**Abstract** Conventional methods and remote sensing were applied for the estimation of reference evapotranspiration and actual evapotranspiration over the Fogera floodplain. Reference evapotranspiration ( $ET_0$ ) by Modified Makkink (MM), Priestly-Taylor (PT) and Abtew (A) simple equations was compared to the Penman-Monteith (PM) estimations, in order to decide which method for  $ET_0$  is the most suitable alternative to PM in data scarce conditions. A comparison was also made to a satellite based energy balance approach that estimated actual evapotranspiration. For the remote sensing approach, images from the Moderate Resolution Imaging Spectroradiometer (MODIS) sensor were selected. For the study, data has been used from Bahir Dar meteorological station at a distance of 50 km from the floodplain and from Woreta weather station that is located in the floodplain. The comparison of results from the conventional methods indicated that the MM method performed best over the floodplain as compared to the PM approach while the PT and Abtew (A) simple equations only produced fair results. The latter two approaches required calibration of site specific coefficients that may have affected the estimation results. Accumulated actual evapotranspiration from the satellite based approach for the year 2008 was about 1,519 mm for rice, while the reference evapotranspiration by the PM approach was 1,498 mm. A comparison of these results with literature values of the crop coefficient of rice indicated that rice transpired at a potential rate.

**Keywords** Evapotranspiration · MODIS · SEBS · Remote sensing · Penman-Monteith · Makkink · Priestley-Taylor · Abtew model · Fogera

---

T. Enku (✉)

Department of Water Resources Engineering, Bahir Dar University,  
Bahir Dar, Ethiopia  
e-mail: enku\_te@yahoo.com; temesgenku@gmail.com

## 8.1 Introduction

Population growth over the past decades in the Lake Tana basin caused the demand for fresh water to increase. Water supply has to meet requirements not only for irrigation and agricultural production but also for domestic uses. Hence, in the area well planned and adequate water resources management is required at local and regional scales. For such management, first quantitative assessments need to be made for meteorological processes of precipitation and evapotranspiration that affect the water balance of the basin at large. This study aims to estimate actual evapotranspiration on the Fogera floodplain, Lake Tana basin, Ethiopia, that probably is the most productive agricultural area in the Lake Tana basin. Also, large scale irrigation is scheduled in the near future.

In the literature, many approaches are available to estimate actual evapotranspiration. Approaches commonly rely on estimated potential evapotranspiration that is estimated from meteorological data. Empirical coefficients in the various conventional methods estimations are usually not transferable to other regions and only have validity for the areas and the period over which estimations are made. As such use of conventional methods results in estimation errors of different magnitude and selecting the most reliable method requires comparison of estimates to select the method that gives best results with preferably minimum data requirement.

### 8.1.1 *Background and Literature Review*

Evapotranspiration is a general term that includes all the processes that water in the liquid state or solid state change into gaseous state. Hence the term includes evaporation from open water surface and from bare soil, transpiration through plant leaves and sublimation from snow and ice surfaces. This phase change is mainly influenced by the availability of solar energy at the evaporating and transpiring surfaces. Both processes occur simultaneously and quantifying these processes separately is complex.

Conventional reference ET estimation methods are commonly applied in specific climatic conditions. For instance, Penman Monteith (PM), Priestly-Taylor (PT), Modified Makkink (MM), and Abtew (A) simple methods were developed for humid areas. In Allen et al. (1998), the Penman-Monteith (PM) method is discussed as a standard method for reference evapotranspiration estimation and is globally most widely used. Conventional methods are ground based and estimate ET using weather station data that is collected at a point scale. Spatial variation of the turbulent fluxes as caused by differences in land cover and topography constrains the translation of ground based methods for  $ET_0$  into  $ET_a$  for larger spatial areas. To overcome the issue of the observation scale, remote sensing is often advocated since an entire area such as a catchment can be covered by satellite images. Nowadays

there are a number of satellite based approaches developed for the estimation of actual evapotranspiration that are all based on solving the land surface energy balance equation. Examples are the Surface Energy Balance Systems (SEBS) (Su, 2002), the Surface Energy Balance Algorithm for Land (SEBAL) (Bastiaanssen, 1998), and the Two Source Energy Balance approach (TSEB) (Norman et al., 1995).

In this chapter, the SEBS approach is selected. In this approach, the latent heat flux is estimated as a residual of net radiation from sensible and soil heat flux estimations. SEBS has applications in various climatic zones with good performance when estimating the surface energy fluxes. In central Arizona, it was tested by Su (2002) and good results were reported. McCabe and Wood (2006) in their study in central Iowa, USA showed that SEBS based latent heat fluxes agree well with the flux tower measurements.

SMEC (2007) reported in a hydrological study of the Tana-Beles sub-basins and estimated ET over the floodplain to be 140, 117, 116 mm, and 129 mm for the months of June, July, August and September, respectively. Water Watch (2005) reports on a satellite based energy balance approach of Tana-Beles sub basins and reported an average  $ET_a$  of 672 mm/year over the entire lake basin area. Hence, this study will be valuable for estimation of the reference and actual ET over the floodplain using both conventional methods and the SEBS approach.

The effects of characteristics that distinguish field crops from the reference grass are integrated in to the crop coefficient ( $K_c$ ). The  $K_c$  of a crop varies with the crop growing stages (Allen et al., 1998). The rice crop coefficient ( $K_c$ ) is estimated here as the ratio of actual evapotranspiration ( $ET_a$ ) to PM reference ET of the rice field in the floodplain.

### 8.1.2 *Objectives*

The main objective of this study is to analyze ET estimations by different conventional methods and estimation of spatiotemporal distribution of actual ET over the Fogera floodplain. The specific objectives are (1) estimation of reference ET using Penman-Monteith (PM), Priestley-Taylor (PT), Modified Makkink (MM) and Abtew (A) equation and (2) the application of Surface Energy Balance Systems (SEBS) for the estimation of actual ET from satellite data.

## 8.2 Study Area

The Fogera floodplain is located in northwestern Ethiopia, about 625 km from the capital Addis Ababa along the shores of Lake Tana. The Ribb and Gumara Rivers with catchment areas of 1,283 and 1,302 km<sup>2</sup> respectively (Abeyou, 2008), pass through the plain and both drain to Lake Tana (Fig. 8.1).

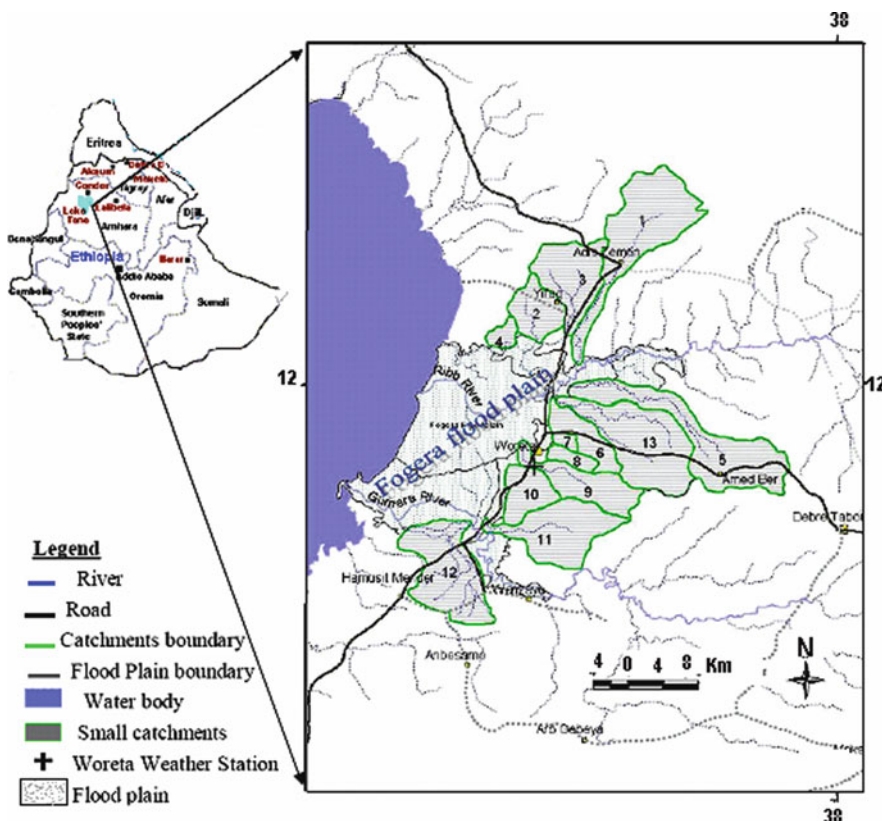


Fig. 8.1 Location map of the Fogera floodplain

The floodplain is bounded by Lake Tana in the west, the Gumara River in south, the Ribb River in the north, and the Bahir Dar-Gondar road in the east. Its latitude ranges from  $11^{\circ}45' N$  to  $12^{\circ}03' N$  while its longitude lies between  $37^{\circ}29' E$  and  $37^{\circ}49' E$ . It stretches about 15 km east-west and 34 km north-south, with an elevation of about 1,800 m amsl, having an inundation area of about 490 km<sup>2</sup>.

### 8.2.1 Climate

Total annual rainfall in the floodplain ranges from about 1,100–1,530 mm. The mean monthly rainfall in the floodplain ranges from 0.4 mm in January to 414 mm in August. The mean monthly temperature of the area is about 19°C, monthly mean maximum temperature of about 27.3°C, and monthly mean minimum temperature is 11.5°C (Dagnachew and Woubet, 2008). The rainy season in the area starts in June and ends in October. About 56% of the Fogera floodplain is covered by rice fields (Temesgen, 2009).

## 8.3 Materials and Data

### 8.3.1 Station Data

For this study, weather station data is collected from Woreta weather station and from Bahir Dar (BD) station that is part of the National Ethiopian Meteorological Network. Woreta weather station (WWS) is located at  $11^{\circ}54' \text{ N}$  and  $37^{\circ}41' \text{ E}$ . Four months data of temperature, relative humidity, atmospheric pressure, incoming solar radiation, and wind speed were collected from this station. These variables were observed at frequency of 1 Hz and automatically recorded at 5-min interval. Bahir Dar station is located at  $11^{\circ}04' \text{ N}$  and  $37^{\circ}25' \text{ E}$  and was used in this study, although its location is some 50 km from the study area. The station was selected to allow for better estimation of ET. Extraterrestrial solar radiation differences computed at the both stations was found less than  $1 \text{ W/m}^2$  (Temesgen, 2009). Also daily temperature and relative humidity were compared and a relation was established between these two stations. The comparison showed that the Bahir Dar station data could be used without significant error in the estimation of ET in the floodplain.

### 8.3.2 Remote Sensing Data

The Moderate Resolution Imaging Spectroradiometer (MODIS) on board of Terra products were collected which were processed in SEBS. Products used include land surface temperature, surface reflectance and leaf area index. The detailed description of the MODIS products are shown in Temesgen (2009).

## 8.4 Theory and Methods

### 8.4.1 Ground Based Evapotranspiration Estimation Models

#### 8.4.1.1 Penman-Monteith Method

The Penman-Monteith equation (Monteith, 1965; Penman, 1948) is a physically based combination approach that incorporates energy and aerodynamic considerations. The Penman-Monteith (PM) equation produces direct estimates of actual ET ( $ET_a$ ), but requires knowledge of the PM canopy resistance (Sumner and Jacobs, 2005). Generally, the PM equation gives acceptable ET estimates for practical applications (Widmoser, 2009), which require measurement of net radiation, soil heat flux, air temperature, relative humidity, and wind speed. The calculation of the net radiation and the assumption of soil heat flux were according to the FAO-56 version. Reference evapotranspiration ( $ET_0$ ) is the potential ET from a hypothetical green grass of uniform height, 0.12 m, well watered, and a constant albedo of 0.23 with fixed surface resistance of 70 s/m (Allen et al., 1998). After the aerodynamic

resistance,  $r_a = 208/u_2$  and the surface resistance  $r_s = 70$  s/m are estimated; for the reference crop, the PM equation can be rewritten as:

$$ET_0 = \frac{0.408\Delta (R_n - G) + \gamma \frac{900}{T+273} u_2 (e_s - e_a)}{\Delta + \gamma (1 + 0.34u_2)} \quad (8.1)$$

where

- $ET_0$  = reference evapotranspiration (mm/day),
- $R_n$  = the net radiation at the crop surface (MJ m<sup>-2</sup>/day),
- $G$  = soil heat flux density (MJ m<sup>-2</sup>/day), assumed zero on daily basis,
- $T$  = mean daily air temperature at 2 m height (°C),
- $u_2$  = wind speed at 2 m height (m/s),
- $e_s$  = saturation vapour pressure (kPa),
- $e_a$  = actual vapour pressure (kPa),
- $e_s - e_a$  = saturation vapour pressure deficit (kPa),
- $\Delta$  = slope vapour pressure curve (kPa/°C),
- $\gamma$  = psychrometric constant (kPa/°C).

#### 8.4.1.2 Priestley-Taylor Method

The PT equation (Priestley and Taylor, 1972) was developed for open water and wet land surfaces, so the PT method gives better results (Brutsaert, 2005) when soil moisture is not a limiting factor for ET. The Fogera plain is wet for a long period in the year. ET<sub>0</sub> estimation with the PT method will be compared with the standard PM ET<sub>0</sub> and a locally calibrated coefficient will be proposed for the study area. The PT equation is expressed as:

$$ET_0 = \alpha \left( \frac{\Delta}{\Delta + \gamma} \right) \left( \frac{R_n - G}{\lambda} \right) \quad (8.2)$$

where  $ET_0$  is in mm/day, and the other input parameters as defined in equation (8.1). It was reported that, the coefficient  $\alpha$  varies in the range of  $1.3 \pm 0.03$  for wetland surfaces (Priestley and Taylor, 1972). For this study,  $\alpha$  value of 1.3 was used.

#### 8.4.1.3 Modified Makkink Method

The Modified Makkink (MM) method is widely used in western Europe. This method is one of the simplest radiation models. The result from this will be compared with PM method and a calibrated coefficient will be proposed. The MM method is defined as (De Bruin, 1981):

$$ET_0 = 0.65 \frac{\Delta}{\lambda(\Delta + \gamma)} R_s \quad (8.3)$$

where  $R_s$  is the incoming solar radiation (MJ m<sup>-2</sup>/day).

#### 8.4.1.4 Simple Abtew Equation

This method requires only solar radiation for estimation of ET. This simple method gives actual ET when soil moisture is not a limiting factor for ET and in drier conditions it gives potential ET (Abtew, 1996). It is formulated as:

$$ET = k \frac{R_s}{\lambda} \quad (8.4)$$

where ET (mm/day) is the daily evapotranspiration,  $k$  is taken as 0.53, this coefficient could be calibrated locally (Abtew and Obeysekera, 1995). A locally calibrated coefficient will be proposed, after comparing with the P-M reference ET.

#### 8.4.2 Surface Energy Balance Systems (SEBS)

The SEBS method developed by Su (2002) is one of the remote sensing methods to estimate turbulent surface energy fluxes. MODIS spectral products and meteorological data were used for the estimation of energy fluxes in SEBS. Actual ET ( $ET_a$ ) is estimated as a residual of mass balance and energy balance equations, which is written as:

$$ET_a = \frac{R_n - G - H}{\lambda} \quad (8.5)$$

where  $R_n$  is the net radiation,  $G$  is the soil heat flux,  $H$  is the sensible heat flux and  $\lambda$  is the latent heat of evaporation (J/kg). Parameterizations of the inputs for the SEBS algorithm are explained in detail in Su (2002) and Temesgen (2009). The instantaneous values obtained with Eq. (8.5) are first extrapolated to daily values using the assumption that the evaporative fraction is constant during the day. Secondly, the daily values are extrapolated to monthly estimates, using the monthly PM estimates based on sunshine hours. All pixels of the floodplain are then averaged to obtain a single monthly  $ET_a$  value.

### 8.5 Results and Discussion

In this section, first, the performance of conventional methods of reference ET estimations are compared to the Penman-Monteith PM equation. Second, the results of the calculation of actual ET with the SEBS approach are discussed. Finally, the results are combined to yield the local crop coefficient of rice.

### 8.5.1 Reference Evapotranspiration

#### 8.5.1.1 Priestley Taylor

Figure 8.2 shows scatter plots of PT versus PM reference ET for two stations: Woreta (left panel) and Bahir Dar (right panel), using an a priori coefficient of  $\alpha = 1.3$ . Table 8.1 shows the statistics of the comparison: the  $R^2$ , the root mean square error (RMSE), the average mean error (AME) and the bias (in mm/day). The table includes both the results for the a priori value of  $\alpha = 1.3$  and a (least square error) calibrated coefficient of  $\alpha = 1.14$ . Calibration obviously improved the results significantly for both the stations: the RMSE, AME and bias are reduced by a factor 2 or more.

#### 8.5.1.2 Modified Makkink

A similar comparison between PM and MM shows that the Makkink method performs very well (Fig. 8.3 and Table 8.1). Even though the Makkink method was

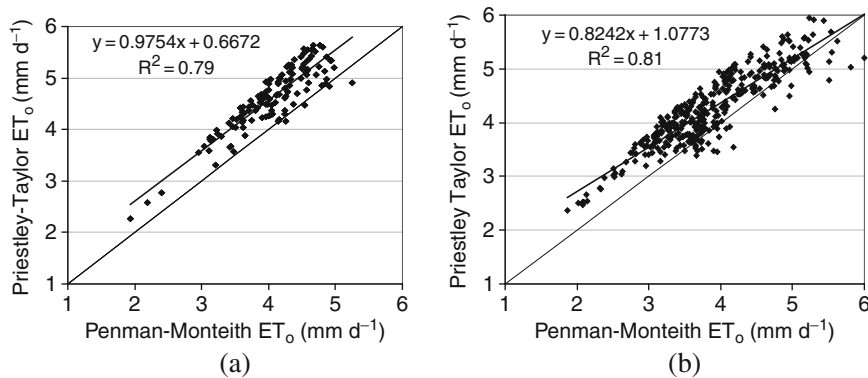


**Fig. 8.2** Scatter plot of PT vs PM  $ET_0$  at stations **(a)** Woreta **(b)** Bahir Dar

**Table 8.1** Comparison of different methods (PT, MM and A) with PM

Methods	$R^2$		RMSE (mm $day^{-1}$ )		AME (mm $day^{-1}$ )		Bias (mm $day^{-1}$ )	
	WWS	BD	WWS	BD	WWS	BD	WWS	BD
PT								
$\alpha = 1.30$	0.79	0.81	0.77	0.63	0.72	0.56	0.71	0.53
$\alpha = 1.14$	0.79	0.81	0.29	0.34	0.25	0.27	0.13	0.01
MM	0.93	0.88	0.19	0.25	0.16	0.19	0.00	0.01
A								
$k = 0.53$	0.90	0.81	0.60	0.63	0.55	0.55	0.54	0.53
$k = 0.48$	0.90	0.81	0.25	0.34	0.21	0.21	0.11	0.11

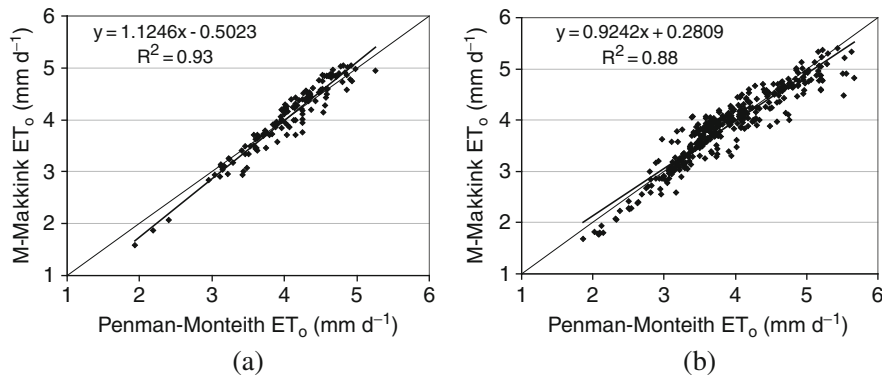


**Fig. 8.3** Scatter plot of MM vs PM ET<sub>0</sub> at stations (a) Woreta (b) Bahir Dar

developed for well-watered grassland in The Netherlands (De Bruin, 1981), the MM equation performs well for both stations without the need for calibration of the coefficient to obtain better matching ET<sub>0</sub> estimations.

#### 8.5.1.3 Abtew Equation

Figure 8.4 and Table 8.1 show the analysis for Abtew's equation. Abtew simple method also requires local calibration of the coefficient. After local calibration with coefficient  $k = 0.48$ , the result improved (Table 8.1). The MM method appears to be slightly better than Abtew's method because it does not require much calibration and hence it would be more generally valid in Ethiopian conditions.

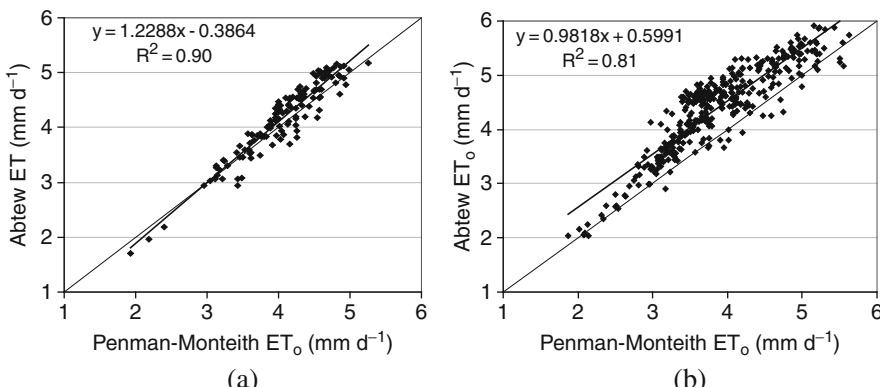


**Fig. 8.4** Scatter plot A vs PM equation at stations (a) Woreta (b) Bahir Dar

### 8.5.2 Actual Evapotranspiration with SEBS

#### 8.5.2.1 Comparison of Remote Sensing (RS) Actual ET to PM ET<sub>0</sub>

Reference evapotranspiration is a climatologic variable characterizing the evaporative demand of the surface, whereas actual evapotranspiration ( $ET_a$ ) represents the effects of soil moisture, land cover heterogeneity and the variability of climatic conditions. Comparing actual to reference evapotranspiration gives insight in the spatial variability of land cover and stress conditions. Differences between time series of actual evapotranspiration and reference evapotranspiration for specific crops indicate the seasonal cycle for the crop coefficient. It is noted that differences also are due to possible effects of water stress that is unaccounted for. We assume that water is sufficiently available not to constrain evapotranspiration. We note that ET estimations are for the wet season where rainfall commonly occurs in heavy daily showers. When comparing remote sensing based  $ET_a$  with ground based  $ET_0$ , one should realize that  $ET_0$  estimates are spatially limited and computed on daily basis, whereas the remote sensing technique estimates of  $ET_a$  are spatially distributed, but they are only valid for the instantaneous time of the satellite overpasses.

Time series of  $ET_0$  and  $ET_a$  are shown in Fig. 8.5. One day per month was analysed. The instantaneous RS  $ET_a$  values were extrapolated to daily and monthly values.

The annual  $ET_a$  estimated from this approach was 1,519 mm, while PM  $ET_0$  was 1,498 mm in the year 2008 (Nov 2007–Oct 2008). The mean annual rainfall over the last 5 years in the Fogera floodplain was 1,296 mm (Temesgen, 2009). This indicates that the annual actual ET was 17% higher than the mean annual rainfall over the area. This is probably due to the spate irrigation practices in the area during the dry seasons, which use water from upstream areas.

In Fig. 8.5, both the remote sensing daily and monthly actual ET and the PM  $ET_0$  daily and monthly estimations follow a similar trend. In the wet season (July to October) the daily estimations from SEBS were larger than the respective PM  $ET_0$ , whereas in dry seasons, the PM  $ET_0$  was larger than SEBS estimations.

This could be explained by the drying out of the top soil layers leading to a reduction of moisture available for evapotranspiration.

April is the driest month in the floodplain and soil moisture is then the limiting factor for  $ET_a$  and reduction in  $ET_a$  is then observed.  $ET_a$  is limited by the available net radiation during the rainy season.

#### 8.5.2.2 Spatiotemporal Distribution of $ET_a$ over the Entire Floodplain

The spatial and temporal variation of ET over the plain was analyzed using three selected images. The spatial variation over the entire area was more pronounced in the dry seasons. The spatial and temporal variation of ET for some selected months is shown in Fig. 8.6.

On January 1st 2008, the actual ET over the plain ranges from 2 mm in a day in bare lands to 4.6 mm a day on wet surfaces, with mean value of 3.3 mm and standard

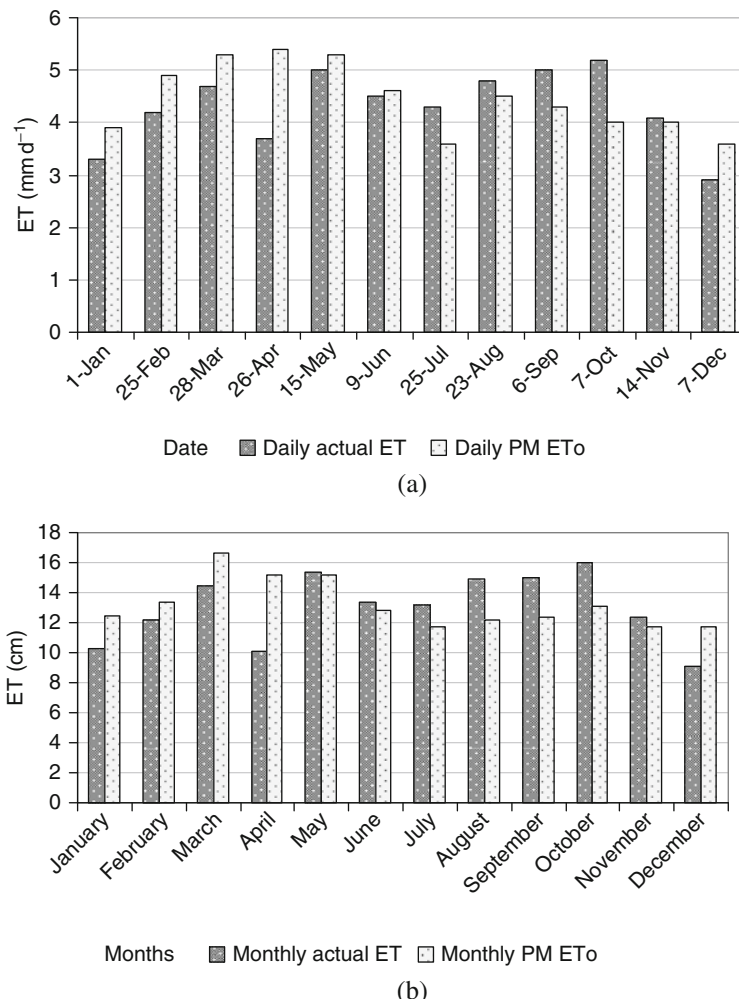


**Fig. 8.5** (a) Daily actual ET and daily PM ET<sub>0</sub> (b) monthly actual ET and PM ET<sub>0</sub>

deviation of 0.59 mm. The evaporative fraction for this day ranges from 0.4 to 0.95, with mean of 0.71 and standard deviation of 0.11.

In the same way, on 26 April 2008 the spatial distribution of ET follows similar pattern as of January 1st 2008, except here more pixels become drier. The minimum and maximum ET was 1.5 and 5 mm a day respectively, with mean value of 3.25 mm and standard deviation of 0.61 mm. The evaporative fraction ranges from 0.3 to 0.9 with mean of 0.55 and standard deviation of 0.11.

On 6 September 2008, daily ET ranges from 4 to 6 mm with mean value of 4.95 mm and standard deviation of 0.37 mm. The evaporative fraction ranges from 0.74 to 0.95 with mean value of 0.83 and standard deviation of 0.05. The lower

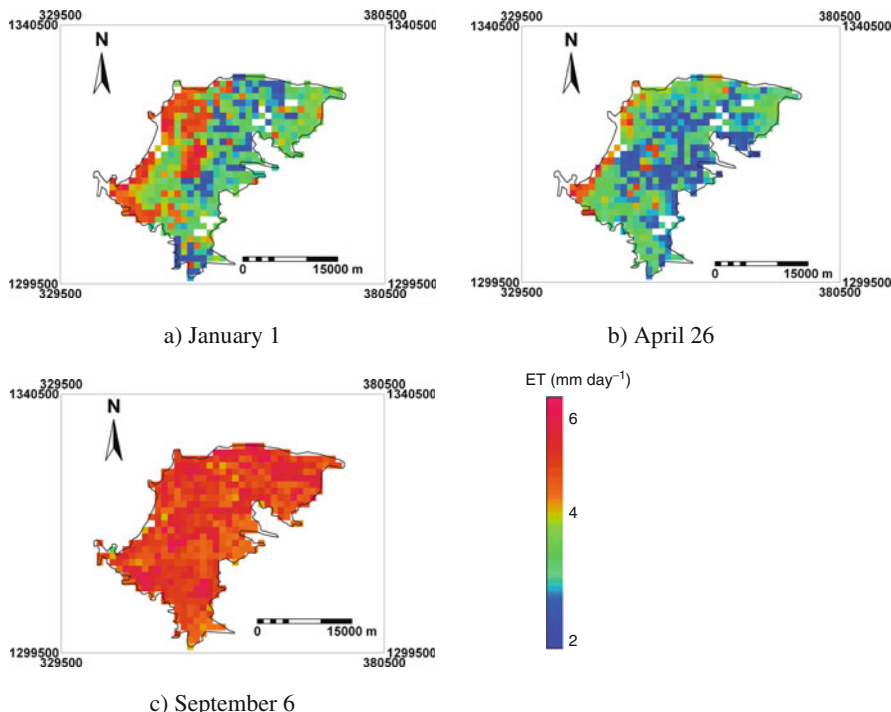


**Fig. 8.6** Spatio-temporal distribution of ET over the floodplain (Projection: UTM, WGS 84)

standard deviation here clearly shows that the spatial variation in wet months is less pronounced.

The high  $ET_a$  values in September clearly show the abundant vegetation growth in the area at the end of the rainy season. The  $ET_a$  values are lowest in April when fields are being ploughed, and conditions are dry. The January values show that vegetation is still growing vigorously near the lake shore, i.e. the lowest part of the floodplain where spate irrigation can be maintained for the longest period of time.

### 8.5.2.3 Spatiotemporal Distributions of Actual ET over Rice Fields

The spatiotemporal distribution of ET over the rice field in the floodplain was analyzed using three selected images. On July 7, the actual ET over the rice field ranges from 2.7 to 4.7 mm/day, with mean and standard deviation of 3.6 mm and 0.27 mm respectively. Similarly, on September 6, ET varies from 3.5 to 5.9 mm in a day, with mean and standard deviation of 4.95–0.37 mm respectively, whereas on December 7 ET varies from 1.5 to 4.7 mm/day with mean 2.88 mm and standard deviation of 0.79 mm. The lower value of standard deviation in July and September indicate that spatial variation in rice field was less pronounced; whereas in December as majority of the rice has been harvested and the spatial variation was more pronounced.

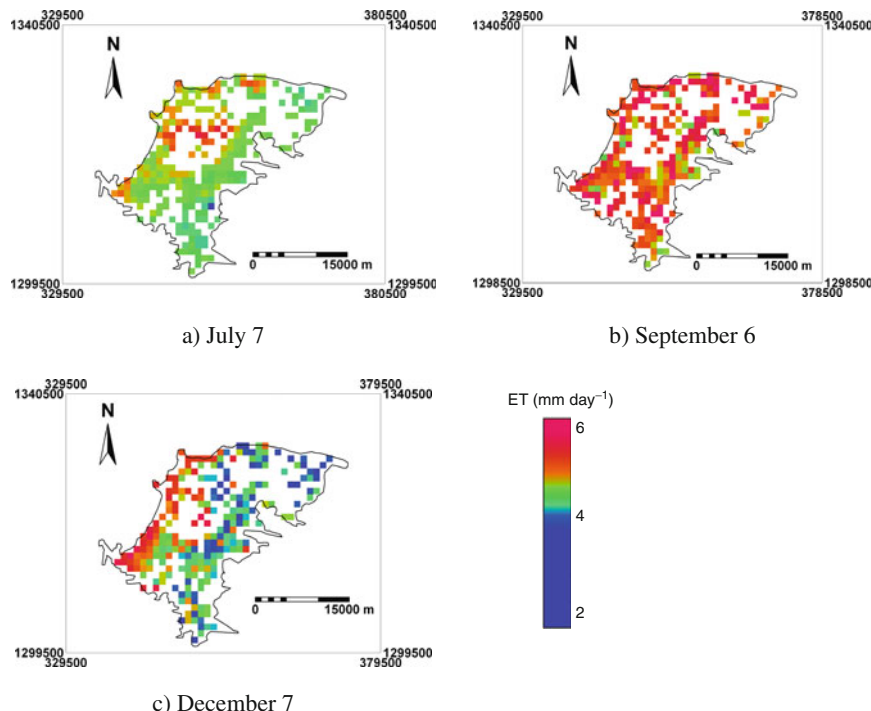


**Fig. 8.7** Spatiotemporal distribution of ET on rice field (a) July 7 (b) September 6 (c) December 7 (Projection UTM, WGS84)

In summary, the spatial variation of ET over the rice field during the seedling and the fully growing seasons was not pronounced; whereas the temporal variation of ET in the rice field was larger. During early and harvesting stage of rice, ET was relatively low compared to its fully growing season. The images of the three selected days are shown in the Fig. 8.7.

#### 8.5.2.4 Single Crop Coefficient (Kc) for Rice Field

The spatial and temporal variation of Kc is shown in selected images of Fig. 8.8. In July, where the rice was in seedling stage, the Kc had an average value of 0.9 with standard deviation of 0.12. In September, when the rice was in its mid growing stage, the Kc value had increased to an average value of 1.16, with standard deviation of 0.13 and during harvesting period, Kc reduced to an average of 0.81 and standard deviation of 0.30. These values agree well with the literature values of 1.0, 1.15 and 0.7–0.45 for initial, mid and harvesting seasons of the cropping period respectively (Allen et al., 1998). It is assumed that, there is no water stress during this period and therefore Ks can be taken as 1. This seems to be realistic because rains are usually

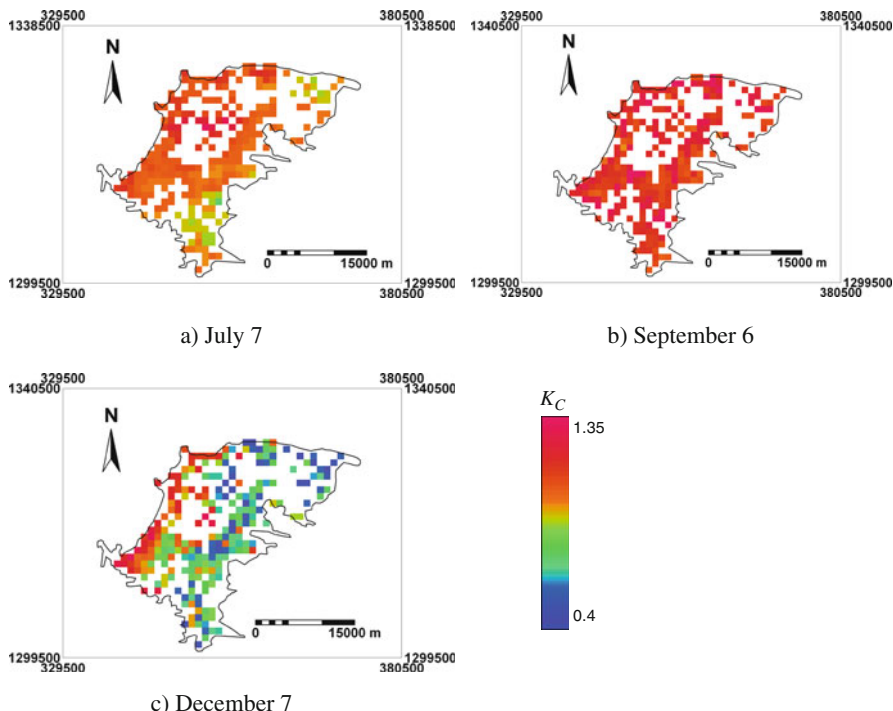


**Fig. 8.8** Spatiotemporal distribution of  $K_c$  on rice field (a) July 7 (b) September 6 (c) December 7 (projection UTM, WGS84)

abundant during the rainy season and surface water is also flowing in from upstream areas. The length of the rice growing season appears to be normal (120–150 days) (Allen et al., 1998).

## 8.6 Conclusions and Recommendations

The two objectives of this study were to compare different  $ET_0$  methods to the (more complete) PM estimate, and to derive remotely sensed based actual ET relative to  $ET_0$  over the Fogera floodplain. MODIS products were used in SEBS. The Woreta and the Bahir Dar weather station data were also used.

Ground based estimations of  $ET_0$  for the year 2008 were carried out using different methods. The different empirical methods were compared to the standard PM reference  $ET_0$ . From the different conventional methods used, the MM method was the only method which does not require local calibration of the coefficient. This method performed the best among the models tested, with a coefficient of determination  $R^2$  of 0.93, RMSE of 0.19 mm, and AME of 0.16 mm. The PT method overestimated  $ET_0$  when the a priori coefficient,  $\alpha = 1.3$  was used. Better estimates

were found when the coefficient  $\alpha$  was reduced to 1.14. The simple Abtew equation also performed well in the area. However it proved necessary to calibrate the coefficient which then gives  $R^2$  of 0.9, an RMSE of 0.25 mm/day, and AME of 0.21 mm/day. The advantage of Abtew's method is that  $ET_0$  can be estimated using radiation data only.

The spatial average of actual ET estimated from remote sensing over the floodplain was smaller than the PM reference  $ET_0$  in relatively drier periods, whereas in wet season the actual ET was larger than the PM reference  $ET_0$ . The annual actual  $ET_a$  over the floodplain was found about 1,519 mm whereas the annual PM reference  $ET_0$  was 1,498 mm. In wet seasons, the spatial variation of actual  $ET_a$  was not well pronounced, whereas in relatively dry months the spatial variation was clearly pronounced.

The crop coefficient ( $K_c$ ) of the rice field was estimated in the three growing stages in 2008. The estimations of  $K_c$  in the seedling, fully grown, and harvesting periods were 0.9, 1.16, and 0.81 respectively, where these values agree well with the literature values. The length of the growing season lies between 120 and 150 days which appear to be in line with values reported by Allen et al. (1998). The crop stress coefficient  $K_s$  has been taken as 1 because rains are usually quite good during the rainy season.

The preliminary results obtained with the MM and A methods appear to be promising. However, further validation and calibration work is required before these simple methods can be routinely applied in the area.

**Acknowledgements** This work was funded by an ITC fellowship grant. The support of Bahir Dar Me-teorological office staff who provided the weather station data is much appreciated. We are grateful to Dr. Assefa M. Melesse and other anonymous reviewers. We thank Abeyou Wale and Alebachew Abreham (both staff members of Bahir-Dar University) for their support during the field campaign.

## References

Abeyou W (2008) Hydrological balance of Lake Tana Upper Blue Nile basin, Ethiopia. ITC, Enschede, p 94

Abtew W (1996) Evapotranspiration measurements and modeling for three wetland systems in South Florida. *Water Resour Bull* 32(3):465–473

Abtew W, Obeysekera J (1995) Lysimeter study of evapotranspiration of cattails and comparison of three estimation methods. *Trans Am Soc Agric Eng ASAE* 38:121–129

Allen RG, Pereira LS, Raes D, Smith M (1998) Crop evapotranspiration: guidelines for computing crop water requirements. Rome, FAO, Report 56

Bastiaanssen WGM (1998) Remote sensing in water resources management: the state of the art. International Water Management Institute (IWMI), Colombo

Brutsaert W (2005) Hydrology: an introduction. Cambridge University Press, Cambridge

Dagnachew L, Woubet G (2008) Flood Hazard and Risk Assessment in Fogera Woreda using GIS & Remote sensing. In: Hydrology and ecology of the Nile Basin under extreme conditions, Addis Ababa, Ethiopia

De Bruin HAR (1981) The determination of (reference crop) evapotranspiration from routine weather data. *Proc Inform Comm Hydr Res TNO Hague* 28:25–37

McCabe MF, Wood EF (2006). Scale influences on the remote estimation of evapotranspiration using multiple satellite sensors. *Rem Sens Environ* 105(4):271–285

Monteith JL (1965) Evaporation and surface temperature. *Quart J Roy Met Soc* 107:1–27

Norman JM, Divakarla M, Goel NS (1995) Algorithms for extracting information from remote thermal-IR observations of the earth's surface. *Rem Sens Environ* 51(1):157–168

Penman HL (1948). Natural evaporation from open water, bare soil, and grass. *Proc R Soc London A* 193:120–145

Priestley CHB, Taylor RJ (1972) On the assessment of surface heat flux and evaporation using large scale parameters. *Monthly Weather Rev* 100(2):81–92

SMEC (2007). Hydrological study of the Tana-Beles sub-basins. Report SMEC International Pty. Ltd

Su Z (2002) The surface energy balance system (SEBS) for estimation of turbulent heat fluxes. *Hydrol Earth Sys Sci* 6(1):85–99

Sumner DM, Jacobs JM (2005) Utility of Penman-Monteith, Priestley-Taylor, reference evapotranspiration, and pan evaporation methods to estimate pasture evapotranspiration. *J Hydrol* 308(1–4):81–104

Temesgen E (2009) Estimation of evapotranspiration from satellite remote sensing and meteorological data over the Fogera Floodplain – Ethiopia. ITC, Enschede, p 89

Water Watch (2005) Remote sensing studies of Tana-Beles Sub Basins, A Nile Basin Initiative project Ministry of Water Resources, Ethiopia

Widmoser P (2009) A discussion on and alternative to the Penman-Monteith equation. *Agric Water Manag* 96:711–721

# Chapter 9

## Flood Hazard and Risk Assessment Using GIS and Remote Sensing in Fogera Woreda, Northwest Ethiopia

Woubet Gashaw and Dagnachew Legesse

**Abstract** Flood is a natural disaster. However human activities in many circumstances change flood behavior. The objective of this study was to assess flood hazard and risk of Fogera woreda (district), which is one of the most severely flood affected areas in Ethiopia in general and Ribb–Gumara Catchment in particular, using Geographic information system (GIS) and remote sensing techniques. Land use/land cover change detection was done for the catchment using the 1973, 1985 and 1999 Landsat images and the general trend showed that vegetative and grass-land areas were mainly changed to agricultural lands. Comparison between long year (1974–2006) annual maximum daily rainfall and annual maximum daily gauge levels (1971–2005) data of Ribb and Gumara Rivers showed that rainfall slightly decreases while gauge level increases, and this can be attributed to land cover conversion especially in the upper catchment. Flood frequency analysis was done using Ribb and Gumara Rivers annual maximum daily gauge levels by Gumbel's, and the likely flood levels in different return periods were found. Digital elevation models (DEM) and the 100 year return period base-flood were combined in the GIS environment in order to produce flood inundation maps. More over, flood causative factors were developed in the GIS and remote sensing environment and weighted and overlaid in the principle of pair-wise comparison and Multicriteria Evaluation (MCE) technique in order to arrive at flood hazard and risk mapping. The major findings of the study from both the two methods revealed that most of the areas in the downstream part of the catchment and the different land uses in these areas were within high to very high flood hazard and risk level. The presence of risk assessment mapping will help the concerned authorities to formulate their development strategies according to the available risk to the area.

**Keywords** Flood risk · MCE · GIS · Remote sensing · Flood frequency · Land use/land cover dynamics

---

W. Gashaw (✉)

Department of Natural Resources Management, Bahir Dar University, Bahir Dar, Ethiopia  
e-mail: wubetga@gmail.com

## 9.1 Introduction

Flood is probably the most devastating, widespread and frequent natural hazard of the world. This problem is more acute in highland areas like Ethiopia under strong environmental degradation due to population pressure. According to UNEP (2002), the major environmental disasters in Africa are recurrent droughts and floods. Their socio-economic and ecological impacts are devastating to African countries, because most of them do not have real time forecasting technology or resources for post-disaster rehabilitation.

Topographically, Ethiopia is both a highland/mountainous and lowland country. It is composed of nine major river basins, the drainage systems of which originate from the centrally situated highlands and make their way down to the peripheral or outlying lowlands. Especially during the rainy season (June-September), the major perennial rivers as well as their numerous tributaries forming the country's drainage systems carry their peak discharges.

Owing to its topographic and altitudinal characteristics, flooding, as a natural phenomenon, is not new to Ethiopia. They have been occurring at different places and times with varying magnitude. Some parts of the country do face major flooding. Most prominent ones include: extensive plain fields surrounding Lake Tana and Gumara and Rib Rivers in Amhara Regional State; areas in Oromia and Afar Regional States that constitute the mid and downstream plains of the Awash River; places in Somali Regional State that fall mainly along downstream of the Wabishebelle, Genalle and Dawa Rivers; low-lying areas falling along Baro, Gilo and Akobo Rivers in Gambella Regional State; downstream areas of Omo River in the Southern Nations, Nationalities and Peoples Regional State (DPPA, 2006).

The country experiences two types of floods: flash floods and river floods. Flash floods are the ones formed from excess rains falling on upstream watersheds and gush downstream with massive concentration, speed and force. Often, they are sudden and appear unnoticed. Therefore, such floods often result in a considerable toll; and the damage becomes especially pronounced and devastating when they pass across or along human settlements and infrastructure concentration. The recent incident (2006 summer) that the Dire Dawa City experienced was typical of flash flood. On the other hand, much of the flood disasters in Ethiopia are attributed to rivers that overflow or burst their banks and inundate downstream plain lands. The flood that has recently assaulted Southern Omo Zone and South Gondar (mainly Fogera woreda) Zone was a typical manifestation of river floods.

It is evident that, the problem of river flooding in Ethiopia is getting more and more acute due to human intervention in the fragile highland areas at an ever-increasing scale. According to United Nation Office for the Coordination of Humanitarian Affairs (UNOCHA) (2006), across Ethiopia, the number of people affected by the floods of 2006 was 357,000 including 136,528 forced to abandon their homes. Ethiopia's northern Amhara region was the worst hit in the giant Horn of Africa nation, with 97,000 people affected, of which 37,000 lost their homes. The

**Photo 9.1** The 2006 flood in Woreta Zuzia



floods swamp large areas of cropped land in this region. Another survey conducted by the Joint Government and Humanitarian Partners Flash Appeal for the 2006 Flood Disaster in Ethiopia (DPPA, 2006) showed that in Amhara Region 40,500 people were vulnerable, 47,100 affected, and 5 were died by this year flood (Photo 9.1 and 9.2).

Fogera woreda (district) (Fig. 9.1), which is located between 11°57' N and 12°30' N latitude & 37°35' E and 37°58' E longitude, is traditionally identified as one of flood prone areas of Ethiopia. This woreda has an aerial extent of 1,110 km<sup>2</sup> and a total population of about 246,541 of which over 90% has rural setting. Elevation in the study area ranges from 1,780 to 2,510 m and it has an average elevation of 1,937 m above mean sea level. The woreda is drained by two major rivers, namely Ribb and Gumara. It totally lays in Ribb–Gumara catchment, which is part of the Blue

**Photo 9.2** Displaced people in the temporary shelter





Fig. 9.1 Location map of the study area

Nile basin. This catchment encloses big flat to gently sloping plains located in the eastern side of Lake Tana. Fogera woreda is particularly found in the downstream part of the above mentioned catchment. Overflow of Ribb and Gumara Rivers and backflow of Lake Tana has affected and displaced 43,127 and 8,728 people, respectively in Fogera woreda in the 2006 summer (UNOCHA, 2006). Some people said that several months of excessive rain has flooded rivers and stranded families in low-lying areas. While others said it is severe environmental degradation of specially the highlands that cause floods in this woreda. This issue needs research in order to design long-lasting solutions for the safety of the population and the natural environment as well.

Geographic information system (GIS) provides a broad range of tools for determining area affected by floods and for forecasting areas that are likely to be flooded due to high water level in a river. Geographic information system was extensively used to assemble information from different maps, aerial photographs, satellite images and digital elevation models (DEM). Census data and other relevant statistical abstract were also used to make the risk map more oriented to need of the local inhabitants. Remote sensing technology along with GIS has become the key tool for flood monitoring in recent years. The central focus in this field revolves around delineation of flood zones and preparation of flood hazard and risk maps for the vulnerable areas. River flooding in the developing countries of Africa is very acute because of their heavy dependence on agriculture but any flood estimation or hazard mapping attempt in this region is handicapped by poor availability of high resolution DEMs. Flood hazard mapping is a vital component for appropriate land

use planning in flood-prone areas. It creates easily read, rapidly accessible charts and maps, which facilitates the administrators and planners to identify areas of risk and prioritize their mitigation/response efforts.

The regulation of flood hazard areas coupled with enactment and enforcement of flood hazard zoning could prevent damage of life and property from flooding in short term as well as in long term. Flood management and control are necessary not only because floods impose a curse on the society, but the optimal exploitation of the land and proper management and control of water resources are of vital importance for bringing prosperity in the predominantly agricultural based economy of this highly populated woreda. This cannot become technically feasible without effective flood hazard and risk mapping. Flood risk mapping is the vital component in flood mitigation measures and land use planning. This study attempts to synthesize the relevant database in a spatial framework to evolve a flood risk map for Fogera woreda in particular and flood hazard map of Ribb and Gumara Catchment in general with the application of multi-criteria evaluation (MCE) technique. Basic aim of this effort is to identify the area chronically suffering from flooding and creates a flood hazard and risk maps based on topographical, meteorological, hydrological, and socioeconomic data. The study has also focused on the identification of factors controlling flood hazard in the study area. A flood risk map based on administrative units is particularly handy for the planners and administrators for formulating remedial strategy. It also makes the process of resource allocation simple resulting in a smooth and effective implementation of the adopted flood management strategy.

## 9.2 Materials and Methods

### 9.2.1 Study Area Description

Ribb–Gumara Catchment, drained by Ribb and Gumara Rivers, is located between  $11^{\circ}43'N$  and  $11^{\circ}53'N$  Latitude and  $37^{\circ}47' E$  &  $37^{\circ}54' E$  Longitude (Fig. 9.2). This catchment is part of the Nile River basin and more particularly that of the Lake Tana basin located on the Northeastern side of Lake Tana. It has an areal extent of about  $3,320 \text{ km}^2$ . Fogera woreda, which has an area of  $1,110 \text{ km}^2$ , totally lies in this catchment. This woreda is found in the down stream part of the catchment where Ribb and Gumara Rivers join to Lake Tana. Overflow of these rivers and back flow of Lake Tana frequently flooded this woreda than other woredas in the Catchment (FWOARD, 2006), and therefore selected for detailed flood risk study. Gumara and Ribb Rivers has their source in a mountainous area and in their lower reaches, these rivers flow through a large flat to very gentle sloping plain which is exposed to serious floods.

Fogera woreda lies to the south-eastern shore of Lake Tana on the road from Bahir Dar to Gondar, 625 km from Addis Ababa and 55 km north of the Regional

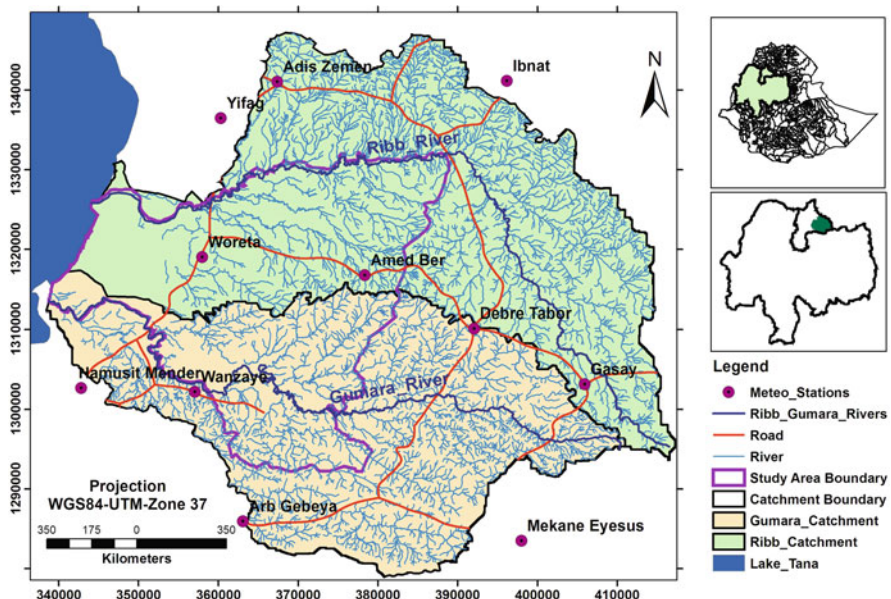


Fig. 9.2 Location map of Ribb–Gumara Catchment

capital of Bahir Dar (Fig. 9.1). The study area has a very flat land, which is known as the Fogera plain, adjacent to the eastern coast of Lake Tana. Altitude ranges from 1,780 to 2,510 m. Total annual rainfall ranges from about 1,100–1530 mm/year. The spatial distribution of rainfall showed that eastern and central part of the woreda receive highest rainfall while the northern portion receives the lowest. The seasonal rainfall has a unimodal distribution with peak in July. This is within the “Meher” season and it receives about 70% of the annual rainfall. The mean annual rainfall is 1,430 mm and mean monthly values varies between 0.6 mm (January) and 415.8 mm (July), which indicate poor temporal distribution of rainfall. The mean monthly temperature of the area is about 19°C, monthly mean maximum temperature is about 27.3°C, and monthly mean minimum temperature is 11.5°C. The major soil types in Fogera woreda exhibit a general relationship with altitude and slopes. Vertisols and Fluvisols are generally dominating the woreda and particularly the lowland flat plains, valley bottoms and river terraces. Texturally these soils are sandy clay and sandy loam respectively (FAO, 2006). Shallow Leptisols are the dominant soil types found in the mountain and hills of the study area. Luvisols dominate the southern and central part of the woreda. There have been many destructive floods in Fogera woreda, including very severe floods of 1996, 1998, 1999, 2000, 2001, 2003 and 2006 (Shiferaw and Wondafrash, 2006). The 1996 flood set a new record for flooded area, while 2006 flood was unprecedented with its long duration and damage.

### **9.2.2 Data Collection**

Contour (20 m interval) was digitized from 1:50,000 scale topographic map obtained from Ethiopian Mapping Authority (EMA). Drainage networks were also digitized from this topographic map. Annual maximum daily gauge level data (1971–2005) of Ribb and Gumara Rivers at Ribb-Addiszemen and Gumara Gauge Stations respectively was obtained from Ministry of Water Resources (MoWR). Annual maximum daily rainfall records (1974–2006) from eleven meteorological stations in and around the catchment were collected from National Meteorological Agency (NMA). Soil type shape file was obtained from Ministry of Water Resources, and Fogera woreda boundary was obtained from International Livestock Research Institute (ILRI) and digitized. The 2007 population record of the woreda was taken from Central Statistical Authority (CSA). Landsat images of February 01, 1973, November 23, 1985 and October 09, 1999 were downloaded from American Global Land Cover Facilities (GLCF) website. Finally, ground truths of the 2006 flood damage and accuracy assessment points were collected with GPS in the field.

### **9.2.3 Methodology**

Software used in this study were selected based on the capability to work on the existing problems in achieving the predetermined objectives. First and for most, Arc Hydro 9 software, which works as an extension on ArcGIS 9× version software, was used to delineate the watershed for which flood hazard analysis was done. MS Excel was used for the flood frequency analysis. Image processing software, ERDAS 9.1 was used for image processing of satellite images. Another image processing software, ENVI 4.3 was used to compute change detection analysis on land use/land cover map of classified images and to do accuracy assessment. The factor map development was carried out using ArcGIS 9.2. The factors that are input for multi-criteria analysis should be pre-processed in accordance to the criteria set to develop flood hazard and risk analysis. So, using Spatial Analyst, 3D Analyst and Geostatistical Analyst extensions, some relevant GIS analyses were undertaken to convert the collected shape files. Eigen vector for the selected factor was computed using Weight module in IDRISI 32 software.

Land cover mapping requires the use of other interpretation elements than just reflectance, particularly positioned in the landscape, with size and association. In addition, knowledge of the land use systems and their extent is essential for attributing spectral reflectance curves to land cover types.

Since the same spectral reflectance curve can represent a variety of land cover types, ground information is essential. Ground information is also needed to determine other land cover characteristics (interpretation elements) such as associations, landscape position, etc. Field visits were consequently undertaken as early as possible in the mapping of the study sites. The principal aim of the field visit was to

understand the image representation of the ground information; to learn what all the image and patterns represent, although areas of uncertainty will always be discovered later. This method was previously used to interpret aerial photography – rather than the black box approach whereby ground information is only recognized from specific training areas.

Flood risk of the woreda was analyzed from the following general risk equation (Shook, 1997).

$$\text{Risk} = (\text{Elements at risk})^* (\text{Hazard}^* \text{Vulnerability}) \quad (9.1)$$

The flood hazard analysis was computed using MCE. To run MCE, the selected flood causative factors such as slope, soil type, elevation, land use/land cover, drainage density, and rainfall were developed and weighted. Then weighted overlay technique was conducted in ArcGIS 9.2 Model Builder to generate flood hazard map. Considering the degree of loss to be total for the study area, the vulnerability is assumed to be one. Finally, to generate flood risk map of the woreda, layers of elements at risk (population density and land use) and flood hazard were overlaid using weighted overlay analysis technique in GIS environment.

Flood frequency analysis is one of the important studies of river hydrology. It is essential to interpret the past record of flood events in order to evaluate future possibilities of such occurrences. The estimation of the frequencies of flood is essential for the quantitative assessment of the flood problem. The knowledge of magnitude and probable frequency of such recurrence is also required for proper design and location of hydraulic structures and for other allied studies. The gauge data which are random variable follow the law of statistical distribution. After a detailed study of the distribution of the random variables and its parameters such as standard deviation, skewness etc. and applying probability theory, one can reasonably predict the probability of occurrence of any major flood events in terms of discharge or water level for a specified return period.

Flood frequency analysis was done in this study by selecting annual maximum daily gauge levels at Ribb-Addiszemen and Gumara gauge site located in the catchment area. Two methods of statistical distribution i.e. Gumbel's extreme value distribution and Log Pearson type III distribution were attempted by selecting peak gauge level data for 35 years (1971–2005) at the two gauge stations above.

*Gumbel's Method:* This extreme value distribution was introduced by Gumbel (1954) and is commonly known as Gumbel's distribution (Gumbel, 1954 as cited by Suresh, 2005). It is one of the most widely used probability analysis for extreme values in hydrologic and meteorological studies for prediction of flood, rainfall etc.

Gumbel defined flood as the largest of the 365 daily flows and the annual series of flood flows constitute a series of largest values of flows. This study attempt to find out water levels at different return period using the Gumbel's equation:

$$x_T = x + k * SDV, \quad (9.2)$$

where

$x_T$  = Value of variate with a return period ‘T’

$x_{avg}$  = Mean of the variate

SDV = Standard deviation of the sample

$k$  = Frequency factor expressed as

$$k = (y_T - 0.577) / 1.2825 \quad (9.3)$$

$y_T$  = Reduced variate expressed by

$$(y_T)/(T - 1) = -(\ln * \ln) \quad (9.4)$$

$T$  = Return period

*Log Pearson Type – III Method:* This method is extensively used in USA for project sponsored by US Government. In this method, the variate is first transformed into logarithmic form (base 10) and the transformed data is then analyzed (Chow et al., 1988). If “X” is the variate of a random hydrologic series, then the series of “Z” variates where  $z = \log x$  are first obtained. For this “z” series, for any recurrence interval “T”, the equation is

$$z_T = z_{avg} + Kz * SDV \quad (9.5)$$

Where,

$K_z$  = Frequency factor taken from table with values of coefficient of skew “ $C_s$ ” and recurrence interval “T”.

SDV = Standard deviation of the “Z” variate sample.

$C_s$  = Co-efficient of skew of variate “Z”

$$= \left\{ N \sum (z - z_{avg})^3 \right\} / \left\{ (N - 1) (N - 2) (SDV)^3 \right\} \quad (9.6)$$

$z_{avg}$  = Mean of the “z” values

$N$  = Sample size = Number of years of record

After finding “ $z_T$ ” with the equation above, the corresponding value of “ $x_T$ ” is obtained by

$$x_T = \text{Antilog } (z_T) \quad (9.7)$$

After obtaining gauge levels by the above two methods for different return period flood, Chi Square test was carried out for “goodness of fit”.

Recurrence Interval can be calculated as:

$$(n + 1) / m, \quad (9.8)$$

where

n is number of samples (years), and  
m-rank of a given gauge level.

## 9.3 Data Processing, Analysis and Result

### 9.3.1 Database Design

The geographic database (geodatabase) is a core geographic information model to organize a spatial data in to thematic layers and spatial representations. Two types of geodatabase architectures are available under ESRI's ArcGIS package: Personal Geodatabase and Multiuser Geodatabase. In this study, personal geodatabase was implemented to store the necessary data that could be applicable to the final analysis for the designed objectives.

### 9.3.2 Land Use/Land Cover Analysis

The 1973 MSS, 1985 TM and 1999 ETM Landsat images of Rib-Gumara catchment were used to define the different classes of land cover types and there by for the land use/land cover change detection.

Supervised image classification which is a widely used technique was applied in this study. Accordingly, the three land use/land cover maps of the year 1973 (Fig. 9.3a), 1985 (Fig. 9.3b) and 1999 (Fig. 9.3c) were generated using maximum likelihood classifier algorithm. The 1973 land use/land cover pattern of the catchment has been classified into five categories- such as agricultural land, bare land, grass land, Shrub and Reed land, and Wood land. Agricultural and wood lands occupy most of the areas in the catchment. While that of the 1985 and 1999 Land use/land cover patterns were classified in to seven classes such as agricultural land, bare land, grass land, plantation forest, Shrub and Reed land, swamp, and Wood land. In the 1985 land use/land cover classes, Agricultural and Grass lands occupy most of the areas while in that of the 1999 agricultural land constitute the largest part.

The ground truth data were utilized in the maximum likelihood report as the independent data set from which the classification accuracy was compared. The accuracy is essentially a measure of how many ground truth pixels were classified correctly. An overall accuracy of 87.63% was achieved with a Kappa coefficient of 0.84 for Landsat 1999 ETM image. The Kappa coefficient represents the proportion

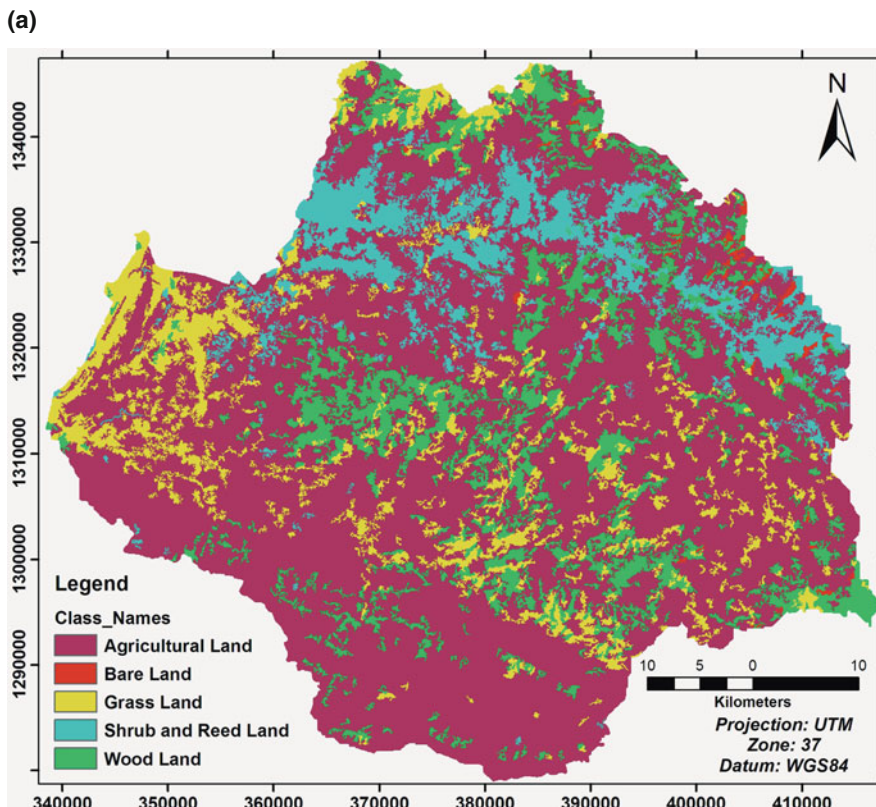


**Fig. 9.3** Land use/land cover maps of Ribb-Gumara Catchment (**a** = Feb. 02, 1973; **b** = Oct. 23, 1985; and **c** = Nov. 09, 1999)

of agreement obtained after removing the proportion of agreement that could be expected to occur by chance (Leica Geosystem, 2000). This implies that the Kappa value of 0.84 represents a probable 84.02% better accuracy than if the classification resulted from a random, unsupervised, assignment instead of the employed maximum likelihood classification. Kappa values are characterized into 3 groupings: a value greater than 0.80 (80%) represents strong agreement, a value between 0.40 and 0.80 (40–80%) represents moderate agreement, and a value below 0.40 (40%) represents poor agreement (Leica Geosystem, 2000). Therefore, the classification in this study meets the specified requirement.

Changes in land cover driven by land use can be categorized into two types: modification and conversion. Modification is a change of condition within a cover type; for example, unmanaged forest modified to a forest managed by selective cutting. Conversion is a change from one cover type to another, such as deforestation to create cropland or pasture.

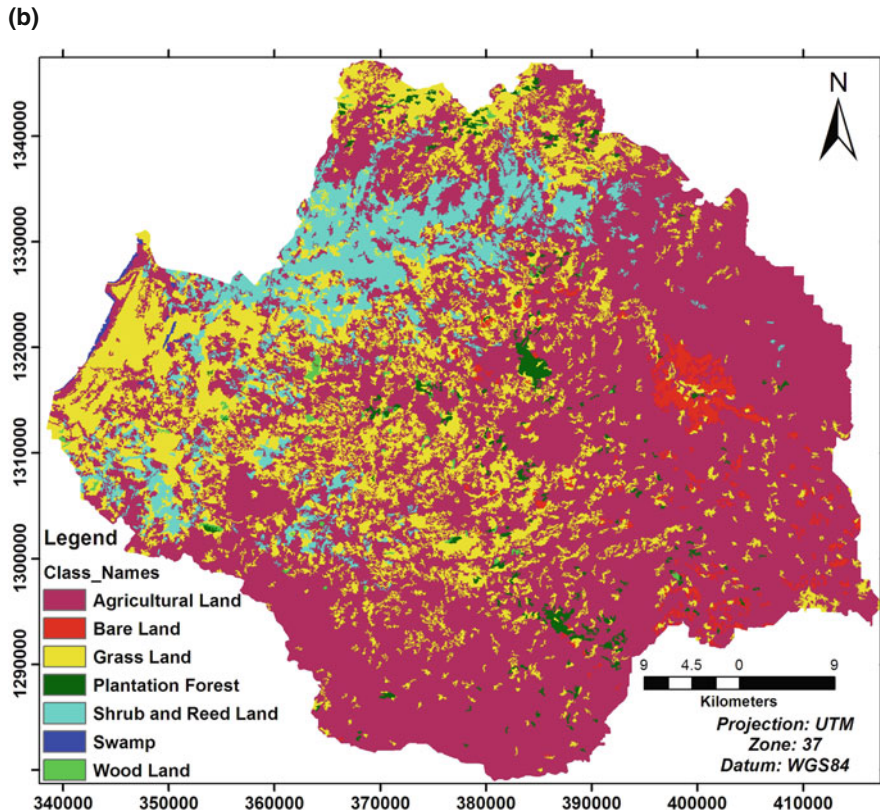


Fig. 9.3 (continued)

The most important change from 1973 to 1985 was observed in the clearance of wood land for agricultural lands, and that of the 1985–1999 was observed in the expansion of swamps and agricultural lands at the expense of grass lands (Table 9.1 and Fig. 9.4). Even bare lands were changed in to agricultural lands. The reason of areal increment of grass land from 1973 to 1985 was that the 1973 MSS image was taken in February 01 (dry season) while that of the 1985 TM image was taken in October 09 (just after the rainy season). Decrement in wood, grass and shrub and reed lands was observed from 1973 to 1999 while there is increment in agricultural land and plantation forest. Note that, most plantation forests during the field survey (May 2007) were cleared for additional agricultural lands and for firewood and construction. These have impacts on the past flooding hazards by decreasing surface roughness which retard the peak flow down stream. Table 9.1 shows areal extent of the different land use/land cover classes in three different periods (1973, 1985 and 1999). It also incorporates the change of the land uses/covers between the given years and their percent change.

(c)

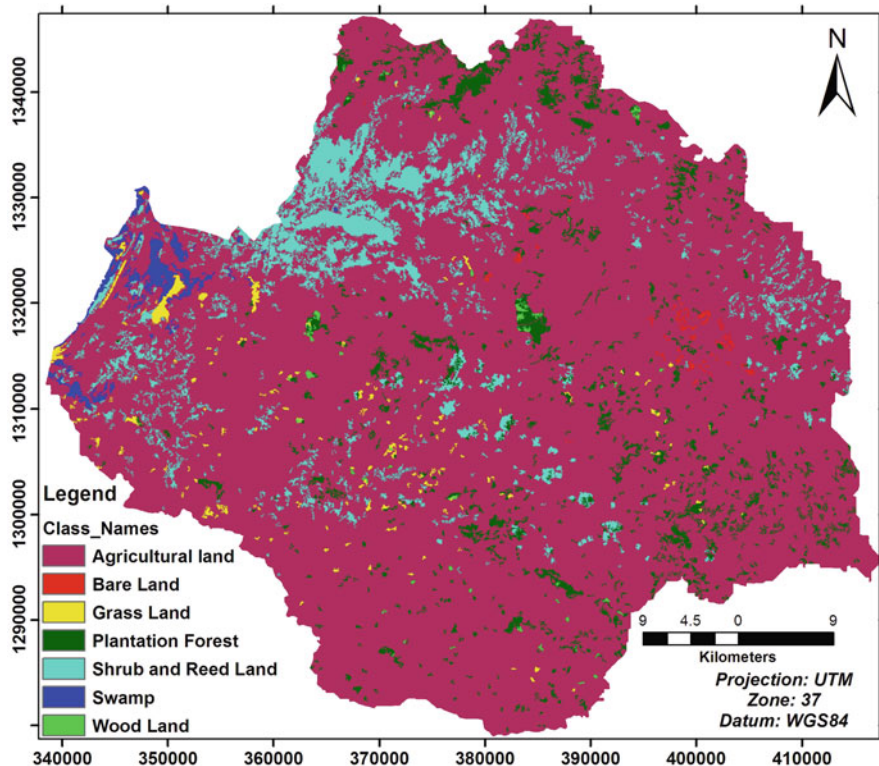


Fig. 9.3 (continued)

### 9.3.3 Flood Hazard and Risk Analysis

#### 9.3.3.1 Factor Development

Flood causative factors particularly in the study area were identified from field survey, and literature. Accordingly, slope, soil type, elevation, land use type, drainage density, and rainfall were listed in order of their importance to flood hazard. Slope has a great influence on flood hazard. The slope raster layer, which was developed from 1:50,000 topographic maps with 20 m contour interval in the GIS environment, was reclassified in five sub-group using standard classification schemes namely Quantiles. This classification scheme divides the range of attribute values into equal-sized sub ranges, allowing you to specify the number of intervals while ArcMap determines where the breaks should be. Finally, the slope was reclassified in to continuous scale in order of flood hazard rating. Soils of the catchment were converted to raster format and reclassified based on their water infiltration capacity. All the processes for the development of the elevation factor are as explained above

**Table 9.1** Land use/land cover changes in Ribb-Gumara Catchment between 1973 to 1985, 1973 to 1999, and 1985 to 1999

LU/LC type	Area coverage (km <sup>2</sup> )			Change			
	1973		1985	1973 and 1985		1985 and 1999	
	km <sup>2</sup>	%	km <sup>2</sup>	%	km <sup>2</sup>	%	km <sup>2</sup>
Agriculture	2,205.6	2,229.7	2,855.8	24.1	626.1	28.1	650.2
Shrub	292.2	271.8	239.2	-20.4	-32.6	-12.0	-53.0
Plantation	0	47.3	160.1	47.3	-	112.8	238.5
Swamp	0	4.3	30.4	4.3	-	26.1	607.0
Grass	349.0	699.4	24.9	350.4	100.4	-674.5	-96.4
Wood	464.5	11.9	7.4	-452.6	-97.4	-4.5	-37.8
Bare	16.9	59.3	6	42.4	250.9	-53.3	-89.9
Total	3,320.2	3,320.2	-	-	-	-	-

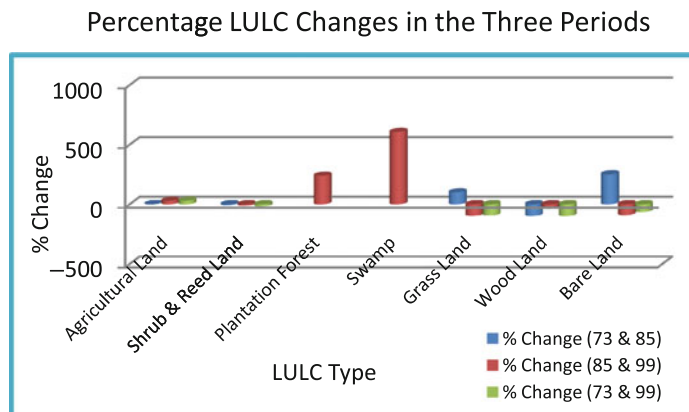


**Fig. 9.4** LULC Percentage changes between the periods 1973 and 1985, 1985 and 1999, and 1973 and 1999

in the slope factor development. The raster layer is then reclassified into a common scale according to their influence to flood hazard. Land use/land cover types of the catchment were reclassified into a common scale in order of their rainwater abstraction capacities for the flood hazard analysis, while that of the woreda were reclassified in order of their vulnerability to flooding for the flood risk analysis. The drainage density layer, which was developed from the same topographic maps explained above in the GIS environment, was further reclassified in five sub-group using standard classification schemes namely equal interval. This classification scheme divides the range of attribute values into equal-sized sub ranges, allowing you to specify the number of intervals while ArcMap determines where the breaks should be. New values (common scale) were re-assigned in order of flood hazard rating. Flood hazard and risk assessment requires an areal rainfall intensity data. However, NMA only provides point rainfall data. In addition, even though rainfall intensity was the best data for flood hazard analysis, this type of data was not available for most of the meteorological stations in Ethiopia; and therefore annual maximum daily rainfall was used. This data was changed into rainfall surface using ordinary kriging in the Geostatistical extension of ArcGIS 9.2 software. Rainfall surface was reclassified into common scale in five sub-group using standard classification schemes namely equal interval. Population density was reclassified in the assumption that the denser the population the more vulnerable it will be to flood hazard. Standardized values of each factor in the reclassification process were listed in Tables 9.2 and 9.3.

### 9.3.3.2 Flood Hazard Analysis

MCE technique was used to assess flood hazard of the catchment using GIS. MCE is a procedure which needs several criteria to be evaluated to meet a specific objective (Malczewski, J., 1999). It is most commonly achieved by one of two procedures.

**Table 9.2** Scaled and waited flood hazard inducing factors

Factor	Weight	Sub-factor	Scale (hazard)
1. Slope (percent)	0.2690	0–0.9	5 (Very high)
		0.9–6.4	4 (High)
		6.4–12.8	3 (Moderate)
		12.8–22.8	2 (Low)
		22.8–88.9	1 (Very low)
2. Soil (based on drainage capacity)	0.1793	Eutric vertisols	5 (Very high)
		Eutric fluvisols	4 (High)
		Haplic luvisols	3 (Moderate)
		Chromic luvisols	2 (Low)
		Eutric leptosols	1 (Very low)
3. Elevation (meter)	0.0860	1,780–2,240	5 (Very high)
		2,240–2,700	4 (High)
		2,700–3,160	3 (Moderate)
		3,160–3,620	2 (Low)
		3,620–4,080	1 (Very low)
4. Land use (level of flood abstraction)	0.0562	Swamp	5 (Very high)
		Agriculture/bare land	4 (High)
		Grass land	3 (Moderate)
		Wood and Shrub land	2 (Low)
		Plantation forest	1 (Very low)
5. Drainage density (km/km <sup>2</sup> )	0.3712	2.8–3.5	5 (Very high)
		2.1–2.8	4 (High)
		1.4–2.1	3 (Moderate)
		0.7–1.4	2 (Low)
		0–0.7	1 (Very low)
6. Daily max rainfall (mm)	0.0383	76.9–70.5	5 (Very high)
		70.5–64.0	4 (High)
		64.0–57.5	3 (Moderate)
		57.5–51.1	2 (Low)
		51.1–44.6	1 (Very low)

The first involves Boolean overlay whereby all criteria are reduced to logical statements of suitability and then combined by means of one or more logical operators such as intersection (AND) and union (OR). The second procedure which was used in the study is known as weighted linear combination (WLC) where continuous criteria (factors) were standardized to a common data model that was raster layer with a resolution of 30 m cell size, and then combined by means of a weighted overlay. The result is a continuous mapping of flood hazard and finally thresholded to yield a final decision.

The standardized raster layers were weighted using Eigen vector that is important to show the importance of each factor as compared to each other in the contribution of flood hazard. The weights for each factor were given through discussion with the concerned bodies and based on literature. Accordingly, the Eigen vector of the weight of the factors was computed in IDRISI 32 software in Analysis menu of the

**Table 9.3** Scaled and weighted flood risk analysis factors

Factors	Weight	Sub-factors	Scale (risk)
1. Flood hazard	0.3333	Very high	5 (Very high)
		High	4 (High)
		Moderate	3 (Moderate)
		Low	2 (Low)
		Very low	1 (Very low)
2. Population density (person/km <sup>2</sup> )	0.3333	2,396–400	5 (Very high)
		400–225	4 (High)
		225–200	3 (Moderate)
		200–175	2 (Low)
		175–149	1 (Very low)
3. Land use types (based on their sensitivity to flooding)	0.3333	Agriculture	5 (Very high)
		Grass land/bare land	4 (High)
		Swamp	3 (Moderate)
		Plantation forest	2 (Low)
		Wood and shrub land	1 (Very low)

Decision Support/Weight module. The Weight module was fed with the pair wise comparison matrix file of the factors in a Pair wise comparison 9 Point continuous scale (Eastman, 2001). And the principal eigenvector of the pair wise comparison matrix using the factors affecting flood hazard was calculated. It was found that the Consistency Ratio to be 0.02, which is acceptable. The computed Eigen vector was used as a coefficient for the respective factor maps to be combined in Weighted Overlay in ArcGIS environment.

The flood hazard maps (Fig. 9.5a, b) shows that 192.8, 502.7, 547.2, 1,099.7, 974.3 km<sup>2</sup> of Ribb–Gumara Catchment, and 141.6, 178.8, 324.3, 355.7, 108.8 km<sup>2</sup> area of Fogera woreda were subjected respectively to very high, high, moderate, low and very low flood hazards.

About three-fourth of area of the catchment under very high flood hazard fall in Fogera woreda while this woreda is only one-third of the catchment. PAs with more than three-fourth of their areas fall under high and very high flood hazard include Wagtera (100%), Nabega (99.6%), Kidiste Hana (98.9%), Shina (93.1%), and Shaga (92.2%). All of these areas lie in the downstream part of Ribb and Gumara Rivers where they join to Lake Tana. Further analysis revealed that 99.7% swamps, 93.8% grass lands, 27.9% shrub lands, and 24.1% Agricultural lands fall under high to very high flood hazard.

### 9.3.3.3 Flood Risk Analysis

As the flood hazard result of the catchment revealed, all of the very high and high hazard areas of the Catchment fall in Fogera woreda. Therefore, it is found important to do the flood risk assessment for this woreda. Flood risk assessment was done for Fogera woreda using the flood hazard layer and the two elements at risk, namely

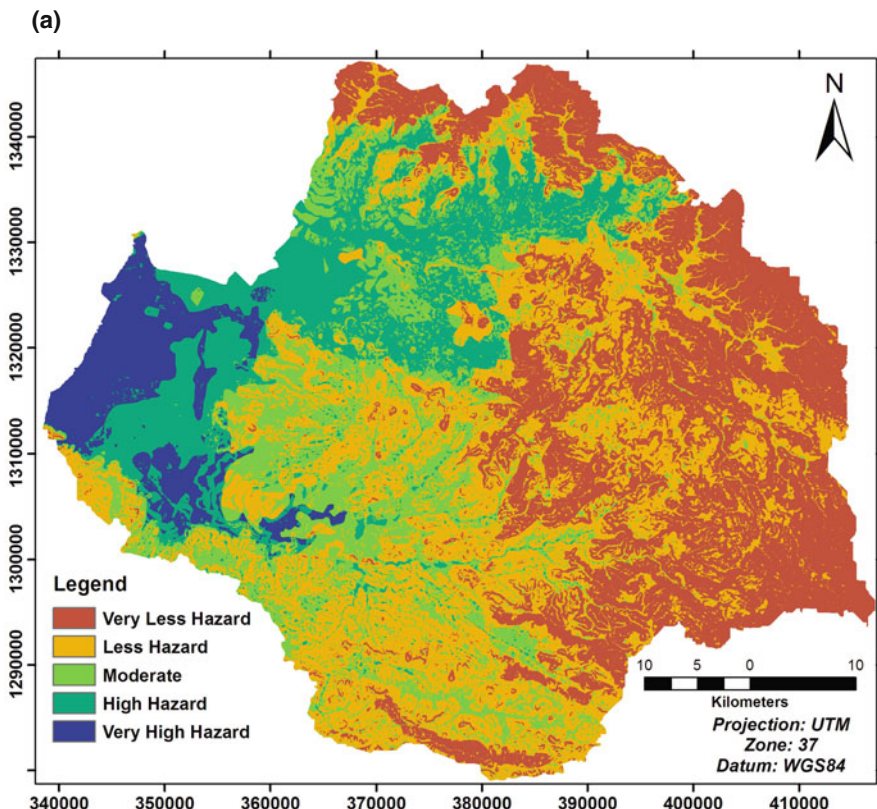


**Fig. 9.5** (a) Flood Hazard map of Ribb-Gumara Catchment, and (b) Fogera woreda

population and land use. Vulnerability was assumed to be one. These three factors remained to be equally important in the Weighted Overlay process (Table 9.3).

Flood risk assessment and mapping was done for Fogera woreda by taking population and land use/land cover elements that are at risk combined with the degree of flood hazards of the woreda.

According to the flood risk map (Fig. 9.6), it was estimated that 40.1, 165.5, 331.3, 385.8 and 186.4 km<sup>2</sup> areas of Fogera woreda were subjected respectively to very high, high, moderate, low, and very low flood risk.

Elements at risk considered in this study show different levels of risk. PAs that are about half of their area under flood risk include Wagtera (96.1%), Shaga (90.3%), Nabega (87.5%), Woreta (65.2%), Bebks (55.8%), Kidiste Hana (53.3%), Shina (49.4%), and Abua Thua (47.1%). With regard to the other element at risk, land use/land cover, 81.8% swamps, 81.6% grass lands, 12.8% agricultural lands are under high to very high flood risk.

The 2006 flood worst hit PAs of Fogera woreda are among the above PAs that are under flood risk. Therefore, the result was in agreement with the reality that is going on in the study area. Specifically, results were compared with ground truth data of

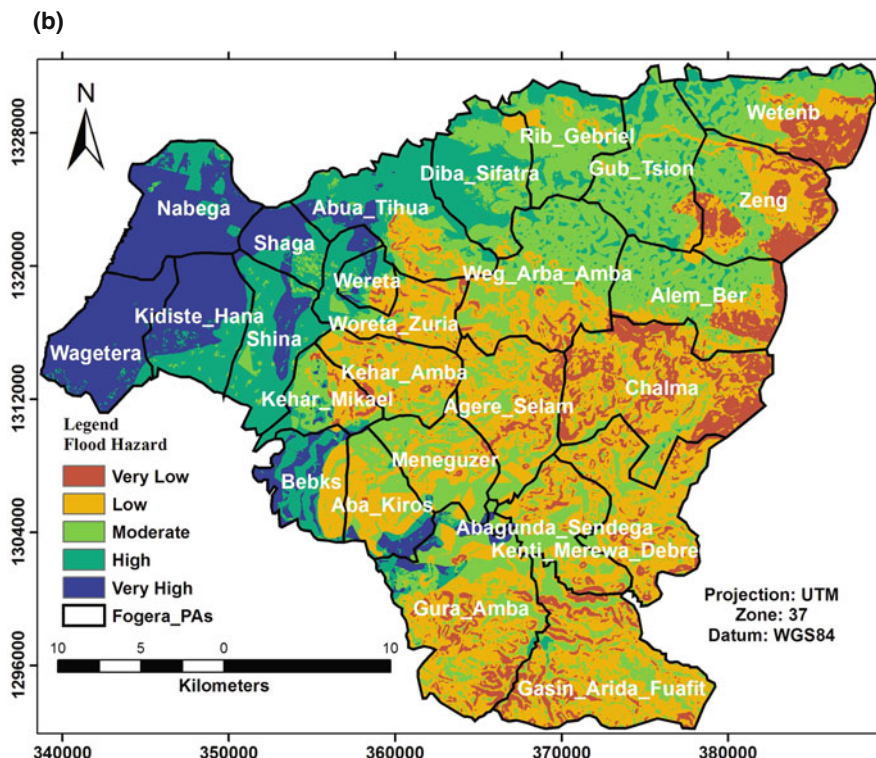


**Fig. 9.5** (continued)

the 2006 flood disaster damaged areas which were collected with GPS during field survey. All these damaged schools, water pumps, crops, and so on fall in the high to very high flood risk areas of the flood risk map of this study. In addition, the above PAs have been traditionally identified as flood prone areas.

### 9.3.4 Flood Frequency Analysis

Hydrologic systems are sometimes impacted by extreme events, such as severe storms, floods and droughts. The magnitude of an extreme event is inversely related to its frequency of occurrence, very extreme events occurring less frequently than more moderate events. According to Chow et al. (1988), the probability of occurrence of an event in any observation is the inverse of its return period;  $P(X \geq X_T) = 1/T$ .

The objective of frequency analysis of hydrologic data is to relate the magnitude of extreme events to their frequency of occurrence through the use of probability distributions. The hydrologic data analyzed are assumed to be independent and identically distributed, and the hydrologic system producing them (e.g., a storm rainfall

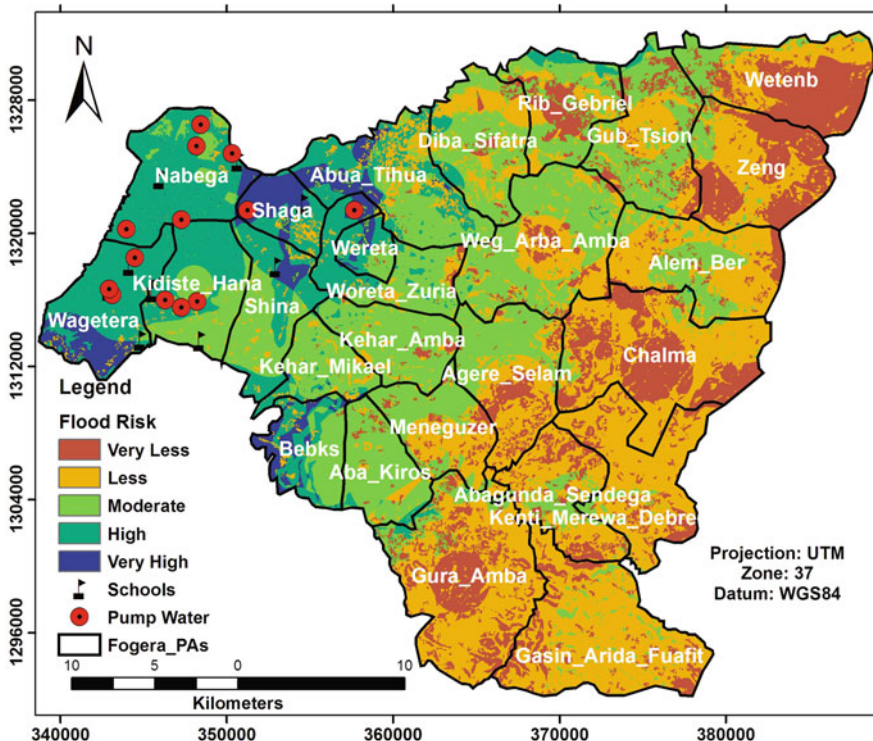


Fig. 9.6 Flood risk map of the study area

system) is considered to be stochastic, space-independent, and time-independent (Chow et al., 1988). The hydrologic data employed should be carefully selected so that the assumptions of independence and identical distribution are satisfied. In practice, this is often achieved by selecting the annual maximum of the variable being analyzed (e.g., the annual maximum discharge, which is the largest instantaneous peak flow occurring at any time during the year) with the expectation that successive observations of this variable from year to year will be independent. The result of flood frequency analysis can be used for many engineering purposes: for the design of dams, bridges, culverts, and flood control structures; to determine the economic values of flood control projects; and to determine flood plains and determine the effect of encroachments on the flood plain.

Flood frequency analysis in this study was done using annual maximum daily gauge level data at Ribb-Addiszemen and Gumara gauge stations (1971–2005). Ribb-Addiszemen gauge station is located at 12°0' N latitude and 37°43' E longitude, and has elevation 1,795 m amsl, while that of Gumara is 11°50' N latitude and 37°38' E longitude, and 1,800 m amsl. Flood frequency calculations were done using the Gumbel's and Log-Pearson Type III methods. CHI Square Test was conducted to test the best fit method to observed data. Using the 100 year base flood level of the best fit distribution, areas that are likely to be inundated in case of

embankment failure of the two rivers were mapped. All the neighborhood pixels in the DEM which has an elevation lower or equal to the specified flood levels were marked likely to be inundated using the Spatial Analyst (Map Calculator) extension of ArcGIS 9.2 software. This result was compared with the result of the flood hazard map done through overlay process of other topographic and meteorological flood causative factors.

By using Gumbel's Method, the calculated Gauge levels of Gumara River for 2, 10, 25, 50 and 100 year return period flood were 5.900, 7.091, 7.685, 8.147, and 8.582 m respectively while that of Ribb-Addiszemen were 6.806, 7.714, 8.166, 8.518, and 8.85 m, respectively. The same gauge data was then analyzed by Log-Pearson Type III Method and gauge levels obtained for 2, 10, 25, 50 and 100 year return period flood for Gumara are 6.075, 7.06, 7.369, 7.553, and 7.706 m respectively, while that of Ribb are 7.016, 7.604, 7.731, 7.793, and 7.836 m, respectively.

The Chi square test comparing computed values with observed values was carried out to find the best fit method and Gumbel's method was found to be the best fit for both rivers. That is, this method has the lower CHI Square value than the Log-Pearson Type III method (0.081 Vs 0.519 for Gumara River, and 0.055 Vs 0.860 for Ribb). Therefore, inundation area mapping was done using the Gumbel's method 100 year return period base flood result.

An 8.582 m gauge level in Gumara River is expected to occur in every 100 year while that of the Ribb is 8.850 m. In other words, the probability of occurrence of an 8.582 m gauge level in Gumara River in a given year is 1/100 or (1%), while with this probability, an 8.85 m gauge level is expected in Ribb River. In Gumara, a 5.900 m gauge level has a 50% probability to occur in any year while in Ribb 6.806 m gauge level is expected with the same probability.

From the Gumbel's distribution result, given the same return periods, gauge levels for Ribb River were found to be a bit greater than that of Gumara (Table 9.4). This is because, river density in the Ribb catchment is relatively greater than that of the Gumara, and again Ribb has more perennial tributaries than that of Gumara.

As discussed previously, in times of embankment failure, inundation will occur in the areas that have an elevation lower than the gauge level and that are connected with the location of the embankment failure. In this study, the 100 year gauge level,

**Table 9.4** Gauge levels for selected return periods

Return period	Gauge level (m)	
	Gumara	Ribb-Addiszemen
2	5.900	6.806
5	6.616	7.352
10	7.091	7.714
25	7.685	8.166
50	8.147	8.518
100	8.582	8.850

which is considered as base flood or project flood, from Gumbel's method for the Ribb and Gumara rivers were taken to map the likely inundation areas in the two respective catchments (Fig. 9.7a, b). These flood maps were merged in the GIS environment so as to see their aggregate effects in the Ribb–Gumara Catchment in general and Fogera woreda in particular. This map was crossed with the maps of elements at risk in Fogera woreda to see its impact on the elements at risk. The quality of the DEM highly limited the inundated area mapping for other return periods. The difference in gauge level between the 2 year and 100 year return periods was calculated as 2.682 m (Gumara) and 2.044 m (Ribb), while the DEM was developed from a 20 m interval contour, therefore failed to show different inundated area maps for different return periods.

For a 100 year return period flood which gage level was calculated as 8.582 m (Gumara) and 8.850 m (Ribb), the total area of the catchment inundated by the flood will be  $352 \text{ km}^2$ . This area is about 12% of the total catchment area, and that of Fogera woreda is  $256 \text{ km}^2$  (23% of the woreda). As the above maps show, almost all the area likely to be inundated by a 100 year return period flood fall in Fogera

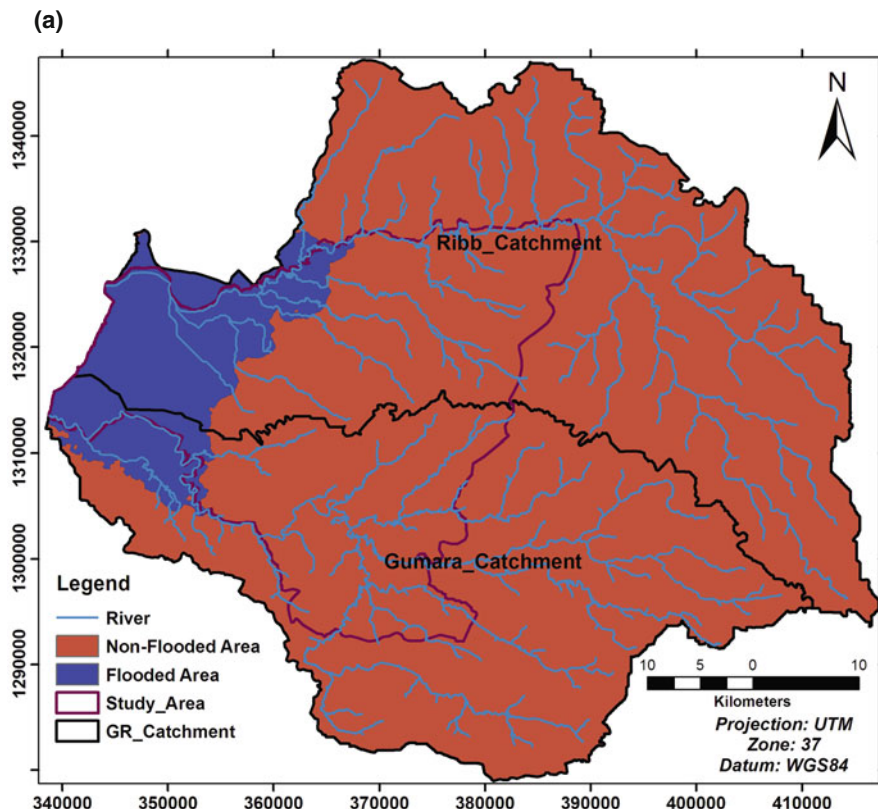


**Fig. 9.7** Flood inundation map of Ribb–Gumara Catchment (a) and Fogera woreda (b) 100 year return period

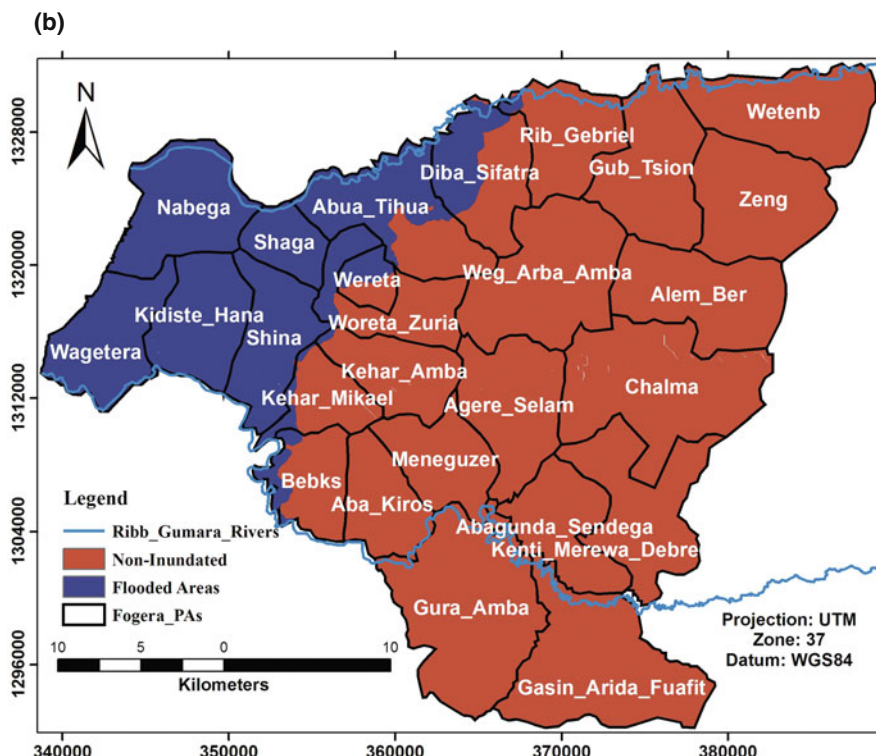


Fig. 9.7 (continued)

woreda. Important to mention here is that the identified areas likely to be flooded by the flood frequency analysis fall in the high and very high flood hazard areas identified by the overlay analysis of the flood hazard assessment. Thus, the result from the frequency analysis soundly agreed with that of the overlay analysis.

The areal comparison above shows that about three-fourth of the inundated area of the catchment (72.7%) fall in Fogera woreda while this woreda is only one-third of the catchment.

With regard to land use classes, with the above mentioned return period flood, 99.8% swamps, 94.0 grass lands, 30.6% shrub land, and 13.9% agricultural lands were found likely to be inundated. 100% of Wagtera, Kidiste Hana, Nabega, Shaga, and Shina and 64.7% of Abua Tihua are likely to be flooded. Most parts of these rural communities were actually inundated by the last year (2006) flood and the people were displaced from their residence. Moreover, agricultural crops including grazing lands of the pastoralist people of these areas were severely damaged by the 2006 flood. As explained before, these areas have been affected by flood almost every year and therefore traditionally identified as flood prone areas.

The return period  $T$  of major flood is the expected value of recurrence interval ( $\tau$ ),  $E(\tau)$ , its average value measured over a very large number of occurrences. For the

**Table 9.5** Years of major floods with their corresponding recurrence intervals

Major flood year	1996	1998	1999	2000	2001	2003	2006	Average
Recurrence interval (years)	2	1	1	1	2	3	1.67	

Ribb-Gumara Rivers data, there are six recurrence intervals covering a total period of 10 years between the first and last occurrences of major flooding, so the return period of major flooding of the Ribb and Gumara Rivers is approximately  $\tau_{av} = 10/6 = 1.67$  years (Table 9.5). Thus the return period of an event of a given magnitude may be defined as the average recurrence interval between events equaling or exceeding a specified magnitude (Chow et al., 1988). As discussed previously, in Fogera woreda major flood peaks occurred in 1996, 1998, 1999, 2000, 2001, 2003 and 2006.

Therefore, from the flood frequency analysis, the calculated 2 year return period gauge level is expected in Ribb-Gumara Catchment in general and Fogera woreda in particular. That is, 6.806 and 5.90 m gauge levels are expected approximately in every 2 year in Ribb and Gumara Catchment, respectively. In other words, these gauge levels have a 60% probability of occurrence in every year in the two respective rivers.

### 9.3.5 Discussion

#### 9.3.5.1 Land Use/Land Cover Change and Flood Hazard and Risk

The land covers (shrub land, wood land, grass land) of the upland sites and the flood plain area have been decreased. Therefore, there is high soil erosion in the upstream and sediments and dissolved substances cumulatively called river load deposited in the river channels and on adjacent flood plains in down stream of the major rivers. Land cover changes increase impervious ground surfaces, decrease infiltration rate and increase runoff rate, hence causing low base flow during the dry seasons (Mustafa Y.M et al., 2005).

According to Shiferaw and Wondafrash (2006), sediments deposited in Ribb and Gumara rivers have changed the rivers gradient, cross-sectional area, average velocity of water flow and discharge of rivers. Therefore, overflow of rivers occurred and flooded the local communities. The cross-sectional areas of Gumara and Rib rivers have been decreasing from time to time as a result of sediment deposition. In some areas the width of Rib River diminished from 35 to 11 m. Deep rooted and tall grasses that had been grown along river banks have been buried by soil sediments, which are transported by rivers. Some agricultural land crops have been buried by the deposited sediments. Overall, the river channels depth and width decreased and the water discharging capacity of the major rivers (Gumara and Rib) and their tributaries minimized in which it leads to overflow of water and flooding consecutively. All this indicates that the rate of erosion and soil loss in the upstream is high due to lack of flood water abstraction.

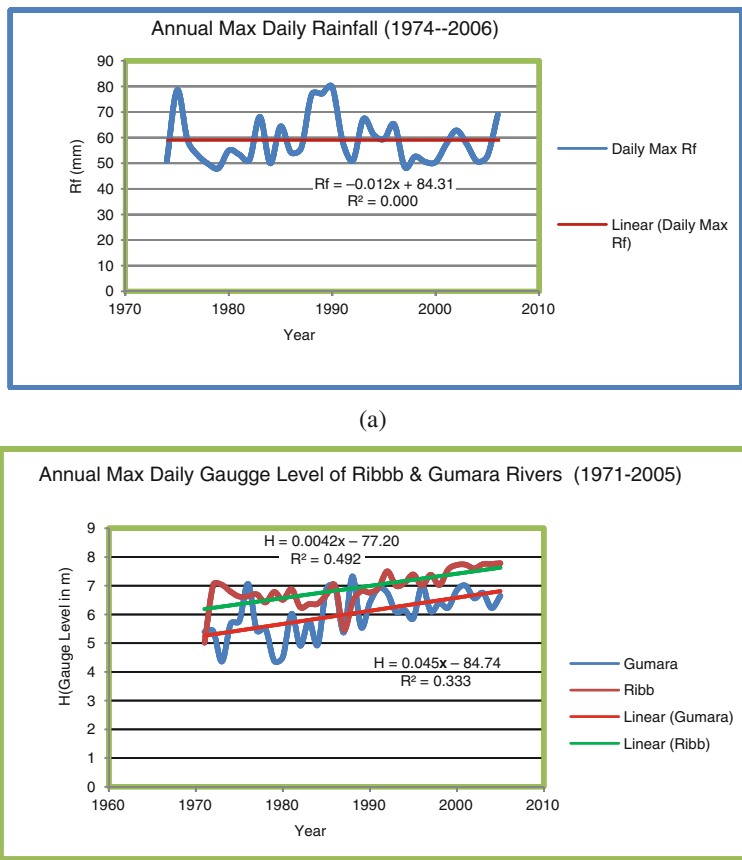


**Fig. 9.8** Trends in (a) annual maximum daily rainfall (1974–2006) from ten meteorological stations in and around Ribb–Gumara Catchment, and (b) annual maximum daily gauge levels (1971–2005) of Gumara and Rib Rivers

The long year daily maximum rainfall trend (Fig. 9.8a) shows that there is a slight decrease in daily maximum rainfall from 1974 to 2006. There were high daily maximum rainfall peaks in the middle of 1970s and around 1990 even though the severe flood in Ribb–Gumara Catchment occurred last summer (2006 Ethiopian main rainy season). Here, one can judge that the recent floods in the catchment in general and Fogera woreda in particular were not caused mainly from rainfall.

As discussed in the previous section, overflow of Ribb and Gumara rivers causes flooding in Ribb–Gumara Catchment. Vast areas that lie below the point where there is a sharp decline in slope (2,200 m) are prone to flooding in the main rainy season. Almost all such areas are found in the so called Fogera Plain just adjacent to Lake Tana where the two rivers empty their water.

According to Fogera woreda disaster prevention and preparedness office (FWODPP), flooding in the woreda has a short history. Flooding, which is the first in its kind in the area occurred some 10 years ago, in 1996. The flooding of that year affected eight PAs of the woreda, namely, Wagtera, Nabega, Kidiste Hana, Shaga, Shina, Woreta Zuria, Kuhar Michael, and Abatihua. From this year onwards, flooding has a regular incidence in some areas especially those PAs adjacent to Lake Tana. Such frequency of the flooding is related to high gauge levels of the two rivers (Fig. 9.8b). Analysis of gauge level data of more than 30 years shows a general increase in daily maximum gauge level. As indicated on Fig. 9.8b, daily maximum gauge level of Ribb and Gumara rivers were increasing at a rate of 0.042 and 0.045 per annum respectively. A relatively higher rate of increase in the daily maximum gauge level is observed in the 1990s and onwards. The 2006 flood was the most severe of all the flood events experienced in the area so far. During this time (1990s and onwards) flood incidence was very high as discussed previously. Therefore, the patterns of gauge level in the catchment reflect the contributions of changes in the physical characteristics particularly land use/land cover changes which is discussed previously. This can be evident from the comparison of trends in the rainfall and gauge level in the catchment. While rainfall was relatively high in the middle of the 1970s and around 1990 (Fig. 9.8a), gauge level was not that much high compared to that of the middle of the 1990s and onwards. This implies that small proportion of the rainfall turns in to runoff thereby increasing the gauge level which can possibly be held by some abstractions such as vegetation and infiltration in to the ground water table.

## 9.4 Conclusion

The basic idea of flood hazard and risk assessment and mapping as undertaken in this study is to regulate land use and population distribution by flood plain zoning in order to restrict the damages. In the light of above discussion, it can be said that flood risk mapping, being an important non-structural flood management technique, will go long way in reducing flood damages in areas frequented by flood.

Pair wise comparison method of flood hazard map generation is a good approach to deduce a sound decision for a forthcoming flood disaster, provided the required data are standardized to a common scale in personal geodatabase. This study confirmed that the method used was capable to integrate all the flood hazard causative factors and the components of flood risk as well in a GIS environment. In this fashion, composite maps were generated to assess flood risk of Fogera woreda. One of the Multi Criteria Evaluation techniques known as Weighted Overlay in GIS environment was shown to be useful for delineating areas at different rating in terms of flood hazard and flood risk. Moreover, factor weight computation in Weight module, that is developed by providing a series of pair wise comparisons of the relative importance of factors to the suitability of pixels for the activity being evaluated, has generated valuable information. This could be useful for disaster studies in

the future. Therefore, it has been shown that MCE-GIS based model combination has potentiality to provide rational and non-biased approach in making decisions in disaster studies.

Satellite images were shown to be very important for land use/land cover change studies with certain limitations like cloud cover and striping. The change statistics of land use/land cover of Ribb-Gumara Catchment showed that clearance of land cover for agricultural expansion has been aggravating flood hazard in the downstream areas of Ribb and Gumara Rivers, Fogera woreda.

Flood frequency analysis of peak hydrological data yielded the return periods of each major peak discharges and the magnitude and probability of occurrence of flood peaks of specified return periods so as to help preparedness to cope with such peaks. Flood frequency analysis combined with GIS was found very important to map the likely inundated areas of a given catchment. In this study, the likely inundated areas mapped using the 100 year return period base flood and DEM, and the flood hazard map obtained from the overlay analysis of flood causative factors in the study area soundly agree to each other. And therefore, the combination of the two results would be a step forward for flood management and mitigation strategies.

This study also showed that recent floods in Fogera woreda, in particular and Ribb-Gumara catchment in general are not mainly due to rainfall but due to vegetation removal. Therefore, environmental issues should be given great emphasis in flood risk management in addition to hydrological parameters.

Although flooding is a natural phenomenon, we can not completely stop it; we can minimize its adverse effects by better planning. The study has shown that automatic flood map delineation can be produced for big river system in short time with the support of GIS and remote sensing.

## References

Chow VT et al (1988) Applied hydrology, McGraw-HILL international edition. Civil Engineering Series, Singapore

DPPA (2006) Joint government and humanitarian partners: flash appeal for the 2006 flood disaster in Ethiopia. <http://www.dppc.gov.et/downloadable/reports/appeal/2006/Flood%20Appeal%20II%20MASTER%20Final.pdf>. Accessed 25 Mar 2007

Eastman JR (2001) IDRISI guide to GIS and image processing, vol 2. [www.gyml.unibas.ch/go/17/pdf2/Guide2](http://www.gyml.unibas.ch/go/17/pdf2/Guide2). Accessed Jan 2007; Clark University, Version 32.20

FAO (2006) World reference base for soil resources: a framework for international Classification, Correlation and Communication, Rome. <http://www.fao.org/docrep/W8594E/W8594E00.htm>. Accessed 12 May 2007

FWOARD (2006) Short description of the 2006 summer flood in Fogera Woreda

Gumbel EJ (1954) Statistical theory of extreme values and some practical applications, Nat Bur Standards Appl Math, Ser. 33, Washington, DC

Leica Geosystem (2000) ERDAS field guide<sup>TM</sup>, 6th edn. Leica Geosystem, Atlanta, GA

Malczewski J (1999) GIS and multi-criteria decision analysis. Wiley, New York, NY

Mustafa YM et al (2005) Evaluation of land development impact on a tropical watershed hydrology using remote sensing and GIS. J Spatial Hydrol 2:1

Shiferaw, Wondafrash (2006) Causes and effects of flooding in the Amhara National Regional State: a case study in Fogera Woreda, Addis Ababa

Shook G (1997) An assessment of disaster risk and its management in Thailand. *Disasters* 21: 77–88

Suresh R (2005) Watershed hydrology: principles of hydrology. Lomus Offset Press, Delhi

UNEP (2002) Africa environmental outlook: past, present and future perspective. United Nations Environmental Program, Nairobi

UNOCHA (2006) Flood affected woredas in Ethiopia. [http://www.ocha-eth.org/Home/downloadables/FD\\_0014\\_RecentFlood\\_www.pdf](http://www.ocha-eth.org/Home/downloadables/FD_0014_RecentFlood_www.pdf). Accessed 25 Mar 2007

# Chapter 10

## Soil Erosion Mapping and Hotspot Area Identification Using GIS and Remote Sensing in Northwest Ethiopian Highlands, Near Lake Tana

**Mulatie Mekonnen and Assefa M. Melesse**

**Abstract** Soil erosion is a critical problem in Ethiopia. The rate of soil erosion at the Debre Mewi Watershed in the upper Blue Nile River basin has occurred at an alarming rate. Estimating soil erosion, identifying erosion hotspot areas and setting priorities are needed by agencies involved in development works of the watershed to plan and implement soil and water conservation measures. Therefore, this research has been carried out to assess soil erosion, identify erosion hotspots and to set priority for conservation measures. The study integrated remote sensing with a Geographic Information System (GIS). Soil, land use/land cover, topography, and climatic data were used to generate the RUSLE factor values. Soil erosion was calculated through overlay analysis, which ranged from 0.0046 to 192 tons/ha/year. About 68% of the watershed experiences from very low to moderate erosion rates, 31% experiences from high to extreme erosion rates and 1% experiences exceptional erosion rates that is greater than 100 tons/ha/year. The results were compared with conventionally collected plot level soil loss data and good agreement was found. Agricultural areas (crop lands) have very high soil erosion followed by grazing lands and bush lands. However, the soil loss is low in eucalyptus plantations and built up areas.

**Keywords** Soil erosion assessment · Erosion hotspot · Watershed · RUSLE · GIS · Debre Mewi watershed

### 10.1 Introduction

Soil erosion is a concern for farmers, development and government agencies throughout the world since it is affecting soil, land and water resources upon which humans depend for their sustenance. Today, soil erosion is universally recognized as a serious threat to man's well – being. The threat is very severe mainly in developing countries, like Ethiopia.

---

M. Mekonnen (✉)

Bureau of Agriculture and Rural Development, Amhara Region, Bahir Dar, Ethiopia  
e-mail: [mulatemekonnen@yahoo.com](mailto:mulatemekonnen@yahoo.com)

In Ethiopia, considerable amount of soil is being lost every year particularly by water erosion. Rates of soil erosion documented in Ethiopia range from 16 to 300 tons/ha/year (Hurni, 1988; Hawando, 1995). According to Berhe (1996), soil loss from the six Soil Conservation Research Projects findings ranges from 18 to 214.8 tons/ha/year.

There are several causative factors that control the spatial pattern and amount of soil loss in an area. The most important of such factors are the erosivity of rainfall, erodibility of soils, vegetation cover, conservation measures and topography of the area. Understanding soil erosion processes, both in time and space, as well as their causes is a prerequisite to design and implement appropriate soil and water conservation approaches and technologies that eventually contribute to sustainable land management (Hurni, 1985).

So as to mitigate the adverse effects of soil erosion, effective soil conservation strategies are required. However, it is not possible to implement soil and water conservation (SWC) measures in large areas at the same time since it requires high technical, financial and management investment. Therefore, spatial information on soil erosion helps to prioritize the conservation strategies and to design effective SWC measures as well as to monitor their effectiveness (Morgan, 2005; Vrieling, 2007).

Several methods have been developed for the spatial assessment of soil erosion. These methods are broadly classified into three approaches. The first approach consists of quantifying erosion from experimental erosion plot measurement. The second approach is to map erosion features by executing erosion survey or by visual interpretation of satellite image or aerial photographs. The third and most widely used approach is through integrating spatial data on erosion factors by using erosion models (Vrieling, 2007). The third approach was applied in this study.

The nature of topography, rainfall and overgrazing compounded with poor farming techniques and depletion of vegetation cover have resulted in severe soil erosion problem at 508 ha Debre Mewi Watershed, Ethiopia (Fig. 10.1) where the study is carried out. Poor management practices including farming on marginal lands have further aggravated the problem. Presently, there are series of active and dead gullies that witness the existence and severity of the erosion problem.

Communities of the watershed identified their problems and prioritized as soil fertility reduction; soil erosion and land slide; shortage of water for livestock consumption and high price of agricultural inputs (SWHISA, 2007, Participatory rural appraisal report of Debre Mewi watershed. IRG – 09. Bahir Dar, Ethiopia, Unpublished). Based on this Participatory Rural Appraisal (PRA) survey and problem prioritization Adet Woreda Office of Agriculture and Rural Development, Sustainable Water Harvesting and Institutional Strengthening in Amhara (SWHISA) and Adet Agricultural Research Center (AARC) planned to treat the watershed by implementing different soil and water conservation technologies.

To design and implement appropriate SWC technologies in the watershed, spatially quantified soil loss and runoff information is essential. Different attempts have been done to estimate soil loss for the northwestern highlands, using conventional methods (i.e. using hydrologically defined runoff plots where runoff and soil loss

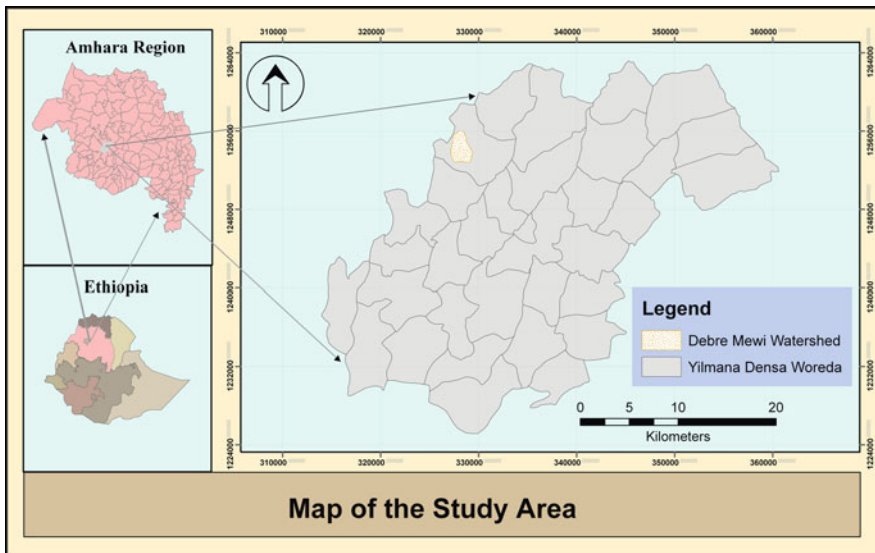


**Fig. 10.1** Location map of the study area

is measured at the exit of the plot by collection tank system and collection of suspended sediment and bed load of the river at watershed scale). For instance, Anjene Soil Conservation Research Unit, which represents the northwestern highlands including the study area, estimated soil erosion that ranges from 40.2 to 199.2 tons/ha/year. Desta et al. (2000) reported that site specific test plots and experiments in 1987 and 1988 at the Soil Conservation Research Project (SCR) stations in the Amhara Region showed soil loss rates between 0.04 and 212 tons/ha/year. Such results are hardly representative for soil and water conservation planning at Debre Mewi watershed, because soil loss and runoff are very different at different locations due to the difference of the controlling factors.

Soil erosion assessment using remotely sensed data and GIS is less time, labor and capital intensive and effective in generating essential quantitative information on soil erosion (Baban and Wan Yusof, 1999). It is also possible to identify the spatial pattern and distribution of soil erosion and categorize erosion risk areas, which is not possible in conventional erosion assessment methods. The Revised Universal Soil Loss Equation (RUSLE) and GIS has been used to estimate soil erosion in Ethiopia (Hurni, 1985; Renard et al., 1997; WBISPP, 2000; Nyssen et al., 2006, Impact of land use and land cover on sheet and rill erosion rates in the Tigray Highlands, Ethiopia, Unpublished).

This study was conducted to estimate soil loss using RUSLE model, to distinguish the spatial distribution of soil erosion and to identify erosion hotspot areas at Debre Mewi watershed, which are indispensable to select, plan and implement appropriate soil and water conservation measures.

The specific objectives of the study reported in this chapter are to (1) estimate soil loss and identify its spatial distribution using GIS integrated with RUSLE model and information derived from high resolution satellite imagery, (2) identify erosion hotspot or erosion risk areas and set priorities for soil and water conservation planning and (3) recommend immediate and long-term natural resource management options.

### ***10.1.1 Soil Erosion in Ethiopia***

Ethiopia is considered to have one of the most serious soil erosion problems in the world. In the highlands of Ethiopia, soil losses are extremely high with an estimated average of 20 tons/ha/year and it can radically exceed this on steep slopes. Measured values range from 0 to 300 tons/ha/year on specific plots (Hurni, 1985; Nyssen et al., 2006, Unpublished). As reported by the Ethiopian Highland Reclamation Study (EHRS, 1984), 27% (over 14 million ha) of the highland area of Ethiopia were seriously eroded and some 6 million ha completely withdrawn from agricultural use and 13 million ha was moderately eroded. Of the remaining 28 million ha, about 54% is susceptible to erosion, requiring some form of soil conservation measures.

Hawando (1995) also estimated that the amount of annual soil movement (loss) by erosion ranges from 1,248 to 23,400 million tons per year from 78 million ha of pasture and rangelands and cultivated fields in Ethiopia. Using conventional soil loss measuring method, the six SCRP sites of Ethiopia found a soil loss ranging from 18 to 214.8 tons/ha/year (Berhe, 1996).

The Amhara National Regional State (ANRS), where the Debre Mewi watershed is located has a total area of 170, 152 km<sup>2</sup>. Soil erosion is one of the major problems affecting food security and natural resources conservation in the region. The destruction of vegetation cover for fuel wood and construction, overgrazing, nature of topography, long history of farming and unsustainable practices are some of the causative factors for soil erosion. A quarter of the highlands of the region are seriously eroded, of which 15% are so severely affected that it will be very difficult to reverse them to be economically productive in the near future (SCRP, 1986).

Desta et al. (2000) reported that site specific test plots and experiments in 1987 and 1988 at SCRP stations in the region showed soil loss rates between 0.04 and 212 tons/ha/year. About 29% of the total area of the region experiences high erosion rates (51–200 tons/ha/year), 31% experiences moderate erosion rates (16–50 tons/ha/year), 10% experiences very high erosion rates (>200 tons/ha/year), and the remaining 30% experiences low erosion rates (<16 tons/ha/year).

Another study by Woody Biomass Inventory and Strategic Planning Project (WBISPP, 2000) indicated that 82% of the ANRS has a soil loss rate of less than 12.5 tons/ha/year while 18% suffers a soil loss of 12.5–200 tons/ha/year. To estimate the soil loss, the WBISPP used the Universal soil Loss Equation adapted for

Ethiopia, which considered rainfall erosivity, soil erodibility, slope gradient, slope length and conservation practice factors.

Results obtained from test plots of the SCRP at Andit Tid (North Shewa) in ANRS indicated that soil loss ranges from 152.4 to 212.4 tons/ha/year. Plot experiment of SCRP at Anjene (West Gojjam) on different slopes and conservation practices showed soil loss between 40.2 and 199.2 tons/ha/year, which can be categorized as extreme and ahead of extreme erosion categories. According to Herweg and Stillhardt (1999) as cited in Zeleke (2000), the long – term average soil loss rates from cultivated plots are highest in the ANRS among nation – wide monitored sites and ranges between 131 and 170 tons/ha/year.

The results of the above studies showed that the ANRS is the most severely eroded than the other regions of the country. Even if the problem existed in Gonder and Wollo areas for the last so many years, by now it is more serious and active in West Gojjam, East Gojjam and Awi Zones and the surrounding areas of Lake Tana, which were considered as the surplus food producing areas of the region as well as the nation.

In Debre Mewi watershed (DMW), farmers consider fertility reduction and soil erosion as their primary and secondary problems, respectively (SWHISA, 2007, Unpublished). Due to lack of precaution, a great number of old and active gullies both shallow, medium and deep sizes were formed and being formed. According to the watershed community, the major causes of such gully formations are overgrazing, roads, absence of immediate treatment while gullies start to form, etc. Gullies represent a severe erosion hazard and are indicatives of an advanced stage of soil erosion. Figure 10.2 shows some of the gullies formed and soil being lost every year in the watershed.

### **10.1.2 Factors Affecting Soil Erosion**

Understanding soil erosion controlling factors is vital to assess the amount of soil loss in a watershed. The four major factors discussed below are erosivity of rain, erodibility of the soil, topography and land cover.

Rainfall is one of the most important erosive agents contributing to soil erosion. Soil particles are detached as well as transported by raindrop and overland flow runoff water. The amount and intensity of rainfall has the greatest influence in the rate of soil erosion (Wischmeier and Smith, 1978; Lal, 1984). Similarly rainfall duration is an important element in soil erosion (Hurni, 1985; Morgan, 2005).

Soil erodibility is the resistance of the soil to detachment as well as to transport. Soil erodibility is a function of the inherent soil properties, including texture, structure, organic matter content and permeability, which can be determined quantitatively through experiment (Wischmeier and Smith, 1978; Renard et al. 1997). Clay sized particles are hard to detach but easy to transport while sand particles are easy for detachment and hard for transportation. Silt and fine sand sized soil particles are most vulnerable to erosion (Lal, 1984; Morgan, 2005).



**Fig. 10.2** Gully formations and soil loss at Debre Mewi watershed (4/9/08)

Slope steepness and slope length are also important factors influencing the rate of soil loss. Slope length is defined as the distance from the point of origin of overland flow to the point where either the slope gradient decreases enough that deposition begins or the runoff water enters a well defined channel. Soil loss generally increases substantially as slope length increases because greater accumulation of runoff on the longer slopes increases detachment and transport capacities (Wischmeier and Smith, 1978; Morgan, 1995). As the length of the slope increases, the rate of soil loss increases because of increase in the volume of runoff water, gathering speed and gaining energy. Similarly, the rate of soil loss increases with slope steepness as a result of increased velocity of runoff water, which in turn facilitates soil detachment and transportation (Wischmeier and Smith, 1978). Field estimation/measurement of slope steepness and slope length factors are more accurate than model calculations from digital elevation model (Millward and Mersey, 1999).

Land cover has significant control over soil erosion. It plays an important role acting as an intercepting agent of rainfall, covering the surface of the soil and reducing the amount and energy of rainfall directly reaching on the soil surface. Hurni (1985) also estimated mean soil loss rates for different land use/land cover types

in Ethiopia as 5, 5, 42, 5, 0, 70, 1, 8 tons/ha/year on grazing land, uncultivable land, crop land, wood/bush land, swampy land, former crop land, forest land and perennial crop land covers, respectively.

### **10.1.3 Field Techniques for Soil Loss Measurement**

According to Sapkota (2008), depending on the spatial scale, there are four fundamental ways of measuring soil erosion at field level: (1) change in weight, (2) change in surface elevation, (3) change in channel cross section and (4) sediment collection from erosion plots and watersheds. Change in weight method is used to measure splash erosion by using funnels or bottles. Change in surface elevation can be used to determine soil loss by using erosion pin. Similarly, rill erosion can be measured by measuring cross-sectional area of rills found in a number of transects. Cross-sectional area of the rill multiplied by the average length of the rill gives the volume of soil loss (Morgan, 2005).

A watershed scale measurement of the quantity of sediment leaving from the river outlet can be used to calculate soil loss for the watershed. The sediment movement in the river takes two forms: suspended sediment and the bed load. Flowing water along with suspended sediment is collected in a bucket of known volume filtered, dried and weighed to calculate the suspended sediment load. Similarly, bed load can be directly measured using pits or collection tanks.

### **10.1.4 Soil Loss Tolerance**

Soil loss tolerance is the maximum rate of annual soil erosion that may occur and still permits a high level of productivity to be obtained economically and indefinitely (Wischmeier and Smith, 1978). Soil loss tolerance depends on the soil type. On very deep and homogeneous soils, the effect of erosion will be less pronounced than on shallow soils.

The soil loss tolerance values are used for the determination of critical area of soil erosion in the watershed by comparing soil loss rates with soil loss tolerance. If the soil loss is less than or equal to the soil loss tolerance, the soil loss is still accepted. However, if the soil loss is more than soil loss tolerance, conservation measures to reduce soil erosion should be taken into account until a level of equal or less than the soil loss tolerance has been reached.

The maximum soil loss tolerance for tropical regions is 25 tons/ha/year (Ringo, 1999, Assessment of erosion in the Turasha catchment in the Lake Naivasha area, Kenya. MSc. Enschede, Unpublished). A commonly used soil loss tolerance rate is 5–12 tons/ha/year for shallow to deep soils (Lal, 1984). The tolerance value for tropical soils has not yet been formulated at international level, but Hurni (1986) and Hudson (1986) established annual soil loss tolerance limits that vary between 0.2 and 11 tons/ha/year (Ringo, 1999, Unpublished).

## 10.2 Study Area and Methods

### 10.2.1 Study Area Description

Debre Mewi Watershed is about 508 ha of land located in Adet Woreda, Western Gojjam Zone, ANRS. Geographically, it is located between  $11^{\circ}20'10''\text{N}$  and  $11^{\circ}21'50''\text{N}$  latitudes, and  $37^{\circ}24'35''\text{E}$  and  $37^{\circ}25'55''\text{E}$  longitudes (Fig. 10.1).

The area is characterized by single maximum rainfall pattern with peaks in July and August and receives on average 1,100 mm of precipitation annually (Fig. 10.3). About 80–90% of the rainfall falls in the main rainy season, which starts in June/July and extends to August/September. The mean minimum and maximum temperature of the area is 8.7 and  $25.4^{\circ}\text{C}$ , respectively (Fig. 10.4).

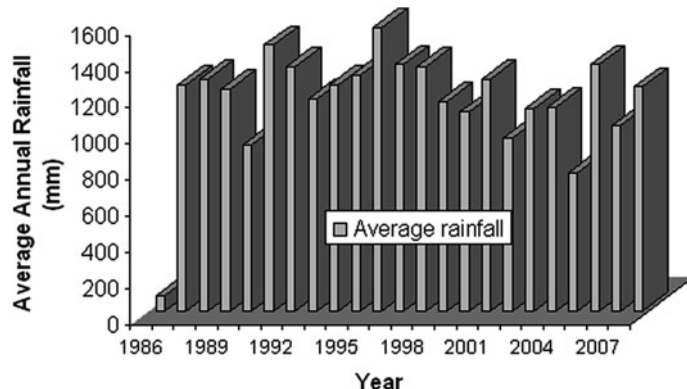


Fig. 10.3 Rainfall and temperature condition of the study area

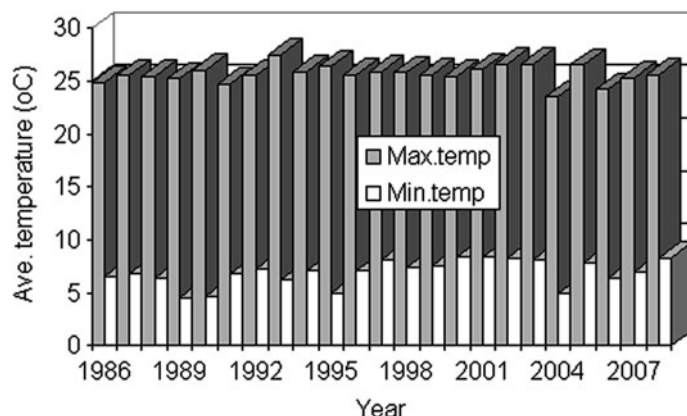


Fig. 10.4 Temperature conditions of the study area

Laboratory analysis result of soil samples indicate that the area is occupied by six soil types according to FAO classification system. Such as Eutric Luvisols on higher elevation and lower slope lands, Pellic Vertisols on lower and flat plains. Eutric Fluvisols are found along river banks whereas Eutric Vertic Cambisols and Eutric Aquic Vertisols are dominant on averagely sloped areas below hilly and steep lands occupied by Eutric Cambisols.

Five major land use/land cover types have been identified in DMW using both QuickBird satellite image and field observation. Such land use/land cover types comprise 70.3% crop land (agricultural area); 6.4% bush land; 19.6% grazing land; 2.5% eucalyptus plantation and 1.2% built up area.

Since slope is the most important terrain characteristic and plays a vital role in runoff process and soil erosion, it is very important to have an understanding of its spatial distribution in the study area. The slope map of the study area was prepared from 1:50,000 scale topographic map. The watershed is characterized by a slope ranging from 1 to 57% and elevation ranging from 2,194 to 2,360 m.

The rural economy of the people in the watershed is based on agricultural production. Only rain fed crops, such as barley, tef, maize, and wheat can grow during the rainy season. In some parts of the watershed, grass pea (*Guaya*) grows by residual moisture. The other source of income is the cattle resource. Population of the cattle is very high, which includes goat, sheep and donkey. This indicates the grazing pressure in the watershed.

### **10.2.2 Methodology**

To attain the objectives of this study, different methods such as satellite image processing, digital terrain analysis, model application, transect walks and field survey were applied.

During the fieldwork, the watershed (study area) and subwatersheds were delineated using GIS with the help of 1:50,000 topographic map and 1:4,000 QuickBird image map. Processing data collected during the field work was conducted together with remotely sensed satellite image data. Firstly, preparation of all the required parameter maps of the model and running the model and secondly, quantifying soil loss and then identification of erosion prone areas were done. Finally, validating the model results, discussions, conclusion remarks and recommendations were given.

#### **10.2.2.1 Topographic Transect Walk**

The rapid rural appraisal technique of the topographic transect walk method was employed for the assessment of the natural resource base of the watershed. In order to obtain as much detail information as possible, the transect walk was applied four times in two directions, east to west and south to north. During the transect walk, observations and estimates of the vegetation density and erosion hazards were done. These were followed by recording land-use/land cover types, slope gradient, slope length, soil color, and drainage patterns over a distance of about 1.73 km

in west – east and 3.26 km in north – south directions. It also provided a good opportunity for informal discussions with farmers working on their plots.

### 10.2.2.2 The RUSLE Model

The original soil erosion model called Universal Soil Loss Equation (USLE) was empirically derived from more than 10,000 plots and years of runoff and soil loss data contributed from 49 locations in the United States (Renard et al., 1997). USLE was designed to provide a convenient tool for soil conservationists and can be used to any geographic region with its modified factors. It has been used in developing conservation plan and land use decisions.

Some recent researches led to a revision of USLE that provides more accurate estimation of soil loss i.e., the Revised Universal Soil Loss Equation (RUSLE). RUSLE has the same formula with USLE but has several improvements in determining factors. Hurni (1985) has modified the USLE to fit the Ethiopian conditions. The modified input factors used by the USLE model include rainfall erosivity (R), land cover (C) and management (P) factors for the Ethiopian condition, which are valuable inputs to the erosion and soil conservation research in Ethiopia since 1980s. Nyssen et al. (2006, Unpublished) examined the application of the RUSLE after Hurni (1985) and Renard et al. (1997) in the Ethiopian Highlands.

In this study, the revised universal soil loss model developed by Wischmeir and Smith (1978) and modified by Hurni (1985), to the Ethiopian conditions, was used because of its less input requirement, computational simplicity and wide applicability. The factors generation flow chart and the mathematical equation used to run the model are indicated in Fig. 10.5 and Eq. (10.1) (Wischmeir and Smith, 1978; Hurni 1985; Foster et al. 2002):

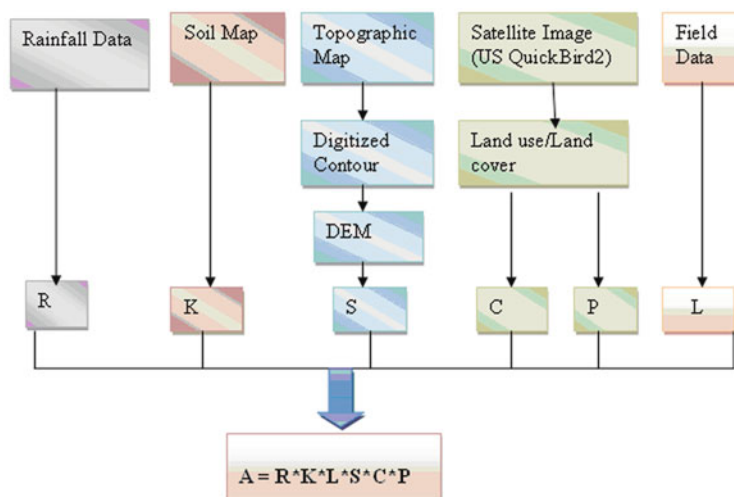


**Fig. 10.5** RUSLE factor generation flow chart

Mathematically, the equation is denoted as follows:

$$A = R \cdot K \cdot L \cdot S \cdot C \cdot P \quad (10.1)$$

Where; A, is mean annual soil loss (in tones/ha), R is rainfall erosivity factor, K is the soil erodibility factor, L is the slope length factor, S is the slope steepness factor, C is crop management or land management factor and P is conservation practice factor.

The soil loss is closely related to rainfall partly through the detaching power of rain drop striking the soil surface and partly through the contribution of rainfall to runoff (Morgan, 1995). According to Wischmeier and Smith (1978), rainfall erosivity is calculated from the kinetic energy of rainfall, which in turn is measured from the mean annual rainfall and 30 min rainfall intensity value. The formula used to calculate rainfall erosivity based on (Morgan, 1995) is:

$$R = EI_{30}/1,000 \quad (10.2)$$

Where, R rainfall erosivity factor, in metric units, E is rainfall kinetic energy,  $J \text{ m}^{-3}$  and  $I_{30}$  is 30 min rainfall intensity, mm/h.

However, rainfall kinetic energy and intensity data are not available in the study area. Therefore, the erosivity factor, R that was adapted by Hurni (1985) for Ethiopian conditions based on the easily available mean annual rainfall was used in this study. It is given by the following equation:

$$R = -8.12 + (0.562 \cdot P) \quad (10.3)$$

Where; P is the mean annual rainfall in mm.

The soil erodibility factor, K measures the resistance of the soil to detachment and transportation by raindrop impact and surface runoff. Soil erodibility is a function of the inherent soil properties, including texture, structure, organic matter content and permeability, which can be determined quantitatively through experiment. In this study, soil types were determined through laboratory analysis and erodibility values of the different soil types developed for the Ethiopian conditions by Hurni (1985) were used.

Slope length, which is the distance from the origin of overland flow along its flow path to the location of either concentrated flow or deposition, was obtained through direct field measurement. According to Millward and Mersey (1999), field estimation/measurement of slope length factor is more accurate than model calculations from digital elevation model (DEM).

Slope gradient (S) in percent were derived from DEM, which is obtained by digitizing 20 m interval contour of 1:50,000 scale topographic map of Adet Woreda. Crop management (C) and conservation practice (P) factors were derived from QuickBird satellite image and the associated factor values were assigned based on Hurni (1985) finding for the Ethiopian conditions.

Plot level conventionally collected soil loss data for validation and rainfall data to calculate mean annual rainfall were obtained from Adet Agricultural Research Center and Ethiopian Meteorological Agency, respectively. Land use/land cover data of DMW was obtained through on screen digitization from QuickBird satellite image.

## 10.3 Results and Discussions

### 10.3.1 Soil Loss (Erosion)

Calculation of the major factors contributing to soil loss, which constitute the main input for the RUSLE model for erosion assessment, were done using the normal procedures that are documented in different sources (Foster et al., 2002; Renard et al., 1997; Hurni, 1985; Wischmeier and Smith, 1978).

The soil erosion map (Fig. 10.6) of the study area was generated by cell to cell multiplication overlay of the raster (grid) maps of the six RUSLE input parameters (rainfall erosivity, soil erodibility, conservation practice, slope gradient, slope length and cropping and management factors). As a result of this analysis, a soil loss ranging from 0.0046 to 192.15 tons/ha/year was obtained. The resulting rate of erosion was classified into seven erosion potential classes (Table 10.1) ranging from very low erosion hazard (<3.125 tons/ha/year) to exceptional erosion hazard

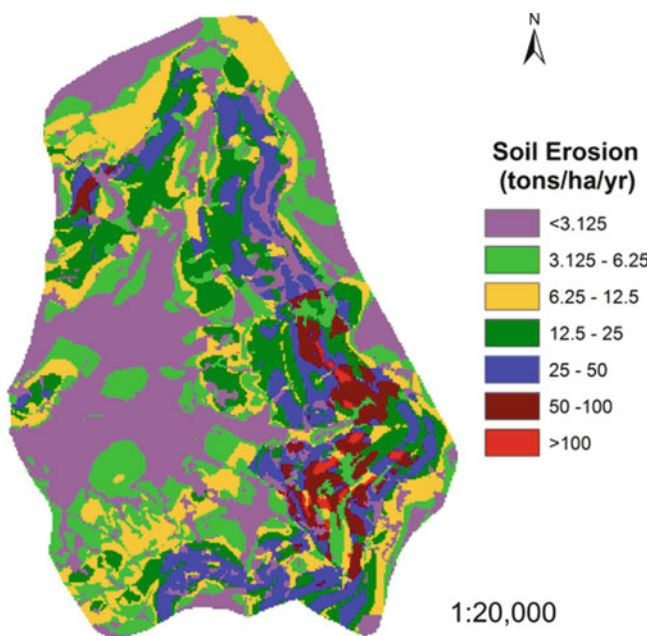


**Fig. 10.6** Soil erosion map of the study area

**Table 10.1** Soil erosion classes of the study area

Erosion class	Soil loss (t/ha/yr)	Erosion potential	Area (ha)	Area (%)
I	< 3.125	Very low	165.0688	32.5
II	3.125–6.25	Low	94.8379	18.68
III	6.25–12.5	Moderate	85.0699	16.75
IV	12.5–25	High	80.3817	15.83
V	25–50	Severe	56.8892	11.20
VI	50–100	Extreme	22.5395	4.44
VII	>100	Exceptional	3.0461	0.60
Total			508	100

(>100 tons/ha/year). Generally, 68% of the study area is under very low to moderate erosion rates and 32% of the land area is found to be between high and exceptional erosion rates.

The estimated soil loss in this study is within the range of soil loss estimated for the Ethiopian high lands by the SCRP, which ranged from 0 to 300 tons/ha/year (Hurni, 1985; Nyssen et al., 2006, Unpublished). It is also within the range of results of site specific test – plots and experiments in 1987 and 1988 at SCRP stations in the Amhara region, which is between 0.04 and 212 tons/ha/year (Desta et al., 2000).

### 10.3.2 Spatial Variability of Soil Erosion in Relation to Topography

The soil loss map was crossed with the slope class map in zonal statistics of ArcGIS 9.2 software to extract the soil loss in different slope classes. The result showed that soil loss is different for different slope classes as indicated in Table 10.2. The highest rate of mean soil loss was found in the slope gradient range of 25–40% that is 45.4 tons/ha/year. It showed a slight reduction for higher slopes (above 40%) and significant reduction for lower slopes.

**Table 10.2** Soil loss by slope category

Slope (%)	Cell count	Area (ha)	Soil loss (t/ha/yr)			
			Minimum	Maximum	Mean	STD
0–1	594	5.05	0.00457	1.9215	1.004	0.43
1–2	1,785	15.95	0.00457	1.9215	0.843	0.5
2–4	10,283	87.49	0.00915	5.124	1.734	0.94
4–6	8,708	74.09	0.01613	16.013	3.327	1.89
6–8	7,669	65.25	0.0275	30.195	6.511	4.06
8–13	15,978	135.95	0.0458	50.325	12.074	8.49
13–25	12,292	104.58	0.128	91.5	29.446	23.34
25–40	2,042	17.37	0.2049	164.4	45.377	41.54
40–55	173	1.47	7.3017	192.15	43.5451	46.21
55–100	70	0.59	9.5618	143.426	19.6747	26.74

Soil erosion reduces for higher slopes above 40%, it might be because of that about 20% of the land having slopes greater than 40% is covered by stone, which can reduce the direct impact of raindrop kinetic energy and serves as stone mulch that reduces runoff effects. Moreover, these areas are not intensively cultivated. Severe to exceptional erosion classes are concentrated around areas having both higher slope gradient and slope length factors. Generally, in this study soil loss increases as slope gradient and length increases that proved the findings of Wischmeier and Smith (1978) and Morgan (1995).

### **10.3.3 Soil Erosion in Relation to Land Use/Land Cover Types**

Soil erosion is found to be different for different land use/land cover types (Table 10.3). Average soil loss is highest (16 tons/ha/year) in crop land and lowest in eucalyptus plantation (0.14 tons/ha/year). For grazing land, bush land and built up areas the soil loss rate is 6.41, 2.28 and 0.34 tons/ha/year, respectively. The reason why high soil loss was recorded on agriculture lands is due to absence of any type of cover during the first rain shower periods including crop residues, which is used for livestock feed. Lack of conservation measures might be the other reason for the increment of soil erosion on crop lands. Soil loss is also high on grazing lands next to crop land because of overgrazing. This finding is in line with Hurni (1985) finding in which soil loss is highest in crop land and followed by grazing, bush and forest lands.

### **10.3.4 Determination of Soil Erosion Prone Areas and Priority Setting for Planning and Implementation of SWC Measures**

Conservation planning depends upon multiple factors like intensity of problems, needs of local people, availability of resources and knowledge of agencies involved in restoration and rehabilitation work. Erosion prone area identification and prioritization is also an important aspect of planning for implementation of the watershed management program due to resource and manpower scarcity to treat the watershed

**Table 10.3** Soil loss by land use/land cover types

Land use	Area (%)	Soil loss (t/ha/yr)			
		Minimum	Maximum	Mean	STD
Crop land	70.3	0.68625	192.15	16.00	20.61
Grazing land	19.6	0.22875	48.8	6.41	8.63
Bush land	6.4	0.04575	9.76	2.28	2.23
Eucalyptus	2.5	0.004575	0.732	0.14	0.15
Built up area	1.2	0.02562	1.83	0.34	0.39

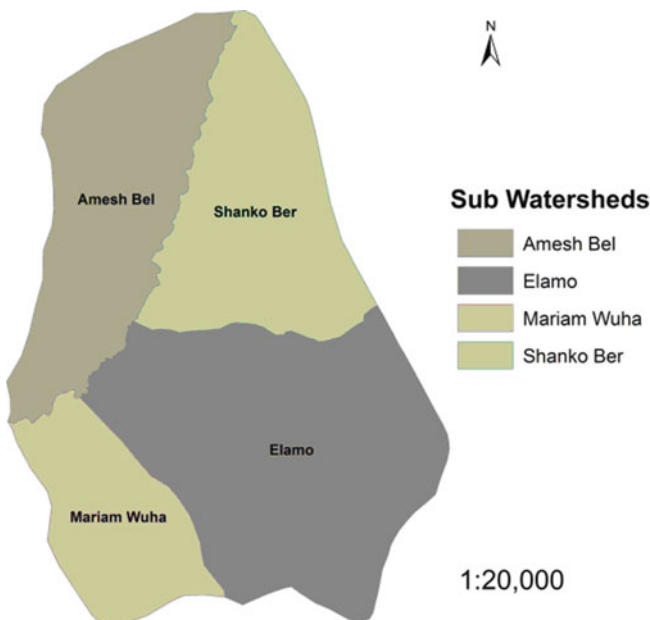


**Fig. 10.7** Sub-watersheds of the study area

at a time. Therefore, dividing the whole watershed into sub-watershed is important to identify priority areas at sub-watershed level for orderly treatment.

In this study, watershed prioritization for treatment is done based on soil erosion amount of each sub-watershed. First, the whole watershed was divided into four sub-watersheds using GPS on the field (Fig. 10.7). Second, the amount of soil loss in each sub-watershed was determined (Fig. 10.8) in ArcGIS 9.2 spatial analyst zonal statistics after soil loss of the whole watershed was estimated. Then priority for soil and water conservation treatment is set among the sub-watersheds based on the amount of soil loss in each sub-watershed.

As indicated in Table 10.4 and observed from soil erosion map by sub-watersheds of Fig. 10.8, soil loss ranges from 0.0128 to 192.14; 0.0046 to 111.26; 0.007 to 61.49 and 0.0235 to 28.18 tons/ha/year at Elamo, Shanko Ber, Amesh Bel and Mariam Wuha sub-watersheds, respectively. The mean annual soil loss rate is highest (18.49 tons/ha/year) at Elamo sub-watershed and lowest (6.93 tons/ha/year) at Mariam Wuha sub-watershed. The mean annual soil loss rate for Shanko Ber and Amesh Bel is 11.47 and 7.79 tons/ha/year, respectively. Therefore, Based on the amount of soil lost from each sub-watershed, Elamo, Shanko Ber, Amesh Bel and Mariam Wuha are prioritized as the first, second, third and fourth sub-watersheds for planning and implementing conservation measures at Debre Mewi watershed.

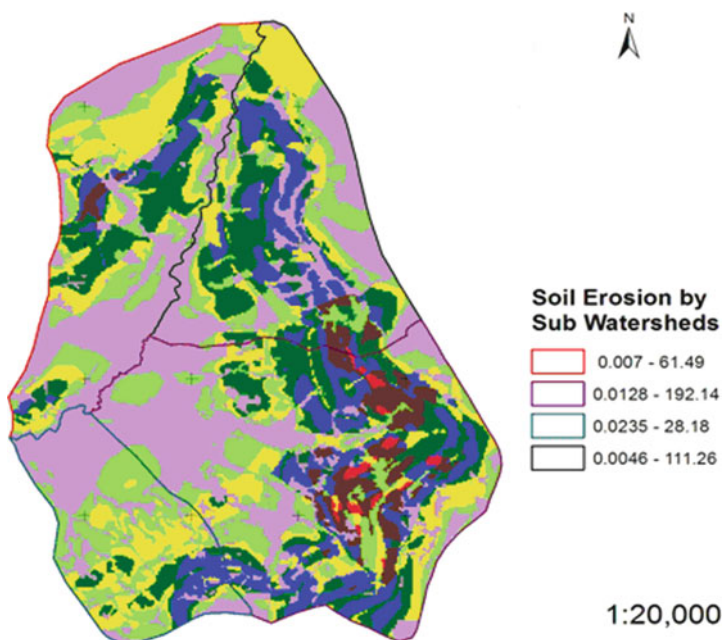


**Fig. 10.8** Soil erosion (t/ha/yr) map by subwatershed in the study area

**Table 10.4** Soil erosion by sub-watershed in the study area

Sub-watershed	Area (%)	Soil loss (t/ha/yr)			
		Minimum	Maximum	Mean	STD
Amesh Bel	24.5	0.0070	61.49	7.79	8.77
Shanko Ber	23.1	0.0046	111.26	11.47	12.92
Elamo	38.7	0.0128	192.15	18.49	25.61
Mariam Wuha	13.7	0.023	28.18	6.93	7.07

### 10.3.5 Validation of Estimated Soil Loss with Measured Values

Adet Agricultural Research Center is conducting research to determine the amount of soil loss in the study area through runoff plot method. One year measured soil loss data obtained from the research center is used to validate model estimated soil loss.

The measured value of soil loss without any conservation measure as a control treatment from the research center is 14.48 tons/ha/year and the model estimated soil loss without conservation practice that is  $p = 1$ , is 18.21 tons/ha/year, having the same slope length, slope gradient, soil type, land use and rainfall amount. The measured soil loss from the treated experiment with physical conservation measure (soil bund) and the model estimated data where  $P = 0.55$  because of terrace

availability, is 6.64 tons/ha/year and 10.56 tons/ha/year, respectively on the same slope length, slope gradient, land use, soil type and rainfall amount.

The above figures indicate that the model estimated soil loss exceeds the measured soil loss by 3.73 tons/ha/year on untreated areas and 3.92 tons/ha/year on treated areas. This is because the research center started to collect data 2 weeks late from the starting date (that is 2 weeks later after the rainfall started). It might be this gap, which reduces the amount of measured soil loss and brings the difference. Therefore, the result of the model prediction is found to be closer to the measured data, despite not exhaustive.

## 10.4 Conclusions

Based upon the above results and discussions, it is possible to draw the following conclusions.

- Debre Mewi watershed is prone to erosion ranging from very low to exceptionally high erosion classes.
- In Debre Mewi watershed, it was possible to notice that different erosion hot spot areas are available.
- Soil loss is different in different land use/land cover types and slope classes. Agricultural areas (crop lands) have very high soil erosion followed by grazing lands and bush lands, respectively. However, the soil loss is lower in eucalyptus plantations and built up areas. Similarly, as slope steepness increases soil loss gets higher.
- From the results of this study, it is clear that RUSLE is a powerful model for the qualitative as well as quantitative assessment of soil erosion with reasonable accuracy.
- DEM, which is derived from digitizing contours of 1:50,000 topographic sheets is found to be a very good data source to find out a better slope gradient.
- Slope length that is measured at the field level was found to be better than that of generated from digitized contour.

**Acknowledgments** We would like to deeply thank the Amhara National Regional State – Bureau of Agriculture and Rural Development (ANRS – BOARD) and SWHISA for the financial support. We extend our thanks to Dr. Birru Yitaferu for his constructive and useful assistance during the study and also to Ayen Mulu, Tigist Getachew, Birara Chekol, Ethiopia Abesha, Nardos Mulate and Kaleab Mulate for their genuine support in creating conducive work environment.

We deeply appreciate and respect the small scale farmers of Debre Mewi Watershed for giving us all the assistance we required and who are struggling all their lives for a better future.

## References

Baban SMJ, Wan Yusof K (1999) Modeling soil erosion in tropical environments using remote sensing and geographical information systems. Department of survey and land information, The University of West Indies, St Augustine, Trinidad, West Indies

Berehe Wolde Aragay (1996) Twenty years of soil conservation in Ethiopia. A personal overview. Regional Soil Conservation Unit/SIDA, Nairobi

Desta H, Kassie M, Benin S, Pender J (2000) Land degradation in the high lands of the Amhara region and strategies for sustainable land management. ILRI, vol II.114P. ISBN 92-9146-090-7. Nairobi, Kenya

Foster GR, Yoder DC, Weesies GA, McCool DK, McGregor KC, Bingner RL (2002) USER'S GUIDE- revised universal soil loss equation version 2 (RUSLE 2). USDA – Agricultural Research Service, Washington, DC

Ethiopian Highland Reclamation Study (EHRS) (1984) Annual Research Report 91983–1984 Ministry of Agriculture, Addis Ababa, Ethiopia

Hawando T (1995) The survey of the soil and water resources of Ethiopia. UNU, Tokyo

Herweg K, Stillhardt B (1999) The variability of soil erosion in highlands of Ethiopia and Eritrea. Average and Extreme Erosion Patterns. CDE Research Report 42, Berne

Hudson NW (1986) Soil conservation, Bats Ford Ltd., London

Hurni H (1985) Erosion – productivity – conservation system in Ethiopia. IV. International Conference on soil conservation, at Mercacy, Venezuela

Hurni H (1986) Degradation and conservation of the soil resource in the Ethiopian highlands. A Paper presented at the first international workshop on African Mountains and Highlands, Ethiopia. 19–27 Oct 1986. Agriculture, CADU Publication No.74

Hurni H (1988) Degradation and conservation of the resources in the Ethiopian highlands. Mountain Res Dev 8(2/3):123–130 University of Bern, Switzerland

Lal RE (1984) Soil erosion: research methods. St. Lucie Press, Soil and Water Conservation Society, Delray Beach, FL, Ankeny, IA

Millward AA, Mersey JE (1999) Adapting the RUSLE to model soil erosion potential in a mountainous tropical watershed. Catena 38:108–129

Morgan RPC (1995) Soil erosion and conservation. Addison – Wesley Longman, Ending burgh, 198pp

Morgan RPC (2005) Soil erosion and conservation. Blackwell Science Ltd., Oxford, 304pp, ISBN 1-4051-178-8

Renard KG, Foster GR, Weesies GA, McCool DK, Yoder DC (1997) Predicting soil erosion by water: a guide to conservation planning with the revised universal soil loss equation (RUSLE). Agriculture Handbook No. 703, US Department of Agriculture, Washington, DC

Sapkota R (2008) Modeling runoff and erosion. Namchun Watershed, Thailand

Soil Conservation Research Project (SCRP) (1986) Fourth progress report (1984) by Hurni H, M. Grunder, University of Berne and UN University in Association with the Ministry of Agriculture, Ethiopia, Series V, Anjene Research Unit (draft)

Vrieling A (2007) Mapping erosion from space. Proefschrift Met Lit.olg. Met Samenvatting in het Engels en Nederland's

WBISPP (2000) Manual for Woody Biomass Inventory and Strategic Planning Project, Ministry of Agriculture, Addis Ababa, Ethiopia

Wischmeier WH, Smith DD (1978) Predicting rainfall erosion loss – a guide to conservation planning. Agricultural Handbook Number 537, USDA

Zeleke G (2000) Landscape dynamics and soil erosion process modeling in the North Western Highlands. GEOGRAPHICA BERNENSIA, Institute of Geography. University of Bern, Switzerland

**Part IV**

**Climate Variability and Hydrologic  
Response**

# Chapter 11

## Application of Hydrological Models for Climate Sensitivity Estimation of the Atbara Sub-basin

**Eman Hasan and Mohamed Elshamy**

**Abstract** Hydrological models have a wide range of applications in water resources planning and management as well as flood forecasting and climate impact assessments. In the latter case, they are usually coupled to meteorological or climate models. In this study, two hydrological models (Hydrologiske Byråen avdeling för Vattenbalans (HBV) and Nile Forecast System (NFS)) are applied to the Atbara catchment, Nile River basin area to study the sensitivity of runoff to changes in rainfall and potential evapotranspiration. The HBV model is a conceptual lumped model while the other NFS is a conceptual distributed model. Atbara River is the last major tributary of the Nile River and has a highly seasonal pattern with very high flows during the flood season and almost zero flows during the dry season. These features pose problems to the calibration of hydrological models. However, both models were able to capture the main features of the monthly flow time series of the Atbara (Nash efficiency index reached 0.92 for HBV and 0.68 for NFS). Results indicate a very high climate sensitivity of the catchment where rainfall increases of 10, 20 and 30% result in runoff increases of 29, 62, and 97%, respectively. The catchment runoff is also sensitive to changes in potential evapotranspiration but to a lesser extent. These results are confirmed by the two used models with slight differences.

**Keywords** Nile · Atbara · Climate sensitivity · Hydrological models · HBV · NFS

### 11.1 Introduction

Hydrological modeling is an area where modeling has been used for a very long time. Applications range from forecasts for the hydropower industry, public safety,

---

E. Hasan (✉)

National Water Research Center, Cairo, Egypt

e-mail: Dr eman30@hotmail.com

This chapter was earlier published in Ain Shams Journal of Civil Engineering, Egypt vol. 2, September 2009, pp. 367–378.

agriculture and environmental monitoring. The HBV model was developed at the Swedish Meteorological and Hydrological Institute (SMHI) in the 1970s. Different model versions of HBV have been applied in more than 40 countries with different climatic conditions all over the world. The model has been applied for scales ranging from lysimeter plots (Lindström and Rodhe, 1992) to the entire Baltic Sea drainage basin (Bergström and Carlson, 1994; Graham, 1999). The model is used for flood forecasting in the Nordic countries, and many other purposes, such as spill-way design floods simulation (Bergström et al., 1992), water resources evaluation (for example Jutman, 1992, Brandt and Bergström, 1994), nutrient load estimates (Arheimer, 1998). Arheimer and Fogelberg (2001) reported that the performance of HBV model is of good accuracy in northern and middle Europe, while it is more difficult to capture the peakiness of the flow in the most southern countries. Booij (2002) reported that the average and extreme discharge behavior at the Borgharen basin outlet is well reproduced by the HBV-15 and HBV-118 in the calibration and validation process. Semmler et al. (2006) used HBV and the Rossby Centre Regional Atmospheric Model (RCA3) to study the effect of climate change on Suir River catchment discharge under different climate scenarios. Suir River catchment is located in the south-east of Ireland. The calibration and validation results of ERA-40 project simulation showed that the HBV model can reproduce the discharge reasonably well. They added that the application of a high resolution regional climate model (RCM) in connection with HBV hydrological model could capture the local variability of river discharge for daily climate. Yemti (2007) tested the performance of HBV-96 by applying ground trust data and satellite data in Gumera sub-catchment (Blue Nile River basin). The simulated hydrograph can reproduce the peak for some event but it was shifted by 2 days. Moreover, the shape of the hydrograph was well represented.

The Nile Forecast System (NFS) is a real-time distributed hydro-meteorological forecast system designed for forecasting Nile flows at designated key points within the Nile; of major interest is the inflow of the Nile into the High Aswan Dam, Egypt. The system is hosted at the Nile Forecasting Center (NFC) of the Ministry of Water Resources and Irrigation (MWRI), Giza, Egypt, which kindly provided a copy of the NFS software (version 5.1 – NFC, 2007) and the available documentation for this research. The performance of the NFS in providing accurate forecasts is thus readily assessed by comparing the issued forecasts with observed flows as soon as they become available and is generally judged as satisfactory (NFC, personal communication, 2004). A recent evaluation of the NFS hydrological component was conducted by Sayed and Saad (2002) for a short period (1997–2002). This evaluation focused on the Diem and Dongola stations and compared simulated and observed daily flows showing a generally good agreement (93 and 90% of the observed daily variance explained by the simulation) but indicated that errors are larger during the Ethiopian rainy season (May–September). The performance of the NFS hydrological component with regard to long-term simulations was also recently assessed for the purpose of conducting climate change scenarios by Elshamy (2006). Using monthly and daily gridded gauge rainfall as available, he assessed the monthly performance of the NFS over the period 1940–1999.

The assessment showed variable performance for the different catchments with better performance for the Blue Nile and Atbara catchments ( $R^2$  was 0.79 and 0.67 respectively and the NFS slightly overestimated the mean annual flow volume).

The overall objective of the study reported in this chapter is to study the sensitivity of the runoff from Atbara catchment area to changes in rainfall and potential evapotranspiration. This is achieved through the application of two hydrological models to the catchment, the HBV and NFS.

## 11.2 Models Description

### 11.2.1 HBV Model

HBV is an acronym formed from Hydrologiske Byråv avdeling för Vattenbalans at SMHI, Sweden. The HBV model is a rainfall-runoff model, which includes conceptual numerical descriptions of hydrological processes at the catchment scale. The general water balance can be described as:

$$P - E - Q = \frac{d}{dt} [SP + SM + UZ + LZ + \text{lakes}] \quad (11.1)$$

Where  $P$  = precipitation (mm),  $E$  = evapotranspiration (mm),  $Q$  = runoff ( $m^3/s$ ),  $SP$  = snow pack,  $SM$  = soil moisture,  $UZ$  = upper groundwater zone,  $LZ$  = lower groundwater zone and  $\text{lakes}$  = lake volume.

The model consists of a precipitation routine representing rainfall and snow, a soil moisture routine determining actual evapotranspiration, overland flow and subsurface flow, a fast flow routine representing storm flow, a slow flow routine representing subsurface flow, a transformation routine for flow delay and attenuation and a routing routine for river flow.

### 11.2.2 Model Modification

The time step is usually 1 day but in this research because of the lack of available daily data of rainfall, runoff and evapotranspiration, the model is modified to be monthly. Moreover, 5 years series version was produced for simplicity of using the model for calibration and verification process.

Input data are observations of precipitation, air temperature and estimates of potential evapotranspiration. The evaporation values used are normally monthly averages. Air temperature data are used for calculations of snow accumulation and melt but in our case it can also be used to adjust potential evaporation when the temperature deviates from normal values, or to calculate potential evaporation. If none of these last options are used, temperature can be omitted in snow free areas.

### 11.2.3 Model Calibration

The model parameters cannot be measured and have to be determined through the model calibration. Calibration is a process in which parameters adjustments are made in order to simulate as closely as possible to hydrological behaviour of the catchment. The goodness of fit is always determined by an objective function. Madsen (2000) concluded that for a proper model calibration it is necessary to consider a good fit between simulated and observed catchment runoff volume, the shape of the hydrograph, the peak flow, and the base flow. All these objectives are taken into consideration during model calibration because a single objective function cannot establish a reasonable match between simulated and observed data. The process of calibration can be done manually by trial and error parameter adjustment.

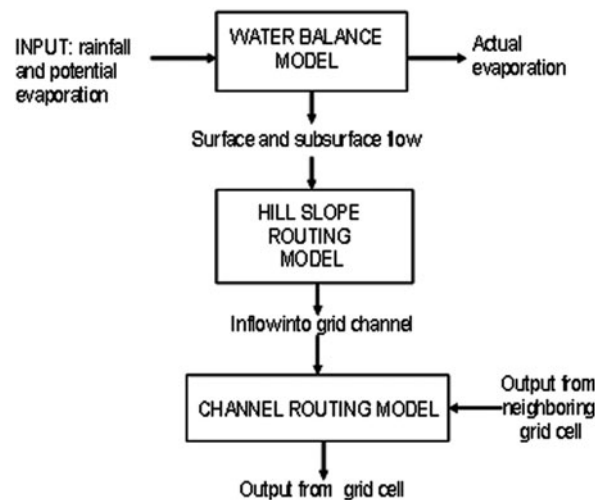
## 11.3 NFS Description

The NFS is composed of six main components that perform the following functions:

1. Rainfall Estimation
2. Hydrological Simulation
3. River Flow Forecasting
4. Assimilation
5. Data Collection and Management
6. GIS Functions

The core of the NFS is a conceptual distributed hydrological model of the whole Nile system including soil moisture accounting, hill slope and river routing, lakes, wetlands, and man-made reservoirs within the basin. The hydrological component of the NFS is defined on the quasi-rectangular grid of the METEOSAT. Each grid cell (pixel) imitates a small basin with generalized hill slopes and stream channels. Input to each grid cell is precipitation and potential evaporation. This input is applied to the water balance model of the grid cell. Based on the moisture deficit in the cell, the water balance model computes the actual evaporation and the surface and subsurface runoff components from the pixel. Surface and subsurface runoffs are subsequently input to the pixel's hill slope routing model, simulating the transfer of water towards the main channel. Then water is routed through this channel to the downstream pixel according to a pre-defined connectivity sequence (established via GIS). Figure 11.1 shows a flowchart of the simulation process in a grid cell. For computational efficiency, the current implementation of the NFS groups used  $4 \times 4$  pixels ( $\approx 484 \text{ km}^2$ ) as the computational unit. All three components (Fig. 11.1) are computed for each unit, and through a predefined channel network, the water is routed through the various tributaries to the outlet points of the Nile River basin

**Fig. 11.1** Hydrological models at the pixel scale of the Nile forecast system (NFS) (After Elshamy, 2006)



taking into account the effect of direct evaporation from river reaches, abstractions for irrigation, and man-made reservoirs (Georgakakos et al., 2001). Special sub-models for lakes and wetlands are called for those pixels designated to fall into these water bodies.

## 11.4 Atbara Catchment Area

River Atbara, which is the last tributary of the Nile, enters the main Nile at about 320 km downstream of Khartoum. It is 880 km long and the greater part of its catchment is situated in Ethiopia. The highest points in the catchment reach more than 3,500 m above mean sea level (a.m.s.l), where as the eastern watershed of the Atbara is, for the most part, more than 2,500 m high (Shahin, 1985). The Atbara does not spring from a lake and relies totally on many small tributaries, of which Tekeze or the Setit is the principal one. Above the Setit junction the Atbara receive a number of tributaries of which the Bahar el Salam is the principle. The Atbara is more strongly seasonal in its flow, compared to the Blue Nile River. Moreover, the big drop in elevation between the head and the junction of the Salam River is responsible for the excessive sediment load of the Atbara in proportion to its flow volume; in this reach the Atbara has a slope of about  $5 \times 10^{-3}$  (Fig. 11.2).

The Atbara River draws its floodwater from the rains on the northern part of the Ethiopian plateau. During the low-water season, which runs from January to June, the Atbara shrinks to a number of pools. But in late summer, during the rainy season (generally June–October), the river is swollen by the summer rains the water level rises more than 5 m above its normal level and provides about one-third of the Nile's total volume of water. It also brings down more than 25 million tons of silt a year. The catchment area of Atbara is 202,652 km<sup>2</sup> as estimated by Nile Forecast Centre.

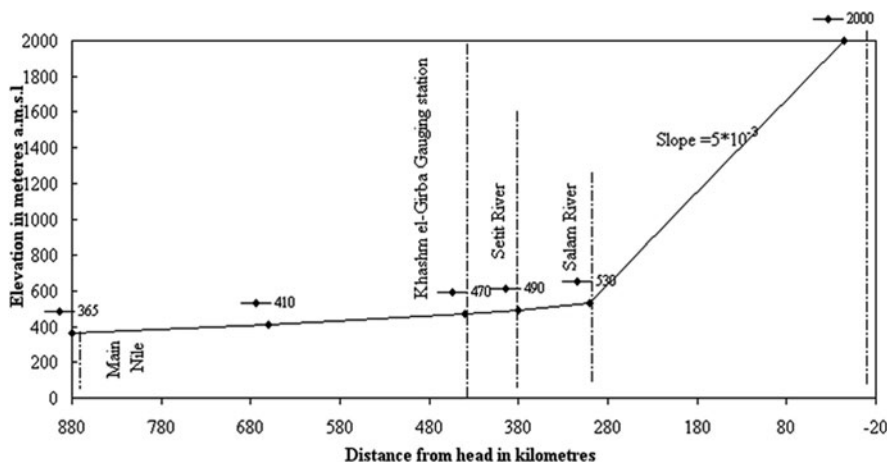


Fig. 11.2 Longitudinal profile of Atbara River (after Zaghloul et al., 2005)

The hydrograph of Atbara catchment area during the period from 1964 to 2000 is shown in Fig. 11.3. From this figure, it is noticed that the peak value of flow equals to about 4.5 billions  $m^3$  during August meanwhile, the maximum rainfall equals to about 150 mm during the same month. The potential evapotranspiration (PET) along Atbara catchment area is also illustrated and it varies from about 128.82 mm in December to 201.93 in May.

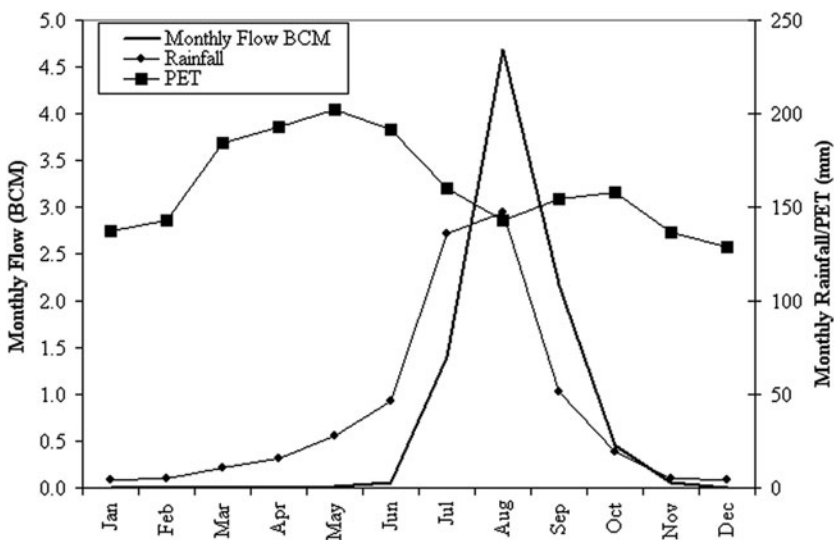


Fig. 11.3 The hydrograph of Atbara catchment area as cumulated monthly average in the (1964–2000)

## 11.5 Analysis

To simulate Atbara catchment area, the HBV model has been calibrated at first with rainfall, runoff and potential evapotranspiration data for the period from 1979 to 1983. This 5-year time series is the only period that has a complete monthly set of data for the model run (especially rainfall stations). Monthly average rainfall is calculated for the stations that included in Atbara catchment area (Fig. 11.4). Monthly observed runoff at the catchment outlet is used for the analysis. Monthly potential evapotranspiration for Gonder station is used, as Gonder is the nearest available station to the catchment (Fig. 11.4).

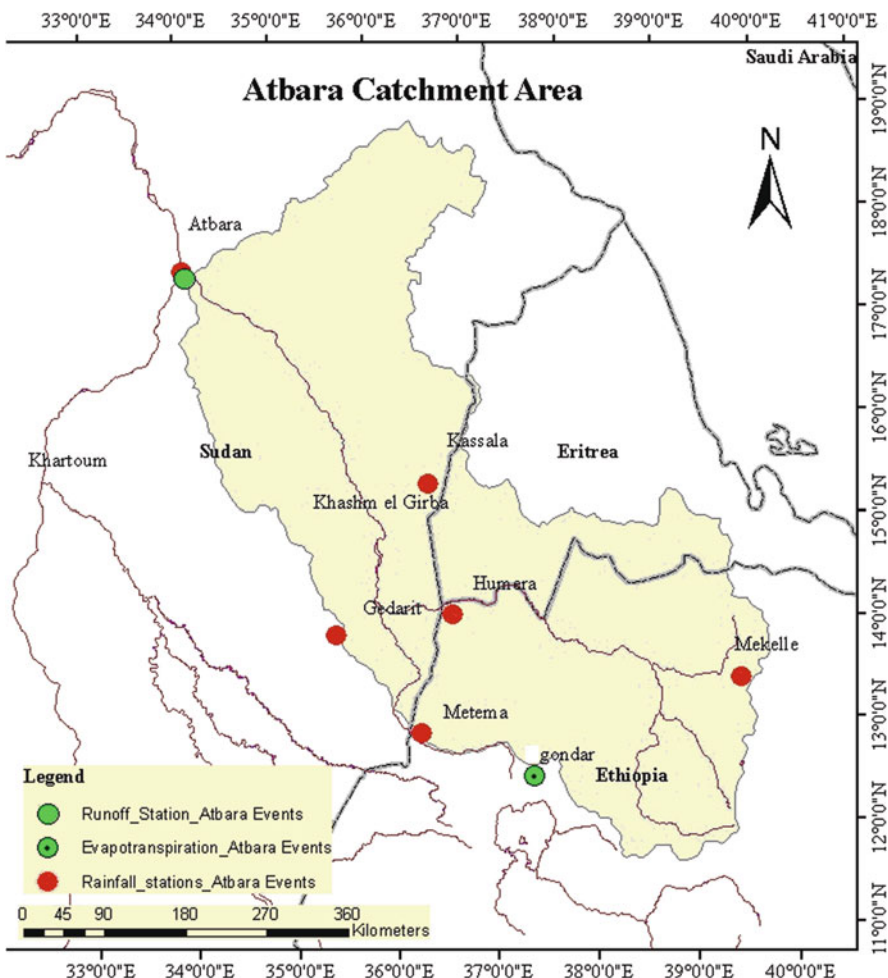


Fig. 11.4 Atbara catchment area

**Table 11.1** Free parameters in HBV – model for Atbara catchment area

Model routine	Free parameters	Symbol	Value	Units
Evaporation	Evaporation factor		0.80	
Precipitation	Rain-correction		0.60	
Soil	Field capacity	FC	400	mm
	BETA	BETA	1.00	
	Threshold evaporation	LP	200	mm
Upper zone	Fast drainage coeff.	KUZ2	0.60	1/day
	Slow drainage coeff.	KUZ1	1.00	1/day
	Threshold	UZ1	0.50	mm
	Percolation	PERC	4.00	mm/day
Lower Zone	Drainage coeff	KLZ	0.00	1/day

HBV model contains a number of free parameters which are adjusted to produce best output during the calibration period, later on; these parameters are kept constant in verification process during the period from 1984 to 1988 to verify the goodness of fit of the model. The performance of the model is assessed qualitatively and quantitatively according to the following equation (Nindamutsa, 2007):

$$NE = 1 - \sum (Q_S - Q_O)^2 / \sum (Q_O^- - Q_O)^2 \quad (11.2)$$

Where  $NE$  = Nash Efficiency,  $Q_O$  = Observed runoff,  $Q_S$  = Simulated runoff,  $Q_O^-$  = observed average runoff during the study period.

Selected HBV free parameters for Atbara catchment area are summarized in Table 11.1.

The NFS was previously calibrated, thus it was used directly to simulate the flow at Atbara using rainfall and potential evapotranspiration data stored in the system. Rainfall data are gridded monthly values while potential evapotranspiration are climatological monthly grids obtained from FAO (LNDFC, 2005).

## 11.6 Results and Discussion

### 11.6.1 Calibration Process

Figure 11.5 illustrates the observed and simulated runoff hydrographs of HBV and NFS models for Atbara catchment area during calibration process for the period from 1979 to 1983, the shape of the simulated hydrographs are well represented and show great similarity to the observed one. The peak and base flow of the observed and HBV model simulated are in close agreement. Both of NFS and HBV models showed an over estimation in the year 1982 and showed an under estimation in the year 1979. The peak flow is during the flood season from August to October and the low or dry season is from January till June. Moreover, the Nash efficiency ( $R^2$ )

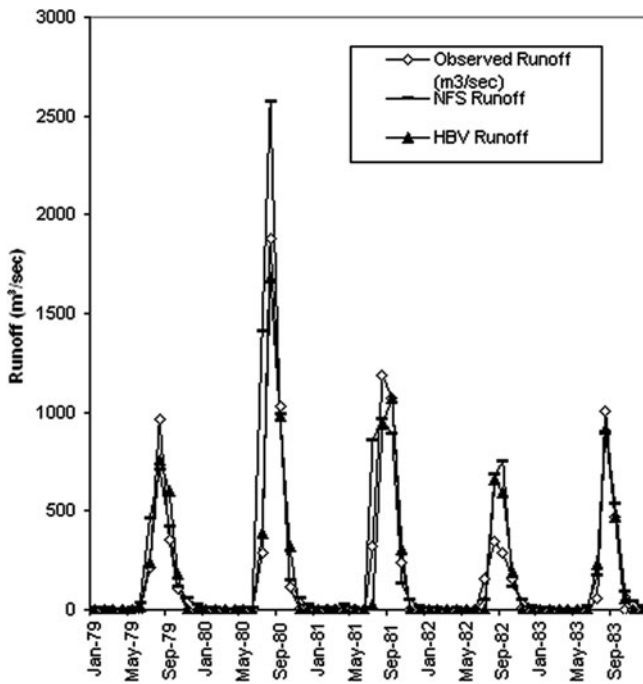


**Fig. 11.5** HBV and NFS models outputs for calibration process

of HBV and NFS equals to 92 and 68%, respectively, which indicates how well the model in simulated the observed runoff from Atbara outlet.

### 11.6.2 Verification Process

The simulated hydrograph of the HBV model shows great similarity to the observed one in most of the time. For HBV model, there is under estimation during the year 1987 and over estimation in the year 1988, Fig. 11.6. While for NFS the hydrograph showed an over estimation in the year 1985 and 1988 and an under estimation in the year 1987. The peak and the base flow are similar for the observed and simulated runoff for the two models.

The Nash efficiency (NE) of HBV and NFS equals to 64 and 71%, respectively during the verification process and these ratios are fair because of the model uncertainties.

#### 11.6.2.1 Peaks Observed and Simulated Runoff (Calibration Process)

Table 11.2 shows the peaks of observed and simulated runoff for HBV model during calibration and the coefficient of determination ( $R^2$ ) between them is 0.865.

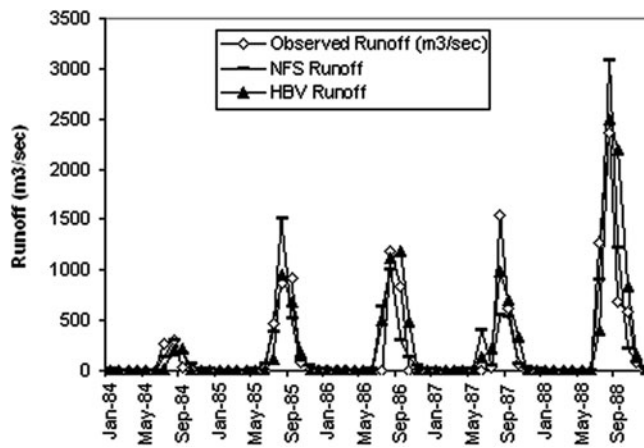


**Fig. 11.6** HBV and NFS models outputs for verification process

**Table 11.2** Linear correlations between peak observed runoff and peak simulated HPV

Date	Peaks observed runoff (m <sup>3</sup> /s)	HBV peaks	R <sup>2</sup>
Aug-1979	963.26	761.73	0.865
Aug-1980	1,877.99	1,682.98	
Aug-1981	1,183.54	937.57	
Aug-1982	343.49	656.09	
Aug-1983	1,008.06	913.05	

**Table 11.3** Linear correlations between peak observed runoff and peak simulated NFS

Date	Peak observed runoff (m <sup>3</sup> /s)	NFS peaks	R <sup>2</sup>
Aug-1979	963.26	711.35	0.7648
Aug-1980	1877.99	2569.71	
Aug-1981	1,183.54	966.76	
Aug-1982	343.49	685.42	
Aug-1983	1,008.06	901.27	

Table 11.3 illustrate that the coefficient of determination between the peaks of observed runoff and the simulated one for NFS model during calibration is 0.7648.

### 11.6.2.2 Peak Observed and Simulated Runoff (Verification Process)

Figures 11.7 and 11.8 show the linear correlation between the peaks observed runoff and the peaks simulated one during verification process for HPV and NFS model respectively. For HPV model the coefficient of determination ( $R^2$ ) between the peaks

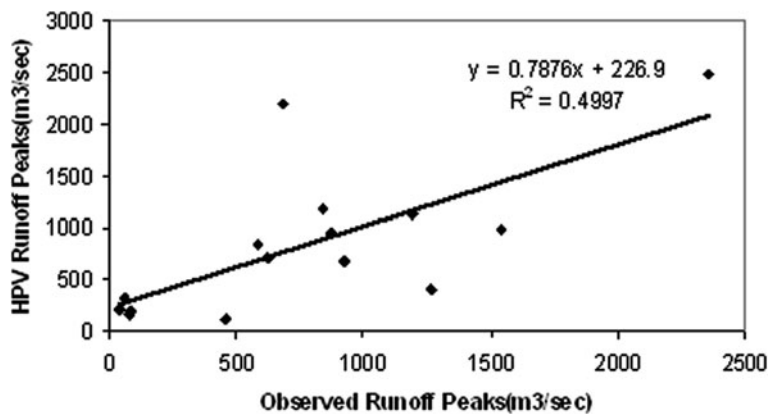


**Fig. 11.7** Linear correlation between the observed runoff peaks and the simulated one for HPV model during verification process

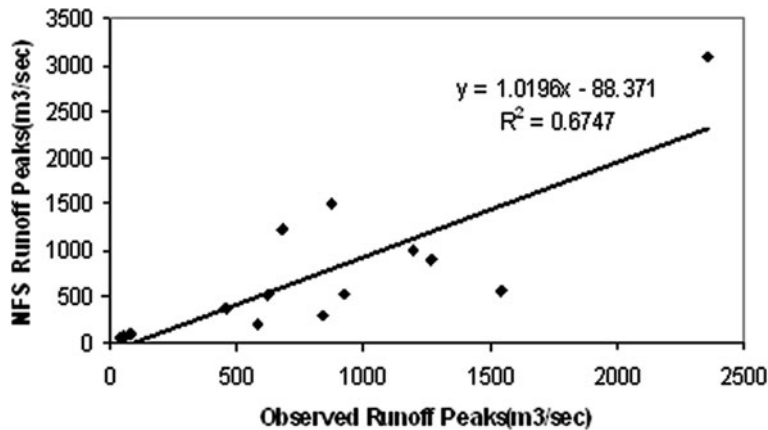


**Fig. 11.8** Linear correlation between the observed runoff peaks and the simulated one for NFS model during verification process

observed runoff and the simulated one by the model is about 0.5 while the linear correlation in case of NFS model is 0.6747.

### 11.6.3 Sensitivity Analysis

This part of the research discusses the sensitivity of the two used models (HBV and NFS) to variation in both rainfall and potential evapotranspiration parameters. Positive and negative changes by 5, 10, 15, 20, 30% for rainfall and potential evapotranspiration are made separately then each model is run again for the period from 1979 to 1984. This means that each model is run ten times for rainfall changes and

the same runs for potential evapotranspiration changes. The changes that occurred in the simulated runoff as a result of rainfall and potential evapotranspiration changes are illustrated in Figs. 11.9 and 11.10, respectively. Figure 11.9 shows that both models predict high sensitivity of runoff for changes in rainfall, while NFS is

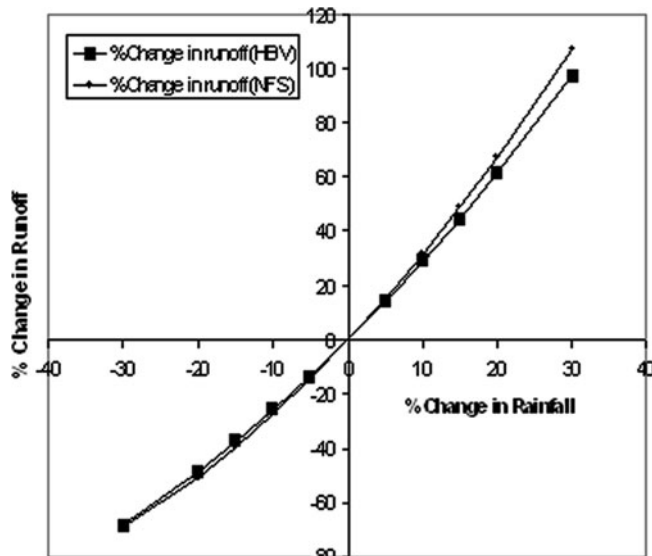


Fig. 11.9 Percentage of changes in simulated runoff of (HBV) and (NFS) for rainfall changes

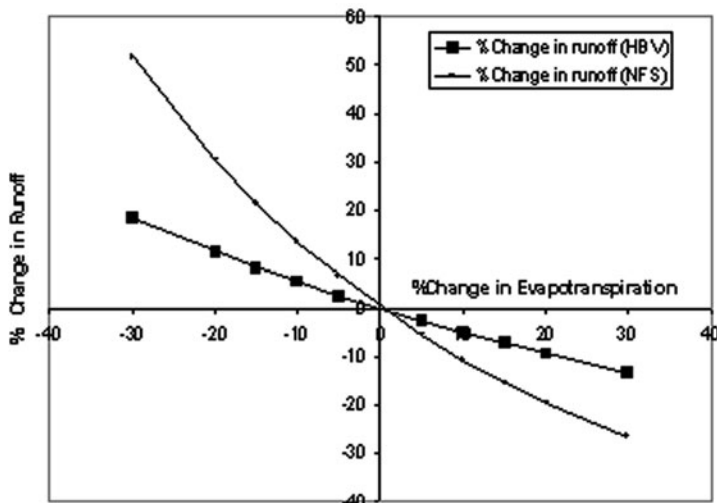


Fig. 11.10 Percentage of changes in simulated runoff of (HBV) and (NFS) for potential evapotranspiration changes

showing slightly higher sensitivity. Changing rainfall by + 10% results in change of runoff by 29.22 and 31.81% for HBV and NFS, respectively. Meanwhile, 30% of increasing or decreasing rainfall affects both model outputs to great extent. Figure 11.10 shows that, increasing potential evapotranspiration by 10% leads to change in runoff by -5.09 and -10.98% for HBV and NFS, respectively. This may be due to the use of climatological evapotranspiration values for NFS, which may not reflect the inter-annual variability. On the other hand, HBV simulations used a time series of potential evapotranspiration values that better reflect the inter-annual variability. In addition, the NFS is a distributed model so the spatial pattern of potential evapotranspiration may be more important than its temporal variability.

## 11.7 Conclusion

HBV and NFS models are used to study the sensitivity of the runoff from Atbara catchment area along the Nile River to changes in rainfall and potential evapotranspiration. Each of the two models was calibrated for Atbara catchment using runoff and the hydro-meteorological data series of 1979–1983. Models verification was carried out for the period from 1984 to 1988 to verify the goodness of fit of the two models. Moreover, sensitivity analysis was carried out to the HBV and NFS models to test the sensitivity of each model output (simulated runoff) to rainfall and evapotranspiration variation.

The study revealed the following:

- Atbara catchment area is very sensitive to climate change (Elshamy et al., 2009).
- HBV – model is more efficient than NFS in simulating Atbara catchment area, as one of the Nile River sub-basin.
- HBV and NFS simulations are more sensitive to rainfall changes than potential evapotranspiration changes.

## 11.8 Recommendation

Based on the results of HBV and NFS, the simulated hydrographs of runoff for Atbara catchment area, it could be concluded that the model simulation results depend on the quality of the input data and on the nature of the catchment itself. This means that data exchange along Nile basin countries is essential for improving research results.

## References

Arheimer B, Fogelberg S (2001) HBV Modeling in several european countries. Internet website <http://euroharp.org/index.htm>

Arheimer B (1998) Riverine nitrogen – analysis and modeling under Nordic conditions. Kanastryckeriet, Motala, p 200

Astere Nindamutsa (2007) Comparison of the performance of rainfall-runoff hydrological models in Ruvubu River Basin. MS.C Thesis, Arba Minch University School of Graduate Studies, Ethiopia

Bergström B, Carlsson B (1994) River runoff to the baltic sea: 1950–1990. *Ambio* 23:280–287

Bergström S, Harlin J, Lindström G (1992) Spillway design floods in Sweden. I: New guidelines. *Hydrol Sci J* 37(5):505–519

Booij MJ (2002) Appropriate hydrological modeling of climate change impacts on River flooding. Water Resources Management Group, Department of Civil Engineering, University of Twente, Enschede, The Netherlands (m.j.booij@ctw.utwente.nl)

Brandt M, Bergström S (1994) Integration of field data into operational snowmelt-runoff models. *Nordic Hydrol* 25:101–112

Georgakakos K, Carpenter TM, Sperfslage JA (2001) Adjusting parameter values for the hydrologic models of the NFS. HRC Technical Note No. 14. Hydrologic Research Centre, San Diego, USA

Graham P (1999). Modelling runoff to the baltic basin. *Ambio* 28:328–334

Jutman T (1992). Production of a new runoff map of Sweden. Nordic hydrological conference, Alta, Norway, NHP report No. 30. pp 643–651

Lindström G, Rodhe A (1992). Transit times of water in soil Lysimeters from modeling of oxygen-18. *Water Air Soil Pollut* 65:83–100

LNDFC (2005) Impact of climate change on the water supply to Egypt. Ministry of water resources and irrigation, Nile Forecasting Center, Lake Nasser Flood and Drought Control Project (LNDFC/ICC)

Madsen H (2000) Automatic calibration of a conceptual rainfall-runoff model using multiple objectives. *J Hydrol* 235:276–288

Mohamed E (2006) Improvement of the hydrological performance of land surface parameterization: an application to the Nile Basin. Ph.D Thesis, Environmental and Water Resources Engineering Department of Civil Engineering Imperial College of Science, Technology, and Medicine London SW7 2BU

Mohamed E, Baligira R, Abdel-Ghaffar E, Moges SA (2009) Investigating the climate sensitivity of different nile sub-basins. Thirteenth international water technology conference, Hurghada, Egypt, 12–15 March

Sayed MAA, Saad B (2002) The Experience of the Nile forecast centre (NFC) in managing floods and setting strategies for knowledge dissemination. The 18th Congress on Irrigation and Drainage. International Commission on Irrigation and Drainage, Montreal, Canada

Semmler T, Wangs M, Mcgrath R, Nolans N (2006) Regional climate ensemble simulation for Ireland impact of climate change on River flooding. Natl Hydrol Seminar

Shahin (1985) Hydrology of the Nile Basin, developments in water science. International Institute for Hydraulic and Environmental Engineering Oude DELT 95, 2601 DA Delt, The Netherlands

Yemti I (2007) Rainfall estimation by remote sensing for conceptual rainfall- runoff modeling in the upper blue Nile Basin. MS.C Thesis, International Institute for Geo-Information Science and Earth Observation. Enschede, The Netherlands

Zaghoul S, El-Moatassem M, Rady AA (2005) The Hydrological interactions between the white and the blue Niles at the confluence region. The international conference of UNESCO friend/Nile project Sharm El-Sheikh, Egypt, 12–15 Nov

## Chapter 12

# Climate Change Impact on Agricultural Water Resources Variability in the Northern Highlands of Ethiopia

Shimelis G. Setegn, David Rayner, Assefa M. Melesse, Bijan Dargahi, Ragahavan Srinivasan, and Anders Wörman

**Abstract** The economy of Ethiopia mainly depends on agriculture, and this in turn largely depends on available water resources. A major effect of climate change is likely to be alterations in hydrologic cycles and changes in water availability. This chapter reports the use of global climate models (GCM's) and application of a hydrological model to investigate agricultural water resources' sensitivity to climate change in the Lake Tana Basin, Ethiopia. Projected changes in precipitation and temperature in the basin for two future seasons (2046–2065 and 2080–2100) were analyzed using outputs from fifteen GCMs. A historical-modification procedure was used to downscale large scale outputs from four GCM models to watershed-scale climate data. The study then investigated how these changes in temperature and precipitation might translate into changes in streamflow and other hydrological components using SWAT model. We interpret the different aspects of the hydrological responses to imply that changes in runoff and other hydrological variables could be significant, even though the GCMs do not agree on the direction of the change indicating high uncertainty.

**Keywords** Climate change impact · Lake Tana · SWAT · Hydrological modeling · GCM · Downscaling · SRES

### 12.1 Introduction

Climate changes pose significant economic and environmental risks worldwide. The economy of Ethiopia mainly depends on agriculture, and this in turn largely depends on available water resources. The country has a fragile highland ecosystem that is currently under stress due to increasing population pressure and land degradation. The Blue Nile River basin is one of the most sensitive basins to changing climate and water resources variability in the region (Kim and Kaluarachchi, 2009). But as

---

S.G. Setegn (✉)

Department of Earth and Environment, Florida International University, Miami, FL 33199, USA  
e-mail: ssetegn@fiu.edu

yet, there is no consensus on the effect of climate change on water availability in the region. Hence it is necessary to improve our understanding of the problems caused by the changing climate.

In recent years, concern has increased over climate change caused by increasing concentrations of carbon dioxide and other trace gases in the atmosphere. A major effect of climate change is likely to be alterations in hydrologic cycles and changes in water availability. Increased evaporation, combined with changes in precipitation, has the potential to affect runoff, the frequency and intensity of floods and droughts, soil moisture, and available water for irrigation and hydroelectric generation. In addition, watershed hydrology is affected by vegetation types, soil properties, geology, terrain, land use practices, and the spatial pattern of interactions among these factors and with climate (Richey et al., 1989; Laurance, 1998; Schulze, 2000; Fohrer et al., 2001; Zhang et al., 2001; Huang and Zhang, 2004, Brown et al., 2005, van Roosmalen et al., 2009, Tu, 2009). The Intergovernmental Panel on Climate Change's (IPCC, 2007) findings suggests that developing countries like Ethiopia will be more vulnerable to climate change due to their economic, climatic and geographic settings. According to IPCC (2007) report, the population at risk of increased water stress in Africa is projected to be between 75–250 and 350–600 million people by the 2020s and 2050s, respectively. Moreover, yields from rain-fed agriculture could be reduced by up to 50%, in countries which depend mainly on rain-fed agriculture.

Assessing the impact of climate change on stream flows, soil moisture, groundwater and other hydrological parameters essentially involves taking projections of climatic variables (e.g., precipitation, temperature, humidity, mean sea level pressure etc.) at a global scale, downscaling these global-scale climatic variables to local-scale hydrologic variables, and computing hydrological components for water resources variability and risks of hydrologic extremes in the future. Projections of climatic variables globally have been performed with General Circulations Models (GCMs), which provide projections at large spatial scales. Such large-scale climate projections must then be downscaled to obtain smaller-scale hydrologic projections using appropriate linkages between the local climates. A number of studies have investigated downscaling methods for establishing a connection between coarse-resolution GCMs and hydrologic models (e.g. Wilby et al., 1998, 2000; Hay and Clark, 2003; Wood et al., 2004; Benestad et al. 2008).

There are limited climate change impact studies in Ethiopia (Tarekegn and Tadege, 2006; Kim and Kaluarachchi, 2008; Abdo et al., 2009; Melesse et al., 2009, Beyene et al., 2010). To make a conclusion about the effect of climate change on the watershed hydrology using a particular GCM may not give clear representation of the future changes. According to IPCC (2007), high uncertainty is expected in climate change impact studies if the simulation results of a single GCM are relied upon (IPCC, 1999). To minimize uncertainties due to GCM model formulations and assumptions, this study downscaled outputs from 15 GCMs. This enabled us to show the future hydrological response to a range of possible changes, as expressed by the outputs from the different models. This study chose to generate daily climate projections by modifying the historical datasets to represent the changes in the GCM climatologies.

From among the different Special Report on Emissions Scenarios (SRES), which were developed by the IPCC, this study used the A1B, A2 and B2 scenarios for this climate change impact study. These scenarios cover a range of future pathways, with respect to global vs. regional development, and environmental vs. economic emphases.

Different studies have been conducted to assess the impact of climate change on hydrology in different parts of the world (Gleick and Chalecki, 1999; Neff et al., 2000; Groisman et al., 2001; Chang et al., 2003; Novotny and Stefan, 2007, Kim and Kaluarachchi, 2009; Abdo et al., 2009). Many of these studies indicated water resource variability associated with climate change.

In this study, we investigated the possible effects of climate change on water resources in Lake Tana Basin, Ethiopia by analyzing outputs from GCM models. To get an indication of the consistency of the projected changes in the region, we first compared projected changes in precipitation and temperature across 15 models for two seasons. The study then investigated how changes in temperature and precipitation might translate into changes in stream flow and other hydrological components, using outputs from the four selected climate models. The physically based Soil Water Assessment Tool (SWAT) model was used to determine the impact of climate change on the surface and ground water resources availability in the Lake Tana Basin. The SWAT model was calibrated and validated using historical data from four rivers which flow into Lake Tana: Gumera, Gilgel Abay, Megech and Ribb rivers (Setegn et al., 2009a).

## 12.2 Materials and Methods

### 12.2.1 Study Area

Lake Tana is located in the country's north-west highlands (Lat 12°0' North, Lon 37°15' East) (Fig. 12.1). The Lake Tana basin comprises an area of 15,096 km<sup>2</sup>, including the lake area. The mean annual rainfall of the catchment area is about 1,280 mm. The climate of the region is "tropical highland monsoon" with the main rainy season between June and September. The air temperature shows large diurnal but small seasonal changes with an annual average of 20°C. The mean annual relative humidity (1961–2004) at Bahr Dar meteorological station is 0.65. Lake Tana occupies a wide depression in the Ethiopian plateau. The lake is shallow, oligotrophic, and freshwater, with weak seasonal stratification (Wood and Talling, 1988; Wudneh, 1998). The lake is believed to have been formed due to damming by lava flow during the Pliocene (Mohr, 1962), but the formation of the depression itself started in the Miocene (Chorowicz et al., 1998). Lake Tana basin comprises a total area of 15,096 km<sup>2</sup> (drainage plus lake area). It is rich in biodiversity with many endemic plant species and cattle breeds; it contains large areas of wetlands; it is home to many endemic birds and cultural and archaeological sites. This basin is of critical national significance as it has great potential for irrigation, hydroelectric power, high value crops and livestock production, ecotourism and more.

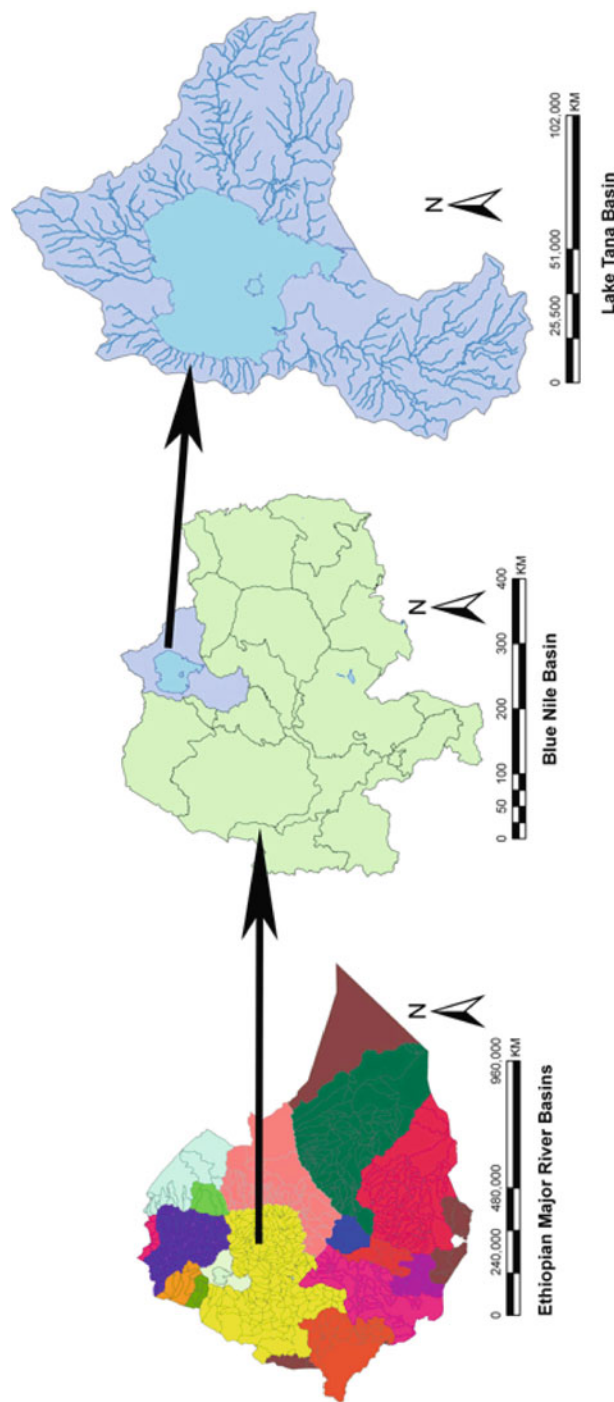


**Fig. 12.1** Location Map of the study area

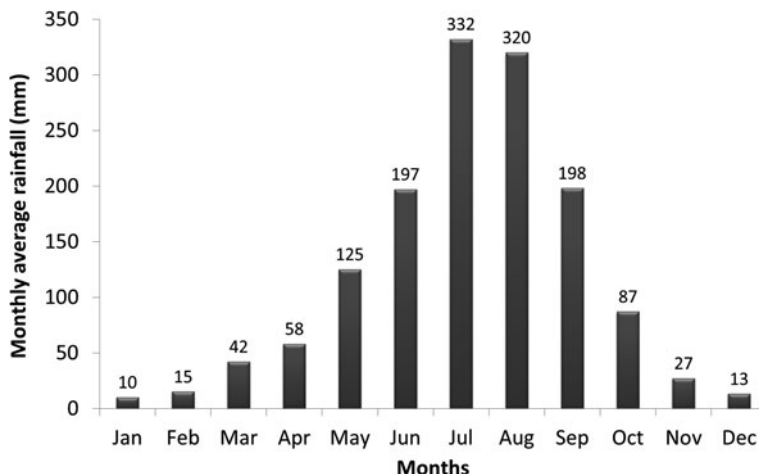


**Fig. 12.2** Upper Blue Nile basin monthly average Rainfall (1960–2002)

The lake is a natural type which covers 3,000–3,600 km<sup>2</sup> area at an elevation of 1,800 m and with a maximum depth of 15 m. It is approximately 84 km long, 66 km wide. It is the largest lake in Ethiopia and the third largest in the Nile Basin. Gilgel Abay, Ribb, Gumera and Megech are the main rivers feeding the lake, and contribute more than 90% of the inflow. The Lake is the main source of the Blue Nile River, which is the only surface outflow for the Lake. The climate of the study area varies from humid to semiarid. Most precipitation occurs in the wet season (locally called *Kiremt*) from June to September. The two other seasons are known as *Bega* (normally dry; from October to February) and *Belg* (normally mild; from March to May). About 70% of annual precipitation is concentrated on *Kiremt*. The annual precipitation has an increasing trend from northeast to southwest. Figure 12.2 shows basin-wide monthly rainfall average. The estimated mean annual precipitation of the study area ranges from 1,200 to 1,600 mm based on data from 1961 to 2000 depending on the studies (Gamachu, 1977; Conway, 1997; Conway, 2000; UNESCO, 2004; Kim et al., 2008; Setegn et al., 2009a). Due to the summer monsoon occurring between June and September, more than 80% of the annual flow occurs from July to October and flows to the downstream countries due to the absence of storage capacity. The observational record from 1980 to 2000 shows a seasonal variation of less than 2°C. The annual mean actual evapotranspiration and water yield of the catchment area are estimated to be 773 and 392 mm, respectively (Setegn et al., 2009a).

### 12.2.2 General Circulation Models (GCMs)

GCM's are numerical coupled models that represent various earth systems including the atmosphere, oceans, land surface and sea-ice and offer considerable potential for the study of climate change and variability. They numerically simulate changes in climate as a result of slow changes in some boundary conditions (such as the

solar constant) or physical parameters (such as the greenhouse gas concentration) (Abbaspour et al., 2009).

GCM output data were obtained from the World Climate Research Programme's (WCRP's) Coupled Model Inter-comparison Project phase 3 (CMIP3) multi-model dataset. The details of the models used in this study are listed in Table 12.1. Monthly precipitation and average surface air temperatures were used to quantify the range of the projected climate changes for the region. A single run was downloaded for each scenario, and data extracted for the pixel containing the observation stations.

Daily data were extracted from the outputs of four models (cccma\_cgcm3\_1, gfdl\_cm2\_1, mpi\_echam5, and ncar\_ccsm3\_0). These data were used for the hydrological modeling and assessing the impact of climate change on stream flows, soil moisture, ground water and other hydrological parameters in the Lake Tana basin.

**Table 12.1** The details of the different GCM are used in this study and their spatial resolutions (IPCC, 2007)

Center	Model	Atmospheric resolution (approx)
Bjerknes Centre for Climate Research Norway (BCCR)	Bergen Climate Model (BCM2.0)	$2.8^\circ \times 2.8^\circ$
Canadian Center for Climate Modelling and Analysis Canada (CCCMA)	Coupled Global Climate Model (CGCM3)	$3.75^\circ \times 3.7^\circ$
Centre National de Recherches Meteorologiques France (CNRM)	CNRM-CM3	$2.8^\circ \times 2.8^\circ$
Australia's Commonwealth Scientific and Industrial Research Organisation Australia (CSIRO)	CSIRO Mark 3.0	$1.9^\circ \times 1.9^\circ$
Australia's Commonwealth Scientific and Industrial Research Organisation Australia (CSIRO)	CSIRO Mark 3.5	$1.9^\circ \times 1.9^\circ$
Max-Planck-Institut for Meteorology Germany (MPI-M)	ECHAM5/MPI-OM	$1.9^\circ \times 1.9^\circ$
Meteorological Institute of the University of Bonn (Germany) (MIUB)	ECHO-G	$3.75^\circ \times 3.7^\circ$
Geophysical Fluid Dynamics Laboratory USA (GFDL)	CM2.0 – AOGCM	$2.5^\circ \times 2.0^\circ$
Geophysical Fluid Dynamics Laboratory USA (GFDL)	CM2.1 – AOGCM	$2.5^\circ \times 2.0^\circ$
Institute for Numerical Mathematics Russia (INM)	INMCM3.0	$5.0^\circ \times 4.0^\circ$
Institut Pierre Simon Laplace France (IPSL)	IPSL-CM4	$3.75^\circ \times 2.5^\circ$
Meteorological Research Institute Japan (MRI)	MRI-CGCM2.3.2	$2.8^\circ \times 2.8^\circ$
National Centre for Atmospheric Research USA (NCAR)	Parallel Climate Model (PCM)	$2.8^\circ \times 2.8^\circ$
National Centre for Atmospheric Research USA (NCAR)	Community Climate System Model, version 3.0 (CCSM3)	$1.4^\circ \times 1.4^\circ$
Hadley Centre for Climate Prediction and Research, Met Office, United Kingdom – UK Met. Office UK (UKMO)	HadCM3	$3.75^\circ \times 2.5^\circ$

Monthly outputs of fifteen GCMs were used for the analysis of changes in major climate variables (precipitation, minimum and maximum temperature) in the Lake Tana basin. The models are the Bergen Climate Model (BCM2.0), Coupled Global Climate Model (CGCM3), CNRM-CM3, CSIRO Mark 3.0, ECHAM5/MPI-OM, ECHO-G, CM2.0 – AOGCM, CM2.1 – AOGCM, INMCM3.0, IPSL-CM4, MRI-CGCM2.3.2, Parallel Climate Model (PCM), Community Climate System Model, version 3.0 (CCSM3) and HadCM3 Global climate change models.

### ***12.2.3 Climate Change Scenarios***

Scenarios are images of the future, or alternative futures. They are neither predictions nor forecasts. Rather, each scenario is one alternative image of how the future might unfold. A set of scenarios assists in the assessment of future developments in complex systems that are either inherently unpredictable, or that have high scientific uncertainties (IPCC, 2007).

The Special Report on Emissions Scenarios (SRES) (IPCC, 2007) are grouped into four scenario families (A1, A2, B1 and B2) that explore alternative development pathways, covering a wide range of demographic, economic and technological driving forces and resulting GHG emissions. The A1 storyline assumes a world of very rapid economic growth, a global population that peaks in mid-century and rapid introduction of new and more efficient technologies. Scenario A1 is divided into three groups that describe alternative directions of technological change: fossil intensive (A1FI), non-fossil energy resources (A1T) and a balance across all sources (A1B). The SRES A1B Emissions Scenarios (a scenario in A1 family) describes “a future world of very rapid economic growth, global population that peaks in mid-century and declines thereafter, and rapid introduction of new and more efficient technologies”. Scenario B1 describes a convergent world, with the same global population as A1, but with more rapid changes in economic structures toward a service and information economy with reductions in materials intensity, and the introduction of clean and resource efficient technologies. B2 describes a world with intermediate population and economic growth, emphasizing local solutions to economic, social, and environmental sustainability. Scenario A2 describes a very heterogeneous world with high population growth, slow economic development and slow technological change. No likelihood has been attached to any of the SRES scenarios (IPCC, 2007). In this study three SRES scenarios (A1B, B1, and A2) were used. These scenarios were constructed to explore future developments in the global environment with special reference to the production of greenhouse and aerosol precursor emissions. Each scenario assumes a distinctly different direction for future developments.

### ***12.2.4 Downscaling Methods***

GCM's are coarse in resolution and are unable to resolve significant sub-grid scale features such as topography, clouds and land use (Grotch and MacCracken, 1991).

For instance, the Canadian Center for Climate Modeling and Analysis Canada (CCCMA), Coupled Global Climate Model (CGCM3) is resolved at a spatial resolution of  $3.75^{\circ}$  longitude by  $3.7^{\circ}$  latitude; the Hadley Centre for Climate Prediction and Research HadCM3 model is resolved at a spatial resolution of  $3.75^{\circ}$  longitude by  $2.5^{\circ}$  latitude, and so on. Table 12.1 above shows the different models and their spatial resolutions. There is a significant gap between the large spatial resolution GCMs and regional and local watershed processes. This scale mismatch causes a considerable problem for the assessment of climate change impact using hydrological models. Hence, significant attention should be given to the development of downscaling methodologies for obtaining high-resolution climate or climate change information from relatively coarse-resolution global climate models (GCMs). This will help for better prediction of climate change consequences at hydrological scale.

Basically, there are two main approaches available for the downscaling of large spatial resolution GCM outputs to a finer spatial resolution, termed dynamical and statistical downscaling. In dynamical downscaling, a higher resolution climate model or regional climate model is forced using a GCM. The statistical approach establishes empirical relationships between GCM-resolution climate variables and local climate.

Statistical downscaling is a tool for downscaling climate information from coarse spatial scales to finer scales. The underlying concept is that local climate is conditioned by large-scale climate and by local physiographical features such as topography, distance to a coast, and vegetation. At a specific location, therefore, links should exist between large-scale and local climatic conditions. Statistical downscaling consists of identifying empirical links between large-scale patterns of climate elements (predictors) and local climate (the predictand), and applying them to output from global or regional models. Successful statistical downscaling is thus dependent on long, reliable series of predictors and predictands. Different studies have shown that the two downscaling methods are usually similar for present day climate, while differences in future climate projections are found more frequently. These differences can be explained by the unwise choice of predictors in the statistical downscaling, for example, predictors that carry the climate signal. It has also been suggested that results from statistical downscaling may be misleading because the projected climate change exceeds the range of data used to develop the model. However, differences between results from statistical downscaling and regional modeling may also result from the ability of statistical downscaling to reproduce local features that are not resolved in the regional models (Draggan, 2010). Major disadvantages of statistical downscaling versus using regional climate model includes: the assumption that observed links between large-scale predictors and local predictands will persist in a changed climate, and difficulties in reproducing observed autocorrelations within climate time-series at daily time-scales. Statistical downscaling does not necessarily produce a physically sound relationship between different climate elements. Similarly some advantages of statistical downscaling versus regional modeling includes: statistical downscaling is less technically

demanding than regional modeling; it is thus possible to downscale from several GCMs and several different emissions scenarios relatively quickly and inexpensive; it is possible to tailor scenarios for specific localities, scales, and problems. The spatial resolution applied in regional climate modeling is still too coarse for many impact studies, and some variables are either not available or not realistically reproduced by regional models.

This study generated daily climate projections by modifying the historical datasets to represent changes in the GCM climatologies. This is different from the approach more usually thought of as “statistical downscaling” (e.g. Benestad et al., 2008) where scenarios are created as a function of the daily outputs from GCMs themselves. The historical-modification approach was used because hydrological models often perform poorly when applied to datasets with distributions of daily climate data that are different from their training data, and statistical downscaling techniques often result in distributions that are noticeably different from observed time-series (e.g. with compressed variance).

This study followed the historical-modification procedure of Harrold and Jones (2003) which produces climate time-series and that have similar statistical properties to the observed datasets. In summary, this method involved calculating the difference between the daily cumulative-frequency-distributions (CFDs) of a GCM output variable for a present-day period and a future period, and then applying these differences to an observed dataset. This simple “downscaling” technique is a good compromise between the requirement to produce realistic time-series, and the desire to represent the effects of climate change across different weather situations, as these are simulated in the GCMs. In addition, the method is easy to implement and fast to run. It is a good solution for producing climate change scenarios for impact assessments.

Our implementation of the Harrold and Jones method was as follows. Cumulative-frequency-distributions for daily precipitation, maximum and minimum temperatures were first calculated for the GCM outputs. The CFDs were calculated independently for each month-of-year, using data from that month-of-year and the preceding and subsequent months. The differences between the present-day period CFD and the scenario-period CFDs were then determined for the cumulative frequencies 0.05, 0.15, 0.25...1.0. Absolute differences were calculated for minimum and maximum temperature CFDs, while for precipitation the changes were derived as ratios with-respect-to the present-period values. Because fractional changes in the low-rainfall end of the CFDs may be large, all GCM rainfall values  $<0.1$  mm/day were considered to be zero, and zero values were omitted from the CDF calculations. The extremes of the CFDs (e.g. 0.001, 0.999) were deliberately not sampled. The time windows used are not long enough to define the tails of the CFDs, or changes in them. The changes in the CFDs sampled at cumulative frequencies 0.05–0.95 were then linearly interpolated and extrapolated to cover the entire cumulative frequency range (0–1). Finally, the historical data were ranked and modified to reflect the changes in the GCM CFDs for each scenario and time-period. The result is “downscaled”, daily climate time-series.

### 12.2.5 SWAT Model Description

SWAT (Soil Water Assessment Tool) is continuous time, spatially distributed model designed to simulate water, sediment, nutrient and pesticide transport at a catchments scale on a daily time step. It is one of the watershed models that play a major role in analyzing the impact of land management practices on water, sediment, and agricultural chemical yields in large complex watersheds. It is a public domain model developed by Arnold et al. (1998). SWAT uses hydrologic response units (HRUs) to describe spatial heterogeneity in terms of land cover, soil type and slope within a watershed. The SWAT system is embedded within a geographic information system (GIS) that can integrate various spatial environmental data including soil, land cover, climate and topographic features. Currently, SWAT is embedded in an ArcGIS interface called ArcSWAT. The Simulation of the hydrology of a watershed is done in two separate divisions. One case is the land phase of the hydrological cycle that controls the amount of water, sediment, nutrient and pesticide loadings to the main channel in each subbasin. The second division is routing phase of the hydrologic cycle that can be defined as the movement of water, sediments, nutrients and organic chemicals through the channel network of the watershed to the outlet. In the land phase of hydrological cycle, SWAT simulates the hydrological cycle based on the water balance equation.

$$SW_t = SW_0 + \sum_{i=1}^t (R_{day} - Q_{surf} - E_a - w_{seep} - Q_{gw}) \quad (12.1)$$

In which  $SW_t$  is the final soil water content (mm),  $SW_0$  is the initial soil water content on day  $i$  (mm),  $t$  is the time (days),  $R_{day}$  is the amount of precipitation on day  $i$  (mm),  $Q_{surf}$  is the amount of surface runoff on day  $i$  (mm),  $E_a$  is the amount of evapotranspiration on day  $i$  (mm),  $W_{seep}$  is the amount of water entering the vadose zone from the soil profile on day  $i$  (mm), and  $Q_{gw}$  is the amount of return flow on day  $i$  (mm).

To estimate surface runoff two methods are available. These are the SCS curve number procedure USDA Soil Conservation Service (USDA, 1972) and the Green & Ampt infiltration method (Green and Ampt, 1911) In this study, the SCS curve number method was used to estimate surface runoff. Hargreaves method was used for estimation of potential evapotranspiration (PET) (Hargreaves, 1985). The SCS curve number is described by equation 12.2.

$$Q_{surf} = \frac{(R_{day} - 0.2S)^2}{(R_{day} + 0.8S)} \quad (12.2)$$

In which,  $Q_{surf}$  is the accumulated runoff or rainfall excess (mm),  $R_{day}$  is the rainfall depth for the day (mm),  $S$  is the retention parameter (mm). The retention parameter is defined by equation 12.3.

$$S = 25.4 \left( \frac{100}{CN} - 10 \right) \quad (12.3)$$

The SCS curve number is a function of the soil's permeability, land use and antecedent soil water conditions. SCS defines three antecedent moisture conditions: 1 – dry (wilting point), 2 – average moisture, and 3 – wet (field capacity). The moisture condition 1 curve number is the lowest value that the daily curve number can assume in dry conditions. The curve numbers for moisture conditions 2 and 3 are calculated from equations 12.4 and 12.5.

$$CN_1 = CN_2 - \frac{20 \cdot (100 - CN_2)}{(100 - CN_2 + \exp[2.533 - 0.0636 \cdot (100 - CN_2)])} \quad (12.4)$$

$$CN_3 = CN_2 \cdot \exp[0.00673 \cdot (100 - CN_2)] \quad (12.5)$$

In which  $CN_1$  is the moisture condition 1 curve number,  $CN_2$  is the moisture condition 2 curve numbers, and  $CN_3$  is the moisture condition 3 curve numbers.

Typical curve numbers for moisture condition 2 are listed in various tables (Neitsch et al., 2005) which are appropriate to slope less than 5%. But in the Lake Tana basin there are areas with slopes greater than 5%. To adjust the curve number for higher slopes an equation developed by (Williams, 1995) was used (equation 12.6)

$$CN_{2S} = \frac{(CN_3 - CN_2)}{3} \cdot [1 - 2 \cdot \exp(-13.86 \cdot slp)] + CN_2 \quad (12.6)$$

In which  $CN_{2S}$  is the moisture condition 2 curve number adjusted for slope,  $CN_3$  is the moisture condition 3 curve number for the default 5% slope,  $CN_2$  is the moisture condition 2 curve number for the default 5% slope, and  $slp$  is the average percent slope of the sub-basin.

The different components of the SWAT model application to the Lake Tana basin are described by Setegn et al. (2009a, 2009b, 2010). More detailed descriptions of the different model components are listed in Neitsch et al. (2005). A comprehensive review of SWAT model applications is given by Gassman et al. (2007).

### 12.2.6 Hydrological Model Input and Setup

The spatially distributed data needed for the ArcSWAT interface include the Digital Elevation Model (DEM), soil data, land use and stream network layers. Data on weather and river discharge were also used for prediction of streamflow and calibration purposes. For the setup of the SWAT model, we have used a 90 m resolution DEM for the delineation of the watershed and to analyze the drainage patterns of the land surface terrain. Sub-basin parameters such as slope gradient, slope length of the terrain, and the stream network characteristics such as channel slope, length,

and width were derived from the DEM. The soil and land use data were used for the definition of the hydrological response units (HRUs). SWAT model requires different soil textural and physico-chemical properties such as soil texture, available water content, hydraulic conductivity, bulk density and organic carbon content for different layers of each soil type. These data were obtained mainly from the following sources: Soil and Terrain Database for northeastern Africa CD-ROM (Food and Agriculture Organization of the United Nations (FAO), 1998), Major Soils of the world CD-ROM (FAO, 2002), Digital Soil Map of the World and Derived Soil Properties CD-ROM (FAO, 1995), Properties and Management of Soils of the Tropics CD-ROM (Van Wambeke, 2003), Abbay River basin Integrated Development Master Plan Project – Semi detailed Soil Survey and the Soils of Anjeni Area, Ethiopia (SCRP report). Figure 12.3 (left) shows the major soil types in the basin.

The land use map of the study area was obtained from the Ministry of Water Resources, Ethiopia. We have reclassified the land use map of the area based on the available topographic map (1:50,000), aerial photographs and satellite images. The reclassification of the land use map was done to represent the land use according to specific land cover types such as type of crop, pasture and forest. Figure 12.3 (right) shows that more than 50% of the Lake Tana watershed is used for agriculture.

SWAT requires daily meteorological data that can either be read from a measured data set or be generated by a weather generator model. The weather variables used in this study for driving the hydrological balance are daily precipitation, minimum and maximum air temperature for the period 1978–2004. These data were obtained from Ethiopian National Meteorological Agency (NMA) for stations located within and around the watershed.

The daily river discharge data were used for model calibration and validation. The river discharges were characterized with high flow periods during June–September and low flow periods during the rest of the year. The highest discharges were for the Gilgel Abay and Gumera Rivers. Daily river discharge values for the Ribb, Gumera, Gilgel Abay, and Megech Rivers and the outflow Blue Nile (Abbay) River were obtained from the Hydrology Department of the Ministry of Water Resources of Ethiopia. The daily river discharges at four tributaries of Lake Tana (Gumera, Gilgel Abay, Megech and Ribb Rivers) from gauging stations were used for model calibration and validation. The peak flows for all inflow rivers occur in August. But the outflow river gets its peak flow at the month of September. There is a 1 month delay of peak flow for outflow from the Blue Nile River. This is due to the influence of the lake, which retards the flow before it reaches the outlet. The record of the outflow river (Abbay) at Bahir Dar gauge station was not used for model calibration and validation. This is because we have seen a significant difference between the default simulated and measured stream flow data at this gauge station. There is abstraction of water from the lake for irrigation and other purposes. But there is no available information on the amount of water losses from the lake.

The details of the input data used for the setup of the SWAT model are documented in Setegn et al. (2009a).

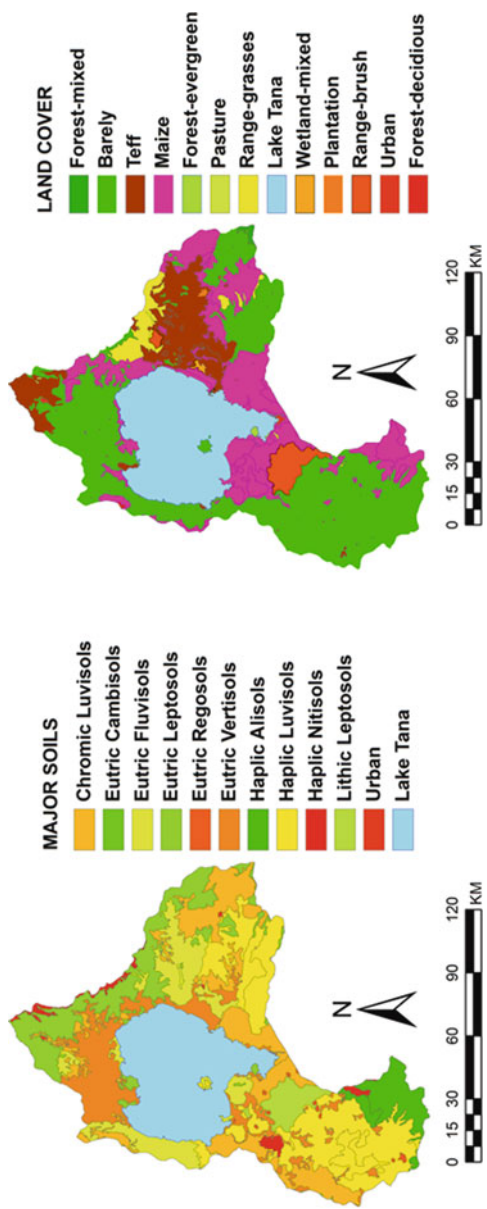


Fig. 12.3 Soil and land use/land cover map of Lake Tana basin

### 12.2.7 Model Setup, Calibration and Evaluation of SWAT Model

The model setup involved five steps: (1) data preparation, (2) sub-basin discretization, (3) HRU definition, (4) parameter sensitivity analysis, (5) calibration and uncertainty analysis. The steps for the delineation of the watershed include DEM setup, stream definition, outlet and inlet definition, watershed outlets selection and definition and calculation of sub-basin parameters. Artificial stations were located during the setup of the SWAT model. This was aimed at quantifying the water fluxes into the lake, which could be used analyzing the water balance of the lake.

Twenty-six hydrological parameters were tested for sensitivity for the simulation of the stream flow in the study area. The data for period 1981–1992 were used for calibration and from 1993 to 2004 were used for validation of the model in the four tributaries of Lake Tana basin. Periods 1978–1980 and 1990–1992 were used as “warm-up” periods for calibration and validation purposes, respectively. The warm-up period allows the model to get the hydrologic cycle fully operational.

The calibration and uncertainty analysis were done using three different algorithms, i.e., Sequential Uncertainty Fitting (SUFI-2) (Abbaspour et al., 2004, 2007), Parameter Solution (ParaSol) (Van Griensven and Mixer, 2006) and Generalized Likelihood Uncertainty Estimation (GLUE) (Beven and Binley, 1992). The details of the methods and application can be found in Setegn et al. (2009a).

## 12.3 Results and Discussion

### 12.3.1 Future Climate Change Projection

In our analysis, we divided the data into a wet-season (June to September) and a dry-season (October to May) so that the results are easier to interpret from the perspective of possible impacts. Projected changes in seasonal mean temperature at the location of Adet station for a range of GCMs are shown in Fig. 12.4. Changes in mean seasonal accumulated precipitation are shown in Fig. 12.5. As represented by the GCMs, the Adet station can be taken to be representative of all stations in the study region, because the study area is relatively small compared to GCM resolution. Temperature changes are given in °C, and precipitation changes as a percentage change on the base-period mean (e.g. a change of 100% would imply a doubling of precipitation). This way of expressing changes has become a de facto convention. The error bars are derived from the 1-standard-deviation error-in-the-mean of seasonal average temperatures or seasonal cumulative precipitation. The error bars can be taken to represent the inter-annual variability in the models. In Fig. 12.4, the bars show plus/minus the quadrature-sum of the errors in the base-period and scenario means. The error-bars in Fig. 12.5 are derived similarly, but have been converted to percentage changes in the base-period mean. The results from Figs. 12.4 and 12.5 are summarized in Tables 12.2 and 12.3. Figure 12.4 shows that the projected temperature at Adet station for the periods 2046–2065 and

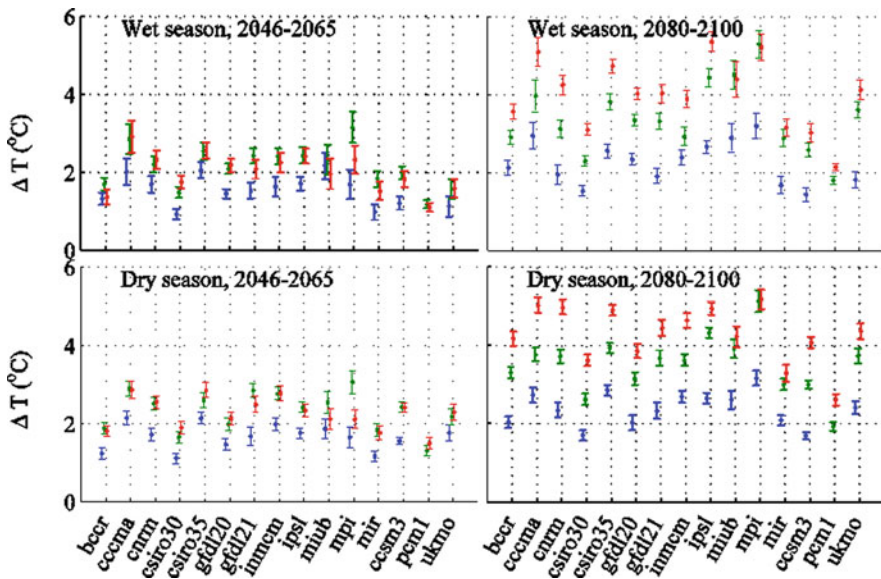


**Fig. 12.4** Projected changes in mean temperature at the location of Adet station for a range of GCMs from the CMIP3 dataset. *Top row* are changes in wet-season temperature, *bottom row* are changes in dry seasons temperature. *Left column* are changes to 2046–2065, *right column* are changes to 2080–2100. Colors denote the SRES scenario used: blue are B1, green are A1b, red are A2. *Error bars* are 1 standard-deviation

2080–2100 for the wet and dry seasons. Figure 12.4 shows that the GCM runs project a wide range of temperature changes for the region. Even so, all the projected changes are for regional warming, and the changes are nearly all statistically-significant. In addition, the ranking of the changes for the three scenarios is consistent with what we expect. That is, for 2080–2100, the smallest changes are for the lowest-emission SRES B1 scenario, and the largest changes are for the highest-emission SRES A2 scenario.

In contrast, Fig. 12.5 suggests that the GCM's do not give us a confident picture of rainfall change in the region. Firstly, approximately half of the models suggest increases in rainfall, and half suggest decreases, so there is no consensus between GCMs. Further, in most cases the projected rainfall changes are less than 3 standard deviations; even though some of the changes are large in absolute terms (greater than 50%), we note that the larger changes are projected in the GCMs with the largest inter-annual variations. Further, for many GCMs, the changes in Fig. 12.5 are not ranked according to the emission scenarios. In fact, for several of the models the changes are similar for all three scenarios; that is, they appear to be independent of the emission scenario. This suggests that for these models the differences between the 1980–2000 base period and the future periods is partly attributable to natural variation with the base-period, because common base-period data were used for all three SRES scenarios.

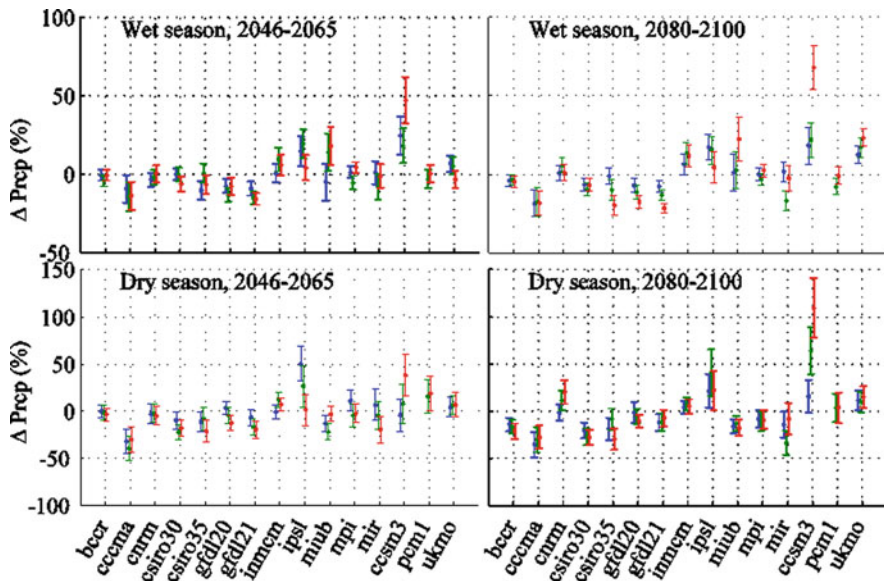


**Fig. 12.5** Projected changes in mean precipitation at the location of Adet station. *Top row* are changes in wet-season precipitation, *bottom row* are changes in dry seasons precipitation. *Left column* are changes to 2046–2065, *right column* are changes to 2080–2100. Colors denote the SRES scenario used: blue are B1, green are A1b, red are A2. Changes are expressed as percentages of the base-period (1980–2000) precipitation. Error bars are 1 standard-deviation

**Table 12.2** The ranges of projected changes (given as 25th–75th percentiles) for the study region for the 2080–2100 period from the 15 GCMs

Scenarios	Rainfall changes		Temperature changes	
	Wet season	Dry season	Wet season	Dry season
SRES B1	-7%–2%	-16%–11%	1.7°C–2.7°C	2.0°C–2.7°C
SRES A1b	-12%–13%	-16%–10%	2.9°C–4.0°C	3.0°C–3.9°C
SRES A2	-18%–12%	-21%–15%	3.3°C–4.7°C	3.9°C–4.9°C

**Table 12.3** The ranges of projected changes (given as 25th–75th percentiles) for the study region for the 2046–2065 period from the 15 GCMs

Scenarios	Rainfall changes		Temperature changes	
	Wet season	Dry season	Wet season	Dry season
SRESB1	-8%–1%	-10%–11%	1.1°C–1.7°C	1.4°C–1.9°C
SRES A1b	-8%–9%	-17%–11%	1.7°C–2.4°C	1.9°C–2.6°C
SRES A2	-7%–4%	-20%–7%	1.6°C–2.3°C	1.9°C–2.6°C

Thus, we conclude from Fig. 12.5 that the GCMs do not project significant changes in rainfall in the region. This is not to say they do not project any changes at all. In our analysis, we compared 20-year seasonal totals, and it is quite possible that a more sophisticated statistical method that could use longer time-periods (for example regressing rainfall against global warming) would yield statistically-significant results. However, from the point-of-view of water users, our finding that the GCMs do not show consistent and statistically significant differences between the rainfall totals for the 1980–2000 period and the 2080–2100 period could be translated as “no consensus on changes in precipitation”.

### 12.3.2 Hydrological Model Setup and Evaluation

The parameter sensitivity analysis was done using the ArcSWAT interface for the whole catchment area. Sensitivity analyses for twenty-six hydrological parameters were conducted within the study area. The most sensitive parameters considered for calibration were soil evaporation compensation factor, initial SCS Curve Number II value, base flow alpha factor, threshold depth of water in the shallow aquifer for “revap” to occur, available water capacity, groundwater “revap” coefficient, channel effective hydraulic conductivity, and threshold depth of water in the shallow aquifer for return flow to occur. The details of the sensitive flow parameters and their fitted values are documented in Setegn et al. (2009a). SUFI-2, GLUE and ParaSol methods were used for calibration of the SWAT model in Gilgel Abay, Gumera, Ribb and Megech inflow rivers. The comparison between the observed and simulated stream flows indicated that there is a good agreement between the observed and simulated discharge which was verified by high values of coefficient of determination ( $R^2$ ) and Nash Sutcliffe efficiency (NSE). Model predictive performances for calibration and validation periods of all inflow rivers discharge for all calibration and uncertainty analysis methods are summarized in Setegn et al. (2009a). Figure 12.6 shows the time-series comparison between measured

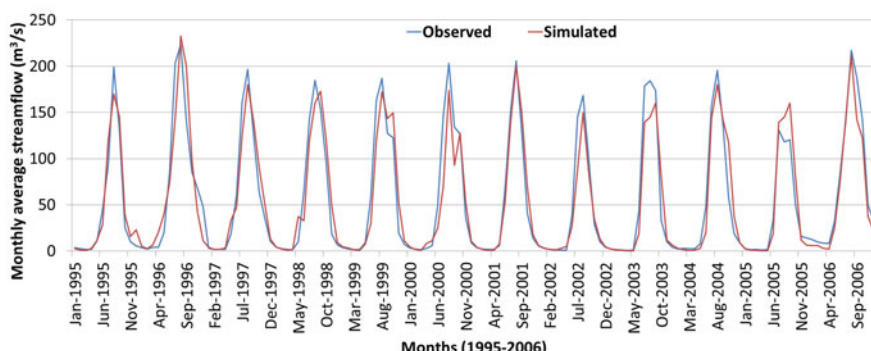


**Fig. 12.6** Time series of measured and simulated monthly flow at Gilgel Abay River station for the validation period (1995–2006)

and simulated monthly flow at Gilgel Abay River gauge station during validation periods. The details of the calibration and validation results can be found in Setegn et al. (2009a). Setegn et al. (2009a) indicated that the water balance of the upland watershed is well represented. The results indicated that 65% of the annual precipitation is lost by evapotranspiration in the basin during the calibration period as compared to 56% during validation period. Surface runoff contributes 31% and 25% of the water yield during calibration and validation periods, respectively. Ground water contributes 45% and 54% of the water yield during calibration and validation periods, respectively.

### 12.3.3 Impact of Climate Change on Stream Flow

River discharge is an important hydrological component that is greatly influenced by climate (rainfall and temperature) and land use. Figure 12.7 shows the projected effect of climate change on annual stream flow, as output from the SWAT model. Using downscaled data from the CCCMA, MPI and GFDL models, the streamflow showed a reduction under all SRES scenarios for both time periods (2046–2065 and 2080–2100). But with the NCAR models there was an increase in streamflow for A2 and B1 scenarios during the two time periods.

The results from the hydrological modeling for the wet-season (June–September) streamflow in the Gilgel Abay River are shown in Fig. 12.8. Wet season streamflow is significantly reduced in the downscaled *ccma\_cgcm3\_1* model for all scenarios for both time periods. For the downscaled *gfdl\_cm2\_1* model there are reductions of around 20% for the 2046–2065 period, and around 50% for the 2080–2100 period, with little variation between scenarios. Results from the downscaled *mpi\_echams5* model show little change. The downscaled *ncar\_ccsm3\_0* model results show little

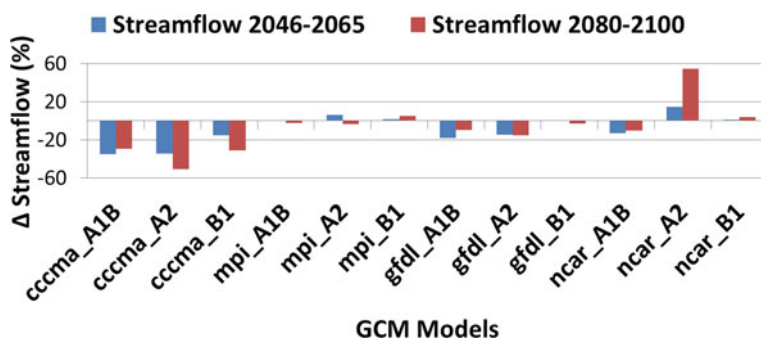


**Fig. 12.7** Change in annual streamflow due to changes in precipitation and temperature for CCCMA, GFDL, MPI and NCAR models under A1B, A2 and B1 scenarios for the periods 2045–2065 and 2080–2100 expressed as a percentage of streamflow in the base period 1980–2000

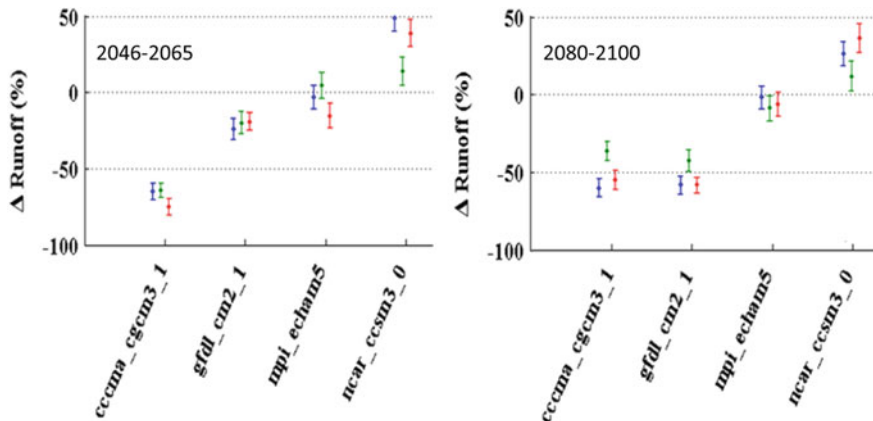


**Fig. 12.8** Projected changes in wet-season runoff in the GilgelAbay River compared to the base-period 1980–2000, calculated with the SWAT model. **Left (a)** changes to 2046–2065, **right (b)** changes to 2080–2100. Colors denote the SRES scenario used: blue are B1, green are A1B, red are A2. Changes are expressed as percentages of the base-period (1980–2000) wet-season runoff

change, except for a streamflow increase of around 60% for the SRES A2 scenario during 2080–2100. However, of the models show similar trends across different scenarios in the 2046–2065 and 2080–2100 periods.

Although the number of GCM outputs examined in the hydrological modeling study is smaller than in the seasonal rainfall and temperature studies shown in Figs. 12.4 and 12.5 (due to both data and time constraints), we can still extract some important points. Firstly, the directions of the streamflow changes follow the changes in rainfall (i.e. decreases for the cccma\_cgcm3\_1 and gfdl\_cm2\_1 models, increases for the ncar\_ccsm3\_0 model for SRES A2 scenario, and no changes for the mpi\_echam5 model). This is expected given the fact that local evapotranspiration does not dominate the water-cycle in the wet-season. But we also see that the streamflow changes are both larger in magnitude and more significant than the rainfall changes. We interpret these aspects of the modeling results to imply that runoff changes in the region could be significant, even though the GCMs do not agree on the direction of the change. The exceptions are the results from the ncar\_ccsm3\_0 model for the SRES A1B and B1 scenarios, where increases in wet-season precipitation are accompanied by streamflow declines. This is presumably not caused by unreasonable increases in modeled evaporation, because the projected temperature changes in ncar\_ccsm3\_0 are lower than average (see Figure 12.4). We note, however, that the ncar\_ccma3\_0-based simulations were downscaled using changes in the GCM daily mean temperature output (for the other models, changes in GCM daily maximum and minimum temperature were used), which may account for these anomalous results. Alternatively, the changes in precipitation and/or temperature as a function of CFD might be substantially different for the ncar\_ccma3\_0 outputs.

### 12.3.4 Impact of Climate Change on Agricultural Water Resources

In this section, we discuss changes in actual evapotranspiration (AET), soil moisture (SW) and ground water (GW) that are of the most important components of the hydrological cycle. Our intention is to understand how the changes in climate variables can affect the different hydrological components of the basin that control the final streamflow.

The possible impact of climate change on the annual changes in actual ET, soil moisture and ground water for the period of 2046–2065 and 2080–2100 periods are shown in Fig. 12.9. The results indicated that AET increases considerably in many models, but especially for GFDL model. This is attributed to the increase in air temperature. It was observed that soil moisture showed little change (between 0 and 2% decrease) for many of the models. Ground water flow is reduced for the downscaled GFDL and MPI models, but the downscaled NCAR model has shown an increase in the groundwater flow.

The increase in ET is probably due to increased air temperatures. The study used the Hargreaves algorithm (Hargreaves et al. 1985) to calculate evapotranspiration from minimum and maximum temperatures. This is consistent with previous

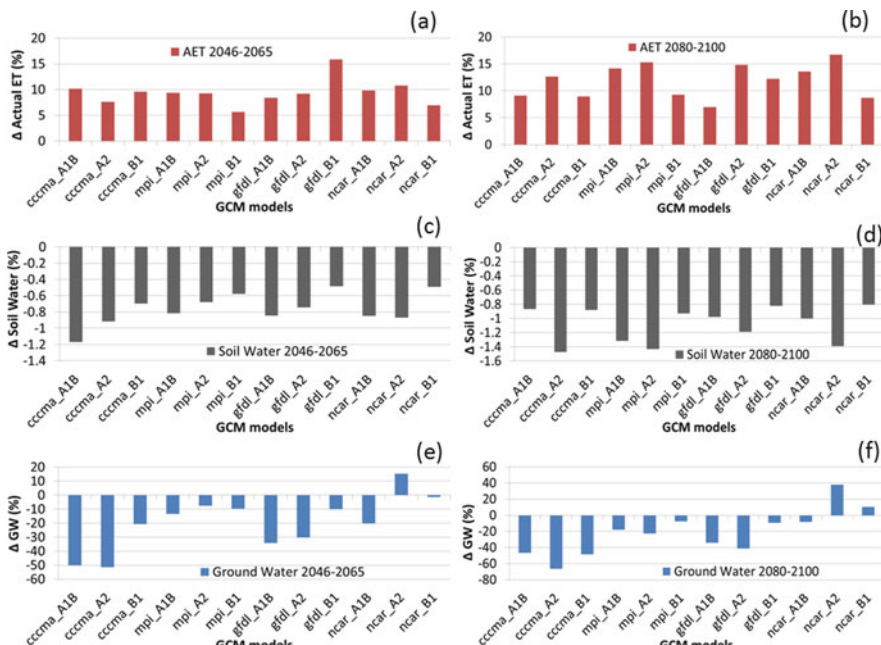


**Fig. 12.9** Annual changes in actual evapotranspiration (AET), soil moisture and ground water due to changes in climate for the 2046–2065 and 2080–2100 periods: (a) changes in AET for 2046–2065 period, (b) changes in AET for 2080–2100 period, (c) changes in soil water content for 2046–2065 period, (d) changes in soil water content for 2080–2100 period, (e) changes in groundwater for 2046–2065 period, (f) changes in groundwater for 2080–2100 period

studies, which have shown that a significant variation in AET is expected to follow changes in air temperature (Abbaspour et al., 2009). The changes in modeled ground water flow clearly influenced the changes in streamflow. This is consistent with the Setegn et al. (2009a), who indicated that 60% of the stream flows from the inflow rivers of Lake Tana are baseflow, and that future reduction in ground water might contribute to reduced streamflow in the basin. Moreover, previous studies have indicated that more than 60% of the hydrological loss in the present system is through evapotranspiration. This suggests that increased evapotranspiration in the future may be a significant factor leading in the direction of decreased streamflow, which may or may not be compensated for by changes in rainfall.

In this study, we have used the same land cover data as the present time. Such a study should not be considered as a realistic actual scenario, because the latter would require including the impact of future land use change. We are conducting further investigations regarding the combined effect of climate and land use change. We note also that in the present study there is no consideration of changes in soil parameters, which could influence the soil properties of the watershed. This may explain the low response of soil moisture to the changes to climate in this study.

Considering the combined effects of land use change and climate change will also raise the question of the effect of climate change on land use changes, and vice versa. Unless we quantify the proportion of the land use changes due to human and those caused by the changing climate (rainfall and air temperature) variability, understanding the combined feedback to the water resources variability will be misleading.

There is much uncertainty in our modeling results. This is a combination of uncertainties in the GCM outputs, as a result of the downscaling, hydrological parameter uncertainty and neglect of land-use changes or potential changes in soil properties. Any or all of these factors may cause the results to deviate from reality. But even so, we are dedicated to perusing a thorough investigation of the combined effect of climate and land use/land cover on the hydrological processes and water recourses in the study area, and we believe this study is an important first-step in this direction.

### ***12.3.5 Implications of Climate Change Impact***

Ethiopia is known to be one of the countries most affected by drought. Given a large part of the country is arid or semi-arid and highly prone to drought and desertification, a further decrease in precipitation could increase the frequency and intensity of droughts in the country. Also, Ethiopia has a fragile highland ecosystem that is currently under stress due to increasing population pressure.

Our analysis suggests that the northern highlands of the country could experience reduced rainfalls, and hence become susceptible to even more severe drought conditions.

A dramatic reduction in precipitation or increase of actual evapotranspiration would cause soil moisture stress. The resulting negative agricultural water balance would reduction both rain-fed and irrigated agriculture productivity. A reduction in rainfall coupled with land degradation and other factors would also significantly reduce effective rainfall; that is, rainfall which could be available for crop consumption. The combined effect has the potential to cause a great agricultural drought, unless there is ample water available for irrigation. However, a reduction in rainfall may cause reduce ground water recharge, which would significantly reduce its contribution to stream flow. Lake Tana is highly sensitive to variations in rainfall, as well as in river inflows and evaporation. Setegn et al. (2009a) showed that inflow river discharge to Lake Tana contributes over 90% of the lake inflow. It is thus very likely that changes in river inflow would also change the volume of the lake and the water balance, which could ultimately adversely impact the lake ecosystem.

## 12.4 Conclusion

The possibility of a reduction in water resources is a major threat in the northern highlands of Ethiopia, due to alterations in hydrologic cycles and changes in water availability. In this study, we investigated the sensitivity of water resources to changing climate in the Lake Tana Basin, Ethiopia. We compared projected changes in precipitation and temperature across 15 GCM models for two future periods to get an indication of the consistency of the projected changes in the region. We found that the models projected temperature increases of around 2–5°C for 2080–2100, depending on the model and emission scenario. However, the models projected a wide range of rainfall changes, both increases and decreases, but the low statistical-significance of the changes combined with apparent systematic effects does not allow us to draw any definite conclusions about rainfall changes in the region. Moreover, the study investigated how changes in temperature and precipitation might translate into changes in stream flows and other hydrological components using downscaled outputs from four climate models. Although the GCM sample examined for this component of the study is small, we note important aspects of the results. Firstly, the direction of streamflow changes followed the direction of changes in rainfall. This is expected, given that local evapotranspiration does not dominate the water-cycle in the wet-season. But we also saw that the changes were both larger-magnitude and more significant than the rainfall changes. The responses of evapotranspiration, soil moisture and ground water were also examined, and it was found that changes in ground water flow may be a significant component of the changes in streamflow.

We interpret the different aspects of the hydrological response and it indicates that changes in runoff and other hydrological variables in the region could be significant, even though the GCMs do not agree on the direction of the rainfall change. This implies that climate change may well impact the surface and ground water resources of the Lake Tana Basin, and the lake may experience a change in water balance due to a change in river inflow in the forthcoming decades.

**Acknowledgments** We acknowledge the modeling groups, the Program for Climate Model Diagnosis and Intercomparison (PCMDI) and the WCRP's Working Group on Coupled Modelling (WGCM) for their roles in making available the WCRP CMIP3 multi-model dataset. We also would like to thank the Ministry of Water Resources of Ethiopia and the Ethiopian Meteorological Agency for the data provided and used in this study.

## References

Abbaspour KC, Johnson CA, van Genuchten MTh (2004) Estimating uncertain flow and transport parameters using a sequential uncertainty fitting procedure. *Vadose Zone J* 3(4):1340–1352

Abbaspour KC, Yang J, Maximov I, Siber R, Bogner K, Mieleitner J, Zobrist J, Srinivasan R (2007) Modelling hydrology and water quality in the pre-alpine/alpine Thur watershed using SWAT. *J Hydrol* 333:413–430

Abbaspour KC, Faramarzi M, Ghasemi SS, Yang H (2009) Assessing the impact of climate change on water resources in Iran. *Water Resour Res* 45:W10434. doi:10.1029/2008WR007615

Abdo KS, Fiseha BM, Rientjes THM, Gieske ASM, Haile AT (2009) Assessment of climate change impacts on the hydrology of Gilgel Abay catchment in Lake Tana basin. *Ethiopia* 23:3661–3669

Arnold JG, Srinivasan R, Muttiah RR, Williams JR (1998) Large area hydrologic modeling and assessment: part I: model development. *J Am Water Resour Assoc* 34(1):73–89

Benestad RE, Chen D, Hanssen-Bauer I (2008) Empirical-statistical downscaling. World Scientific Publishing, Singapore, 300pp

Beyene T, Lettenmaier DP, Kabat P (2010) Hydrologic impacts of climate change on the Nile River Basin: implications of the 2007 IPCC scenarios. *Clim Change* 100:433–461

Beven K, Binley A (1992) The future of distributed models: model calibration and uncertainty prediction. *Hydrol Process* 6:279–298

Brown AE, Zhang L, McMahon TA, Western AW, Vertessy RA (2005) A review of paired catchment studies for determining changes in water yield resulting from alterations in vegetation. *J Hydrol* 310:28–61

Chang H (2003) Basin hydrologic response to changes in climate and land use: the Conestoga River Basin, Pennsylvania. *Phys Geogr* 24:222–247

Chorowicz J, Collet B, Bonavia F, Mohr P, Parrot J-F, Korme T (1998) The Tana basin, Ethiopia. Intra-plateau uplift, rifting and subsidence. *Tectonophysics* 295:351–367

Conway D (1997) A water balance model of the Upper Blue Nile in Ethiopia. *Hydrol Sci J* 42(2):265–286

Conway D (2000) The climate and hydrology of the Upper Blue Nile, Ethiopia. *Geogr J* 166:49–62

FAO (1995) Digital soil map of the world and derived soil properties (CDROM). Food and Agriculture Organization of the United Nations, Rome

FAO (1998) The soil and terrain database for northeastern Africa (CDROM). FAO, Rome, 1998.

FAO (2002) Major Soils of the World. Land and Water Digital Media Series (CD-ROM). Food and Agricultural Organization of the United Nations, Rome

Fohrer N, Haverkamp S, Eckhardt K, Frede HG (2001) Hydrologic response to land use changes on the catchment scale. *Phys Chem Earth B* 26:577–582

Gamachu D (1977) Aspects of climate and water budget in Ethiopia. Addis Ababa University Press, Addis Ababa

Gassman PW, Reyes MR, Green CH, Arnold JG (2007) The soil and water assessment tool: historical development, applications, and future research directions. *Trans ASABE* 50(4): 1211–1250

Gleick PH, Chalecki EL (1999) The impacts of climatic changes for water resources of the Colorado and Sacramento-San Joaquin River basins. *J Am Water Resour Assoc* 35: 1429–1441

Green WH, Ampt GA (1911) Studies on soil physics, 1. The flow of air and water through soils. *J Agric Sci* 4:11–24

Groisman PY, Knight RW, Karl TR (2001) Heavy precipitation and high streamflow in the contiguous United States: trends in the twentieth century. *Bull Am Meteorol Soc* 82: 219–246

Grotch SL, MacCracken MC (1991) The use of general circulation models to predict regional climatic change. *J Clim* 4:286–303

Hargreaves GL, Hargreaves GH, Riley JP (1985) Agricultural benefits for Senegal River basin. *J Irrigat Drain Eng* 111(2), 113–124.

Harrold TI, Jones RN (2003) Generation of rainfall scenarios using daily patterns of change from GCMs. *IAHS-AISH Publ* 280:165–172

Hay LE, Clark MP (2003) Use of statistically and dynamically downscaled atmospheric model output for hydrologic simulations in three mountainous basins in the western United States. *J Hydrol* 282:56–75

Huang MB, Zhang L (2004) Hydrological responses to conservation practices in a catchment of the Loess Plateau, China. *Hydrol Proc* 18:1885–1898

IPCC (Intergovernmental Panel on Climate Change) (1999) In: Penner JE, Lister DH, Griggs DJ, Dokken DJ, McFarland M (Eds.) Prepared in collaboration with the Scientific Assessment Panel to the Montreal Protocol on Substances that Deplete the Ozone Layer. Cambridge University Press, Cambridge, UK. p 373

IPCC (Intergovernmental Panel on Climate Change) (2007) In: Parry ML et al (eds) Climate change 2007: impacts, adaptation, and vulnerability—contribution of working group II to the third assessment report of the Intergovernmental Panel on Climate Change. Cambridge University Press, Cambridge, UK

International Arctic Science Committee (Content Partner); Sidney Draggan (Topic Editor) (2010) Statistical downscaling approach and downscaling of AOGCM climate change projections. In: Cleveland CJ (ed) Encyclopedia of Earth. Environmental Information Coalition, National Council for Science and the Environment, Washington, DC [First published in the Encyclopedia of Earth 8 Sept 2009; Last revised 8 Feb 2010; Retrieved 4 Sept 2010]

Kim U, Kaluarachchi JJ, Smakhtin VU (2008) Generation of monthly precipitation under climate change for the Upper Blue Nile River Basin, Ethiopia. *J Am Water Resour Assoc* 44(5): 1231–1274. doi:10.1111/j.1752-1688.2008.00220.x

Kim U, Kaluarachchi JJ (2009) Climate change impacts on water resources in the Upper Blue Nile River Basin, Ethiopia. *J Am Water Resour Assoc (JAWRA)* 45(6):1361–1378. doi:10.1111/j.1752-1688.2009.00369.x

Laurance WF (1998) A crisis in the making: responses of Amazonian forests to land use and climate change. *Tree* 13 (10):411–415

Melesse AM, Loukas AG, Senay G, Yitayew M (2009) Climate change, land-cover dynamics and ecohydrology of the Nile River Basin. *Hydrol Proc* 23(26):3651–3652

Mohr PA (1962) The Geology of Ethiopia. University-College Press, Addis Ababa, 268p

Neff R, Chang H, Knight CG, Najjar RG, Yarnal B, Walker HA (2000) Impact of climate variation and change on Mid-Atlantic region hydrology and water resources. *Clim Res* 14: 207–218

Neitsch SL, Arnold JG, Kiniry JR, Williams JR (2005) Soil and water assessment tool, theoretical documentation: version. USDA Agricultural Research Service and Texas A&M Blackland Research Center, Temple, TX

Novotny EV, Stefan HG (2007) Stream flow in Minnesota: indicator of climate change. *J Hydrol* 334:319–333

Richey JE, Nobre C, Deser C (1999) Amazon River discharge and climate variability: 1903–1985, *Science* 246:101–103

Setegn SG, Srinivasan R, Melesse AM, Dargahi B (2009a) SWAT model application and prediction uncertainty analysis in the Lake Tana Basin, Ethiopia. *Hydrol Proc* 23(26):3738–3750

Setegn SG, Srinivasan R, Dargahi B, Melesse AM (2009b) Spatial delineation of soil erosion vulnerability in the Lake Tana Basin, Ethiopia. *Hydrol Proc* 24(3):357–367

Setegn SG, Dargahi B, Srinivasan R, Melesse AM (2010) Modeling of sediment yield from Anjeni-gauged watershed, Ethiopia using SWAT model. *J Am Water Resour Assoc (JAWRA)* 46(3):514–526. doi:10.1111/j.1752-1688.2010.00431.x

Schulze RE (2000) Hydrological responses to land use and climate change: a southern African perspective. *Ambio* 29 (1):12–22

Tarekegn D, Tadege A (2006) Assessing the impact of climate change on the water resources of the Lake Tana sub-basin using the WATBAL model. CEEPA discussion paper no. 30, Centre for Environmental Economics and Policy in Africa, University of Pretoria

Tu J (2009) Combined impact of climate and land use changes on stream flow and water quality in eastern Massachusetts, USA. *J Hydrol* 379:268–283

UNESCO (United Nations Educational, Scientific and Cultural Organization) (2004) National Water Development Report for Ethiopia, UN-WATER/WWAP/2006/7. World Water Assessment Program, Report, MOWR, Addis Ababa, Ethiopia

USDA Soil Conservation Service (1972) National engineering handbook: section 4. Hydrology, Chapters 4–10 USDA-SCS, Washington, DC

Van Griensven A, Meixner T (2006) Methods to quantify and identify the sources of uncertainty for river basin water quality models. *Water Sci Technol* 53(1):51–59

Van Roosmalen L, Sonnenborg TO, Jensen KH (2009) Impact of climate and land use change on the hydrology of a large-scale agricultural catchment. *Water Resour Res* 45:W00A15. doi:10.1029/2007WR006760

Van Wambeke A (2003) Properties and management of soils of the tropics, FAO Land and water digital media series no. 24. FAO, Rome

Wilby RL, Wigley TML, Conway D, Jones PD, Hewitson BC, Main J, Wilks DS (1998) Statistical downscaling of general circulation model output: a comparison of methods. *Water Resour Res* 34(11):2995–3008

Wilby RL, Hay LE, Gutowski WJ, Arritt RW, Takle ES, Pan Z, Leavesley GH, Clark MP (2000) Hydrological responses to dynamically and statistically downscaled climate model output. *Geophys Res Lett* 27(8):1199–1202

Williams JR (1995) The EPIC model. In: Singh VP (ed) Computer models of watershed hydrology. Water Resources Publications, Highlands Ranch, CO, Chapter 25, pp 909–1000

Wood RB, Talling JF (1988) Chemical and algal relationships in a salinity series of Ethiopian inland waters. *Hydrobiologia* 158:29–67

Wood AW, Leung LR, Sridhar V, Lettenmaier DP (2004) Hydrologic implications of dynamical and statistical approaches to downscaling climate model outputs. *Clim Change* 62:189–216

Wudneh T (1998) Biology and management of fish stocks in Bahir Dar Gulf, Lake Tana, Ethiopia. PhD dissertation. Wageningen Agricultural University, Wageningen, 144p

Zhang L, Dawes WR, Walker GR (2001) The response of mean annual evapotranspiration to vegetation changes at catchment scale. *Water Resour Res* 37:701–708

# Chapter 13

## Climatic Factors Modulating Nile River Flow

Mark R. Jury

**Abstract** This chapter presents a review of climatic factors modulating variability of Nile River flow. Through composite analysis of seasons with high and low flow, the Atlantic zonal overturning atmospheric circulation is seen as a dominant feature. When upper easterlies and lower westerlies prevail, convection is enhanced over the highlands of Northeast Africa. This atmospheric cell is shown to be coupled with the Pacific Ocean thermocline oscillation that comprises the El Niño Southern Oscillation. At the event scale, floods are produced by an enhanced southerly monsoon over the West Indian Ocean that is reflected back toward Northeast Africa by an Arabian ridge. Diurnal forcing is evident in surface heating and a mid-day strengthening of northwesterly winds over Sudan. During the 1970s and early 1980s, droughts caused the Nile River flow to decline. This appears related to a multi-year cool phase in the North Atlantic and a southward retreat of the near-equatorial trough. Sympathetic responses of rainfall extend from Ethiopia to India and across the West African Sahel, suggesting that climatic variability in the Nile catchment is part of a global pattern. Although some predictability is uncovered, more than half of the variance in Nile River flow is apparently random and unresolved by either statistical or numerical models. Thus coping mechanisms and strategies for resource switching in wet and dry phases are needed, to put countries bordering the Nile on sound economic footing.

**Keywords** Nile River flow variability · Climatic factors · Ethiopian highlands rainfall

### 13.1 Introduction

The Nile River flows through arid northeastern Africa, nurturing life with its water. Each year it rises and falls  $\sim 5$  m in Sudan following seasonal rains over Ethiopia.

---

M.R. Jury (✉)

Physics Dept, University of Puerto Rico, Mayagüez, Puerto Rico; University of Zululand, KwaDlangezwa, South Africa  
e-mail: mark.jury@upr.edu

In some years the flow doubles in others it is halved, bringing socio-economic stress to agrarian communities of the African savannah. The year-to-year variability arises from the coupling of slowly evolving ocean conditions and large-scale atmospheric circulation. Equatorial ocean upwelling displaces the overlying atmospheric convection, altering the position of large-scale hydrological sources and sinks (Philander et al., 1987; Nicholson and Grist, 2001). Past studies have attributed African climate variability to north–south patterns of Atlantic SST (Folland et al., 1986; Lough, 1986; Palmer, 1986; Semazzi et al., 1996), and to the Pacific El Niño–Southern Oscillation (ENSO; Eltahir, 1996; Eltahir and Wang, 1999). In addition to ocean–atmosphere coupling, evapo-transpiration from surface vegetation offers additional memory (Zeng and Eltahir, 1998; Zeng et al., 1999). Research on climatic modulation of Nile River flow is extensive (Quinn, 1992; Wang and Eltahir, 1999; Eldaw et al., 2003; Potter, 2004; Korecha and Barnston, 2007) and points to the ENSO and Indian Ocean monsoon as influential (Camberlin, 1997; Camberlin et al., 2001; Segele et al., 2009). During ENSO cool (warm) phase upper easterly (westerly) wind anomalies prevail over the equatorial Atlantic that generate rising (sinking) motion over Africa and India (Hastenrath, 2000).

The Nile River collects flow from the Abay (Blue Nile) River of central Ethiopia (54 km<sup>3</sup>/year), Sudd wetlands of southern Sudan (15), Baro River of southern Ethiopia (13) and Atbara River of northern Ethiopia (12), according to Ahmed and Ismail (2008; their figure 13.4). Thus 85% of the Nile River flow derives from rainfall over the Ethiopian highlands, where run-off efficiency is ~18% (Roskar, 2000; Dettinger and Diaz, 2000). The Blue Nile catchment is elevated ~2,000 m above the surrounding areas (Fig. 13.1a, b) and orographic convection prevails in summer (June–September) as the southwest monsoon draws moist tropical air from the Congo River basin. Concurrently, the Indian monsoon generates an upper

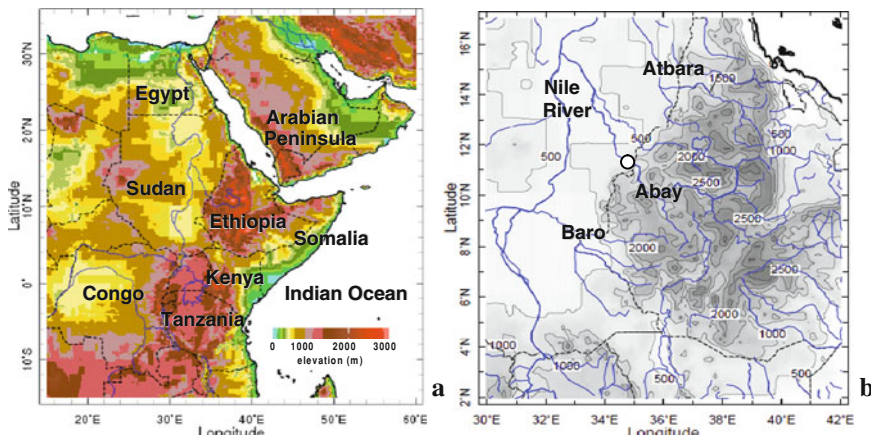


**Fig. 13.1** (a) Topographic map of northeastern Africa, (b) close-up of Nile River catchment with shaded contours at 500 m and rivers (blue). River flow gauge is circled near the Sudan-Ethiopia border (dashed)

easterly jet that crosses the Arabian Sea, pulsing Ethiopian highlands rainfall every few weeks. Diurnal heating promotes evapo-transpiration and afternoon thunderstorms that contribute >2/3 of total rainfall (Seleshi, 1991).

The objective of this chapter is to review how the large-scale environment modulates Nile River flow using historical data sets and statistical analyses. Other objectives include an estimation of current levels of predictability and a review of intra-seasonal and diurnal factors contributing to floods. In Section 13.2, the data and methods are outlined. Section 13.3 gives results of time series analysis, composite patterns, seasonal predictability, and intra-seasonal to diurnal aspects of flood events. The conclusions are given in Section 13.4 within a conceptual framework.

## 13.2 Data and Methods

To study variability of the Nile River, river gauge data were obtained from two stations (cf. Fig. 13.1b): Roseires, Sudan ( $11^{\circ}43'N$ ,  $35^{\circ}23'E$ ) and Eldeim, Ethiopia ( $11^{\circ}09'N$ ,  $35^{\circ}08'E$ ). The two records are closely related (Conway et al., 2009) and provide a complete record from 1912 to 2002. Supplementing the monthly flow data are gauge rainfall from the World Climate Research Program Global Precipitation Climatology Center (GPCC; Rudolf and Schneider, 2005) averaged over the catchment area ( $5$ – $16^{\circ}N$ ,  $32$ – $40^{\circ}E$ ) in the period 1912–2007. The monthly rainfall data are averaged to seasonal or annual blocks to study inter-annual variability. To investigate the nature of climatic oscillations, the time series are subjected to wavelet spectral analysis following the methods of Yeshanew and Jury (2007). Large-scale environmental patterns are studied by ranking the top 6 wet and dry summers (June–September) since 1960 based on an average of flow and rainfall standardized departures. Wet summers include: 1961, 1964, 1998, 1988, 1999, 1967; dry summers are 2002, 1984, 1987, 1972, 1986, 1990 as shown in Table 13.1. Composite difference fields are calculated using monthly re-analyzed atmospheric fields (Kalnay et al., 1996) of National Center for Environmental Prediction (NCEP) for wind, stream function and velocity potential as maps and vertical sections, serving to update the findings of Yeshanew and Jury (2007). Composite

**Table 13.1** Wet and dry summers from ranking of Nile flow and catchment rainfall since 1960

Wet		Dry	
JJAS	St. dep.	JJAS	St. dep.
1961	1.98	1984	-2.52
1964	1.80	1987	-1.65
1998	1.42	1972	-1.55
1988	1.39	1986	-1.48
1999	1.04	1990	-1.43
1967	0.76	2002	-1.43

St. dep. = Standardized departures.

difference fields are also calculated for NOAA extended sea surface temperature (SST; Smith et al., 2008) and GPCC rainfall. From the resulting patterns, key areas are identified and standardized annual time series are extracted for statistical tests. To quantify environmental influences on Nile River flow, a multi-variate regression is made using three parameters at concurrent time and 1-year lead, following statistical methods similar to Eldaw et al. (2003). Numerical predictability is evaluated by extraction of annual Nile catchment rainfall simulated by six coupled general circulation models (cGCM) in the period 1960–2000. Comparisons are made with GPCC catchment rainfall and Nile River flow by cross-correlation, with values  $> 0.28$  significant at 95% confidence. The model data (from COLA, CCM3, ECHAM, NCEP, NSIPP, GFDL) are extracted from the IRI Forecast Division via the climate library. Details of the cGCM are given at: [iridl.ideal.columbia.edu/SOURCES/IRI.FD/](http://iridl.ideal.columbia.edu/SOURCES/IRI.FD/) Simulations are at concurrent time and based on observed SST fields. Intra-seasonal variability is reviewed from Jury (2009), based on daily GPCP gauge-satellite blended rainfall (Huffman et al., 2001) over the Nile catchment in the period 1997–2007. Two flood events are identified by objective ranking: 23–28 July 2006 and 26–31 July 2007. Composite NCEP reanalysis anomaly fields are analyzed by subtracting the historical mean for those days, and diurnal amplitude is quantified by subtracting 08h00 from 14h00 LST fields. 3-hourly multi-satellite estimated catchment rainfall (Joyce et al., 2004) for the two floods is analyzed for diurnal cycles. Wavelet spectral analysis is again applied to daily time series of rainfall and meridional wind to characterize the intra-seasonal oscillations present.

## 13.3 Results and Discussion

### 13.3.1 Temporal Analysis

There is a large seasonal cycle in Blue Nile River flow (Fig. 13.2a) induced by Ethiopian highlands rainfall that peaks in July. Flows rise from June to August, followed by a gradual decline to December. The mean flow is  $49 \text{ km}^3/\text{year}$  and the range over the period 1912–2002 is of similar value. The standard deviation is  $9.5 \text{ km}^3/\text{year}$  and the coefficient of inter-annual variability is  $\sim 30\%$ . Annual time series of flow and catchment rainfall (Fig. 13.2b) and wavelet co-spectra (Fig. 13.2c) reveal significant oscillations in the twentieth century around 3 years. Other significant oscillations include: 6–7 years up to 1930 and after 1985, 16–18 years from 1960 to 1985, and 34 to 40 years after 1930. Using longer records of annual flow Currie (1987) and Fraedrich et al. (1997) confirm the presence of oscillations at  $\sim 18$  and  $\sim 40$  years. The river flow closely follows catchment rainfall as expected, except in the period around 1980 when flow dropped early. The 3-year cycle is associated with large-scale ocean-atmosphere coupling, as will be shown later. The lowest frequency appears related to the North Atlantic multi-decadal oscillation (Enfield et al., 2001), which contributed to drought in the early 1980s.

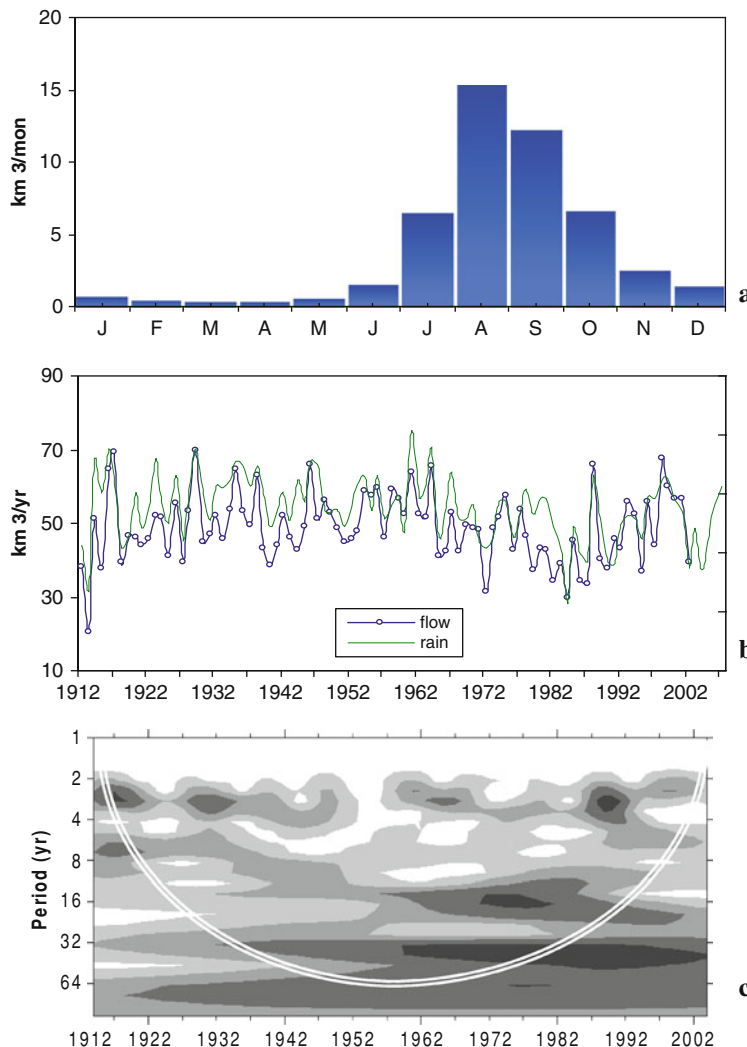


**Fig. 13.2** (a) Seasonal cycle of Blue Nile River flows averaged over the study period, (b) comparison of annual catchment rainfall and Blue Nile River flow (*solid*), (c) wavelet co-spectra of annual flow and rainfall with power shaded at 25% intervals. Cone of validity is outlined

### 13.3.2 Large-Scale Patterns

The composite difference fields with respect to Nile River flow are given in Fig. 13.3 for wet and dry seasons as indicated in Table 13.1. The SST pattern exhibits a cool tongue  $<-2^{\circ}\text{C}$  in the east Pacific consistent with La Niña conditions (Fig. 13.3a). SST differences across the Atlantic and Indian Ocean are trivial in comparison. The summer rainfall pattern (Fig. 13.3b) reveals sympathetic wet conditions across

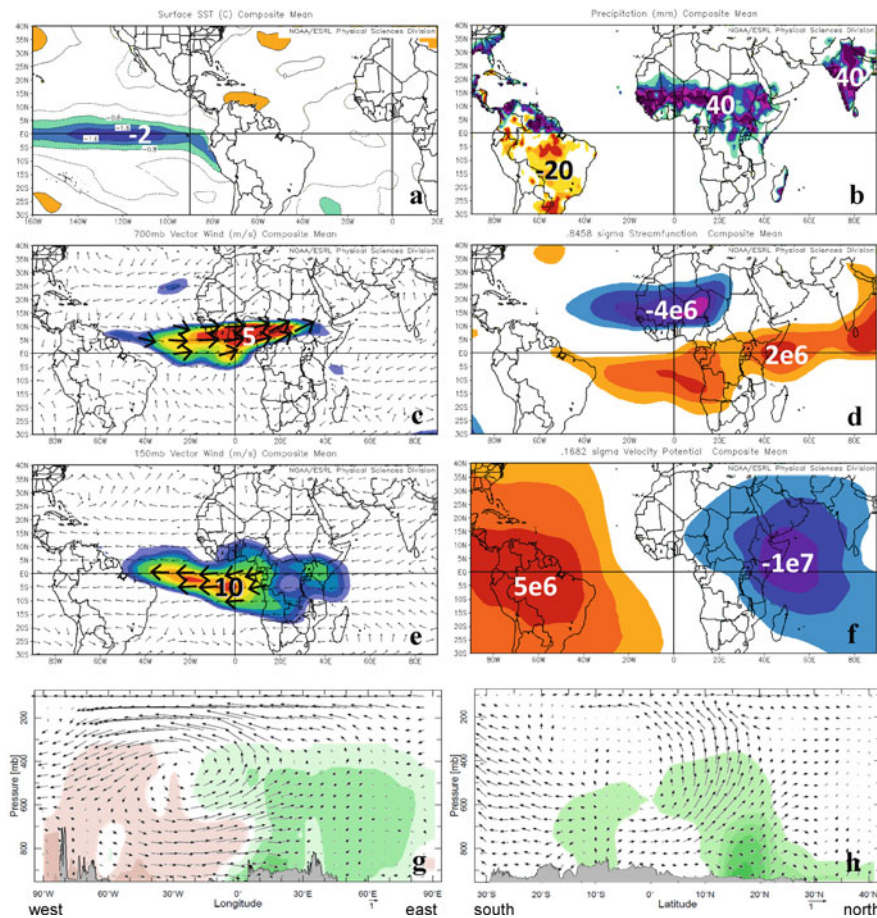


**Fig. 13.3** Composite difference maps for 6 wet minus 6 dry seasons (June–September) as defined in Table 13.1, for (a) SST, (b) rainfall, (c) 700 hPa wind with vectors  $> 5 \text{ m/s}$  bold, (d) 700 hPa streamfunction, (e) 150 hPa wind with vectors  $> 10 \text{ m/s}$  bold, and (f) 150 hPa velocity potential. Composite difference vertical sections for (g) zonal wind averaged 5S–10N, and (h) meridional wind averaged 20E–55E, shading refers to specific humidity surplus (green) or deficit (brown). Sections are averaged 20E–50E, vertical motion is  $\times 10$ ; key vector and terrain profile are given

the African Sahel and India, and drier conditions across South America below the equator. This reflects a convective polarity between the two continents as outlined by Yeshanew and Jury (2007). Composite 700 hPa ( $\sim 3 \text{ km}$ ) winds exhibit low-level westerlies across the Atlantic from Brazil to Ethiopia (Fig. 13.3c). This circulation is emphasized by twin rotors in the 700 hPa streamfunction field (Fig. 13.3d) over the Sahel (counter-clockwise) and southeastern Africa (clockwise). The clockwise southern rotor is zonally elongated and tilted NE, linking the east Atlantic and India as described by Kucharski et al. (2009). Upper easterly differences are found (Fig. 13.3e) over the tropical Atlantic, connecting two distinct centres of action in the velocity potential composite (Fig. 13.3f). A zonal overturning (Walker)

circulation modulates Nile River flow as seen in the vertical section (Fig. 13.3g), with upper (lower) differences of 10 m/s (4 m/s) over the eastern equatorial Atlantic. The southern meridional overturning (Hadley) circulation also participates (Fig. 13.3h), with differences of 1 m/s over the equator during June–September seasons with extreme Nile River flow.

The patterns show how African convection is related to large-scale environmental features; but what is the dominant coupling between ocean and atmosphere? Depth-longitude sections of sea temperature in ocean reanalysis fields have been analyzed for principal components by Yeshanew and Jury (2007). The 1st Pacific mode is an ENSO dipole (Fig. 13.4a) reflecting the “see-saw” of tropical ocean

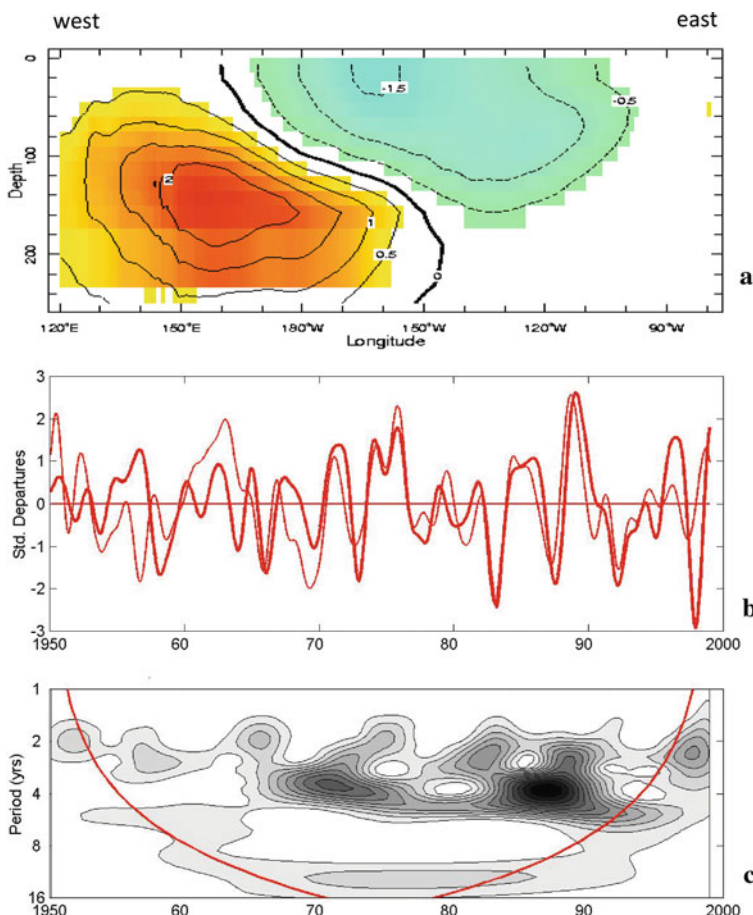


**Fig. 13.4** (a) First principal component loading pattern for Pacific sea temperature (PC1) as longitude-depth section, averaged 10S–10 N; (b) 1.5–16 year wavelet filtered Pacific PC1 time score compared with the Atlantic zonal overturning circulation (thin line) as represented by Fig. 13.3g; (c) wavelet co-spectral energy with shading at 10% power intervals and cone of validity. Adapted from Yeshanew (2003)

thermocline. Its filtered time score matches the Atlantic overturning (700–150 hPa) atmospheric circulation (Fig. 13.4b) in amplitude and frequency. There is no systematic delay between the two records, but co-spectral energy evolves over time (Fig. 13.4c) indicating a degree of random behavior. 3-year oscillations prevail as they do for Nile River flow (cf. Fig. 13.2c) and Indian Ocean Rossby wave evolution (Jury and Huang, 2004).

Seven key variables from the composite analysis are extracted for comparison with the Nile River flow. Pair-wise cross-correlations are rather similar ( $r = |0.42–0.58|$ ), but multi-variate regression indicates that African velocity potential (coefficient = –0.38), Pacific SST (–0.31), and Southern streamfunction (+0.16) have greatest influence at concurrent time (Table 13.2). The scatterplot (Fig. 13.5a) reveals a 45% fit. Thus upper divergence related to the Africa–America dipole is most important, followed by Pacific La Niña conditions. A third influence is southern streamfunction, highlighting the need for equatorial westerly wind anomalies from the Atlantic to India. At 1-year lead (Fig. 13.5b) the key variables are upper zonal wind (–0.51), Pacific SST (+0.36) and Venezuela SST (+0.22). Early development of the upper limb of the Atlantic Walker cell is seen to be the most important predictor of Nile River flow. Significantly Pacific SST changes sign from

**Table 13.2** Multi-variate statistical fit of environmental variables to Blue Nile flow at concurrent and 1-year lead time. Variables are: AfricaVP=150 hPa velocity potential averaged over 15S–25N, 20E–65E; se.Afr.Strm=700 hPa streamfunction 10S–5N, 10E–60E; PacSST=SST 5S–5N, 160W–80W; VenezSST=SST 10N–15N, 75W–50W; 150U=150 hPa zonal wind 10S–5N, 42W–20E. Compare with Fig. 13.5a, b

<i>Concurrent model</i>					
Adj R Sq	0.41				
Std. Error	0.74				
Sample	48				
ANOVA	<i>df</i>	<i>SS</i>	<i>MS</i>	<i>F</i>	
Regression	3	19.37	6.46	11.91	
Residual	43	23.84	0.54		
<i>Variable</i>	<i>Coeff.</i>	<i>Std. Error</i>	<i>t Stat</i>	<i>P-value</i>	
AfricaVP	–0.38	0.14	–2.64	0.01	
se.Afr.Strm	0.16	0.14	1.16	0.25	
PacSST	–0.31	0.11	–2.81	0.01	
<i>1-year lead model</i>					
Adj R Sq	0.26				
Std. Error	0.83				
Sample	47				
ANOVA	<i>df</i>	<i>SS</i>	<i>MS</i>	<i>F</i>	
Regression	3	13.37	4.46	6.42	
Residual	43	29.83	0.69		
<i>Variable</i>	<i>Coeff.</i>	<i>Std. Error</i>	<i>t Stat</i>	<i>P-value</i>	
PacSST	0.36	0.15	2.46	0.02	
VenezSST	0.22	0.13	1.72	0.09	
150U	–0.51	0.14	–3.54	0.00	

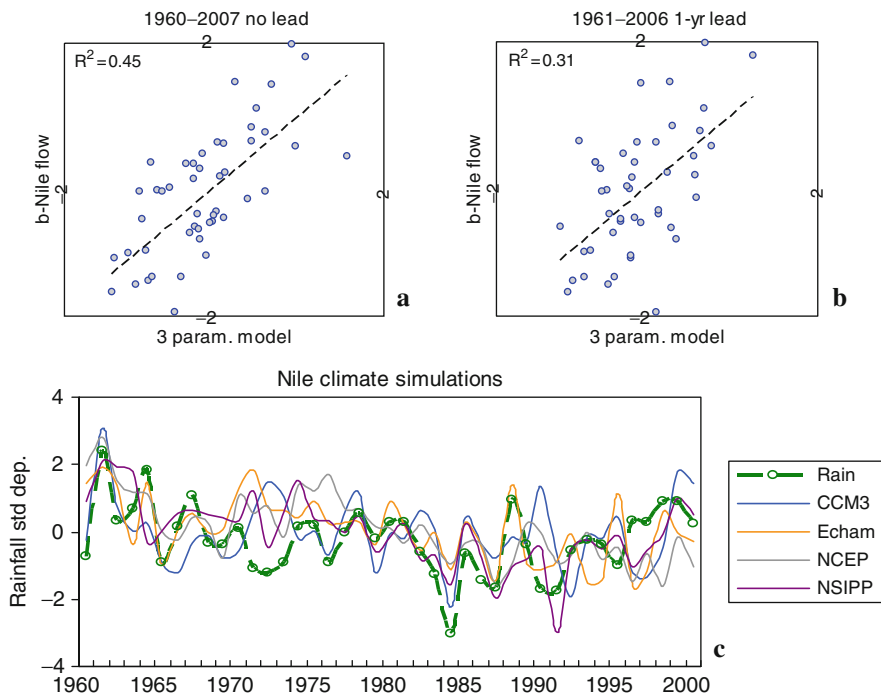


**Fig. 13.5** Scatterplot of 3 parameter statistical model (x-axis) versus Blue Nile flow for (a) concurrent time, and (b) 1-year lead; as described in Table 13.2. (c) Time series of coupled GCM simulations of Blue Nile annual catchment rainfall (thin solid) and observed (thick dashed), as described in Table 13.3

**Table 13.3** Cross-correlation of time series of GPCC catchment rainfall, Nile River flow and cGCM simulated catchment rainfall in the period 1960–2000. Significant values are bold. See Fig. 13.5c

	Rain	Flow
Flow	<b>0.77</b>	
COLA	0.01	0.01
CCM3	<b>0.35</b>	<b>0.30</b>
ECHAM	<b>0.43</b>	<b>0.39</b>
NCEP	<b>0.34</b>	0.17
NSIPP	<b>0.53</b>	<b>0.40</b>
GFDL	0.23	<b>0.31</b>
ENS	<b>0.51</b>	<b>0.39</b>

the concurrent model, reflecting a biennial component in tropical climate (Meehl and Arblaster. 2002). Venezuela SST has a weak pair-wise correlation, but appears in the multi-variate model as an indicator of reduced Atlantic trade-winds prior to years of high river flow. The 1-year lead statistical model has a 31% fit.

Numerical model simulations of Nile catchment rainfall are evaluated in Table 13.3 and Fig. 13.5c. Of the six models considered, only the COLA model fails to capture the inter-annual signal ( $r = 0.01$ ). In the next tier are the NCEP

(0.17–0.34) and GFDL (0.23–0.31) models. CCM3, ECHAM and NSIPP all exhibit significant ability to simulate year-to-year fluctuations of catchment rainfall and Nile River flow (0.30–0.53). The ensemble average of five models is consistent with the best model, but is weaker than the statistical model at concurrent time ( $r^2 = 26\%$  vs. 45%). This may be attributed to coarse model resolution ( $\sim 2^\circ$ ), distant influence of the Pacific ENSO and indeterminate coupling with the Atlantic Walker circulation.

### 13.3.3 Examples of Local Forcing

The local pattern of winds and rainfall for composite wet minus dry years is given in Fig. 13.6. Low level winds are southwesterly, confluent and rise from Sudan onto the Ethiopian highlands (Fig. 13.6a), generating orographic convection. Annual rainfall differences  $>+3\sigma$  spread across the Baro River catchment (Fig. 13.6b), while surpluses  $>+2\sigma$  cover the Abay and Atbara catchments. Although seasonal composites are useful, it is necessary to consider shorter time scales important to hydrological processes such as run-off. In 2006 and 2007 daily rainfall  $> 100$  mm and seasonal accumulations up to 2,000 mm were reported [www.ethiomet.gov.et](http://www.ethiomet.gov.et). Numerous mud-slides caused  $\sim 1,000$  fatalities and displaced  $\sim 476,000$  people, exposing over 3 million to flood-related diseases [www.re liefweb.int](http://www.re liefweb.int). The Blue Nile River rose to levels similar to the floods of 1988 and 1998. Nile catchment daily rainfall displays two peaks at the end of July 2006 and July 2007 (Fig. 13.7a). There is spectral energy around 40 days related to Madden Julian Oscillations of the Indian monsoon

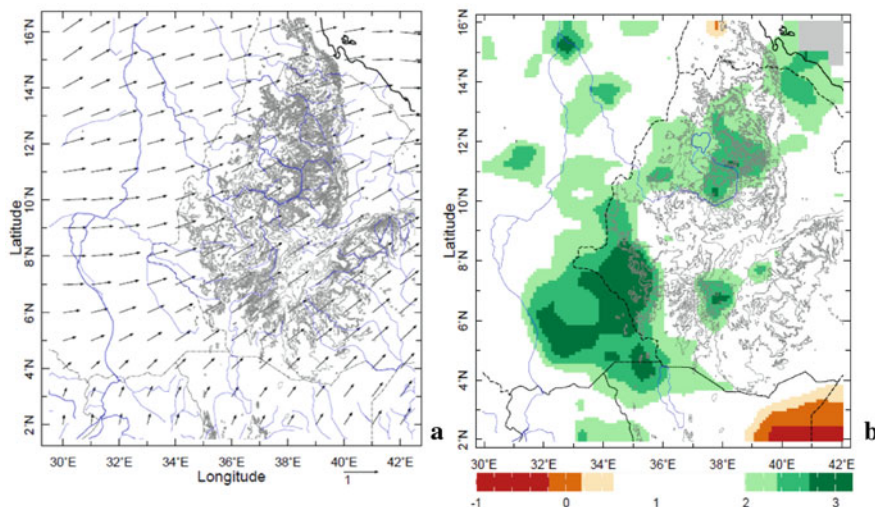


**Fig. 13.6** Composite difference maps for 6 wet minus 6 dry years for (a) 700 hPa wind and (b) rainfall standardized departures

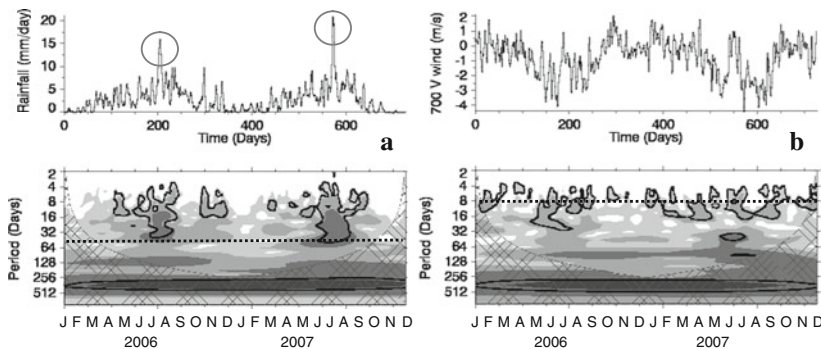


**Fig. 13.7** Wavelet spectral analysis for 2006–2007 of (a) Ethiopian highlands daily rainfall, and (b) Ethiopian 700 hPa meridional wind. Energy is shaded at 25% power intervals; cone of validity given; outline denotes statistical significance w.r.t. red noise at 90% confidence. *Dashed lines* highlight key cycles at 10- and 40-days; *circles* in (a) identify flood events: 23–28 July 2006 and 26–31 July 2007

that “pulse” the tropical circulation (Hulme and Tosdevin, 1989; Camberlain, 1997; Hoyos and Webster, 2007). On the other hand, low level meridional winds fluctuate at intervals around 10 days over the 2 year period (Fig. 13.7b) and northerlies are conspicuous in the wet season.

Regional scale circulation anomalies during the 2006–2007 floods are illustrated in Fig. 13.8. Low level wind anomalies exhibit a cyclonic vortex centered on Ethiopia (Fig. 13.8a). The southerly monsoon over the West Indian Ocean is stronger than usual. This anomalous flow extends toward the Arabian Peninsula, and turns westward across the Red Sea then southward toward the Blue Nile catchment. 700 hPa geopotential height anomalies are positive over the Arabian Peninsula (Fig. 13.8b) and encircle the aforementioned cyclonic vortex. Thus an anomalous Arabian ridge deflects part of the “Somali jet” back towards Africa. Diurnal amplitude is analyzed by subtracting 08h00 from 14h00 LST fields during peak floods. Air temperatures increase 12°C over the northeastern Sahara desert (18–30°N) and also over the highlands of southern Africa (Fig. 13.8c). The wind response to diurnal heating is evident over southern Egypt and northern Sudan, with northwesterly differences  $> 3$  m/s (Fig. 13.8d). Hence there is anomalous orographic lifting during afternoon hours along the Sudan-Ethiopia border, consistent with increased rainfall there (cf. Fig. 13.6b). The time series of rain rates based on 3-hr multi-satellite estimates averaged over the Blue Nile catchment is given in Fig. 13.8e, f. Heaviest rainfall is between 18h00 and 24h00 LST following the typical sequence of solar radiation and evapotranspiration stimulating growth in boundary layer height and convective available potential energy. Mesoscale thunderstorm clusters reaching  $-70^{\circ}\text{C}$  propagate westward across the Ethiopian highlands according to Meteosat imagery (Jury, 2009). Whilst the July 2006–2007 flood patterns are noteworthy, it is unnecessary to conclude that all Nile floods derive from similar local-scale forcing.

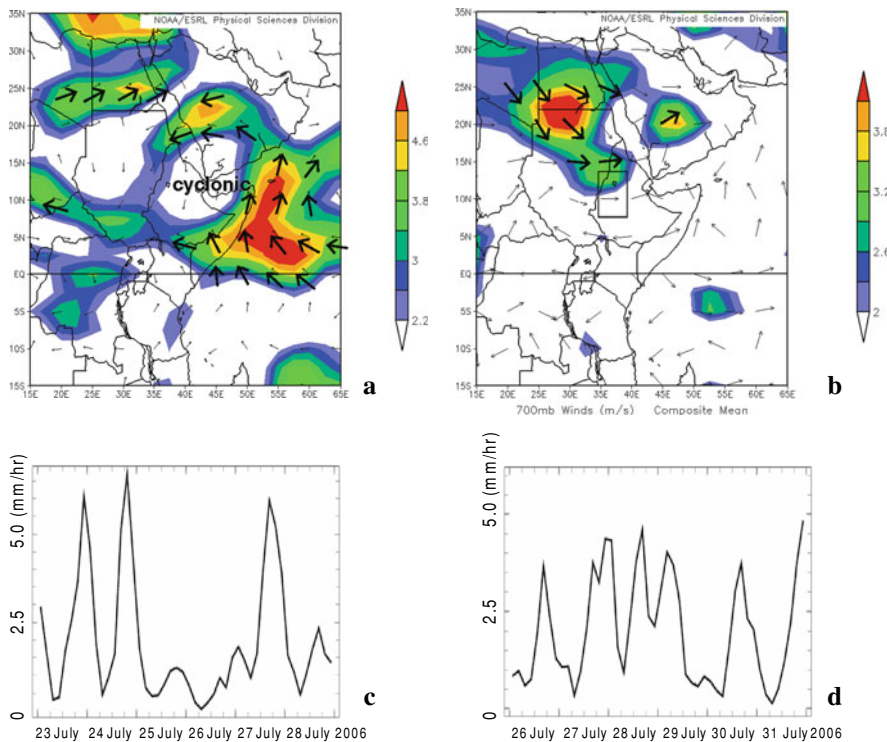


**Fig. 13.8** Composite anomalies of NCEP reanalysis fields on peak flood days in 2006–2007 for (a) 700 hPa winds with  $> 3$  m/s bold. Composite differences of diurnal amplitude (14h00 minus 08h00 LST) on flood days for (b) 700 hPa winds with  $> 3$  m/s bold (from Jury 2009). Three-hourly satellite rainfall rate averaged over the Nile catchment (box in b) for the 2006 (c) and 2007 (d) flood events. Peaks tend to occur after sunset

### 13.4 Conclusions

This review has sought to characterize the climatic forcing of Nile River flow variability. The dominant feature is the Atlantic zonal overturning circulation, with upper easterlies and lower westerlies inducing (suppressing) large scale convection over Africa (South America). This atmospheric cell is coupled with the Pacific thermocline oscillation that comprises the ENSO, as described in Camberlin et al. (2001) and shown here in Fig. 13.4. It is during La Niña that the Nile River rises due to heavy rainfall over the Ethiopian highlands. At the event scale, floods are produced by an enhanced southerly monsoon over the West Indian Ocean that is deflected cyclonically toward Northeast Africa by an Arabian ridge. Diurnal forcing is evident in surface heating and northwesterly winds over Sudan. During the 1970s and early 1980s, droughts caused the Nile River levels to drop. This appears related to a multi-year cool phase in the North Atlantic and a southward retreat of the near-equatorial trough. Indeed, there are widespread sympathetic responses of rainfall that extend from Ethiopia to India and across the Africa Sahel (and Atlantic

Ocean) toward Central America (cf. Fig. 13.3b), suggesting that climatic variability in the Nile catchment is not unique but part of a global oscillation of the Hadley cell.

Further research progress will depend on open access to daily and monthly Nile River flow data, increased mesoscale observations involving weather radar and routine aircraft profiles, the calibration and operational use of mesoscale weather prediction models, and the establishment of regional science networks. Already researchers have open access to mesoscale satellite data, and rewards are there – particularly for studies on intra-seasonal forcing. Although some predictability has been uncovered here, more than half of the variance in Nile River flow is apparently random and unlikely to be resolved by more technology. Thus coping mechanisms and strategies for resource switching in wet and dry phases is needed, to put countries such as Ethiopia on a stronger economic footing.

**Acknowledgments** The author thanks Declan Conway, Univ. East Anglia for provision of Nile River flow data.

## References

Ahmed A, Ismail U (2008) Sediment in the Nile River system, UNESCO-IHP report, Khartoum, Sudan, 93pp

Camberlin P (1997) Rainfall anomalies in the source region of the Nile and their connection with Indian summer monsoon. *J Climate* 10:1380–1392

Camberlin P, Janicot S, Poccard I (2001) Seasonality and atmospheric dynamics of the teleconnection between African rainfall and tropical sea surface temperature: Atlantic vs. ENSO. *Int J Climatol* 21:973–1005

Conway D, Persechino A, Ardoine-Bardin S, Hamandawana H, Dieulin C, Mahé G (2009) Rainfall and water resources variability in sub-Saharan Africa during the twentieth century. *J Hydrometeor* 10:41–59

Currie RG (1987) On bistable phasing of 18.6-year induced drought and flood in the Nile records since AD 650. *Int J Climatol* 7(4):373–389

Dettinger MD, Diaz HF (2000) Global characteristics of stream flow seasonality and variability. *J Hydrometeor* 1:289–310

Eldaw AK, Salas JD, Garcia LA (2003) Long-range forecasting of the Nile River flows using climatic forcing. *J Appl Meteor* 42:890–904

Eltahir EA (1996) El Niño and natural variability in the flow of the Nile River. *Water Resour Res* 32:131–137

Eltahir EAB, Wang G (1999) Nilometers, El Niño and climate variability. *Geophys Res Lett* 26(4):489–492

Enfield DB, Mestas-Nunez AM, Trimble PJ (2001) The Atlantic Multidecadal Oscillation and its relationship to rainfall and river flows in the continental US. *Geophys Res Lett* 28:2077–2080

Folland CK, Palmer TN, Parker DE (1986) Sahel rainfall and world-wide sea temperature, 1901–85. *Nature* 320:602–607

Fraedrich K, Jiang J, Gerstengarbe F-W, Werner PC (1997) Multiscale detection of abrupt climate changes: application to River Nile flood levels. *Int J Climatol* 17(12):1301–1315

Hastenrath S (2000) Inter-annual and longer-term variability of upper air circulation over the tropical Atlantic and West Africa in boreal summer. *Int J Climatol* 20:1415–1430

Hoyos CD, Webster PJ (2007) The role of intra-seasonal variability in the nature of Asian monsoon precipitation. *J Clim* 20:4402–4424

Huffman GJ, Adler RF, Morrissey M, Bolvin DT, Curtis S, Joyce R, McGavock B, Susskind J (2001) Global precipitation at one-degree daily resolution from multi-satellite observations. *J Hydrometeor* 2:36–50

Hulme M, Tosdevin N (1989) The tropical easterly jet and Sudan rainfall: a review. *Theor Appl Climatol* 39:179–187

Joyce RJ, Janowiak JE, Arkin PA, Xie PP (2004) cMorph: a method that produces global precipitation estimates from passive microwave and infrared data at high spatial and temporal resolution. *J Hydrometeorol* 5:487–503

Jury MR, Huang B (2004) The Rossby wave as a key mechanism of Indian Ocean climate variability. *Deep Sea Res* 51:2123–2136

Jury MR (2009) Meteorological scenario of Ethiopian floods of 2006–07. *Theor Appl Clim.* doi: 10.1007/s00704-010-0259

Kalnay E et al (1996) The NCEP/NCAR 40-year reanalysis project. *Bull Am Meteorol Soc* 77:437–471

Kucharski F, Bracco A, Yoo JH, Tompkins AM, Feudale L, Ruti P, Dell'Aquila A (2009) A Gill-Matsuno-type mechanism explains the tropical Atlantic influence on African and Indian monsoon rainfall. *Q J R Meteorol Soc* 135(640):569–579

Lough JM (1986) Tropical Atlantic sea surface temperatures and rainfall variations in sub-Saharan Africa. *Mon Weather Rev* 114:561–570

Meehl GA, Arblaster JM (2002) The tropospheric biennial oscillation and Asian–Australian monsoon rainfall. *J Clim* 15:722–744

Mutai CC, Ward MN (2000) East African rainfall and the tropical circulation/convection on intraseasonal to interannual timescales. *J Clim* 13:3915–3939

Nicholson SE, Grist JP (2001) A conceptual model for understanding rainfall variability in the West African Sahel on interannual and interdecadal timescale. *Int J Climatol* 21: 1733–1757

Philander S, Hurlin W, Seigel A (1987) Simulation of the seasonal cycle of the tropical Pacific Ocean. *J Phys Oceanogr* 17:1986–2002

Palmer TN (1986) Influence of Atlantic, Pacific, and Indian Oceans on Sahel rainfall. *Nature* 322:251–253

Potter C, Zhang P, Klooster S, Genovese V, Shekhar S, Kumar V (2004) Understanding controls on historical river discharge in the world's largest drainage basins. *Earth Interact* 8:1–21

Quinn WH (1992) A study of southern oscillation-related climate activity 622–1990 incorporating Nile River flow data. In: Diaz HF, Markgraf V (eds) *El Nino: historical and paleoclimate aspects of southern Oscillation*. Cambridge University Press, Cambridge, pp 119–142

Roskar J (2000) Assessing the water resources potential of the Nile River based on data at the Nile forecasting center Cairo. *Geogr J Slovakia* :31–80

Rudolf B, Schneider U (2005) Calculation of gridded precipitation data for the global land-surface using in-situ gauge observations. Proceedings of the International Precipitation Working Group, Monterey, Eumetsat contribution. ISBN 92-9110-070-6

Segele ZT, Lamb PJ, Leslie LM (2009) Seasonal-to-interannual variability of Ethiopia/Horn of Africa monsoon, part I: associations of wavelet-filtered large-scale atmospheric circulation and global sea surface temperature. *J Clim* 22:3396–3421

Seleshi Y (1991) Statistical analysis of Ethiopian droughts in the 20th century based on monthly and yearly precipitation totals. MSc thesis, Vrije University, Brussels, Belgium

Semazzi HFM, Burns B, Lin NH, Schemm JE (1996) A GCM study of teleconnections between the continental climate of Africa and global sea surface temperature. *J Clim* 9:2480–2497

Smith TM, Reynolds RW, Peterson TC, Lawrimore J (2008) Improvements to NOAA's historical merged land-ocean surface temperature analysis (1880–2006). *J Clim* 21:2283–2296

Wang G, Eltahir EAB (1999) Use of information in the medium-and long-range forecasting of the Nile floods. *J Clim* 12:1726–1737

Yeshanew A, Jury MR (2007) North African climate variability, part 2: Tropical circulation systems. *Theor Appl Climatol.* doi:10.1007/s00704-006-0243-7

Zeng N, Eltahir EAB (1998) The role of vegetation in the dynamics of West African monsoons. *J Clim* 11:2078–2096

Zeng N, Neelin JD, Lau KM, Tucker CJ (1999) Enhancement of interdecadal climate variability in the Sahel by vegetation interaction. *Science* 286:1537–1540

**Part V**

**Water Resources Management, Allocation  
and Policy I**

# Chapter 14

## Hydrological Water Availability, Trends and Allocation in the Blue Nile Basin

Seleshi B. Awulachew, Fasikaw Dessie Wubet, Matthew McCartney, and Yilma Sileshi Shiferaw

**Abstract** Within the Blue Nile River basin rainfall varies significantly with altitude and is considerably greater in the Ethiopian highlands than on the plains of Sudan. The river is the principal tributary of the main Nile River providing 62% of the flow reaching Aswan in Egypt. Flow and sediment variation are large, with unimodal peaks. Significant water development therefore requires considerable investment in water control and management to offset variability. This chapter provides an overview of the basin characteristics, hydrology and hydrological variability of the Blue Nile, as well as a brief evaluation of the current and future status of water resource development and implications for water availability.

**Keywords** Abbay · Blue Nile · Hydrological variability · Sediment · Water allocation · Water use potential

### 14.1 Introduction

The Blue Nile<sup>1</sup> Sub-basin covers an area of 311,548 km<sup>2</sup> (Hydrosult et al., 2006). The river is the principal tributary of the main Nile River, providing 62% of the flow reaching Aswan (World Bank, 2006). The river and its tributaries drain a large proportion of the central, western and south-western highlands of Ethiopia before dropping to the plains of Sudan. The confluence of the Blue Nile and the White Nile is at Khartoum. The Dinder and Rahad rise to the west of Lake Tana and flow westwards across the border joining the Blue Nile below Sennar in Sudan. The basin is characterized by highly rugged topography and considerable variation of altitude

---

S.B. Awulachew (✉)

International Water Management Institute (IWMI), Addis Ababa, Ethiopia  
e-mail: s.bekele@cgiar.org

<sup>1</sup>The Blue Nile is a sub-basin of the main Nile. The sub basin is called Abbay in Ethiopia and Blue Nile in the Sudan. Generally, Blue Nile basin is widely understood to represent the Abbay-Blue Nile upstream of its confluence with the White Nile.

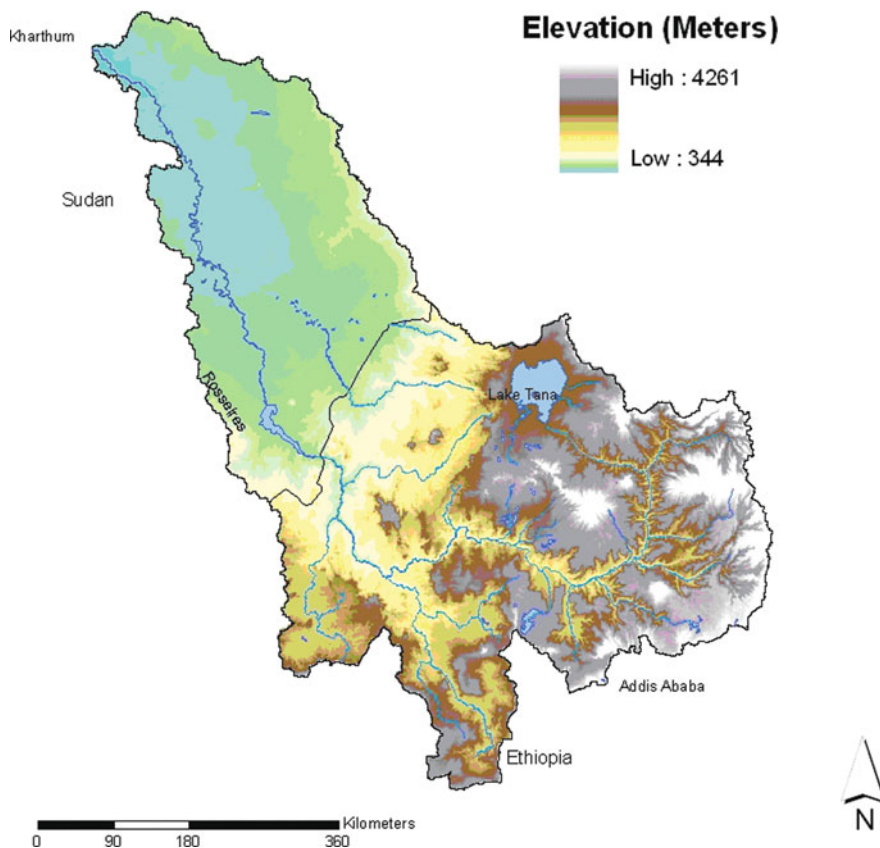


**Fig. 14.1** Map of the Blue Nile showing elevation, main tributaries and key geographic features (Awulachew et al., 2008)

ranging from about 350 meters above sea level (masl) at Khartoum to over 4,250 masl in the Ethiopian highlands (Fig. 14.1).

Until the 1990s, Egypt and Sudan were the only countries in the Nile Basin that, significantly exploited Nile water and regularly addressed issues of apportionment. In 1959, the two countries signed a binding agreement fixing the allocation of the total Nile flow. This treaty, entitled “The Full Utilization of the Nile”, apportioned the entire “utilizable flow” of the Nile, estimated to be  $74 \text{ km}^3$ , between the two countries. The treaty was based on the premise that  $10 \text{ km}^3$  of the entire Nile flow at Aswan (i.e.  $84 \text{ km}^3$ ) would be lost in evaporation and seepage from the soon to be constructed Lake Nasser and so was not utilizable. The basic allocation of the water was  $55.5 \text{ km}^3$  for Egypt and  $18.5 \text{ km}^3$  for Sudan (Waterbury, 2002). No allowance was made for upstream riparian states. However, it was recognized that 1 day these countries might make claims on the Nile water and the agreement stipulated that, in this event, Egypt and Sudan would negotiate jointly with any other claimants. Not

surprisingly, none of the upstream riparian states formally recognize the “rights” of Egypt and Sudan in this agreement.

In 1999, following a long process of development and with assistance from the World Bank and the United Nations Development Program (UNDP), the Nile Basin Initiative (NBI) was instigated. The intention of the initiative is to develop a cooperative framework that will ultimately lead to the establishment of a Nile River Basin Commission incorporating all ten riparian states. The principles proposed in the draft of December 1999, but not yet adopted by the member states, give prominence to “equitable” utilization of the water among all ten states. However, the importance of prevention of “significant harm” to existing water utilization is also stressed. The intention is to, as far as possible, develop win-win projects (e.g. infrastructure development, trade, tourism, industrial promotion, environmental protection and watershed management) that benefit all states. However, as yet, it is not clear what criteria will be used to assess rival or contradictory principles and claims. Currently, Ethiopia and upstream countries are insisting on a new set of allocation and use principles that could replace the 1959 *status quo*. By August 2010, five of the seven upstream countries had signed a new agreement, but both Egypt and Sudan have refused to sign.

Despite the current failure to establish a commonly agreed treaty between all the countries, the NBI has led to more general cooperation. After intensive dialogue and consultation, the Nile Basin countries have agreed on a Shared Vision that seeks “to achieve sustainable socio-economic development through the equitable utilization of, and benefit from, the common Nile Basin water resources”. This vision recognizes that only cooperation can unlock the development potential of the river, provide win-win benefits to all, increase access to food, energy, water supply, and enhance trade and international relations. However, in order to unlock the development potential, understand opportunities and establish an agreed framework of investments, it is essential to have a good understanding of the river hydrology and the likely implications of water resource development. Against this background, this paper reports on the hydrological variability and water availability in the Blue Nile sub-basin. It also describes an investigation of possible development scenarios in the Ethiopian Highlands, evaluating the impacts on water availability.

## 14.2 Variability in Blue Nile Basin

### 14.2.1 Rainfall Variability

Within the basin, rainfall varies significantly with altitude and rainfall amount is considerably greater in the Ethiopian highlands than on the Plains of Sudan (Fig. 14.2). Within Sudan, the average annual rainfall over much of the basin is less than 500 mm. In Ethiopia, the average annual rainfall is about 1,600 mm. It increases from about 1,000 mm near the Sudan border to between 1,400 and 1,800 mm over

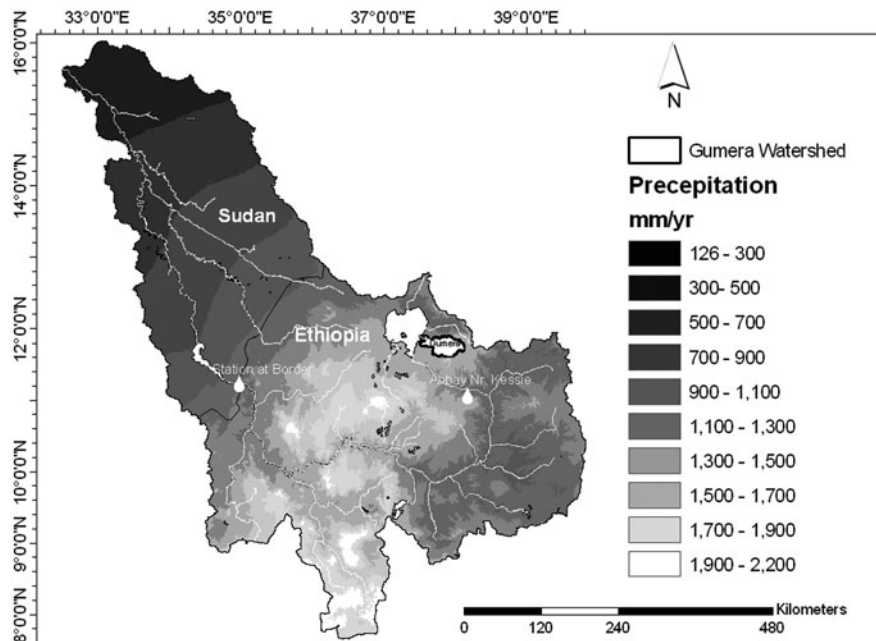


**Fig. 14.2** Mean annual rainfall across the Blue Nile basin

parts of the upper basin and in a few places, in the south-west of the catchment, it exceeds 2,000 mm.

The temporal distribution of rainfall is governed to a large extent by the movement of air masses associated with the Inter-Tropical Convergence Zone (ITCZ). The main rains (known in Ethiopia as the *Kiremt*) occur in the summer, between June and September, when the ITCZ moves north and the south-west air-stream extends over the entire Ethiopian highlands. This is also the main rainy season in Sudan, though being further north and at lower altitude, the period of rainfall is foreshortened and totals are considerably less than in Ethiopia. Shorter rains (known in Ethiopia as the *Belg*) fall between March and May. Inter-annual variability in rainfall is considerable and several consecutive years with below average rainfall is not uncommon.

The dynamics of the ITCZ over most of Ethiopia are known to be teleconnected to El Niño occurrence (Seleshi and Zanke, 2009, “Recent changes in rainfall and rainy days in the Upper Blue Nile basin”, Unpublished report). Studies have shown that in general El-Niño years are accompanied by below average *Kiremt* rainfall in large parts of Ethiopia (Haile, 1988; Beltrando and Camberline, 1993; Seleshi and Demaree, 1995; Nicholson and Kim, 1997). Years of abnormally low frequency of tropical cyclones over southwest Indian Ocean are associated with heavy *Belg* rainfall in Ethiopia (Shanko and Camberline, 1999).

As the economy of Ethiopia depends largely on rain-fed agriculture, it is highly sensitive to variability of rainfall across time and space. Recent major drought years (i.e. 1972/1973, 1983/1984 and 2002/2003) resulted in low agricultural production and significantly reduced Nile flow. These droughts affected millions of rural poor farmers and pastoralists as well as domestic and wild animals. Furthermore, there was serious degradation of the environment.

### 14.2.2 Runoff Variability

Throughout the Blue Nile basin, flow data are generally limited because of the remoteness of many of the catchments and the lack of economic resources and infrastructure to build and maintain monitoring stations. In Ethiopia, although there are over 100 flow gauging stations in the basin, most of these are located on relatively small tributaries and/or near the headwaters of the main rivers. Very few gauging stations are located on the main stem of the river or on the major tributaries close to their confluence with the Blue Nile. Table 14.1 presents summary statistics and naturalized flow estimates for each of the major tributaries. As with rainfall there is considerable inter-annual and seasonal variability in flow (Fig. 14.3a, b). Typically, 80–85% of discharge occurs in the 4 months July–October (Fig. 14.4).

The average annual flow of the Blue Nile at the Sudan border (El Diem) is reported to range from about 20 to 70 km<sup>3</sup>, with an average around 50 km<sup>3</sup>. Despite inflows from the Dinder and Rahad, the mean annual flow of the Blue Nile at Khartoum (48.2 km<sup>3</sup>) is slightly less than at the border. The reduction in flows between the border and Khartoum, despite the increased catchment area, is a consequence of both water abstractions (primarily for irrigation) and high transmission losses. It is estimated that annual transmission losses (i.e. both evaporation and percolation) between Rosieres and Khartoum are about 2 km<sup>3</sup>, with an additional 0.5 km<sup>3</sup> of evaporation from the Sennar and Roseires reservoirs (Sutcliffe and Parks, 1999). Figure 14.5 shows, the runoff variation at Khartoum and El Diem and the Khartoum flow minus the El-Diem flow. This figure illustrates both the high inter-annual variability and the increasing impact of water resource development, particularly from 1960. The annual discharge for the Blue Nile oscillated around the mean between 1920 and 1960. From 1960 to 1984 there was a general decrease in discharge. Thereafter annual discharge has gradually increased (Ahmed, 2006; Hydrosult et al., 2006).

In addition to large inter-annual variability there are also considerable seasonal variations in river flow. The mean monthly low flow of the Blue Nile at Khartoum is 302 million m<sup>3</sup>/month in February and the peak flow is 13,151 million m<sup>3</sup>/month in August (Fig. 14.6). Consequently, meaningful use and development of water resources in the basin requires water management/storage facilities that provide a mechanism for managing both the seasonal and the inter-annual variability in the availability of water.

**Table 14.1** Summary statistics for the major sub-basins of the Blue Nile

No	Sub-basin	Catchment area (km <sup>2</sup> )	Mean annual rainfall (mm)	Mean annual potential evapotranspiration (mm)	Mean annual runoff (mm)	Mean annual flow (Mm <sup>3</sup> )	Coefficient of runoff
<i>Ethiopia</i>							
1	Guder	7,011	910	1,307	312	2,187	0.34
2	Dabus	21,030	2,276	1,112	297	6,246	0.13
3	Finchaa	4,089	1,766	1,290	438	1,719	0.25
4	South Gojam	16,762	1,633	1,183	299	5,012	0.18
5	Anger	7,901	1,813	1,318	298	2,355	0.16
6	Beles	14,200	1,655	1,274	306	4,345	0.18
7	Didessa	19,630	1,816	1,308	289	5,673	0.16
8	Muger	8,188	1,347	1,210	298	2,440	0.22
9	North Gojam	14,389	1,336	1,242	305	4,389	0.23
10	Jemma	15,782	1,105	1,059	304	4,798	0.28
11	Lake Tana	15,054	1,313	1,136	253	3,809	0.19
12	Welaka	6,415	1,072	1,263	323	2,072	0.30
13	Beshilo	13,242	982	1,140	296	3,920	0.30
14	Wombera	12,957	1,660	N/A	299	3,874	0.18
15	Dinder	14,891*	N/A	N/A	188	2,797+	N/A
16	Rihad	8,269*	N/A	N/A	133	1,102+	N/A
<i>Sudan</i>							
1	Upper Blue Nile	33,804	674	1,480	135	4,563	0.20
2	Dinder-Rahad	38,851*	620	1,570	124	4,817	0.20
3	Lower Blue Nile	5,530	430	1,960	68.8	380	0.16

Source: for Ethiopia data are taken from MOWR (1998) and Tesfahun (2007). For Sudan: data are taken from Hydrosult et al. (2006). Note here that there are significant variations in estimates of the area of the Blue Nile basin. The overall estimated area is 311,548 km<sup>2</sup>, while the defined tributaries account for just 277,995 km<sup>2</sup>. The difference is attributable to smaller rivers and areas draining directly into the river.

### 14.2.3 Sediment Variability

The other critical parameter in the Blue Nile water resources is the extent of erosion and hence sediment in the river. According to Hydrosult et al. (2006), the erosion in the Blue Nile is extreme and the sediment delivery ratio is at 45%. As a result Roseires and Sennar reservoirs have suffered extensively from sedimentation, and the reservoir volumes have declined significantly (Awulachew et al., 2008). The Rosaries reservoir is currently being heightened by 10 m to compensate for storage lost through sedimentation.

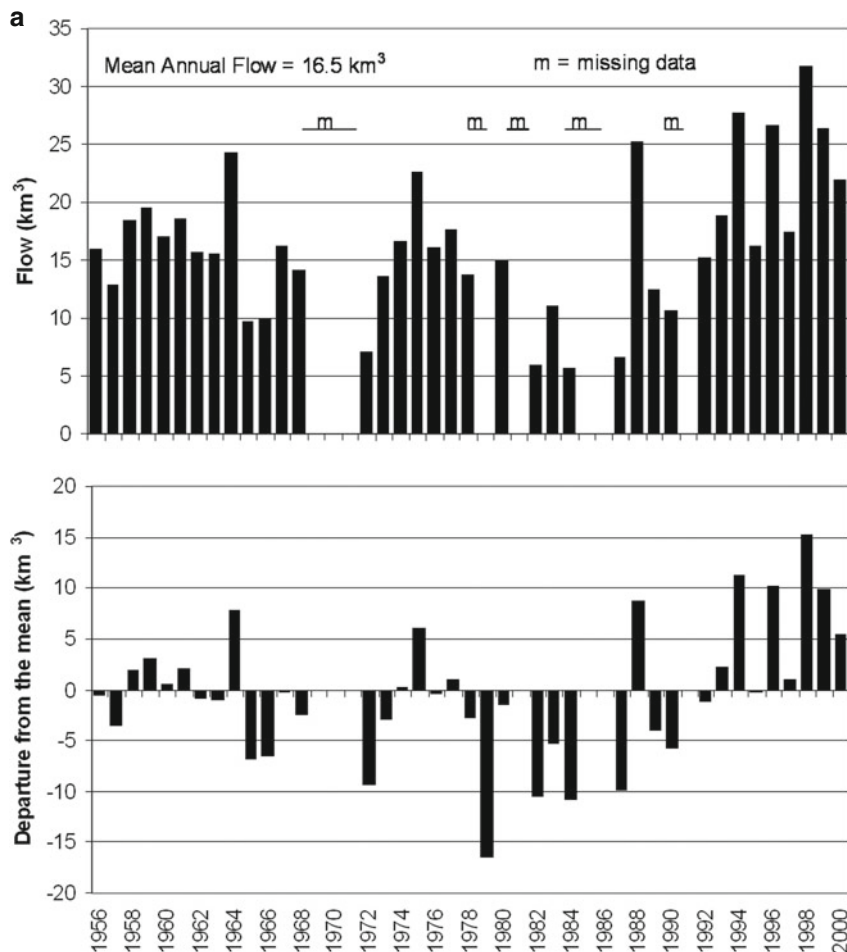


**Fig. 14.3** Flow and departure from the mean as measured on the Blue Nile River at two locations:  
**a** Kessie in Ethiopia and **b** El diem in Sudan

Temporal variations in sediment are investigated by looking at measurements made at various sediment measuring stations. Sediment concentrations in the Ethiopian highlands peak at 20,000 ppm (part per million) or mg/l at Addis Zemen in the Ribb River watershed in the month of July. At the border with Sudan, peak concentrations of 12,300 ppm were measured in 2003 and 2004. Figure 14.7, shows a typical sediment cumulative graph for the Ribb watershed based on average concentration and runoff. This distribution is typical of the Blue Nile as a whole. Typically sediment concentration in the Blue Nile peaks before that of both rainfall and runoff. The greatest concentration and yield of sediment occur during the early period and onset of the major (*kiremt*) rainy season.

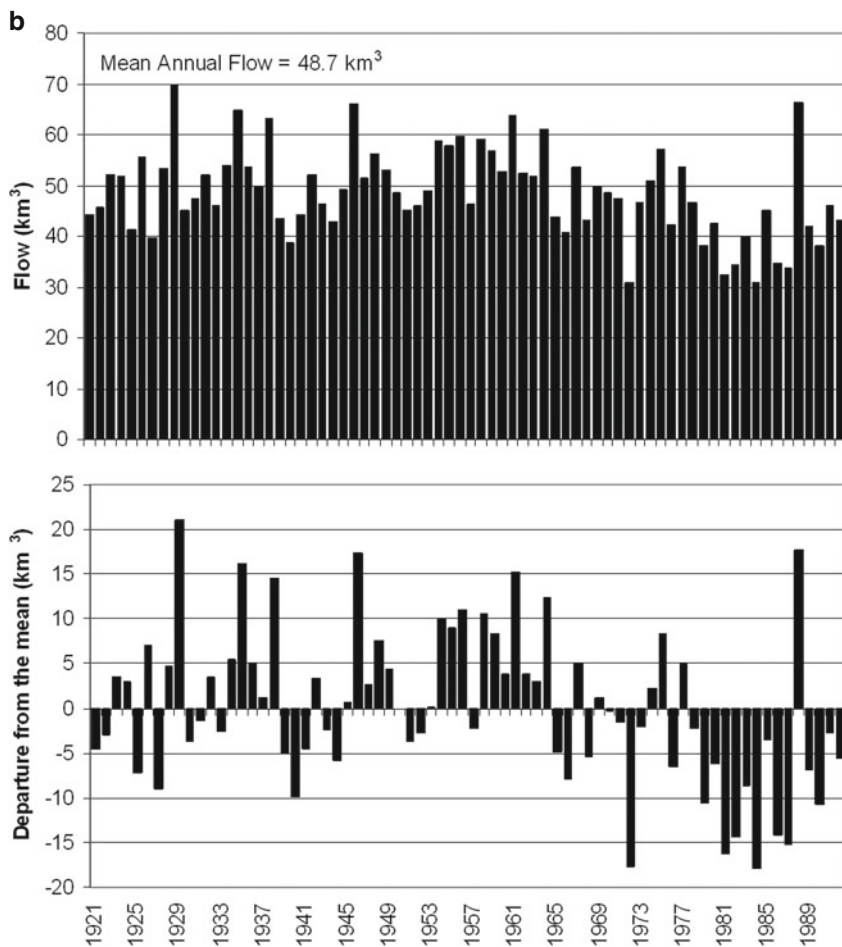
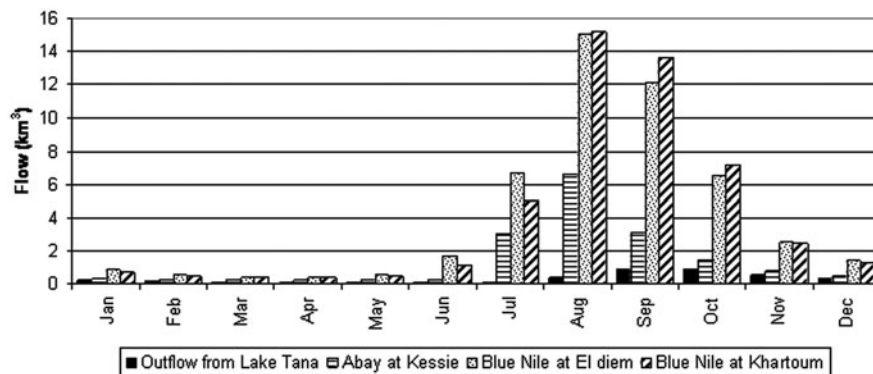


Fig. 14.3 (continued)

### 14.3 Water Demand, and Trends in the Blue Nile Basin

Ethiopia currently utilizes very little of the Blue Nile water, and to date only three relatively minor hydraulic structures have been constructed in the Ethiopian Blue Nile catchment. The Chara Chara weir and the Finchaa dam were built primarily to provide hydropower. The Koga dam was constructed to supply water for a small-holder irrigation scheme. Formal irrigation is in the Abbay is currently estimated to be less than 20,000 ha. However, this does not include the small-scale traditional schemes so is certainly an underestimate of the overall total.

In contrast to Ethiopia, Sudan utilizes significant volumes of Blue Nile water both for irrigation and for hydropower production. Both the Sennar and Roseries dams have been constructed on the main river. These provide hydropower (primarily for



**Fig. 14.4** Mean monthly flow ( $Mm^3$ ) at gauging stations located on the main stem of the Blue Nile

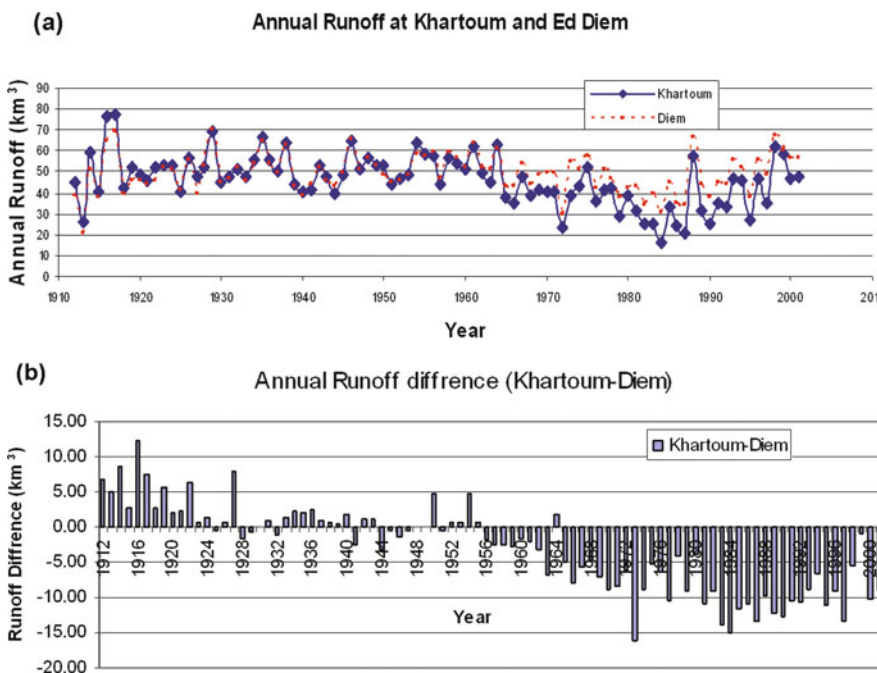


**Fig. 14.5** Runoff variability and change of runoff availability with water resources development in the Sudan (a) runoff at Ed Diem and Khartoum (b) annual runoff difference at Khartoum minus Ed Diem

Khartoum) as well as water for the huge Gezira irrigation scheme (882,000 ha) and other irrigation schemes. The estimate for the total currently irrigated area in the Blue Nile catchment of the Sudan is 1,305,000 ha. Approximately 90% of the water abstracted from the Blue Nile in Sudan is used for irrigation, with domestic, industry and other uses accounting for the remaining 10% (World Bank, 2000).

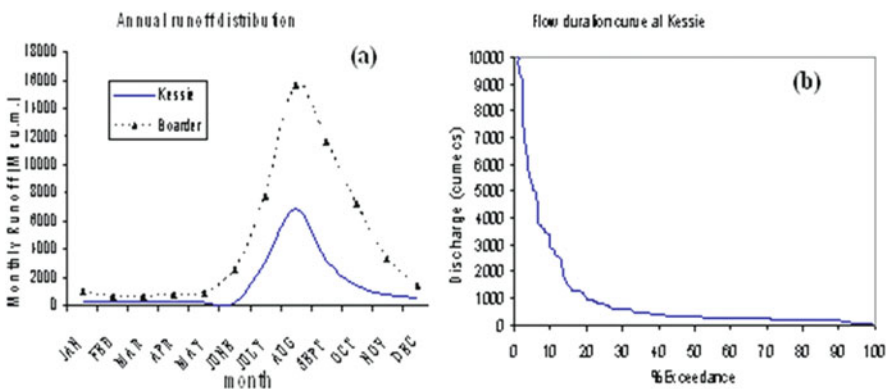
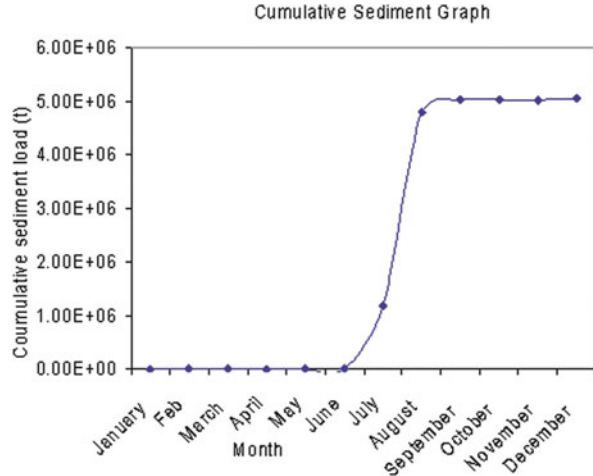


**Fig. 14.6** **a** Variations of runoff of Blue Nile (notice periods of large volume of flow) **b** flow duration curve

**Fig. 14.7** Over years averaged cumulative sediment load of typical watershed in the Blue Nile basin (Ribb Watershed, measured at Addis Zemen)



In Ethiopia, possible irrigation projects have been investigated over a number of years (e.g. Lahmeyer, 1962; USBR, 1964; JICA, 1977; EVDSA, 1980; HALCROW, 1982; WAPCOS, 1990; BCEOM, 1998). In the Abbay basin, the Master Plan identified a potential of about 2.5 millions ha of large and medium-scale irrigation schemes, of which 526,000 ha were deemed to be economically feasible (Fig. 14.8). That potential comprises 93 different irrigation schemes identified in more than 10 sub-basins. The mode of water supply for these projects varies from pumping from lakes (e.g. Lake Tana), run of river diversions and storage dams.

The Lake Tana and Beles sub-basins contain half of the total potential. Unlocking the Beles potential requires an intra-basin water transfer from the Tana sub-basin through a tunnel that can also be used for hydropower production. The hydropower

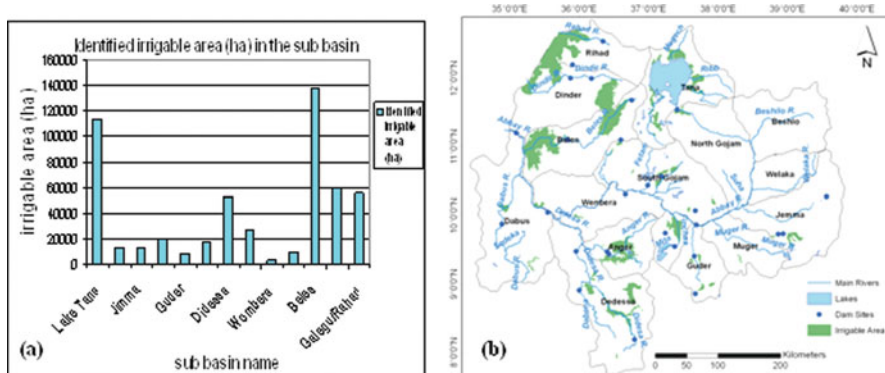


**Fig. 14.8** **a** distribution of the 526,000 ha irrigation potential and **b** location of irrigation potential in the Abbay basin

development (460 MW) has recently been completed and water is currently being diverted from Lake Tana to the Beles sub-basin.

The hydropower potential in the Blue Nile exceeds 12,000 MW, with major power stations on the main stem of the Blue Nile (i.e. Karadobi, Beke Abo, Mandaya and Border) having potential installed capacities of between 3,643 MW and 7,629 MW. These sites have been identified as priority sites, and feasibility studies are currently being undertaken.

An analysis of the water resources required to support the Ethiopian irrigation development, proposed in the Abbay River Master Plan (BCEOM, 1998), indicates that approximately 5,750 Mm<sup>3</sup> would be needed to irrigate between 370,000 and 440,000 ha. This represents approximately 11–12% of the mean annual flow in to Sudan.

In the Sudan, there is no planned hydropower development in the Blue Nile. However, additional new projects and extension of existing irrigation schemes are anticipated to add an additional 889,340 ha of irrigation. Based on current irrigation efficiencies in the Gezira and other schemes, the additional development in Sudan will require an average of 9,300 Mm<sup>3</sup> more water than is abstracted at present.

#### 14.4 Demand and Variability Management

As indicated above, the rainfall-runoff-sediment variability in the Blue Nile is considerable. Consequently, any meaningful development requires mechanisms for managing the hydrological variability.

For this chapter, 17 priority irrigation development sites with total irrigation area of 240,416 ha were identified. The irrigation water requirements were determined from BCEOM (1999) which specifies the crop water requirements for selected crops. Available water at the sites was estimated based on specific discharge, the

area-ratio method or using a rainfall runoff model, whichever provided the best estimates for a particular site, based on past studies. See Tesfahun (2007), Awulachew (2000), BCEOM (1999) and Rumenik (1996) for details of the methods.

ArcGIS with the integrated MIKE Basin modeling environment was used to simulate water demand and supply under two major scenarios. These were (1) without reservoirs, where only the natural stream flow is considered (2) with reservoirs, where characteristics of the reservoirs were obtained from master plan studies. Objective functions were established to prioritize drinking water supply, environmental flows, irrigation and hydropower development. The reservoir operation zones considered were flood control, normal operation, reduced operation and conservation operation.

In the simulation without reservoirs, it was found that, with the exception of the Dabus sub-basin, irrigation demand cannot be satisfied. In the simulation with reservoirs it was found that most irrigation demands can be satisfied. To satisfy the demand for 240,416 ha of irrigation the amount of water extracted from the reservoirs is 1,624 Mm<sup>3</sup>/year. This would result in an average annual flow reduction in the Abbay at the Sudan border of about 3.04%. This is also assumes that one cropping season could be fully satisfied by rainfall alone (i.e. there would be no need for supplemental irrigation during the rainy season). This compares with another recent study which estimated that the water required for the 220,416 ha of highest priority irrigation would be between 2,200 and 3,830 Mm<sup>3</sup> (Endale, 2006).

Without reservoirs the deficit in the various sub-basins is shown in Fig. 14.9. With the reservoirs as currently planned, there remains a small deficit of 173 Mm<sup>3</sup>.

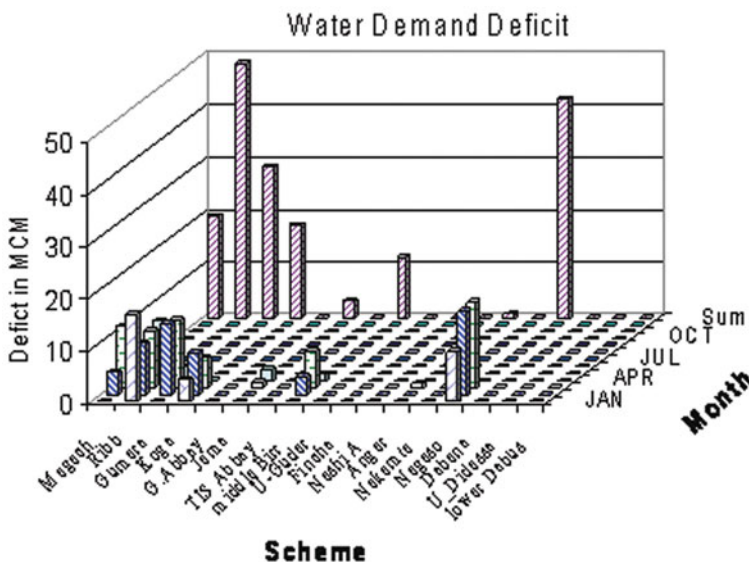


**Fig. 14.9** Water demand deficit in million cubic meter for runoff without storage by sub-basin and month for planned irrigation in Ethiopia part of Blue Nile, considering 240,416 ha priority developments

This deficit occurs at the sites of Negesso and some of Lake Tana Sub-basin sites; six sites in total.

It can be concluded that due to high rainfall and runoff variability substantive development of irrigation as planned is only possible with reservoirs. Furthermore, some of the currently planned reservoirs are not adequate to fully satisfy the irrigation water demand.

## 14.5 Conclusions

Temporal and spatial variability in rainfall, runoff and sediment in the Blue Nile is considerable. Rainfall, runoff and sediment vary seasonally with peaks occurring in the period mid-June to mid September. The highest sediment concentrations occur in July, before the peaks of rainfall and runoff which usually occur in August. Despite significant water resources availability on an annual basis, water resources development in the Ethiopian highlands has been very limited. However, pressure on water resources is likely to increase in the near future due to high population growth and increasing development-related water needs.

Because of the high variability, any meaningful development of the Blue Nile water resources requires provision of storage infrastructure. Current irrigation development in Ethiopia is insignificant. Future development of the full potential in the Blue Nile would result in total water abstraction of 5,000–6,000 Mm<sup>3</sup> (i.e. 10–12% of the mean annual flow at the Sudan border). However, the highest priority irrigation, which is most likely to be completed in the near to medium future, will only result in withdrawals of between 1,624 and 3,830 Mm<sup>3</sup>. The use of the water for further irrigation development in the Sudan may lead to an additional water withdrawal of 9,000–10,000 Mm<sup>3</sup>.

This sort of analysis, which provides quantitative insights into the needs and expectations of countries in the Nile Basin, can be used to avoid conflicts and to assist in the development of agreements on the extent of water resources development in each country. Cooperation between the countries is pre-requisite for equitable use of the water in a manner that contributes to the rapid socio-economic transformation so desired in the region.

**Acknowledgments** This chapter presents findings from the project Upstream-Downstream in the Blue Nile, a part of the CGIAR Challenge Program on Water and Food. The study was conducted with financial support of Challenge Program on Water and Food CPWF).

## References

- Ahmed AA (2006) Multipurpose development of the eastern Nile, one system inventory, ENTRO report, Sudan
- Beltrando G, Camberline P (1993) Interannual variability of rainfall in the eastern horn of Africa and indicators of atmospheric circulations. *Int J Climatol* 13:533–546
- BCEOM (1998) Abbay River basin integrated development master plan project. Report to Ministry of Water Resources, The Federal Democratic Republic of Ethiopia

Block P (2007) Integrated management of the Blue Nile basin in Ethiopia: hydropower and irrigation modeling. IFPRI discussion paper 07000. International Food Policy Research Institute, Washington, DC

Conway D (2000) The climate and hydrology of the Upper Blue Nile River. *Geogr J* 166(1):49–62

Endale YD (2006) Assessment of Water Demand for irrigation development in Abay Basin (A case of tributary development scenario). In: The Nile Development Forum (2006) proceeding. Addis Ababa, Ethiopia

Haile T (1988) Causes and characters of drought in Ethiopia. *Ethiop J Agric Sci* 10:1–2, 85–97

Hydrosult, Tecslult, DHV, Nile Consult, Comatax Nilotica and T & A Consulting (2006) Cooperative regional assessment (CRA) for watershed management. Transboundary analysis Abay-Blue Nile sub-basin. Report to Eastern Nile Technical Regional Office, Nile Basin Initiative

JICA (Japanese International Cooperation Agency) (1977) Feasibility report on power development at Lake Tana Region, Ethiopia

Johnson PA, Curtis PD (1994) Water balance of Blue Nile River basin in Ethiopia. *J Irrigat Drain Eng ASCE* 120(3):573–590

Nicholson S, Kim J (1997) The relationship of the ENSO to African rainfall. *Int J Climatol* 17: 117–135

Norconsult (2006) Karadobi Multipurpose project, pre-feasibility study. Report to Ministry of Water Resources, The Federal Democratic Republic of Ethiopia

Norplan, Norconsult and Lahmeyer International (2006) Karadobi multipurpose project pre-feasibility study. Project report to the Ministry of Water Resources, Federal Democratic Republic of Ethiopia

Seleshi Y, Demarée GR (1995) Rainfall variability in the Ethiopian and Eritrean highlands and its links with the southern Oscillation Index. *J Biogeogr* 22:945–952

Shanko D, Camberlin P (1998) The effects of the southwest Indian Ocean tropical cyclones on Ethiopian drought. *Int J Climatol* 18:1373–1388

Sutcliffe JV, Parks YP (1999) The hydrology of the Nile. IAHS Special Publication 5. IAHS, Wallingford, Oxfordshire

Tesfahun D (2007) Catchment water balance for Blue Nile River basin. MSc thesis, Arba Minch University

USBR (1964) Land and water resource of the Blue Nile basin, Ethiopia. Appendix V – power

WAPCOS (1990) Preliminary water resource development master plan for Ethiopia, vol III, annex – a hydrology and hydrogeology, vol V annex J – hydropower

Waterbury J (2002) The Nile basin: national determinants of collective action. Yale University

World Bank (2000) Sudan – options for the sustainable development of the Gezira scheme. World Bank sector report 20398, Washington DC

World Bank (2006) Ethiopia: managing water resources to maximize sustainable growth. World Bank Agriculture and Rural Development Department, Washington DC

# Chapter 15

## Livestock-Water Productivity in the Nile Basin: Solutions for Emerging Challenges

Tilahun Amede, Katrien Descheemaeker, Everisto Mapedza, Don Peden, Paulo van Breugel, Seleshi B. Awulachew, and Amare Haileslassie

**Abstract** The competition for water between different uses and users is increasing, particularly in the Nile basin where about 90% of the production systems comprise livestock. There is an ongoing debate on how to increase water productivity in these crop-livestock systems. This paper presents a comprehensive framework to provide policy guidance and promote action to improve returns from water investments through: (i) provision of sufficient watering points for livestock across the basin; (ii) improving water productivity through promoting water-saving technologies, ensuring system integration and control of transboundary flux of livestock diseases; and (iii) formulating participatory basin scale regulatory frameworks on water use and sharing. It also argues that improving water productivity through integrated technological, policy and institutional interventions offers an opportunity for smallholders in both upstream and downstream countries to adapt to climate and market risks.

**Keywords** Nile · Livestock · Water depletion · Interventions

### 15.1 Introduction

The Nile River Basin comprises ten riparian countries, occupies an area of about 3.3 million km<sup>2</sup> and receives an average annual rainfall of about 2,000 billion m<sup>3</sup>. It stretches over different geographical, climatological and topographical regions. Out of the 300 million people living in the Nile basin, about 160 million depend on the Nile River for their livelihoods (Appelgren et al., 2000). On average, 85% of the water is utilised for agricultural purposes and over 70% of the Nile population depends directly or indirectly on farming for their incomes and livelihoods

---

T. Amede (✉)

International Livestock Research Institute (ILRI), International Water Management Institute (IWMI) and Challenge Programme on Water for Food (CPWF), Addis Ababa, Ethiopia; International Livestock Research Institute (ILRI), Addis Ababa, Ethiopia  
e-mail: t.amede@cgiar.org

(Appelgren et al., 2000). One major characteristic of the basin is that livestock grazing is the dominant land use occupying about 60% of the total land areas while mixed crop-livestock systems cover about one third of the basin (Peden et al., 2009).

The competition for water between different uses and users in the Nile basin is increasing. Moreover, water utilization in the Nile basin has been unilateral, and there are no comprehensive inter-riparian legal or institutional modalities that can facilitate cooperative development and joint planning activities between upstream and downstream riparian areas. Possible and mutually beneficial options to the unilateral and conflicting water utilization approaches are not yet being seriously addressed (Arsano, 2007). The demand for water in domestic and industrial sectors is expected to substantially increase in the next decades (Postel, 2000). However, agriculture will remain the largest water user, accounting for ca. 75% of current human water use (Wallace, 2000). Major trade-offs are forecasted between agriculture and ecosystem services (e.g. Lemly et al., 2000), including trade-offs between alleviating poverty and increasing food security on the one hand and safeguarding ecosystems on the other hand (de Fraiture et al., 2007). With growing concerns about climate change, crop production for energy generation (the so-called bio-fuels) is also becoming more important in using more water. Moreover, lack of adequate upstream-downstream water utilization and management in the riparian countries have been challenged by cross-boundary challenges of excessive soil erosion and land degradation in upstream Ethiopia, flood and silt accumulation in the midstream Sudan and excessive water loss through evaporation in downstream Egypt (Arsano, 2007).

The ongoing challenges and the solutions to water scarcity are complicated by several challenges. There is a huge loss of water in various agricultural and non-agricultural systems in the Nile basin, which are associated with uncontrolled evaporation particularly in the extensive land use systems, water depletion through excessive run-off in the upstream countries, and water pollution due to excessive use of agro-chemicals in the downstream countries (Descheemaeker et al., 2009). Water management interventions at farm, landscape and higher scales are often poorly adopted and implemented, which leads to high social and environmental costs (Molden et al., 2007). Policies in the region are not giving priority to improved use and management of water, but serve the interest of getting the highest share of water for irrigation and hydropower stations. The absence of adequate and fair treaties and international arrangements dealing with shared water resources is likely to result in increasing water conflicts (Postel, 2000; Postel and Wolf, 2001), which will further undermine the future sustainable use of the water resources. In most cases, planning Nile water resources is commonly done nationally with no or little regard to the overall water resource balance along the watershed. However, consequences of environmental degradation and resource scarcity are not restricted to the national borders rather will inevitably affect riparian countries.

Climate change puts an extra pressure on sustainable water resources management (Molden et al., 2007), through probable increases in temperature, rainfall variability and occurrence of extreme events (IPCC, 2001). The still remaining uncertainty on the actual characteristics and the extent of climate change and on

its effects on water supply and agricultural production makes it difficult to develop the right adaptive measures (Bruinsma, 2003; Kurukulasuriya et al., 2006), particularly in the resource poor Nile basin countries. The globally increasing importance of the livestock sector is believed to be another important factor that may aggravate water scarcity and competition as livestock production systems are blamed for depleting, degrading and polluting enormous quantities of water (Steinfeld et al., 2006).

Also changing nutritional needs, driven by growing incomes and demographic transitions, result in rising needs for livestock products on a global scale (Speedy, 2003; Steinfeld et al., 2006). Over the last decades, demands for animal products increased two to three times faster in developing countries as compared to developed countries (Delgado, 2003). According to Peden et al. (2009), the annual growth in consumption and production of animal products was 2–4% in developing countries, while only 0.5% in developed countries. Delgado (2003) predicted a rise in meat production from 233 million Mt in 2,000–300 million Mt in 2,020 and in milk production from 568 to 700 million Mt over the same time span. Within the group of animal-derived products, the highest growth rates are achieved in poultry, pigs, eggs and milk production (Speedy, 2003).

Taking into account projected population and income growth, food demands are estimated to grow by 70–90% by 2050 (Molden et al., 2007), particularly due to increased demand for livestock products. Population growth, urbanization, economic growth, and flourishing markets all lead to increasing demands for animal products (Delgado, 2003; Costales et al., 2006; Steinfeld et al., 2006). The additional food required to feed the growing population would require an extra 5,000–6,000 km<sup>3</sup>/year of water, as compared to the 7,000 km<sup>3</sup>/year of water that is used globally today to produce food and fodder (Falkenmark, 2007). As a result, water demands by the agricultural sector will also increase, which calls for integrated approaches to improve livestock and water productivity. Moreover, with increasing demands for animal products, along with increasing global water scarcity and competition for water, there is a pressing need to increase livestock production, without depleting more water, and while safeguarding the environment. Improving water productivity in livestock production systems can benefit both the environment and people's livelihoods (Bossio, 2007; Cook et al., 2009).

### ***15.1.1 The Need for Improved Water Productivity***

The major concern in the basin is that water resources management was not top on the policy agenda up to very recently, particularly in the upstream countries. For instance, the Ethiopian national water policy document acknowledges that the water resources management in the country failed to bridge the spatial and temporal variability of the total annually available water. It also admits that poor performance in the nation's water development sector is the cause for its slow agricultural development and low crop productivity (Arsano, 2007).

Water productivity defined as the ratio of agricultural outputs to the amount of water consumed is a well-known concept that has been successfully used in crop sciences. Plant breeders and agronomists were applying principles of genetics and plant physiology to develop germ plasm adaptable to drought-prone regions and responsive to irrigation inputs. They have also identified phenotypic traits that could be used to identify appropriate inbred lines and gene pools to extract the desired genes and transfer them to the crop ideotypes and preferred varieties. These traits could be phenotypic, those including stay-green, early maturity, harvest index and root depth to mention few, or physiological, those including stomatal regulation, osmotic adjustment and developmental plasticity (Amede, 1998). Recent discussion on water productivity (WP) in agriculture highlights livestock as a key area for WP improvement (cf. Molden et al., 2007). Peden et al. (2007, 2009) define livestock water productivity (LWP) as the ratio of net beneficial livestock-related products and services to the water depleted in producing them. The concept acknowledges the importance of competing uses of water but focuses on livestock-water interaction. Livestock water productivity is a systems concept that would require an understanding and application of integrated approaches (Amede et al., 2009a).

This chapter focuses on water productivity in mixed crop-livestock systems of the Nile basin countries, with a major emphasis on Ethiopia, Sudan and Uganda. Crop-livestock systems are defined as those in which crop and livestock production activities are managed by the same economic entity, such as a household, with animal inputs (for example, manure or draft power) being used in crop production and crop inputs (for example, residues or forage) being used in livestock production (Williams et al., 2000). In this paper, we treat LWP as an innovation, and consider in what ways it may be introduced and/or developed amongst the crop-livestock agricultural systems by drawing on successful examples of change from this area. In the first part of this paper, we introduce relevant tenets of livestock-water literature; in the second part we display the major hydrological, governance and local characteristics of the three countries and its implication on water productivity. In the third section we present selected technologies that would improve water productivity at farm and higher scales and in the final section, we draw implications of these various components on the economic and environmental benefits of the basin.

## 15.2 The Role of Livestock in the Nile Basin

### 15.2.1 *The Livestock-Based Systems*

Livestock production contributes about 40% of the gross value of agricultural production worldwide, while this is about 30% in developing countries, 37% in East Africa and 25% in Southern Africa (Parthasarathy et al., 2005). The often used classification system developed by Seré and Steinfeld (1996) and slightly modified by Thornton et al. (2002) differentiates the farming systems with livestock into

4 broad groups, including (1) rainfed mixed systems, (2) irrigated mixed systems, (3) landless or industrial systems and (4) pastoral, rangeland-based grazing systems. These groups are further subdivided according to agro-ecological characteristics. Mixed crop-livestock systems are widespread in semi-arid and sub-humid regions in the tropics (Steinfeld et al., 2006) and with increasing population density and land scarcity, crop and livestock activities tend to integrate more intensively (Thornton and Herrero, 2001, Parthasarathy et al., 2005). These classifications also hold true for the majority of the Nile basin countries.

The most important livestock production systems in the Nile basin comprise the pastoral rangeland systems (56% of the Nile basin) and the mixed rainfed crop-livestock systems in arid, humid and temperate highland climates (20, 5 and 8% of the Nile basin area respectively) (Herrero et al., 2008; van Breugel et al., 2009 Recommendation domains and key aspects of livestock-water productivity in the Nile basin. ILRI working paper, unpublished). Livestock densities in the Basin vary widely between production systems. The highest cattle and small ruminant densities of more than 50 TLU km<sup>-2</sup> are found in the mixed irrigated systems, followed by the mixed rainfed systems with densities ranging between 30 and 44 TLU km<sup>-2</sup>. The rangeland systems have densities between 9 and 19 TLU km<sup>-2</sup>, and the lowest densities are found in the hyperarid grazing systems with 2 TLU km<sup>-2</sup> (Wint and Robinson, 2007; Herrero et al., 2008). In Sudan, very high livestock densities are recorded around the irrigation schemes of the White Nile and Aj Jazira and west of the Sudd. In Ethiopia, the mixed crop-livestock systems in the highlands south of Lake Tana, are characterized by high livestock densities. Around Lake Victoria, livestock densities are very high in the mixed farming systems in Kenya, in the pastoral and mixed farming systems in Tanzania and in the mixed farming systems in Burundi, Rwanda and Uganda (Fig. 15.1).

On the other hand, livestock densities are low in the vast area of hyperarid rangelands north of the agricultural belt in Sudan, due to the harsh conditions and the low availability of feed and water. In the rest of the basin, pockets with low livestock density in spite of sufficient feed availability are characterized by inadequate livestock drinking water (Junqoley district and the Western Bahr Al Gazal and Western Equatoria districts in Sudan, the areas north-west of Lake Tana in Ethiopia and the mixed farming systems in Uganda) or the occurrence of diseases like trypanosomosis (the area north-west of Lake Victoria, near the borders of Uganda and DR Congo in Sudan and the western slopes of the Ethiopian highlands) (van Breugel et al., 2009, unpublished).

### **15.2.2 Livestock Products and Services**

Livestock have a great economic and social importance for the majority of the Nile basin population. It provides many different products and services to people (Thornton and Herrero, 2001; ILRI, 2002; Peden et al., 2007). Livestock have an important economic role as they are major sources of income and wealth in the

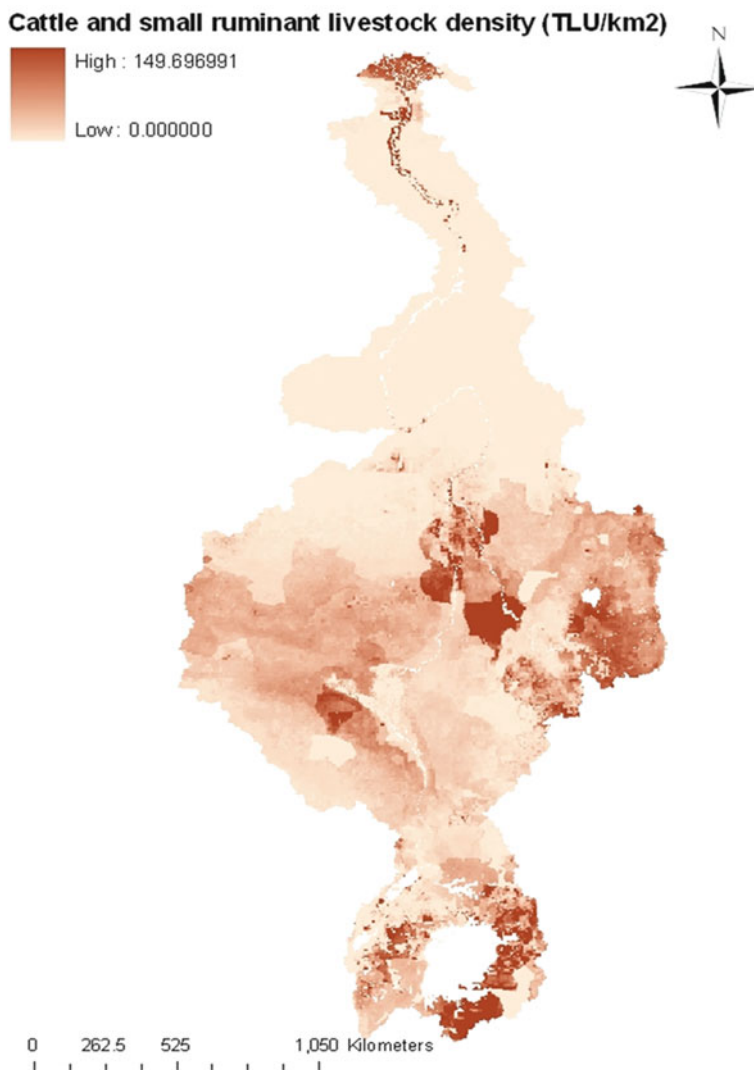


**Fig. 15.1** Cattle and small ruminant combined livestock density in the Nile basin. Source: Gridded livestock of the world (Wint and Robinson, 2007)

basin. Within agriculture, the livestock sub-sector contributes up to 30% of the GDP involving a majority of the rural population. About 15% of farmers' income in mixed systems and 80% in agropastoral systems come from livestock and livestock products. Similarly, in other SSA countries, e.g. Botswana Livestock contributes 88% of the total agricultural output while in Chad livestock makes up over one third of exports. Hides and skins make up over 10% of the export earnings in Burkina Faso, Eritrea and Ethiopia.

The consumption of animal products can alleviate nutrition problems, which are still widespread in the basin and secure a better child physical and mental development (Delgado, 2003; Speedy, 2003). Besides the obvious products like meat, milk, and eggs, satisfying the human nutritional requirements, livestock also provide energy in the form of draught power for land preparation and threshing, transport facilities and manure for fuel. Manure fulfils also another important role through nutrient cycling between and within farms, which enabled the continual use of farm land in the small holder farms. Animals also assume various socio-cultural roles (ILRI, 2002). For instance in the Ethiopian highlands, Oxen exhibit locally highly valuable outputs among the herd thanks to their draught power supply. Farmers who own oxen can plough on time to capture soil moisture and runoff and plant early, which enables crops to escape late season drought. Other farm practices like weeding and thinning is also done by oxen / horses, releasing a huge amount of labour for other activities. On the other hand, dairy cows in Kenya are the most important income generating enterprises.

Livestock productivity is generally low in the basin. The causing factors differ across locations and systems, but generally include climate variability, high mortality rates, inadequate feed availability and quality and poor market access. The more intensive and market-oriented systems in the floodplains and irrigated areas in Egypt and some pockets in Sudan and Kenya are the only exceptions. However, if besides milk and meat production, the other livestock benefits, like draught power, manure, insurance, etc. would be taken into account; livestock productivity would be significantly higher or comparable to crop productivity in monetary terms (Haileslassie et al., 2009).

### **15.2.3 Livestock-Water Nexus**

Animals derive their water from three sources (McGregor, 2004 cited in Peden et al., 2007): water directly consumed by drinking, water consumption through the feed and water formed during the metabolism of feed and body tissues. The metabolic water is produced as a consequence of stress through loss of body weight. For instance, a goat losing one kg of body weight per week will generate about 139 ml of metabolic water per day (Teixeira et al., 2006). The amount of drinking water used per animal varies with species, dry matter intake, composition of feed, water content of the feed, live weight of the animal, level of milk and meat production, physiological status of the animal and the climate in which the livestock is managed (Gigar-Reverdin and Gihad, 1991). Goats and sheep are regarded as having a more efficient water metabolism than large ruminants (Wilson, 2007). Moreover, livestock systems depending on grain-based feed, as it is the case in the developed world, are more water intensive than systems which rely on crop-residues and pasture lands as it is the case in SSA and SA. Livestock systems dominated by small ruminants are also found to be more water efficient than those with large ruminants and equines (Gigar-Reverdin and Gihad, 1991).

Although water for livestock drinking and servicing might be the most obvious water use in livestock production systems, it constitutes only a minor part of the total water consumption (Peden et al., 2007). There are many ways in which livestock affect water use across a landscape, but the two key areas are through the feed that they consume, and the damage they can potentially cause to a landscape's hydrology (Amede et al., 2009a). The amount of water transpired to produce animal feed accounts for more than 95% of the total water used by livestock (Singh et al., 2004; Peden et al., 2009). About 450 m<sup>3</sup> of water is required annually to produce the feed needed to maintain one Tropical Livestock Unit (TLU: measured at 250 kg live weight). When animals are growing, working, stressed or lactating, they use even more. Indeed, the complexity and diversity of livestock production systems create great uncertainty regarding the actual amounts of water used by livestock (Peden et al., 2007).

The impact of livestock keeping on water resources at farm, watershed and landscape scales in SSA has been rarely quantified. The impact of high livestock densities on a landscape are also thought to affect its hydrology profoundly, causing erosion of varying intensity, widespread degradation of the vegetative cover and other damage. The linear relationship between stocking densities and erosion, "desertification" and other landscape damage is frequently contested – see, for example, Rowntree et al., 2004. In one study, Mwendera et al. (1997) reported that high grazing pressure significantly increased seasonal run-off and decreased water infiltration, the effect being much more than the effect of slopes alone. This result is particularly relevant for the context of the Nile basin highlands as the livestock is kept in the upper slopes during the rainy season as the downstream valley bottoms and flat fields are covered by annual crops. Again, there is immense variability in how and where high livestock densities affect landscape hydrology, but a key area for concern is damage to landscapes surrounding livestock water points, and underutilized fodder in landscapes away from such water sources.

### 15.3 Characteristics of Livestock-Water Schemes in the Nile Basin

In a recent paper, Amede et al. (2009a) presented a conceptual framework for LWP innovation system, which draws on broad drivers of technological, institutional and policy innovations. Improving LWP includes several challenges, located on different fronts and usually not straightforward to meet (Descheemaker et al., 2009). First of all, given the growing water scarcity and the rising demands for animal products, appropriate water allocation is needed in order to both satisfy these demands and at the same time safeguard environmental services of ecosystems. As the latter also largely depend on water availability, meeting these competing demands is very challenging and raising the water productivity of livestock production systems only will not be sufficient (Bouman, 2007). Intensification and vertical integration of

different components in the product chain usually lead to higher productivities, but also tends to marginalize the poor (Peden et al., 2009). In the following sections we display the livestock hydrology of the basin, the governance structures of Ethiopia, Uganda and the Sudan from the perspectives of livestock-water and how it affects water productivity in these countries.

### ***15.3.1 Livestock Hydrology in the Nile Basin***

Rainfall in the Nile basin is highly variable in amount and distribution, with annual precipitation ranging from practically zero in the desert areas to more than 2,000 mm in the mountainous areas in the south and east (Fig. 15.2). Moving south to north, humid climates supporting rainforests change to less humid and semi-arid climates with a variety of savannah and grassland vegetations, to arid climates, supporting practically no vegetation (Moustafa and Gichuki, 2003). The pattern of potential ET is approximately the inverse of that for rainfall. Potential ET is relatively low in the mountains and gradually increases as one move northwards. Low levels of humidity and long hours of sunshine in the northern desert areas result in potential ET values of up to 3,000 mm/year (Moustafa and Gichuki, 2003). Also runoff volumes vary a lot within the basin with the highest values (up to 1,600 mm/year) recorded in the Ethiopian highlands and in the Kenyan highlands east of Lake Victoria. Other high runoff areas are found in the mountainous areas of Rwanda and Burundi and south west Sudan (data not presented).

Based on remote sensing analyses, earlier work suggested 15 land and water use classes for the Nile basin, including natural land cover, managed land use and managed water use (Mohamed, 2009, Water budgets of the Nile basin, IWMI, unpublished). For each of these classes, rainfall, actual evaporation and transpiration and biomass production were determined. Looking at the Nile sub-basins and aggregating all land uses within them, actual evapotranspiration (ET) ranges from 45 mm/year in the el Allaqi sub-basin to 1,409 mm/year in the Lake Albert sub-basin (1,760 mm is for Lake Nasser) (FAO, 2000). For the same sub-basins, applying the water balance allows to calculate the actual outflow (precipitation + inflow – actual ET – drainage) from the basin. In areas with large irrigation schemes, outflow values are negative as actual ET is higher than precipitation and inflow together. Very high positive values for outflow are recorded for sub-basins along the White and the Blue Nile with high inflow of water from upstream and low values of depleted water for production (FAO, 2000). At the overall basin scale, results indicate that the major part of the Nile water is consumed (98% or 1,716 km<sup>3</sup> of water/year), mainly by natural land cover (1,458 km<sup>3</sup> of water/year) and managed land uses (189 km<sup>3</sup> of water/year), which comprise beneficial (1,305 km<sup>3</sup> of water/year) and non-beneficial uses (411 km<sup>3</sup> of water/year) (Mohamed, 2009, unpublished; van Breugel et al., 2009, unpublished). Biomass production in the Nile basin logically follows the actual ET pattern, as biomass production is directly related to transpiration.

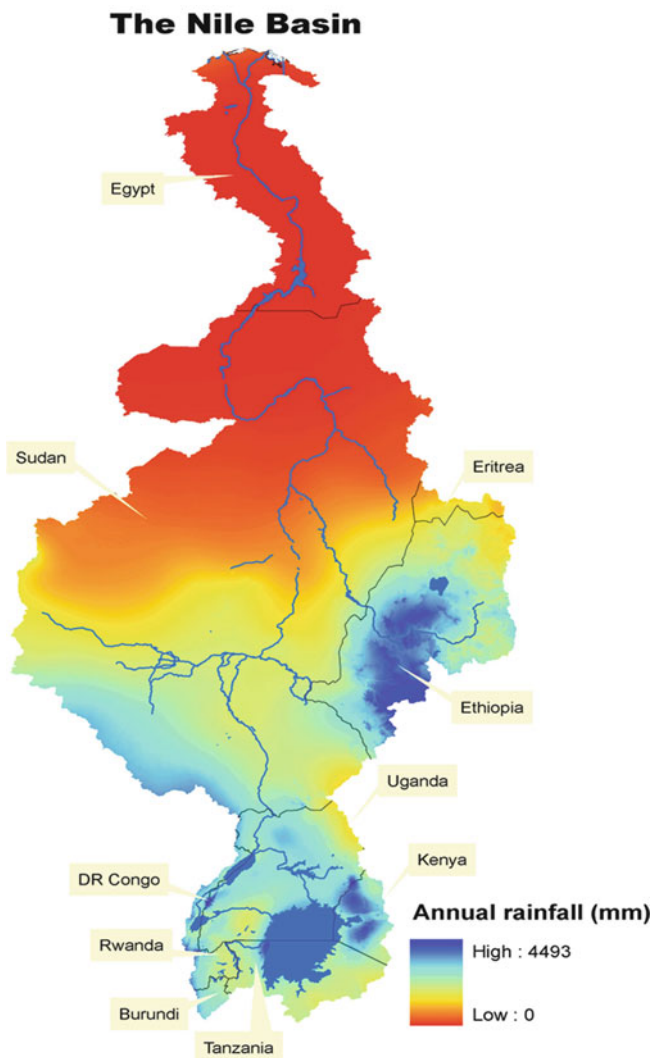


**Fig. 15.2** Annual rainfall distribution in the Nile basin

Livestock water consumption is quite variable between livestock production systems and animal types. For cattle, annual water requirements vary from 1,300 to 2,600 m<sup>3</sup>/year/TLU in mixed rainfed systems to 3,300–4,200 m<sup>3</sup>/year/TLU in mixed irrigated systems and 1,900–1,320 m<sup>3</sup>/year/TLU in the pastoral systems (Fig. 15.3). For small ruminants, the water requirements per TLU are higher as compared to cattle in each of the production systems (van Breugel et al., 2009, unpublished). Considering the spatial variability of livestock water requirements at basin scale, it is clear that there is a strong correlation with livestock density.

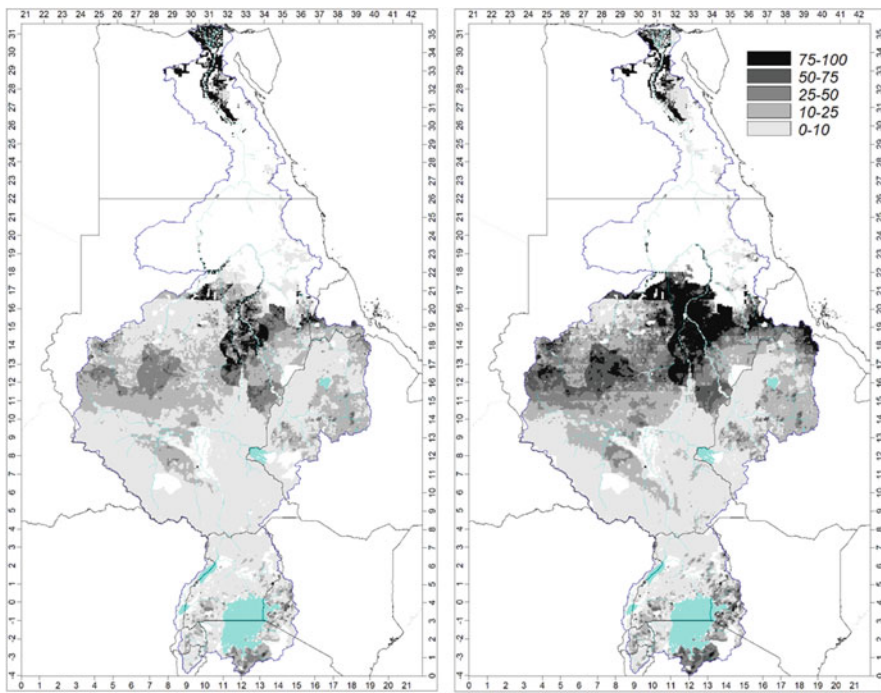


**Fig. 15.3** *Left:* Total annual livestock water use expressed as percentage of the total annual evapotranspiration. Note that the areas with percentages >100% are irrigation areas. *Right:* The same but assuming water available for AET equal to the rainfall in the historical lowest rainfall year. Source: van Breugel et al. (2009, unpublished)

Figure 15.3 presenting the ratio of livestock water requirements to actual ET (van Breugel et al., 2009, unpublished) suggests areas in deficit, where the requirements are much higher than the actual ET. These areas are predominantly located in the Nile Delta, along the Nile River in Egypt and in the agricultural belt in Sudan. Smaller pockets of high ratios are found in North Ethiopia, areas south east of Lake Tana, and along Lake Victoria in Kenya and Tanzania. On the other hand, where the ratio is low, water requirements are lower than actual ET, which implies that there are underutilized feed resources due to low livestock densities.

In the mixed crop-livestock systems of the basin, large amounts of water are saved by the use of crop residues as animal feed as the water used for growing crops is already accounted for by the crop enterprises. Contrastingly, some irrigation schemes like the White Nile and Aj Jazira districts in Sudan are characterized by very low livestock water productivity values (van Breugel et al., 2009, unpublished). Among other causes, the inadequate integration of crop and livestock production and inadequate provision of drinking points might create hotspots as well. Not only because livestock loose a lot of energy by walking to these points, but also because the concentration of livestock around a few drinking points leads to degradation of

land, vegetation and the water sources itself. Van Breugel et al. (2009, unpublished) indicated that from the Nile basin countries, Sudan has the largest areas where drinking water availability is a problem, followed by Ethiopia. Uganda exemplifies a much better situation where drinking points are all within a 5–10 km radius.

Areas of concern include those Nile basin areas where the current livestock density in terms of livestock water requirements is higher than the actual ET. In order to avoid permanent and irreversible degradation in these areas, either livestock densities have to be reduced, access to additional watering sources developed and/or water productivity of the vegetation and crops has to be increased. For instance, the Ethiopian highlands with high rainfall and accentuated topography, are prone to erosion and high runoff, which is exacerbated by high livestock grazing pressure. Besides the areas with high runoff, underutilized hydrological potential is manifested where water storage is inadequate.

### ***15.3.2 Livestock-Water Governance in the Basin***

As observed by Norse and Tschirley (2000), policy makers in the basin didn't necessarily know what kind of information they can reasonably expect or ask for from the R&D community to improve crop-livestock productivity. For example, the majority of political leaders and policy-makers in Uganda were not well informed about the existing byelaws and NRM policies, their regulations and implementation mechanisms, and the process of formulating byelaws (Sanginga, 2006). Thus, proactive role was essential in assessing the information needs of policy makers and develop effective communication strategies for guiding and informing debate and fostering public understanding of the policy process that would enable improved livestock and crop production at farm, landscape and higher levels.

A review on the nature, functions and gaps of organizations, policies and institutions related to Livestock-water in the three riparian countries viz. Ethiopia, Sudan and Uganda indicated that the organizational set up affecting livestock-water stretches from national level policy/strategy-making ministerial offices to local micro-planning and implementing offices (Amede et al., 2009b). Despite its contribution in enhancing economic and social well-being in the basin, livestock remains a subsidiary sector and all possible interventions, policies and plans are subordinated with other sectors such as water and agriculture (dominantly crops). In addition, policies for livestock development are poorly provided, biased towards commercialization and have very little to do with small holder farming. Livestock research in general and livestock-water interaction in particular are yet at rudimentary state in country level policy researches. Improving livestock water productivity is barely mentioned in national livestock policies at all. The existing livestock/animal feed policies lack in-depth analysis of the steps that have to be taken to improve efficiency of livestock-water use.

The concept of national versus local is the major difference among the three countries. In Ethiopia and Sudan, local organizations are responsible to sub-national (regional) organizations that, except for few strategic national issues, are relatively

autonomous to plan and execute their own priorities. The local organizations in these two countries are more of implementing partners to their respective regional superiors. In the case of livestock, the policies initiated in all the three countries are national in nature and lack local input in their build up. The three countries have Non-governmental Organizations (NGOs) and Community Based Organizations (CBOs) directly and indirectly working in livestock and water related issues with varied intensity. Traditional institutions are particularly active in resolving livestock and water related conflicts arising from competing land and water uses by different clans and ethnic groups.

In the case-countries, organizations related to livestock are either inadequately funded and/or politically weak compared to other sectors such as infrastructure development or food security. As a result, policies/provisions made at national level are poorly implemented and weekly monitored at local levels. On the other hand, organizations related with livestock but dealing with broader issue such as irrigation, food security and resources management are well formulated with clear mandate and detailed terms of reference but mostly each organization pursues its own mandate with minimum coordination. There exists weak institutional arrangement and lack of requisite in human, financial and material resources as well as viable and clear administrative rules and regulations to appreciate the positive and negative roles of livestock in the basin hydrology and economy. This gap is more vivid at the local and grass roots levels, where policy elements are carried out with lack of clear understanding of local needs and with inadequate, fragmented and thinly distributed resources.

Albeit differences from one another, institutions affecting the basic inputs for livestock production such as access to feed, water and insurance receive low attention. Secured access to these inputs is one of the key incentives that enable poor and vulnerable livestock holders to positively respond to market needs. There exists limited coordination role in guiding local organizations towards integrated and sustainable water efficient livestock development. The key improvement areas pertaining to livestock-water governance strategies in the three countries could be as follows:

1. The majority of the population in the basin is engaged in systems where livestock plays a critical economic and environmental role. In the rangelands, where the potential for rainfed or irrigated agriculture is limited, livestock form the basic means of subsistence and livelihood for the people. However, the overall awareness of policy makers and planners as well as donors as to the role of livestock and their keepers in poverty alleviation and sustainable resources management appear to be modest. Participatory policy development (one that allows consultation with livestock keepers), with an intent to forge sound policies for guiding/leading the livestock water improvement, has therefore to be in place. There is therefore a need to raise the awareness of policy makers so that the livestock-water issues get the attention it deserves.
2. In the three countries studied, policies related to livestock and water are not adequate and whenever they exist, they are not supplemented with efficient

and well-authorized institutions to enforce designated policies. This means that when policies are designed, an adequate effort has to be paid to establish sound and efficient institutions that can facilitate the implementation of those policies. It is also essential that the institutions be supplemented with sufficient budget and power as well as mandates. This is because, there appear to be too much “organizations” that require vertical and horizontal linkages (particularly in Ethiopia) but with mixed mandates and without proper means of communications. Building an appropriate legal and regulatory framework of the livestock-water sector with measures to encourage the emergence of CBOs and civil society including actions to better equip them in implementing policies on the ground also remains one of the priorities.

3. The tendency observed in the three countries is that the issue of export-oriented livestock management is in a “kick-start” and is being intermittently mentioned in policy arenas. To promote the livestock sector in a sustainable manner, national policies/strategies need to be wary of not giving “the wrong incentives” that may relieve current shortage but end up putting pressure on land and water. Policies promoting cost-sharing arrangements (e.g. water pricing) are commonly effective. Responding to recurrent and more appealing needs such as strategic distribution of watering points for pastoralists need to be reviewed in light of their long term impact on land degradation, climate change and managing vulnerability. Concentration of too many herds of livestock around small watering points could escalate conflicts, land degradation and ultimately reduce resources use efficiency.
4. Research and development interventions related to improved management of livestock and water need to be disseminated to end users timely and with uncompromised standards. Improving access to information exchange, particularly a system that facilitates international/regional institutions to disseminate improved practices to local institutions and one that allows the former to access follow-up information from the later on regular basis has to be in place.
5. Evidences show that good access to markets and reasonable as well as efficient taxation systems are not in place in the three countries studied (Amede et al., 2009b). Transportation of livestock and their products to market outlets takes too much time which compromises the quality of items and their market returns. In addition, taxes are levied at different points (e.g. upto eight times in the Sudan) and are in most cases excessive. Measures to encourage livestock productivity such as by avoiding prohibitive tax system and improving local and international marketing outlet have therefore to be carefully crafted.

### ***15.3.3 Livestock-Water-Gender Nexus in the Basin***

Gender is a central organizing principle of societies and often governs the processes of production and reproduction, consumption and distribution. Gender roles are the “social definition” of women and men, and vary among different

societies and cultures, classes and ages, and during different periods in history (Mapedza et al., 2008a). They vary greatly across the Nile Basin and Sub-Saharan Africa at large. Gender-specific roles and responsibilities are often conditioned by household structure, access to resources, political stability and ecological conditions. Gender research in livestock-water is therefore essential in poverty reduction and sustainability of development interventions.

As part of the BMZ-supported project on “Improving water productivity in SSA” and Challenge Program on Water and Food Project (CP 37), a survey of key informants on the relative contribution and benefits accruing to men and women in livestock and related farming activities was undertaken in the three case study countries of Ethiopia, Sudan and Uganda (Mapedza et al., 2008b). Accordingly men have more access and the corresponding benefits for the water resources in Ethiopia and Uganda. In Sudan, perceived access to agricultural water is equal (50% for men and 50% for women) with the benefits accruing from water also equally shared between men and women. The benefits from rivers included domestic uses, livestock watering and crop irrigation.

Access to land and water resources is also tilted in the favor of men. It is only in Ethiopia where women get a similar proportion of benefits as they have access to the land resources. In the remaining case studies of Uganda and Sudan, women even get fewer benefits from land resources which favor male access. Another set of research done by ILRI and IWMI, drawn upon the Gendered Sustainable Livelihood Framework (GSLF) van Hoeve and van Koppen (2006) attempted to analyze the overall labor requirements of new livestock-water interventions, disaggregated along gender lines. For instance, if a new “cut and carry” scheme is introduced for livestock keeping, depending on the specific circumstances, it might result in increased labor requirements for women through collecting fodder for the livestock. If cattle herding was previously the responsibility of boys and men, the result is an increased workload for the women (cf. van Hoeve and van Koppen, 2006). Such extra labor requirements have also to be further juxtaposed on the different types of households. *De jure* female headed households tend to have labor constraints for their agricultural activities when compared with *de facto* female headed households where the male heads of household are based in urban areas and tend to send remittances which can then be used to hire extra labor. Male headed households tend to have more labor reserve than the two types of female headed households (cf. ICRISAT, 2007; van Hoeve and van Koppen, 2006). It is however, important that the intra-household assessments also look at the impact of women labor contribution in male headed households. Other studies have demonstrated that in some irrigated areas in the Awash River Basin of Ethiopia women in male headed households were worse off than women who headed their own households and had access to irrigation plots (Aredo et al., 2006).

Often women and children are contributing most of the labor requirements for livestock and water management, but the income distribution does not reflect that contribution (Mapedza et al., 2008b). The access and control of benefits terrain is also shaped by the political, economic and institutional contexts of the respective countries. Laws and rules on livestock and land tenure will directly and indirectly

impinge on who has access and who benefits from the improved livestock water productivity. As presented above, Institutions - from local to community level - and how they are nested to national level, also has an important implication in access and control of benefits by both women and men.

In general, LWP needs to be viewed using a gendered lens that will enable an assessment of the differential impact of the proposed interventions on both poor women and men. There are concerns that rural development in sub-Saharan Africa has often only improved the well being of well-off male-headed households, leaving poor females and males worse off (van Hoeve and van Koppen, 2006).

## 15.4 Technologies Effecting Water Productivity

### 15.4.1 “In Situ Water Conservation” for Improving Water Productivity

Water conservation, which involves decreasing the unproductive water losses from a system while increasing the system’s water use efficiency, has the potential to increase water productivity. Water conservation is often achieved through integrated interventions, which simultaneously lead to erosion control, as these are conceived to break the water flow energy and facilitate infiltration of the runoff water. Within soil and water conservation measures (WOCAT, 2007, for an overview) a distinction can be made between physical structures on the one hand and vegetation management on the other hand.

One key intervention to overcome the problems of low water availability in semi-arid areas is the use of different water harvesting structures that fit with the existing socio-economic situations. Excess runoff can be temporarily stored in the soils or micro-basin water harvesting structures and diverted to livestock drinking and plant growth in various forms. These structures retain excess soil moisture, increase the time for infiltration and encourage crop growth. In addition, they reduce sediment load and minimize erosion effects on downstream sites (Deribe et al., 2009). The impacts of different types of micro-basin water harvesting structures have been tested and found to be successful in improving seedling survival and crop yield in countries like Kenya (Mugwe et al., 2001) and northern Ethiopia (Deribe et al., 2009). Similarly, Zaï is a traditional water conservation practice developed in Burkina Faso and commonly used in the Sudano-Sahelian areas for rehabilitating eroded and completely crusted fields, where the infiltration is too low to sustain vegetation (Roose et al., 1999). The pits combine water harvesting and targeted application of organic amendments (Fatondji et al., 2007). Zaï pits, typically comprise holes dug during the dry season and then filled with handfuls of dry dung (corresponding to about 1–3 t ha<sup>-1</sup> of dry organic matter). These are then seeded with approximately a dozen cereal seeds after the first storms. They have been shown to alleviate the adverse effects of dry spells and result in a three to fourfold increase in grain yield compared to

flat planting, mainly as a consequence of in situ water conservation (Fatondji et al., 2007). A study conducted with the objectives of evaluating the effects of Zai pits on water productivity of Potato (*S. tuberosum*) and beans (*P. vulgaris*) in Southern Ethiopia, in combination with using different sources of fertilizers (Amede et al., 2011) revealed that Zai pits improve the water productivity of crops by a factor of three, which is in agreement with Fatondji et al. (2007). The yield gains in Zai were not only due to increased nutrient supply but also caused by improved water availability at the critical growth stages.

In a recent paper, Deribe et al. (2009) reported that in degraded landscapes of northern Ethiopia where growth of vegetation is becoming very slow due to land degradation, micro basins, particularly trenches and eye-brow treatments were effective in promoting seedling survival and growth of acacia seedlings. The effect was due to water saving of these micro-basins and minimizing runoff effects as the water from upstream was flowing towards the pits.

#### ***15.4.2 Effects of Area Exclosures on Water Productivity: The Case of Lenche Dima, Ethiopia***

Land degradation is acknowledged as a major challenge in improving land and water productivity of the Ethiopian highlands. The low return of crop, livestock, fuel and other enterprises is partly associated with low soil fertility and poor soil water holding capacity. Similarly, the major problems and production constraints of the Lenche Dima watershed in Northern Ethiopia is land degradation reflected in the form of recurrent water scarcity, low livestock and crop productivity, soil erosion and shortage of livestock feed and fuel. As part of a USAID funded development project implementing integrated watershed management, exclosures (Fig. 15.4) were established in the watershed in 2003 with the overall aim of rehabilitating degraded hill slopes (Benjamin et al., 2008).



**Fig. 15.4** Degraded open access grazing land (left) and protected exclosures, 3 years after closing (right)

From 2004 to 2007, degraded hillslopes, ranging in size from 20 to 100 ha, were being closed for grazing and distributed among individual farmers. A total of 208 ha (out of 542 ha of rangeland) was protected and distributed equally among 530 farmers in the watershed. To speed up the rehabilitation of the degraded hillslopes, contour trenches were made for improved water infiltration and multipurpose trees were planted at the time of closing. Tree species planted included *Grevillea robusta* A.Cunn. ex R.Br., *Acacia saligna* (Labill.) H.L.Wendl., *Olea europaea* subsp. *Africana* (P. Mill.) P. Green, *Cajanus cajan* (L.) Millsp., *Sesbania sesban* (L.) Merrill and *Leucena leucocephala* (Lam.) de Wit. They have also introduced high quality multipurpose grasses for livestock feed, which was used as an entry point to attract the interest of the community to rehabilitate degraded lands and to provoke institutional innovation at various scales. The community was responsible for the protection of the area by guarding and institutionalized through written bylaws. Thanks to the protection from grazing, herbaceous and woody biomass production in exclosures recovered drastically (Fig. 15.4 and Table 15.1) within few years, which was also documented in other areas (Asefa et al., 2003; Yayneshet et al., 2009). Farmers harvested the grass for haymaking. The average herbaceous biomass production in the study area was about  $1.2 \text{ t DM ha}^{-1} (\pm 0.69)$  (Table 15.1), which lies within the range of  $1.1\text{--}1.8 \text{ t DM ha}^{-1}$  reported by Yayneshet et al. (2009) for exclosures in North Ethiopia. However, according to Asefa et al. (2003) hay production from hillside exclosures can amount upto  $2\text{--}3.5 \text{ t DM ha}^{-1}$ . Once the fodder trees start producing enough biomass, branches and leaves were also harvested and fed to the livestock. Apart from the benefits derived from harvesting grass and haymaking, exclosures are also known for their beneficial effects on land rehabilitation, biodiversity restoration and soil and water conservation (Asefa et al., 2003; Descheemaeker et al., 2006).

In addition to improvements in LWP, vegetation restoration in the protected areas leads to increased infiltration and decreased runoff (Descheemaeker et al., 2006), with higher transpiration and increased overall biomass production as a result (Descheemaeker et al., 2009). Other positive effects of reduced runoff from the steep slopes include the protection of downstream farmland against damaging floods, reduced erosion and less peak flows in gullies and streams. In some instances, the groundwater table can be recharged (Descheemaeker et al., 2009) and new springs start to appear (Nyssen et al., 2002), which was also observed in Lenche Dima. Farmers' interests in feed and woody biomass could be harmonized with these long-term environmental services by enabling farmers to make better use of the natural resources present in the exclosures. This could be done by consolidating the cut and carry activities for hay making and allowing farmers to harvest woody biomass as part of a selective and careful forest management plan (Yayneshet et al., 2009). Other opportunities lie in the promotion of non-wood forest production like honey. In our evaluation of water productivity we only took into account feed production and its potential effects on milk production. However, if the woody biomass and environmental benefits were also considered, water productivity improvements would have been even stronger.

**Table 15.1** Scenario analysis for enclosure establishment and two levels of hay production for the rangelands (542 ha) in Lenche Dima watershed in terms of water depletion for livestock feed, feed biomass and metabolizable energy production and water productivity (WP)

		Depleted water for		Metabolizable			
Hay production in enclosures (t DM ha <sup>-1</sup> )		livestock feed production (10 <sup>6</sup> m <sup>3</sup> )		Biomass production (ton) <sup>b</sup>		Energy WP (MJ m <sup>-3</sup> )	
	Scenario <sup>a</sup>			(10 <sup>6</sup> MJ ME)	energy production (10 <sup>6</sup> MJ ME)	(1,000 kg) <sup>c</sup>	Milk production (1,000 kg)
1.2 (measured)	Without	2.3	867	7.93	3.5	1,454	
	With	1.7	784	6.88	4.0	1,263	13
2.5 (Asefa et al., 2003)	Without	2.3	867	7.93	3.5	1,454	
	With	1.8	1,054	9.04	4.9	1,660	40

<sup>a</sup>scenarios: without enclosure establishment: 542 ha open-access grazing land; with enclosure establishment: 334 ha open-access grazing land and 208 ha enclosures with cut and carry of herbaceous biomass for hay making.

<sup>b</sup>biomass production calculated using the hay production in enclosures as reported in the table and 1.6 t DM ha<sup>-1</sup> for the grazing lands (based on measurements in the study area).

<sup>c</sup>milk production: assuming all energy produced is converted into milk at 5.45 MJ ME kg<sup>-1</sup> of milk. DM= dry matter, ME= metabolized energy.

## 15.5 Introducing Change

15.5.1 Increased and complementary cooperation among the riparian nations for shared use of the basin is of paramount importance considering the poverty level and developmental stages of the nations in the basin. Although the Nile Basin Initiative (NBI) can be considered as a step forward in creating forum to maintain cooperation and reduce conflict among the riparian countries, there is a clear gap in terms of formulating legal regulatory frameworks that are aimed at improving the management and productivity of livestock and water use at basin level. In addition, despite the fact that the NBI is designed to explicitly include involvement of local communities and local governments, the lower level governments seem to be less involved in the process, partly because the NBI is rather a top-down process that is not well designed for stakeholder involvement (Pottinger, 2006). The cooperation between administration levels is consequently underdeveloped. Generally, historical disputes could make joint decision-making between the riparian countries a difficult element to deal though the NBI provides a firm basis for cooperation in decision-making. There is a need for a regional policy that would ensure equitable and sustainable use of the Nile water including (i) the provision of sufficient watering points for grazing animals across the Nile basin. It is important not only to ensure that animals don't loose too much energy walking long distances looking for water, but also to avoid that too many animals concentrate around one watering point, causing soil degradation and water contamination (Peden et al., 2007). Restricting the access of too many animals to the watering points lies in the same line with this; (ii) ensuring control of transboundary flux of livestock diseases through improved quarantine and monitoring systems and; (iii) Minimizing illegal livestock trade across borders through designing a common marketing and pricing strategy; promoting rather a virtual trade.

15.5.2 There is a need for an over-arching, comprehensive Livestock-water framework to provide policy guidance and promote action. For instance in the case-countries, the "health aspect" is much more emphasized in Uganda while "market/tax aspect" received huge emphasis in the Sudan. Such isolated emphasis will not bring over all improvement in the livestock sector because gain in one side could be "compensated" by a loss at another side. Without a long-term vision and adequate political support, the livestock sector under water scarcity may not survive challenging issues such as climate change, devastating disease outbreaks or rapid changes in market conditions. Furthermore, all three case studies demonstrate that local participation is needed to avoid sector investments being captured by special interests whether it being populist politicians, state enterprises, or large businesses with special access to politicians.

15.5.3 Enhancing rehabilitation of livestock-based watersheds in upstream communities/ countries thereby minimizing land degradation, deforestation and water depletion. Rehabilitated landscapes are becoming the major sources

of livestock feed without competing with crop lands. This could be done through well designed and negotiated scheme including “payment for environmental services” (Haileslassie et al., 2008) and enclosures of degraded systems through collective action by the respective communities, as it is now practiced in the Ethiopian highlands.

15.5.4 While the Ethiopian highlands remain under great pressure in terms resources degradation due to slope effects and the current agricultural practices, it is also the major sources of water in the basin that should attract investment and capacity building. The livestock systems in the sub-basin must undergo major transformation in terms dissemination and adoption of appropriate water-saving technologies that could increase economic returns while positively influencing the hydrology of the basin to ensure that local and downstream peoples benefit. As mentioned above integrated agricultural water management, including water harvesting together with feed development is becoming a necessity to minimize effects of recurrent drought, conflicts and the unforeseen impacts of climate change. In all three countries, investments on animal health and marketing infrastructure are critical to improve water productivity at farm, community and higher scales.

## References

Amede T (1998) Analysis of Drought Resistance in grain legumes: the case of *Vicia faba* L., *Pisum sativum* L., *Phaseolus vulgaris* L., and *Cicer arietinum* L. PhD thesis, University of Hohenheim, Ulrich Grauer Publishing, Stuttgart, 135pp

Amede T, Geheb K, Douthwaite B (2009a) Enabling adoption of interventions to enhance livestock-water productivity in the crop-livestock systems of Eastern Africa: gender, institutions and action. *Rangeland J* 31:223–230

Amede T, Tamene L, Habte E, Yimer A (2009b) Policies and institutional arrangements affecting livestock-water productivity in the Nile basin: case studies from ethiopia, sudan and uganda. A synthesis report, IWMI/ILRI/CPWF, June, 2009, Addis Ababa

Amede T, Menza M, Awlachew SB (2011) “ZAI” for improving nutrient and water productivity in high rainfall ethiopian high lands. *Exp Agric* 47:7–20

Arsano Y (2007) Ethiopia and the nile: dilemmas of national and regional hydropolitics. PhD thesis. Center for security studies, Swiss Federal Institute of Technology, Zurich ETH Zentrum SEI, Switzerland. ISBN 3-905696-14-2

Appelgren B, Klohn W, Alam U (2000) Water and agriculture in the Nile basin Nile basin initiative report to ICCON background Paper prepared by FAO, Land and Water Development Division, Rome

Aredo D, Peden D, Taddese G (2006) Gender, irrigation and livestock: exploring the nexus. ILRI Report

Asefa DT, Oba G, Weladji RB, Colman JE (2003) An assessment of restoration of biodiversity in degraded high mountain grazing lands in northern Ethiopia. *Land Degrad Dev* 14:25–38

Benjamin ML, Yitayew A, Oloro VM, Collick A, Brhane G, Steenhuis T (2008) Hydrological assessment and integrated water resources management with special focus on developing countries. *Phys Chem Earth* 33 (1–2):14–21

Bossio D, Critchley W, Geheb K, van Lynden G, Mati B (2007) Conserving land – protecting water. In: Comprehensive assessment of water management in agriculture. Earthscan, London, and International Water Management Institute, Colombo, pp 551–583

Bouman B (2007) A conceptual framework for the improvement of crop water productivity at different spatial scales. *Agric Syst* 93:43–60

Bruinsma J (ed) (2003) World Agriculture: towards 2015/2030 an FAO perspective. Food and Agriculture Organization and Earthscan, London

Cook S, Andersson M, Fisher M (2009) Assessing the significance of livestock water use in basins. *Rangeland J* 31:195–206

Costales A, Gerber P, Steinfeld H (2006) Underneath the livestock revolution. In: Livestock report 2006. Food and Agriculture Organization, Rome, pp 15–27

de Fraiture C, Wichelns D, Rockström J, Kemp-Benedict E (2007) Looking ahead to 2050: scenarios of alternative investment approaches. In: David Molden (ed) Comprehensive assessment of water management in agriculture. Earthscan, London, and International Water Management Institute, Colombo, pp 91–145

Delgado CL (2003) Rising consumption of meat and milk in developing countries has created a new food revolution. *J Nutr* 133:3907S–3910S

Deribe DS, Tewodros A, Belete B, Gete Z (2009) Impacts of micro-basin water harvesting structures in improving vegetative cover in degraded hillslope areas of north-east Ethiopia. *Rangeland J* 31:259–265

Descheemaeker K, Nyssen J, Poesen J, Raes D, Mitiku H, Muys B, Deckers J (2006) Runoff processes on slopes with restored vegetation: a case study from the semi-arid Tigray highlands, Ethiopia. *J Hydrol* 331:219–241

Descheemaeker K, Raes D, Nyssen J, Poesen J, Haile M, Deckers J (2009) Vegetation restoration on degraded hillslopes leads to groundwater recharge and increased water productivity at the landscape scale in semiarid highland areas in northern Ethiopia. *Rangeland J* 31: 237–249

Falkenmark M (2007) Shift in thinking to address the 21st century hunger gap moving focus from blue to green water management. *Water Resour Manag* 21:3–18

FAO (2000) Land resource potential and constraints at regional and country levels. Land and Water Development Division, FAO, Rome, 114p

Fatondji D, Martius C, Bielders CL, Vlek P, Bationo A, Gerard B (2007) Effect of planting technique and amendment type on pearl millet yield, nutrient uptake and water use on degraded land in Niger. In: Bationo A (eds) Improving human welfare and environmental conservation by empowering farmers to combat soil fertility degradation African Soils Network (AFNet), Springer, The Netherlands, pp. 179–193

Gigar-Reverdin S, Jihad EA (1991) Water metabolism and intake in goats. In: Morand-Fehr P (ed) Goat nutrition. Wageningen, Pudoc, pp 37–45

Haileslassie A, Peden D, Gebreslassie S, Wagnew A, Amede T, Tadesse G (2009) Livestock water productivity in the Blue Nile basin: assessment of farm scale heterogeneity. *Rangeland J* 31:213–222

Haileslassie A, Hagos F, Mapedza E, Sadoff C, Aulachew SB, Gebreslassie S, Peden D (2008) Institutional settings and livelihood strategies in the Blue Nile basin: implications for upstream/downstream linkages. IWMI working paper 132. International Water Management Institute, Colombo, 81p

Herrero M, Thornton PK, Kruska R, Reid RS (2008) Systems dynamics and the spatial distribution of methane emissions from African domestic ruminants to 2030. *Agric Ecosyst Environ* 126 (1–2):122–137

ICRISAT (2007) Challenge program on water and food project 1: baseline survey report: South Africa and Zimbabwe. ICRISAT, Bulawayo

ILRI (International Livestock Research Institute) (2002) Livestock – a pathway out of poverty: ILRI's strategy to 2010. ILRI, Nairobi

Intergovernmental Panel on Climate Change (IPCC) (2001) Climate change 2001: impacts, adaptation, and vulnerability. Cambridge University Press, Cambridge

Kurukulasuriya P, Mendelsohn R, Hassan R, Benhin J, Diop M, Eid HM, Fosu KY (2006) Will African agriculture survive climate change? *World Bank Econ Rev* 20(3):367–88

Lemly AD, Kingsford RT, Thompson JR (2000) Irrigated agriculture and wildlife conservation: conflict on a global scale. *Environ Manage* 25:485–512

Mapedza E, Moraradet S, Cheron, C, Magombeysi M (2008a) Socio-economic conditions and agricultural water management practices of smallholders in quaternary catchment B72A, Olifants River Basin. IWMI, Pretoria

Mapedza E, Amede T, Geheb K, Peden D (2008b) Why gender matters: reflections from the livestock-water productivity research report. In: Humphreys E et al (eds) (2009) Fighting poverty through sustainable water use, vol II. Proceedings of the CPWF 2nd international forum on water and food, Addis Ababa, 10–14 Nov 2008, pp 97–100

Mohamed Y (2000) Water budgets of the Nile basin, IWMI, (forthcoming) Addis Ababa, Ethiopia

Molden D, Frenken K, Barker R, de Fraiture C, Mati B, Svendsen M, Sadoff C, Finlayson C (2007) Trends in water and agricultural development. In: Molden D (ed) Comprehensive assessment of water management in agriculture. Earthscan, London and International Water Management Institute, Colombo, pp 57–89

Moustafa M, Gichuki F (2003) The Nile basin profile: strategic research for enhancing agricultural water productivity. Challenge Program on Water and Food, Colombo

Mwendera EJ, Saleem MAM (1997) Hydrologic response to cattle grazing in the Ethiopian highlands. *Agric Ecosyst Environ* 64:33–41

Mugwe J, Mick O, Samuel G, Jonathan M, Jack M (2001) Participatory evaluation of water harvesting techniques for establishing improved mango varieties in smallholder farms of Mbeere District, Kenya. In: Stott DE, Mohtar RH, Steinhart GC (eds) Sustaining the global farm. 10th International Soil Conservation Organization meeting, pp 1152–1157. <http://topsoil.nserl.Pudue.edu/nserlweb/isco99/pdf/ISCOdisc/SustainingTheGlobalFarm/P066-Mugwe.pdf>. Accessed 6 Nov 2007

Norse D, Tscharley JB (2000) Links between science and policy making agriculture. *Ecosystems and Environment* 82:15–26

Nyssen J, Moeyersons J, Poesen J, Deckers J, Haile M (2002) The environmental significance of the remobilisation of ancient mass movements in the Atbara-Tekeze headwaters, Northern Ethiopia. *Geomorphology* 49:303–322. doi:10.1016/S0169-555X(02)00192-7

Parthasarathy RP, Birthal PS, Ndejunga J (2005) Crop–livestock economies in the semi-arid tropics: facts, trends and outlook. International Crops Research Institute for Semi-Arid Tropic, Patancheru, 68pp

Peden D, Tadesse G, Misra A (2007) Water and livestock for human development. In: Comprehensive assessment of water management in agriculture. Earthscan, London and International Water Management Institute, Colombo, pp 485–514

Peden D, Tadesse G, Haileslassie A (2009) Livestock water productivity: implications for Sub-Saharan Africa. *Rangeland J* 31:187–194

Postel S (2000) Entering an era of water scarcity: the challenges ahead. *Ecol Appl* 10:941–948

Postel S, Wolf A (2001) Dehydrating conflict. *Foreign Policy* 126:60–67. <http://www.globalpolicy.org/security/natres/water/2001/1001fpol.htm>

Pottinger L (2006, Aug) Africa's perfect storm: extreme vulnerability to climate change increases pressure on rivers. *World Rivers Rev* 21(4):15

Roose E, Kabore V, Guenat C (1999) Zai practice: a West African traditional rehabilitation system for semiarid degraded lands, a case study in Burkina Faso. *Arid Soil Res Rehab* 13(4):343–355

Rowntree K, Duma M, Kakembo V, Thornes J (2004) Debunking the myth of overgrazing and soil erosion. *Land Degrad Dev* 15:203–214

Sangina P, Kamugisha R, Kakuru A, Stroud A (2006) Facilitating participatory processes for policy change in NRM: lessons from the highlands of SW Uganda. In: Amede TL, German S, Rao CO, Stroud A (eds) Integrated natural resource management in practice: enabling communities to improve mountain livelihoods and landscapes. Conference proceedings 12–15 October 2004 Nairobi, Kenya. African Highlands Initiative, Kampala, Uganda, 390pp.

Seré C, Steinfeld S (1996) World livestock production systems: current status, issues and trends. FAO Animal Production and Health Paper 127. FAO, Rome

Singh OP, Sharma A, Singh R, Shah T (2004) Virtual water in dairy economy. *Econ Polit Wkly* 39:3492–3497

Speedy AW (2003) Global production and consumption of animal source foods. *J Nutr* 133:4048S–4053S

Steinfeld H, Gerber P, Wassenaar T, Castel V, Rosales M, de Haan C (2006) Livestock's long shadow. Environmental issues and options. FAO, Rome, 390p

Teixeira IA, Pereira Filho JM, Murray PJ, Resende KT, Ferreira ACD, Fregadolli FL (2006) Water balance in goats subjected to feed restriction. *Small Rumin Res* 60(1–2):20–27

Thornton P, Herrero M (2001) Integrated crop-livestock simulation models for scenario analysis and impact assessment. *Agric Syst* 70:581–602

Thornton P, Kruska R, Henninger N, Kristjanson P, Reid R, Atieno F, Odero A, Ndegwa T (2002) Mapping poverty and livestock in the developing world. International Livestock Research Institute, Nairobi

Van Breugel P, Herreor M, van de Steeg J, Peden D (2010) Livestock water use and productivity in the Nile Basin. *Ecosystems* 13:205–221

Van Hoeve E, van Koppen B, (2006) Beyond fetching water for livestock: a gendered sustainable livelihood framework to assess livestock-water productivity. ILRI working paper number 1. ILRI, Nairobi

Wallace J (2000) Increasing agricultural water use efficiency to meet future food production. *Agric Ecosyst Environ* 82:105–119

Williams TO, Hiernaux P, Fernández-Rivera S (2000) Crop–livestock systems in Sub-Saharan Africa: determinants and intensification pathways. In: McCarthy N, Swallow B, Kirk M, Hazell P (eds) Property rights, risk, and livestock development in Africa. International Food Policy Research Institute, Washington DC, and International Livestock Research Institute, Nairobi, pp. 132–151

Wilson T (2007) Perceptions, practices, principles and policies in provision of livestock water in Africa. *Agric Water Manag* 90:1–12

Wint W, Robinson T (2007) Gridded livestock of the world. FAO, Rome, ix, 131p

WOCAT (World Overview of Conservation Approaches and Technologies) (2007) Where the land is greener – case studies and analysis of soil and water conservation initiatives worldwide. In: Liniger H, Critchley W (eds) CTA, FAO, UNEP, CDE on behalf of WOCAT, Bern

Yayneshet T, Eik LO, Moe SR (2009) The effects of exclosures in restoring degraded semi-arid vegetation in communal grazing lands in northern Ethiopia. *J Arid Environ* 73:542–549. doi:10.1016/j.jaridenv.2008.12.002

# Chapter 16

## Blue Nile (Abbey) Hydropower Potential, Prioritization, and Trade-Offs on Priority Investments

Dereje T. Desalegn, Seleshi B. Awulachew, and Semu A. Moges

**Abstract** The low level of access, rising fuel costs, and increasing effects of climate change are reinvigorating the policy-makers' interest in Africa in renewable energy sources such as hydropower. Ethiopia is among countries which have very low modern energy sources, but possesses one of the highest hydropower potential, next to Congo. The topographic feature and the availability of water in Ethiopia permit a large hydropower potential. However, as the available runoff in rivers has very high hydrological variability, tapping into this potential requires investment on storage to smooth out the temporal hydrological variability. In this chapter, first the behavior of this hydrological variability and implication of water resources development are discussed. Second, various documents and reports providing varying values of hydropower potential of Ethiopia and Abbey are summarized. To improve the existing understanding of sites, topographical and hydrological evaluation of 129 hydropower potential sites has been carried out. These sites were identified in previous studies having a total capacity of 13,845 MW. After evaluations, 91 possible sites with total potential of 12,148 MW from various tributary rivers were identified and mapped. Dabus sub-basin stands first among the 16 sub-basins with 13 hydropower potential sites and a total capacity of 3,524 MW, and similarly the other sub-basins are also ranked. The ranking of these sites has been carried out based on cost per kilowatt hour of the hydropower potential (HP) sites. Furthermore, the chapter discusses the benefits and trade-offs for four priority developments identified as Eastern Nile regional fast-track projects.

**Keywords** Hydrological variability · Abbey · Hydropower · Potential · Trade-offs · Renewable energy

### Abbreviations

ARB	Abbey River Basin
ARBIDMPP	Abbey River Basin Integrated Development Master Plan Project

---

D.T. Desalegn (✉)

Water Works Design and Supervision Enterprise, Addis Ababa, Ethiopia

e-mail: der\_tadesse@yahoo.com

cost/kWh	Cost of electricity production per kilowatt hour
EEPCO	Ethiopian Electric Power Corporation
ENTRO	Eastern Nile Technical and Regional Organization
GDP	Gross Domestic Product
HP	Hydropower project
MW	Megawatt
TWh/year	Terawatt hour per year
WAPCOS	Water and Power Cooperation

## 16.1 Introduction

Water plays an important role in producing renewable energy sources both directly in the form of hydropower and indirectly in the form of biomass. At present, the share of renewable energy sources in total global energy supply is only about 13%. Of this, biomass accounts for the major share (10%) followed by hydropower (2.2%). Although the share of renewable energy sources including hydropower is only modest at present, many countries aim to increase this significantly. For instance, in China, where renewable sources account for only 8% of the present energy supply, the government aims to double this by 2020, particularly through the development of additional hydropower capacity. Much more important is the case of Africa, where there is tremendous untapped economically and technically feasible potential for hydropower development (McCormick et al., 2007). While the total technically feasible hydropower potential of the continent is estimated to be about 1,750 terawatt-hour (TWh)/year, current use is just about 5% (BMZ, 2007).

In recent times, the non-renewable and exhaustible sources of energy are getting depleted at a very fast rate, which has focused attention on the non-exhaustible and renewable sources of energy. Sustainable energy development is essential and necessary for socio-economic development of a country. Satisfying the energy needs of the population through sustainable energy-based approach helps to avoid deforestation and improve the living standards in developing countries. Hydropower is one of the most common renewable sources, abundantly available in the hilly region provided that there is adequate rainfall that could form runoff.

Ethiopia has not only a very low energy per capita but also most of this is in the form of biomass. Notably, such a low per capita energy with an extreme dependence on biomass occurs despite the vast energy potential in the country. Despite significant developments in the last half of the decade, few years back only 17% of the population, mainly in urban areas, had access to electricity. Low coverage and poor quality of power also cause heavy economic losses. For instance, during the drought of 2002–2003, it was estimated that with each day of lost service in energy provision the GDP for that day reduced by up to 15% (World Bank, 2006). Equally serious are also the environmental consequences of the present energy composition. Due to intensive biomass exploitation, it is reported that only less than 3% of the natural forest remains at present. Siltation from land degradations

has led to the storage loss of Koka Reservoir (World Bank, 2006), and to date, more than 30% of the total volume has been lost to sedimentation (Michael, 2004). Recognizing the importance of hydropower as crucial source of energy and rapidly growing demand, hydropower development in Ethiopia is given priority and connectivity has increased rapidly toward achieving universal access. According to the Ethiopian Electric Power Corporation (EEPCO, 2009), access to hydropower connectivity increased from 401,000 customers in 1991 to 1,677,000 customers in 2008, and the electric energy demand growth was 5–6% during 1995–2001, 13% during 2002–2007, and 24% in 2008–2009. Accordingly, the development of hydropower increased from 640MW in 2008 to additional 1,180MW hydropower energy from Tekeze I (300MW) in 2009, Ghibe II (420MW in 2010), and Tana Belese (460MW in 2010) and a total of 1820MW. Furthermore, Ghibe III, which is expected to supply 1,870 MW hydropower, is planned to be completed in 2013.

Ethiopia has significant water resources, which can be further exploited to enhance the socio-economic development of its people (MoWR, 2002). Based on topography, Ethiopia is subdivided into 12 major drainage basins. Theoretical hydropower potential in Ethiopia is about 650 TWh/year, with technically feasible potential of 40% of the theoretical potential; this constitutes about 15% of the total technically feasible potential of Africa. Among these, Abbay River Basin (ARB) is one of the major and largest river basins, and it is divided into 16 sub-basins. Based on various factors such as the energy potential, the quantity of water, and its trans-boundary implications, Abbay River Basin is the most important river basin in Ethiopia. The hydrology of the ARB and Nile is dominated by Abbay which rises in the center of the catchments of ARB and develops its course in a clockwise spiral.

## 16.2 Description of the Study Area

The study area, ARB, is found in the north-west part of Ethiopia, between  $7^{\circ}45'$  and  $12^{\circ}45'N$  and  $34^{\circ}05'$  and  $39^{\circ}45'E$  (Awulachew, 2000). This river basin covers about 17.58% of Ethiopia's land area, 43.11% of total average annual runoff of the country, and 25% of its population. It has an average annual runoff of about 52.60 billion m<sup>3</sup>. The location of the basins is shown in Fig. 16.1; it constitutes 16 sub-basins including the largest lake in Ethiopia. The annual rainfall varies between about 800 and 2,200 mm with a mean about 1,420 mm. The mean temperature of the basin is 18.5°C with minimum and maximum average daily temperatures of 11.4°C and 25.5°C, respectively (BCEOM, 1998).

Closer examinations of hydrological features of Ethiopian rivers reveal that meaningful exploitations of the rich water resources require investment on water storage. Since the rainfall is non-uniformly distributed, the runoff in the rivers which significantly depends on direct runoff reflects the rainfall patterns. Figure 16.2 shows the flow duration curve of a typical gauging station which reflects that the dependable flow of the river is small. The 95 to 50% mean flow ratio is 0.44. Increasing meaningful development, resilience of systems against climate variability, and climate change therefore require investment on storage.

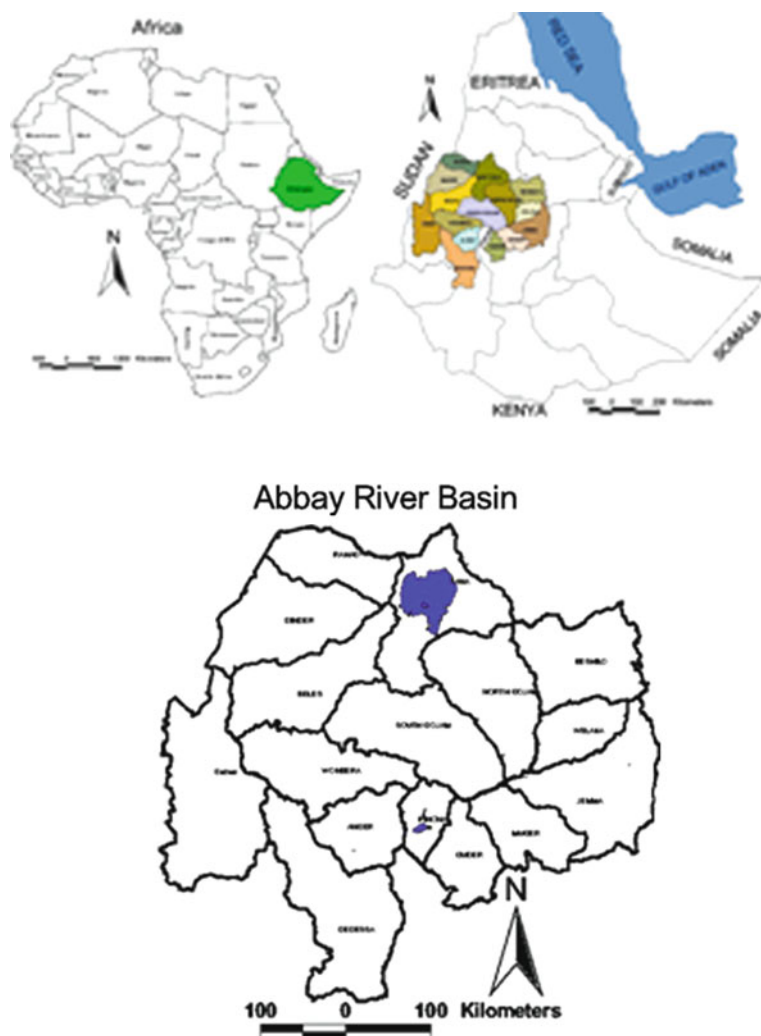


**Fig. 16.1** Map showing location of the study area (Africa, Ethiopian, and Abbay River Basin and sub-basins)

### 16.3 Objective of the Study and Methodology

The main objectives of the study reported in this chapter are (1) to accurately geo-reference the potential hydropower sites, (2) evaluate the potential capacities of the sites, (3) identify any pertinent challenges and problems, and (4) rank the sites with respect to their capacity and sub-basin.

The selection of the hydropower potential site is governed by the topography of the area, hydrology of the catchments, geological condition, and distance from

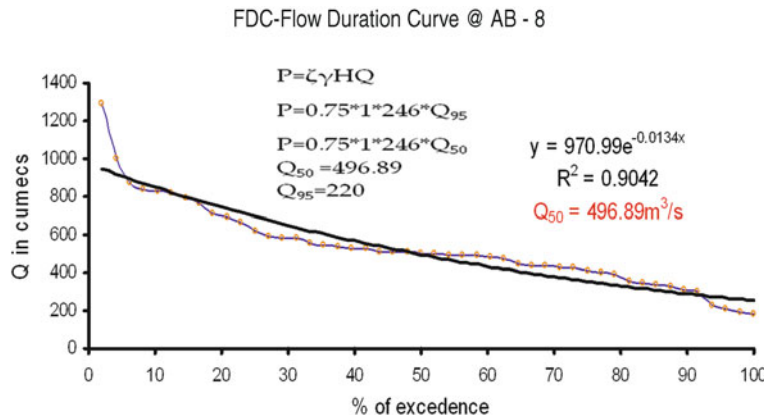


**Fig. 16.2** Flow duration curve at site AB-08

the grid system. It is the sum of all these components which helps us to decide the potential of the site and its economical feasibility.

The methods used include collection of relevant data from various institutions such as Ministry of Water Resources, Ethiopian Mapping Authority, and EEPCO; desk study to review previous recommendations; and data processing and analysis of collected information using various tools such as statistical packages and geographic information system (GIS) to obtain spatial and temporal hydrological and physical parameters. The collected, computed, and analyzed data are used to identify the possible potential sites and ranking of the sites.

## 16.4 Data Sets

The two important datasets for estimation of hydropower potential are the available discharge and hydraulic head. The discharge data used in this study include monthly stream flow data of 90 stream gauging stations found in the basin for estimation of the dependable flow for power production. Fifty percent dependable flow is employed for storage-type hydropower plant and ninety percent dependable flow for runoff river-type hydropower plant. The available hydraulic head is determined from digital terrain analysis and/or simple topographic map surveying techniques; moreover, from these datasets drainage basin areas are defined and some important features such as slopes and stream patterns are measured for hydrologic analysis.

## 16.5 Evaluation of Selected Hydropower Potential Sites

In addition to the head and discharge other useful data for evaluation of technical aspects of the hydropower structures and reservoir include geology, topography, and drainage patterns of the area. In the study area while hydrological and topographical

data are reasonable, geological data are very scanty and evaluation relies on the available data based on 1:2,000,000 scale of the geological map, which is too coarse to undertake reliable evaluations. Therefore, the evaluations reported in this chapter exclude the geological suitability of the given site.

The site evaluation was performed for potential HP sites which are selected/ identified by Water and Power Cooperation (WAPCOS) in the 1990 report. Most of the possible hydropower potential sites which are mentioned in other documents and reports except the WAPCOS (1990) and the BCEOM (Abbey River Basin Integrated Development Master Plan Project) (1998) reports do not have the description of the sites, rather only the technically available power and number of possible potential sites. As a result other documents are not considered in this work. Furthermore, the report of the Abbey River Basin Integrated Development Master Plan Project (ARBIDMPP) document provides assessment of partial sites.

## 16.6 Site Evaluation Criteria

The general criteria employed for the evaluation of the selected hydropower potential sites are listed:

1. As far as possible, harness the available head on the site optimally or maximize the use of the available head. There should be also adequate discharge on the site for the developed hydropower.
2. For storage-type hydropower development, the submergence and water surface area should be minimum; narrow gorge areas are advantageous.
3. In case there is a confluence of two rivers in the selected reach, the site should be located downstream of the confluence point to take advantage of the flow of both rivers.
4. The site should be easily accessible considering access to road and transport.
5. Distance from the load center (national grid system) should be considered.

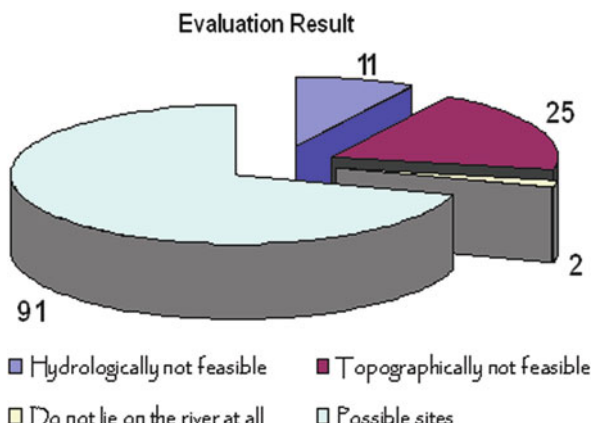
Any combination of head and flow can be used to develop a hydropower, and more emphasis is given for these two main factors. Moreover, if hydropower is to be generated from dam water, then selecting suitable dam sites requires careful consideration of economy. Smaller length of the dam will reduce the quantities of fill material and the cost of dam construction. Hence, the site has to be the one where the river valley has the narrow and neck-like formation.

## 16.7 Result and Discursion

### 16.7.1 Screening of Sites

With the above criteria for site evaluation in mind, the following problems are identified during the evaluation of the previously identified sites by WAPCOS and used to screen the inappropriate potential sites:

**Fig. 16.3** Evaluation of the sites result



- The site may not lie on the river, i.e., it lies on a bare land, such as sites AB-13 and AB-48. Even though most of the selected hydropower potential sites needed coordinate adjustment, these sites did not lie on a river after coordinate adjustment.
- The sites lie on a small (flash) river, which emerges or originates from a mountainous area. In such cases, there is no sufficient amount of discharge to suggest such sites as potential sites.
- The sites lie on a plain area and it is difficult to get the suggested head without construction of a costly dam. Such sites are also rejected.
- The downstream site affects the upstream site due to submergence of reservoirs in cascaded system. There may be feasible hydropower potential sites considering topographical and hydrological factors. However, if the downstream site has an effect on the upstream site due to submergence, such sites are also excluded.

Accordingly, the sites are screened as shown in Fig. 16.3, categorized into four groups, representing 91 feasible sites and 38 non-feasible sites, due to the above-discussed problems related to hydrological, topographical, and coordinate locations.

### 16.7.2 Capacity Evaluation Result

A total of 129 sites, which have been identified by WAPCOS (1990), have been evaluated. The following charts describe the result of the evaluation in different categories. The majority of the sites (64.84%) have potential capacities greater than 10 MW, but less than 200 MW (Fig. 16.4). Only 11 sites have capacities exceeding 200 MW. Head classification for the basin and capacity distribution, head, potential, and construction features by sub-basins are also used to categorize the potential of the ARB and are provided in Figs. 16.5, 16.6, 16.7, 16.8, and 16.9.

**Fig. 16.4** Number of sites by capacity groups

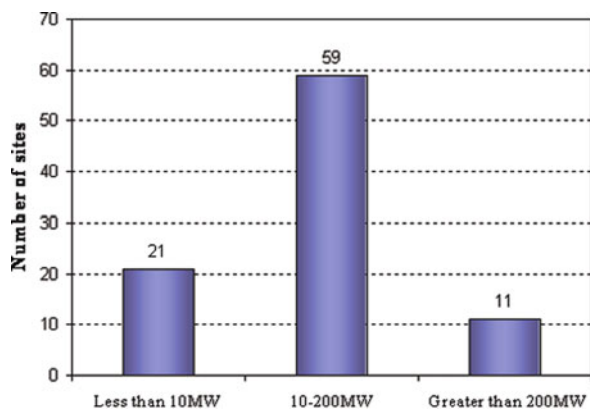
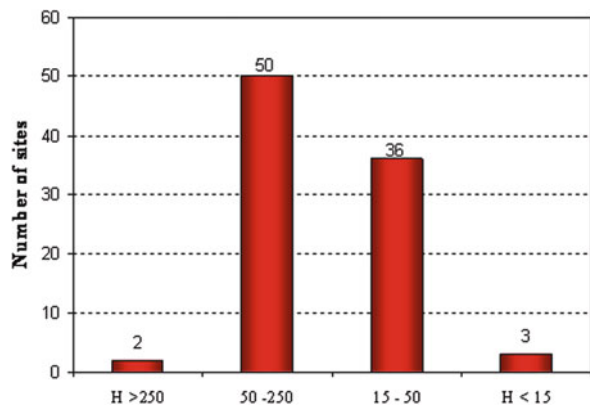


**Fig. 16.5** Number of sites by head groups



### 16.7.3 Mapping of the Selected Sites

The 91 possible hydropower potential sites in the 16 sub-basins of the ARB are mapped with improved accuracy with respect to geo-referencing and site suitability. The mapping of the sites improves the understanding in terms of distribution and locations of the sites. Figure 16.10 shows the possible hydropower potential sites of the Abbay River Basin.

### 16.7.4 Ranking of the Evaluated Potential Sites

In order to exploit the hydropower potential economically and under prevailing socio-economic conditions, it is useful to prioritize and rank the available hydropower potential sites. The sole criterion used for ranking the potential sites (to be further studied) was the “normalized” cost per kilowatt hour (Table 16.1).

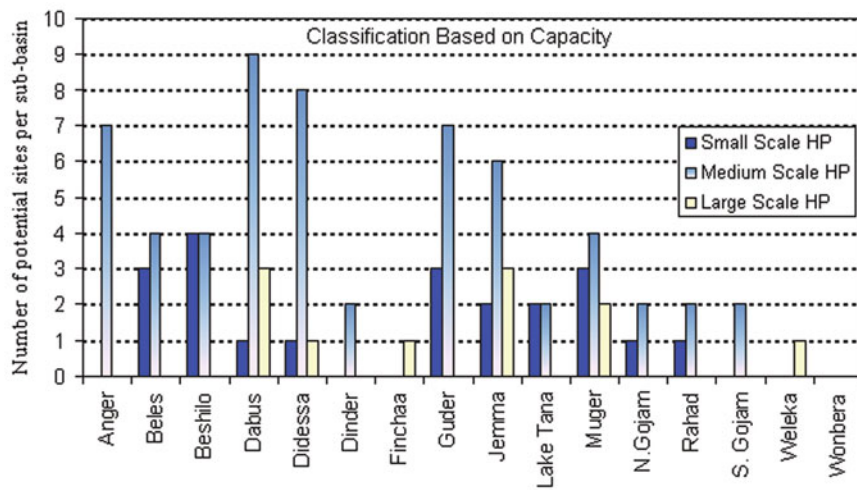


**Fig. 16.6** Number of sites by capacity groups for the sub-basins

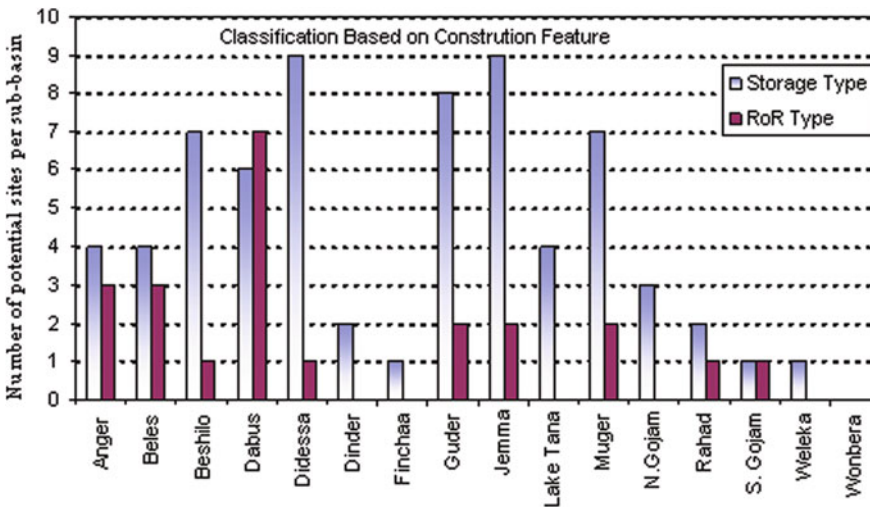


**Fig. 16.7** Number of sites by available head for the sub-basins

Estimate of costs of electricity production in birr per kilowatt hour is available in various sources of documents for most of the projects identified in the initial list. However, these costs refer to different base years, as adopted by the individual consultants undertaking the studies. Therefore, the production costs have been adjusted to the year 2005, with 11% interest rate.

$$F = P [1 + i]^n \quad (16.1)$$

where  $F$  = present value,  $P$  = past value,  $i$  = discount rate, and  $n$  = number of years.

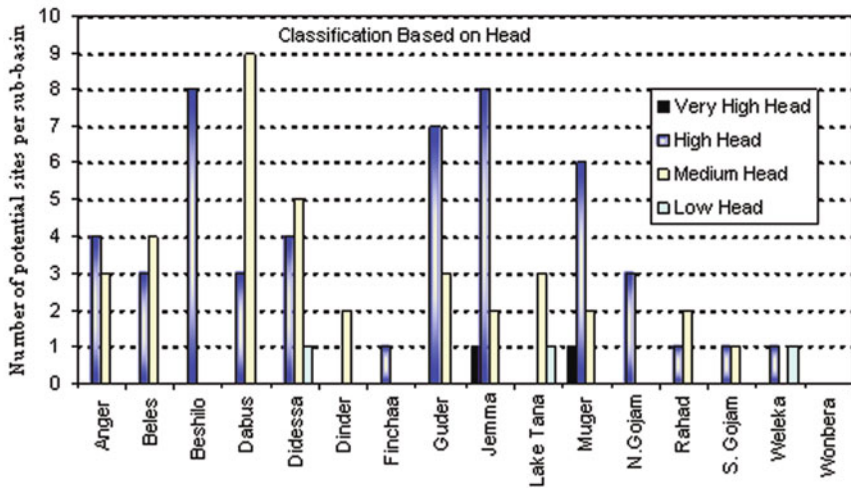


Fig. 16.8 Number of sites by construction feature for the sub-basins

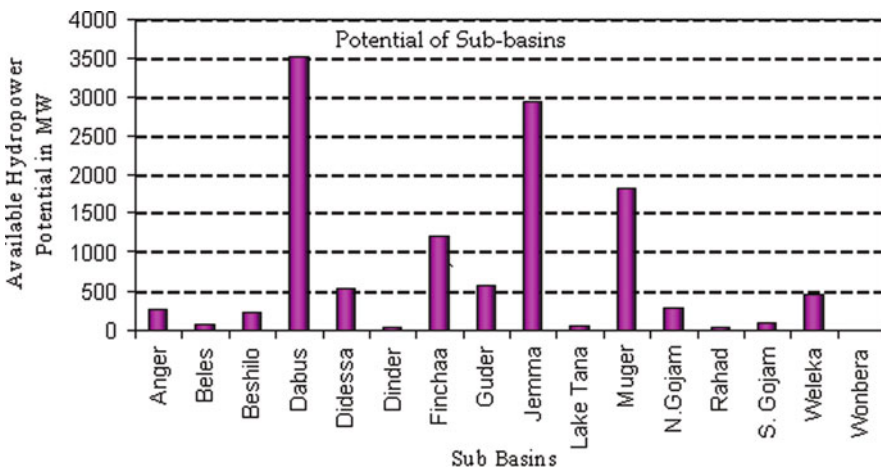
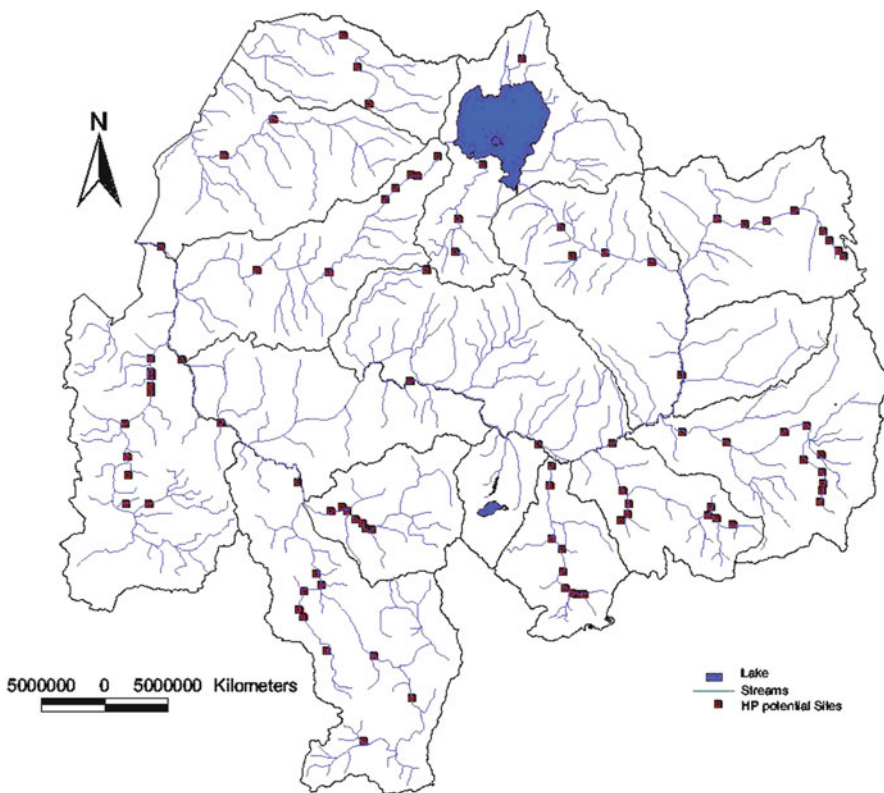


Fig. 16.9 Available potential of the sub-basins in MW

The reference costs are taken from the BCEOM (1998) and WAPCOS (1990) main reports. Using these values, two model equations are developed: one for runoff river type and the other for storage-type scheme. The parameters which are employed to develop these model equations are the available head ( $H$ ), the available discharge ( $Q$ ), available power ( $P$ ), distance from the access road (AR), and distance from the load center (LC).



**Fig. 16.10** GIS-based mapping of the potential site

The developed equation for storage-type hydropower potential sites is

$$C = \alpha_1 H + \alpha_2 Q + \alpha_3 P + \alpha_4 AR + \alpha_5 LC \quad (16.2)$$

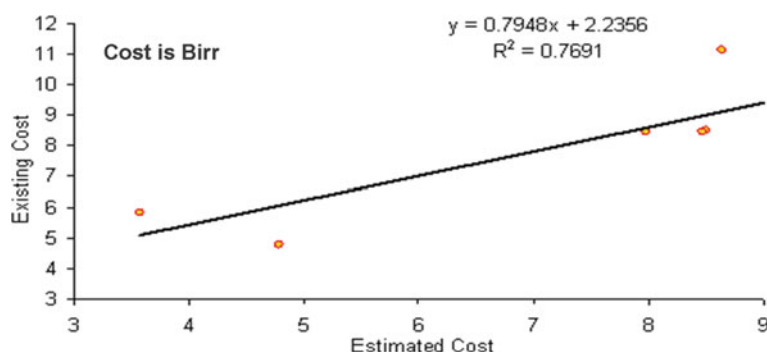
$$C = -0.015H - 0.006Q - 0.002P - 0.134AR + 0.347LC \quad (16.3)$$

where  $C$  = cost of electric power production (birr/kWh),  $H$  = the available head (m),  $Q$  = the available discharge ( $m^3/s$ ),  $P$  = the available discharge (MW),  $AR$  = distance from the access road (km), and  $LC$  = distance from the load center (km).

Based on Eq. (16.3) and Eq. (16.5), the estimated cost of electric power production for selected hydropower potential sites have been carried out for storage type and runoff river type HP sites respectively (Table 16.1). Prior to cost estimation, a correlation relationship between the estimated cost and the existing cost has been done to verify the correlation factor ( $R$ ) as shown in Fig. 16.11 and Fig. 16.12 for storage and run off river type respectively.

**Table 16.1** Ranking of the possible sites based on different criteria

WAPCOS site designation	Ranking based on cost (birr/kWh)	WAPCOS site designation	Ranking based on cost (birr/kWh)	WAPCOS site designation	Ranking based on cost (birr/kWh)
AB-1	39	AB-37	7	AB-86	37
AB-2	29	AB-38	46	AB-87	38
AB-3	41	AB-41	35	AB-88	82
AB-4	42	AB-42	43	AB-91	67
AB-5	58	AB-43	57	AB-93	87
AB-6	77	AB-44	73	AB-94	44
AB-8	14	AB-49	11	AB-95	51
AB-9	15	AB-52	21	AB-96	78
AB-10	8	AB-53	24	AB-98	31
AB-11	16	AB-54	25	AB-99	40
AB-12	63	AB-55	23	AB-100	76
AB-14	3	AB-57	48	AB-101	83
AB-15	9	AB-59	32	AB-102	80
AB-16	30	AB-60	91	AB-103	64
AB-17	62	AB-61	89	AB-104	86
AB-19	72	AB-62	90	AB-105	68
AB-20	85	AB-63	18	AB-106	69
AB-21	13	AB-65	66	AB-107	88
AB-22	26	AB-67	20	AB-109	17
AB-24	71	AB-69	81	AB-111	36
AB-25	6	AB-70	60	AB-112	79
AB-26	4	AB-72	84	AB-115	45
AB-27	5	AB-75	65	AB-117	10
AB-28	28	AB-76	19	AB-119	52
AB-29	59	AB-77	27	AB-120	2
AB-31	47	AB-79	49	AB-122	53
AB-32	74	AB-81	61	AB-124	54
AB-33	33	AB-82	75	AB-125	70
AB-34	22	AB-83	50	AB-128	55
AB-35	34	AB-84	1	AB-129	56
AB-36	12				

**Fig. 16.11** The relationship of the estimated and existing cost (birr/kWh) for storage type

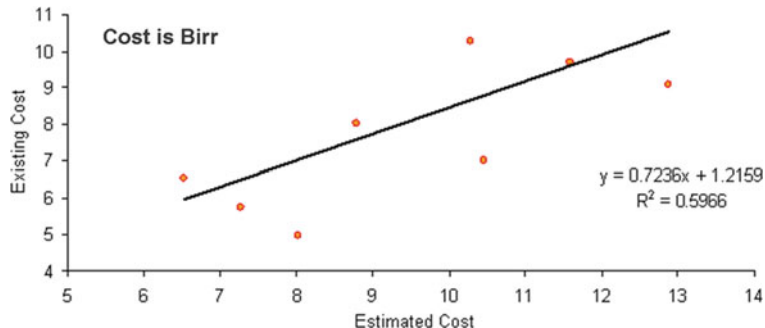


**Fig. 16.12** The relationship of the estimated and existing cost (birr/kWh) for runoff river type

The developed equation for runoff river hydropower potential sites is

$$C = \alpha_1 H + \alpha_2 Q + \alpha_3 P + \alpha_4 AR + \alpha_5 LC \quad (16.4)$$

$$C = 0.042H + 0.350Q - 0.158P + 0.091AR - 0.151LC \quad (16.5)$$

Among these sites, four sites were identified by the Eastern Nile Technical and Regional Organization (ENTRO), see also Block (2007). Recently, the Tana Beles hydropower scheme generating a maximum of 460 MW energy was completed, which is among the identified potential sites. The power production is designed based on 0.48 plant factor and diversion of average 77 m<sup>3</sup>/s of water and maximum discharge of 130 m<sup>3</sup>/s. The available head at the Tana Beles transfer is over 300 m. In order to realize the large potential of Abbay, it is important to harness potentials not only in the main stems of the Abbay but also in the tributary rivers, which are provided in the various sub-basins.

## 16.8 Conclusion and Recommendations

This particular chapter provides an overview of the energy condition of Ethiopia, the hydropower potential, the ranking of the potential sites, and identification of the specific sites of the Abbay basin. The result, in addition to providing consolidated information about the basin energy source, serves as a base reference to undertake further studies leading to pre-feasibility and feasibility studies. Some specific conclusions and recommendations include the following:

- The topographical and hydrological evaluation lowers the selected sites (129) by about 29.45% to 91 potential sites.
- The total theoretical potential of the basin according to WAPCOS (1990) study was 13,540MW, however according to this study, the total 91 HP sites gives 12,480MW.

- Ranking these possible potential sites will facilitate to exploit the available potential of the basin in priority order.
- Site evaluation based on geology of the area and also field visit may change the value, so further detailed study should have to be carried out.
- The evaluation has been done only from the point of view of hydropower; however, the sites may serve as a multipurpose project so that the sites should have to be evaluated from other water resource development benefits.
- The same procedure can be followed for other major drainage basins of the country as well.
- The study needs a detailed hydrological study for each site to get the actual power potential of the sites, considering efficiencies of conveyance and generation.
- The cost considered for ranking purposes is not the exact cost of the sites, but it can serve as a representative for economical evaluation of the potential sites. The developed equation can serve only for preliminary determination of cost/kWh of the sites, so one can change the equation to logarithmic or exponential form.

## References

Awulachew SB (2000) Investigation of water resources aimed at multi-objective development with respect to limited data situation: the case of Abaya-Chamo Basin, Ethiopia. PhD thesis, TU Dresden

BCEOM – French Engineering Consultants, in association with ISL and BRGM (1998) Abbay river basin integrated development master plan project (ARBIDMPP), phase 2 Volume I Main report, volume II part 1 climatology, part 2 Hydrology, Volume VI part 2 Large dams and Hydropower schemes, phase 3 volume IV part 7 hydropower schemes

Block P (2007) Integrated management of the Blue Nile Basin in Ethiopia: hydropower and irrigation modeling. International Food Policy Research Institute. IFPRI Discussion Paper 00700

Michael A (2004) Lesson learned from existing hydro schemes, case study: Koka Dam. First National Water Forum conference proceeding paper, Ministry of Water Resources, Addis Ababa, Ethiopia, pp 49–58

McCormick PG, Awulachew SB, Abebe M (2008) Water–food–energy–environment synergies and tradeoffs: major issues and case studies. *Water Policy* 10(S1):23–26

MoWR (Ministry of Water Resources) (2002) Ethiopia water sector development programme 2002–2016, main report

WAPCOS (1990) Preliminary water resource development master plan for Ethiopia, vol III, annex – a hydrology and hydrogeology, vol V annex J – hydropower

World Bank (2006) Ethiopia: managing water resources to maximize sustainable growth: country water resources assistance strategy. The World Bank, Washington, DC

**Part VI**

**Water Resources Management, Allocation  
and Policy II**

# Chapter 17

## Concepts of Environmental Flow Assessment and Challenges in the Blue Nile Basin, Ethiopia

Bianca Reitberger and Matthew McCartney

**Abstract** The degradation of riverine ecosystems, resulting from changes in natural flow regimes, is increasingly recognized as being amongst the most significant negative effects of hydraulic structures. Environmental flows are managed releases from a reservoir intended to mitigate these impacts. Numerous techniques have been developed to estimate environmental flows but, for a variety of reasons, these methods are rarely applied in developing countries. The Ethiopian Government is planning major hydropower and irrigation development in the catchment of the Blue Nile River. This paper reports the findings of a first attempt to rigorously quantify environmental flows in the Blue Nile River. Three desktop hydrological methods, the *Global Environmental Flow Calculator*, the *Desktop Reserve Model*, and the *Tennant Method*, were applied at three locations. With reasonable consistency they indicate that 21–28% of the mean annual flow may be sufficient to sustain basic ecological functioning. The results, which are low-confidence estimates, need to be confirmed with much more detailed studies, but provide a basis for discussion and can contribute to the early phases of planning.

**Keywords** Environmental flows · Blue Nile · Ethiopia · Water resources development

### 17.1 Introduction

In the past, water resources have been managed primarily from a supply perspective, with a focus on meeting accelerating demands for irrigation and hydropower as well as industrial and domestic needs. These demands, together with the manipulation of flows for navigation and flood control, require hydraulic infrastructure such as dams and weirs, as well as inter-basin water transfers, run-of-river

---

B. Reitberger (✉)

Faculty of Biology and Geography, Applied Hydrogeology/Hydrobiology,  
University of Duisburg-Essen, Essen, Germany  
e-mail: bianca.reitberger@gmail.com

abstractions and exploitation of aquifers. All of these can cause severe alterations to natural hydrological regimes (Tharme, 2003).

Past studies indicate that over half of the world's rivers are fragmented and regulated by dams and other hydraulic structures (Revenga et al., 2000; Nilsson et al., 2005). Many of these provide substantial benefits to human societies and economies. Hydropower schemes currently provide about 19% of the global electricity supply and dams related to irrigation schemes are estimated to contribute directly to 12–16% of food production worldwide (Richter and Thomas, 2007).

Although there are benefits, the alteration of natural flows results in a number of severe ecological effects ranging from genetic isolation through habitat fragmentation to declines in biodiversity. In turn these ecological impacts can have severe effects on ecosystem services (e.g. water purification, flood attenuation, fisheries, flood recession agriculture and recreational and cultural opportunities) often with profound consequences for the people who depend on them (Tharme, 2003). In many cases, the negative impacts extend for hundreds of kilometers downstream of the hydraulic structure (Richter and Thomas, 2007). These impacts are of particular significance in developing countries, where large proportions of the rural population are often directly dependent on the natural resource base and, so-called, common property resources, for their livelihoods (Millennium Ecosystem Assessment, 2005).

Due to the inter-linkages between the state of aquatic ecosystems and human welfare the topic of sustainable freshwater and related resources management ranks high on the international political agenda. With the exception of the EU Water Framework Directive, no international, legally enforceable, policies have been ratified to date. However, at the national level more progressive developments are occurring and policy frameworks that prioritize the allocation of water for ecosystem maintenance have been developed in several countries. In the Southern Hemisphere, South Africa and Australia have led the way and accordingly have the most advanced methodological and legislative frameworks relating to environmental flows. Several other African countries (e.g. Ethiopia, Tanzania and Kenya) have introduced new water legislation in recent years that is built on the general principles of sustainable and equitable resource use.

In this context, the growing recognition of the significance of the natural flow regime has driven the evolution of the science of environmental flow assessment (EFA) (Arthington et al., 2006; Dyson et al., 2003; Tharme, 2003). The goal of EFAs is to determine a flow regime that provides adequate patterns of flow quantity, quality and timing for achieving or sustaining a predefined condition of ecosystem functioning. These predefined objectives may be predicated on the conservation or rehabilitation of an entire river system, at maximizing commercial fisheries, at conserving certain key species, or elements of scientific, cultural or recreational value (Tharme, 2003). By preserving critical ecosystem functions (e.g. fisheries) the livelihoods and wellbeing of poor rural communities dependent upon such services can be safeguarded. Hence, EFAs make possible the incorporation of the interests and needs of these communities in water resource development plans.

In recent years numerous EFA methodologies have been developed. Each method is applicable under specific conditions of time, data, and financial and

technical resource availability and the specific issues to be addressed (Tharme, 2003). The types of methods range from relatively simple, quick and cheap hydrological approaches to more resource-intensive methods that incorporate comprehensive ecological assessments (e.g. habitat simulation and holistic methods). With this multitude of possible approaches the suitability of specific methods and their results have to be evaluated on a case-by-case basis. This chapter discusses environmental flows within the context of developing countries and presents a case study from the Blue Nile basin in Ethiopia.

## 17.2 Approaches to Environmental Flow Assessment

Early applications of EFA methods focused mainly on the maintenance of economically important target fish species, or other highlighted ecological features, neglecting other ecosystem components. However, the importance of flow management with regard to entire ecosystems has repeatedly been advocated in limnological research (e.g. Junk et al., 1989; Hill et al., 1991) and intensive studies relating to the development and advancement of EFA methods are progressing on a global scale. A recent inventory of EFA methods recorded 207 different approaches in use in 44 countries (Tharme, 2003).

Broadly there are four types of methods ranging from relatively simple, quick and cheap hydrological approaches, such as hydrological index and hydraulic rating methods, to more resource-intensive methods that incorporate ecological assessments (e.g. habitat simulation and holistic methods) (Table 17.1).

Hydrology-based EFA methods are the simplest and most commonly used methods, especially in situations where ecological data are scarce (Tharme, 2003). As the name implies, these methods rely solely on historical hydrological data, such as long-term daily or monthly discharge records. The recommended environmental flows are usually given as specific flow percentiles from a flow duration curve

**Table 17.1** Types of environmental flow assessment

	Advantages	Disadvantages
Hydrological index	<ul style="list-style-type: none"> <li>• Rapid</li> <li>• Few monetary and human resources</li> </ul>	<ul style="list-style-type: none"> <li>• Recalibration of parameters necessary</li> <li>• Low resolution</li> </ul>
Hydraulic rating	<ul style="list-style-type: none"> <li>• Rapid, simple, flexible</li> <li>• Moderate resource requirements</li> </ul>	<ul style="list-style-type: none"> <li>• Solely based on hydrologic data</li> </ul>
Habitat simulation	<ul style="list-style-type: none"> <li>• Flexible</li> <li>• Data processing efficiency</li> <li>• Multi-disciplinary</li> <li>• Natural flow paradigm</li> <li>• Flexible, robust, pragmatic</li> </ul>	<ul style="list-style-type: none"> <li>• Focus on target biota</li> <li>• High resource requirements</li> <li>• Focus on target biota</li> <li>• Substantial resource requirements</li> <li>• Recalibration parameters necessary</li> </ul>
Holistic		

or some other fixed percentage of the annual, seasonal, or monthly flow (King et al., 1999). Worldwide, the Tennant (or Montana) Method is the most widely applied of these methods (Tharme, 2003). It aims to satisfy environmental flow needs by linking specific percentages of the average annual flow to different conditions of instream habitat. Perhaps the most advanced hydrology-based EFA method is the Desktop Reserve Model (DRM) that has been developed by Hughes and Münster (2000) and further refined by Hughes and Hannart (2003). This method was developed to generate rapid, low-confidence estimates of environmental flow requirements for rivers in South Africa.

The advantages of this type of method are that they can be applied in a relatively short period of time and require few monetary and human resources. However, because they are often based on research conducted in specific geographical locations they are not easily transferable between different regions. Strictly they should be re-calibrated whenever they are used in locations in which they were not developed. Additional criticisms are their low temporal resolution regarding natural flow variability and the absence of ecological input data.

Hydraulic rating methods are based on the assumption that habitat integrity of riverine ecosystems is directly linked to changes in various hydraulic variables (wetted perimeter, width, depth, velocity), which are dependent on discharge. Measured stage-discharge data for one or more cross-sections and other hydraulic data (e.g. water depth, average velocity) in combination with ecological expertise are required to generate environmental flow recommendations from this type of approach. Environmental flows are usually determined in the form of a discharge value that is presumed to represent the optimal minimum flow, below which the available habitat (for many species) decreases rapidly (King et al., 1999). In this category, the wetted perimeter method (Reiser et al., 1989) is reported to be the most commonly applied method globally (Tharme, 2003).

The main advantage of these methods is that they are generally relatively rapid and simple procedures, flexible enough to accommodate the habitat requirements of various species, with only moderate resource requirements. Despite these strengths and their apparent improvement over hydrological index methods (e.g. by making use of ecologically based data such as physical instream habitat requirements), in recent years hydraulic rating methods have been surpassed by more sophisticated habitat simulation methods or incorporated within holistic methods that use micro-habitat and biological information in addition to pure hydrologic data (King et al., 1999).

Habitat simulation methods, the second most widely used type of EFA approach, are based on hydrological, hydraulic and biological response data. They aim to generate environmental flow recommendations with respect to habitat availability and its suitability for target species, life stages or assemblages over time and space. The most common technique is the use of habitat/flow curves and the determination of a so-called “diminishing return” point, where proportionately more habitat is lost with decreasing flow than is gained with increasing flow (Jowett, 1997).

By far the most widely used approach in this category is PHABSIM (Physical Habitat Simulation Model) (Bovee, 1982). The beneficial characteristics of high

flexibility, data processing efficiency and the possibility of creating dynamic hydrological and habitat time series at high spatial and temporal resolutions are counterbalance by the very high resource requirements in terms of time, data and expert knowledge. Furthermore, habitat simulation methods still focus almost entirely on target biota and therefore only partially provide the tools for fully-fledged, holistic EFA. Generally speaking, habitat simulation methods are most appropriate in trade-off situations, where the degree of habitat alteration can be weighed against the gains from resource use (Jowett, 1997).

Holistic methods are essentially integrated frameworks, consisting of a combination of hydrological index, hydraulic rating and habitat simulation methods, rather than separate approaches. They focus on the entirety of riverine ecosystems, including floodplains, estuaries, and coastal systems that are linked through riverine processes. As a consequence, comprehensive primary hydraulic and hydrological data, combined with as much supporting ecological data as possible, are pre-requisites for their implementation. In addition, information on the needs of local people dependent on riverine common property resources should also be used (King et al., 1999).

The South African Building Block Methodology (BBM) (King and Louw, 1998) and the Australian Holistic Approach (Arthington et al., 1992) were the first attempts of this kind and served as foundation for the development of more recent, innovative scenario-based approaches, such as the Downstream Response to Imposed Flow Transformation (DRIFT) method (King et al., 2003). The major advantage of holistic methods is that they address all components of riverine ecosystems and their links to flow regimes, and they can also incorporate socio-economic aspects. Furthermore, these flexible, robust and pragmatic methods can generate outputs at several levels of spatial and temporal resolution. However, a substantial amount of expert input and primary data collection is required, rendering holistic methods very time and resource intensive. Generally, these approaches require extensive fieldwork and lots of data and inputs from teams of experts with detailed local knowledge over prolonged periods of time.

Globally, North America is at the forefront of the field of EFAs and the first attempts towards the realization of the concept can be traced back to the late 1940s (Tharme, 2003). In North America and other developed Northern Hemisphere countries the application of habitat simulation methods predominates primarily because of the presence of economically important game fish species (e.g. salmon) and associated lobby groups (King et al., 1999). However, these methods are of limited importance in developing countries where data availability is scarce and analyses of the impact of flow regulations on the livelihoods of rural people dependent on natural resources have to be prioritized.

King et al. (1999) and Tharme (2003) identified a trend towards a hierarchical application of EFA methods, comprising two major steps. Often basin-wide scoping, planning or reconnaissance studies are conducted first, based on hydrological methods using historic flow records. These are then followed by more comprehensive assessments applying either habitat simulation or holistic methods. Examples for such a two-step approach are provided for Alaska (Estes, 1996) and the Czech

Republic (Bernadová, 1998). In other countries, such as Australia (Arthington and Zalucki, 1998), South Africa (Tharme, 1997), Lesotho (King and Brown, 2003) and the UK (Petts et al., 1996), an adaptable multiple-step method is applied, starting with simple hydrological methods proceeding to more comprehensive methods as additional resources become available.

### **17.3 Challenges to Environmental Flow Assessment in Developing Countries**

EFAs are an essential component of Integrated Water Resources Management (IWRM). Many developing countries are in the process of drafting new water laws that are underpinned by IWRM principles. For example in Asia, various countries are reforming their water sectors in accordance with these principles (e.g. Turner, 2008; Lincklaen and Arriens, 2004). Similarly many countries in Africa have, in recent years, re-drafted water legislation in compliance with these currently widely accepted notions of best practice, focusing on integrated catchment-wide approaches to management and emphasizing the need for environmental sustainability. Recognition of environmental requirements in water resources policies and legislation provides an essential foundation for their inclusion in basin and catchment water resource plans (Brown and Watson, 2007).

Against this background there is increased interest in environmental flows and numerous case studies for the development of national environmental flow tools have been conducted (e.g. Sri Lanka (Smakhtin and Weragala, 2005), Nepal (Smakhtin and Shilpkar, 2005), India (Venot et al., 2008; Smakhtin et al., 2007; Smakhtin and Anputhas, 2006), South Africa (King et al., 2000) and Tanzania (Kashaigili et al., 2006)). However, there remain significant constraints to the successful application of EFAs in many developing countries. These arise for technical reasons as well as limitations in human, financial and institutional capacity.

The lack of data, even basic biophysical data (e.g. on river flows), is often a key limitation to the successful application of EFAs. Even today, despite the recognition of the importance of well-managed water resources, the acquisition of basic hydro-metric data is rarely given high priority by government institutions (Houghton-Carr, 2006). Often data are not of sufficiently high spatial or temporal resolution to assist planning and decision-making at a local level. Even where it exists, administrative challenges of accessibility to data, including lack of familiarity of government officials with requests for information, deficient protocols for requesting data and lack of common data standards that promote data sharing, all hinder its use. In some instances, particularly in transboundary basins (e.g. the Nile), issues of national security also lead to restrictions on data sharing. There is need for much greater efforts in data collection, which is vital for EFA methods. There is also need for better coordination among different data collection agencies and improved data sharing.

Limited understanding of the complex environmental and social interactions, caused by changes in flow regimes is in developing countries, as elsewhere in the world, a major constraint to the planning and design of environmental flow regimes. To address this requires much more research into the links between modified flow regimes and the environmental and social impacts caused by changes in flow. It is also important that specific evaluation of uncertainty and risk should, as far as possible, be key components of EFA methods.

In addition, the limited pool of qualified professionals to develop and implement EFAs is often a major constraint to their application in developing countries. Technical capacity in the fields required (e.g. water resources, hydrology, botany, fisheries, ecology, public health, socio-economics etc.) and, particularly in the integration of different disciplines, is frequently insufficient. To address this challenge requires comprehensive professional training and capacity building programs. Sufficient training, retention of qualified personnel, continuing education and long term capacity building must all be part of a general educational strategy targeted at improving the management of water resources. There is particular need for cross-disciplinary programs that can provide future engineers and scientists with holistic understanding of EFA methods. Wider dissemination of existing guidance materials is also essential.

## 17.4 Case Study: EFA in the Upper Nile River Basin

### 17.4.1 Basin Characteristics

The Blue Nile basin, which is situated in the central, western and south-western highlands of Ethiopia and in the eastern plains of Sudan (Fig. 17.1) is the major tributary of the Nile River. Known as the Abay River in Ethiopia it supplies 62% of the flow reaching Aswan, with a mean annual discharge of 48.3 km<sup>3</sup> (at Khartoum) from a total drainage area of 311 and 548 km<sup>2</sup>.

The basin is characterized by considerable variation of altitude (350–4,250 m) and corresponding temperature variations with an average temperature fall of 5.8°C for every 1,000 m increase in elevation. A monsoonal climate results in high inter- and intra-annual variability in precipitation. Within the basin rainfall varies significantly with altitude and is considerably greater in the Ethiopian highlands than on the Plains of Sudan. Within Sudan, the average annual rainfall over much of the basin is less than 500 mm. In Ethiopia, it increases from about 1,000 mm near the Sudan border to between 1,400 and 1,800 mm over parts of the upper basin and exceeds 2,000 mm in some places. The flow of the Blue Nile is characterized by extreme seasonal variability. Typically, more than 80% of the flow occurs during the flood season (July–October) while only 4% of the flow occurs during the dry season (February–May) (Awulachew et al., 2008).

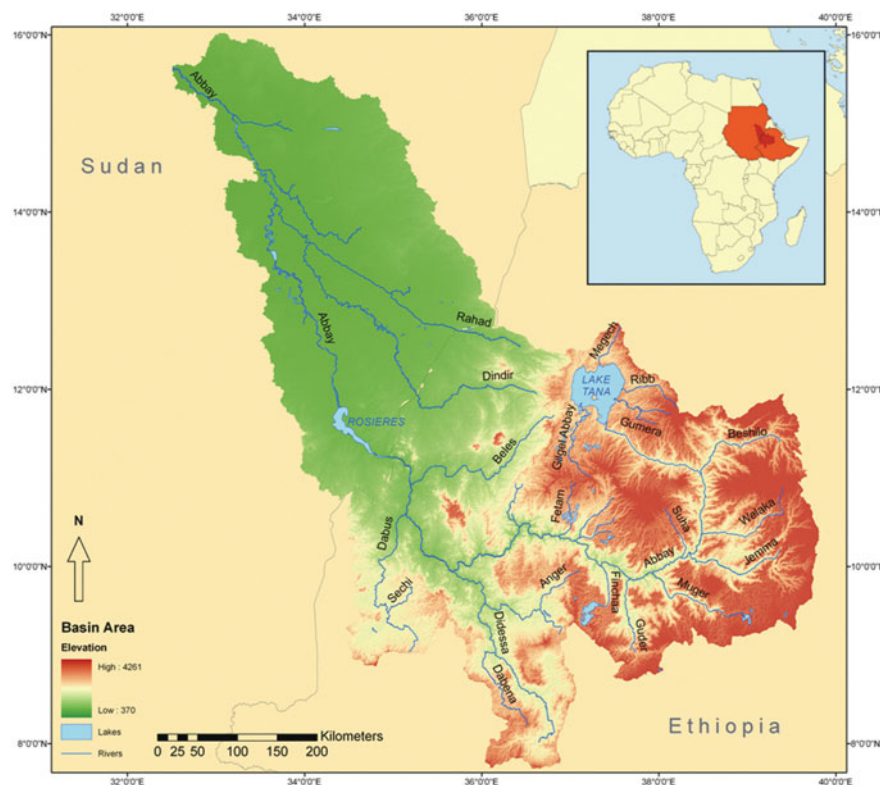


**Fig. 17.1** Location and topography of the Blue Nile basin

#### **17.4.2 Water Resources Use and Development**

To date, only two minor hydraulic structures have been built in the Ethiopian part of the basin (Table 17.2). One of the two is the Chara Chara weir, a dam built on the outlet of Lake Tana to regulate flow for hydropower production at the downstream Tis Abay power station. The second is the Finchaa scheme which comprises one dam and a somewhat larger hydropower station on the Finchaa River and another smaller reservoir on the Amerty River, from which water is transferred to the Finchaa. Together the Tis Abay and Finchaa power stations have an installed capacity of 218 MW, which represents approximately 27% of the total 814 MW grid based electricity-generating capacity of the country (EEPCo, 2009).

Only a very small area in the Abay basin is under formal irrigation. At present, the only modern irrigation schemes in the Abay are the Finchaa sugarcane plantation with an area of roughly 8,000 ha and the Koga irrigation scheme which will cover an area of 7,200 ha once fully operational in 2010 (McCartney et al., 2009).

Currently, the water resources of the Abay are mainly used to sustain the capabilities, assets (including both material and social resources) and activities that are

**Table 17.2** Existing hydrologic structures in the Abay catchment area

Dam	River	Storage (Mm <sup>3</sup> )	Year of construction	Purpose
Chara chara	Abay	9,100	1996	Hydropower production (installed capacity 84 MW)
Finchaa	Finchaa	2,395	1971	Hydropower production (installed capacity 134 MW) Sugarcane irrigation (8,145 ha)
Koga	Koga	83	2008	Smallholder irrigation (7,200 ha)

Modified from Awulachew et al. (2008) and McCartney et al. (2009).

required for the means of living of the rural population. Rainfed and floodplain agriculture, agro-pastoralism and artisanal fisheries play the most important role. The high percentage of 84% out of the total 77 million Ethiopians (2008 census) living in a rural setting (AFP, 2008) and therefore being dependent on the natural resource base, gives a measure of the importance of water resources and the related ecosystem services for subsistence-based livelihoods in Ethiopia.

In the context of a lack of significant fossil fuel reserves (Larson and Larson, 2007), presumed national water abundance, and an urgency to harness these resources to increase the national level of development and alleviate poverty the Ethiopian government has developed comprehensive Development Master Plans for all of the major river basins (Yohannes, 2008). The Abay River Master Plan (1998) identified various potential sites for future “modern” irrigation schemes. The currently planned projects will cover approximately 174,000 ha, corresponding to 21% of the total 815,581 ha that are estimated to be suitable for irrigated agriculture in the basin. Furthermore, over 120 potential sites for hydropower schemes have been identified within the Abay catchment area with a total potential capacity of over 30,000 MW (Larson and Larson, 2007). Of these 26 were investigated in detail during the preparation of the Abay River Basin Master Plan and several have now advanced to the stage of feasibility studies.

The growing demand for power and irrigation will certainly increase the pressure on water resources and related ecosystems in the Blue Nile basin in the near future. Accelerating population growth rates and development-related water needs in Ethiopia as well as downstream in Sudan, where there are plans to increase substantially the already high levels of irrigation (McCartney et al., 2009), will further aggravate this trend.

### 17.4.3 Water Resources Management Policy

With the water resources development sector on the rise, in 1999 the Ethiopian Government prepared a Water Resources Management Policy in order to enhance

economic growth and to optimize the use of the country's resources. The officially stated goal of the Policy is:

... to enhance and promote all national efforts towards the efficient, equitable and optimum utilization of the available water resources of Ethiopia for significant socio-economic development on sustainable basis (MoWR, 1999).

In five subsections the Policy addresses fundamental management principles regarding general water resources, water supply and sanitation, irrigation, hydropower, and institutional arrangements. A series of highly relevant and progressive ideas, founded upon the Integrated Water Resources Management (IWRM) concept, are incorporated. In general terms, the policy marks a shift away from purely supply side management and the prioritizing of industrial and urban users. With regard to water allocation, the Policy recognizes basic human and livestock needs as well as the environmental reserve as highest priority users. Water allocation plans have to be built around these key requirements. By using the term "environmental reserve" the Policy shows strong parallels with the water management philosophy adopted in South Africa, where ecological water requirements have to be determined before any flow alteration takes place. Consequently, only the difference between the total available water resource (natural flow regime) and the environmental reserve can be considered available for other uses.

In addition, the Policy calls for the minimization or mitigation of adverse environmental impacts and identifies Environmental Impact Assessments (EIA) as critical parts of any water resources project.

Despite the overall progressive nature of the Water Policy, there are numerous problems related to its implementation. On the ground practices deviate a lot from the written policy. There tends to be a lack of coordination between the various implementing agencies and in many cases requirements stipulated in the policy are neglected (Haileselassie et al., 2008). Often EIAs (including EFA) are either not conducted at all or insufficient resources and attention are given to them. Environmental standards regarding water quality as well as quantity are not acted upon due to a lack of monitoring and enforcement mechanisms. Hence, despite a modern legal framework, it is clear that environmental considerations are currently of relatively low priority in Ethiopian water resources planning and development.

#### ***17.4.4 Environmental Flow Assessment***

##### **17.4.4.1 Selection of Key Locations**

As discussed above, significant hydraulic development is planned in the Abay basin. The sites of potential future flow alteration present focal points for EFAs. In addition to proposed dam sites on the main stem of the river, those on major tributaries are also sites of interest since these rivers contribute significant amounts of water to the main stem and so influence its hydrological characteristics.

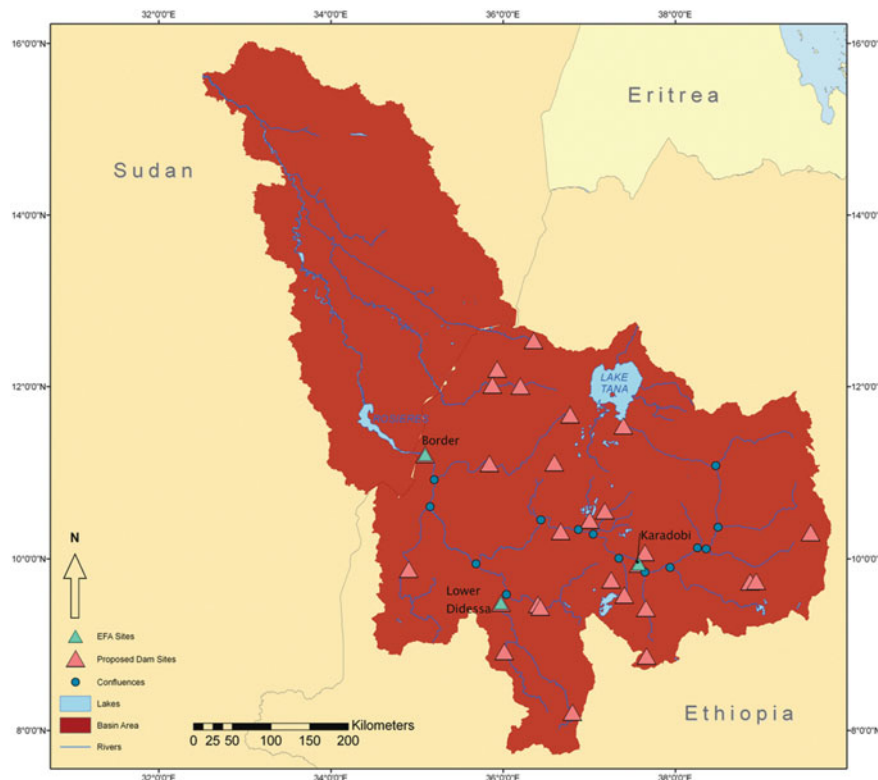


**Fig. 17.2** Location of sites of interest for EFA (proposed dam sites, major confluences) and the three EFA sites selected for this study

Within the Abay 33 locations of interest for EFA can be identified (19 proposed dam sites; 14 major confluences) (Fig. 17.2). From these locations of interest, three key sites were selected for this study. These were selected based principally on their significance in terms of the dimension of the dam planned or the size of the joining river branch.

Two of the selected study sites are situated on the main stem of the Abay. The first at Karadobi and the second near the Sudanese border. Both are planned locations for large hydropower dams.

The Karadobi scheme will be located roughly two kilometers downstream of the confluence with the Guder tributary approximately 300 km downstream of Lake Tana (Norconsult, 2006). With an intended dam height of 250 m and an anticipated total reservoir volume of 40,220 Mm<sup>3</sup>, the Karadobi scheme is the biggest of the currently planned dams in the Abay basin.

The Border dam will be located approximately 21 km upstream of the border with Sudan (Block et al., 2007). The dam planned for this site will have a height of approximately 90 m and a total storage capacity of 11,100 Mm<sup>3</sup>.

The third site chosen is situated on the lower Didessa River close to its confluence with the Abay. The Didessa River is the largest tributary of the Abay. A hydropower scheme is planned on the Lower Didessa, which if constructed could impact significantly the flow regime of the main stem of the river.

#### 17.4.4.2 Availability of Hydrological and Ecological Data

A data inventory for the Blue Nile basin revealed constraints in the availability of both hydrological and ecological data. Hydrological data are only available at a few locations and are limited to discontinuous records.

For the EFA sites at Karadobi and near the Sudanese border, flow data were obtained from Norconsult (2006). These data records were created in the course of a pre-feasibility study for the Karadobi dam. Using the incomplete time series available, all records were in-filled and extended over a 50-year period (1954–2003) with a monthly time step by applying multi-site, multiple regression procedures (Norconsult, 2006).

There are no streamflow data for the EFA site on the Lower Didessa River because there is no flow gauge located close to the confluence. However, monthly time-step estimates of the flow were derived for the Abay River Basin Master Plan based on rainfall-runoff modelling (BCEOM, 1998). These data were used in the current study. However, the length of record only covers the period from 1960 to 1992 (33 years). Thus, time-coincident data from both sources (MoWR and BCEOM) for these 33 years were used for the environmental flow assessments.

Despite the notion of rich biodiversity and high endemism in the basin, site-specific data on local ecology or habitat requirements for target biota are non-existent. This limited the EFA method applied to those which do not require ecological data.

#### 17.4.4.3 EFA Method Selection

Choosing the right EFA method from the plethora of methods available is not straightforward. Each method has advantages and disadvantages. Essentially, the choice for an appropriate approach depends on the data and resources available and the type of issue to be addressed (Dyson et al., 2003).

In common with the situation in many other developing countries, environmental flow initiatives in Ethiopia are still in their infancy. Country-specific EFA methods have not been developed, nor have existing methods been adapted to Ethiopian conditions (compare Tharme, 2003).

Based on a literature survey and the data availability three hydrologic index EFA methods were selected for the current study. Specifically, these were the Global Environmental Flow Calculator (GEFC), the Desktop Reserve Model (DRM) and the Tennant Method.

The GEFC was selected due to its fast and straightforward applicability, and the additional option to use its internal flow database in comparison to user-defined data. In contrast to this first, very simple model, the DRM was chosen because

it is considered to be the most advanced hydrology-based desktop method to date (Smakhtin and Shilpkar, 2005). In addition, the Tennant Method was applied, since it is the most commonly applied hydrologic index method worldwide (Tharme, 2003). Further details and underlying principles of each of the methods are given below.

### Global Environmental Flow Calculator

The Global Environmental Flow Calculator (GEFC) is a software package complemented by a global database of simulated flow time series. The EFA technique incorporated in the GEFC involves a number of successive steps and essentially relies on flow duration curves (FDCs) – cumulative probability distribution functions of flows – that reflect the natural, unregulated flow pattern based on flow time series with a monthly time step. FDCs in the GEFC can be created by accessing either the default simulated flow time series from the package's internal global database or by importing a user defined file containing observed or otherwise simulated flow records. In the case of site-specific assessments user-defined flow data records should greatly improve the precision of the results and – if available – should always be chosen as the preferred option. For a detailed description of the computation procedures applied in the preparation of the global default data refer to Smakhtin and Eriyagama (2008).

FDCs show the percentage of time that a certain flow rate is equaled or exceeded. In the GEFC, 17 fixed percentiles are used (0.01, 0.1, 1, 5, 10, 20, 30, 40, 50, 60, 70, 80, 90, 95, 99, 99.9 and 99.99%) to adequately cover the whole range of flow variability and to ease further application in the context of the subsequent steps (Smakhtin and Eriyagama, 2008).

The GEFC incorporates six environmental management classes (EMCs). EMCs relate to the desired ecological condition of the river. The six classes range from “unmodified and largely natural” rivers (classes A and B) where future developments should be restricted to “seriously and critically modified” rivers (classes E and F). Classes E and F are deemed ecologically unsustainable so class D (i.e. “largely modified”) is usually set as the lowest allowed management “target” for future status. The higher the class, the more water is allocated for ecosystem maintenance and the greater the range of flow variability preserved (Smakhtin and Eriyagama, 2008).

In GEFC, unique FDCs can be generated and subsequently translated into more tangible, physical data (e.g. monthly flow time series in  $m^3/s$ ) for each of the six EMCs based on site-specific natural flow records. Details of the lateral shifting method for the estimation of environmental FDCs for different EMCs can be found in Smakhtin and Anputhas (2006) and Smakhtin and Eriyagama (2008). The spatial interpolation procedure applied in the computation of the associated simulated monthly time series is explained in Hughes and Smakhtin (1996).

### Desktop Reserve Model

The Desktop Reserve Model (DRM) is a hydrology-based method using monthly natural flow records, which has been developed by Hughes and Münster (2000) and

further refined by Hughes and Hannart (2003) to provide a method for generating low-confidence, initial environmental flow requirements for rivers in South Africa.

The DRM is based on the principles of the Building Block Methodology (BBM) (King et al., 2000). The BBM is underpinned by the concept that different components of a river's natural flow regime are essential for the creation of an ecologically acceptable, modified flow regime. These so-called "Building Blocks" (BBs) of the flow regime are low or base flows, small increases in flow (freshets) and high flow or flood events, which are required for channel maintenance (Hughes et al., 1997). In this context, flow variations between normal ("maintenance") and dry ("drought") years play a fundamental role and are defined individually. As a result, four BBs of the natural flow regime are defined in the model output for each of the 12 calendar months:

- Maintenance base flows;
- Drought base flows;
- Maintenance high flows and freshets;
- Drought high flows and freshets.

In addition to this table of monthly requirements for maintenance and drought flows, the model also combines these parameters to monthly assurance or frequency curves. The DRM includes parameters for 21 regionalized assurance curves (e.g. Cape, Karoo, Drakensburg, Zululand, etc. regions), which were established for the natural flow regimes of 1,946 quaternary catchments in South Africa (Hughes and Hannart, 2003). These assurance rules define the frequency with which maintenance and drought years occur in specific regions and principally depend on the prevailing climatic conditions. Consequently, maintenance years dominate (60–70%) in wetter areas with rivers comprising a stable flow regime, whereas they are less common ( $\leq 20\%$ ) in semi-arid and arid rivers (Kashaigili et al., 2006).

Similar to the GEFC, the DRM uses the classification of management targets divided into EMCs for the computation of suitable environmental flows. However, the DRM incorporates only four possible EMCs (A–D), because classes E and F are not regarded as acceptable management goals. In addition, the DRM offers the possibility of opting for transitional EMC categories (e.g. A/B, B/C), which increases the range of possible management scenarios within the model.

### Tennant Method

The Tennant Method was developed in the United States by Tennant (1976) together with the US Fish and Wildlife Service. Environmental flow recommendations resulting from this method are based on specific percentages of the average annual runoff (MAR) related to qualitative fish habitat, as well as to recreational, wildlife and other environmental resources attributes. The impacts of changing discharge rates on stream width, depth, velocity, temperature, substrate, etc., were determined empirically for 11 streams in Montana, Wyoming and Nebraska and translated into an easy to use look-up table (Table 17.3) that suggests the quality of flow-related

**Table 17.3** Environmental flow requirements for fish, wildlife, and recreation

Description of flows	Percentage of MAR	
	Dry season	Wet season
Flushing or maximum	200	
Optimum range	60–100	
Outstanding	40	60
Excellent	30	50
Good	20	40
Fair or degrading	10	30
Poor or minimum	10	10
Severe degradation	0–10	

From Tennant (1976).

ecosystem conditions on a seasonal basis (i.e. wet and dry season flow requirements). For example, it was found that below the critical dry season flow rate of 10% of MAR water depth was insufficient for fish migration leading to a decline in or loss of sensitive species, whereas flow rates of roughly 30% of MAR sustained satisfactory width, depth and velocity to allow for migration (Gordon et al., 2004).

#### 17.4.4.4 Comparison of EFA Methodologies

The environmental flow recommendations for the three key EFA sites were calculated using the three hydrologic index methods, i.e. the GEFC, DRM and Tennant Method. Their similarities and differences were examined and their applicability in a developing country context with severe data constraints was assessed.

For an unbiased comparison, the EMC used in GEFC and DRM, and the Tennant quality category respectively, had to be set to an equivalent management target. Based on a scoring chart that utilizes aggregate environmental indicators to assess the ecological condition of a river (Smakhtin et al., 2007), the most realistic environmental status of the Blue Nile and its tributaries was assessed as EMC C/D (i.e., moderately to largely modified). This reflects the need to balance socio-economic development needs in Ethiopia with the requirement to protect basic ecological services. It means that the flow regime should be allowed to change in such a way that there is likely to be loss and change of natural habitat and biota (possibly including fish) but the basic ecosystem functions of the system will only be moderately altered (Kleynhans, 1996).

As the GEFC does not allow for transitional management classes the average flow value for EMC C and D was calculated and used for comparison. In case of the DRM, the direct simulation of a monthly flow series for EMC C/D was possible and was used accordingly. For the Tennant Method the environmental quality category “fair or degrading” was assumed to be most comparable to EMC C/D and the respective thresholds (10% of MAR as dry season flow and 30% of MAR as wet season flow) were used for the generation of a monthly environmental flow series for further evaluation and comparison.

#### 17.4.4.5 Model Adjustments

As the three hydrologic index methods applied were developed for other regions, initially a reconfiguration of internal model parameters was undertaken to make the models more applicable to the conditions in the Blue Nile basin.

Within the DRM the estimations of the annual totals of the BBs are based on a fixed-internal setting regarding the seasonal distribution of high and low flows, which was determined according to the prevailing flow patterns of South African rivers (c.f. Midgley et al., 1994). The primary dry season is defined as occurring from June to August and the wet season months are January to March. However, the Blue Nile basin is characterized by a different climatic pattern, with the wet season primarily concentrated from July to October and the key dry season flow from February to April. Therefore, the input flow series was shifted by 6 months (i.e. January became July, February became August, etc.). The output time series was then corrected accordingly in order to assign the flow values to the appropriate months. The assurance parameters chosen were those attuned to the conditions in the Drakensburg region of South Africa as its natural flow regime was most comparable to that of the Blue Nile basin due to similar climatic and geological characteristics.

The Tennant Method was developed for the climatic conditions in the western United States with low streamflows in fall and early winter (October to March) and high flows in summer (April–September) (Tennant, 1976). Therefore, similar to the procedure with the DRM, the timing of occurrence for the wet and dry season was altered to December to May (dry season) and June to November (wet season). Additionally, in contrast to the other two EFA methods applied, the Tennant method only yields a point value (MAR) for each environmental quality category. In order to link the Tennant MAR categories with flow variability, its environmental flow recommendations were applied and examined in relation to the monthly streamflow series in a so-called “extended” version of Tennant’s original concept (Smakhtin and Shilpkar, 2005). Thereby, the natural flow record itself provides for the maintenance of characteristic elements of the hydrograph, whilst Tennant provides the percentage of acceptable flow reduction for each month. Furthermore, a prerequisite for successful application of the Tennant Method in an area different from that for which it was originally developed, is the morphologic similarity (e.g. width, depth, velocity) of the streams (Gordon et al., 2004). Since no morphologic data were available for the Blue Nile basin, the direct transfer of the method without additional field investigations and revaluation of Tennant’s original measurements was necessary, but means that results must be treated with extra caution.

In case of the GEFC no site-specific model adjustments were made.

#### 17.4.4.6 EFA Results

The application of the GEF, DRM and Tennant Method to the three study sites in the Blue Nile basin resulted in three different environmental flow time series for each site.

Table 17.4 shows the monthly averages of the three environmental flow series for each EFA site. The annual average values indicate that the maintenance of EMC C/D or “fair or degrading” conditions would require roughly 28, 24 or 21% of the observed MAR according to Tennant, GEFC and DRM, respectively. Furthermore, it can be seen that the DRM consistently results in the lowest flow recommendations, which are approximately 25% lower than the flow recommendations from the Tennant Method (which suggests the highest annual flows) for all three EFA sites. The GEFC computes intermediate annual flow recommendations that are 4, 22 and 16% below Tennant’s flows for the EFA sites Karadobi, Lower Didessa and Border, respectively.

In a month-by-month analysis it can be seen that the environmental flow series derived from the Tennant Method exhibits the largest seasonal flow variations. It shows the lowest values for recommended monthly flows in the dry season (December–May) for all three study sites, where the suggested flows are up to 80% lower than the environmental flows recommended by the two other methods. On the other hand, the recommended flows during the wet season (June to November) exceed the environmental flow series derived from GEFC and DRM by up to 60%.

The differences and similarities of the results from the three individual methods for each of the sites under investigation are illustrated in Fig. 17.3.

#### 17.4.5 Conclusions and the Way Forward

The maintenance of natural hydrological regimes is highly relevant in developing countries, such as Ethiopia, where the livelihood security of a large part of the population is strongly dependent on environmental goods and services. At the

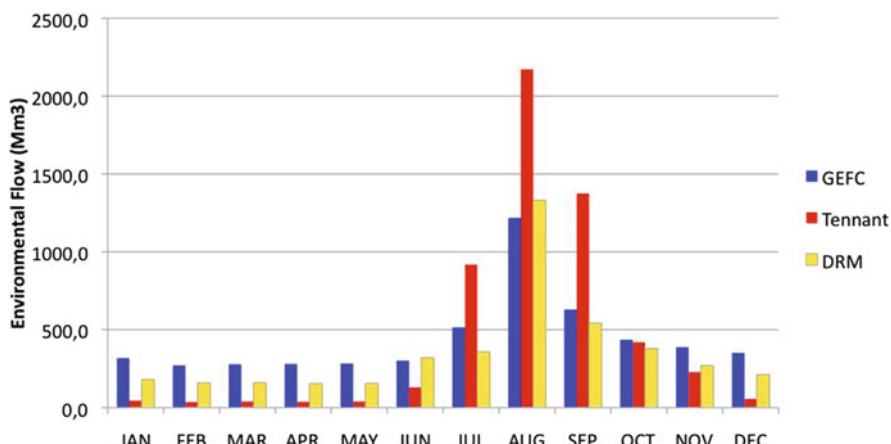


**Fig. 17.3** Comparison of results (mean monthly flow requirements in  $\text{Mm}^3$  for EMC C/D or “fair” conditions) from different environmental flow assessment (EFA) methods for the EFA site at **a** Karadobi, **b** Lower Didessa and **c** near the Sudanese border

**Table 17.4** Monthly averages of observed flows and environmental flow time series ensuring EMC C/D or Tennant's ecological category "fair or degrading", which were generated for the three key EFA sites in the Blue Nile basin

EFA site/method	Environmental flow requirements (Mm <sup>3</sup> )											
	Jan	Feb	Mar	Apr	May	Jun	Jul	Aug	Sep	Oct	Nov	Dec
<i>Kardabi</i>												
Observed	449.1	376.2	398.6	380.8	397.6	432.9	3,061.1	7,241.8	4,583.5	1,399.5	762.4	553.7
GEFC	317.1	270.9	278.2	279.7	282.2	301.5	514.8	1,218.3	629.3	435.2	388.1	350.8
DRM	179.5	157.6	159.2	153.5	155.2	319.4	357.4	1,330.9	541.6	378.5	268.4	211.3
Tennant	44.9	36.7	39.9	38.1	39.8	129.9	918.3	2,172.5	1,375.1	419.9	228.7	55.4
<i>Didessa</i>												
Observed	109.8	63.8	52.6	56.5	95.9	289.4	954.8	1,810.1	1,774.3	1,111.9	355.0	185.8
GEFC	28.0	15.0	13.4	14.5	23.8	69.6	150.9	444.8	409.6	214.2	80.5	48.4
DRM	51.7	34.2	29.4	27.6	33.2	110.1	123.7	381.6	220.9	221.3	129.1	83.1
Tennant	11.0	6.4	5.3	5.7	9.6	86.8	286.4	543.0	532.3	333.6	106.5	18.6
<i>Border</i>												
Observed	511.1	351.4	301.8	284.9	337.2	888.1	1,215.5	3,190.5	1964	1,623.4	1,169.2	757.4
GEFC	318.4	215.2	188.9	180.3	241.0	476.3	1,313.3	3,076	2,196.4	1,066.7	609.0	403.2
DRM	420.5	283.4	244.3	225.6	259.0	740.8	917.5	2,657.0	1,477.9	1,370.4	946.7	614.1
Tennant	84.9	51.0	41.6	39.0	59.2	538.1	2,227.4	3,880.2	3,321.5	1,871.2	795.7	132.7

same time it is recognized that the implementation of environmental flows can also involve some costs related to reduced hydropower and irrigation supply, which is in high demand and essential for national socio-economic development. Despite the national benefits of water resources development, hydraulic structures and related flow alterations also pose an equity problem as the part of the population that is mainly affected and pays the price of such developments (due to lost ecosystem services and displacement) rarely benefit from the supply of electricity. These conflicting interests should be thoroughly evaluated prior to finalizing the planning and design of the numerous water resource developments, proposed for the Abay basin.

In order to achieve compliance with the Ethiopian Water Resources Management Policy potential adverse environmental and socio-economic impacts from hydraulic structures and other water uses have to be minimized or mitigated. Thus, the concept of environmental flows is a pre-requisite for finding a compromise between environmental, economic and social demands on the available water resources.

This study attempted the quantification of a full range of environmental flows (i.e. both high and low flows) using three desktop hydrological methods in the Abay basin. It demonstrated that, in the absence of ecological information, hydrological data can be used to produce coarse, initial estimates of environmental flow requirements. The different approaches produced broadly similar results. Nevertheless all the model results must be treated with caution and they should not be used for anything more than very preliminary planning. Much more detailed studies, including ecological surveys are necessary to provide estimates which can be accepted with more confidence. As indicated by the overassesssd flow recommendations from the DRM, such information is essential to recalibrate the models for the monsoon-driven flow regime of the Blue Nile. Further studies and the development of region-specific model parameters are required to improve the accuracy of the first estimates derived from this study.

Furthermore, the calculation of environmental flows based purely on hydrologic indices has to be restricted to preliminary assessments. Links between flow regime and ecological response are merely assumed, whereas links between flow regime and social impacts are not considered at all. Because of the high proportion of the Ethiopian population living in a rural setting and dependent on subsistence livelihoods, the reliance of these communities upon river flows and related ecosystems has to be assessed. While in the short term hydrology-driven methods provide quick estimates for initial planning, they have to be supported by more comprehensive approaches (e.g. holistic methods) in order to achieve more accurate and (legally) defensible results in the longer term.

Ethiopia's progressive Water Resources Management Policy provides an enabling foundation for sustainable water resources management including the implementation of environmental flows. As basic human and environmental needs are recognized as the highest priority users, in principle further data acquisition relating to these aspects should be promoted. However, a lack of effective monitoring and enforcement mechanisms, as well as the general perception that environmental considerations hamper development, still pose major constraints for

the success of environmental flow assessments in Ethiopia and other developing countries.

In future, as more dams are constructed, difficult choices will need to be made. Informed decisions are only possible with at least a basic understanding of the requirements of all the components of the water system. Greater understanding of flow-ecology-livelihood linkages is essential if water resources are to be used in a sustainable and equitable manner.

## References

AFP (Agence France Presse) (2008) Ethiopia population soars to near 77 million: census. <http://www.eastafricaforum.net/2008/12/04/ethiopia-population-soars-to-near-77-million-census/>. Accessed 12 Sep 2009

Arthington AH, Zalucki JM (eds) (1998) Comparative evaluation of environmental flow assessment techniques: review of methods. Occasional Paper No. 27/98, Land and Water Resources Research and Development Corporation, Canberra

Arthington AH, Bunn SE, Pusey BJ et al (2006) The challenge of providing environmental flow rules to sustain river ecosystems. *Ecol Appl* 16:1311–1318

Arthington AH, Bunn SE, Pusey BJ et al (1992) Development of a holistic approach for assessing environmental flow requirements of riverine ecosystems. In: Pigram JJ, Hooper BP (eds) Proceedings of an international seminar and workshop on water allocation for the environment, The Centre for Water Policy Research, University of New England, Armidale, 282pp

Awulachew SB, McCartney M, Steinhaus T et al (2008) A review of hydrology, sediment and water resource use in the Blue Nile Basin. IWMI Working Paper 131, Colombo

BCEOM (1998) Abbay river basin integrated development master plan project. Report to ministry of water resources, The Federal Democratic Republic of Ethiopia

Bernadová I (1998) Methods for determination of minimum flows in the CR watercourses. In: Blazkova S, Stalnaker C, Novicky O (eds) Hydroecological modelling, research, practice, legislation and decision-making. Report by US geological survey, biological research division and water research institute, Fort Collins, and Water Research Institute, Praha, VUV, Praha, pp 31–32

Block PJ, Strzepek K, Rajagopalan B (2007) Integrated management of the Blue Nile basin in Ethiopia – hydropower and irrigation modelling. International Food Policy Research Institute Discussion Paper, Environment and Protection Technology Division, Washington, DC

Bovee KD (1982) A guide to stream habitat analysis using the instream flow incremental methodology. Instream flow information paper 12, U.S.D.I Fish & Wildlife Services, Office of Biological Services, FWS/OBS-82/26, 248pp

Brown, C, Watson P (2007) Decision support systems for environmental flows: lessons from Southern Africa. *Intl J River Basin Manag* 5:169–178

Dyson M, Bergkamp G, Scanlon J (2003) Flow – the essentials of environmental flows. IUCN, Gland, Switzerland and Cambridge

EEPCo (Ethiopia Electric Power Corporation) (2009) About EEPCo. <http://www.eepco.gov.et/eepco.htm>. Accessed 28 Oct 2009

Estes CC (1996) Annual summary of instream flow reservations and protection in Alaska. Alaska Department of Fish and Game, Fishery Data Series No. 96–45 m Anchorage

Gordon ND, McMahon TA, Finlayson BL et al (2004) Stream hydrology: an introduction for hydrologists, 2nd edn, Wiley, London, 429pp

Haileselassie A, Hagos F, Mapedza E et al (2008) Institutional settings and livelihood strategies in the Blue Nile basin: implications for Upstream/Downstream Linkages. IWMI Working Paper 132, Colombo

Hill MT, Platts WS, Beschta RL (1991) Ecological and geomorphological concepts for instream and out-of-channel flow requirements. *Rivers* 2:198–210

Houghton-Carr HA (2006) The decline of hydrological data collection for development of integrated water resource management tools in Southern Africa. Proceedings of the fifth international conference on FRIEND, Havana

Hughes DA, Hannart P (2003) A desktop model used to provide an initial estimate of the ecological instream flow requirements of rivers in South Africa. *J Hydrol* 270:167–181

Hughes DA, Münster F (2000) Hydrological information and techniques to support the determination of the water quantity component of the ecological reserve. Water Research Commission Report TT137/00, Pretoria

Hughes DA, Smakhtin V (1996) Daily flow time series patching or extension: a spatial interpolation approach based on flow duration curves. *Hydrol Sci* 41:851–871

Hughes DA, O'Keeffe J, Smakhtin V et al (1997) Developing of an operating rule model to simulate time series of reservoir releases for instream flow requirements. *Water SA* 23: 21–30

Jowett IG (1997) Instream flow methods: a comparison of approaches. *Regul Rivers Res Manag* 13:115–127

Junk WJ, Bayley PB, Sparks RE (1989) The flood pulse concept in river-floodplain systems. In: Dodge DP (ed) Proceedings of the international large river symposium (LARS), Can Spec Publ Fish Aquat Sci 106:110–127

Kashaigili JJ, McCartney MP, Mahoo HF et al (2006) Use of a hydrological model for environmental management of the Usangu wetlands, Tanzania. IWMI Research Report 104, Colombo

King JM, Brown CA (2003) Environmental flows: case studies. In: Davis R, Hirji R (eds) Water resources and environment, Technical Note C.2, The World Bank, Washington DC

King JM, Louw MD (1998) Instream flow assessment for regulated rivers in South Africa using the building block methodology. *Aquat Ecosyst Health Manag* 1:109–124

King JM, Brown CA, Sabeth H (2003) A scenario-based holistic approach to environmental flow assessments for rivers. *River Res Appl* 19:619–639

King JM, Tharme RE, Brown CA (1999) Definition and implementation of instream flows. Thematic Report for the World Commission on Dams, Southern Waters Ecological Research and Consulting, Cape Town

King JM, Tharme RE, De Villiers MS (2000) Environmental flow assessments for rivers: manual for the building block methodology. Water Research Commission (WRC) Technology Transfer Report No. TT 131/00, Pretoria

Kleynhans CJ (1996) A qualitative procedure for the assessment of the habitat integrity status of the Luvuvhu River (Limpopo System, South Africa). *J Aquat Ecosyst Health* 5:41–54

Larson S, Larson S (2007) Index-based tool for preliminary ranking of social and environmental impacts of hydropower and storage reservoirs. *Energy* 32:943–947

Lincklaen Arriens WT (2004) Introducing a framework for national water sector apex bodies to assess their effectiveness. <http://www.pacificwater.org/userfiles/file/TWRM/Toolboxes/Framework%20for%20NWC.pdf>. Accessed 11 Sep 2009

McCartney MP, Alemayehu T, Shiferaw A, Awulachew SB (2010) Evaluation of current and future water resources development in the Lake Tana Basin, Ethiopia. International Water Management Institute, Colombo (IWMI Research Report 134), 39pp

Midgley DC, Pitman WV, Middleton BJ (1994) Surface water resources of South Africa. Vols I, II, III, IV, V and VI, Report No's 298/1.1/94, 298/2.1/94, 298/3.1/94, 298/4.1/94, 298/5.1/94 and 298/6.1/94, Water Research Commission, Pretoria

Millennium Ecosystem Assessment (2005) Ecosystem change and human well-being. <http://www.millenniumassessment.org/documents/document.274.aspx.pdf>. Accessed 10 Sep 2009

MoWR (Ministry of Water Resources) (1999) Water resources management policy. Ministry of Water Resources, Addis Ababa, 33pp

Nilsson C, Reidy CA, Dynesius M et al (2005) Fragmentation and flow regulation of the world's large river systems. *Science* 308:405–408

Norconsult (2006) Pre-feasibility study of the karadobi multipurpose project. Volume 1 – main report, draft final. Report to the Federal Democratic Republic of Ethiopia, Ministry of Water Resources

Petts GE, Saccardo I, Crosato A et al (1996) Natural/artificial floods connected with river habitat. In: Leclerc M, Capra H, Valentin S et al (eds) *Ecohydraulics 2000. Proceedings of the 2nd international symposium on habitat hydraulics*, INRS-Eau, Quebec, pp B175–186

Reiser DW, Wesche TA, Estes C (1989) Status of instream flow legislation and practices in North America. *Fish* 14:22–29

Revenga C, Brunner J, Henninger N et al (2000) Pilot analysis of global ecosystems: freshwater ecosystems. World Resources Institute, Washington DC

Richter BD, Thomas GA (2007) Restoring environmental flows by modifying dam operations. *Ecol Soc* 12:12

Smakhtin V, Anputhas M (2006) An assessment of environmental flow requirements of Indian river basins. IWMI Research Report 107, Colombo

Smakhtin V, Eriyagama N (2008) Developing a software package for global desktop assessment of environmental flows. *Environ Model Softw* 23:1396–1406

Smakhtin VU, Shilpkar RL (2005) Planning for environmental water allocations – an example of hydrology-based assessment in the East Rapti River, Nepal. IWMI Research Report 89, Colombo

Smakhtin V, Weragala N (2005) An assessment of hydrology and environmental flows in the Walawe River basin, Sri Lanka. IWMI Working Paper 103, Colombo

Smakhtin V, Arunachalam M, Gehera S et al (2007) Developing procedures for assessment of ecological status of Indian River Basins in the context of environmental water requirements. IWMI Research Report 114, Colombo

Tennant DL (1976) Instream flow regimes for fish, wildlife, recreation and related environmental resources. *Fish* 1:6–10

Tharme RE (1997) Review of IFR methodologies. In: Task 1 Report: IFR Methodology and Parameters, Consulting Services for the Establishment and Monitoring of the Instream Flow Requirements for River Courses Downstream of LHWP dams, Metsi Consultants, Lesotho Highlands Water Project. Report No. 648-02. Lesotho Highlands Development Authority: Lesotho

Tharme RE (2003) A global perspective on environmental flow assessment: emerging trends in the development and application of environmental flow methodologies for rivers. *River Res Appl* 19:379–441

Turner T (2008) Water governance in central Asia. Inception Report, Europe Aid/125803/SER/MULTI

Venot JP, Sharma BR, Rao KVGK (2008) The lower Krishna basin trajectory: relationships between basin development and downstream environmental degradation. IWMI Research Report 125, Colombo

Yohannes O (2008) Water resources and inter-riparian relations in the Nile basin: the search for an integrative discourse. Suny Press, New York, NY, 256pp

# Chapter 18

## Geospatial Mapping and Analysis of Water Availability, Demand, and Use Within the Mara River Basin

Christina Hoffman, Assefa M. Melesse, and Michael E. McClain

**Abstract** The Mara River Basin (MRB) is an international river basin between the bordering countries of Kenya and Tanzania in Eastern Africa. This study looks at several consumptive water-use factors that exist within the basin, as well as established environmental flow requirements, and quantifies the amount of water demanded. Subsequently, this quantity is compared to existing records of water availability for the dry season months of December through March. Hydrologic records, site interviews, population census data, and spatial datasets were used in combination with a geographic information system to determine water demand. Results show that the total current water demand within the basin does not appear to exceed water supply during periods of maintenance or average flow. However, current water requirements do exceed supply during periods of low flow for each of the dry season months, posing a serious threat to water resources within the MRB.

**Keywords** Mara river · Water supply and demand · GIS

### Abbreviations

DRSRS	Department of Resource Survey and Remote Sensing
ESRI	Environmental Systems Research Institute
FDC	Flow Duration Curve
GIS	Geographic Information System
GLOWS	Global Water for Sustainability
GPS	Global Positioning System
MMNR	Masai Mara National Reserve
MRB	Mara River Basin
NMM	North Mara Mine
NOAA	National Oceanic and Atmospheric Administration
RFE	Rainfall Estimate

---

C. Hoffman (✉)

School of Natural Resources, University of Nebraska, Lincoln NE, USA; Department of Earth and Environment, Florida International University, Miami, FL, USA  
e-mail: christina.hoffman@huskers.unl.edu

SNP	Serengeti National Park
UNEP	United Nations Environment Program
UNESCO	United Nations Educational, Scientific, and Cultural Organization
WWF	World Wildlife Fund

## 18.1 Introduction

Fresh water shortages are expected to appear and intensify in many regions of the world over the coming decades. Signs of over-exploited water resources are already apparent in many areas of the world and will only worsen if current consumption and use patterns are not modified and adapted. The Mara River Basin (MRB), a part of the larger Nile River Basin, is one such area where water resources are an ongoing concern. The MRB is an important hydrologic system that not only serves the bordering countries of Kenya and Tanzania but also exists as a valuable input to Lake Victoria, the world's second largest freshwater lake and the recognized source of the White Nile River. Growing water demands and unsustainable use of natural resources in the region are placing an increasing strain on the hydrology of the basin, threatening the livelihood of the many populations that rely on the Mara River as a main source of water.

This study looks at the entire MRB, an area that covers approximately 13,750 km<sup>2</sup>, 65% of which is located within Kenya and the remaining 35% within Tanzania (Fig. 18.1). The Mara River originates on the Mau Escarpment in Kenya's Nakuru District and flows approximately 400 km through the districts of Bomet, Narok and Transmara before crossing into Tanzania where the river flows through the administrative districts of Tarime, Serengeti and Musoma. On the Kenyan side of the basin, the Mara River flows through the Masai Mara National Reserve (MMNR) and then enters Tanzania through the Serengeti National Park (SNP) before ending at Lake Victoria. The MRB includes the entire area of the MMNR as well as the northern portion of the SNP, which is listed as a UNESCO World Heritage site.

Sustaining escalating water demands of the growing population within the basin, as well as meeting the requirements of the Mara-Serengeti ecosystem, is vital to the region. Flora and fauna that populate the MMNR and the SNP rely on the Mara River for survival, for it is the only perennial river in these protected areas. Overall, the Mara River contributes approximately 5% of the total amount of water that flows into Lake Victoria; however, it is probably one of the most important rivers in regards to conservation for it supports both the MMNR and SNP (Nile Basin Initiative 2004).

In addition to human and wildlife demands for water, livestock populations and pressures from large-scale irrigation farming are also placing mounting strain on the river. Water demands from numerous lodges within and around the MMNR and large-scale mining activities in the southern portion of the basin add to the long list of water needs. Rainfall is the driving force that supports life within the MRB;



**Fig. 18.1** Mara River and its main tributaries: the Amala River, Nyangores River, Engare Ngobit River, Talek River and Sand River

however, rainfall within the basin varies greatly across seasons as well as annually. During dry periods, which exist between June and October and December to mid March, insufficient rainfall places strain on the water users of the basin. It is estimated that droughts occur every seven years within the MRB, although variations to this are quite possible (Gereta et al., 2002). Droughts are a contributing factor to the loss of livestock as well as to decreases in wildlife, including both residential and migrating wildlife populations that inhabit the Mara-Serengeti ecosystem.

Currently, a number of factors contribute to the degradation of the MRB. Deforestation, changing land-use patterns, increased human population, poor management of water abstractions and wastewater discharges in both Kenya and Tanzania are threatening sustainability. Deforestation on the Mau Escarpment is being caused by human population increase, small-scale agricultural expansion and timber collection for fuel and construction materials. These factors, in combination with poor soil conservation efforts and overgrazing of livestock, result in increased erosion throughout the region.

Soil erosion and run-off have been associated with sediment build-up at the mouth of the river, increased turbidity which harms aquatic life, decreased soil fertility, and contamination of the river due to releases of pesticides and pollutants into the water system (Mati et al., 2005b). Increased inputs of fertilizers, such

as nitrogen and phosphorus, augment the threat of eutrophication (Muir 2007). Furthermore, uncontrolled small-scale artisanal mining in the southern portion of the basin threatens water quality.

In addition to water quality, water quantity is also a major concern within the MRB, especially during the dry season when the threat of drought is high. According to surveys conducted within the MRB, 62% of households use water from the Mara River for both their domestic and livestock use (Aboud 2002). While the Mara River and its tributaries are the dominant water source within the basin, other water sources include springs, rainwater, wells, and boreholes. However, the MRB is considered to have low potential of groundwater resources. For example, of the nine boreholes in the Narok District analyzed in the National Water Master Plan, none were considered to have a safe yield (JICA 1992 and Krhoda 2001). Adding to the challenge, the water abstraction system within the basin is poorly planned and loosely monitored, causing abstractions to occur in an uncontrolled manner and often times without permits.

While the MRB draws much attention from researchers due to the biodiversity and ecological significance associated with both the MMNR and the SNP, limited studies on water quantity have been conducted to date. Furthermore, there have been no studies that have attempted to quantify the total consumptive water demand placed on the MRB from the various users that exist within the system.

Kenya is already deemed to be in a “water stressed” condition (1,000–1,700 m<sup>3</sup> of water/person/year) and is predicted to reach “water scarce” status (less than 1,000 m<sup>3</sup> of water/person/year) in less than 25 years. Furthermore, the United Nations projects that Tanzania will become a “water stressed” nation by 2025 (UNPFA 2003 and UNEP 2002a).

In order to establish a more comprehensive understanding of the surface water availability and demand that exists within the MRB, the goals of this research are to: (1) investigate the current hydrologic situation within the MRB and map relevant water-demand factors within the basin, (2) estimate the cumulative consumptive water demand in the MRB based on current uses, and (3) compare total consumptive water demand, in combination with environmental flow requirements, to records of surface water availability within the basin to see if there are any instances when water demand eclipses supply.

## 18.2 Datasets and Methodology

### 18.2.1 *Hydrometeorological Analysis*

#### 18.2.1.1 Rainfall

The MRB has both a short and long rainy season. The short rains can begin as early as September and extend to December, while the long rains usually begin in mid-March and extend to June (with a peak in April). Rains falter beginning in June and

dry conditions may extend to October. Similarly rains may falter in December and very dry conditions may extend through January (Krhoda 2001).

In Kenya, the mean annual rainfall in the upper portion of the basin (the Mau Escarpment) averages between 1,000 mm and 1,750 mm, while mean rainfall in the southern portion is between 300 mm and 800 mm/year. The northern and western portions of the basin receive the most rain, which ranges from 1,200 mm to 1,800 mm/year (Krhoda 2001). In Tanzania, the district of Tarime and a portion of the Serengeti district receive between 1,250 mm and 2,000 mm of rainfall annually, which is more than surrounding areas due to orographic effects. Much of the Musoma district and the eastern parts of Serengeti receive annual rainfall ranging from 900 mm to 1,300 mm/year (Yanda and Majule 2004). Table 18.1 shows the descriptive statistics of temperature, rainfall and evaporation within the basin based on historical records while Fig. 18.2 depicts the locations of select gauging stations within the MRB. Additionally, Fig. 18.3 shows the high variability in long-term monthly average rainfall values for each month for Kiputunga Forest in Kenya and Nyabassi in Tanzania.

**Table 18.1** Descriptive statistics within the MRB (a) flow ( $\text{m}^3/\text{s}$ ), (b) rainfall, air temperature and evaporation were acquired and analyzed as part of the Mara Environmental Flows Assessment (EAC 2009)

(a)	Amala <sup>a</sup>	Nyangores <sup>a</sup>	Mara mines <sup>a</sup>
Min	0.004	0.4	0.89
Max	71.7	27.2	102.9
Mean	8.1	8.5	24
STD	12.4	6.5	22.8
Skewness	2.6	0.66	1.4
Kurtosis	7.2	-0.65	1.3

(b)	Average monthly rainfall (mm) <sup>b</sup> at Kiputunga (1961–2003)	Average monthly rainfall (mm) <sup>b</sup> at Nyabassi (1944–1993)	Average daily air temperature ( $^{\circ}\text{C}$ ) <sup>b</sup> at Narok (1995–2003)	Average daily evaporation (mm) <sup>b</sup> at Narok (1995–2003)
	Min	41.7	62	15
Max	283	207	19.6	8.7
Mean	107	116	17.5	5.2
STD	38	27.5	0.99	1.1
Skewness	2.2	0.8	-0.5	0.3
Kurtosis	8.1	1.4	-0.5	0.1

<sup>a</sup>Flow data was acquired from the Ministry of Water and Irrigation (Kenya) and Ministry of Water (Tanzania).

<sup>b</sup>Rainfall, temperature and evaporation were acquired from Kenyan Meteorological Department and Tanzanian Meteorological Agency.

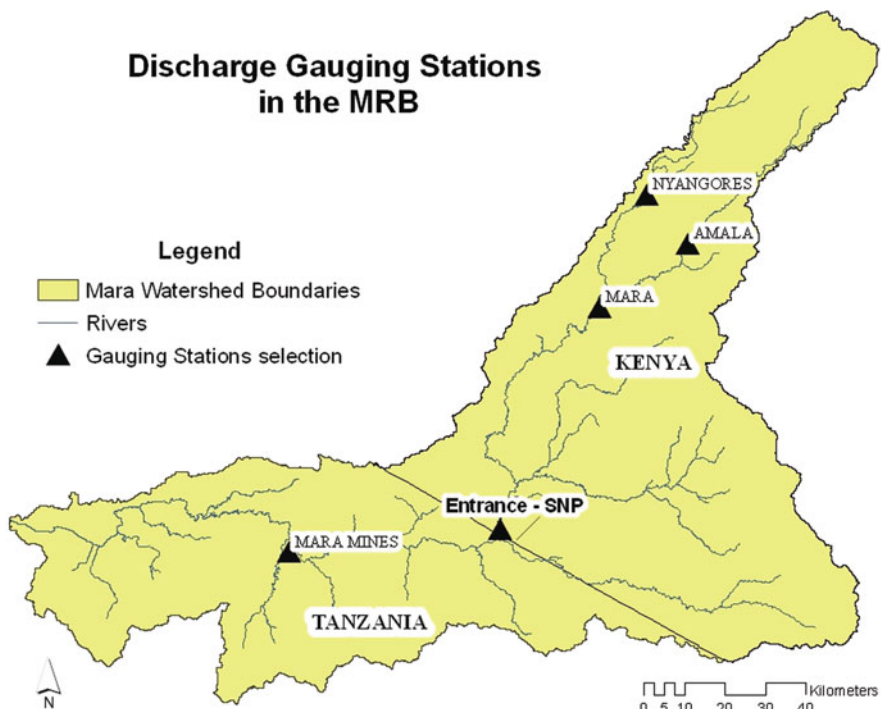


Fig. 18.2 Discharge gauging stations and drainage lines within the MRB

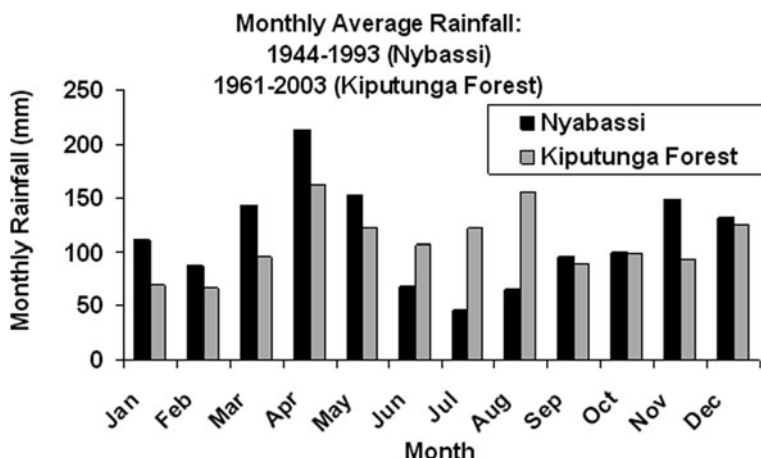


Fig. 18.3 Long-term monthly average rainfall values for each month for Kiputunga Forest in Kenya and Nyabassi in Tanzania

### **18.2.1.2 Hydrological Analysis**

A flow duration curve (FDC) shows the percentage of time that a given flow rate is equaled or exceeded for a particular value. The shape of the FDC can indicate the hydrogeological characteristics of a watershed. Flow duration curves from the mean monthly flow data of the Amala, Nyangores and Mara Mines were constructed to understand the low and high flow end of the rivers and also to characterize the rivers based on the slopes of the two ends of the curve. High slopes in the low flow tail will indicate a less sustained low flow during the dry seasons than a low slope FDC. This indicated less and/or variable base flow in the dry seasons.

A low-flow frequency analysis shows the number of years when a low-flow rate is exceeded. This depicts the recurrence interval, the average interval (in years) that the river discharge falls below a given rate, and can also be used to represent base flow conditions. The curve is generated from the series of annual minimum flow values extracted from the stream monitoring data. A high slope of the low-flow curve can be taken as an indicator of variable low flow.

### **18.2.2 Use of GIS**

This research used a Geographic Information System (GIS) to explore water demand factors within the MRB. Specifically, ESRI's ArcGIS was used to visually define the study area, give spatial attributes to water-demand factors and to incorporate quantitative data for water-demand factors considered in the study. This analysis integrates available research, as well as new data and information collected in the field, in an effort to spatially represent water use in the basin. General techniques utilized include topological modeling, map overlay and data extraction for each of the six water demand sectors.

### **18.2.3 Data Collection**

Data for this research were collected over the length of the MRB, from the Mau Forest in Kenya to the mouth of the Mara River at Lake Victoria in Tanzania, as well as in the capital cities of Nairobi and Dar es Salaam during June-July 2006. Data were collected in a number of ways including literature reviews of scholarly journals and articles, meetings with organizations and agencies involved in the study area, site visits to irrigation schemes, mining operations, lodges and tent camps, as well as site visits and interviews with local and state agencies associated with the MRB. Data obtained through these efforts included notes from on-site interviews, information on water policies and regulations collected from organizations and agencies, water permitting data from regulating agencies, river gauging data, digital data including various GIS datasets, statistical data, and onsite GPS points taken with a mobile GPS unit.

### **18.2.4 Estimation of Water Demand**

Six major water demand factors were identified within the MRB, including water demanded for: (1) domestic water supply, (2) livestock, (3) wildlife, (4) lodges and tent camps, (5) large-scale irrigation farming and (6) large-scale mining. The methodology utilized is described specific to each factor.

#### **18.2.4.1 Human Population**

The human population is multiplying in all areas of the MRB, with an average projected population growth rate of 2.4% for the Kenyan districts of Nakuru, Bomet, Transmara, and Narok and an average 2.5% annual population growth rate for the Tanzanian districts of Tarime, Serengeti and Musoma. (Kenya NBS 2006; Tanzania NBS 2005; Tanzania NBS 2003).

National population census counts conducted in 1999 in Kenya and 2002 in Tanzania were utilized to spatially determine the human population existing within the natural boundaries of the MRB (Kenya CBS 2001; Tanzania NBS 2005). For wards fully incorporated within the boundaries of the MRB, the population count was taken directly from the respective census data. However, for wards extending beyond the basin boundary, the relevant population was determined through the use of ArcGIS. Population counts at the ward level were spatially associated with an administrative boundary shapefile of the study area and were clipped to determine the new area. The population density associated with the original ward was then used to determine the human population of the clipped ward (Fig. 18.4).

To estimate the quantity of water required to sustain the human population within the MRB, population counts were multiplied by daily per person water usage estimates. Since the majority of the population residing within the basin is rural, an average water quantity of twenty liters per person per day was used. This is considered the average in both Kenya and Tanzania as the year-round availability for per capita domestic water consumption, including water used for drinking, bathing, washing, and cooking (Mati et al., 2005a; Zaba and Madulu 1998). However, it is important to note that the 20 liters per person per day used in this study is slightly below the value specified in Kenyan water law, which is 25 liters per person per day.

#### **18.2.4.2 Livestock Populations**

Livestock production is a major source of income throughout the MRB, providing both employment opportunities and food supply to inhabitants, as well as serving important social and cultural values. Livestock rearing, which mainly consists of cattle, goat, and sheep, is undertaken as small and middle scale enterprises in the upper portions of the basin while activity in the mid region is more closely associated with extensive ranching enterprises.

Livestock population counts for this research were derived from a variety of sources for varying years based on data availability (Department of Livestock Production, Bomet District 2006; UNEP Report 2002b; District Livestock Office,

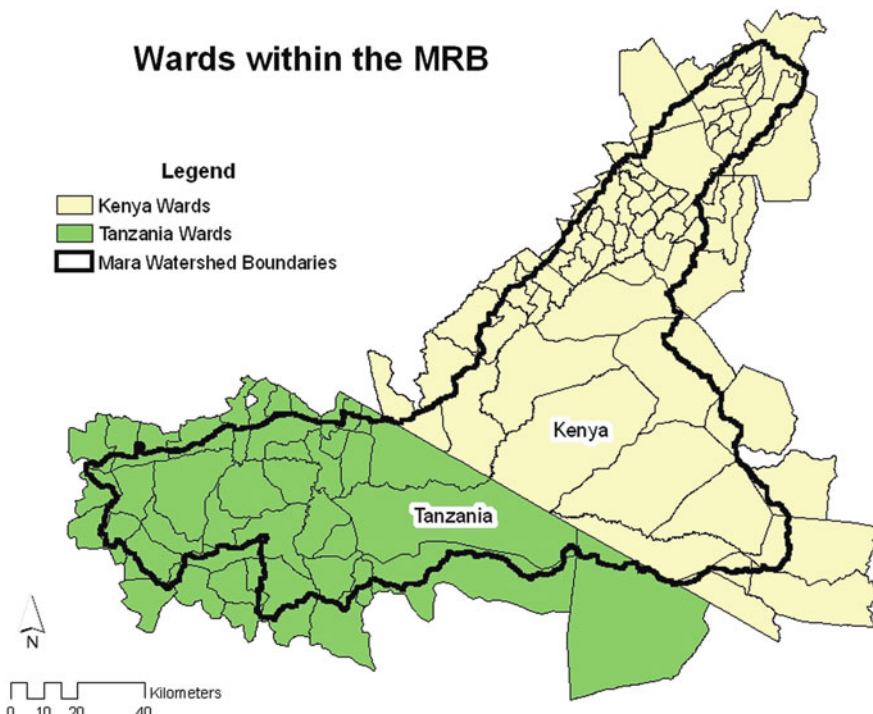


**Fig. 18.4** Administrative boundaries at the ward level for both Kenya and Tanzania with an overlaying boundary of the MRB

Nakuru 1996; URT 2003). Subsequently, livestock population counts for the MRB were determined at the district level using a methodology similar to that used in calculating the human population. For districts fully incorporated within the boundaries of the MRB, the population count was taken directly from the respective census data. However, for districts extending beyond the basin's boundary, population counts were derived by applying the districts population density to the area of the clipped ward. Daily drinking water requirements were based on estimates established for non-lactating livestock under African ranching conditions determined by King (1983) as depicted in Table 18.2. As defined by King (1983), a practical guideline for daily drinking water requirements for development purposes reflects the maximum requirements of the animal, both in terms of its daily requirements and the amount it can drink in one visit.

#### 18.2.4.3 Wildlife Populations

Wildlife in the MMNR and SNP is the backbone for tourism within the MRB and the region's annual migration of over 1 million wildebeest, Thompson Gazelles, and zebras is one of the magnificent spectacles that fuel this industry. Much of the

**Table 18.2** Estimated daily drinking water requirements for non-lactating livestock under African ranching conditions (King 1983)

Species	Weight (kg)	Daily drinking water requirements (liters)	
		Mean	Practical guideline for development
Zebu bovine	350	16.4	25
Goat	30	2.0	5.0
Sheep	35	1.9	5.0
Donkey	120	12.4	Not provided

wildlife within the MRB depend on the Mara River as a dry season water source. This is especially true in drought years, when water shortages severely affect water and forage availability, causing declines in wildlife populations through reduced reproduction, starvation, and/or insufficient water consumption (Gereta et al., 2002).

Due to the complexity of wildlife movements over the landscape and the limited availability of wildlife population census data specific to the area of the MRB, wildlife populations counts for this study are limited to (1) wildlife populations within the Narok and Trans Mara districts of Kenya (which includes the MMNR in entirety) and (2) population counts for the migrating species that enter into the MRB during the dry season. The migrating species included in this analysis are those that make up the annual migration, which enters into the MRB for an approximate 4 month span between the months of July and October (Gereta et al., 2002). For this 4 month period, the annual migration numbers of one million wildebeest and 300,000 of each Thompson Gazelle and zebra were used (Wolanski et al., 1999) in combination with resident population counts for wildebeest, Thompson Gazelle, zebra, buffalo, eland, elephants, Grant's Gazelles, Maasai Giraffe, impala, hartebeest, topi, warthog, and waterbuck.

Wildlife population counts for the Narok and Trans Mara districts of Kenya were taken from a study conducted by the United Nations Environment Program (UNEP 2002b) using data provided from aerial censuses conducted by the Department of Resource Surveys and Remote Sensing (DRSRS) in Kenya. It is important to note that the 2,000 wildlife population counts taken from the UNEP study were taken at the height of the year 2000 drought. During this drought a more than 50% decline in wildlife population numbers was seen when compared to 1996 census data (UNEP 2002b) which indicates a potential underestimate of quantified wildlife water demand.

Wildlife population numbers were then used in combination with estimated daily water requirements for the considered species. Daily water requirements for each species was calculated at 4% of the body weight of an adult male as adapted from du Toit (2002). While water consumption rates vary by species, consumption is directly proportional to each animal's body weight (Peden et al., 2003).

#### 18.2.4.4 Lodges and Tent Camps

Rapid increases in tourism to the MRB have raised demands for tourist lodging facilities. Between 1995 and 2004, tourism increased by 80% in the MMNR and by 535% in the SNP between 1990 and 2002. As a result, the water resources required to support this industry have also multiplied, leading to greater abstractions from flowing rivers or streams located near the facility or from boreholes drilled into underlying aquifers.

While no lodging facilities exist within the SNP portion of the MRB, at the time of research, sixty-five lodges and tent camps were found to be operating within the Kenyan portion of the MRB. Of this number, thirty-six were considered basic in regards to the types of facilities and amenities offered, usually consisting of short-drop toilets and safari showers (where water is hand-carried to the room). While the cumulative water use from these basic sites is likely to augment overall demand, this research solely quantified water demand from the twenty-nine high-end accommodations found to offer running water and flush toilets to their guests.

The accommodation facilities considered in this analysis, which are depicted in Fig. 18.5, make available a combined total of approximately 1,000 rooms and 2,116 beds to tourists visiting the MMNR and/or the SNP. Using bed availability and monthly bed occupancy rates (based on a sample of lodges and camps in the MMNR from 1997 through 2000), daily bed occupancy was calculated and then multiplied with daily per person water consumption averages (Walpole et al., 2003). While the amenities and facilities offered by lodges and tent camps in and around the MMNR vary to some degree, a general guideline for water demand for non-residential use estimates the average daily water use per person staying at a luxury camp to be between 380 to 570 liters per day (Water Systems Design Manual 2001). For the purpose of this study, it was assumed that the average water use per day per guest is 380 liters.

#### 18.2.4.5 Large-Scale Irrigation Farming

Agricultural water demand was calculated for large-scale irrigation farms operating within the MRB. While smallholder mixed farming also exists, it takes place primarily on the subsistence level and is typically rain fed. At the time of research (2006), large-scale irrigation was limited to the Kenyan portion of the MRB. In total, 690 hectares were under irrigation from four farms: Olerai Limited Mara Farm, Lemontoi, Shimo Limited and Ndakaini Farm Limited (Fig. 18.6). Of this total, 660 hectares were under pivot irrigation and 30 hectares were under floppy irrigation, a South African method of overhead irrigation. Combined, these farms used ten irrigation pivots; all fed by water abstracted directly from the river via large, diesel pumps. In 2006, there were five pumps abstracting water from the river, which was the sole source of irrigation for these farms.

Major crops within the basin include seed maize, French beans and gum trees, of which only seed maize and French beans are irrigated. While irrigation timeframes

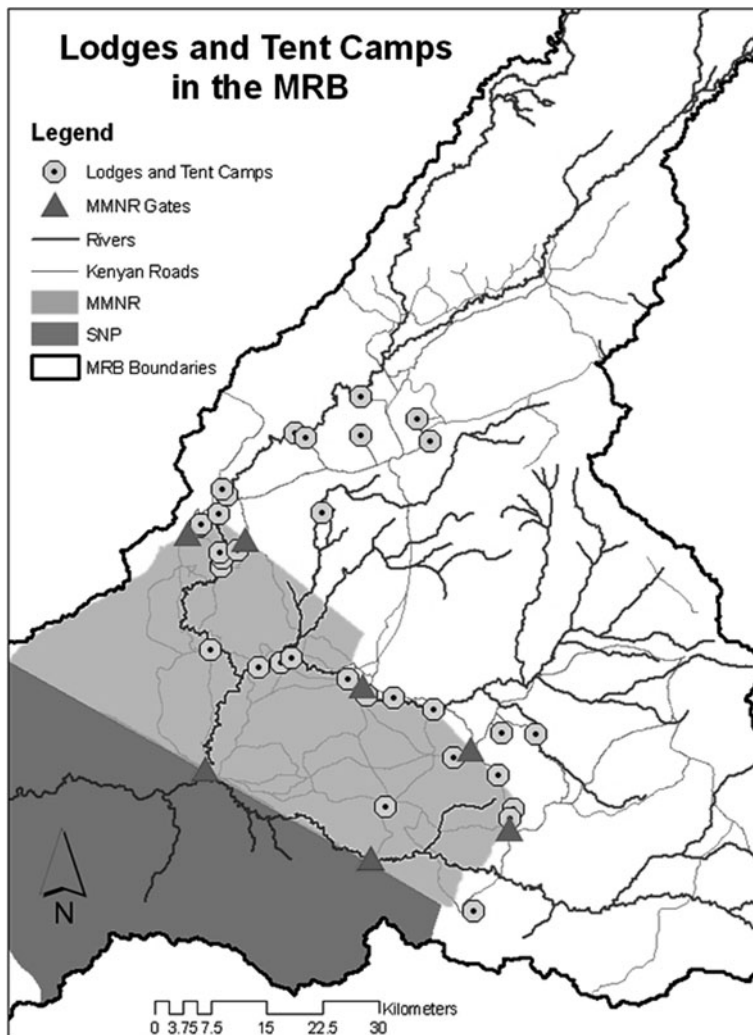


**Fig. 18.5** Locations of lodges and tent camps in and around the MMNR

and quantities vary with rainfall, it is estimated that each hectare of land under irrigation requires approximately five to seven mm of water per day during the growing season (personal communication, Tarquin Wood of Olerai Limited Mara Farm). GIS data layers showing 2006 satellite daily rainfall amounts in 123 km<sup>2</sup> blocks were used to ascertain the amount of daily rainfall received and therefore determine the daily irrigation required to make up for insufficient rainfall (assuming a daily irrigation requirement of seven mm). For irrigation areas falling within several blocks, the average rainfall between blocks was calculated and utilized.

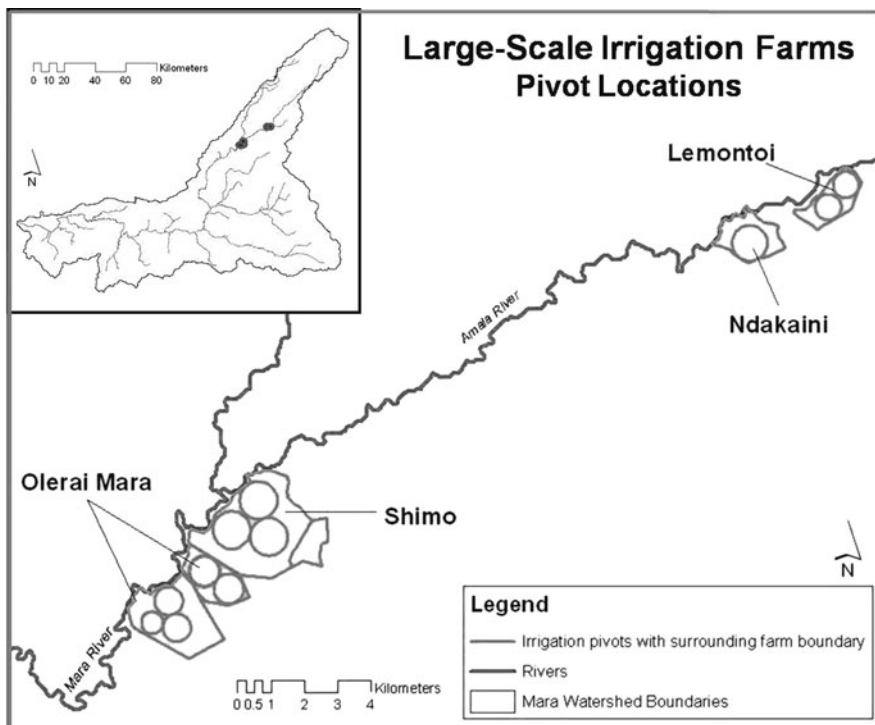


**Fig. 18.6** Large-scale irrigation farms within the MRB and their associated pivot locations. Note: Although the map depicts a total of eleven irrigation pivots, at the time of research (2006), only 10 pivots were operating. Shimo Limited has two pivots to date, with a third pivot planned. Source: Shapefile of pivot locations and farm boundary locations provided by Ramani Communications, Ltd

Rainfall data for this analysis were taken from the National Oceanic and Atmospheric Administration's Rainfall Estimate (NOAA RFE) database. The NOAA Climate Prediction Center has been using a technique to generate daily precipitation by merging daily rain gauge observations with satellite estimates over the African continent since 1982 (NOAA 2007).

#### 18.2.4.6 Large-Scale Mining

Of the two large-scale mining facilities in operation within the MRB (Fig. 18.7), only the North Mara Mine (NMM) was considered in this analysis. The Buhemba Mine, which is not considered, is located near the edge of the MRB and does not appear to have proximity to the Mara River or its tributaries. This would seem to be especially true during the dry season since the Mara River is the only perennial river in the lower portion of the basin. The NMM on the other hand, is located in the Tanzanian portion of the MRB, approximately 10 km south of the Kenyan-Tanzania border.

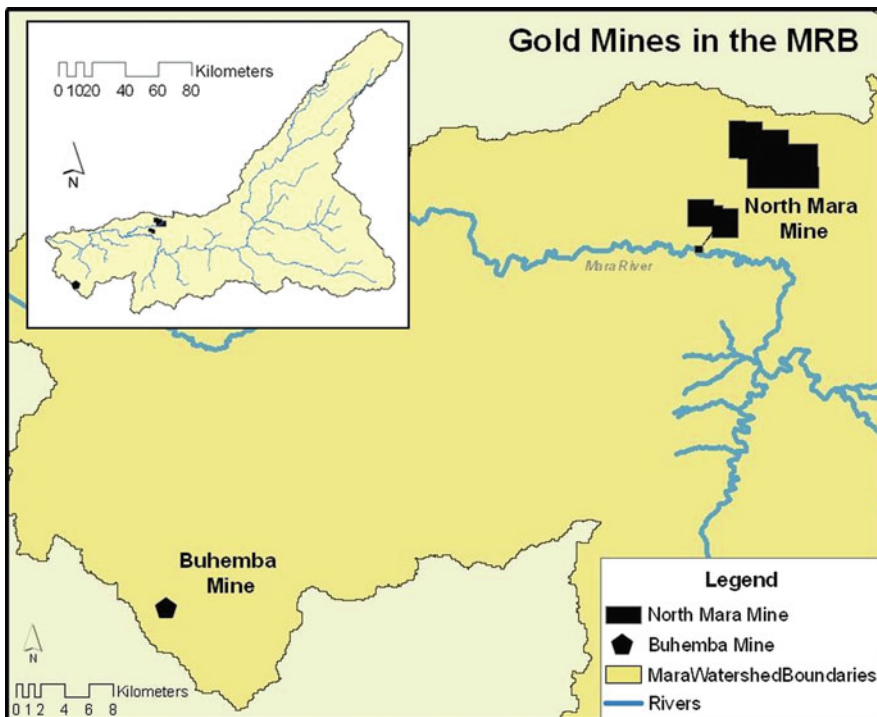


**Fig. 18.7** Large-scale mining operations within the Tanzanian portion of the MRB

Water used in the operation of the NMM is pumped directly out of the Mara River to be used in the mining process. While the NMM recycles the resulting waste water back into the mining cycle, the waste water is not sufficient for all processes as there needs to be a continuous supply of clean water to aid in the gold washing cycle, as well as a supply of water used in the operation of the facility (i.e. bathrooms, living quarters, etc.). For this portion of the analysis, the NMM 2005 Environmental Monitoring Report provided water-abstraction data from the Mara River (North Mara Mine 2006).

#### 18.2.4.7 Water Demand and Supply Comparisons

In order to compare the water demand results found in this analysis to water supply within the MRB, flow data from the Ministry of Water and Irrigation in Kenya were utilized. It is important to note that there are many gaps and discontinuities in existing gauging data, but the data used are the best available for discharge. Furthermore, gauging stations do not exist in all tributaries, which somewhat limits the analysis.

As mentioned, there are five main tributaries contributing to the main stem Mara River, and the integrated flow of all is represented by the discharge at the Mara Mines gauging station. This is also the closest station to the mouth of the

Mara River, thus water demand based on its historical average monthly flows is the most appropriate estimate of surface water supply to use for comparison with the demand calculated in this study. Consumptive water use was determined by looking at the cumulative demand from the six water-use factors. In addition, estimated environmental flow requirements were considered as a component of water demand in this analysis. This is an essential consideration when looking at water quantity requirements since rivers must maintain a flow regime that is sufficient to sustain the aquatic and riparian species that depend on them (WRI 2007). A recent study conducted in conjunction with the Global Water for Sustainability (GLOWS) team establishes minimum environmental flow requirements for the MRB (EAC 2009). Minimum environmental flow requirements describe the proportion of flow intended to maintain river condition at some designated acceptable level on an annual/seasonal/monthly basis (IWMI 2007). The environmental flow data incorporated into this study include minimum average monthly base flow necessary to support targeted ecological functions and maintain flow-related water quality.

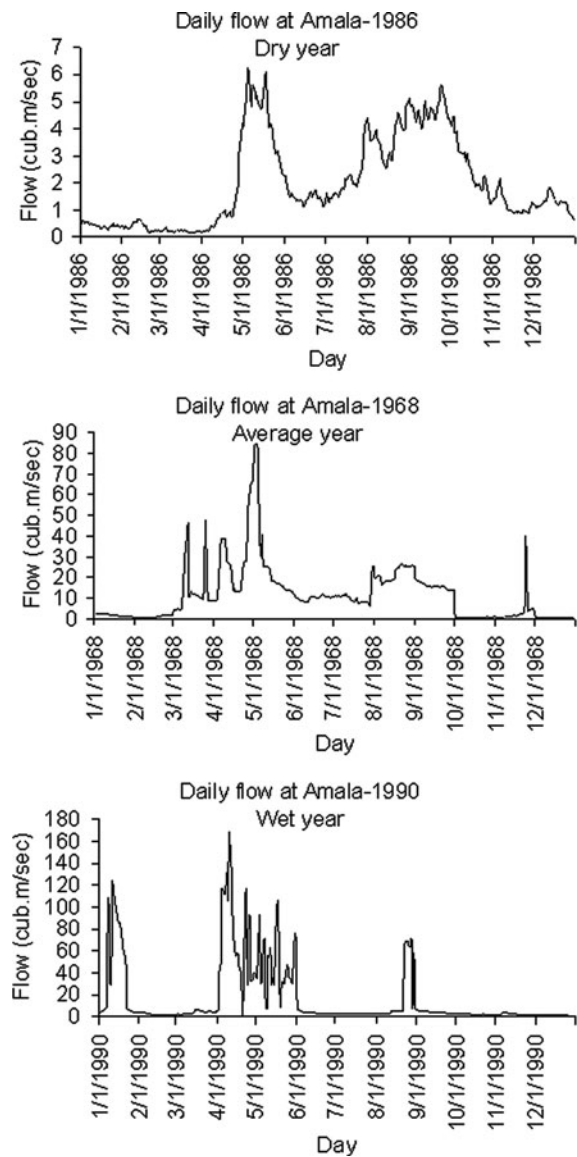
## 18.3 Results and Discussion

### 18.3.1 Hydrometeorological Analysis

Data were obtained from the Amala River, Nyangores River and Mara River at Mara Mines documenting the annual and inter-annual flow variability, the recurrence interval of selected low flows and also estimates of the available average flows during the drought years and average years (Table 18.1). Figures 18.8 and 18.9 show hydrographs for selected drought, average and wet years at the Amala and Nyangores gauging stations. The record reveals different levels of hydrologic variability from extreme drought years as seen in 1986 to wet years in 1990. The river discharges are a reflection of the rainfall in the basin, mainly in the upstream areas. Declines in the dry season flows during recent years were also observed at the Amala gauging station with no corresponding declines in annual precipitation total, possibly. The lower dry season flows may be associated with reduced headwater recharge due to some land use change, especially conversion of forest to agricultural in the headwaters of the Amala River. Historical flow data show the Amala to have lower dry season flows and higher wet season flows than the adjacent Nyangores River with a similar drainage area.

The monthly flow duration curves (FDC) for the two headwater rivers and main-stem Mara are shown in Fig. 18.10. The rivers have different characteristics during low flow seasons. The flow below 50% recurrence interval shows a steeper slope for Amala than Nyangores and Mara Mines indicating a less sustained flow. Similarly the 7-day low flow data (Fig. 18.11) show that Amala has lower values for the lowest flow for 7 days from the historical records than Nyangores. Analysis of the 7-day low flow recurrence interval shows that the 10-year 7 day low flow was  $4 \text{ m}^3/\text{s}$  for Nyangores and  $1.3 \text{ m}^3/\text{s}$  for Amala (Fig. 18.12).

**Fig. 18.8** Hydrographs for selected drought, average and wet years at the Amala gauging station



### 18.3.2 Demand Analysis

The total annual consumptive water use calculated within the MRB is 23,812,454 m<sup>3</sup>, with the largest use being large-scale irrigation, followed by human domestic use, livestock watering, wildlife, large-scale mining, and lodges and tent camps (Fig. 18.13).

**Fig. 18.9** Hydrographs for selected drought, average and wet years at the Nyangores gauging station

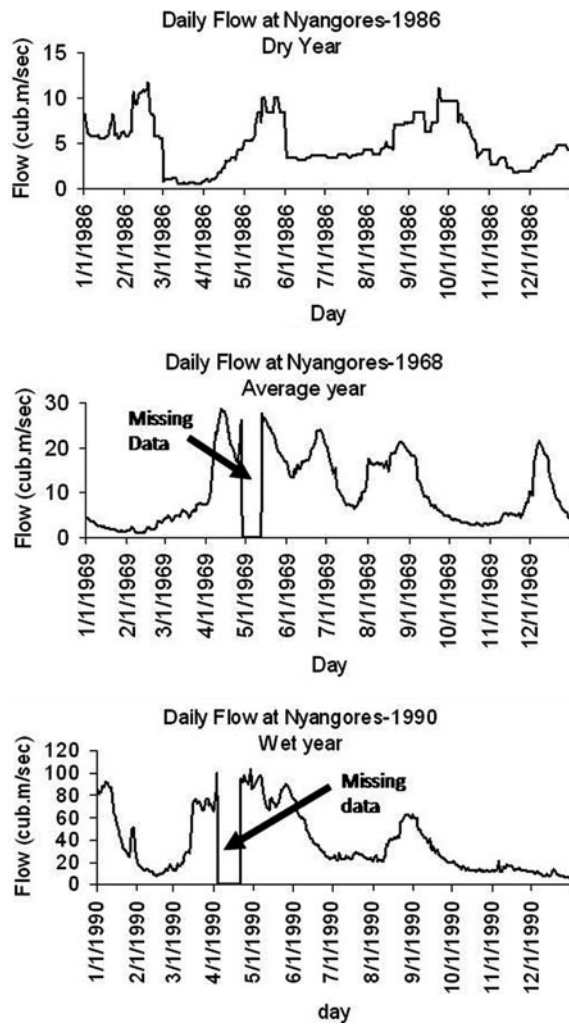
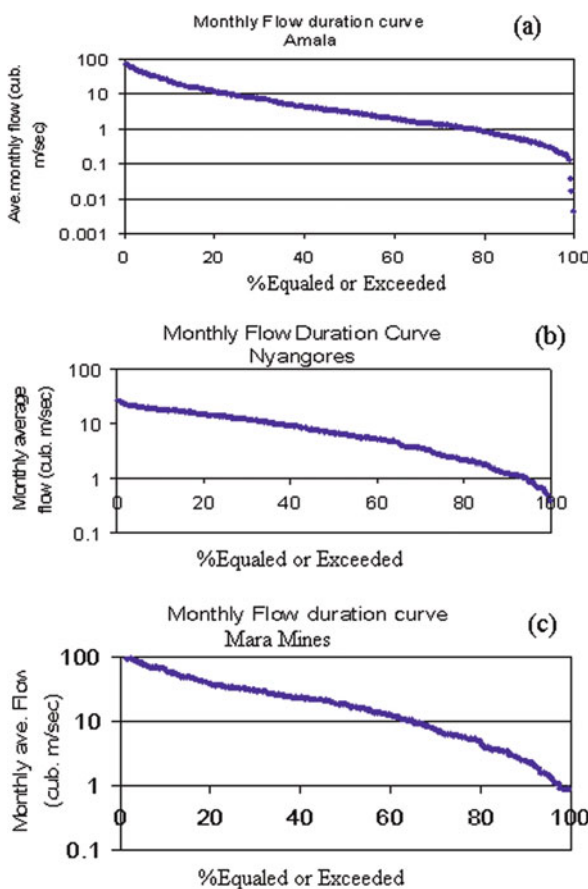


Table 18.3 quantifies the estimated monthly and annual consumptive water use for the factors considered in this analysis. The greatest water demand is seen over dry season months, mainly January through February and June Through October. The water demand from large-scale irrigation as well as from lodges and tent camps peaks during both the early (January through February) and late (June through October) dry season periods while the wildlife demand peaks during the dry season months of July through August (as a result of the annual migration). Water demand from mining operations escalates in July and remains high through November. However, due to low river flows, abstraction was not possible for the months of September and December, and therefore, demand was not assessed. Monthly water

**Fig. 18.10** Monthly flow duration curves (FDC) for Amala, Nyangores and Mara Mines



demand variation is not seen within the human and livestock demand columns because annual census data were utilized.

Table 18.4 compares the historical monthly average flow of the Mara River at Mara Mines (1970–1990) to the amount of water needed to meet environmental flow requirements and consumptive water use demands. The comparison suggests that the historical flows in the river are sufficient to support the present demand for water in the basin while preserving necessary environmental flows. Moreover there is an estimated surplus of flow which if well managed can contribute to further development of the basin. It is informative to note, however, that more than 50% of the surplus occurs during just 3 months of the year (April, May, and June). Thus, storage during these months will be important for meeting increased future water demands during the other months of the year when runoff is reduced. The largest increase in demand is likely to come from the expansion of irrigated agriculture. Kenya water law already requires that all irrigators store a volume of water

**Fig. 18.11** 7-day low flow data for the Nyangores and Amala Rivers

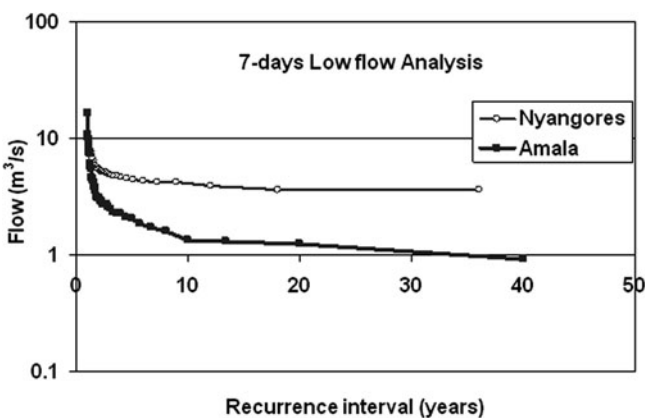
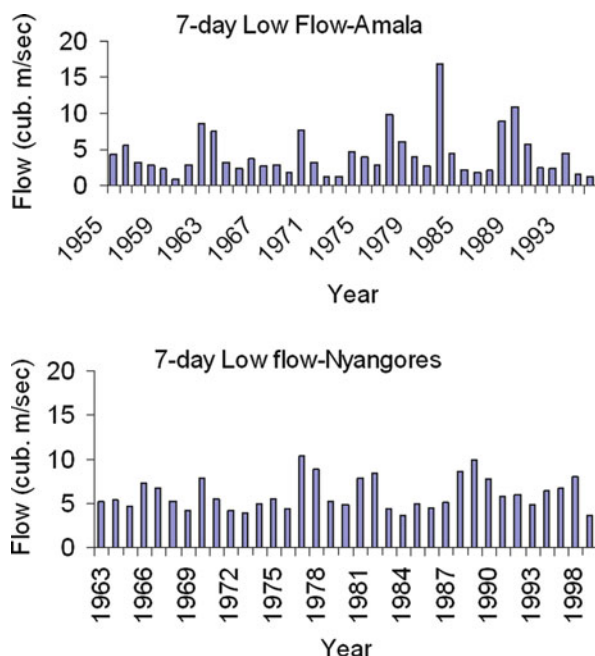


**Fig. 18.12** 7-day low flow recurrence interval for the Nyangores and Amala Rivers

equivalent to at least 3 months demand. Off-channel storage is preferred because this would cause minimal environmental damage to the Mara River system.

While the historical flow record presents an optimistic view of overall water supply in the MRB and opportunities for water-dependent development, it is important to note that the situation is quite different during drought years. As mentioned earlier, it is estimated that drought occurs on average once every 7 years within

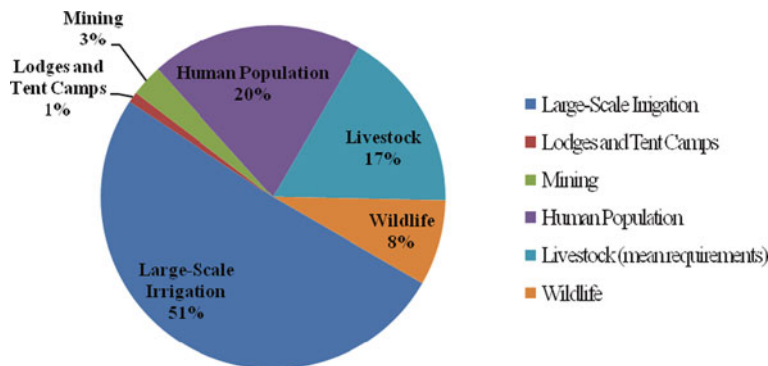


**Fig. 18.13** Annual consumptive water use within the MRB

the MRB (Gereta et al., 2002). During drought years, flows in the Mara River at Mara Mines have fallen as low as  $1 \text{ m}^3/\text{s}$ . Past droughts have caused widespread mortality of both domesticated and wild animals in the basin, and orders have been issued to stop irrigation. Kenyan water law is quite explicit in stating that priority in water allocations is devoted first to the basic domestic water needs of people (25 l/person/day) and second to meeting the minimal environmental flow requirement.

At the time of research, several site interviews were conducted with representatives from MRB lodges and tent camps. While this research focuses on surface water resources within the MRB, site interviews revealed that lodges and tent camps using ground water resources within the basin also experience water shortages during dry months. During January and February of 2006, the borehole at Mara Fig Tree dried out and the camp had to borrow water from its neighbor, Sikanani River Camp. During this same period, Keekorok Lodge had to borrow water from Sarova Mara Lodge. Furthermore, both the Mara Simba and Keekorok Lodges ran into challenges when trying to obtain water from boreholes. Mara Simba Lodge attempted to drill a borehole onsite but was unsuccessful. They drilled 150 m into the ground (well below the river bed) but got no water. In December 2005, after experiencing water shortages, Keekorok Lodge reported that they had to expand their borehole further into the ground, from a depth of 45 m to its current depth of 110 m.

Both future climate change and land use/land cover changes also need to be factored into the water demand and supply equation. The most recent International Panel on Climate Change synthesis report on climate change projects increased precipitation in East Africa by the end of the 21st Century, which could increase water supply somewhat (IPCC 2001). However, it is important to consider that large population growth is projected over this same period and that changes in land use/land cover are also important contributors to climate change and variability (CCSP 2006). This is of definite concern within the MRB, for recent research

**Table 18.3** Estimated monthly and annual consumptive water use (m<sup>3</sup>) in the MRB

Month	Human population	Livestock (mean requirements)	Wildlife	Lodges and tent camps	Large-scale irrigation	Mining	Total consumptive water use per month (m <sup>3</sup> )
January	409,398.4	344,360.4	54,392.9	12,463.2	1,297,200	0 <sup>a</sup>	2,117,814.9
February	369,779.2	311,035.2	49,129.1	13,065.9	1,007,400	15,064	1,765,473.4
March	409,398.4	344,360.4	54,392.9	11,721.1	696,900	5,208	1,521,980.8
April	396,192.0	333,252.0	52,638.3	10,499.4	621,000	0 <sup>a</sup>	1,413,581.7
May	409,398.4	344,360.4	54,392.9	8,104.6	910,800	0 <sup>a</sup>	1,727,056.3
June	396,192.0	333,252.0	52,638.3	12,061.2	1,400,700	52,830	2,247,673.5
July	409,398.4	344,360.4	355,894.0 <sup>b</sup>	6,456.7	1,407,600	180,017	2,713,726.5
August	409,398.4	344,360.4	355,894.0 <sup>b</sup>	9,201.4	1,262,700	136,121	2,527,675.2
September	396,192.0	333,252.0	344,413.5 <sup>b</sup>	13,873.8	1,214,400	0 <sup>a</sup>	2,302,131.3
October	409,398.4	344,360.4	355,894.0 <sup>b</sup>	13,711.9	1,373,100	110,794	2,607,258.7
November	396,192.0	333,252.0	52,638.3	10,248.6	614,100	124,680	1,531,110.9
December	409,398.4	344,360.4	54,392.9	11,226.3	517,500	93 <sup>a</sup>	1,336,971.0
Annual water	4,820,336.0	4,054,566.0	1,836,711.1	152,634.1	12,323,400	624,807	23,812,454.2

quantity demanded (m<sup>3</sup>)

<sup>a</sup>Abstraction was not possible for September and limited in December due to insufficient rainfall and was not needed in January, April, and May due to sufficient rainfall (NMM, 2006).

<sup>b</sup>Assumes the annual migration is within the MRB for the 4 month period from July through October (Gereta et al., 2002).

**Table 18.4** Supply and demand comparisons for the Mara River for years characterized by normal rainfall and low rainfall.

Month	Average minimum flow at mara mines (m <sup>3</sup> /s)	Consumptive water demand <sup>a</sup> (m <sup>3</sup> /s)	Environmental flow estimate <sup>b</sup> (m <sup>3</sup> /s)	Estimation of available supply (m <sup>3</sup> /s)
Jan	16.4	0.8	9.9	5.7
Feb	15.6	0.7	9.8	5.1
Mar	26.7	0.6	12.9	13.3
Apr	69.4	0.5	24.5	44.4
May	59.2	0.6	24.5	34.1
Jun	31.1	0.9	15.3	14.9
Jul	21.8	1.0	10.8	10.0
Aug	22.6	0.9	11.1	10.6
Sep	27.4	0.9	13.4	13.1
Oct	16.3	1.0	9.8	5.5
Nov	23.0	0.6	11.2	11.2
Dec	20.4	0.5	9.9	9.9

<sup>a</sup>The water demands are basin-wide.

<sup>b</sup>Environmental flow estimate derived from EAC (2009).

shows that land use/land cover changes are rapidly occurring. Between 1973 and 2000, rangelands (savannah, grasslands and shrublands) were reduced by 53% and forests were reduced by 32%. Furthermore, during the same period, agricultural land area more than doubled (203%) (Mati et al., 2008).

## 18.4 Conclusions

This study concluded that during normal rainfall years, the supply of water in the Mara River is sufficient to meet current extractive demands and protect environmental flows. Moreover, we estimate that there is surplus water available for continued development in the basin, although more than half of this surplus flow is concentrated during just 3 months of the year. It is vital to realize that during drought years the situation is quite different, as past droughts have already caused serious impacts in the basin and with increasing future water demands the impacts of prolonged droughts are likely to be even more severe.

Water demand within the MRB is greatest during the dry season months, mainly January through February and June through October. This trend is seen when looking at the amount of water required from wildlife, lodges and tent camps, large-scale irrigation, and mining. Large-scale irrigation is by far the largest current extractive water demand factor within the basin, with a demand 39% higher than the next largest demand factor (human domestic use). With increases in human population, tourism, large-scale irrigation and mining expected, it can be assumed that the quantity of water demanded from each of these sectors will continue to escalate.

Improvements in data collection and monitoring throughout the basin are critical to producing a more accurate idea of the water resources within the basin, as well as

an increased knowledge of the limitations of the hydrologic system. Implementing a hydrometric monitoring network to better monitor the components of the hydrologic cycle, as well as water quality and flow characteristics, is one possible solution. Such daily and continuous data would alleviate current data gaps and provide a fundamental resource for sound integrated water resource management.

**Acknowledgments** This research was conducted as part of the USAID Global Water for Sustainability (GROWS) program. We thank the Florida International University Geographic Information System – Remote Sensing Centre, the WWF – East African Regional Program Office (EARPO), and WWF-Tanzania Program Office for critical analytical and field support. Daniel Gann, Heather Singler, Mohamed Awer, Batula Awale, Adams Dikirr and William Kasanga are acknowledged for their individual contributions to this project. Essential hydrological data was obtained from the Kenyan Ministry of Water and Irrigation, the Tanzanian Ministry of Water and Livestock Development, the Kenyan Meteorological Department, and the Tanzanian Meteorological Agency. Financial support was provided by the United States Department of Agriculture (USDA CSREES International Agricultural Sciences Program) and the United States Agency for International Development.

## References

Aboud AA (2002) A rapid socioeconomic assessment of the mara river basin. Environmental studies and natural resources. Egerton University, Njoro

Central Bureau of Statistics (CBS) (2001) Ministry of finance and planning. 1999 population and housing census – counting our people for development, vol 1. CBS, Nairobi

Climate Change Science Program (CCSP) (2006) Temperature trends in the lower atmosphere: steps for understanding and reconciling differences. In: Karl TR, Hassol SJ, Miller CD, Murray WL (eds) A report by the climate change science program and the subcommittee on global change research. CCSP, Washington DC, 164 pp

Department of Livestock Production, Bomet District (2006)

District Livestock Office, Nakuru (1996)

East African Community (EAC) (2009) Assessing Reserve Flows for the Mara River, Kenya and Tanzania. Technical Report under the auspices of the Lake Victoria Basin Commission

Gereta E, Wolanski E, Borner M, Serneels S, (2002) Use of an Ecohydrology model to predict the impact on the serengeti ecosystem of deforestation, irrigation and the proposed amala weir water diversion project in Kenya: Transboundary Issue. Ecohydrol Hydrobiol 2(1-4):127-134

Intergovernmental Panel on Climate Change (2001) Synthesis report. Cambridge Press, Cambridge

International Water Management Institute (2007) Environmental flow methodologies. <http://www.LK.IWMI.ORG/EHDB/efm/visitors/ViewAllEFMType.asp>. Accessed 15 Jan 2007

Japan International Cooperation Agency (JICA) (1992) The study on the national water master plan. JICA, Ministry of Water Resources and Management, Nairobi

King JM (September, 1983) Livestock water needs in Pastoral Africa in Relation to Climate and Forage. ILCA Research Report No.7. International Livestock Centre for Africa

Krhoda GO (2001) Preliminary Phase: Project Development and Stakeholder Analysis – The Hydrology of the Mara River. WWF Eastern Africa Regional Program Office – Mara River Catchment Basin Initiative

Mati BM, Muchiri JM, Njenga K, de Vries FP, Merrey DJ (2005a) Assessing water availability under pastoral livestock systems in Drought-prone Isiolo District, Kenya. Working Paper 106. International Water Management Institute (IWMI), Colombo

Mati BM, Mutie S, Gadain H, Home P, Mtalo F (2008) Impacts of land-use/cover changes on the hydrology of the transboundary Mara River, Kenya/Tanzania. Lakes & Reservoirs: Res Manag 13:169–177

Mati BM, Mutie S, Home P, Mtalo F, Gadain H (September 6–9, 2005b) Land use changes in the transboundary mara basin: A threat to pristine wildlife sanctuaries in East Africa. Paper for presentation at the 8th International River Symposium, Brisbane, Australia

Muir PS (January, 2007) Eutrophication. Oregon State University. <http://oregonstate.edu/~muirp/eutrophi.htm>. Accessed 1 Feb 2007

National Bureau of Statistics (NBS) Online (2003) Key statistics by regions of the United Republic of Tanzania. NBS, Tanzania. <http://www.nbs.go.tz/stregions.htm>. Accessed 10 Jan 2007.

National Bureau of Statistics (NBS) (June, 2005) 2002 Population and housing Census – Village and Street Statistics – Mara Region VII. Central Census Office. Dar es Salaam, Tanzania

National Bureau of Statistics (NBS) Online (2006) Ministry of planning and development. population and housing statistics. NBS, Nairobi. <http://www.cbs.go.ke/>. Accessed 10 Jan 2007

Nile Basin Initiative (September, 2004) Mara River Basin Transboundary Integrated Water Resources Management and Development Project – Project Document

NOAA (2007) Rainfall estimate (RFE). [http://www.cpc.ncep.noaa.gov/products/african\\_desk/AFM.shtml](http://www.cpc.ncep.noaa.gov/products/african_desk/AFM.shtml). Accessed Mar 2007

North Mara Mine (NMM) (2006) Environmental Monitoring 2005 Annual Report. Placer Dome. Environment Department, North Mara Mine. Report No. PDT/ENV – 1/06

Peden D, Tadesse G, Mammo M, (2003) Improving the water productivity of livestock: An opportunity for poverty reduction. In: McCornick PG, Kamara AB, Tadesse G, (eds) Integrated water and land management research and capacity building priorities for Ethiopia. Proceedings of a MoWR/EARO/IWMI/ILRI International Workshop held at ILRI, Addis Ababa, Ethiopia, 2–4 December 2002. Colombo, Sri Lanka and Nairobi: International Water Management Institute (IWMI) and International Livestock Research Institute (ILRI). [http://www.ilri.org/publications/cdrom/integratedwater/TWMI/Documents/Print\\_version/WMI\\_Pro.pdf](http://www.ilri.org/publications/cdrom/integratedwater/TWMI/Documents/Print_version/WMI_Pro.pdf). Accessed 30 May 2007

du Toit JG, Water Requirements (2002) Game Ranch Management. J. du P Bothma. 4th ed. South Africa J L Van Schaik, 2002. 98–99

United Nations Environment Program (UNEP) (2002a) Africa Environment Outlook: Past, Present and Future Perspectives. <http://www.unep.org/dewa/Africa/publications/aoe-1/index.htm>. Accessed 1 June 2006

United Nations Environment Program (UNEP) (February, 2002b) Devastating Drought in Kenya: Environmental Impacts and Responses

United Nations Population Fund (UNPFA) (2003) State of World Population 2003. Making 1 Billion Count: Investing in Adolescents' Health and Rights. [http://www.unfpa.org/upload/lib\\_pub\\_file/221\\_filename\\_swp2003\\_eng.pdf](http://www.unfpa.org/upload/lib_pub_file/221_filename_swp2003_eng.pdf). Accessed 1 June 2006

The United Republic of Tanzania (URT) (2003) Macroeconomic Policy Framework for the Plan/Budget 2003/04 and 2005/06, President's Office, Planning and Privatisation, Dar es Salaam, Tanzania

Walpole M, Karanja G, Sitati N, Leader-Williams N (2003) Wildlife and People: Conflict and Conservation in the Masai Mara, Kenya. Wildlife and Development Series No. 14. International Institute for Environment and Development, London

Water Systems Design Manual (August, 2001) Guide for non-residential water demand. [http://www.ecy.wa.gov/programs/wr/cro/images/pdfs/gpm\\_estimate.pdf](http://www.ecy.wa.gov/programs/wr/cro/images/pdfs/gpm_estimate.pdf). Accessed 7 Nov 2006

Wolanski E, Gereta E, Borner M, (November/December 1999) Water, migration and the serengeti ecosystem. *Am Sci* 87(6):526–33

World Resources Institute (WRI); Department of Resource Surveys and Remote Sensing, Ministry of Environment and Natural Resources, Kenya; Central Bureau of Statistics, Ministry of Planning and National Development, Kenya; and International Livestock Research Institute (2007) Nature's benefits in Kenya, an Atlas of ecosystems and human well-being. World Resources Institute, Washington, DC and Nairobi

Yanda PZ, Dr. Majule AE, (June 2004) Baseline Studies on Socio Economic and Cultural Aspects on The Mara River Basin – Final Report. WWF – Tanzania Programme Office (TPO)

Zaba B, Madulu N (1998) A Drop to Drink? Population and Water Resources: Illustrations from Northern Tanzania. American Association for the Advancement of Science

## Chapter 19

# Impacts of Irrigation on Soil Characteristics in Selected Irrigation Schemes in the Upper Blue Nile Basin

**Mekonnen Getahun, Enyew Adgo, and Asmare Atalay**

**Abstract** Assessing soil and water qualities for salinity and other related problems and suggesting remedies are fundamental in irrigation management decision options. The analysis reported in this chapter provides the necessary information to predict the soil and water related problems as consequences of irrigation practices undertaken at various irrigated command areas in the upper Blue Nile River basin, Ethiopia. The study presented in this chapter was conducted in five selected irrigation schemes which have been constructed before 20 years in the Upper Blue Nile basin, Ethiopia. Farmers' perception of changes in crop yield as a result of changes in soil characteristics and water logging problems were compared with soil physical and chemical analyses. Soil profile pits were opened from selected representative sites in the respective irrigation command areas and from non-irrigated fields adjacent to the irrigated area for the purpose of comparison. The soil pH at Mendel and Tikurit schemes ranges mildly alkaline to moderately alkaline in both irrigated and non-irrigated sites and pH increased with depth due to the corresponding increase in bicarbonate. Infiltration rate and bulk densities in all schemes showed some variation between irrigated and non-irrigated sites. Farmers perceive changes in land productivity as a result of irrigation activities compared with non-irrigated plots especially, onion crops decreased from time to time. Furthermore, seasonal water logging was observed in some of the schemes during the rainy season as a result of flat topography and vertic nature of the soils of the command area. Total nitrogen, organic carbon and to some extent available phosphorus contents are generally found to be in the range of low to very low status while potassium is found to be more or less enough for the current low yield levels.

**Keywords** Soil salinity · Water quality · Irrigation schemes · Command area

---

M. Getahun (✉)

Amhara Design and Supervision Works Enterprise, Bahir Dar, Ethiopia  
e-mail: mekonnengetahun2001@gmail.com

## 19.1 Introduction

When compared to neighbouring countries, Ethiopia is endowed with significant amount of water resources, with a mean annual flow of about 110 Billion m<sup>3</sup> (BCM) that drain in to 12 drainage basins. Among these river basins, Blue Nile (201,000 km<sup>2</sup>), Tekeze (82,000 km<sup>2</sup>), Baro-Akobo (74,104 km<sup>2</sup>), Mereb-Gash (23,900 km<sup>2</sup>) make up Ethiopia's contribution to the Nile waters. These river basins cover more than 381,000 km<sup>2</sup> geographical area and contribute more than 86% of the total Nile water. Its groundwater resources are insignificant with an estimated annual renewable potential of only 2.6 BCM when compared to surface water potential (MoWR, 1998).

In developing countries like Ethiopia, population growth often exceeds growth in food production leading to food deficit mainly because of natural causes, where conventional rain fed agriculture has become unreliable and the return from inputs applied is highly influenced by the moisture constraints that crops are facing at different growth stages. In order to have, sustainable development and to alleviate food insecurity, irrigated agriculture is going to play a vital role in agricultural development in Ethiopia and, specifically in Amhara Region.

The Amhara Region (Fig. 19.1) is dominated by rain-fed agriculture in a country where the mean annual rainfall exceeds the average 1,200 mm in the highlands and middle altitudes. Blue Nile, Tekeze and Awash are the major river basins found in the region. About 80% of the region is drained with Blue Nile and

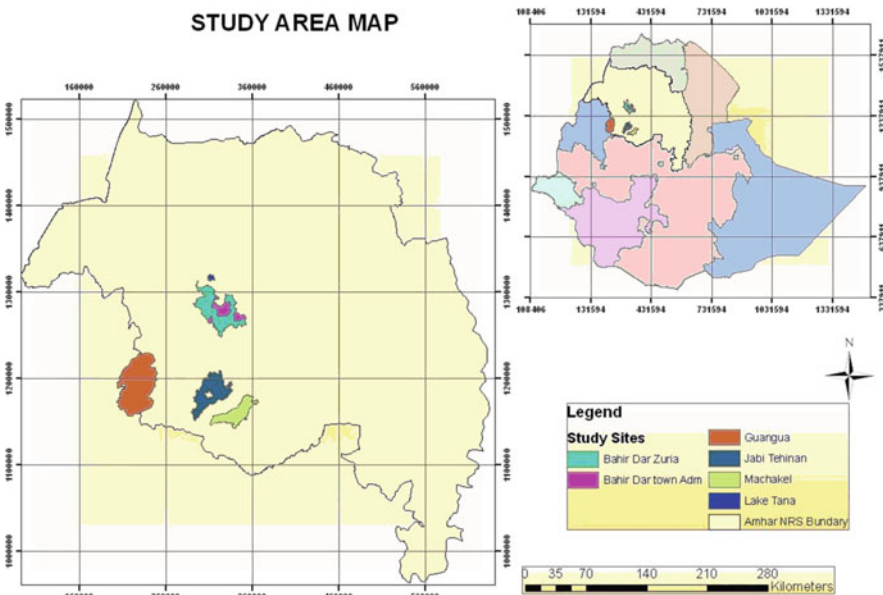


Fig. 19.1 Amhara region and the study area map

the remaining (slightly less than 20%) are drained by Tekeze-Anger and Awash main basins and very few portion of the region is drained by the Afar drainage basins.

The region constitutes the major source of water in the country and the Nile River. Some studies indicate that the regional surface water potential is estimated to be 35 BCM, of which less than 2% is utilized for irrigation. In the eastern part of the region, moisture is relatively scarce and hence storage mechanisms shall be used to develop the available land potential through small-scale irrigated agriculture. Though moisture deficit is the major problem in the area, there are more than 200 small streams flowing perennially and can be utilized for small-scale irrigated agricultural development (WWDSE, 2001). The region has got considerable land potential for the development of both small-scale and medium and large scale irrigation agricultural developments. Land and Water Resources Inventory Report (Irrigation sub-sector 2004/2005) indicates that there is well over 657,500 hectares of land suitable for irrigated agriculture and ample water resources that can be utilized for irrigation. The current irrigated area in the region is insignificant share of the potential. Currently, there is a good start to intensify irrigated agriculture. However, most of irrigation practices in the region are run traditionally without considering the spatial and temporal supply of water that in turn affects growth, quality and quantity of crop production.

The irrigation system of the study area is mainly traditional and has not been supported by improved technologies that could help framers maximize productivity and water use efficiency. The ultimate economic and environmental consequence of poorly managed irrigation is the destruction of an area's productive base because application of too little water is an obvious waste as it fails to produce the desired benefit. Excessive flooding of the land is still more harmful as it tends to saturate the soil for too long, inhibit aeration, leach nutrients, induce greater evaporation and salinity, and ultimately raise the water table to a level that suppress normal root and microbial activity and that can only be drained and leached at great expense (Hillel, 1997).

Based on field visit and gathered information from beneficiary farmers, causes of non-sustainability of irrigation and drainage schemes are degradation of irrigation land (alkalinization, water logging and soil acidification), increased incidences water related disease, poor water quality (Co-SAERAR, 1999).

Methodical approaches towards sustainable use of water and soil resources and prevention of development of saline soils is very essential in transforming rainfall dependant traditional agriculture to sustainable irrigated agriculture. Assessing soil and water qualities for salinity and other related problems and suggesting remedies are fundamental in management decision options. Therefore, this research was initiated to provide the necessary information to predict the soil and water related problems as consequences of irrigation practices undertaken at various irrigated command areas within Amhara region, upper Blue Nile River basin.

## 19.2 Materials and Methods

### 19.2.1 Description of the Study Areas

The study were conducted at three different administrative zones in the Amhara National Regional State, namely, West Gojjam, East Gojjam and Awi Zones (Fig. 19.2). The study sites are Mendel and Tikurit irrigation sites in West Gojjam

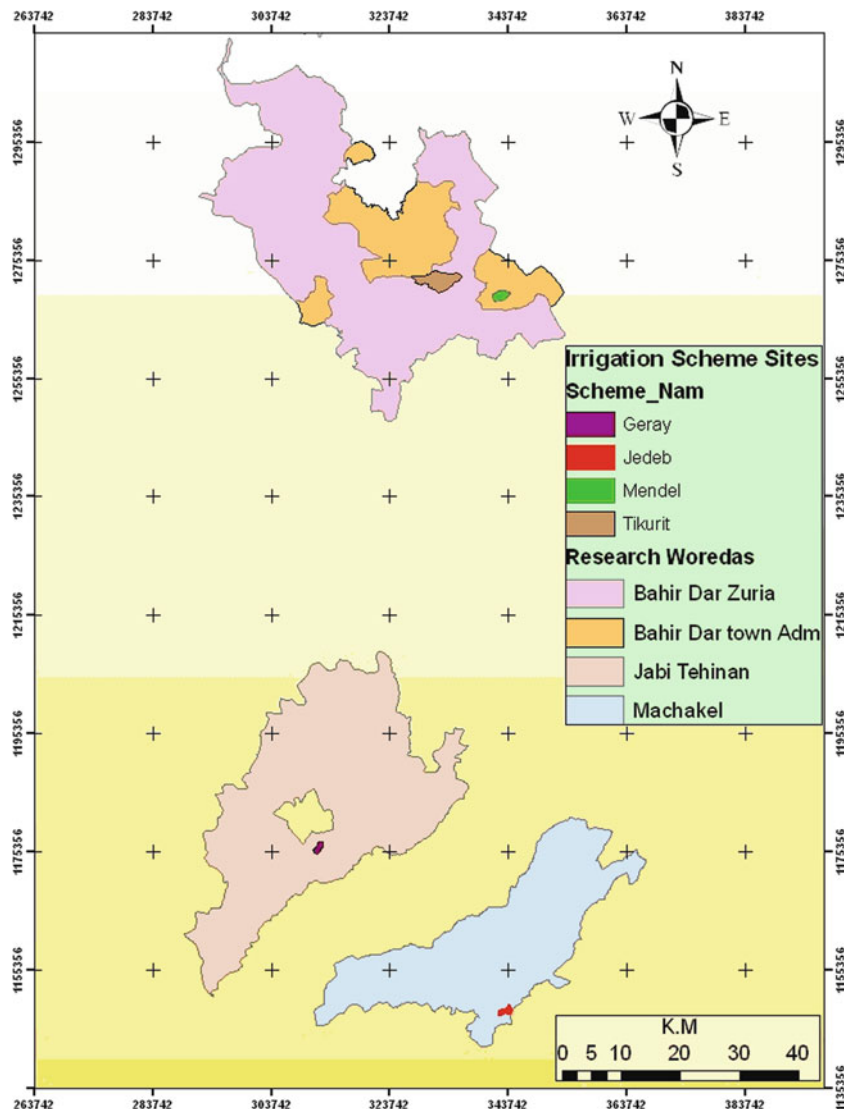


Fig. 19.2 Map of the irrigation schemes

(Tis-Abay woreda), Jedebe is found in Machakel woreda and Geray is found in Jabi-tsehnan woreda and Fetam is located in Guangua woreda in Awi Zone. Table 19.1 describes the environmental setting and specific information of the irrigation schemes.

The research sites are positioned on flat topography with moderate to imperfect drainage. The main parent materials are basalt, volcanic ash materials and some alluvial deposits. The major crops grown include, teff, wheat, sugar cane, maize, onion, Garlic, potato and others. As it is shown in Table 19.1, areas planned to develop irrigation agriculture were 770, 268, 210, 100 and 100 hectares in Geray, Jedebe, Fetam, Mendel and Tikurit, respectively, however actual command areas are being irrigated are 30.4, 16.8, 23.8, 64 and 30% in Geray, Jedebe, Fetam, Mendel and Tikurit, respectively. It is clear that actual irrigated areas are being by far lower than what was actually planned. The reasons for this could be planning problems as well as water management problems in the respective irrigation schemes. Some of the major factors include water shortage for dry season irrigation, seepage or percolation losses at head work and main canals and poor irrigation performances, poor water management of the schemes (water logging and drainage problems), lack of awareness on managing and controlling the schemes by beneficiary farmers and water users committees.

### 19.2.1.1 Description of the Soil Profiles

Two representative pedons at each scheme were dug on irrigated and non-irrigated areas adjacent to irrigated areas. The site was selected based on similarity of their topographic feature, slope and soil type. Soil samples were collected at two depths on the basis of observable differences. Field observations, soil profiles (freshly dug pits) were described and the horizons were designated according to the guideline of FAO (2006). Soil colour notation was according to Munsell colour chart (KIC, 1994). Soil samples were collected from each horizon of freshly dug pits. In general, disturbed and undisturbed soil samples were collected at all selected areas for laboratory analyses. The soil sampling started from the bottom of the pits up the profiles.

### 19.2.1.2 Physical and Chemical Analyses

Physical and chemical properties were determined for the soil samples that were air dried, crushed and sieved to pass  $\leq 2$  mm. Particle size was determined by hydrometer method (Bouyoucos, 1951); pH of the soil samples were determined using 1:2.5 soil-water solution; organic carbon was determined using the method of wet digestion (Walkley and Black, 1934) and total N by Kjeldahl Method (Cottenie, 1980).

The available phosphorous content of the soil was determined by 0.5 M sodium bicarbonate extraction solution (pH 8.5) method of Olsen as outlined in Van Reeuwijk (1993). Exchangeable cations content and the cation exchange capacity (CEC) of the soils were determined by the 1 M ammonium acetate (pH 7) method

**Table 19.1** The study sites and their environment

Details	Units	Schemes			
		Geray	Jedeb	Fetam	Mendel
Command areas	Planned irrigated, ha	770	268	210	100
	Actual irrigated, ha (% of planned)	235 (30.8%)	45 (16.8%)	50 (23.8%)	64 (64%)
Rainfall	mm	850			900–1,400
Temperature	°C	19		20	20
Elevation	Meter at sea level	1,875	2,175	2,321	1,750
Year of construction	1979–1980	1993	1985	1987	1985
Number of beneficiaries	Family head	660	572	400	130
					301

Source: Regional Land and Water Resources Inventory (March 2005).

according to the percolation tube procedure (Van Reeuwijk, 1993). Base saturation was calculated by sum of exchangeable bases divided by the CEC and multiplied by 100. The CEC of clay was calculated by dividing the CEC by the clay percent and multiplied by 100.

The infiltration rates were determined using the double ring infiltrometer method described in FAO soil Bulletin No.42 (FAO, 1979). At each location, the measurement site was pre-wetting on the afternoon preceding each test. This is normal procedure to avoid unrealistically high initial infiltration rates that can result from a test began on dry soils and to fill the cracks on soils with vertic properties. The bulk densities of the soils were determined using undisturbed cores samples collected. Samples were collected from the topsoil and subsoil and at approximately 50 cm and 100 cm depths.

## 19.3 Results and Discussions

### 19.3.1 Physical Properties

#### 19.3.1.1 Soils of the Study Sites

All the studied soils except that of Fetam irrigation scheme have very deep profiles (>200 cm). As a whole, the soils in Mendel and Tikurit manifested a high degree of similarity in morphology and physical characteristics. Invariably, they were clay in texture greater or equal to 58%, very deep, and uniform through the major part of the profiles which is attributed to marked pedoturbation resulting from the characteristic shrink-swell properties of the soils, with changes in moisture content, very hard, firm, very sticky and very plastic. The soils crack widely during the dry season, but the cracks close up again on rewetting. The resulting expansion and contraction is responsible for the formation of grooved shiny faces (slickenside) and wedge shape structures at depth (Fig. 19.3a).

At Mendel and Tikurit both at irrigated and non-irrigated command areas, calcium carbonate/bicarbonate nodules and concretions were distributed throughout



**Fig. 19.3** Pictorial representation of different profiles (a) deep crack (Tikurit and Mendel) (b) salt crystals at Mendel (c) calcareous nodules

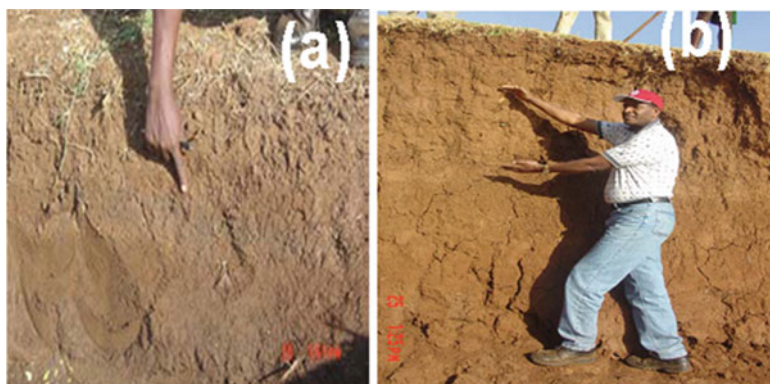


**Fig. 19.4** Pictorial representation of profile description (a) Jedeb irrigate site (visible Iron and Mn nodules) (b) profile description of Alisols

the profiles. The intensity of carbonates increases with depth throughout the profiles. It was interesting to observe that at Mendel and Tikurit sites carbonate precipitation were observed (Fig. 19.3b, c) along with the profile. Iron (Fe) and Manganese (Mn) nodules were apparent in all profiles of Jedeb and Fetam schemes, which may be explained by intermittent anaerobic conditions caused by water logging as is evident from the imperfect drainage of the soils (Fig. 19.4a). By both bacterial and chemical actions, Fe and Mn are reduced to ferrous and managanous forms and become soluble and more mobile, where seasonal drying allows the re-oxidation of these materials, they are re-deposited as yellow and rusty' spots and streaks of ferric iron or as black manganese concretions (Crompton, 1967).

The soils in Jedeb, Geray and Fetam irrigated areas also have very deep and uniform profiles, however, the soils have different morphological characteristic which have not visible shrink-swell properties as compared to Mendel and Tikurit. As shown in Fig. 19.4a, the soils at Jedeb having plinthite (Iron rich-it commonly occurs as red mottles) within 125 cm of the surface, shows gleyic and stagnic properties within 100 cm and 50 cm of the surface, respectively.

As presented above in Fig. 19.4b, soil profiles dug at Alisols have a brown ochric (to light in colour) A-horizon. The surface soil structure is rather weak, particularly where the organic matter content of the A-horizon is low. The structure of the Bt (accumulation of clay)- horizon is clearly more stable than that of the surface horizon(s). The profile also shows the presence of an argic B-horizon, a mixed clay assemblage that is in a state of transition to high aluminium levels in the subsoil, and a general paucity of bases (Table 19.2).

The field survey information of the sites shows water logging and drainage are the main problems in all study areas. The main causes of water logging in all schemes are flat topographic position, more clayey soils, poor drainage systems, and others management.

As shown below in Table 19.2, particle size distribution, on irrigated and non-irrigated command areas do not show variations except Jedeb, Fetam and Mendel

**Table 19.2** Some physical properties of the selected schemes

Site name	Depth (cm)	Texture (%)		Infiltration rate, (cm/h)		Bulk density (gm/cm <sup>3</sup> )	
		Irrigated	Non-irrigated	Irrigated	Non-irrigated	Irrigated	Non-irrigated
Geray	0-19	Clay	Clay loam	1.3	2.3	1.14	1.1
	0-15	Sand clay loam	Clay	3.6	2.1	1.21	1.29
Fetam	0-20	Sandy loam	Loam			1.26	1.2
	0-15	Clay	Clay loam	1.1	1.4	1.37	1.22
Mendel	0-20	Clay	Clay	1.3	2.5	1.1	1.02
Tikurit							

which shows minor differences. However, these variations are not strong enough to be emphasized.

Infiltration tests were carried out in the major soil units in the Mendel, Geray and Jedeb command areas and the result in irrigated sites were smaller than non-irrigated whereas measured bulk densities at irrigated command areas become larger and this shows more of compaction problems. As indicated in Table 19.2, at Geray, Mendel and Tikurit sites the infiltration tests results at irrigated command become slower than at non-irrigated command areas, this might be due to clay texture, however at Jedeb infiltration result at irrigated site become faster and this is also related with soil textures. Generally, optimum basic infiltration rates for surface irrigation are considered to be in the range of 0.7 to 3.5 cm/h, although an acceptable value normally ranges from about 0.3 to 6.5 cm/h.

The bulk densities at Geray, Jedeb, Fetam, Mendel and Tikurit top soils at both irrigated and non-irrigated sites ranges from 1.02 g/cm<sup>3</sup> for Tikurit to 1.37 g/cm<sup>3</sup> at Mendel. The bulk density variation between irrigated and non-irrigated schemes resulted from effects of cultivation and other physical works.

### **19.3.2 Chemical Properties**

#### **19.3.2.1 Soil Reaction (pH)**

As shown in Table 19.3, the soil pH increasing trends with depth at all schemes at irrigated and non-irrigated sites. However, higher soil pH values at Mendel and Tikurit schemes ranges mildly alkaline to moderately alkaline and increasing trends along with the soil profile for both irrigated and non-irrigated sites were observed, due to the corresponding increase in carbonates. On the other hand, the laboratory results at Fetam become medium acidic to slightly acidic, and Jedeb become very strong acidic to slightly acidic. The level of acidity at Fetam and Jedeb decreases along the soil profiles.

#### **19.3.2.2 Salinity (EC, dS/m)**

The electrical conductivity of the soils in all study schemes were very low and shows increasing tendency along the profile for Geray, Fetam, Mendel and Tikurit irrigated sites (Table 19.3). The low EC values indicate that the total soluble salt content of the soils of the area is generally very low. It is therefore can be concluded that a salinity effect is not critical problems for the time being in all irrigation sites.

#### **19.3.2.3 Organic Carbon and Total Nitrogen**

Total nitrogen contents in the cases of Geray and Tikurit found to be in the range of low to very low in both irrigated and non-irrigated sites and shows decreasing trend along with the soil profiles (Landon, 1991). In the case of Jedeb and Fetam, the nitrogen contents changes from low to very low at irrigated sites and medium to low

Table 19.3 Soil chemical characteristics of different schemes

Site name	Depth (cm)	pH 1:2.5 H <sub>2</sub> O		EC 1:2.5 dS/m		TN, %		OC, %		C/N		Av. P, -ppm (Olsen's method)	
		Irrigated	Non-irrigated	Irrigated	Non-irrigated	Irrigated	Non-irrigated	Irrigated	Non-irrigated	Irrigated	Non-irrigated		
<b>Geray</b>	0-19	7.1	7.1	0.09	0.196	0.155	0.08	2.31	1	1.5	1.3	16.4	
	19-45	6	7	0.055	0.054	0.069	0.077	0.897	0.624	13	8	0.44	
	45-95	5.9	6.8	0.079	0.048	0.066	0.074	0.78	0.897	12	12	2.58	
	95-145	6.5	6.9	0.064	0.038	0.06	0.033	0.39	0.293	7	9	3.58	
	145-200	6.6	6.5	0.078	0.04	0.049	0.029	0.371	0.291	8	10	0.78	
<b>Jedeb</b>	0-15	6.5	4.1	0.05	0.232	0.136	0.242	0.987	1.873	7	8	6.54	
	15-45	6.5	5.9	0.04	0.075	0.105	0.175	0.722	1.307	7	7	5.58	
	45-95	6.7	6.1	0.03	0.067	0.088	0.095	0.761	0.78	9	8	7.62	
	95-145	6.4	6.4	0.04	0.072	0.072	0.072	0.56	0.56	8	8	7.02	
<b>Fetam</b>	145-200	6.5	0.05	0.034				0.237		7	7	7.7	
	0-20	6.1	5.9	0.02	0.015	0.17	0.349	2.75	3.179	16	9	11.28	
	20-50	6.3	6.1	0.03	0.018	0.129	0.102	1.541	1.19	12	12	16.52	
<b>Mendel</b>	0-15	6.7	7.1	0.121	0.471	0.066	0.644	0.936	0.644	14	9	3.32	
	15-50	7	7.6	0.06	0.096	0.049	0.839	0.791	0.839	16	13	2.62	
	50-110	7.6	7.9	0.089	0.086	0.042	1.443	0.429	1.443	10	10	6.56	
	110-150	8.1	0.155			0.033		0.39		12	12	13.1	
<b>Tikurit</b>	150-200	7.8	0.273			0.035		0.351		10	10	4.76	
	0-20	7.5	0.278			0.149		2.243		15	15	16.4	
	20-60	8.1	0.151			0.057		0.878		15	15	4.38	
	60-112	8.8	0.598			0.04		0.585		15	15	3.32	
	112-160	9.4	0.907			0.034		0.488		14	14	trace	

Table 19.3 (continued)

Site name	Depth (cm)	Exchangeable cations, C mol(+) / Kg						CEC, C mol(+) / Kg	BS, %		
		Na		K		Ca					
		Irrigated	Non-irrigated	Irrigated	Non-irrigated	Irrigated	Non-irrigated				
<b>Geray</b>	0-19	0.39	0.89	0.9	1.29	5.51	6.08	2.71	21.4		
	19-45	0.72	1.71	0.31	0.41	3.94	3.97	1.77	25		
	45-95	2.32	2.1	0.31	0.61	3.23	4.43	1.73	24.2		
	95-145	0.85	0.61	0.37	0.61	4.12	4.53	2.34	21.8		
	145-200	2.21	1.87	0.31	0.63	3.23	3.33	2.81	1.4		
								20.4	34.68		
<b>Jedeb</b>	0-15	0.01	0.12	0.63	0.36	2.18	10.1	4.86	42.8		
	15-45	0.2	0.36	0.54	0.26	1.97	15.3	5.59	5.1		
	45-95	0.34	0.36	0.5	0.27	14.92	24.8	5.76	9.13		
	95-145	0.35		0.52		14.52		5.43			
	145-200	0.21		0.58		14.47		5.84			
								33.6	66.5		
<b>Fetam</b>	0-20	0.91	0.59	0.7	0.24	7.45	6	1.4	38.4		
	20-50	1.65	0.39	0.52	0.29	6.32	5.19	1.44	1.03		
	50-110	0	0.12	0.5	0.58	50.05	36.9	21.8	20.23		
	110-150	0.22	0	0.61	0.63	51.9	36.9	17.3	20.07		
	150-200	0.56		0.67	0.76	63.67	38	21	11.51		
								71.6	70.6		
<b>Mendel</b>	0-15	0	0.12	0.5				64.1	52.4		
	15-50	0	0.12	0.61				68.6	50.6		
	50-110	0.22	0	0.67	0.76			70	56.6		
	110-150	0.54		0.78		55.74			103		
<b>Tikurit</b>	112-160	9.11		0.93		55.89			96		
	0-20	0.07	0.95			38.7			27		
	20-60	1.54	0.6			35.1			24		
	60-112	5.4	0.67			26.2			21		

at non-irrigated sites, however, the amounts N have decreasing trends along with the soil profiles. At Mendel, even though the N content in irrigated site have very low and decreasing trends along with profiles, in the case of non-irrigated site the trends become increased along with depth from medium to very high concentration (Table 19.3).

The results of organic carbon at Geary showed low at irrigated and very low in non-irrigated sites and decreasing trends along with the profiles. In the case of Jedeb and Mendel, the concentration at both irrigated and non-irrigated sites become very low at the surface and decreasing down with the profiles; however Fetam and Tikurit decreases from low to very low for both irrigated and non-irrigated sites. Also Fetam and Tikurit are rich in organic carbon. Generally, the organic carbon content of the research areas showed a regular decrease along with increasing soil depth.

#### 19.3.2.4 Phosphorus Content

As presented in Table 19.3, available P concentration is higher in irrigated than non-irrigated sites. This might be due to P transported from the upper catchment along with sediments. In the case of Tikurit, since pH increases along with the profile depth, the available phosphorus content decreases, and the reason might be at high pH phosphorus becomes insoluble. This can be also due to the presence of Ca, and phosphate tends to be converted to calcium phosphate, and availability of P to plants is reduced. In general, the soils of Geray have high phosphorous contents as compared to soils at Mendel, Tikurit and Fetam.

#### 19.3.2.5 The CEC and Exchangeable Cations

Cation-exchange capacity (CEC) measurements are commonly made as part of the overall assessment of the potential fertility of a soil, and possible response to fertilizer application. As indicated in Table 19.3 above, the topsoil values for the cations exchangeable capacity (CEC) measured on whole sites were rating medium to very high (Landon, 1991). The measured top soil (0–45 cm soil depth) values of CEC at Geray on irrigated and non-irrigated sites become 21.4–25 cmolc/kg 31.8–24.8 cmolc/kg, respectively. The CEC value is increasing at irrigated sites with soil profile, but in the case of non-irrigated the value become decreasing. This is true for all other schemes (Table 19.3).

#### 19.3.2.6 Exchangeable Potassium (K), Sodium (Ca), Sodium (NA) and Magnesium (Mg)

The exchangeable K ranged between 0.3–0.9 and 0.63–1.29 cmolc/kg for irrigated and non-irrigated site at Geray, 0.5–0.63 and 0.27–0.36 cmolc/kg for irrigated and non-irrigated at Jedeb, 0.52–0.7 and 0.24–0.29 cmolc/kg for irrigated and non-irrigated at Fetam, 0.5–0.67 and 0.58–0.76 cmolc/kg for irrigated and non-irrigated at Mendel and 0.72–0.95 cmolc/kg for irrigated at Tikurit. As shown in Table 19.3, it is clear that in Geray, Jedeb, Fetam and Tikurit, exchangeable K shows decreasing

trends along with soil depth profiles in both irrigated and non-irrigated sites except at Fetam and Mendel at non-irrigated which shows increase trends along with soil depth. All schemes exhibited higher levels of exchangeable K than the range of 0.25–0.5 cmolc/kg, which was indicated as a medium level by Metson (1956).

As obtained from the result, the exchangeable Ca in Geray irrigated ranged from (5.51–3.23 cmolc/kg) and non-irrigated (6.08–3.33 cmolc/kg), Fetam irrigated (7.45–6.32 cmolc/kg) and non-irrigated (6.00–5.19 cmolc/kg) and Tikurit (38.7–5.64 cmolc/kg). Generally, the values were decreasing with increasing soil depth along the soil profiles, whereas, at Jedebe irrigated (2.18–14.92 cmolc/kg) and non-irrigated (10.1–24.8 cmolc/kg) as well as Mendel in irrigated (50.05–63.67 cmolc/kg) & (36.9–38.0 cmolc/kg) in non-irrigated sites exchangeable Ca shows that increasing trends along with the soil profile. As shown in Table 19.3, exchangeable Ca of Tikurit at lower depth decreasing very much, on the other hand the exchangeable Na increase, the reason may be fixation of Ca with P and more soluble Na in the soil. The distribution of exchangeable Ca at Geray decreased from the plough layer to the third horizon and increases thereafter.

The exchangeable Na content of the soils regularly increases with increasing soil depth in irrigated and non-irrigated sites with some inconsistency. This indicates that exchangeable Na is concentrated in the subsoils. However, the very low exchangeable sodium (Na) content of the soil at the surface in both irrigated and non-irrigated sites indicates that there is no sodicity problem in these soils.

Exchangeable Mg ranged between 1.73–2.71 and 1.69–2.55 cmolc/kg for irrigated and non-irrigated site at Geray, 4.86–5.43 and 4.28–9.13 cmolc/kg for irrigated and non-irrigated at Jedebe, 1.40–1.44 and 1.03 cmolc/kg for irrigated and non-irrigated at Fetam, 17.3–21.8 and 11.51–20.23 cmolc/kg for irrigated and non-irrigated at Mendel and 32.1–46.1 cmolc/kg for irrigated at Tikurit. As shown in Table 19.3, it is clear that at Geray and Mendel a decreasing trend from plough layer to the third horizon and increased afterward is exhibited. At Jedebe, Fetam and Tikurit exchangeable Mg shows increasing trends along with soil profiles both for irrigated and non-irrigated sites except Jedebe, in which the exchangeable Mg on non-irrigated site shows a decreasing trend along with soil depth. All schemes exhibited higher levels of exchangeable Mg than the range of 0.28–0.51 cmolc/kg, which was indicated as a medium level by Metson (1956). Generally, the range of critical values (points above which crop response is not extracted and no fertilizer is recommended) for K, Ca and Mg is from, 0.25 to 0.5, 1.25 to 2.5, 0.25 to 0.5 and 0.28 to 0.51 cmolc/kg, respectively.

Percent base saturation (PBS) was very high at Mendel and Tikurit. Its values decreased along with soil profile with few minor inconsistencies. The PBS values exceeding 100% in these studies indicates inflated condition. It could be due to underestimated CEC's of the soils which are calcareous. As has been discussed by Chapman (1965), calcareous soils present a problem with ammonium acetate method as a consequence of the solubility of  $\text{CaCO}_3$ , in the ammonium acetate solution giving lower values of CEC. This is because the dissolved Ca present in the  $\text{NH}_4\text{OAC}$  solution prevents complete saturations of the exchange positions with ammonium. The above explanations suggest for trying methods other

**Table 19.4** Water quality result analysis

Parameter	Geray	Site name					
		Jedeb					
Temp, oc	21.84	19.77	24.24	22.81	23.12	25.12	24.25
EC, dS/m	290.1	174.7	232.9	216.5	263.7	860.8	613
TDS, g/l	202.6	114	152.6	147.4	181.4	558.2	404.4
pH	6.52	7.55	8.56	9.45	8.61	8.65	8.11
DO, %	142.7	133	115.9	129.5	128.7	116	122.1
ORP, mv	149.5	71.9	158.6	53.2	39.3	155.2	106.2

TDS = Total dissolved solids, DO = dissolved oxygen, ORP = Oxidation-reduction potential.

than  $\text{NH}_4\text{OAC}$  to estimate the CEC of calcareous soils. The PBS at Fetam, Geray and Jedeb however, lower at the surface and increased down with soil profiles (Table 19.3).

### 19.3.2.7 Irrigation Water Quality Characterization

Irrigation water sources were also analysed to assess their contribution in the salinization process. Water used for irrigation can be varying greatly in quality depending upon type and quantity of total dissolved salts, the Sodium Adsorption Ratio (SAR) and Residual Sodium Carbonate Content. The criteria were used to assess the quality of irrigation water in the areas.

It was observed that the pH in the analysed water samples, especially at Jedeb, Fetam and Mendel was higher than in other sites (Table 19.4). This might be because of the presence of alkali ions mainly bicarbonate. An increase in alkalinity is accompanied by an increase in pH (Gupta and Abrol, 1990). Potential impacts on crop yields may result from the exceedence of this irrigation guideline.

Majority of electrical conductivity measurements of all sample areas were showed low salt concentration. As per the guideline for water quality for irrigation and drainage paper, FAO 29 showed that electrical conductivity of all sites is found within the low range, hence, irrigation water coming from the highlands of Western Amhara in the Upper Blue Nile basin which is dominated by basaltic rocks is not carrying salts that might cause soil salinity.

## 19.4 Conclusions and Recommendations

All the studied soils except that of Fetam irrigation scheme have very deep profiles ( $>200$  cm). As a whole, the soils in Mendel and Tikurit manifested a high degree of similarity in morphology and physical characteristics; they were clay in texture and calcium carbonate nodules and concentrations were distributed and the intensity of carbonates, whereby, increases with depth throughout the profiles. These

areas are located on the flat plain and receive water containing basic cations (Ca, Mg, K, Na), resulting in higher amount of cations compared with other schemes. Especially, in these schemes drainage, seasonal flooding as well as water logging problems was common, the reason could be poor infiltration capacity of the soil due to clayey textured and flat topographic position of the areas. Hence, close follow-up and water management practice in the case of Mendel and Tikurit and vertisols management, appropriate ploughing, and planting early and lately according to moisture requirement of crops is important to use Vertisols and to improve their suitability for irrigated and rain-fed agriculture.

Higher soil pH values at Mendel and Tikurit areas and increasing trends along with the soil profile at both irrigated and non-irrigated sites were observed. The major effect of basic pH is to reduce the solubility of micronutrients like Fe, Zn, Cu and Mn. Also as shown in Table 19.3, at Tikurit, the available phosphorus content decreases along with the soil profile, this might due to high pH values. This can be also due to the higher amount of Ca, resulting in phosphorus to be converted to calcium phosphate reducing availability of P to plants.

From the results discussed so far, it can thus be concluded that the studied areas have low to very low organic matter, total nitrogen, and low available phosphorous for high demanding crops. So that applications of organic and inorganic as well as nitrogen fertilizer are very crucial for plant growth in all schemes.

## References

Bouyoucos GH (1951) A recalibration of the hydrometer method for making *mechanical* analysis of soils. *Agron J* 43:434–438

Chapman HD (1965) Cation-exchange capacity. In: Black CA (ed) *Methods of soil analysis – Chemical and microbiological properties*. *Agronomy* 9:891–901

Co-SAERAR (August 1999) Socio-economic report on problem identification and need assessment. Bahir Dar, Ethiopia

Cottenie A (1980) Soil and plant testing as a basis of fertilizer recommendations. *FAO Soils Bull 38/2*. FAO, Rome

Crompton E (1967) Soil formation. In: Drew JV, (1967) *Selected papers in soil formation and classification*. Soil science society of America, Inc. Madison, Wisconsin, USA, pp3–15

FAO (1979) Soil survey investigations for irrigation. *FAO Soils Bulletin No. 42*. FAO, Rome, 188 p

FAO (2006) Manual on participatory rapid diagnosis and action planning of irrigated agricultural system (PRDA) – APPIA project, IWMI sub-regional office for the Nile Basin and Eastern Africa, Italy, Rome

Gupta RK, Abrol IP (1990) in *Advances in Soil Science: Soil Degradation* (eds) Lal R, Stewart BA, Springer, Berlin, pp 223–288

Hillel D (1997) small-scale irrigation for arid zones: Principles and options, FAO Development technical Report 2, Rome

Kollmorgen Instruments Corporation (KIC) (1994) MunSell soil color charts, Macbeth Division of Kollmorgen instruments corporation 405 little Britain road, New Windsor, NY12553 (1994 revised edition)

Landon JR (Ed) (1991) *Booker tropical soil manual : a handbook for soil survey and agricultural land evaluation in the tropics and subtropics*. Longman, New York NY, 185p

Metson AJ (1956) Methods of chemical analysis for soil survey samples. N.S.I.R. Bureau Bulletin 12

MoWR (Ministry of Water Resources) (1998) Integrated development of Abbay River basin master plan study, Vol.III: part 2, Vol. VI: Part 1, Vol. VI: part 3, Addis Ababa: Ethiopia

Regional Land and Water Resources Inventory (March 2005) Irrigation sub-sector 2004/05, Bahir Dar, Ethiopia

Van Reeuwijk (1993) Procedure for Soil Analysis, 4th Edition, ISRIC Technical Paper 9. Soil Reference and Information Centre, Wageningen, The Netherlands

Walkley A, Black CA (1934) an examination of the Degtjareff method for determining soil organic matter, and a proposed modification of the chromic acid titration method. *Soil Science* 37: 29–38

Water Works Design & Supervision Enterprise (WWDSE) (2001) V-4, Subsector reports on irrigation development, Dec., (2001), Addis Ababa, Ethiopia

# Chapter 20

## Critical Water Resources Issues in the Nile River Basin

Muluneh Yitayew and Assefa M. Melesse

**Abstract** The central water management issue for the Nile River basin, as in many other river basins throughout the world, is sustainability of water supply in the context of intense population growth, recurring drought, and increasing competition for water. The issue gets complicated as a result of global climate change that is taking place at an alarming rate. A serious discussion of these and other important water resource issues and the challenges in the basin is necessary and needs our attention to seek solutions and insure sustainability of the water supply. This chapter addresses the physical and hydrological conditions of the basin as a background and present the cross-cutting issues of concern in the basin. The uncertainty of availability of water in the face of climate variability and increased land degradation will be also discussed. The challenges to obtain, protect, and manage the basin's water supply and ecosystem will also be discussed. Even though one cannot make a meticulous coverage of all the issues and challenges in the basin, a serious attempt was made to present possible solutions at local and regional scale. The solution will be geared towards getting more of the water, using it as much, and making it sustainable.

**Keywords** Nile river · Water management · Sustainability · Climate change · Hydropolitics

### 20.1 Introduction

Sustainability of water supply in a given basin implies that the present water needs of the population in the basin are met without compromising the ability of the future generations to meet their needs. The situation with respect to Nile water need and supply is getting critical and growing worse. The demand for the water is increasing

---

M. Yitayew (✉)

Agricultural and Biosystems Engineering Department, University of Arizona, Tucson AZ, USA  
e-mail: myitayew@email.arizona.edu

significantly as a result of increased population and the effect of global warming. New water demands for various uses by upstream countries are increasing the tension among the Nile countries. Some of the basin states have already experienced critical water shortage as a result of some extreme events such as recurring drought while some had occasional flooding. Shortage of water occurs when the needed amount of quality water is not available at the right time and place of need. It can be due to drought or due to contamination of the available water. In the latter case, the water can become degraded to an extent it is not safe for human consumption.

Considering a threshold value of 1,000 m<sup>3</sup> per person per year, it is projected that some of the Nile Basin countries: Burundi, Rwanda, Egypt, Ethiopia, and Kenya will be considered as water “scarce” by 2025 (Falkenmark, 1989; Falkenmark and Widstrand, 1992). This is based on a continuous population growth at the present rate. If the present trend of water shortage continues, which is likely to happen, the result will be that socio-economic development will be restrained and the potential for water conflict will be increased. What this also means is that hydrologists, engineers, sociologists, politicians, water resources managers, decision makers, and other water resources interest groups would have to be knowledgeable about the river water to develop, protect, keep, share and use it in an efficient and equitable manner. This may require a shift in paradigm, developing and adopting new ways of technically, legally, and administratively handling the Nile water. There may be a need to think regionally and act locally. Most of the Nile water issues today transcend one country, and the basin. In many cases even the region. Yet, a great portion of the solution must be attained at the country level. It is the authors’ belief that most of the basins problems are not the result of the people living in the basin countries rather more and more of the basin’s future water issues and problems will be driven out of a more regional and global environment. To this end, this chapter will discuss some of the critical issues in the management of the water resources of the Nile River basin that need attention and need to be addressed at this point in time. There are many issues such as water scarcity, water quality, water policy, good governance, institutional and financial capacity, poverty reduction, food security etc. that affect management of the basin’s water directly or indirectly and needs to be considered seriously in any discussion of the basin’s water resources management. Recognizing that, it is very hard to make a meticulous coverage of all the issues. This chapter only addresses three of the most critical ones and will suggest possible solutions for achieving sustainable water resources development and management in the basin. The physical and hydrological conditions are described first.

## 20.2 The Nile Basin Geography

The Nile River Basin (Fig. 20.1) with its diverse ecosystem is one of Africa’s largest and most important river basin. It is located in a region with varied geographical, topographical, climatological, hydrological, political, and physical characteristics. It extends through 35°C of latitude of the north-eastern African quadrant as it flows from the south highlands through alluvial plains and desert sands into the eastern



**Fig. 20.1** Map of the Nile River basin

Mediterranean to the north. It starts from its headwaters at elevation 1,135 m above sea level in Lake Victoria and above 1,800 m above sea level in the Ethiopian highlands resulting in a drainage area of about 3,007,000 km<sup>2</sup>. The basin spans over ten countries: Burundi, Egypt, Ethiopia, Eritrea, Kenya, Tanzania, Rwanda, Sudan, and the Democratic Republic of Congo. The total drainage area is nearly 10% of Africa's landmass. From the headwater source, the river flows 6,700 km to end up in the Mediterranean Sea. This makes the Nile the longest river in the world. Geographically, as stated earlier, the downstream states Egypt and Sudan have a flatter terrain while upstream states such as Ethiopia located at a river's headwaters are more mountainous. This gives the downstream states a skewed advantage for agricultural development that uses a large quantity of water for irrigation compared to the upstream states.

There are three major tributaries to the Nile: the Blue Nile, the White Nile, and the Atbara Rivers. The Blue Nile is the main tributary and starts in Lake Tana,

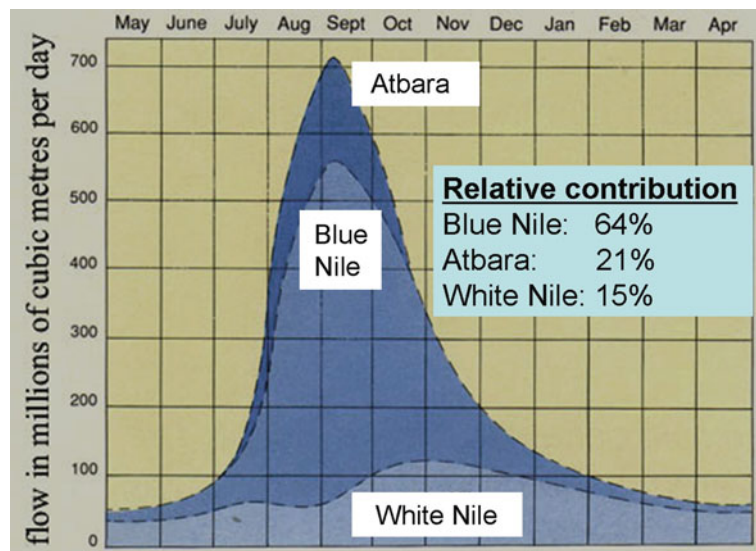


**Fig. 20.2** Average daily flow rate in millions of m<sup>3</sup>/day (Source: <http://www.mbaron.net/Nile/>)

Ethiopia before it travels northwest and joins the White Nile in Khartoum, Sudan. The Atbara drains also from Ethiopia as Tekeze before it joins the main Nile about 300 km north of Khartoum. The White Nile originates from the Equatorial Lakes region and joins the Blue Nile at Khartoum. The Ethiopian headwater contributes about 85% of the Nile water through the Blue Nile, Atbara, and Baro-Akobo (Sabot) Rivers (Table 20.1) with the remaining 15% coming from the Equatorial lakes headwater. The contribution of White Nile is very important as it provides a sustained flow throughout the year. Figure 20.2 gives the average flow rates contribution of the total flow the Nile (<http://www.mbaron.net/Nile/>).

The Nile Basin can be divided into two main sub-basins, the White Nile and the Blue Nile. The White Nile sub-basin consists catchment areas in Burundi, Kenya, Rwanda, Sudan, Uganda, and Congo while the Blue Nile sub-basin consists catchments from Ethiopia and Sudan (Fig. 20.1). The Nile River basin ecosystem has

**Table 20.1** Ethiopia's three rivers contributing to the Nile River system

River basin	Catchment area (Km <sup>2</sup> )	Annual runoff (BM <sup>3</sup> )	Specific discharge (l/s/km <sup>2</sup> )
Abbay (Blue Nile)	199,800	52.6	7.8
Baro-Akobo	74,100	23.6	9.7
Tekeze	90,000	7.6	3.2
Total	363,900	83.8	

Source: Compiled from various river basin master plan studies and river basin surveys. Ministry of Water Resources, Ethiopia, 1999. Water Sector Strategy Document.

the two lakes i.e., Lake Victoria and Lake Tana. Lake Victoria is the second largest freshwater lake in the world.

### 20.3 Hydrology of Lake Tana and Lake Victoria

Lake Tana and Lake Victoria are the two most important lakes of the Nile River basin. Lake Tana, the largest lake in Ethiopia and the source of Blue Nile, has a surface area of 3,156 km<sup>2</sup> (20% of the 16,000 km<sup>2</sup> drainage area). The river inflows from Gilgel Abay, Rib, Gumera, and Megech Rivers account about 93% of the inflow into the lake, and at the outlet starts the Blue Nile. Historical records of the lake's stage and data from satellite has shown that Lake Tana has shown a historical variation in its level (Fig. 20.3a). This change is believed to stem from various factors including hydrologic alterations within its basin due to reduction in dry season flows attributed to human and climate-induced changes (Chebudi and Melesse, 2009).

With a surface area of 68,800 km<sup>2</sup>, Lake Victoria is Africa's largest lake by area, and it is the largest tropical lake in the world. Lake Victoria is also the world's second largest freshwater lake. Lake Victoria receives almost all (80%) of its water from direct precipitation. Average evaporation on the lake is between 2,000 and 2,200 mm (79–87 in) per annum. Approximately, 25 major rivers flow into Lake

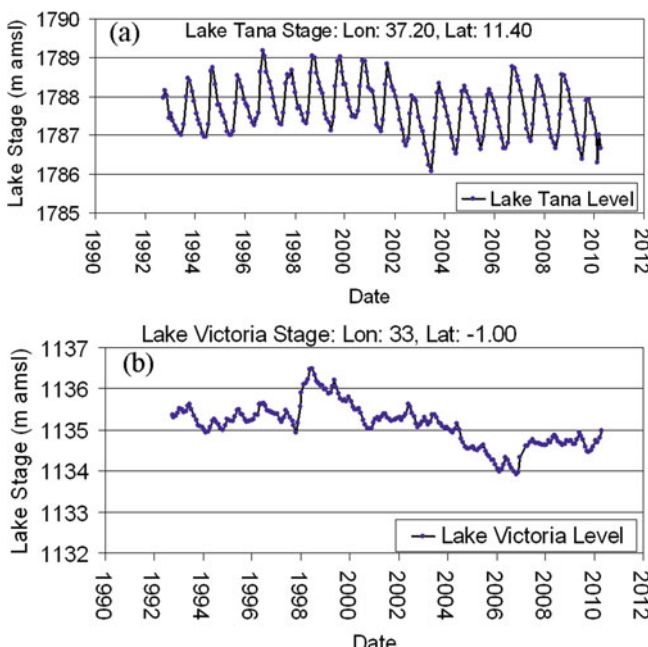


Fig. 20.3 Historical lake levels (a) Lake Tana and (b) Lake Victoria

Victoria from the 194,000 km<sup>2</sup> basin surrounding the lake. Historical water level of the lake has shown variability (Fig. 20.3b). Rainfall on the lake being the major source of lake's recharge, the lake level is highly sensitive to the rainfall pattern in the basin. As shown from Fig. 20.3b, the lake level is declining since 1998. The increased hydropower capacity at Nalubaale and Kiira power stations in Uganda allowed more water to be released for power generation and recently lowered lake levels to unsustainable levels below 11 m at the Lake Victoria outlet. Historically, the lake maintained equilibrium of 11.9 m for many years.

## 20.4 Nile Hydro-Climatology

The Nile hydrology shows a high degree of temporal and spatial variation. There is abundant rainfall in the headwaters and very low rainfall in the arid Sudan and Egypt. Although the watershed is large, the portion contributing to stream flow is almost half of the entire basin (only  $1.6 \times 10^6$  km<sup>2</sup>) due to the fact that north of 18°N latitude, rainfall is almost zero (Teodoru et al., 2006). Precipitation increases towards the headwaters to over 1,200 to 1,600 mm/yr on the Ethiopian Plateau and in the region of the Equatorial lakes: Victoria, Albert, Kayoga, and Edward (Mohamed et al., 2005). The seasonal pattern of rainfall follows the Inter-Tropical Convergence Zone (ITCZ), where the dry northeast winds meet the wet southwest winds and are forced upward causing water vapor to condense. The ITCZ follows the area of most intense solar heating and warmest surface temperature and reaches the northern part of the Ethiopian Plateau by late July. The southward shift of the ITCZ results in the retreat of the rainy season towards the central part of the basin after October. Therefore, the monthly distribution of precipitation over the basin shows one single but long wet season over the Ethiopian Plateau and two rainy seasons over the Equatorial Lakes Plateau (Mohamed et al., 2005).

Nicol (2003) identified three major hydrological characteristics of the Nile River. These are first its two major origins: in the highlands of Ethiopia and in the Nile equatorial lakes region. The former provides the major flow of the Nile north of Khartoum – the Blue Nile – and the latter the far lower and slower flows of the White Nile. The second major feature of the hydrological system is the huge seasonality of the Blue Nile's flows. A third major feature of the river system is caused by virtue of the river's situation in hot, arid areas where evaporation losses are high.

Subject to seasonal variations, about 80% of the total annual discharge of the River Nile occurs during the summer rainy season (July to October) mainly with the Blue Nile and the Atbara River (Woodward et al., 2001). Atbara River runs dry at times of the year while the White Nile maintains the flow in the Nile over the entire year. Without the discharge of the upper White Nile, the Nile River would probably run dry in May.

More than 95% of the mean annual suspended sediment load of the Nile River upstream of the Aswan High Dam (120 millions tons per year) (Woodward et al., 2001) comes with the Blue Nile (72%) and the Atbara River (25%) whereas the

White Nile contributes only 3% of the total load. Apart from seasonal variations, the total annual discharge of the Nile River is subject to intense annual variations with the highest annual flows of  $154 \text{ km}^3/\text{year}$  recorded in 1878 (Abu Zeid, 1987) and  $120 \text{ km}^3/\text{year}$  measured in 1984 (Woodward et al., 2001). The lowest annual flow on record was observed in 1913 with only  $42 \text{ km}^3/\text{year}$  (Abu Zeid, 1987). The mean annual flow of the Nile River and the three tributaries calculated over the period 1901–1995 (Mohamed et al., 2005).

As a result of increased water surface area being exposed to arid climate conditions, the evaporation from the lake behind the Aswan High Dam (AHD) was estimated to vary between 18 and 21% (19% in average) of the total river input (Aly et al., 1993). A review of earlier literature established a large range for evaporation from Lake Nasser between  $1.7 \text{ m/year}$  and  $2.9 \text{ m/year}$  (Sadek et al., 1997). Based on water balance, energy budget and modeling, narrower range of  $2.1\text{--}2.6 \text{ m/year}$ , with an average of  $2.35 \text{ m/year}$ , was calculated by Sadek et al., (1997). It was estimated that the annual evaporation from the AHD Reservoir varied between 12 and  $12.6 \text{ km}^3/\text{year}$  which correspond to an evaporation rate of  $2.0\text{--}2.1 \text{ m/year}$  (Roskar, 2000). Compared to the reservoir volume of  $162 \text{ km}^3$ , the evaporation represents about 8% per year but more than 15% of the river inflow of  $84 \text{ km}^3/\text{year}$ .

The hydro-climatological studies show the variability in flow of the Nile both in time and space. Unless there is a way to regulate this flow condition, it is difficult to plan a meaningful sustainable water resources development and management program. It is also apparent that in a basin as big as the Nile, a concerted effort to gather data that can be used to forecast the hydrologic and climatologic variables is absolutely necessary. Integrated basin-wide cooperation must go parallel with the rest of the effort to bring the riparian countries to work together with a shared vision of benefiting socio-economically and politically. With this as a goal, the next section addresses some of the critical issues that need to be considered in the basin.

## 20.5 Critical Water Resources Issues

The Nile basin is one of the fastest growing areas in Africa. There is an increase in population and recurring drought, floods, food insecurity and poverty in most of the riparian countries. Continued growth in population and new demands emanating from the growing economies of the upstream counties like that of Ethiopia, which has shown a growing interest in boosting its agricultural production, will place severe pressures on the water resources of the basin.

Agriculture plays a major role in the future of the basin. It is the largest consumer of water especially in the downstream countries of Sudan and Egypt. The agricultural industry in both these countries depends upon irrigation water from the Nile. Urban use is also becoming one of the largest consumer of the Nile water. A change in the mix of water uses in these two countries has a serious implication on the overall water availability of the region. This is particularly true if the present status quo arrangement for water sharing in the basin remains unchanged. New interest and projects to harness Blue Nile by Ethiopia for hydroelectric power production and

irrigation projects will be issues of concern by lower basin countries. Increasing irrigated agricultural productivity to ensure food security and power generation to meet the countries energy demand to support the economic activities are the focus of Ethiopia.

Water shortage in the upstream basin countries caused mainly by drought is the major problem in the basin. Other problems for these countries include lack of regulating infrastructure like reservoirs, lack of coordinated water policy both in-country and basin wide, lack of scientific data and information to predict drought and floods, and the absence of basin wide integrated water management system. Resolving water shortage issue cannot be a one-state, two-state or three-state affair. It has to involve development of new paradigm of looking at the problem across the basin. A new method of addressing water shortage issues have to be crafted that is responsive to the growing needs for the Nile water across the basin not just country by country. There is also a need to look at water right issues alongside issues such as water shortage, drought, floods and water quality. It is also important to resolve these outstanding issues before they become acute in the basin and become the causes of water conflicts. What ever we see at the present time are warning flags for what is worse problems to come as a result of the global climate change. Collective goodwill and collaborative efforts of the basin states are urgently needed before these warnings come true. This requires addressing the cross-cutting issues described below.

## 20.6 Hydropolitics

With the basin comprising areas from ten countries: Burundi, Ethiopia, Egypt, Kenya, Uganda, Rwanda, Tanzania, Congo, Sudan, and Eritrea, and claims for the portion of the river water by most of these countries increasing, it is obvious to expect the complexity of dealing with sharing of the water in an equitable manner. What most think and know about the Nile is that the water is used solely by Egypt and Sudan. There is and has been for a long time a clear inequitable distribution of the Nile water resource in the upstream and the downstream countries. For the most part, the hydropolitics of the Nile has been dominated by a single country, Egypt that is totally dependent on the Nile water that is generated in the upstream countries. It has the upper hand diplomatically, militarily and economically of all the riparian countries. On the other hand, the upstream countries though they may have geographic advantage, are some of the least developed and poorest countries in the world facing poverty, recurring drought, and famine. This disparity between the upstream and the downstream countries lead to an unbalanced level of development within the basin as reflected by the gross domestic product (Table 20.2).

From the nineteenth to the middle of the twentieth century, the hydropolitics was also influenced by colonial power with the British Empire as the major player. Most of the agreements on the Nile basin were made either between colonizers or bilateral agreement between Sudan and Egypt. With the blessing of the British,

**Table 20.2** Renewable water resources and GDP of the Nile basin countries

Country	Percent of NRB (%)	Percent of country in NRB (%)	Population total (million)	GDP per capita (2005)	Renewable water resources, (m <sup>3</sup> /person)
Sudan	63.6	79	31.7	2,100	1,981
Ethiopia	11.7	32.4	65.8	900	1,666
Egypt	10.5	32.6	65.2	3,900	830
Uganda	7.4	98	22.8	1,800	2,663
Tanzania	2.7	8.9	34.4	700	2,472
Kenya	1.5	7.9	30.7	1,100	947
Eritrea	0.8	20.5	4.2	1,000	1,578
DR Congo	0.7	0.9	52.4	700	23,639
Rwanda	0.7	75.5	7.9	1,500	638
Burundi	0.4	47.6	6.9	700	538

Source: NBI ([2006](#)).

Egypt was able to dictate most of the treaties and bilateral agreements that are still in the books ratified by Sudan but never been accepted by the other riparian countries. Most importantly, Ethiopia has never been a party to most of these agreements.

In the 1990s, greater effort was invested by the riparian countries, the World Bank, and donor agencies, to forge a cooperative approach to the Nile water development and management. With the formation of the Nile Basin Initiative (NBI) in 1999, the hydro-political environment has changed. This came about as a result of the realization by the major players that the status quo is neither in their (Nile basin countries) best interest nor is sustainable. It is also the result of their willingness to move from “unilateralism” to “multilateralism” in resource development (Nicol, [2003](#)). With the formation of the Nile Basin Initiative, representatives of the riparian countries have been negotiating to develop a regional partnership for the cooperative development of the water resources in the Nile Basin with the goal of the initiative being “To achieve sustainable socioeconomic development through the equitable utilization of, and benefit from the common Nile Basin water resources” (NBI – [www.nilebasin.org](http://www.nilebasin.org)). The future for such cooperation in the basin will depend on the acceptance of benefit sharing over water sharing as guiding principle by the countries in the basin and also in recognizing “equitable and reasonable” allocations along with historical precedence of water usage. Two realities about the Nile water that needs to be considered are (1) it is going to get scarce as a result of the population pressure and climate change, and (2) riparian countries are going to compete among each other for the scarce and limited water in the Nile River system. If the recurrent drought that has plagued most of the upper countries for the last three decades continues, scarcity is going to mount and the competition is going to get intense. This can cause anxiety among all countries especially with the Eastern Nile countries with unpredictable consequences. The downstream countries will not

have certainty that they will get the amount of water they claim the right for in the existing water right arrangement.

As stated above, over the last three decades, cooperation over the Nile water management has been the focal point for most of the riparian countries and the international community. This cooperation to develop and manage the river water will become even more important as the basin face uncertain but increasingly evident challenges that the global climate change will bring. The recurring drought in most of the countries is a likely harbinger of tough times ahead making sustainable water management more difficult. The increasingly stressful environmental and demographic conditions will require much more cooperative action now than has been delivered thus far.

These challenges will necessitate formulation and presentation of strong rationales for working together cooperatively to assure adequate water supplies. All the individual countries interest for the Nile water need to be treated in a pragmatic manner. Most people take cooperation to have a positive value, on its face. To argue against would seem an untraditional thought. The issue is to what extent individual countries influence the decision making about sharing the transboundary water resources. It is also important to clearly understand the value and the limits of cooperation for the individual countries such as Ethiopia that contributes approximately 85% of the river water, the second populous country of the continent with over 85 million people and aspiring for self sufficiency in food production as one of its major short term national economic goal. One should not stretch cooperation to a point where it does lose its meaning. The question is what should the role of the upstream and downstream countries be in this cooperation and how can the countries maximize the value of their involvement and reach the best and informed decisions for the sake of their own population? At some point in the near future, each country has to see if cooperation is working for it requiring some measure of success in cooperative outcomes. This will help each decide on future investment in cooperative management of the natural resources. It will also help continue to put a sustained effort by the riparian countries.

Nile Basin Initiative brought the countries together which for a long time were not in talking terms at all. While they were able to work out their differences and reach some win-win consensus agreements, it has not changed the basic equation of equitably sharing of the Nile water. The most important challenge in this case is establishing the legal and institutional framework. To this end, there has to be some mechanism to bring each of the countries at the table and draw the expertise of the international community as the third party. This is the sticking point in the hydropolitics of the Nile basin and of all the pillars of the shared vision which may derail the movement towards continued cooperation and might even reverse the situation back to upstream and downstream squabble with the “zero-sum game” position back at work.

The May 2010 agreement signed by Ethiopia, Tanzania, Rwanda and Uganda without Egypt and Sudan on the Nile River cooperative framework to collectively work towards conserving Nile River and equitably using its water is a big and very important step in the right direction. Egypt and Sudan’s dependence on historic right

and no harm legal principles has been and will be used as a stalling mechanism for unified agreement. Both, while aware of the importance of the Nile water to the upstream countries, still looks at the situation as a zero-sum game, which in the face of international water law principles such as equitable utilization and the obligation not to cause significant harm will not have the legal ground to stand alone. Historical right, equitable distribution and the no harm principles should not be seen as mutually exclusive principles. Instead, they should be looked at with the goal of coming out with an inclusive optimum approach that will benefit both upstream and downstream countries without harming any. Joint management of the river or equal per capita shares of the water are some of the ways that need to be considered to perhaps achieve this goal.

In 1997, the UN Convention on the Non-Navigational Uses of International Water Courses was adopted by the United Nations – considered to be an international framework agreement for use by states in negotiating water disputes. Perhaps most notably the Convention has officially put to rest the historic conflict between the two extreme principles of absolute territorial sovereignty (the right of an upstream state to do as it wishes with the waters in its territory regardless of the adverse affect on downstream states) and absolute territorial integrity (the right of a downstream state to an uninterrupted flow of a fixed quantity of usable water from upstream states). Instead, it adopted the limited territorial sovereignty principle, which introduces equitable utilization and the obligation not to cause significant harm (Dinar et al., 2007). The Nile basin countries should adopt these two principles to go forward and have a lasting negotiated agreement with a spirit of striking a reasonable balance between the historical downstream uses with the new need to use by the upstream countries i.e., the historic rights and the no-harm principle Egypt and Sudan relies and the equitable utilization principle the upstream countries depend upon.

## 20.7 Climate Change and Water Resources

Global climate change is an accepted reality by many scientists around the world. Since the industrial revolution, the mean surface temperature of Earth has increased an average of 1°C per century mainly due to the accumulation of greenhouse gases in the atmosphere. Furthermore, most of this change was in the past 30–40 years, and the rate of increase is accelerating. Seen over the last millennium, this rapid warming represents a strong deviation from the norm. Increase in temperature by several degrees is expected over the next century (Mitchell et al., 1995; Wigley and Raper, 1992; Houghton et al., 1992).

Intergovernmental Panel on Climate Change (IPCC) predicts this change to be in the order of 1.5–6°C per 100 years. A change of this magnitude is unprecedented and will result in significant impacts that will be felt at a global scale, potentially disrupting the overall ecosystem. Some believe global climate change as a result of the effect of greenhouse gas concentration is already evident (Thomson, 1995). The

twentieth century's ten warmest years all occurred in the last 15 years of the century (Colby et al., 2005).

Hulme et al. (2001) used observed data to analyze past and future climates for the African continent using four greenhouse gas (GHG) emission scenarios and 7 global circulation model (GCM) outputs. The study confirmed temperatures have risen during the previous century and that this is expected to continue in the twenty-first century. The study also found a slight increase in rainfall volumes over the equatorial lakes. Future rainfall uncertainty, especially for the Ethiopian Plateau was high. Setegn et al. (2011) studied the watershed level hydrologic response due to the predicted climate change (increase in temperature and decline in precipitation) in the upper Blue Nile River basin. Using 4 scenarios and 15 GCMs, the downscaling analysis for the periods 2046–2065 and 2080–2100 resulted a mixed prediction in terms of precipitation decline and temperature increase. High uncertainty and less conformity among the GCMs were observed. Based on the outputs from the Soil Water Analysis Tool (SWAT) model using the predicted rainfall and air temperature, an increase in evapotranspiration, decline in river flows, groundwater level and soil moisture was observed at the watershed scale in the Lake Tana basin for selected gauging stations. Chapter 12 discusses the detailed analysis of this study.

In a separate study, based on the watershed scale modeling result using outputs from three GCMs, Conway and Hulme (1996) also predicted that Lake Victoria outflows will range from –9.2 to +11.8% in 2025. For the Blue Nile, outflow varied from –8.6 to +15.3% in the same period. Various studies have found that fluctuations in the main Nile River are mainly caused by changing rainfall patterns within the Blue Nile basin.

The fourth assessment report of the IPCC gives mostly quantitative prognoses for climate change (Boko et al., 2007). This report indicated that temperature rises is likely to be larger for Africa than for the rest of the world throughout the entire continent and in all seasons. Dryer subtropics (e.g. the Ethiopian Plateau) warm more than wetter tropics. Tate et al. (2004) analyzed the sensitivity of the water balance of Lake Victoria to climate change using HadCM3 A2a and B2 emission scenarios, and indicated that changes in annual rainfall and evaporation derived from HadCM3 implied that declines in water levels would occur during the 2021–2050 time horizon.

IPCC summarized hydrologic changes that can be expected as a result of global warming to include changes in precipitation levels, seasonal patterns of regional precipitation, and flood frequencies. Specifically, their analysis suggested that a projected increase in the average temperature will have the effect such that the frequency and severity of droughts could increase in some areas as a result of decrease in total rainfall, more frequent dry spells, and higher evaporation. They also pointed out that the hydrology of arid and semi-arid areas is particularly sensitive to climate variation such that small variations in temperature and precipitation in these areas can result in a large percentage changes in runoff, increasing the likelihood and severity of droughts and floods.

Most studies indicate climate change in the basin will occur and will shift and reshape the annual and seasonal climate patterns. It is inevitable that runoff and

water supply will change. More important is also the fact, in the Nile basin, climate variability is amplified by the complexity of the hydrology of the basin. For example, precipitation varies from close to about 2,000 mm/year in the Ethiopian highlands and valley lakes to almost zero in the Egyptian deserts. Climate variability can bring large changes in the reliability of the existing reservoirs yield from small changes in precipitation and runoff. Climate changes can also reduce the productivity of hydroelectric dams by causing fluctuations in hydroelectric generation. The challenge is thus developing basin wide strategies to minimize the adverse effects of climate change and implementing it before it occurs. This is a serious consideration as the whole basin heavily depends on hydroelectricity and drought will affect the availability and cost of electricity.

Climate change has also a serious implication on sharing of the Nile water. It should be considered in all the negotiations and decision-making regarding the equitable water allocation. There should, for example, be an anticipation of droughts and prepare for it. Climate forecasting, monitoring and evaluating hydrologic variables will also help the parties adapt changes that will address water allocation in wet and dry years. It will help negotiate priorities of deliveries of the available river water especially during dry years.

Most of the Nile basin countries are more prone to climate change by the nature of their weak economy, poor infrastructures, and limited institutional capacity, as well as their greater reliance on climate-sensitive sectors like agriculture. They are least able to cope with it and are poised to suffer most. Adaptation to the ongoing and potential effects of global climate change must be a key consideration basin wide if these countries are to develop their economies.

The challenge is responding to the anticipated climate change to minimize the adverse effect of such changes. To this end, both structural and non-structural measures have to be considered. Flexible anticipatory adaptation policies with full consideration to the uncertainties of predicting the different types of climate change must be put in place. Climate change should be incorporated in long-term basin water management planning. Use of inter-basin water transfers should be considered. Water conservation practices should be put in place. Changes in design and construction of hydraulic structures and proper dam sites selection should be adapted. Above all change of attitude on the use and conservation water should be an important component of adaptation strategies.

## 20.8 Information Sharing

Solutions to water management problems in the basin start and end with reliable data and information. Data gathering on the flow of the Nile, the quality of the water, control, and distribution is absolutely a prerequisite for any cooperation in managing shared water resources. At present, the collection and processing of hydrometeorological data and modeling work for forecasting hydrologic responses in the basin are limited to the downstream states with very inadequate systems in the upstream states. This imbalance has created anxiety among some countries to an

extent they are not willing to exchange information with the downstream countries. This is based on the belief that information provides power to whoever owns it. This sometimes can create an apparent sense of control and advantage for the owner but can also create unnecessary suspicion for those who do not have it. Sharing data and information enable people to think together in solving problems, in building trust essential for cooperative efforts towards sustaining shared vital natural resources and in avoiding conflict. Naff (1999) summarized advantages of sharing data and information in that it enables people to think together in solving problems, to build trust, and avoid conflict. Sharing is the foundation of good neighborliness. The ideal of peaceful, cooperative use of water and the environment cannot be achieved in the absence of sharing. Shared data is the most productive and efficiently used data. Solutions to water problems must be commensurate with their complexity; this is not possible without adequate, shared data. Equitable distribution of water among the users of transboundary water is not possible without shared data. Cooperative data collection and sharing prevents unnecessary duplication and reduces costs for all involved parties.

The Nile water resource management requires that the countries share data that is useful for planning, modeling, and management of a shared resource. This includes collecting relevant data, conducting water availability, and sustainable water yield analysis. The challenge is to establish a protocol for collecting and analyzing data, managing, and sharing information among the ten riparian countries without a single country dominating and taking advantage of the others. To this end, the priority should be to identify and acquire the necessary technology for monitoring, information and data gathering, build capacity and skills of the manpower needed in each country, and create the incentives for local data collection and data sharing. As an example, at a basin level, countries upon recognizing or anticipating specific water resources problem or combination of problems should initiate information and data gathering to determine the exact nature and extent of the water problems (including quantification of availability of the water resource and the past, present and projected water demands) and determine whether those problems warrant basin wide or local attention.

## 20.9 The Way Forward

The Nile water is critical for long-term economic development, health and social welfare of the population in the basin. Any water shortage in the future is likely to restrain socio-economic development and to become a potential source of conflict between the basin countries. Solutions to existing and potential problems of the Nile water resources sustainability therefore should be viewed with the desire to minimize such possibilities.

The Nile basin countries have been negotiating for decades over the amount of water each country to use. These negotiations involved some mutually shared goals. Some countries have distinct and often conflicting objectives on what they want to accomplish with the negotiation. Despite these conflicting objectives, emphasis

should be given to addressing the common goals of all the basin countries. These goals include secured access to water, water projects for economic development, stable, comprehensive and lasting water agreement, coordinated and integrated water management, improved relationship and communication among the riparian countries, and a well defined process for conflict resolution within the basin.

To address these mutual goals, the way forward for the basin is to focus on benefit sharing rather than water sharing, multilateralism instead of unilateralism, and enhancing more cooperative approach. Establishing the NBI legal and institutional framework agreement with full consideration of the hydropolitics of the basin is urgently needed if the countries are to overcome their differences and attain a sustainable water development and management system. Improving the understanding of past climate conditions based on a collaborative information and data sharing system with the goal of improving the ability to predict the future effect of global climate change is also necessary. One should be optimistic and hopeful that the constructive measures suggested would be put to work to respond to the crucial issues of sustainable water resource development and management in the basin with a shared vision of developing and managing the Nile water, fight poverty, advance socioeconomic development, and promote peace and stability in the region.

## References

Abu Zeid M (1987) Environmental impact assessment for the aswan high dam. In: Biswas A, Geping Q (eds) Environmental impact assessment for developing countries . Water Research Center, Ministry of Irrigation, London, pp 168–190

Aly AIM, Froehlich K, Nada A, Awad M, Hamza M, Salem WM (1993) Study of environmental isotope distribution in the aswan-high- dam lake (Egypt) for estimation of evaporation of lake water and its recharge to adjacent groundwater. *Environ Geochem Health* 15:37–49

Boko M, Niang I, Nyong A, Vogel C, Githeko A, Medany M, Osman-Elasha B, Tabo R, Yanda P (2007) Africa. In: Parry ML, Canziani OF, Palutikof JP, van der Linden PJ, Hanson CE (eds) Climate change 2007: impacts, adaptation and vulnerability. Contribution of working group II to the fourth assessment report of the Intergovernmental Panel on Climate Change. Cambridge University Press, Cambridge, UK, pp 433–467

Chebud YA, Melesse AM, (2009) Modeling lake stage and water balance of Lake Tana, Ethiopia. *Hydrol Process* 23(25):3534–3544

Colby BG, Thosser J, Britton S (2005) Negotiating Tribal Water Rights: Fulfilling Promises in the Arid West. University of Arizona Press

Conway D, Hulme M (1996) The impacts of climate variability and future climate change in the Nile Basin on water resources in Egypt. *Int J Water Resour Dev* 12(3):277–296

Dinar A, Dinar S, McCaffrey S, McKinney D (2007) Understanding Transboundary Water Conflict, Negotiation and cooperation. World Scientific on Energy and Resource Economics. Vol. 3. World Scientific Publishing Co. Ptc. Ltd.

Falkenmark M (1989) The massive water scarcity now threatening Africa-why isn't it being addressed? *Ambio* 18(2): 112–118

Falkenmark M, Widstrand C (1992) Population and water resources: a delicate balance, *Population Bulletin*, Population Reference Bureau.

Houghton JT, Callander BA, Varney SK (1992) Climate change -1992- the supplementary report to the IPCC Scientific assessment. WMO/UNEP intergovernmental panel on climate change. Cambridge University Press, Cambridge

Hulme M, Doherty R, Ngara T, New M, Lister D (2001) African climate change: 1900–2100. *Clim Res* 17(2):145–168

Mitchell FB, Johns TC, Gregory JM, Tett SFB (1995) Climate response to increasing levels of greenhouse gases and sulphate aerosol. *Nature* 376: 501–504

Mohamed YA, Van der Hurk BJM, Savenije HH, Bastiaanssen WGM (2005) Hydroclimatology of the Nile: results from a regional climate model. *Hydrol Earth Syst Sci* 9:263–278

Naff T (1999) Data sharing for international water resource management: eastern Europe, Russia and the CIS. Kluwer Academic Publisher, The Netherlands

Nicol A (2003) The Nile: moving beyond cooperation. UNESCO-IHP-WWAP IHP-VI Technical Documents in Hydrology PC-CP Series No. 16.

Nile Basin Initiative (NBI) (2006) [www.nilebasin.org](http://www.nilebasin.org). Accessed Mar 2010

Roskar J (2000) Assessing the water resources potential of the Nile River based on data, available at the Nile forecasting center in Cairo. Hydrometeorological Institute of Slovenia UDC: 556.53 (282.263.1) 36. Ljubljana, [http://www.zrc-sazu.si/giam/zbornik/roškar\\_40.pdf](http://www.zrc-sazu.si/giam/zbornik/roškar_40.pdf)

Sadek MF, Shahin MM, Stigter CJ (1997) Evaporation from the reservoir of the High Aswan Dam, Egypt: a new comparison of relevant methods with limited data. *Theor Applied Climatol* 56:57–66

Setegn S, Rayner D, Melesse AM, Dargahi B, Srinivasan R (2011) Impact of climate change on the hydro-climatology of Lake Tana basin. *Ethiopia Water Resources Research*. doi:10.1029/2010WR009248, in press.

Tate E, Sutcliffe J, Declan C, Farquharson F (2004) Water Balance of Lake Victoria: update to 2000 and Climate change Modeling to 2100. *Hydrol Earth Syst Sci* 49(4):563–574

Teodoru C, Wuest A, Wehrli B (2006) Independent review of the environmental impact assessment for the Merowe Dam project (Nile River, Sudan) Eawag, Seestrasse 79, 6047 Kastanienbaum, Switzerland

Thomson DJ (1995) The seasons, global temperature, and precession. *Science* 268:59–68

Wigley, TML Raper SCB (1992) Implementation for climate and sea level of revised IPCC emissions scenarios. *Nature* 357:293–324

Woodward JC, Macklin MG, Welsby DA (2001) The Holocene fluvial sedimentary record and alluvial geoarchaeology in the Nile Valley of northern Sudan. In: Madday D et al (eds) *River basin sediment systems: archives of environmental change*. Rotterdam, Balkema, pp 327–355

# Index

## A

Abbey, 4, 31, 34–35, 100–102, 105, 252, 290, 292–294, 321–334, 404

Abtew Model, 164–165, 169, 171, 177

Agriculture, 4, 21, 40, 42, 64–66, 131, 147, 182, 192, 194–195, 208, 220, 223, 228, 242, 252, 262, 287, 298, 300, 302, 308–309, 338, 345, 376, 384–385, 387, 398, 407, 413

Agroecological zones, 19–20

Atbara, 227–239, 268, 276, 403–404, 406

## B

Bathymetry, 70, 74, 87

Blue Nile River basin, 3–35, 228, 241, 385, 412

Blue Nile River flow, 28–30, 32, 35, 270–271

Brightness temperature, 96–99, 102–103, 105–106

## C

Classification, 19, 24, 44–46, 53, 58–59, 66, 188–189, 191, 193, 215, 252, 300–301, 327, 350

Climate

change, 411–413

impact, 241–262

sensitivity, 227–239

Climatic factors, 267–279

Climatic teleconnections, 22–24

Cloud area and volume index, 104–105

CMAP, 110, 112, 114–116, 124

CMORPH, 110, 112–113, 115, 120, 122–124

Cold Cloud Duration (CCD), 97–101, 105, 113

Command area, 383

Convective activity, 95–96

Convective cloud tracking, 96–97

## D

Debre Mewi Watershed, 208–212, 214, 221, 223

Desktop Reserve Model, 340, 348–350

Downscaling, 242, 247–249, 261, 412

## E

El Niño Southern Oscillation (ENSO), 23–29, 35, 268, 273, 276, 278

Environmental flows, 337–356, 363, 376, 380

Erosion hotspot, 209–210

Ethiopia, 19, 69–88, 131, 147, 158, 163–177, 179–205, 210–211, 241–263, 268, 288–289, 313–315, 337–356, 409

Ethiopian highlands rainfall, 269–270

Evapotranspiration, 63, 163–177, 260, 288, 307, 412

Extreme rainfall intensity, 95, 102

## F

Flood

frequency, 185–186, 197–202, 205

risk, 183, 186, 193, 195–198

Fogera, 163–177, 179–205

## G

Geographic Information System (GIS), 45–46, 179–205, 207–223, 230, 250, 325, 331, 365, 370

Gilgel Abbay, 100–102, 105

Global Climate Models (GCM), 242–243, 245–249, 254, 259, 261–262, 275, 412

Global Environmental Flow Calculator (GEFC), 348–354

Global Precipitation Climatology Project (GPCP), 110, 112, 114, 116–117, 119, 124, 270

Gridded products, 111, 114–117, 122, 124, 126  
 Gurer Island, 73, 95–96, 106

**H**  
 Hillslope hydrology, 145, 314  
 Hydrological modeling/models, 41–44, 45–46, 48, 53, 59–63, 100, 130, 139, 155, 227–239, 246, 248–249, 251–253, 257–259  
 Hydrological variability, 3–35, 285, 293, 321  
 Hydrologiske Byråns avdeling för Vattenbalans (HBV), 74–75, 79, 228–229, 233–239  
 Hydro-meteorology, 39–66  
 Hydropolitics, 408–411  
 Hydropower, 290, 292–294, 321–334, 338, 344–348, 355, 406

**I**  
 Infiltration excess, 151–153  
 Interventions, 298, 308, 310–312  
 Irrigation, 290–295, 298–300, 307, 309, 311, 346, 355, 360, 366, 369–372, 374–375, 378–381, 403, 407–408 schemes, 291–293, 301, 305, 307, 338, 344–345, 365, 383–398

**K**  
 Kenya, 40–42, 48, 53–54, 213, 301, 303, 307, 312, 338, 360–368, 372, 402–404, 408–409

**L**  
 Lake Tana, 29–31, 42, 69–88, 93, 95–97, 100, 102, 105–106, 146, 164–166, 180, 182–184, 195, 203–204, 207–223, 243, 246–247, 251–254, 261–262, 283, 288, 292–293, 295, 301, 307, 344, 347, 403–406, 412  
 Lake Tana basin, 29, 42, 71–73, 81, 95, 164, 183, 243, 246–247, 251, 253–254, 262, 412  
 Lake Victoria, 26, 41, 48, 301, 305, 307, 360, 365, 403, 405–406, 412  
 Land cover, 21–22, 40, 44–46, 50, 53, 57–59, 132, 164, 172, 185–186, 188–190, 192–193, 196, 202–205, 207, 209, 211–212, 215–216, 218, 220, 250, 252–253, 261, 305, 378, 380  
 mapping, 57–60  
 Landsat, 44, 46, 59, 66, 185, 188

Land use/land cover dynamics, 182–183, 185–186, 188–190, 192–193, 196, 202–205, 212, 215, 218, 220, 253, 261, 378, 380  
 Livestock, 300–303, 360–362, 366–368, 374, 376, 379  
 water productivity, 297–317

**M**  
 Makkink, 163–165, 168, 170–171  
 Mara River, 39–66, 359–381  
 Moderate Resolution Imaging Spectroradiometer (MODIS), 167, 169, 176  
 Multicriteria Evaluation (MCE), 183, 186, 193, 205

**N**  
 Nile Basin Initiative (NBI), 285, 316, 360, 409–410  
 Nile Forecast System (NFS), 227–231, 234–239  
 Nile hydrology, 129–141, 406  
 Nile River basin, 3–35, 230–231, 239, 285, 297, 343–356, 401–415  
 Nile River flow variability, 267–279  
 Nile water, 160, 284, 288, 290, 295, 298, 305, 316, 384, 401–402, 404, 407–411, 413–415

**P**  
 Penman-Monteith, 163–165, 167, 169–171  
 Perched water table, 153–155  
 Potential, 321–334  
 Priestley-Taylor, 43, 165, 168, 170

**R**  
 Rainfall estimation (RFE), 48, 93–106, 110–111, 113, 230  
 Rainfall frequency analysis, 4  
 Regionalisation, 70, 74, 79, 83–86, 350  
 Remote sensing, 45, 52, 94–96, 105–106, 163–177, 179–205, 207–223, 305, 359, 368  
 Renewable energy, 322–323  
 The Revised Universal Soil Loss Equation (RUSLE), 209–210, 216–218

**S**  
 Satellite, 93–106, 129–141, 163–165, 182, 185, 205, 208  
 rainfall, 109–126, 278, 371, 405  
 Saturation excess, 151, 153, 155–156

Sediment, 41–44, 63, 65, 202, 209, 213, 231, 250, 283, 288–290, 292–293, 295, 312, 361, 406

Soil and Water Assessment Tool (SWAT), 40, 42–45, 47–48, 50, 52–53, 59–60, 66, 130–132, 134, 136–140, 146, 243, 250–252, 254, 257–259, 412

Soil(s), 20–21, 45, 47, 389–392  
    erosion assessment, 209  
    salinity, 397

Spatial Report on Emissions Scenarios (SRES), 243, 247, 255–256, 258–259

Surface Energy Balance System (SEBS), 73, 165, 167, 169, 172, 176

Sustainability, 247, 311, 342, 361, 373, 381, 385, 401, 414

**T**

Tanzania, 39–41, 53–54, 268, 301, 307, 338, 342, 360–367, 371, 403, 408–410

Tennant Method, 348–353

Topography, 3, 18–21, 42, 45, 70, 77, 110, 131, 148–149, 164, 208, 210–211, 219, 247–248, 308, 323–325, 344, 387

Transboundary river basin, 342

TRMM-3B42, 110, 112–113, 120, 124

TRMM multi-satellite precipitation analysis (TMPA), 113, 129–130, 139–140

**U**

Uncertainty, 50, 52, 87, 186, 242, 254, 257, 261, 298, 304, 343, 412

Ungauged watersheds, 72, 86

**V**

Variable source area, 160

**W**

Water  
    allocation, 304, 346, 378, 413  
    balance closure, 70  
    budget, 3–35, 39–66, 69–88  
    depletion, 298, 315–316  
    management, 24, 287, 298, 311, 346, 387, 398, 408, 410, 413, 415  
    quality, 52, 346, 362, 373, 381, 385, 397, 402, 408  
    resources development, 291, 295, 321, 345–346, 355, 402, 407  
    supply and demand, 359–381  
    use, 298, 304–305, 307–308, 312, 316, 365, 369, 373–376, 378–379, 385, potential, 283–295

Watershed  
    hydrology, 145–161  
    modeling, 145–161, 163–177, 179–205, 207–223

Wildlife, 40, 350–351, 360–361, 366–368, 374–375, 379–380